

## **General Disclaimer**

### **One or more of the Following Statements may affect this Document**

- This document has been reproduced from the best copy furnished by the organizational source. It is being released in the interest of making available as much information as possible.
- This document may contain data, which exceeds the sheet parameters. It was furnished in this condition by the organizational source and is the best copy available.
- This document may contain tone-on-tone or color graphs, charts and/or pictures, which have been reproduced in black and white.
- This document is paginated as submitted by the original source.
- Portions of this document are not fully legible due to the historical nature of some of the material. However, it is the best reproduction available from the original submission.





## Technical Memorandum 78063

# The GISS Sounding Temperature Impact Test

(NASA-TM-78063) THE GISS SOUNDING  
TEMPERATURE IMPACT TEST (NASA) 448 P HC  
A19/MF A01 CSCI 04E

N78-31667

Unclas

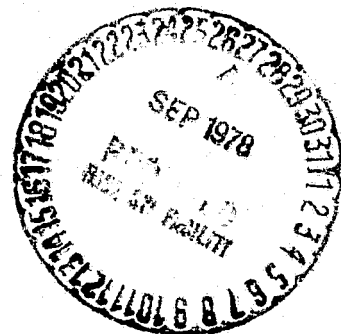
G3/47 31855

**Milton Halem  
Michael Ghil  
Robert Atlas  
Joel Susskind  
W. J. Quirk**

**JANUARY 1978**

National Aeronautics and  
Space Administration

**Goddard Space Flight Center**  
Greenbelt, Maryland 20771



## THE GISS SOUNDING TEMPERATURE IMPACT TEST

M. Halem, M. Ghil, R. Atlas, J. Susskind and W.J. Quirk,  
with the collaboration of GTE staff.

January, 1978

### PRINCIPAL CONTRIBUTORS:

R. Dilling, D. Edelmann, D. Sakal, Y. Sud, R. van Norton, H. Carus, R. Mosebach,  
P. Suchanick, L. Peng, B. Shkoller, L.-C. Tsang, A. Smith, I. Morrow, E. Tobenfeld,  
N. Rushfield, C.-Y. Tung, M. Economedes, C. Ryan, J. Majewski, K.K. Wong, T. Kern,  
E. Umland, J. Forkosh, J. Searl, P. Anolick, T. Kimmel and R. Kinkhabwala.

GODDARD SPACE FLIGHT CENTER  
NATIONAL AERONAUTICS AND SPACE ADMINISTRATION

# TABLE OF CONTENTS

	<u>Page</u>
PREFACE . . . . .	i
SUMMARY . . . . .	vi
CONCLUSION . . . . .	xii
CHAPTER 1.	
INTRODUCTION . . . . .	1-1
1.1 Background . . . . .	1-1
1.2 Assessment of Factors Influencing the Sounder Impact on Forecasting . . . . .	1-3
1.3 Operating Approach . . . . .	1-8
CHAPTER 2.	
SOUNDING TEMPERATURE STUDIES (STS) . . . . .	2-1
2.1 Introduction . . . . .	2-1
2.2 Operational Temperature Retrievals for DST-5 and DST-6 . . . . .	2-9
2.2.1 NIMBUS-6 HIRS, SCAMS, THIR . . . . .	2-9
2.2.1.1 Overview . . . . .	2-9
2.2.1.2 Data Systems Test-5 . . . . .	2-10
2.2.1.2.1 Yield . . . . .	2-10
2.2.1.2.2 Accuracy . . . . .	2-14
2.2.1.3 Data Systems Test-6 . . . . .	2-14
2.2.1.3.1 Yield . . . . .	2-17
2.2.1.3.2 Accuracy . . . . .	2-17
2.2.2 NOAA-4 VTPR . . . . .	2-18
2.2.2.1 Overview . . . . .	2-18
2.2.2.2 DST-5 and DST-6 Yields . . . . .	2-18
2.2.2.3 DST-5 and DST-6 Accuracies . . . . .	2-22
2.3 GISS Approach to Temperature Sounding: Theoretical Consideration . . . . .	2-22
2.3.1 Temperature Retrievals Given Clear Column Radiances . . . . .	2-25
2.3.2 Cloud Effects . . . . .	2-26
2.3.2.1 Cloud Filtering . . . . .	2-27
2.3.2.1.1 Dual Field of View Approach . . . . .	2-28
2.3.2.1.2 Determination of $\eta$ - Infrared Channels . . . . .	2-28
2.3.2.1.3 Apparent Temperature Profiles . . . . .	2-29

# TABLE OF CONTENTS (Continued)

	<u>Page</u>
2.3.2.1.4 Sensitivity of $\eta$ to Initial Guess	2-30
2.3.2.1.5 Dual Frequency Principle	2-31
2.3.2.1.6 Determination of $\eta$ - Microwave Channels	2-33
2.3.3 Use of Microwave Channels for Temperature Sounding.	2-34
2.3.4 Cloud Height Determination	2-35
2.3.5 Alternate Temperature Inversion Scheme	2-36
2.4 GISS Operational Procedures for Data Reduction	2-40
2.5 Determination of Temperature Profiles	2-41
2.5.1 VTPR	2-41
2.5.2 NIMBUS-6 Sounders	2-42
2.5.2.1 Overview	2-42
2.5.2.2 Stratospheric Sounding Channels	2-44
2.5.2.3 Tropospheric Sounding and Cloud Filtering Channels	2-44
2.5.2.3.1 Microwave Alone	2-44
2.5.2.3.2 HIRS Alone	2-45
2.5.3 Results of HIRS and SCAMS Retrievals	2-47
2.5.4 Combined HIRS-SCAMS Retrievals	2-54
2.5.5 Comparison of VTPR and NIMBUS Soundings	2-55
2.5.6 NIMBUS 6 Soundings in the Winter DST Period	2-59
2.5.6.1 Winter Retrieval Procedures	2-59
2.5.6.2 Results of Winter Retrieval	2-60
2.5.7 Comparison of Quality of Winter and Summer Soundings	2-63
2.6 Assessment of Retrievals in the Arctic	2-64
2.7 Cloud Height Retrievals	2-68
2.8 Comparison of GISS and NESS NIMBUS 6 Retrievals	2-72
2.8.1 Yield	2-72
2.8.2 Accuracy of Retrievals	2-75
2.8.3 Dependence of Retrievals on the Initial Guess	2-75
2.9 Conclusions	2-77
2.9.1 Expectations for FGGE	2-80

## CHAPTER 3.

ANALYSIS AND ASSIMILATION	3-1
3.1 Introduction	3-1
3.2 Methods	3-4
3.2.1 Direct Insertion Method (DIM)	3-4

# TABLE OF CONTENTS (Continued)

	<u>Page</u>
3.2.1.1 Introduction . . . . .	3-4
3.2.1.2 Quality Control of Insertion Data . . . . .	3-4
3.2.1.3 Description of DIM Experiments . . . . .	3-7
3.2.1.4 Results of DIM Experiments . . . . .	3-9
3.2.1.5 Conclusion . . . . .	3-10
3.2.2 Automated Consistency Check . . . . .	3-11
3.2.2.1 Introduction . . . . .	3-11
3.2.2.2 Procedure . . . . .	3-11
3.2.2.3 Results . . . . .	3-16
3.2.2.4 Conclusions and Recommendations . . . . .	3-17
3.2.3 Local Interpolation Procedure (LIP) . . . . .	3-18
3.2.3.1 Introduction . . . . .	3-18
3.2.3.2 The Method . . . . .	3-18
3.2.3.3 Preliminary Results . . . . .	3-20
3.2.3.4 Conclusion . . . . .	3-23
3.2.4 Successive Correction Method (SCM) . . . . .	3-23
3.2.4.1 Introduction . . . . .	3-23
3.2.4.2 The Analysis Method . . . . .	3-24
3.2.4.3 Applications and Results . . . . .	3-26
3.2.4.4 Conclusions and Recommendations . . . . .	3-32
3.2.5 Asynoptic Variational Method for Satellite Data Assimilation . . . . .	3-32
3.2.5.1 Introduction . . . . .	3-32
3.2.5.2 The Method . . . . .	3-35
3.2.5.3 Preliminary Results . . . . .	3-39
3.2.5.4 Application to Large Regions . . . . .	3-46
3.2.5.5 Concluding Remarks . . . . .	3-49
3.2.6 Filtered Equations Method (FEM) . . . . .	3-50
3.2.6.1 Filtered Equations Method, I: Preliminary Tests of a Global Balance-Equation Model . . . . .	3-50
3.2.6.1.1 Introduction . . . . .	3-50
3.2.6.1.2 The Model . . . . .	3-53
3.2.6.1.3 Method of Solution . . . . .	3-56
3.2.6.1.4 Some Preliminary Tests . . . . .	3-61
3.2.6.1.5 Summary and Concluding Remarks . . . . .	3-70
3.2.6.2 Filtered Equations Method, II: The Balance- Equation Model as a Data Assimilation Tool . . . . .	3-79
3.2.6.2.1 Introduction . . . . .	3-79
3.2.6.2.2 The Method . . . . .	3-80
3.2.6.2.3 Preliminary Results . . . . .	3-82
3.2.6.2.4 Concluding Remarks . . . . .	3-87

## TABLE OF CONTENTS (Continued)

	<u>Page</u>
3.2.7 Statistical Assimilation Method . . . . .	3-89
3.2.7.1 Introduction . . . . .	3-89
3.2.7.2 The Method . . . . .	3-91
3.3 Results . . . . .	3-98
3.3.1 Description of the Experiments . . . . .	3-98
3.3.1.1 Introduction . . . . .	3-98
3.3.1.2 Summer Experiments . . . . .	3-100
3.3.1.3 Winter Experiments . . . . .	3-107
3.3.1.4 Computational Aspects of Experiments . . . . .	3-111
3.3.2 Comparison of Results . . . . .	3-113
3.3.2.1 Introduction . . . . .	3-113
3.3.2.2 DST-5 Results . . . . .	3-115
3.3.2.3 DST-6 Results . . . . .	3-141
3.4 Conclusions and Recommendations . . . . .	3-165

## CHAPTER 4.

FORECAST MODEL DEVELOPMENT . . . . .	4-1
4.1 Approach . . . . .	4-1
4.2 Development of the Ultrafine Model . . . . .	4-3
4.3 Testing the Ultrafine Forecast Model . . . . .	4-9
4.4 Implementation of the Ultrafine Assimilation Cycle with DST-6 Data . . . . .	4-14
4.4.1 Introduction . . . . .	4-14
4.4.2 Assimilation and Forecast Experiments Used to Test the Ultrafine Model . . . . .	4-15
4.5 Problems of Statistical Evaluation . . . . .	4-19
4.6 Statistical Evaluation of the Ultrafine Model and Assimilation Cycle . . . . .	4-20
4.7 Synoptic Evaluation of Ultrafine Forecasts . . . . .	4-23
4.8 Conclusions . . . . .	4-35

## CHAPTER 5.

EVALUATION AND VERIFICATION TESTS . . . . .	5-1
5.1 Introduction . . . . .	5-1
5.2 Background . . . . .	5-3
5.2.1 Preliminary Subjective Evaluation . . . . .	5-3
5.2.2 The Computerized Forecasting Model . . . . .	5-7
5.3 Impact of Satellite Data on Analyses . . . . .	5-21

# TABLE OF CONTENTS (Continued)

	<u>Page</u>
5.3.1 Initial State Differences . . . . .	5-21
5.3.2 Isentropic Cross Section Analyses . . . . .	5-26
5.3.3 The Energy Spectrum of the Satellite and No-Satellite Analyses . . . . .	5-31
5.4 Impact of Satellite Data on Prognostic Flow Patterns . . . . .	5-40
5.4.1 Statistical Comparisons . . . . .	5-40
5.4.2 Synoptic Comparisons . . . . .	5-45
5.4.2.1 Forecast Differences . . . . .	5-45
5.4.2.2 Case Studies . . . . .	5-46
5.5 Impact of Satellite Data on Actual Weather Forecasts . . . . .	5-78
5.6 Conclusions and Recommendations . . . . .	5-80

## PREFACE

This report documents the findings obtained from the DST Temperature Sounding Impact Test Project conducted at GISS between April 1976 and April 1977. The objective of the project was to determine the impact on weather forecasting that can result from operational use of temperature profiles obtained from satellite soundings.

The project stemmed from the recommendation of an ad-hoc advisory committee that met at GISS in March 1976 to review the meteorological research program. The consensus of the committee was that among GISS meteorological programs, the sounder impact study had the highest priority, in terms of Agency objectives.

Results from the project tests show the impact of sounding data to be substantial and beneficial for a one-month winter test period, according to all the verification criteria applied. Results for a two-week summer test period show positive impacts of considerably smaller magnitude with much less statistical significance. The magnitude of the monthly mean impact in the winter forecasts is comparable with that of improvements made in NMC operations over the past decade.

The largest magnitude of the sounder data impact was obtained (1) using the combined data from two satellites and (2) applying a time-continuous four-dimensional assimilation procedure developed at GISS and based on statistical weighting ("optimal interpolation") of temperatures. Significantly smaller (but positive) forecast impacts resulted when conventional data assimilation methods were used.



These smaller positive impacts from conventional assimilation techniques agree in magnitude with results recently reported by NMC for this same DST period.

*This study leads us to believe that adoption of the GISS assimilation techniques, plus operational use of simultaneous data from two satellites should result in a significant increase in the accuracy of 48 and 72 hour forecasts.*

## DESCRIPTION OF EXPERIMENTS

Sounder Impact experiments were carried out for the DST-5 and DST-6 periods of Data System Testing. The periods over which the DST data were used extended from Aug. 18 through Sept. 4, 1975, for DST-5, and Jan. 29 through Feb. 21, 1976, for DST-6. The data sets contained all the conventional operational upper air and surface data collected by the National Meteorological Center in a ten-hour window about synoptic times, as well as special aircraft reports, cloud-tracked winds and temperature sounding data. The temperature sounding data sets included the NESS operational sounding data from the VTPR instrument on the NOAA-4 satellite and NESS-processed sounding profiles obtained from the HIRS and SCAMS instruments on the NIMBUS-6 satellite.

Each impact experiment consisted of a distinct analysis/forecast cycle for the entire period. The same forecast model was used in all the impact experiments. The analysis scheme treated all the data identically in every experiment except for the handling of sounding temperature profiles. The basic cycle which serves as the control experiment is the "NO SAT" case and consisted of omitting all satellite sounding data. Every other experiment reported involved asynoptic assimilation of the sounding data within ten-minute intervals of the time of

observation. Experiments differed from each other either in respect to the number of satellite sounders from which data were used or in the method by which the data were assimilated. In no experiment were the cloud-track wind data from the University of Wisconsin included in the study.

## RESULTS OF EXPERIMENTS

The major impact results summarized below are derived from the experiment in which optimal statistical weighting procedures were applied to the sounding data. The results are presented for the 48 and 72 hour forecast comparisons using the GISS analysis technique and forecast model.

The evaluation of the impact is assessed according to the following criteria:

- (i) Magnitudes and locations of initial-state differences in the analyzed fields produced *with and without satellite data*,
- (ii) Statistical measures of forecast accuracy (i.e.,  $S_1$  skill scores and rms errors) obtained from numerical integrations starting from the initial states prepared *with and without satellite data*;
- (iii) Verifications of local precipitation and surface temperature forecasts based on prognostic charts produced *with and without satellite data*.

The principal findings obtained for the winter test period are:

- Satellite data generate large initial state differences in data sparse regions which lead in turn to significantly different forecasts.
- Forecasts started from initial states obtained with the aid of satellite data show a mean improvement of about 4 points in the 48 and 72-hour  $S_1$  skill scores as verified over North America and Europe. This corresponds to an 8 to 12 hour forecast improvement in the forecast range at 48 hours.
- Satellite data lead to substantial differences in the 72 hour forecast errors over North America in 83% of the winter forecasts. Of these, 77% of the impacts were beneficial resulting in a 38-75% reduction of errors at 500mb.
- An automated local precipitation forecast model applied to 128 cities in the United States showed an average 15% improvement when satellite data had been used for the numerical forecasts. Over the midwest, where the difficulties in modeling mountain and coastal effects can be avoided in the precipitation model, there was a 75% improvement obtained from the use of satellite data.
- The statistical impact of data from two satellites is greater than that from either satellite alone and is proportional to the combined sounding yield of both satellites.
- Satellite soundings do not systematically smooth potential temperature gradients.

In the coming year, more detailed studies of certain aspects of the data assimilation method are planned. In addition, similar tests will be conducted employing a higher resolution model. Among the problems which still require study and clarification are the removal of the statistical bias of satellite data, the treatment of the large-distance tail in the statistical covariance error function, the propagation speed of disturbances in the model, and the effect of balancing techniques on initial states. From the outset of the project, many promising experiments had to be abandoned or deferred in order to meet the firm schedules leading to this report. It is hoped that some of these unfinished studies including the testing and operational use of GISS derived sounder temperature profiles can be completed in time for FGGE.

The instruments scheduled to become the operational system on TIROS-N are essentially the same as the present HIRS and SCAMS temperature sounders; it is expected therefore that the data processing and assimilation techniques developed for these sounders during the Data System Test may also be used for the future operational system. This means that the data assimilation technology developed for the present sounders will carry over to the TIROS sounding systems; it is hoped that the experimental results reported herein for the assimilation methods will then prove themselves operationally.

## SUMMARY

1. *Initial-State Differences.* Forecasting is an initial-value problem. If satellite data are expected to lead to improved forecasts, then a necessary condition is that they produce significant differences in the initial description of the atmospheric states. Earlier reports by NMC and GISS showed occasional large differences (of up to 60m in the 500mb heights) in data sparse regions. In the impact experiments employing the statistical assimilation method, the magnitude of the differences between initial states obtained with satellite data and without was found to be on the order of 90 to 120 meters in the 500mb heights at mid-latitudes in seven of the eleven initial forecast days during the winter test. Such a height difference corresponds roughly to a 5C mean virtual temperature difference in the 1000 to 500mb column. The differences occurred mainly in data sparse regions and range over areas between  $10^6$  and  $4 \times 10^6 \text{ km}^2$ . At low latitudes the areas where differences are observed were even larger, and so was the magnitude of the differences. The initial state differences in the summer were smaller, of the order of 30 to 60 meters over regions of areas from  $10^5$  to  $5 \times 10^5 \text{ km}^2$ . (See difference charts in Chapter 5, Figures 16a and 16b.)

The differences produced by the assimilation of satellite sounding temperatures showed a warm bias in the 1000 to 500mb thickness over the oceans in the mid to high latitudes of the northern hemisphere in ten of the eleven winter cases. It is not clear whether this systematic bias represents correct observations of a warmer synoptic situation or whether it is a spurious feature of the sounding system.

2. *Effect of Sounding Data on Analysis.* In a report by S. Tracton and R. McPherson (NMC Office Note 136), it is claimed that "the NIMBUS 6 soundings underestimate the variance in the thermal structure of the atmosphere, and this deficiency acts to the detriment of the analyses which incorporate the satellite data." This effect has been investigated in this report in terms of detailed subjective and automatic examinations of isentropic cross-sections throughout the winter period and also in terms of an analysis of the available potential energy budgets for the various experiments, as well as for NMC's own analysis. GISS studies do not seem to substantiate the claim that the sounder data analyses are affected in any serious way by a smoothing of the atmosphere's thermal structure.

Evaluations of isentropic cross-sections in the winter show that 406 cases of moderate to intense potential temperature gradients (greater than  $8^{\circ}/400\text{km}$ ) occurred along longitudes  $170^{\circ}\text{W}$  and  $150^{\circ}\text{W}$  for the North Pacific. Among these cases, 40 percent were weaker in the SAT system while 24 percent were more intense, the remainder being about the same. In 119 cases along longitude  $85^{\circ}\text{W}$  over the United States, 27 percent were weaker and 8 percent were more intense. This indicates that the sounding data are not leading to any systematic smoothing of the temperature fields in data sparse regions. Similar case results were obtained for cross-sections along specific latitudes in the N. Pacific. A tendency toward warmer temperatures was observed in the SAT analysis but no systematic smoothing of potential temperature gradients was evident. (Examples of isentropic variance are shown in Chapter 5, Figures 17 and 18.)

In subsection 5.3.3 we show that the 10-15 percent difference in eddy available potential energy between SAT and NO SAT analyses is primarily due to the differences in the Aleutian Low. To determine which analysis is correct, one would need more complete data in order to do a detailed study of the Aleutian areas. On the other hand, the GISS and NMC analyses differ by 25 to 50 percent, and they differ all over the globe. The NMC analysis scheme seems to considerably underestimate the available potential energy in the atmosphere. This could be a significant source of error in NMC forecasts, if underestimation of the variance in the thermal structure of the atmosphere indeed has a detrimental effect on the analyses.

3. *Net Statistical Impact.* The average improvement in the  $S_1$  skill scores of sea-level pressure and 500mb heights for the statistical assimilation experiment in the winter test was 5 percent when verified over North America and Europe; the corresponding improvement in rms error is 10 percent. (See Chapter 3, Tables 41 and 42, respectively.) This could represent an 8- to 12-hour forecast improvement. The statistical significance of these impacts was greater than two standard deviations. (See Chapter 3, Tables 40 and 43.) The statistical improvements in the summer were 2 percent and 5 percent respectively, (see Chapter 3, Tables 35 and 37, respectively) with smaller error significance attached to the impact. (See Chapter 3, Tables 36 and 38.)

The impact of the statistical assimilation method was approximately twice that obtained from the use of successive correction methods both in terms of percent impact and statistical significance. Compared with a direct insertion method the percent impact was roughly

four times as great and even more so in terms of statistical significance. (See Chapter 3, Tables 41 through 43.) The improvement in the statistical magnitude of forecast impact resolution just from optimal statistical weighting of sounding data compared with direct insertion is also in qualitative agreement with recent simulation studies reported by N. Philips of NMC. Since NMC reports a small but positive impact for the winter test roughly comparable to our impact with the successive correction method, there is good reason to believe that an adaption of the GISS statistical assimilation method will produce a similar improvement in the forecast accuracy of NMC operational forecasts.

A substantial positive impact occurred in a number of winter cases: 3 cases out of 11 showed improvements of more than 20 percent in  $S_1$  skill score and of 30 percent in rms errors. A longer sequence of impact tests is needed, however, to establish whether these cases are random occurrences or whether they are related to weather systems periodically missed in data-sparse regions by the current operational systems.

A further experiment was designed to test the conjecture that the impact is not a result of random disturbances produced by the four-dimensional temperature assimilation and wind balancing techniques of our method but mainly to actual information content extracted from the satellite data. In this experiment, simulated satellite data were generated at each time step from the 12 hour forecast fields, and temperature profiles computed at the position of each Nimbus sounding location were introduced; these profiles had the vertical error structure of actual satellite data. The errors used to generate the profiles were a function of height and latitude; they were obtained from regional comparisons with co-located radiosonde profiles. Assimilating these "fabricated" data led to negligible statistical impacts in both the sea-level and 500mb heights confirming the fact that the sounders provide real atmospheric information. (See Chapter 5, Table 4.)



4. *Subjective Interpretation of Forecast Impact.* Verification of prognostic charts of the 72-hour forecast errors for the SAT and NO SAT system analyzed over North America showed seven examples of synoptically better verifications of 500mb heights for the SAT system and two with the NO SAT system. The percent reduction in the forecast error in regions where the satellite had an impact ranged from 38 to 75 percent from day-to-day. Sea-level pressure differences were generally not as systematically favorable with the major deficiencies occurring over the North Atlantic. These regional impacts lead us to conclude that in general satellite data make larger and more consistent impacts in the 500mb height forecasts than in surface forecasts.

A computerized local precipitation forecast model was developed to test the impact of satellite data in terms of local weather forecasts. The model is based on calculations using quantities produced by the numerical model, such as vorticity advection, temperature advection; it also makes use of an algorithm embracing conventional practices employed for operational precipitation forecasting. The automatic precipitation model was applied to the SAT and NO SAT forecast outputs for the eleven cases and precipitation forecasts made for the same 128 cities in the United States used by the National Weather Service in their monthly regional forecast. The model indicated a net 15 percent improvement for the SAT system among all the occurrences of different yes/no precipitation forecasts. In particular, when there were restrictions on the number of cities to the midwest, in order to avoid the effects of mountains and coastal precipitation which are more difficult to model, there was a four-fold improvement in precipitation forecasting. (See Chapter 5, Table 6.)

5. *Dependence of Impact on Sounder Coverage.* Experiments were conducted to test the impact of each of the sounders separately. The statistical impact of temperature data from either the NOAA-4 or the NIMBUS-6 sounder alone was less than the impact when both were combined; the magnitudes were in proportion to the respective yields of the two sounder systems separately, and of the combined system.

This result supports earlier simulation studies reported by GISS where it was shown that (i) two satellites damp down wind errors more effectively than one, and (ii) that two satellites with observational errors of approximately  $2^{\circ}\text{C}$  have a comparable effect to one satellite with  $1^{\circ}\text{C}$  observational error.

## CONCLUSIONS

GISS impact test results point to two major areas which, if improved, can bring about larger forecast impacts from satellite sounder systems.

First, technology must be developed to improve the accuracy and vertical resolution of the sounder temperature profiles themselves. At present, the accuracy of vertical temperature sounding profiles derived from satellite radiance data when compared with co-located radiosonde profiles have rms errors of approximately 2-2.5°C. Although these accuracies fall short of meeting GARP data requirements, the data are still capable of producing the modest impacts demonstrated in this report when properly utilized. However, the deficiencies in the quality of the data can only partially be compensated for by special processing and assimilation methods. While continuous data monitoring and close interaction between the processing of raw data and the assimilation of processed data will remain as major considerations, the need for more accurate temperature profiles under all conditions is still the most important requirement.

Second, numerical prediction models themselves must be improved to make better use of the sounding data. In order to successfully assimilate synoptic data and have them contribute to more accurate forecasts, it is necessary that the model be able to convey information accurately over extended distances and periods of time from one region of the globe to another. Improvements in model forecasts can only proceed by a judicious combination of higher grid resolutions, more accurate numerical discretization methods, and better representations of atmospheric processes in the model.

A concerted effort in designing better observing instruments and systems, refining the methods for processing and assimilating their observations, and developing better numerical models will lead to considerable improvements in numerical weather prediction and to a better understanding of the atmospheric circulation; these are the goals of the Global Atmospheric Research Program.

## CHAPTER I

# 1. INTRODUCTION

## 1.1 BACKGROUND

Complete atmospheric temperature profiles with global coverage have been available from spaceborne IR grating spectrometers since SIRS 1 flew on NIMBUS-3 in 1969. Since that time, NASA and NOAA supported the evolution and flight testing of a series of instruments, each possessing significantly improved technological capabilities with respect to horizontal spatial resolution, spectral resolution, and scanning coverage. This effort led to the introduction of the VTPR instrument in December 1972, as the first operational sounder to become part of the data base of the National Weather Service. These operational sounders have been producing roughly 1000 VTPR sounding temperature profiles per day for use by NMC; this number is equivalent to half the total number of radiosonde reports, and they are routinely incorporated into the operational analysis.

More recently, prototypes of advanced sounders, which are expected to replace the current operational VTPR instrument, were flown and tested on NIMBUS-6. In spite of further technological improvements in sounders, the accuracies of temperature profiles have improved only marginally while the yield has been greatly increased. This quality of information has led to downward revisions for the expected accuracy of the TIROS sounders and in turn has led to a growing concern in the meteorological community about the effectiveness and usefulness of the sounder capability for the First GARP Global Experiment (FGGE).

During this period NOAA and NASA have conducted a limited number

of experiments on the operational impact of sounding data. Studies conducted at NMC with temperature data from the original SIRS and VTPR instruments and, more recently, from the new NIMBUS instruments, find no impact of satellite sounding data on forecast accuracy. Some scientists at NMC suggest that sounding data will actually degrade the forecast skill when numerical models with higher resolution are introduced into operational forecasting.

These findings run counter to conclusions reached from similar sounder studies conducted earlier at GISS. The studies reported by GISS find small but favorable forecast impacts in 48 to 72 hours when the full yeild of satellite data is inserted into the analysis.

This concern with sounder performance evidenced itself at a GISS program review held in March 1976, where a steering committee composed of scientific consultants and NASA management personnel recommended that program priority be given to tests of forecast impact from the NIMBUS-6 sounding data.

In accordance with this recommendation, a DST Sounding Temperature Impact Test Project was set up at GISS and a work plan submitted on April 15 was approved. That plan specified a definite assessment by December 31, 1976, and a preliminary assessment was delivered to the NASA administrator on December 6, 1976. This report serves to document that assessment and presents more recent results and investigations bearing on the interpretation of the sounding impacts.

## 1.2 ASSESSMENT OF FACTORS INFLUENCING THE SOUNDER IMPACT ON FORECASTING

*Accuracy.* The most important factor in forecast impact would seem to be the accuracy of the sounding data. Simulation studies confirm that data accuracy is in fact a significant element in forecast impact. RMS errors for sounding temperatures as compared with co-located radiosondes are about  $2.5^{\circ}\text{C}$  well above the desired accuracy levels specified in GARP documents. However, the yield of data, i.e., the amount of sounding data available as input for data assimilation, has turned out to be of comparable importance, both in the simulation study and in the real data tests. The importance of yield relative to accuracy was one of the surprises in this series of tests.

*Yield and Coverage.* The importance of yield in terms of forecast impact was a major consideration in the design of the GISS assimilation method. In simulation studies and in later real VTPR data tests, studies consistently showed that the magnitude of the impact was proportional to the quantity (frequency of insertion per gridpoint per day) of data inserted in the model. For example, results of the simulation study shown in Figure 1 indicate that sounding temperature profiles from two satellites having  $2.5^{\circ}\text{C}$  error accuracies yield initial states of comparable accuracy that would be provided from one satellite sounder having  $1^{\circ}$  accuracy.

The trade-off between accuracy and yield has never been fully exploited by the operational groups responsible for providing temperature sounding data, nor by the groups responsible for incorporating the sounding profiles into operational forecast systems. Part of the reason this idea apparently failed to take hold in operational



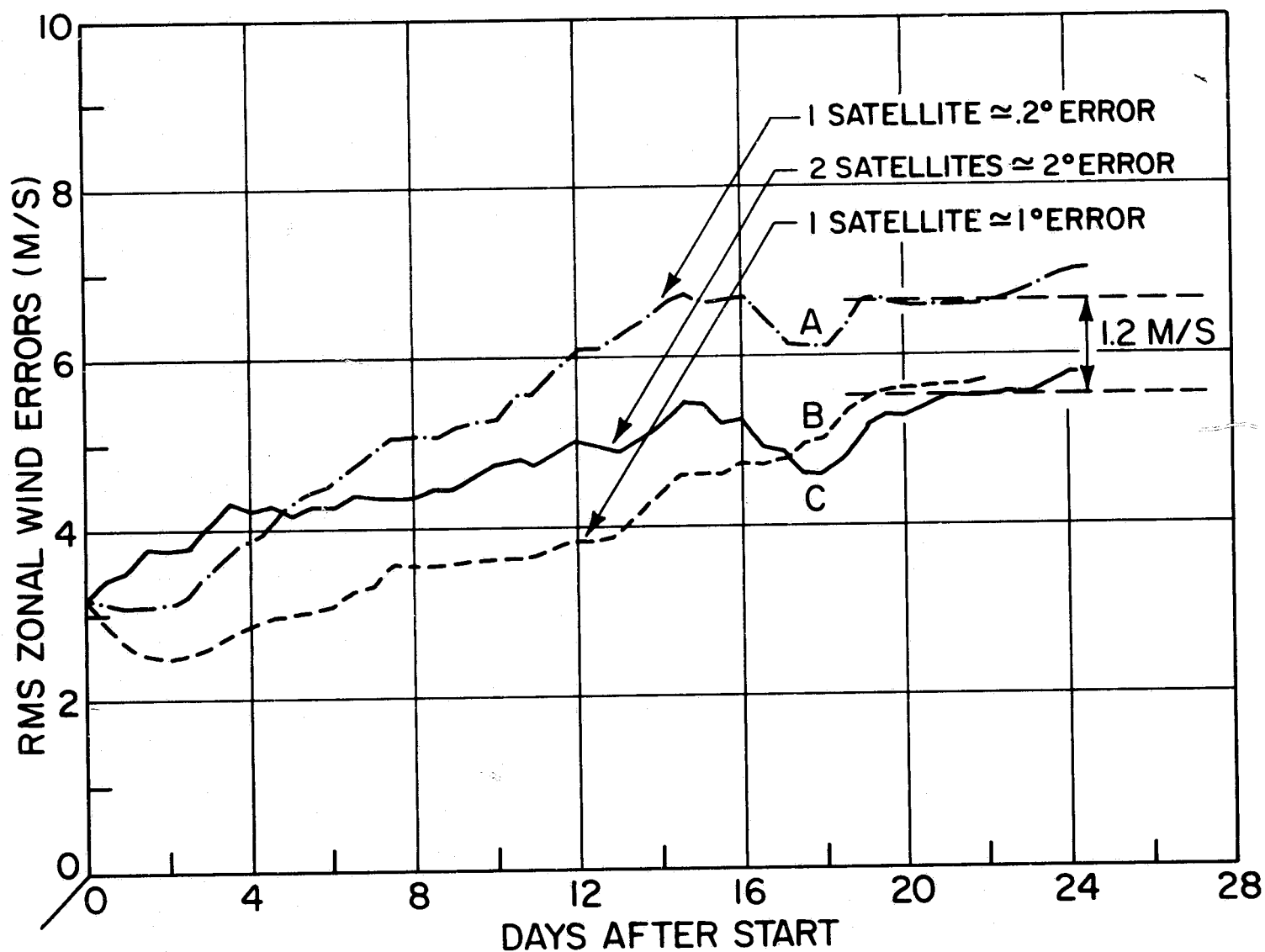


Figure 1. Trade-Off: Accuracy vs. Coverage.

practice was the fact that processing procedures were developed to toss out data which were perceived to be suspect by cloud contamination thereby reducing the yield. Alternative techniques were proposed by GISS which could have greatly increased the yield without degrading the overall accuracies. Similarly, techniques utilizing the full field of observations, based on four-dimensional assimilation and horizontal temperature gradients corrections that could be used to adjust the mass field, were also tested and recommended.

The NIMBUS-6 sounding data and the processing techniques developed by W. Smith et al., for the DST-6 data, led to a different situation. The HIRS and SCAMS sounder systems provided roughly 5000 soundings per day with overall accuracies comparable to the VTPR. Moreover, the information in these data is much less correlated with the first guess fields supplied than the current VTPR operational systems, which use the NMC forecast as the first guess. There does not seem to be in the NIMBUS system, any consistent bias or significant reduction of yield in the presence of clouds.

Although the GISS studies analyzing the effect of clouds on the accuracies of the temperature profiles are incomplete, no evidence of a cold bias in cloudy regions was detected. To the contrary, there may be a compensating bias everywhere on the warm side to account for clouds. Confidence in the quality of these data is enhanced by similar findings obtained with our own processing techniques developed for these data. The GISS methods for the HIRS/SCAMS sounders are radically different from those of NESS, yet, the comparisons of temperature data quality seem to give consistent results as is shown in Chapter 2. As a result of the increased yield, the impact studies produced substantial differences in the initial

states and those differences led to a beneficial average forecast impact for the system with satellite data.

A recent point raised by analysts at NMC concerns the ability of sounding data to specify the thermal structure of the atmosphere. Isentropic cross-section analyses performed on these data by NMC reveal significant reductions in the variance of the fields due to a smoothing of the temperature gradients as compared with the structure shown in the radiosonde analysis. The GISS investigation of this problem, as shown in Chapter 5 shows no systematic smoothing of potential temperature gradients in data-sparse regions.

*Data Assimilation.* The design and development of proper satellite data assimilation techniques is a major aspect of the total analysis system. The reason special efforts are required in this area is the enormous volume of satellite data that is available and the large errors in these data, which have to be assimilated along with conventional in situ observations. If one applied the conventional technique of intermittent synoptic insertion of all the data, then most of the information content of the asynoptic data will be lost as a result of time-space averaging. Automatic quality control checks are desirable but difficult to apply in data-sparse regions. As a result of experience gained over many years of experimenting with satellite data assimilation methods, a scheme was developed based on theoretical findings and practical results reported in the recent meteorological literature. The method implemented a time-continuous, four-dimensional assimilation procedure based on statistical weighting of temperatures and on geostrophic wind corrections; it modified the technique so as to deal with the practical problems imposed by the available real data.

Of all the components used in the assimilation scheme, the impact resulting from statistical weighting procedures may be the most significant. Serious mathematical and computational problems associated with this method were encountered and considerable care went into the solution of these problems. The methods are described in some detail in Chapter 3 of this report and also appear in the earlier Phase I Study Report.

The main point to be commented on here is that the GISS technique is adaptable and transferable to an operational forecast system. If this scheme or reasonable facsimile thereof were introduced into an operational practice, then significantly improved initial state determinations and forecast accuracies could result by 1978 when applied to the TIROS-N sounding data.

*Forecast Model.* The magnitude of forecast impact is highly dependent on the skill of the forecast model. Clearly, if the forecast model breaks down well before 48 to 72 hours, no matter how well the data in the northern hemispheric oceans is specified, the impact will be negligible. Predictability studies show that today's forecast models will have a significant downstream response to finite amplitude differences in the initial states over the oceans in 48 to 72 hours, when the differences in the initial states are as large as those produced by the satellite data. The major concern is to what extent can the improvement in skill of the large scale synoptic forecast at 72 hours be useful to local weather forecast operations. To the extent that the numerical weather forecasts are improved on these time scales by better models, the impact of satellite data is expected to be additive to that of model improvement.

NMC is currently engaged in an intensive effort to develop a high resolution model. Results with a limited-area forecast model for the past year show skill score improvements in sea-level pressure and 500mb heights on the order of 5 to 10 percent. This translates into a 12-hour forecast gain in the accuracy of large-scale synoptic predictions. The GISS studies with a higher resolution model show similar forecast improvements (Chapter 4).

Forecast improvements of these magnitudes using NIMBUS-6 and NOAA-4 sounding data were obtained without any increase in the model resolution (Chapter 5). Tracton and McPherson (1977) speculate that the performance of high resolution models will be degraded by satellite data. In the few limited forecasts made with a higher resolution GISS model results do not substantiate these speculations. In fact, to the contrary, the GISS high resolution model (250km mesh size) produced somewhat more substantial impacts in the forecast skill than the low resolution model as a result of using satellite data. Results seem to suggest that the combined effects of resolution and temperature sounding data may be additive. If this is confirmed by further tests, it could produce a major increase in the skill of operational 72-hour forecasts.

### 1.3 OPERATING APPROACH

It was recognized from the outset of this project that the success of the program ultimately rests on the quality of the data and the forecast skill of the model. The winter DST data sets offered the best chances of showing an impact because of the active systems originally in data sparse regions and moving over land in 48 to 72 hours. Although the satellite-borne instruments were seriously degraded during the winter period, losing all 15 $\mu$ m

channel capability the sounding data were reprocessed by NESS so as to include special efforts to filter the instrument noise. As a back-up system in case the NESS procedures were not effective, GISS developed its own temperature retrieval techniques. As a result of the quality of the sounding data, additional quality controls to check the data were added to the GISS data assimilation schemes. Furthermore, because the volume of data was so large, balancing techniques were developed and tested in order to minimize the shock effects produced by data insertion. In addition, it was desirable to use an improved forecasting model, if possible, which might be more responsive to differences in the initial states.

An important constraint imposed on the project was to demonstrate in operational terms the impact of sounding data on forecast operations. This meant the development of product outputs and verification techniques that are standard practice at NMC.

The project has been organized into the following four activities. The general approach to meeting these program objectives is described below and the specific programs to develop and demonstrate sounding capabilities are detailed in the subsequent chapters. A brief description of the specific program objectives of the four groups are:

● **Sounder Temperature Studies:** This group had two tasks. First, to assess the quality of the IR and microwave data with respect to their dependence on initial guess, clouds and atmospheric effects, such as sea-level albedo and other uncertainties in the

calculations of transmission functions; and second, to develop an alternative to the NESS retrieval processing system for the HIRS and SCAMS sounders based on Chahine's dual frequency principle.

● Assimilation and Analysis: This group was responsible for developing an analysis scheme and new assimilation techniques which would make use of the error structure of the satellite data in blending them with conventional data. It also was to develop filtered models which minimize the shocks of imbalanced sounding data.

● Forecast Model Development: To develop a higher resolution (vertical and horizontal) numerical forecast model in order to improve the accuracy of forecasts up to four days.

● Evaluation and Verification Test: To evaluate the impact of satellite data on medium-range forecasts in the context of a real-time forecast operation. Emphasis in evaluation tests was on practical utility, i.e., usefulness to a local forecaster in the field.

In each area listed above the report will show the development of a significant technological capability which we believe will lead to a further improvement in the forecast impact in the future tests with FGGE data sets.

## CHAPTER II



## 2. SOUNDING TEMPERATURE STUDIES (STS)

(J. Susskind, Scientist; D. Edelman, Manager)

### 2.1 INTRODUCTION

The DST operational data set of temperature profiles derived from satellite borne observing systems (VTPR on NOAA 4 and HIRS and SCAMS on NIMBUS 6) was produced at NOAA/NESS. Most of the impact studies discussed in the remaining sections of this report use the operational temperatures of these as their data base. The accuracies and yields of these operational temperatures are presented in Section 2.2 of this Chapter.

The remainder of this chapter of the report discusses the theory of temperature sounding, presents an alternate method developed at GISS, for deriving temperature profiles from sounder data, and finally gives the results of a number of studies for measuring and assessing the quality of the retrieved temperature profiles. The quality of temperatures retrieved using the methods of GISS and NESS are compared and shown to be generally comparable to each other.

The theoretical section of this report deals primarily with the two main problems facing temperature sounding from satellites; the effects of clouds on the radiances, and limited inherent vertical resolution, even when the clear column radiances are known. These problems are amplified by noise of an instrumental nature, affecting the accuracy of a measurement, and noise of a computational nature, affecting the ability to accurately reproduce the physics giving rise to the measurements as a function of temperature.

The limited vertical resolution of the measurements is a result of the fact that the photons entering into the observed signal arise from a wide portion of the atmosphere. Figures 1 to 4 show the weighting function and Planck-weighted weighting functions for the temperature sounding channels on the VTPR, SCAMS, and HIRS sounders used in the DST experiment. The latter curves indicate the portion of the total signal arising per unit height from each pressure. The broader the curve, the less specific the measurement. The peaks of the weighting functions and Planck-weighted weighting functions for the channels are summarized in Table 1. The resolution cannot be higher than the spacing between adjacent peaks.

There has been much discussion of the relative merit of microwave and infrared sounders. Microwave sounders such as SCAMS have the advantage that, given a temperature profile, their observations are essentially unaffected by clouds in the field of view. As seen from Figure 4 and Table 1, SCAMS is characterized by limited vertical resolution, having only two sounding channels in the troposphere. Microwave sounders also have a potentially large source of computational noise due to a low and variable surface emissivity, which must be determined accurately before meaningful microwave sounding can be made.

Infrared sounders, such as VTPR and HIRS, have the potential of achieving higher vertical resolution and are less affected by variations in surface properties. The presence of clouds in the sounder's field of view has a major effect on observed infrared

Table 1. Peaks of Weighting Function in Mb.

CHANNEL	FREQUENCY (CM <sup>-1</sup> )	WT. PEAK	B WT. PEAK
<u>HIRS-SCAMS</u>			
1	669.0	30	20
2	679.0	60	50
3	690.0	100	100
4	700.0	280	360
5	716.5	475	575
6	732.0	725	875
7	749.5	surface	surface
8	2190.0	surface	surface
9	2210.5	650	surface
10	2243.5	340	675
11	2271.5	170	425
12	2357.0	15	2
13=M1	22.235 GHZ	window	
14=M2	31.400 GHZ	window	
15=M3	52.850 GHZ	surface	
16=M4	53.850 GHZ	500	
17=M5	55.450 GHZ	200	
<u>VTPR</u>			
2	668.0	30	3
3	679.8	60	60
4	696.9	140	140
5	707.2	400	475
6	725.1	725	900
7	748.9	surface	surface

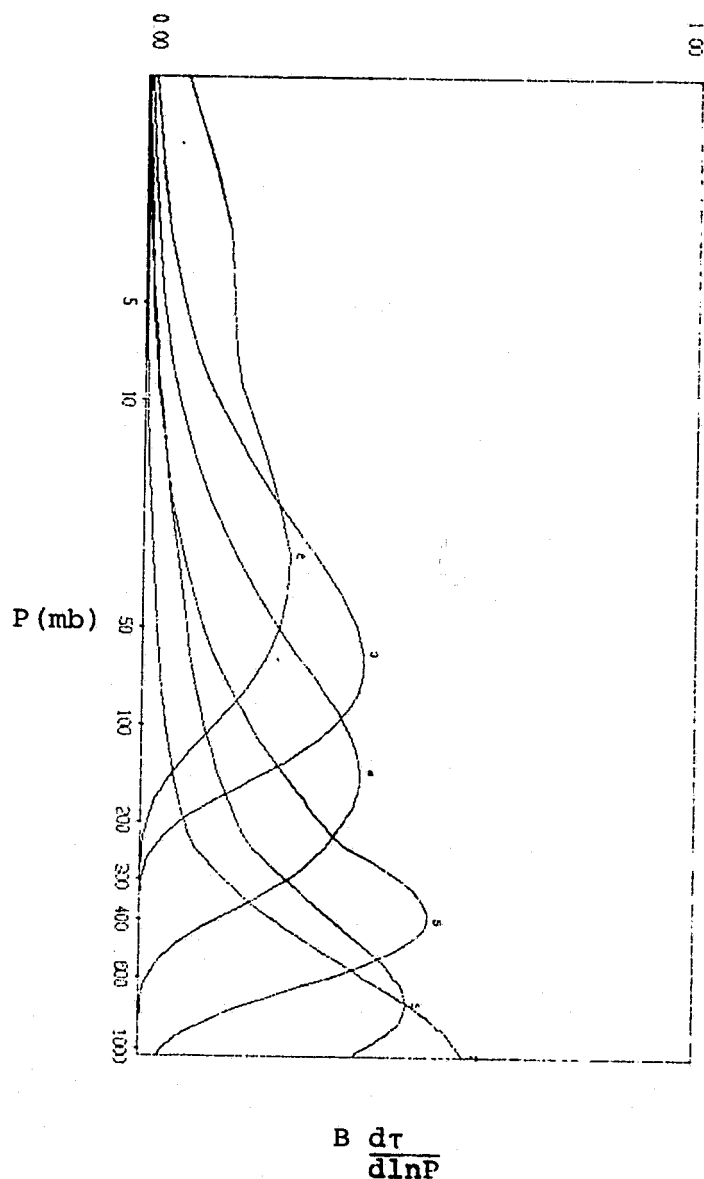
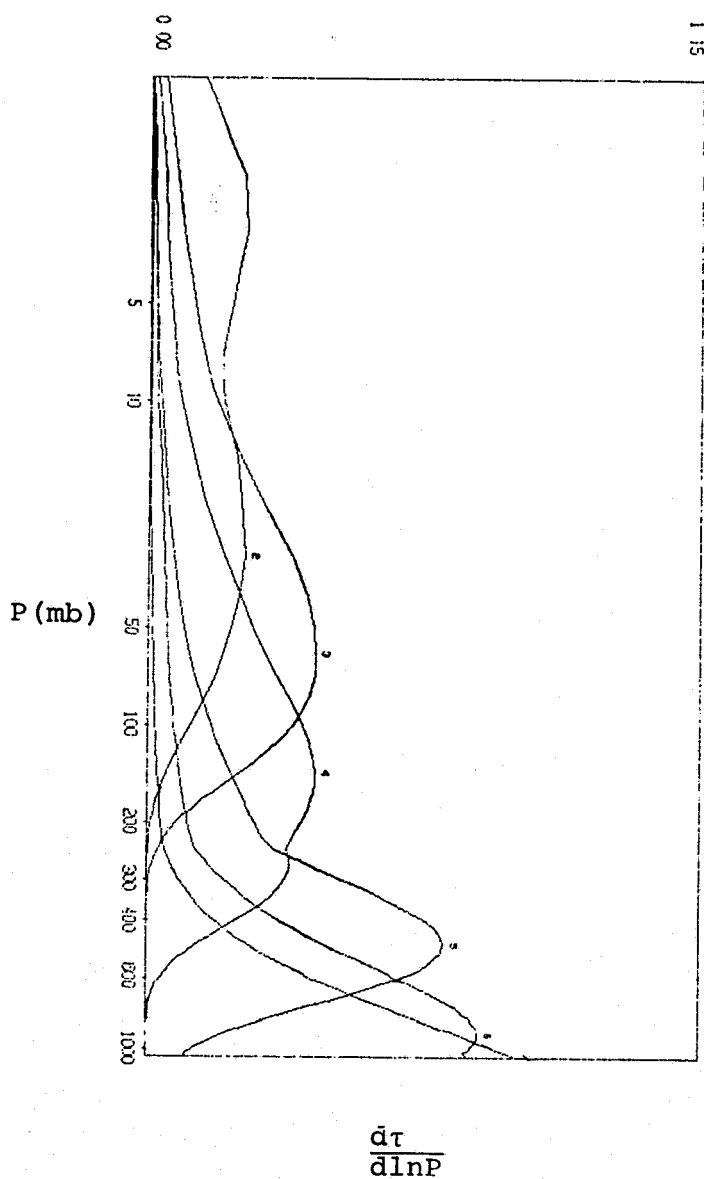


Figure 1. Unweighted and Planck-Weighted Weighting Functions for VTPR Temperature Sounding Channels. Dry Standard Atmosphere. Nadir Viewing.

ORIGINAL PAGE IS  
OF POOR QUALITY

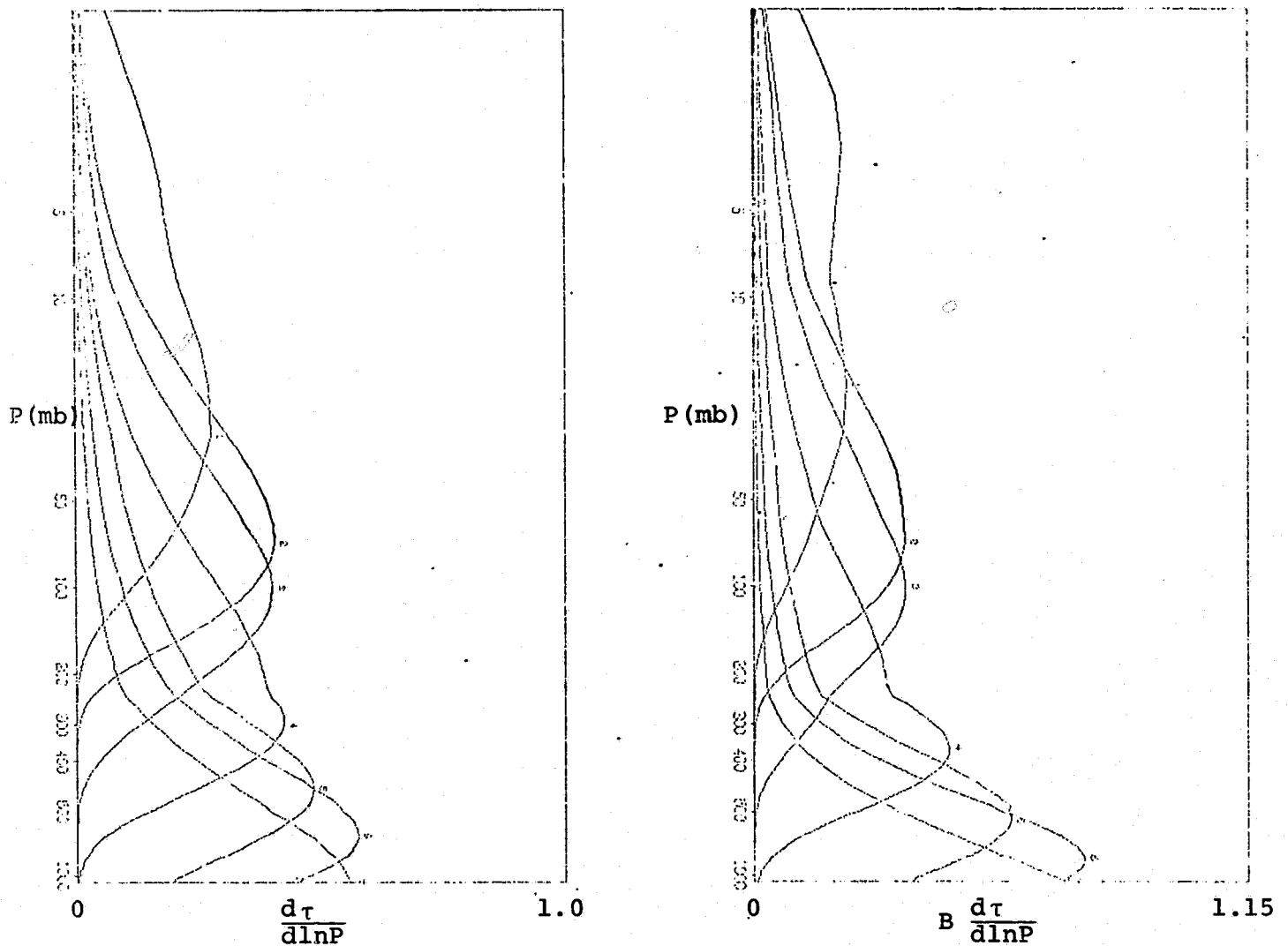


Figure 2. Unweighted and Planck-Weighted Weighting Functions for HIRS 15μm Channels. Dry Standard Atmosphere. Nadir Viewing.

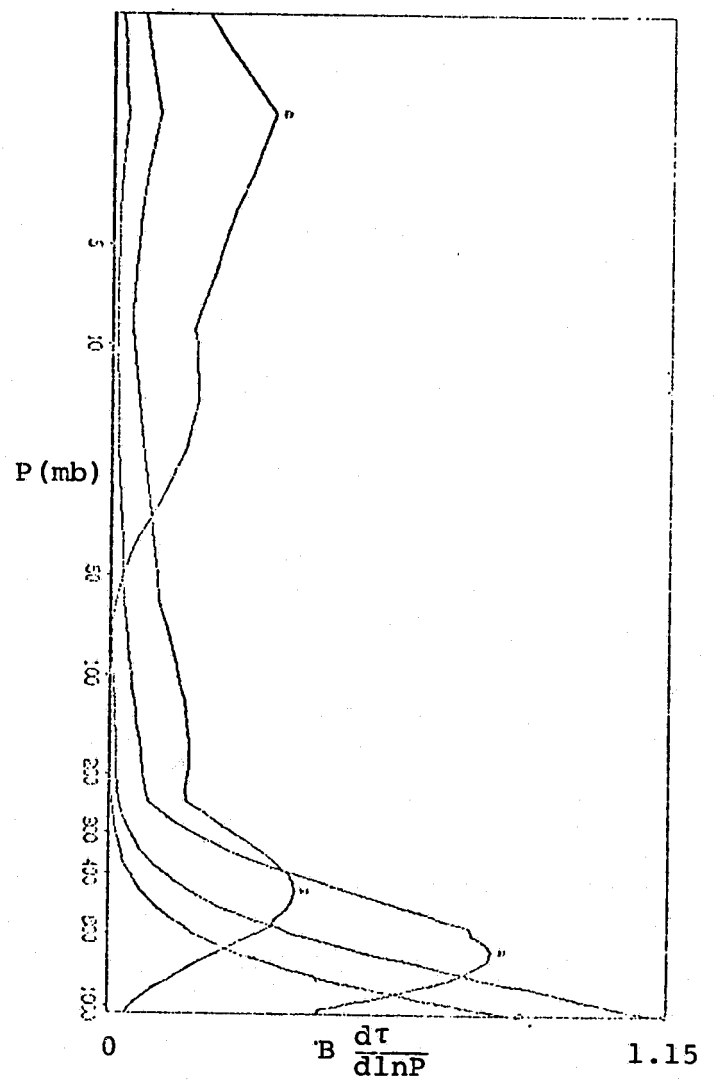
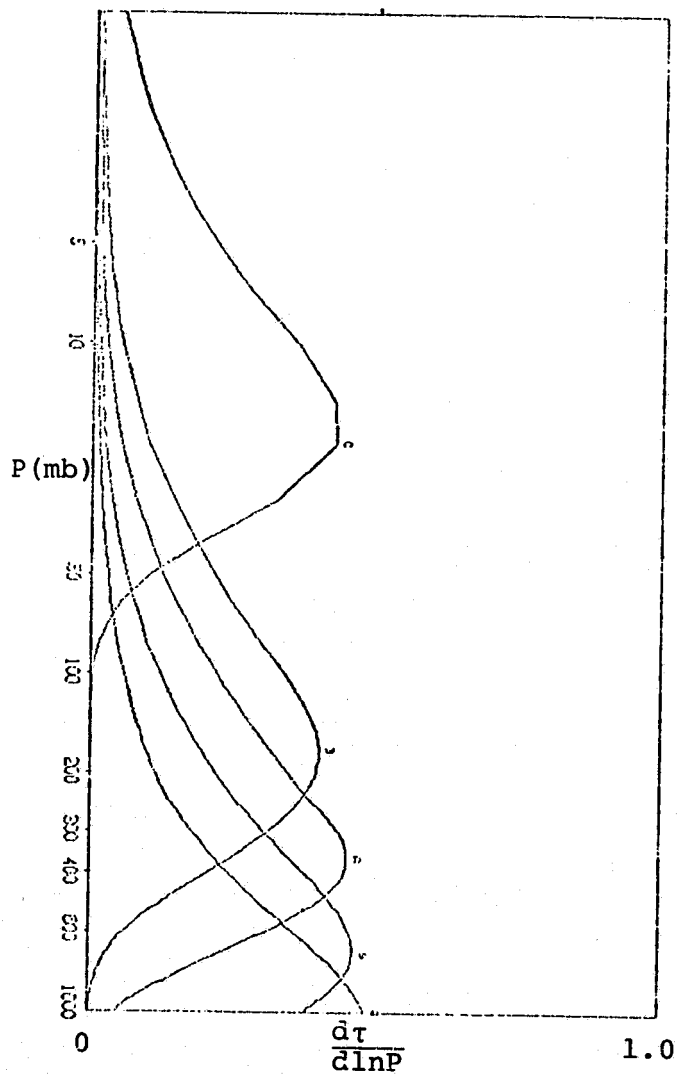


Figure 3. Unweighted and Planck-Weighted Weighting Functions for HIRS 4.3μm Channels. Dry Standard Atmosphere. Nadir Viewing.

ORIGINAL PAGE IS  
OF POOR QUALITY

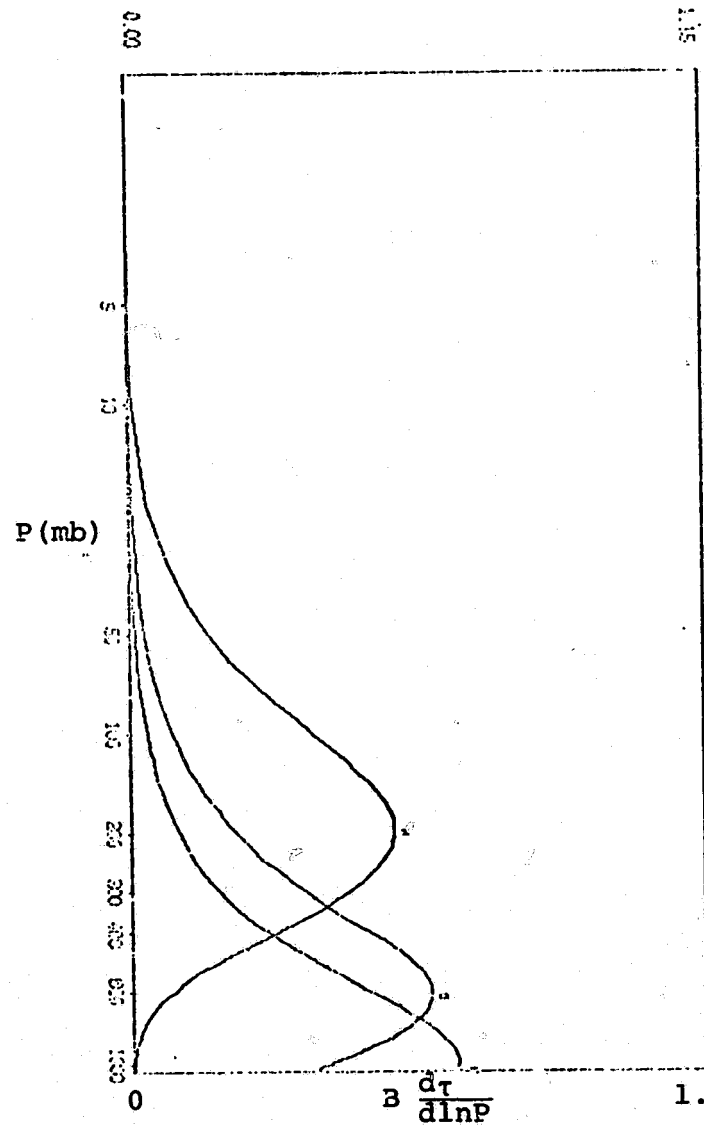
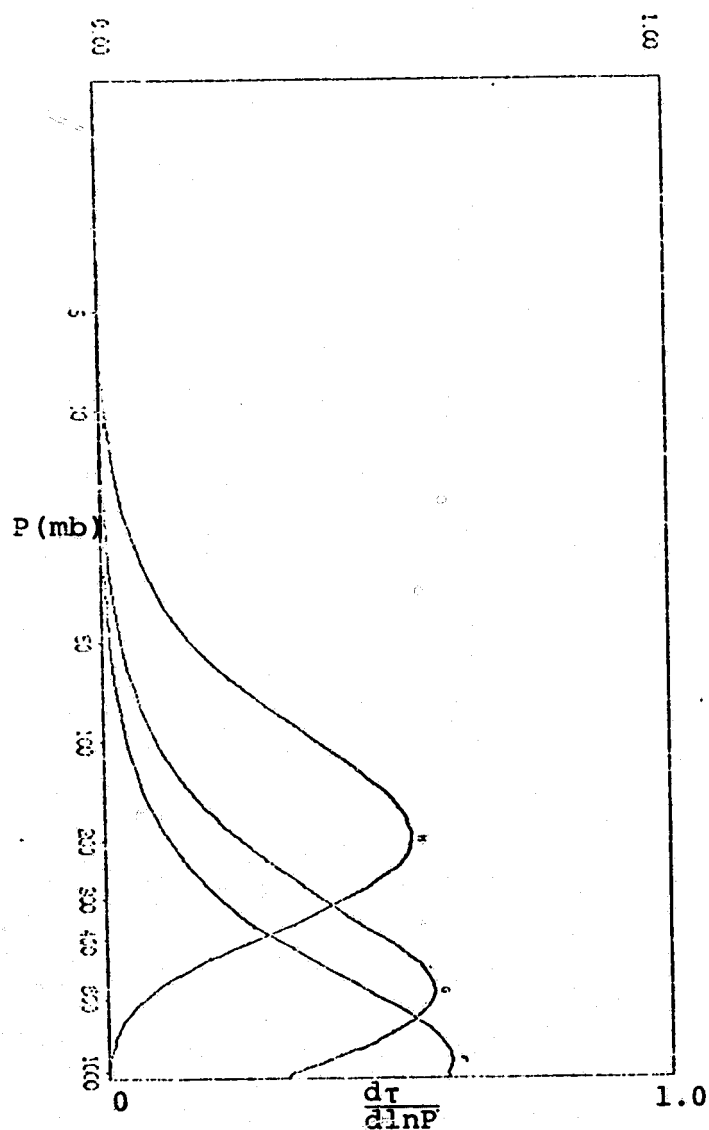


Figure 4. Unweighted and Planck-Weighted Weighting Functions for SCAMS Temperature Sounding Channels. Dry Standard Atmosphere. Nadir Viewing.

radiances, however, and this factor must be dealt with accurately before meaningful infrared soundings can be achieved.

This study has also addressed the ability of the VTPR temperature sounder on NOAA 4 along with the combined HIRS-SCAMS temperature sounder on NIMBUS 6 to deal with the problems of clouds, vertical resolution, and the accuracy of temperature retrievals for each instrument. Our conclusions show that effective cloud filtering (i.e., determination of clear column radiances) can be obtained by use of combined HIRS-SCAMS observations or by use of either instrument separately. The VTPR instrument, however, has no cloud filtering ability of its own and hence cannot give information about surface or lower tropospheric temperatures independent of outside information. Both sounder systems have only moderate vertical resolution below 400 mb and contain very little information at the levels of 300, 250, and 200 mb.

The HIRS and SCAMS sounders give comparable quality retrievals when used separately indicating, on the one hand, that clouds are not seriously degrading the quality of infrared retrievals, and, on the other hand, that HIRS is not realizing the potential for significant improvement in results when the full complement of HIRS channels can be used. During the winter DST periods, when the 15- $\mu$ m channels on HIRS malfunctioned, HIRS alone retrievals were impossible and combined HIRS-SCAMS retrievals were only marginally better than SCAMS alone.



## 2.2 OPERATIONAL TEMPERATURE RETRIEVALS FOR DST-5 AND DST-6

### 2.2.1 NIMBUS-6 HIRS, SCAMS, THIR

#### 2.2.1.1 OVERVIEW

In August 1975, and again in January 1976, GISS initiated real-time processing operations of NIMBUS 6 sounding data for the GARP Data Systems Tests (DST) -5 and -6, respectively. The raw sounding data were processed into calibrated, Earth-located radiances and then into temperature and humidity profiles by a technique developed by NESS/NOAA (Smith, Hayden, Woolf, et al.) and integrated into a DST-supportable system by GSFC personnel (Gary, Iobst, et al.)

Although plans called for a 60-day DST-5 data set of amalgamated temperature and humidity profiles from the HIRS, SCAMS, and THIR sounders, and a 65-day data set of equivalent DST-6 profiles, neither test generated a full data base.

Processing operations for the summer test were discontinued on September 5, when excessive noise was detected in the 15  $\mu$ m long-wave channels. This condition, which persisted through the DST-6 period, required major changes in the temperature extraction technique to compensate for the loss of these channels.

The start of DST-6 was delayed until late January when a malfunction in either the HIRS instrument or in the data recording device on board NIMBUS 6 caused a bit slippage in the structure of the raw data. This problem was overcome by changes to the INGEST section of the software and real-time processing operations commenced on January 23.

Subsequent analysis of the processed microwave sounding data by NOAA programmers, revealed that the algorithm which co-locates microwave with infrared soundings, contained an error in the scanning direction of the microwave instrument. A management decision by the GARP Project Office was made in April 1976, to reprocess both DST data sets from the raw data archived in the tape library at GISS. These activities came to a successful completion in March 1977.

### 2.2.1.2 DATA SYSTEMS TEST-5

Data Systems Test-5 was planned to start in mid-August and run for 60-days' duration. However, due to the difficulties in the 15 $\mu$  channels, which forced the premature termination of the test, the final data set only contains profiles from 21Z August 17, to 12Z September 4 for a total of 17.6 days.

#### 2.2.1.2.1 YIELD

Table 2 and its graphic equivalent in Figures 5 and 6, show the daily composition of the data in terms of time gaps and profile counts.

With the exception of August 21, 22, 25, 30, and September 2, for which at most one orbit of data is missing, the remaining days contain rather large data gaps with the worst cases occurring from August 26 through August 29. These are large discontinuities, especially when compared against similar DST-6 statistics, which account for almost 23 percent of the total data set and which are reflected in the large daily fluctuations in the number of retrieved profiles. For those days for which the data are most complete,

Table 2. Missing Data and Profile Count for DST-5 NIMBUS

Date	August														September				Totals
	18	19	20	21	22	23	24	25	26	27	28	29	30	31	1	2	3	4 <sup>1</sup>	
Missing Data (Hours)	6.4	9.7	7.4	1.8	1.7	5.3	4.3	1.8	10.9	7.4	8.4	9.9	0.4	7.5	6.9	1.9	3.2	1.9	96.8
Profile Count	4163	4546	3693	5842	6055	5178	5083	5912	4353	3311	3923	3867	5100	4859	3996	5623	4745	3994	84,243

<sup>1</sup>Data available to 12 GMT only.

Table 3. Missing Data and Profile Count for DST-6 NIMBUS

Date	February																					
	1	2	3	4	5	6	7	8	9	10	11	12	13	14	15	16	17	18	19	20	21	22
Missing Data (Hours)	0	3.7	0.9	0.5	1.5	3.6	2.3	3.7	1.2	0.9	0	0.6	2.2	0	0	5.0	0	3.8	0	4.0	1.9	0
Profile Count	5755	5220	5501	5525	5872	5146	4797	5581	5265	6020	6091	6110	5518	5108	5929	4813	5551	4638	5923	5103	4728	6334

Date	March											Totals
	23	24	25	26	27	28	29	1	2	3	4	
Missing Data (Hours)	0	2.6	5.6	0.3	2.1	4.4	0	1.9	1.8	0	0	54.5
Profile Count	6361	5716	4845	6177	5674	4602	5943	5819	5755	5955	6159	183,534

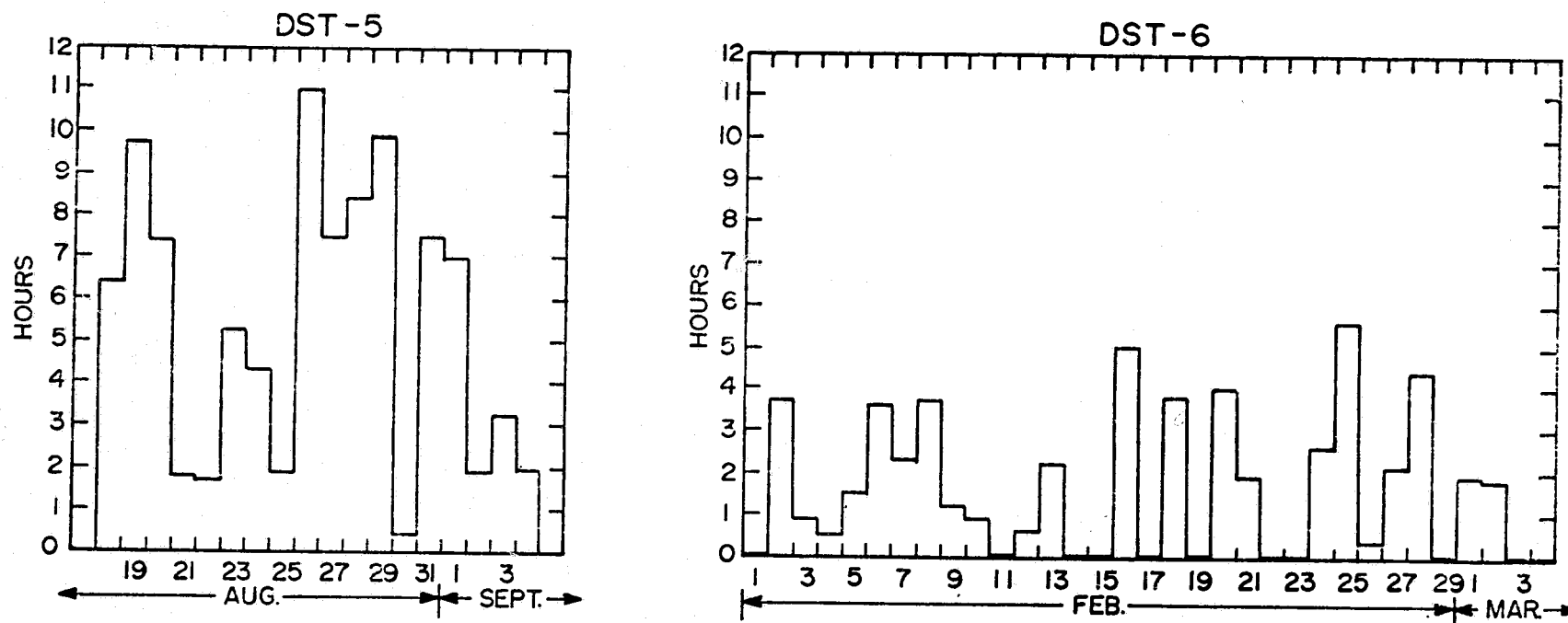


Figure 5. Missing Data From DST-5 and DST-6 NIMBUS Temperature Data Sets

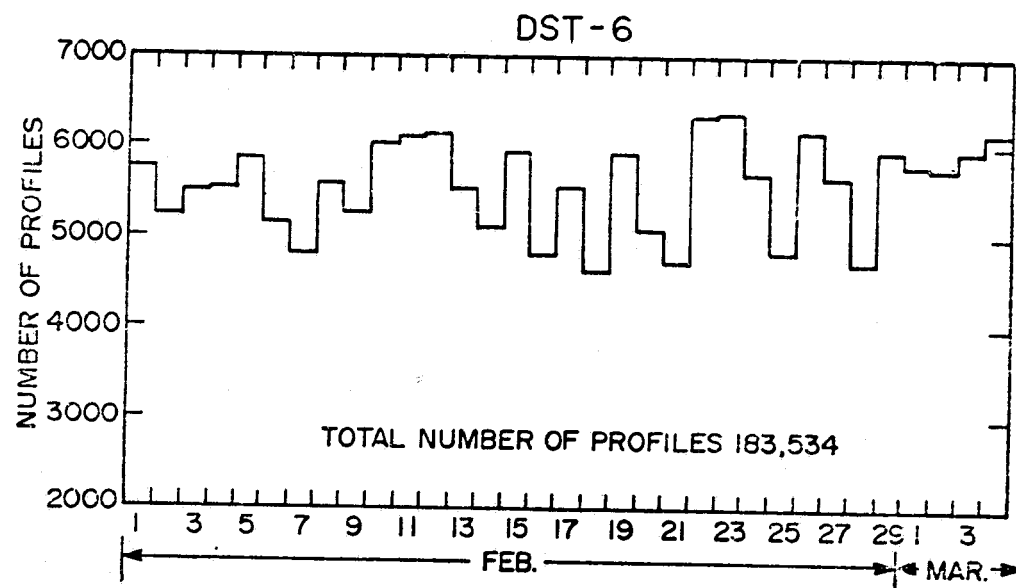
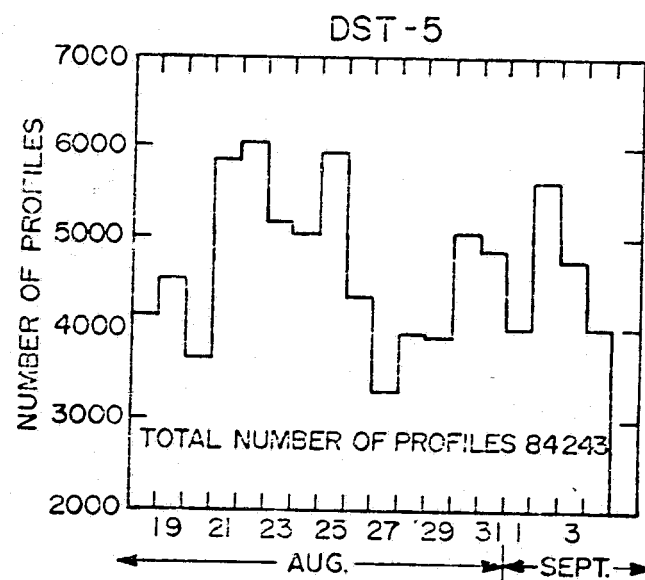


Figure 6. Daily Yield of NIMBUS Temperature/Humidity Profiles for DST-5 and DST-6

the average global profile count of approximately 5700 retrievals compares closely with the average number of profiles obtained during DST-6.

#### 2.2.1.2.2 ACCURACY

Figure 7 shows the weekly RMS errors of profiles retrieved over water and colocated to within  $\pm 110$  km and  $\pm 3$  hours of radio-sonde observations. The overall accuracy for the entire period is of the order of  $2.29^\circ$ , and as can be seen from the Figure, only within the tropopause region (250 mb to 100 mb) do the errors increase to  $3^\circ$ .

It must be noted that these errors (and those given in Figure 8 for DST-6) were computed by restricting the observations in the sample to those profiles that do not exceed  $5^\circ$  errors for the column and  $7^\circ$  errors for the individual levels.

#### 2.2.1.3 DATA SYSTEMS TEST-6

Data Systems Test-6 was planned to start on January 1 and run for 65-days' duration. Problems with bit slippage and the consequent modifications made to the software, delayed the start of real-time operations to January 23; final reprocessing, subsequent to software corrections for the microwave scanning direction error, was also started from this date.

The final archived data set does not contain profiles before February 1, because a one week start-up period is required to generate accurate multi-level and surface analysis fields for fine tuning the retrieved temperatures.

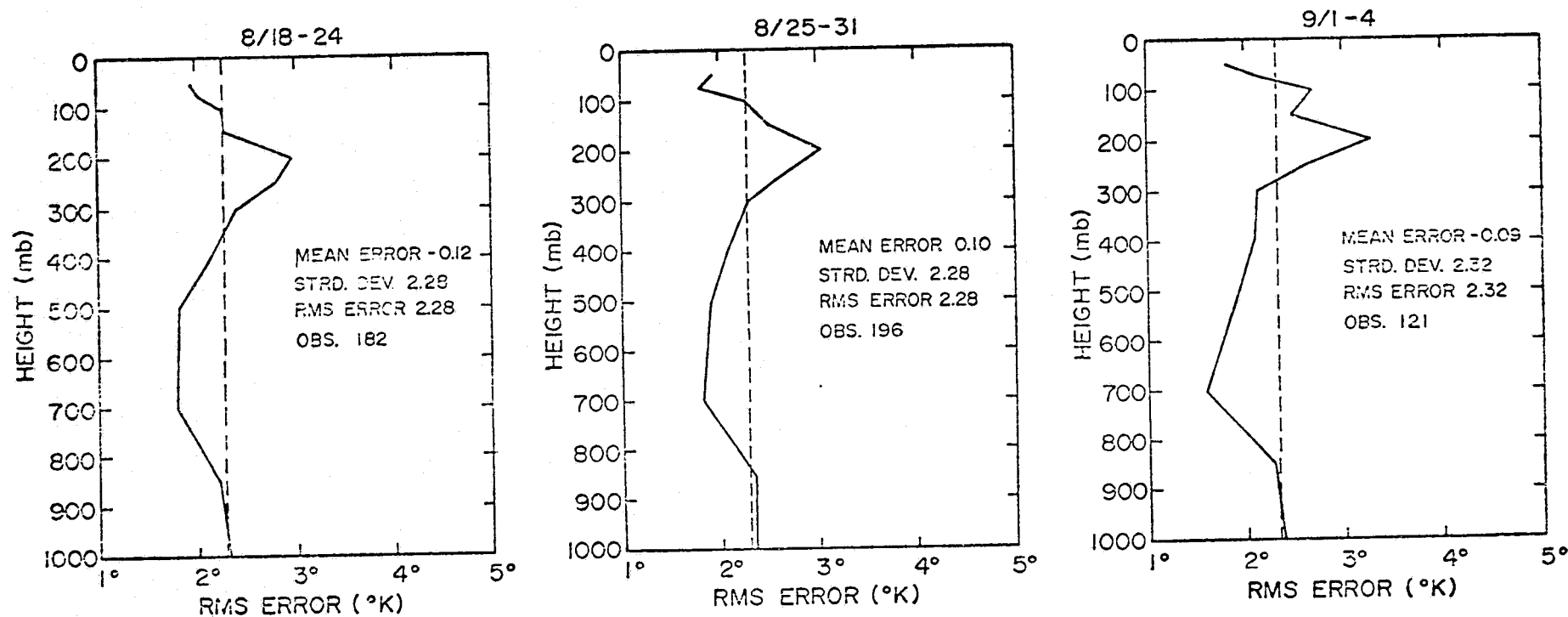


Figure 7. DST-5 Weekly NIMBUS Accuracies  
Temperature Error Versus Height  
±3 Hours, 110 km, Water, 18°N-70°N Latitude

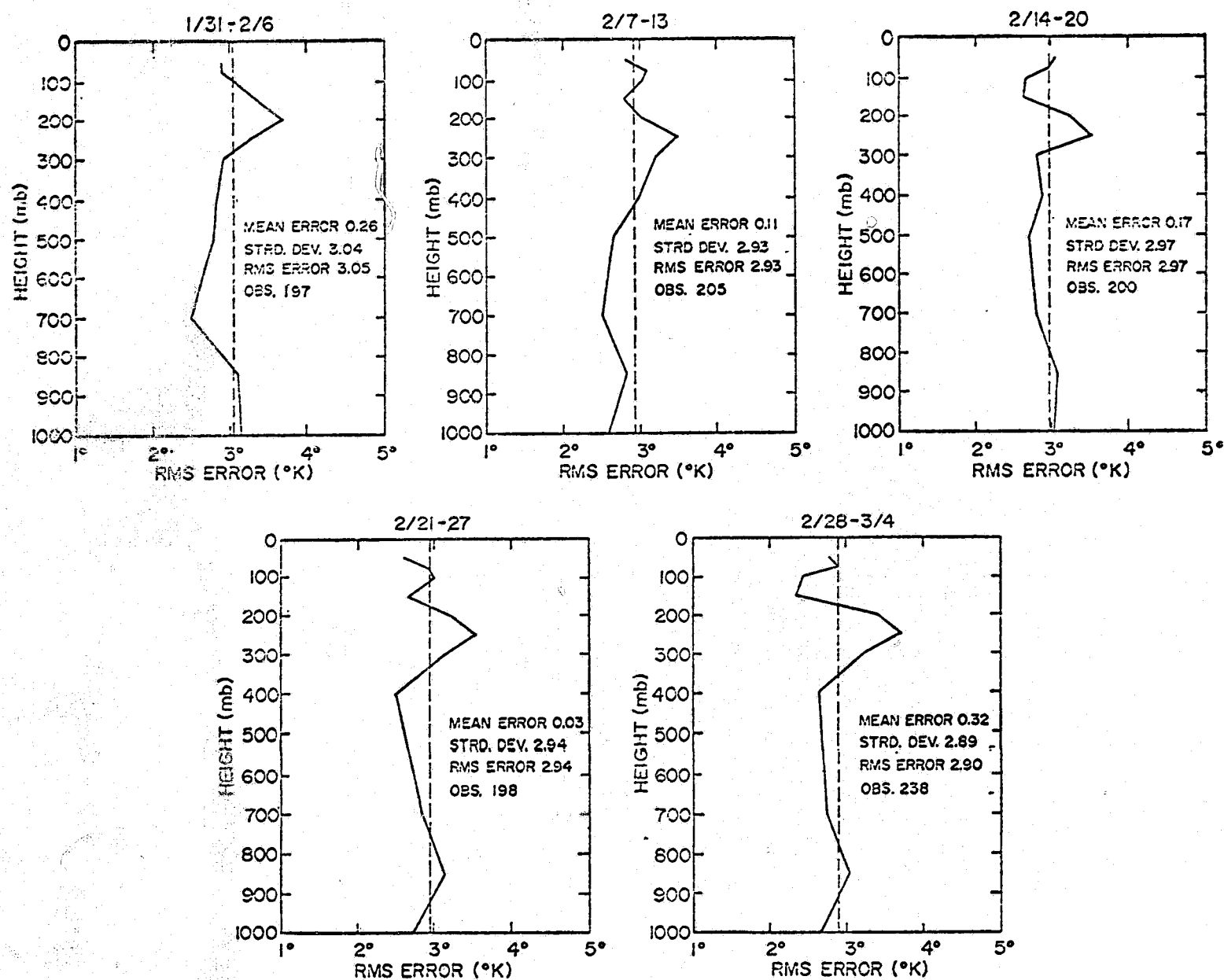


Figure 8. DST-6 Weekly NIMBUS Accuracies  
 Temperature Error Versus Height  
 ±3 Hours, 11 km, Water, 18°N-70°N Latitude



### 2.2.1.3.1 YIELD

Table 3 and its graphic equivalent in Figures 5 and 6, shows, in contrast to DST-5, that the data for this period is extremely continuous in its coverage. There are 21 days for which at most one orbit of data is missing, and for these the global average is 5800 retrievals per day.

The continuity of this dataset is the result of a coordinated effort between GISS and MHDS (the NIMBUS 6 archives at GSFC) to recover and process every available orbit. Similar efforts for DST-5, were not as successful due to problems in the date-time identification of the HIRS and SCAMS orbits. The subsatellite tracks of the missing orbits, the actual time and date of the data gaps, and the complete count of profiles for DST-6, are presented in Appendix A.

### 2.2.1.3.2 ACCURACY

The weekly DST-6 accuracies, shown in Figure 8, indicate that these temperatures are of poorer quality, in an RMS sense, than those for DST-5, by approximately  $0.7^{\circ}$ .

This reflects the fact that for the latter period all instruments were functioning properly, while the former operated with the  $4.3\mu$  and microwave channels only.

## 2.2.2 NOAA-4 VTPR

### 2.2.2.1 OVERVIEW

The VTPR instrument, which became operational in December 1972, has been returning usable global temperature and humidity soundings taken from on-board the NOAA 2,3 and 4 satellites. The Level I radiances, the first guess temperature values used in the NESS technique, and the NESS operational retrieved profiles, have been routinely archived at GISS during the operational life of the instrument and used in the 4-dimensional GISS assimilation scheme directly as an operational product, and as GISS-derived temperature profiles.

This section reviews the quality and coverage of the operational NESS temperatures for the DST-5 and DST-6 test periods.

### 2.2.2.2 DST-5 AND DST-6 YIELDS

Tables 4 and 5 and their graphic equivalent in Figures 9 and 10 show the daily composition of the data in terms of time gaps and profile counts.

As can be seen from Table 4, the data coverage for DST-5, with the exception of August 28 when 50% of the orbits are missing, is fairly continuous. For the 18-day period the number of retrievals, which are obtained only over water points, average to a little over 1000 profiles per day.

Table 5 for DST-6 on the other hand, shows the data coverage to be much less continuous after February 21 than during the first

Table 4. Missing Data and Profile Count for DST-5 VTPR

Date	August														September				Totals
	18	19	20	21	22	23	24	25	26	27	28	29	30	31	1	2	3	4	
Missing Data (Hours)	1.8	2.5	4.7	2.8	3.4	2.6	1.2	6.5	2.0	2.1	12.0	3.9	1.9	4.6	1.8	1.8	4.6	7.5	67.7
Profile Count	1106	1104	1003	1144	1024	1116	1125	1017	1146	1132	715	1034	1064	997	1136	1144	1047	890	18,944

Table 5. Missing Data and Profile Count for DST-6 VTPR

Date	February																					
	1	2	3	4	5	6	7	8	9	10	11	12	13	14	15	16	17	18	19	20	21	22
Missing Data (Hours)	3.3	6.6	5.5	5.1	9.7	3.0	3.4	2.1	7.6	4.3	3.2	6.5	6.2	11.3	6.2	1.5	3.2	3.3	2.9	5.9	15.3	9.2
Profile Count	1258	1087	1097	1181	863	1250	1241	1231	1024	1134	1272	1073	1059	785	1073	1241	1253	1279	1237	1114	498	902

Date	March											Totals
	23	24	25	26	27	28	29	1	2	3	4	
Missing Data (Hours)	16.5	20.4	11.9	13.5	8.7	13.6	14.3	16.8	11.8	6.6	15.6	284.7
Profile Count	632	217	708	620	917	623	506	438	695	958	453	30,413

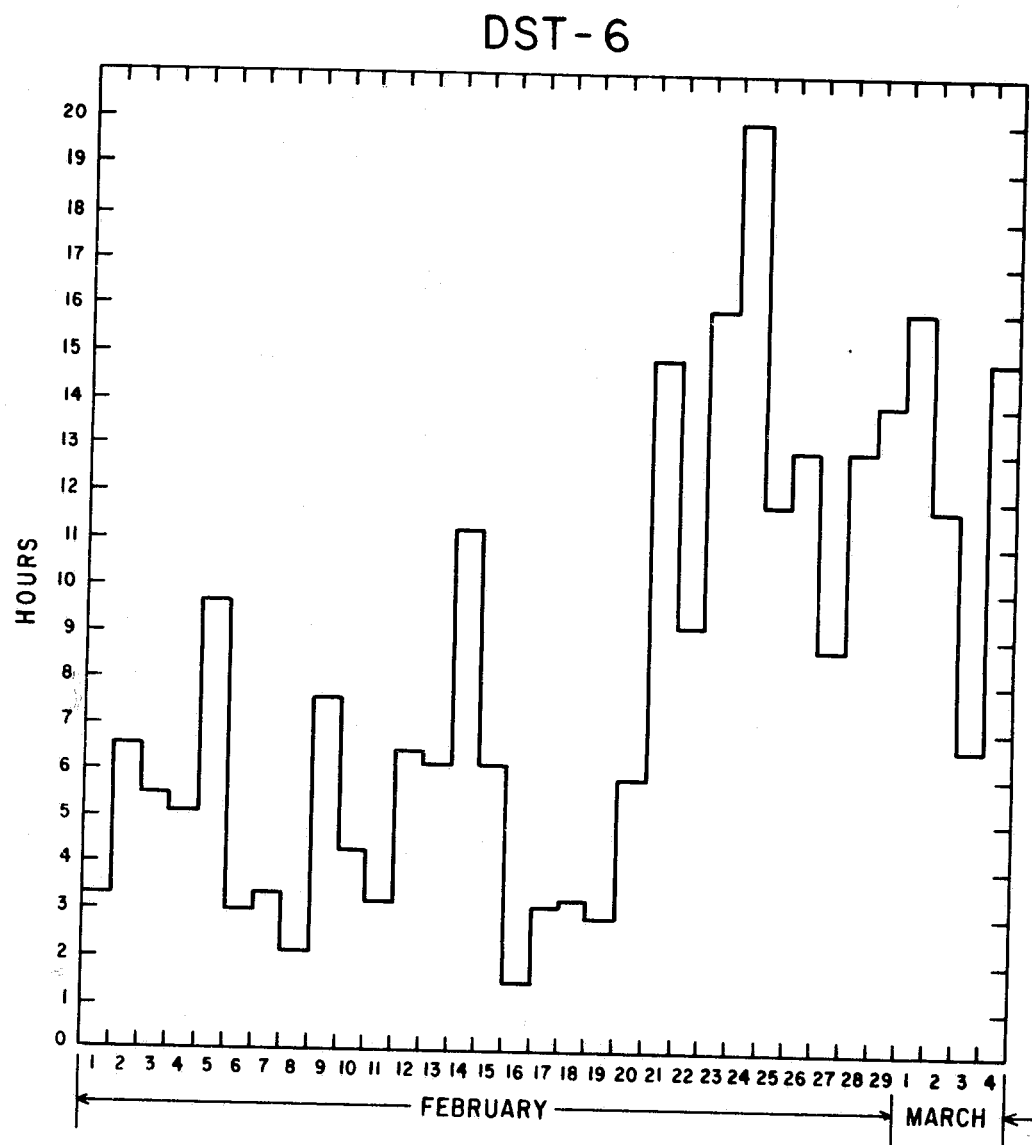
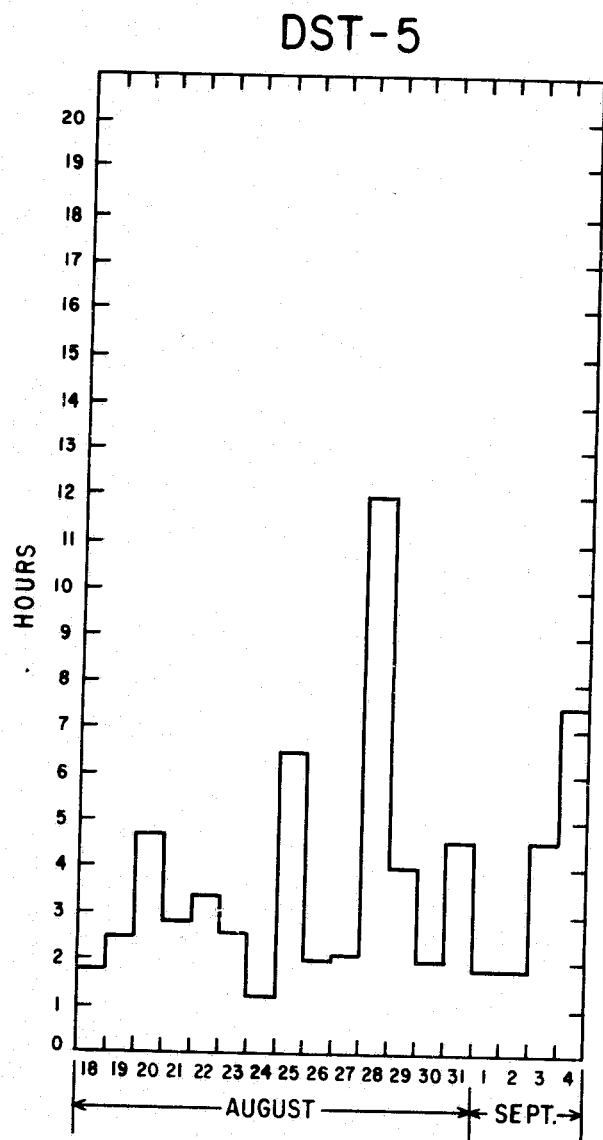


Figure 9. Missing Data from DST-5 and DST-6 VTPR Temperature Data Sets

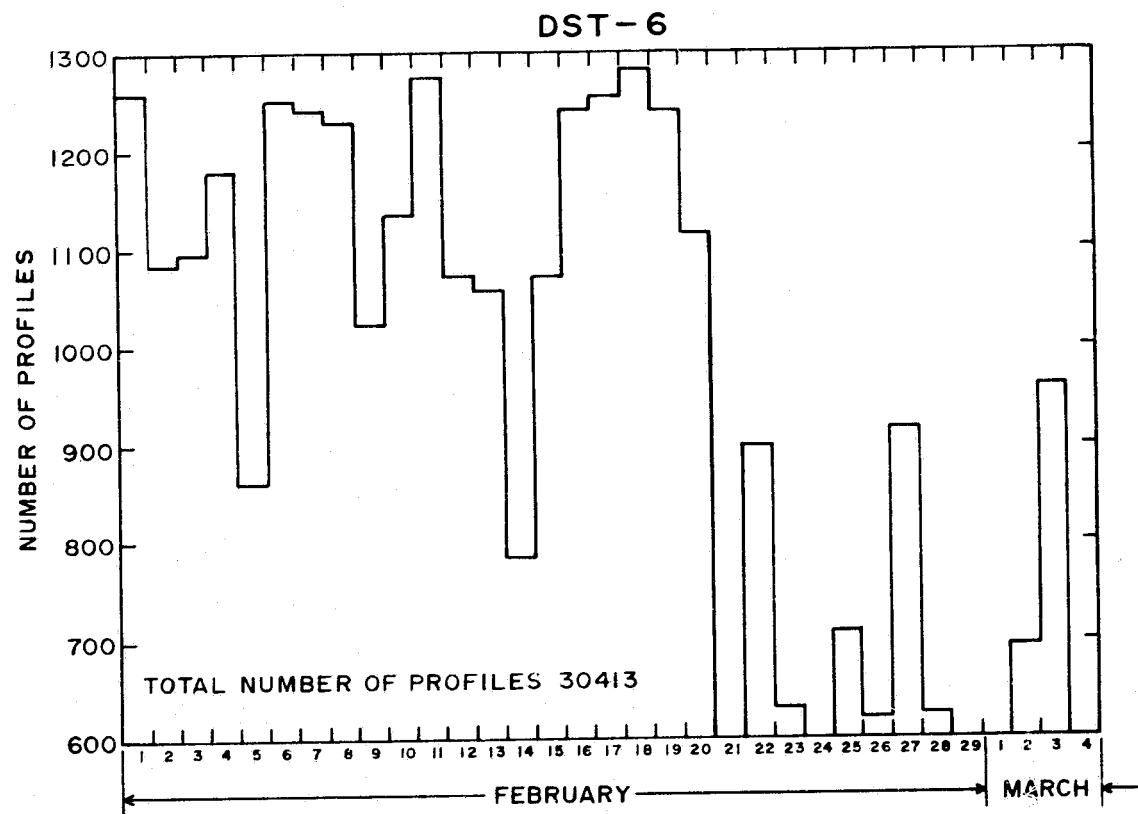
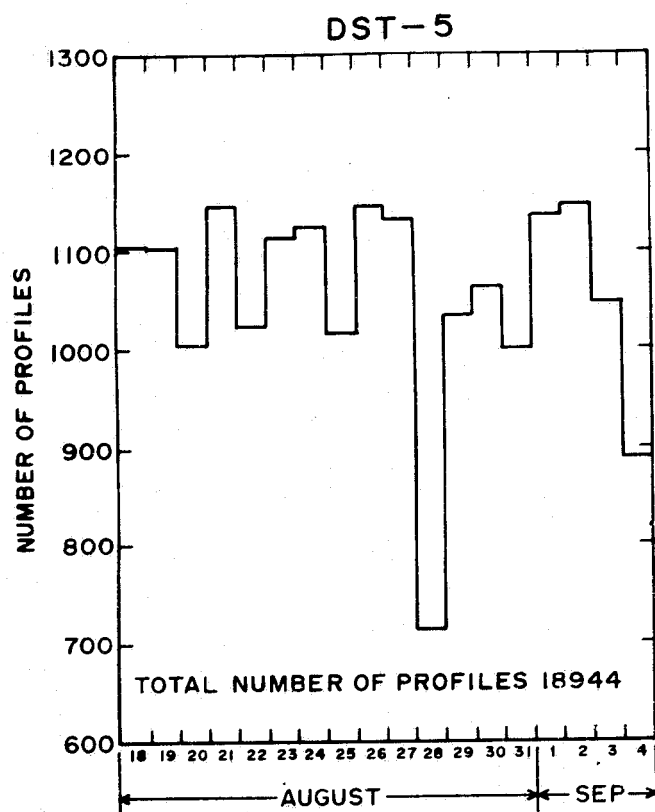


Figure 10. Daily Yield of VTPR Temperature Profiles for DST-5 and DST-6

part of the test period. These time gaps are the result of problems encountered during the transmission of the data from NESS to GISS, and the almost complete breakdown in data link communications towards the end of the experiment. Although from February 1-20 the average number of retrievals is over 1100 profiles per day, the yield is reduced to an average of only 620 daily profiles for the latter part of the test.

### 2.2.2.3 DST-5 AND DST-6 ACCURACIES

Figure 11 and Figure 12 show the weekly RMS errors of profiles retrieved over water and colocated to within  $\pm 3$  hours and  $\pm 110$  km of radiosonde observations. Also shown are the RMS errors of the initial guess used in these retrievals. The same error cutoff criteria applied to the NIMBUS accuracies (Sections 2.2.1.2.2 and 2.2.1.3.2) have been used here to evaluate the VTPR retrievals.

Both periods show good accuracies, with DST-6 errors roughly  $0.10^\circ$  worse than in the summer. The initial guesses, coming from a 12-hour forecast, are also very good in the regions near radiosondes. The accuracies of retrievals in data poor regions, where the forecast guess is of poorer quality, is of unknown quality.

## 2.3 GISS APPROACH TO TEMPERATURE SOUNDING: THEORETICAL CONSIDERATIONS

The basic theory for temperature retrievals and the techniques developed at GISS for their implementation are discussed in detail by Susskind et al. (1977). The theory discussed in this report will deal primarily with special considerations for the HIRS and SCAMS sounders.

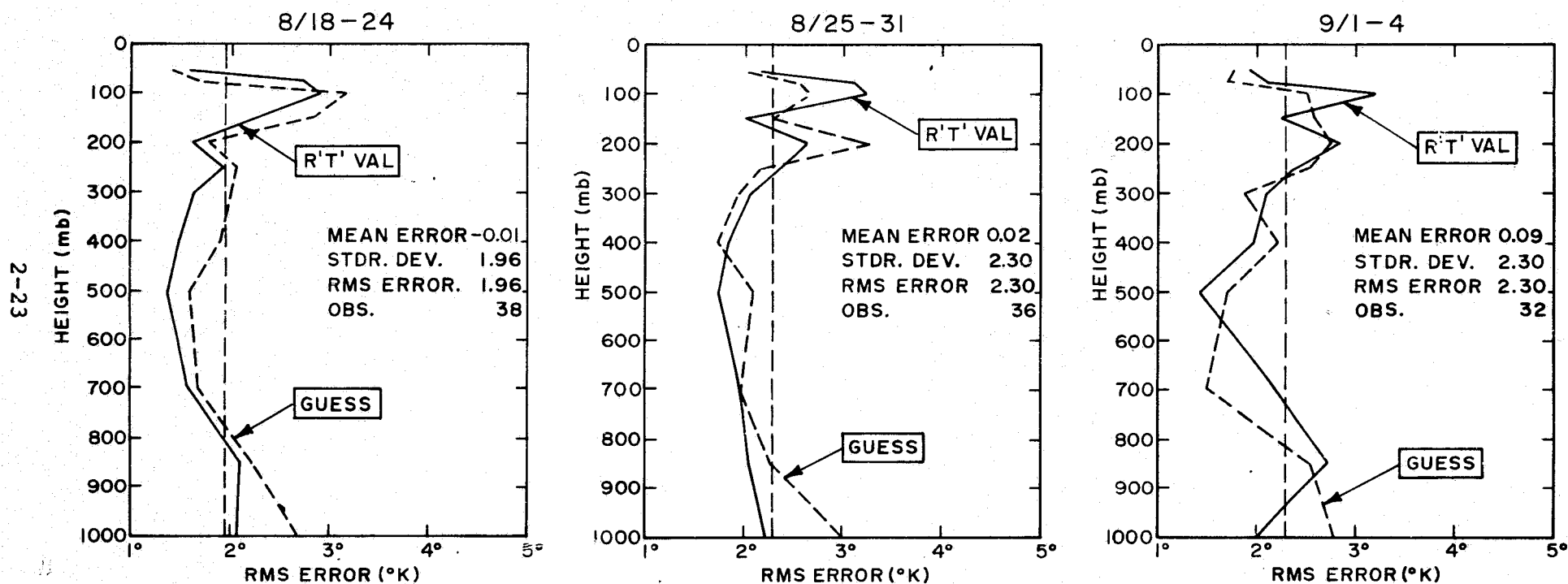


Figure 11. DST-5 Weekly VTPR Accuracies  
Temperature Error Versus Height  
±3 Hours, 110 km, Water, 18°N-70°N Latitude

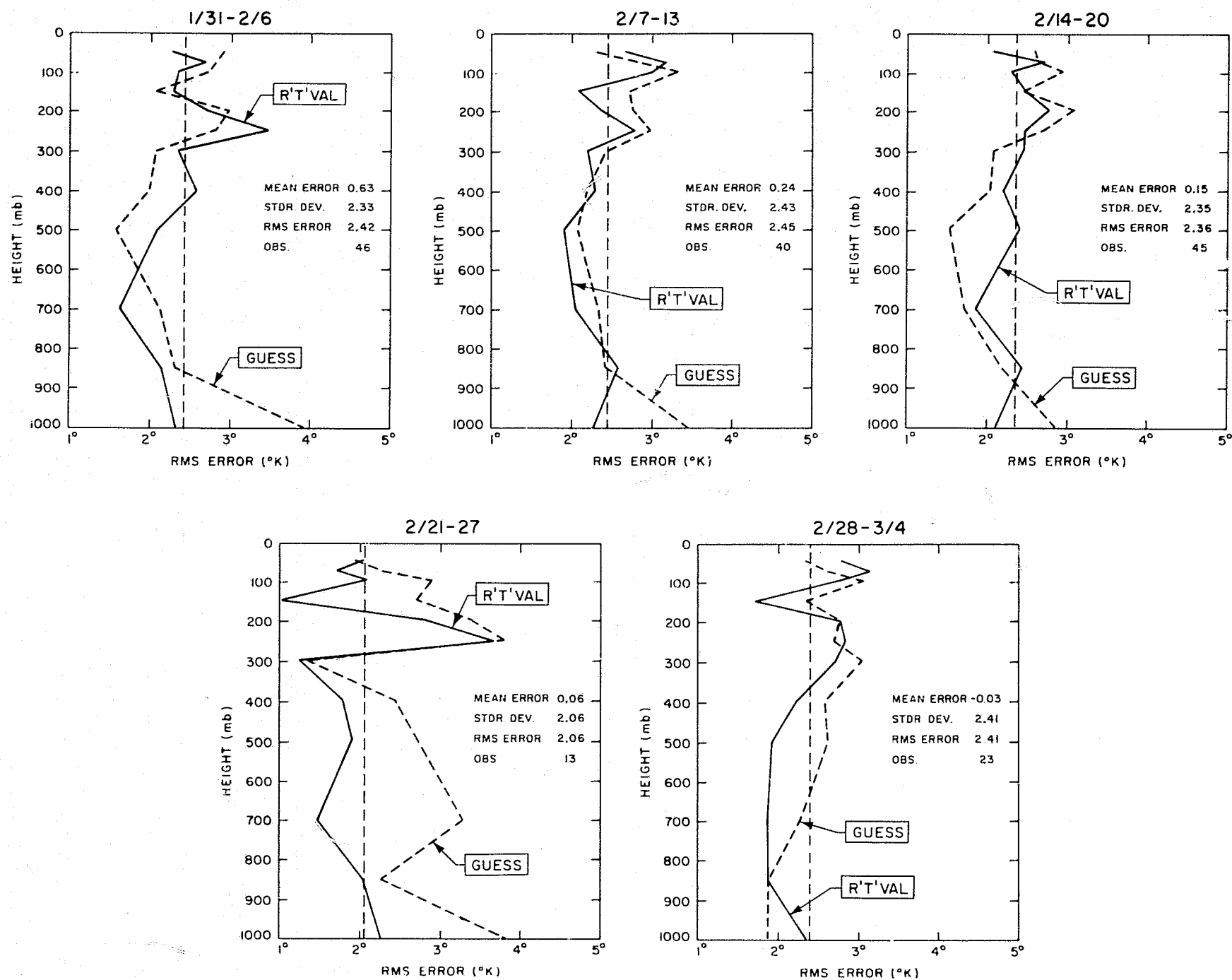


Figure 12. DST-6 Weekly VTPR Accuracies  
Temperature Error Versus Height  
±3 Hours, 110 km, Water, 18°N-70°N Latitude



### 2.3.1 TEMPERATURE RETRIEVALS GIVEN CLEAR COLUMN RADIANCES

There are many techniques for retrieving atmosphere temperature profiles from radiance observation. The approach used by NESS in creating the operational DST temperature profiles involves the use of statistics, i.e., tabulation of past radiance observations together with colocated radiosonde temperature measurements. The approach used at GISS is based on the method developed by Chahine (1972, 1974, 1975), and does not rely on past statistics. Avoiding the use of statistics gives one a greater chance of finding unusual meteorologically significant temperature profiles, such as those indicating passing fronts, which would have a great impact on a forecast. It also places a greater emphasis on being able to theoretically reproduce the atmospheric physics giving rise to the measurements.

The approach involves taking an initial guess temperature profile, calculating clear column radiances, comparing with the observations, and modifying the guess profile iteratively until agreement is reached.

For each sounding channel used, the guess is modified according to the equation

$$B_i [T^{n+1}(P_i)] = \frac{R_{i,clr}}{R_i(n)} B_i [T^n(P_i)]; \quad (1)$$

where  $B_i[T]$  is the Planck black body function evaluated at sounding frequency  $i$  and temperature  $T$ ;  $P_i$  is a characteristic pressure for channel  $i$ , typically the peak of the weighting function for that channel;  $T^n(P_i)$  is the  $n^{\text{th}}$  guess temperature at  $P_i$ ;  $R_i^n$  is the clear

column radiance calculated for channel  $i$  using  $T^n(P)$ ; and  $R_{i,clr}$  is the "observed clear column radiance," i.e., the radiance which would have been observed if the field of view of the observation were completely clear. In fact, the field of view is in general at least partially cloud covered, and the "observed clear column radiance" is in fact not an observation but must be constructed from the observation by filtering out the cloud effects. Two techniques for doing this are described in the following section. One uses only infrared observations and the other uses combined infrared and microwave soundings.

### 2.3.2 CLOUD EFFECTS

Consider a field of view which is otherwise homogeneous but partially cloud covered with cloud fraction  $\alpha$ . The radiance observed by a sounding channel  $i$  can be written as

$$R_i = (1-\alpha)R_{i,clr} + \alpha R_{i,cld} \quad (2)$$

where  $R_{i,clr}$  is the radiance which would have been observed if the entire field of view were clear, and  $R_{i,cld}$  the radiance if the entire field of view were cloudy. The clear column radiance can be written (neglecting solar radiation) as

$$R_i = [\epsilon_i B_i(T_s) + (1-\epsilon_i) \hat{R}_i^\downarrow] \tau_i(P_s) + \int_{\ln \bar{P}}^{\ln P_s} B_i[T(P)] \frac{d\tau_i}{d \ln P} d \ln P \quad (3)$$

where  $\epsilon_i$  is the surface emissivity;  $B_i(T)$  is the Planck black body function evaluated at sounding frequency  $\nu_i$  and temperature  $T$ ;  $\hat{R}_i^\downarrow$  is an effective downward flux of thermal radiation;  $\tau_i(P)$  is the channel-averaged transmittance from pressure  $P$  to the top of the atmosphere; and  $\bar{P}$  is a pressure above which there is little atmos-

spheric absorption. The term  $\frac{d\tau}{d\ln P}$  is called the weighting function for channel  $i$  (see Figures 1 to 4) and is a measure of the extent that the temperature at a particular pressure level contributes to the integral in Equation (3), and hence to the signal in channel  $i$ .

$R_{i,cl\bar{d}}$  can be written as

$$R_{i,cl\bar{d}} = \tau_{i,c} R_{i,clr} + [\epsilon_{i,c} B_i(T_c) + \eta_{i,c} \hat{R}_{i,c\downarrow}] \tau_i(P_c) + (1 - \tau_{i,c}) \int_{\ln \bar{P}_c}^{\ln P_c} B_i[T(P)] \frac{d\tau}{d\ln P} d\ln P, \quad (4)$$

where  $\tau_{i,c}$  is the transmissivity of the cloud at  $\nu_i$ ,  $\epsilon_{i,c}$  is its emissivity,  $\eta_{i,c}$  is its reflectivity,  $\hat{R}_{i,c\downarrow}$  is an effective downward flux striking the cloud,  $P_c$  is the cloud top pressure, and  $T_c$  is the cloud temperature. If  $\tau_{i,c} \approx 1$ , as in the microwave region, the cloud radiance becomes equal to the clear column radiance (because  $\eta_{i,c} + \epsilon_{i,c} + \tau_{i,c} = 1$ ) and Equation 2 becomes independent of cloud fraction  $\alpha$ . For microwave channels, the temperature profile then can be constructed directly with no cloud filtering, as described previously, provided  $\epsilon_i$  is known or can be determined.

### 2.3.2.1 CLOUD FILTERING

In the infrared, however,  $\tau_{i,c} \approx 0$ , and one must be able to either calculate  $R_{i,cl\bar{d}}$  directly or to otherwise determine clear column radiances from the observations.  $R_{i,c}$  can be calculated assuming  $\epsilon_{i,c}$ ,  $\eta_{i,c}$ ,  $P_c$ , and  $T_c$  are known. In the 15- $\mu\text{m}$  region,  $\epsilon_{i,c} \approx 1$  for most clouds so  $R_{i,cl\bar{d}}$  can be evaluated as a function of  $P_c$  (and  $T_c$ ). Cloud properties are more variable in the 4.3- $\mu\text{m}$

region and evaluation of  $R_{i,clr}$  becomes more difficult. Evaluation of  $R_{i,clr}$  is unnecessary, however, if measurements are made in dual fields of view.

### 2.3.2.1.1 DUAL FIELD OF VIEW APPROACH

If measurements are taken in two adjacent, otherwise homogeneous fields of view but with different cloud fractions  $\alpha_1$  and  $\alpha_2$  then it follows from Equation (2) that

$$R_{i,clr} = R_{i,1} + \eta(R_{i,1} - R_{i,2}) \quad (5)$$

where  $R_{i,j}$  is the observation in channel  $i$  in field of view  $j$  and

$$\eta = \frac{\alpha_1}{\alpha_2 - \alpha_1} \quad (6)$$

Since  $\eta$  depends only on the ratio of the physical cloud cover in each field of view, it is channel (and spectral region) independent. Determination of  $\eta$  is equivalent to determination of the clear column radiances for all channels through Equation 5 without having to make any assumption of the cloud properties. In the above, field of view 1 is always taken as the clearer (warmer) field of view and  $\eta$  should be a positive quantity.

### 2.3.2.1.2 DETERMINATION OF $\eta$ - INFRARED CHANNELS

If the clear column radiance is known for channel  $i$ ,  $\eta$  can be calculated according to

$$\eta_i = \frac{R_{i,clr} - R_{i,1}}{R_{i,1} - R_{i,2}} \quad (7)$$

In general,  $R_{i,clr}$  is not known but can be approximated from the  $n$ th guess temperature profile and  $\eta$  determined according to

$$\eta_i^{(n)} = \frac{R_{i,clr}^{(n)} - R_{i,1}}{R_{i,1} - R_{i,2}} \quad (8)$$

where  $R_{i,clr}^{(n)}$  is calculated from Equation (3). Neglecting instrumental noise on  $R_{i,1}$  and  $R_{i,2}$  and computational noise on  $R_{i,clr}^{(n)}$ ,  $\eta_i^{(n)}$  will be incorrect only insofar as the iterative temperature profile is incorrect. The sensitivity of  $\eta$  to temperature errors can best be assessed by considering apparent temperature profiles.

### 2.3.2.1.3 APPARENT TEMPERATURE PROFILES

Chahine (1975) has shown that if one treats cloud contaminated radiances as clear column radiances and retrieves an "apparent temperature profile," then the true temperature profile is related to the apparent temperature profiles in the two fields of view according to

$$B_i[T(P)] = B_i[T_1(P_i)] + \eta \{B_i[T_1(P_i)] - B_i[T_2(P_i)]\} \quad (9)$$

where  $P_i$  is the pressure corresponding to the peak of the weighting function for channel  $i$ ,  $T_1(P)$  is the apparent temperature profile in field of view 1,  $T_2(P)$  is the apparent temperature profile in field of view 2, and  $T(P)$  is the true temperature profile.

If the true temperature  $\bar{T}$  is known (or guessed) at a characteristic pressure  $P_j$ , then  $\eta_j$  can be calculated according to

$$\eta_j = \frac{B_j[\bar{T}(P_j)] - B_j[T_1(P_j)]}{B_j[T_1(P_j)] - B_j[T_2(P_j)]} ; \quad (10)$$

and a subsequent temperature profile,  $T_j(P_i)$  is obtained by substituting  $\eta_j$  into Equation (9). For best cloud filtering one must find the appropriate channels  $j$  and  $\{i\}$  such that errors in the initial guess  $\bar{T}(P_j)$  produce the smallest errors in the retrieved temperatures  $T_j(P_i)$ . Note, for example, that if channel  $j$ , used to determine  $\eta$ , is also one of the channels  $\{i\}$  used to determine apparent temperature profiles, it follows from Equations (9) and (10) that  $T_j(P_j) = \bar{T}(P_j)$ , i.e., the retrieved temperature at  $P_j$  is equal to the guessed value at that level, giving maximum sensitivity to initial guess errors.

#### 2.3.2.1.4 SENSITIVITY OF $\eta$ TO INITIAL GUESS

The error in  $\eta_j$ , as calculated from Equation (10), caused by an error in the guessed temperature,  $\bar{T}(P_j)$ , can be approximated as

$$\Delta\eta_j = \frac{\partial\eta}{\partial\bar{T}} \Delta\bar{T}(P_j) = \frac{\partial B_j(\bar{T})}{\partial\bar{T}} \left[ \frac{\Delta\bar{T}(P_j)}{B_j[T_1(P_j)] - B_j[T_2(P_j)]} \right] \quad (11)$$

Approximating the Planck black body function in the infrared as

$$B_i(T) = a_j e^{-\ell v_j/T} \quad (12)$$

and expressing the apparent temperature in field of view  $i$  at pressure  $P_j$  as obeying the relationship (Chahine 1975)

$$B_j[T_i(P_j)] = (1-\alpha_i)B_j[T(P_j)] + \alpha_i B_j(T_c) \quad ; \quad (13)$$

where  $T(P_j)$  is the actual temperature at  $P_j$ , and  $T_c$  is an effective cloud temperature, one obtains

$$\frac{\Delta \eta_j}{\Delta \bar{T}} = \frac{\ell v_j}{(\alpha_1 - \alpha_2) T^2} \frac{B_j[T(P_j)]}{B_j(T_c) - B_j[T(P_j)]} =$$

$$\frac{\ell v_j}{(\alpha_1 - \alpha_2) T^2} \left[ \frac{1}{e^{-\frac{\ell v_j}{T(P_j) T_c}} [T(P_j) - T_c]} \right] \quad (14)$$

The sensitivity of  $\eta_j$  to guess temperature errors is minimized by choosing a channel which minimizes  $v_j$ , while at the same time sounds as deeply as possible into the atmosphere so as to maximize  $T(P_j) - T_c$ .

### 2.3.2.1.5 DUAL FREQUENCY PRINCIPLE

As stated earlier, if a set of channels, e.g., 4.3  $\mu\text{m}$  channels, are used to construct the apparent temperature profile, and one of those channels, e.g., the surface channel, is used to get  $\eta$ , then the retrieved temperature equals the guess temperature at the characteristic level, in this case the surface. We see from Equation (14) that  $\eta$  determined from a 15  $\mu\text{m}$  surface channel is less sensitive to guess errors than if determined from a 4.3  $\mu\text{m}$  surface channel. Using the 4.3  $\mu\text{m}$  channels to determine apparent temperature profile, and the 15  $\mu\text{m}$  surface channel to determine  $\eta$  will therefore produce a retrieved surface temperature which is better than the guess (provided other sources of error are sufficiently small). The degree of improvement can be estimated by linearizing Equation (10) to give

$$\frac{\hat{T}(P_s) - T(P_s)}{\bar{T}(P_s) - T(P_s)} = \frac{\eta_{15} - \eta}{\eta_{4.3} - \eta} = \frac{\Delta \eta_{15}}{\Delta \eta_{4.3}} \quad (15)$$

where  $\hat{T}(P_s)$  is the retrieved surface,  $\bar{T}(P_s)$  is the guess,  $T(P_s)$  is the actual temperature, and  $\eta$  is the true  $\eta$ . The right-hand side of Equation (15) can be evaluated from Equation (14) to give

$$\frac{\Delta\eta_{15}}{\Delta\eta_{4.3}} = \frac{v_{15}}{v_{4.3}} \left[ \frac{e^{-\ell v_{4.3} \left[ \frac{T_s - T_c}{T_s T_c} \right]} - 1}{e^{-\ell v_{15} \left[ \frac{T_s - T_c}{T_s T_c} \right]} - 1} \right] = \frac{v_{15}}{v_{4.3}} \left[ \frac{1 - x^{(v_{4.3}/v_{15})}}{1 - x} \right], \quad (16)$$

where  $x = e^{-\ell v_{15} \left[ \frac{T_s - T_c}{T_s T_c} \right]}$ ,  $\ell = 1.439$ , and  $\frac{v_{4.3}}{v_{15}} \approx 3$ . The smaller the right-hand side of Equation (16), the more improvement of the retrieved temperature over the guess. The right-hand side of Equation (16) varies from  $\frac{\eta_{15}}{\eta_{4.3}} \approx \frac{1}{3}$  as  $x$  approaches zero ( $T_c$  very cold compared to  $T_s$ ) to 1 as  $x$  approaches 1 ( $T_c$  almost the same as  $T_s$ ). Therefore, with very cold (high) clouds, a factor of 3 improvement in initial guess temperature error can be obtained in this fashion, while for low clouds, the improvement becomes small. Table 6 gives  $\frac{\Delta\eta_{15}}{\Delta\eta_{4.3}}$  evaluated from Equation (16) as a function of  $T_s$  and  $T_s - T_c$ . We see that at least  $\frac{1}{3}$  of the guess error can be removed,  $\left( \frac{\Delta\eta_{15}}{\Delta\eta_{4.3}} \leq .67 \right)$  provided  $x$  is less than 0.6, i.e., the clouds are at least  $30^\circ$  colder than the surface. An iterative process, whereby  $\hat{T}^n(P)$  is used as  $\bar{T}^{n+1}(P)$  to evaluate  $\eta_{15}^{n+1}$  from equation (8) or (10), will further decrease dependence of the retrieved temperatures on the guess but is potentially sensitive to noise.



Table 6 . Potential Surface Guess Improvement Factor Using Infrared Only.

$T_s - T_c$	$T_s = 300$		$T_s = 280$		$T_s = 260$	
	x	$\frac{\Delta\eta_{15}}{\Delta\eta_{4.3}}$	x	$\frac{\Delta\eta_{15}}{\Delta\eta_{4.3}}$	x	$\frac{\Delta\eta_{15}}{\Delta\eta_{4.3}}$
10	.90	.90	.88	.88	.86	.87
30	.69	.72	.65	.69	.61	.66
50	.51	.59	.46	.56	.40	.52
70	.36	.50	.30	.46	.24	.43

#### 2.3.2.1.6 DETERMINATION OF $\eta$ - MICROWAVE CHANNELS

An alternate approach to the determination of  $\eta$  involves the use of the microwave channels. This procedure has the advantage of being independent of the initial guess surface temperature, but has the disadvantage of being sensitive to computational microwave noise, i.e., errors in computed surface emissivity. To the extent that the latter is not significant, use of microwave channels to determine  $\eta$  is superior to use of  $15\mu$  channels.

One will have determined from Equation (9) a different temperature profile  $T_\eta(P)$ , depending on the choice of  $\eta$ . Given this temperature profile, one can calculate the microwave brightness temperature  $R_i(\eta)$  for a given channel, e.g., 15, the surface channel, according to Equation (3), assuming  $\epsilon_i$  is known or has been determined.

$\eta_i$  is chosen so that  $R_i(\eta) = R_i$ , the observed microwave brightness temperature.

The surface emissivity  $\epsilon_i$ , can be determined according to the method of Waters et al. (1975) from the observations in microwave channels 1 and 2, a knowledge of whether you are looking at land or water, and a guess atmospheric temperature. We have tested the procedure by comparison of brightness temperature observed near radiosondes with those calculated using the radiosonde temperature profile and the emissivity calculated from the observations. The resultant calculation shows small systematic differences with observation, but with standard deviation lower than  $1^\circ$  K. This indicates that the microwave computational noise is not, in general, much worse than the instrumental noise of about  $0.6^\circ$  K. The systematic differences for each microwave channel were calculated for each of the summer and winter periods for five latitude zones. The systematic differences were subtracted from each observation in the handling of the data according to channel, season, and zone.

### 2.3.3 USE OF MICROWAVE CHANNELS FOR TEMPERATURE SOUNDING

In addition to the determination of  $\eta$ , the microwave channel 17(M5) is an excellent stratospheric channel having a sharp weighting function peaking at about 150 mb which can be used in temperature sounding, either in conjunction with infrared channels or with microwave alone. In the case of microwave alone soundings, there are only three channels, giving information at the surface, 500 mb, and 150 mb for the determination of temperature profiles. To the

extent that the shape of the initial guess is correct, excellent tropospheric temperatures can be retrieved, provided the error in calculated surface emissivity is small. Features in the actual profile not in the initial guess will cause serious degradation of the results.

### 2.3.4 CLOUD HEIGHT DETERMINATION

Use of any of the three techniques described previously, (i.e., 4.3  $\mu\text{m}$  channels to get the apparent temperature profile and 15  $\mu\text{m}$  channels to get  $\eta$ , 4.3  $\mu\text{m}$  channels to get the apparent temperature profile, and microwave channels to get  $\eta$ , or microwave channels to get the temperature profile directly) will have produced temperature profiles which are independent of assumption of cloud properties and basically the same as each other up to noise affects and slightly different vertical resolution. Cloud height and percent cloud cover can now be determined from the observation and retrieved temperature profile from Equations (2) and (4), provided assumptions are now made about the cloud properties. Clouds act as essentially black bodies ( $\epsilon=1$ ) in the infrared spectral region. The assumption of unit emissivity is not valid enough for accurate temperature determination but is sufficiently valid for determination of reasonable cloud parameters. If we assume a black cloud whose top is at  $P_c$  with temperature  $T(P_c)$ , where  $T(P)$  is the retrieved temperature profile, then Equation (4) can be evaluated at any assumed cloud top pressure to give

$$R_{i,\text{cld}}(P_c) = B_i[T(P_c)]\tau_i(P_c) + \int_{\tau_i(P_c)}^1 B_i(\tau)d\tau \quad (17)$$

Using Equation (2), a cloud fraction, consistent with the assumed cloud pressure,  $\alpha_i(P_c)$ , can be determined for channel  $i$  according to

$$\alpha_i(P_c) = \frac{R_{i,clr} - R_i}{R_{i,clr} - R_{i,cld}(P_c)} \quad (18)$$

where  $R_i$  is the observation for channel  $i$  and  $R_{i,clr}$  is the calculated clear column radiance using the retrieved temperature profile and equation (3). Channel  $i$  should sound as deeply into the atmosphere as possible to maximize the numerator and denominator of Equation (18) and minimize the affects of errors. For any pair of channels,  $P_c$  and  $\alpha$  can be determined such that  $\alpha_i(P_c) = \alpha_j(P_c) = \alpha$ .

### 2.3.5 ALTERNATE TEMPERATURE INVERSION SCHEME

An alternate inversion technique--the "Residual Error Method"--has been developed as a replacement for equation (1). The procedure is an iterative process of perturbing an initial guess temperature profile such that the radiances computed from a set of radiative transfer equations approximately equals the corresponding set of measured radiances.

Let  $P_c$  = cloud top pressure

$P_s$  = surface pressure

$P_o$  = pressure where radiances are measured

$R_i^m$  ( $i = 1, \dots, N$ ) = a set of measured radiances

$\alpha$  = the cloud fraction

$T(p)$  = an initial guess for the temperature profile

$\tau(\nu_i, p)$  = the transmission (for frequency  $\nu_i$ )

$B$  = the Planck function

$PK_i$  = the peak of the weight function  $d\tau_i/d\ln p$ , where

$$P_0 < PK_1 < PK_2 < \dots < PK_N = P_S$$

A set of computed radiances is obtained using the initial temperature profile guess:

$$R_i^C = (1-\alpha) \left( B_S \tau_S + \int_{P_S}^{P_0} B d\tau \right) + \left( B_C \tau_C + \int_{P_C}^{P_0} B d\tau \right) \quad (19)$$

(The determination of cloud parameters is essentially the same as in previous methods, and we omit discussion of them.)

We seek a temperature profile for which

$$|(R_i^C - R_i^m)/R_i^m| < \epsilon, \quad (i = 1, \dots, N)$$

for some given  $\epsilon$ . We describe the procedure graphically as shown in Figure 13.

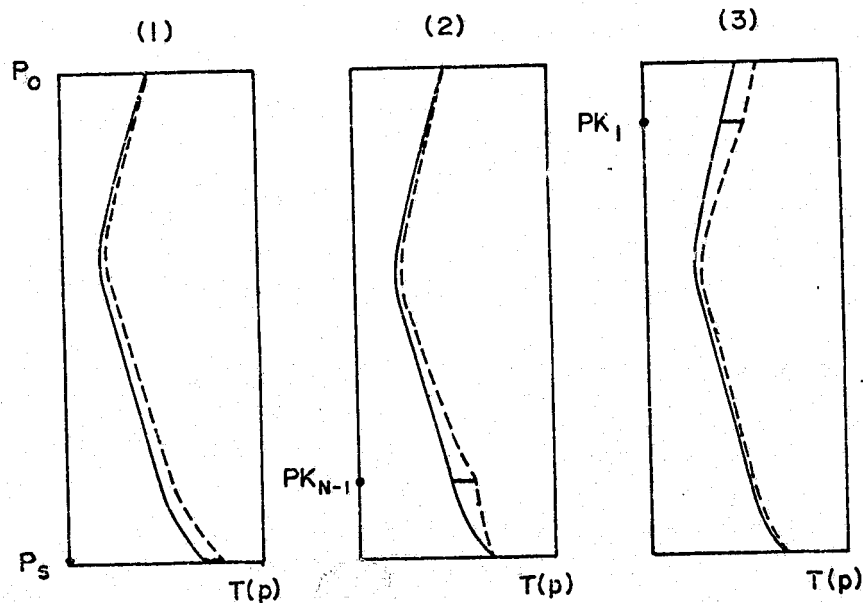


Figure 13. Perturbation Procedures Used in Residual Error Method

Basic to our procedure is the fact that if  $T_1(p) > T(p)$  for all  $p$  ( $P_0 < p < P_s$ ), then  $R_1^C(T_1) > R_1^C(T)$ . The first step (chart 1) is to rotate  $T(p)$  about  $P_s$  to obtain  $T_1(p)$  such that

$$T_1(PK_N) = T(PK_N) + \Delta T,$$

where  $\Delta T$  is some positive or negative quantity accordingly as  $R_N^m - R_N^C(T)$  is positive or negative. We repeat this process until we find that the signs of  $R_N^m - R_N^C(T_j)$  and  $R_N^m - R_N^C(T_{j-1})$  differ. We then interpolate to find the  $\Delta T$  such that  $R_N^m - R_N^C(T_{j+1}) = 0$ , where  $T_{j+1}$  is a rotation of  $T_{j-1}$  such that

$$T_{j+1}(PK_N) = T_{j-1}(PK_N) + \Delta T.$$

Our next step (chart 2) varies from the first step only in that we perturb  $T_{j+1}(p)$  (our current temperature profile) by rotations from  $P_0$  (above  $PK_2$ ) and from  $P_s$  (below  $PK_2$ ). Upon completing step 2 and obtaining a new temperature profile  $T(p)$  such that

$$R_{N-1}^C(T) = R_{N-1}^m,$$

we have put an error into Equation 19 (for  $i = N$ ), i.e.,

$$R_N^C(T) \neq R_N^m.$$

If the weight functions had sufficiently sharp peaks, then the integrals  $R_i^C$  would be almost independent of perturbations of  $T(p)$  outside of a small interval about the corresponding  $PK_i$ . This leads us to an iterative process. After applying our perturbation method (as per chart 2) to obtain the required  $R_i^C$ 's ( $i' = N, N-1, \dots, 2$ ) and obtaining  $R_1^C = R_1^m$  according to chart 3, where the perturbations above  $PK_1$  are linear shifts, we repeat the entire process until we obtain  $\max |(R_i^C - R_i^m)/R_i^m| < \epsilon$  (for  $i = 1, 2, \dots, N$ ) for some given  $\epsilon$ .

Preliminary indications show that improvements can be made over the old iterative scheme in the far north where inversions at 850 mb have been determined through use of this method.

## 2.4 GISS OPERATIONAL PROCEDURES FOR DATA REDUCTION

The basic operational procedures used at GISS for temperature retrieval were described in Susskind et al. (1977). Temperature retrievals are done at the GISS gridpoints using averaged radiances over the grid area for each channel. Initial guesses for the retrievals are taken from a 12-hour forecast. The retrieved temperatures are considered to be typical of the entire grid area and are used for assimilation into the model at the grid points. To implement the dual field of view retrieval scheme, spots falling into a grid area were ordered according to the ratio of the observed radiances of channel 7 to channel 5 for either the VTPR or HIRS observations. Those spots lying in the half with the highest ratio form the relatively clear field of view; the remainder the relatively cloudy field of view. This procedure is used so as to maximize contrast between the fields of view (minimize  $\eta$  from Equation (7)) and also provide the greatest homogeneity of temperature profiles in the field of view. The ratio is used to account for the dependence of radiance on the zenith angle of the observation (the radiance is roughly linear with the secant of the angle for uniform temperature profiles along the scan line). In the winter DST period, HIRS channels were very noisy and not suitable for use. The spots were then ordered in terms of the observed radiance for channel 8, the 4.3  $\mu\text{m}$  surface channel. The effective zenith angle for each field of view is determined according to the arc secant of the average secant of the zenith angle of each spot included in the field of view. This is needed for calculation of effective atmospheric transmission functions for each field of view. The SCAMS brightness



temperatures are averaged into only one field of view because they are not affected by clouds. The HIRS radiances are taken from the output of the NESS operational INGEST program. The SCAMS observations obtained from the INGEST program are antenna temperatures and differ by  $1^\circ$  to  $2^\circ$  from the needed brightness temperatures. We obtain the brightness temperatures from a program by Dr. Rosenkrantz at M.I.T. which makes appropriate corrections to the antenna temperatures. The brightness temperatures are expected to have further small systematic errors due to calibration. Systematic errors determined as described in the text are subtracted from the brightness temperatures before use. The systematic errors are actually systematic differences between observation and calculation and therefore are region dependent.

## 2.5 DETERMINATION OF TEMPERATURE PROFILES

### 2.5.1 VTPR

As shown in Figure 1 and Table 1, VTPR has six  $15\text{-}\mu\text{m}$  temperature sounding channels, 2 through 7, sounding progressively deeper in the atmosphere. Because the sounding channels are all in the  $15\text{-}\mu\text{m}$  region, cloud effects cannot be filtered out and retrievals are strong functions of the initial guess in the lower troposphere. If, after apparent temperature profiles are obtained,  $\eta_7$  is determined according to Equation (10) and used in Equation (9), the retrieved temperature matches the guess at the surface. If  $\eta_6$  is determined and used, the retrieved temperature matches the guess at 700 mb. If, in fact  $\eta_7 = \eta_6$ , then the retrieved temperature matches the guess from 700 mb to the surface. In general  $\eta_7$  and

$\eta_6$  are slightly different because of noise and guess errors. To cancel out noise somewhat,  $\eta$  is chosen as  $\eta = 1/3\eta_6 + 2/3\eta_7$ . This has the property of closely matching the guess near 850 mb.

*Redundant or Highly Overcast Field of View.* As shown in equation (9), the larger  $\eta$ , the more extrapolation must be done from the apparent temperature profiles to the true one. The procedure is thus more sensitive to noise. Also, the further the apparent surface temperature in the clear field of view is from the true (or approximately, the forecast) surface temperature, the more extrapolation is needed. To guard against extreme cases, the dual field of view approach is not done if  $\eta > 3$  or if the apparent surface temperature is more than  $30^\circ$  colder than the guess surface temperature. The former case corresponds to redundant fields of view ( $\alpha_2 < 4/3\alpha_1$ ) and the latter corresponds to highly overcast conditions or very cold clouds. In either of these cases, a single field of view retrieval is done as described in Susskind et al. (1977).

## 2.5.2 NIMBUS-6 SOUNDERS

### 2.5.2.1 OVERVIEW

As seen in Figures 2 to 4 and Table 1, the HIRS-SCAMS sounder complex has many potentially redundant temperature sounding channels. Because of cloud effects, the lower tropospheric  $15\text{-}\mu\text{m}$  channels on HIRS, channels 5 through 7, can only be used for determination of  $\eta$ . Channel 1 was always extremely noisy and not usable. Channel 2 through 4 are potentially usable for stratospheric sounding. The tropospheric  $4.3\text{ }\mu\text{m}$  channels on HIRS, 8 through 10,

have signals coming from relatively sharp portions of the atmosphere (see figure 3b) and have the potential of high vertical resolution in the lower troposphere. The channel 10 radiance does have non-negligible contribution from above 10 mb, however, and is potentially affected by non-thermodynamic equilibrium near 4.3  $\mu\text{m}$  in the upper stratosphere. Channels 11 and 12 are affected to even greater extents. Channel 11 also receives its signal almost uniformly over the entire atmosphere so as to be essentially useless for temperature sounding. The microwave has, aside from two surface channels necessary to determine surface emissivity (and humidity and liquid water content), channels sounding at 1000 mb, 500 mb, and 200 mb. The stratospheric channel, M5 (also called 17) is the sharpest stratospheric channel in the HIRS-SCAMS complex. The tropospheric channels can be used for cloud filtering in conjunction with the 4.3 $\mu\text{m}$  channels or alone for temperature profile determination.

We have considered the three different systems -- HIRS alone, SCAMS alone, and combined HIRS/SCAMS soundings to assess the information content and accuracies of infrared and microwave sounders used separately or in conjunction with each other. In actuality, we were primarily concerned with accuracies of tropospheric soundings. Because these are affected somewhat by stratospheric temperatures, a common set of stratospheric channels was used for all the experiments. Slightly different techniques were developed for the winter DST period because of the poor quality of the 15 $\mu\text{m}$  channel soundings during this period. The summer period will be discussed first.

### 2.5.2.2 STRATOSPHERIC SOUNDING CHANNELS

The best set of stratospheric sounding channels for the summer period were found to be channels 2 (15  $\mu$ m) and 17 (microwave) sounding at 50 mb and 150 mb. Channel 12, sounding at 2 mb, was found to be slightly erratic, possibly due to the effects of non-thermodynamic equilibrium which were not taken into account in analysis of the data. Channels 3 (70 mb) and 4 (250 mb) were found to be too close to channel 17 to produce stable solutions. Channel 4 has the additional problem of cloud contamination for high clouds.

### 2.5.2.3 TROPOSPHERIC SOUNDING AND CLOUD FILTERING CHANNELS

#### 2.5.2.3.1 MICROWAVE ALONE

The microwave alone sounding system consists of channels 2, 17, 16, and 15. The main problems are the effects of surface emissivity and the low tropospheric resolution. To the extent that the emissivity is calculated accurately and the initial guess has the correct shape between 1000 and 500 mb, in particular, the proper lapse rate between 1000 mb and 850 mb, accurate temperature retrievals will be obtained. If, for example, the true profile has a temperature inversion at 850 mb that is not present in the guess, or vice versa, there is no way that it can be determined from the observation, and, in general, the result will be poor retrieved temperatures at 850 and 1000 mb.

The procedure for analyzing microwave only data is to obtain the apparent temperature profile for the single field of view using the characteristic pressure for each channel to be the peak of its

weighting function. Five iterations are performed, and the procedure is then terminated. To guard against very poor retrievals, possibly due to poor surface emissivity, the retrieval is rejected if the retrieved surface temperature differs from the forecast by more than  $6^{\circ}$  K. This quality control is also used with all other retrieval schemes which do not match retrieved surface temperatures to the surface guess.

### 2.5.2.3.2 HIRS ALONE

The HIRS alone temperature retrieval system consists of channels 2, 17, 10, 9 and 8 for apparent temperature profile and 6 and 7 ( $15\text{ }\mu\text{m}$  channels) for determination of  $\eta$ . The characteristic pressures for channels 10 and 8 are taken at the peaks of  $B$  times the weighting function, typically 650 and 1000mb, with the pressure for channel 9 set halfway between those of 10 and 8. The characteristic pressure for channel 10 is never allowed to go beneath 700 mb. Apparent temperature profiles are obtained from the initial guess for each field of view.  $\eta_6^{(0)}$  and  $\eta_7^{(0)}$  are calculated from Equation (8), using the initial guess temperature profile. A new temperature profile is obtained by applying Equation (9) at the characteristic pressures. To help account for possible multiple cloud layers with different effective  $\eta$  as a function of height,  $\eta$  is chosen as a function of  $\eta_6$  and  $\eta_7$  for different  $4.3\text{ }\mu\text{m}$  channels.  $\eta_8$  is taken as  $.75\eta_7 + .25\eta_6$ ,  $\eta_9 = .5(\eta_7 + \eta_6)$ , and  $\eta_{10} = .25\eta_7 + .75\eta_6$ . Temperatures between the characteristic levels are obtained by a shape-preserving interpolation from the initial guess (Susskind et al, 1977). As described previously,  $\eta$  calculated from Equation (8) and  $T_s$ , calculated from Equation (9), are somewhat de-

pendent on the initial guess, particularly if the cloud temperature is close to the surface temperature. To minimize this dependence, the procedure is iterated five times, using the retrieved profile from Equation (9) to calculate  $15\text{ }\mu\text{m}$  radiances to be used in Equation (8) to calculate new  $\eta$ 's, which in turn provide a new profile from Equation (9). The apparent temperature profiles are not iterated.

*Quality Controls.* The HIRS retrievals have the advantage over the SCAMS retrievals in that variable surface emissivity is not a problem and the the retrievals have the potential of finding structure in the lower troposphere, i.e., a different shape profile between 1000 mb and 500 mb than was found in the guess. HIRS has the disadvantage of being affected by clouds. To filter out clouds  $\eta$  must be determined, and in turn multiply a difference in apparent temperatures. The larger the value of  $\eta$ , or the difference in apparent temperatures, the further one has to extrapolate in Equation (9) to get the correct temperature and the more sensitive one is to noise and other errors. To protect against this, HIRS retrievals are rejected if  $\eta > 5$  and the apparent surface temperature in the clear field of view differs from the initial guess surface temperature by more than  $3^\circ$ , or, if the apparent surface temperature in the two fields of view differ from each other by more than  $15^\circ$  but less than the difference between the clear apparent surface temperature and the initial guess. The first case signifies redundant information (but not clear), while the second signifies highly overcast, even in the clear field of view, with insufficient discrimination between fields of view. If  $\eta > 5$  and the apparent "clear" surface temperature is within  $3^\circ$  of the guess, the fields of view are treated as

completely clear and  $\eta$  is taken as zero, i.e., the clear field of view temperature profile is taken as the solution. Another potential problem in retrievals using 4.3  $\mu\text{m}$  channels is the effect of a "hot" surface due either to reflected solar radiation or ground temperatures which are considerably warmer than the air at the surface. The HIRS sounder does not have sufficient information to distinguish ground temperatures from surface air temperatures (two 3.7  $\mu\text{m}$  window channels are needed for this) and the two temperatures are assumed equal in the calculation. Large differences produce very warm apparent surface temperatures. To protect against this, all cases are rejected where the apparent surface temperature in the clear field of view is  $8^\circ$  greater than the guess temperature. If the apparent surface temperature is between  $3^\circ$  and  $8^\circ$  greater than the guess, the case is not rejected but treated specially in that  $\eta$  is allowed to become very negative, thus possibly giving temperatures colder than those in the "cloudy" (cooler) field of view. Ordinarily,  $\eta$  is not allowed to be less than  $-.2$ . A last additional criterion for rejecting a sounding arises if the iterative procedure for calculating apparent temperature profile does not converge within 15 iterations for either field of view.

### 2.5.3 RESULTS OF HIRS AND SCAMS RETRIEVALS

Global HIRS alone and SCAMS alone temperature retrievals with a 12 hour forecast initial guess were run using the techniques described. Figures 14 to 16 show locations of successful (that is,

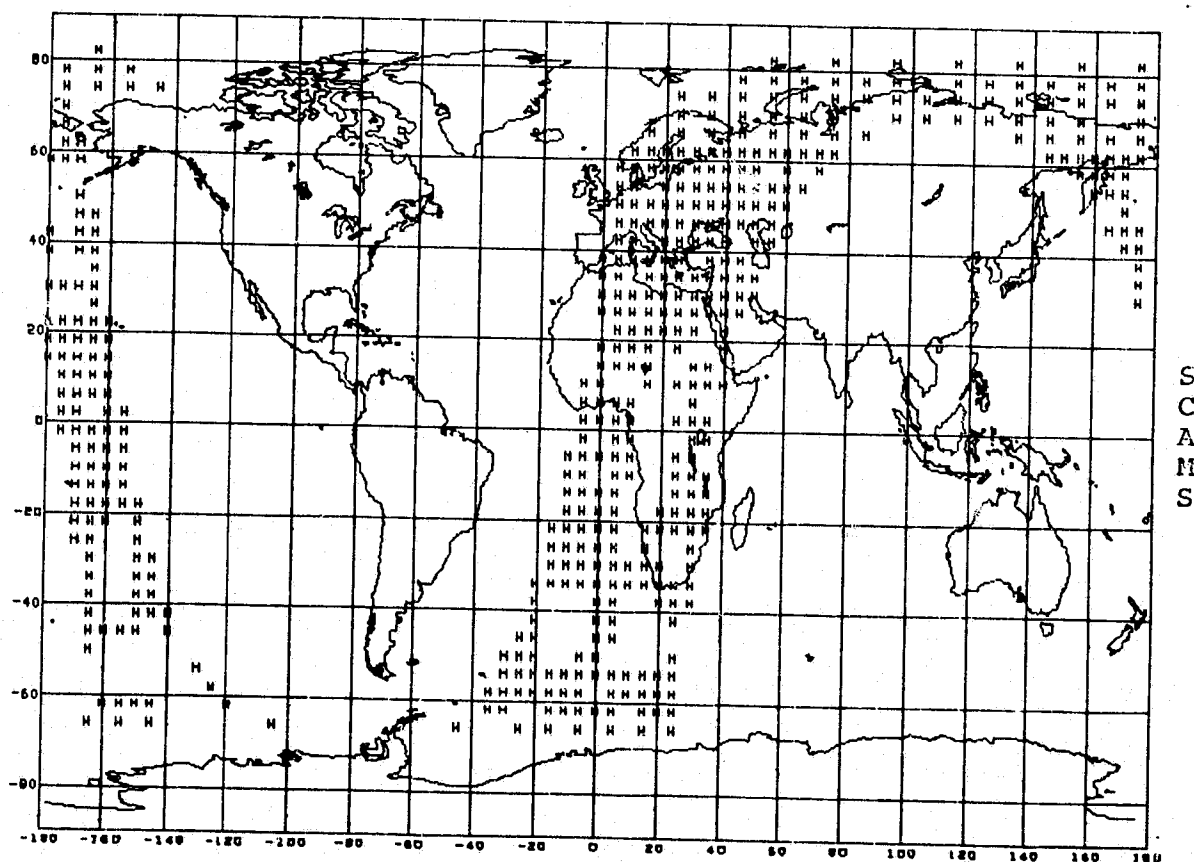
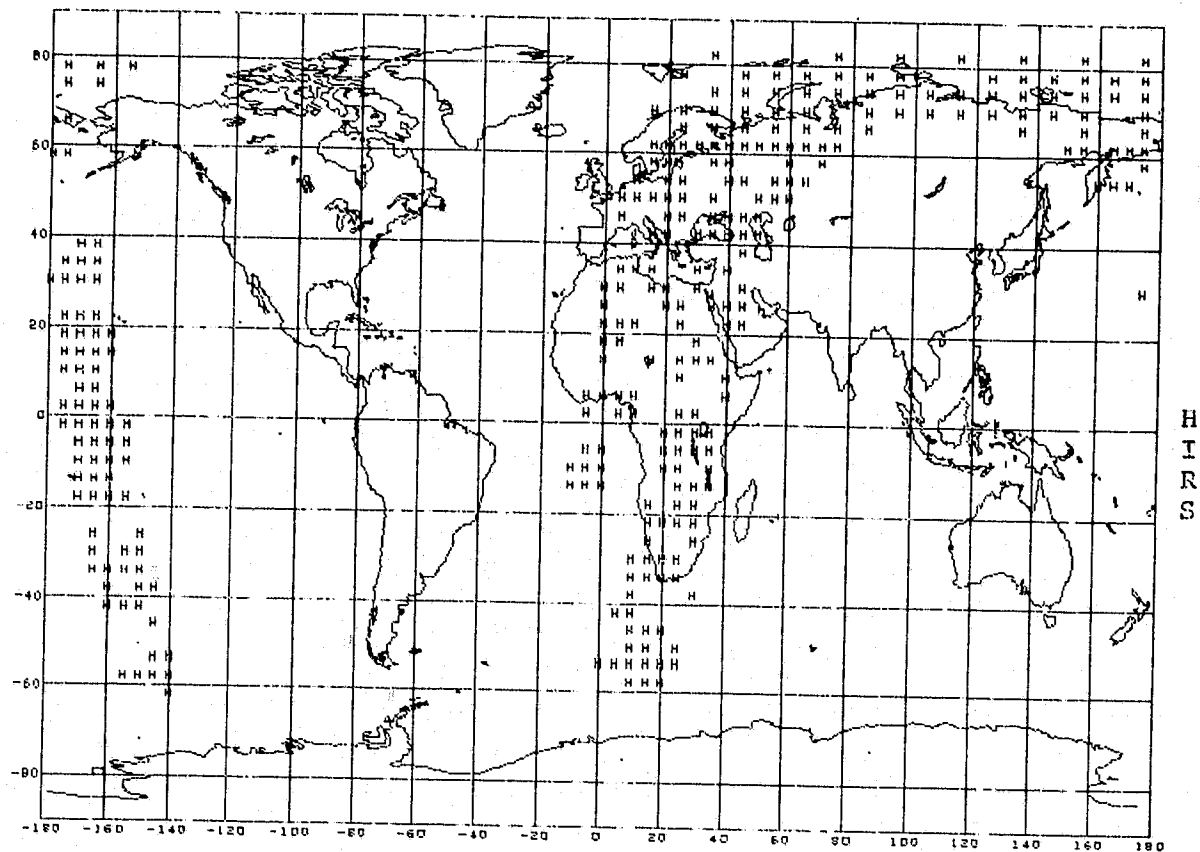
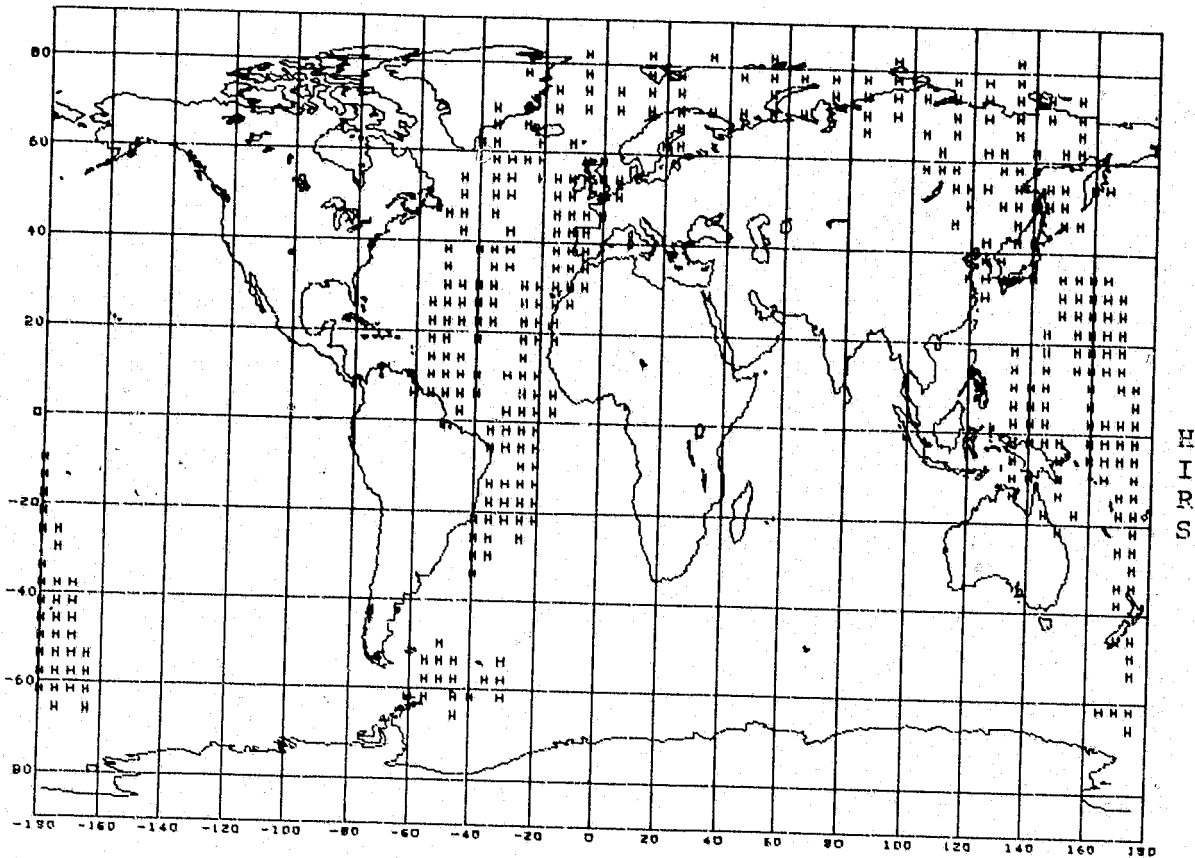


Figure 14. Acceptable HIRS and SCAMS Retrievals for  
Aug. 20 21Z - Aug. 21 0Z





ORIGINAL PAGE IS  
OF POOR QUALITY

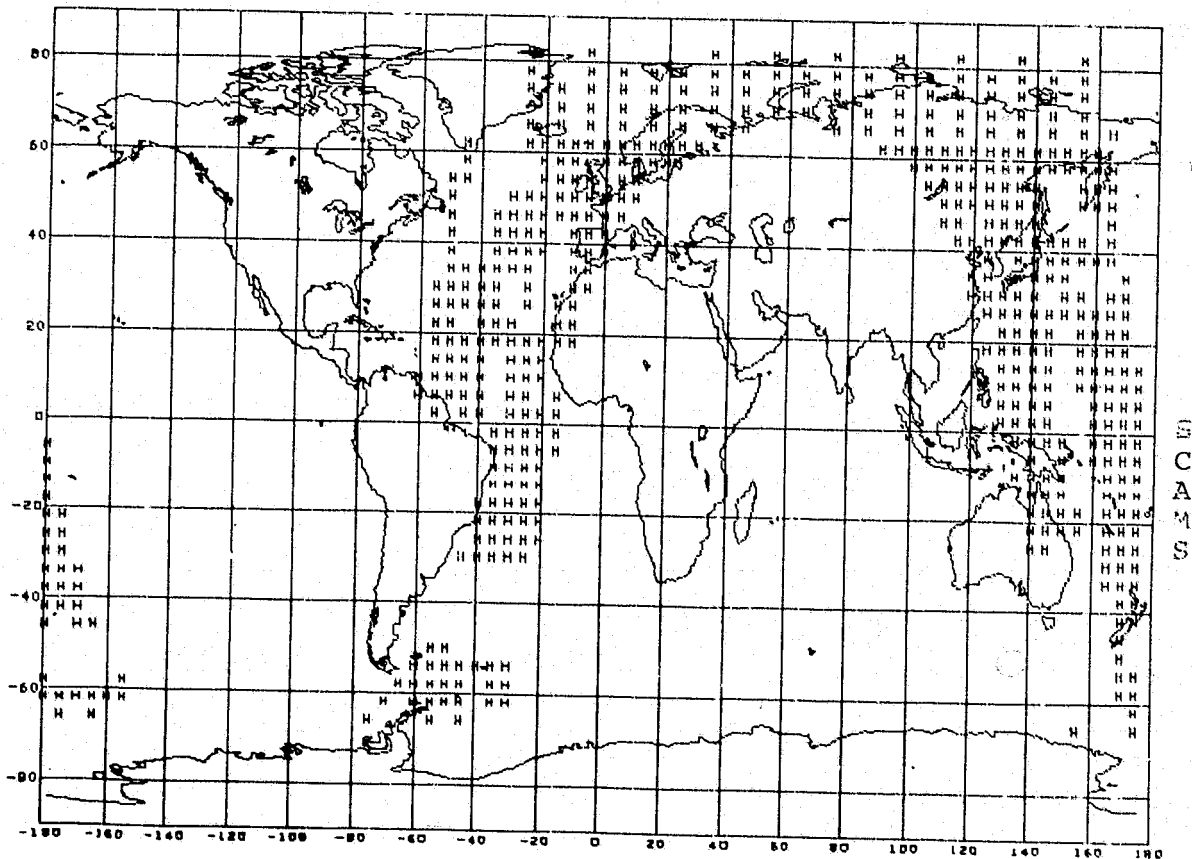
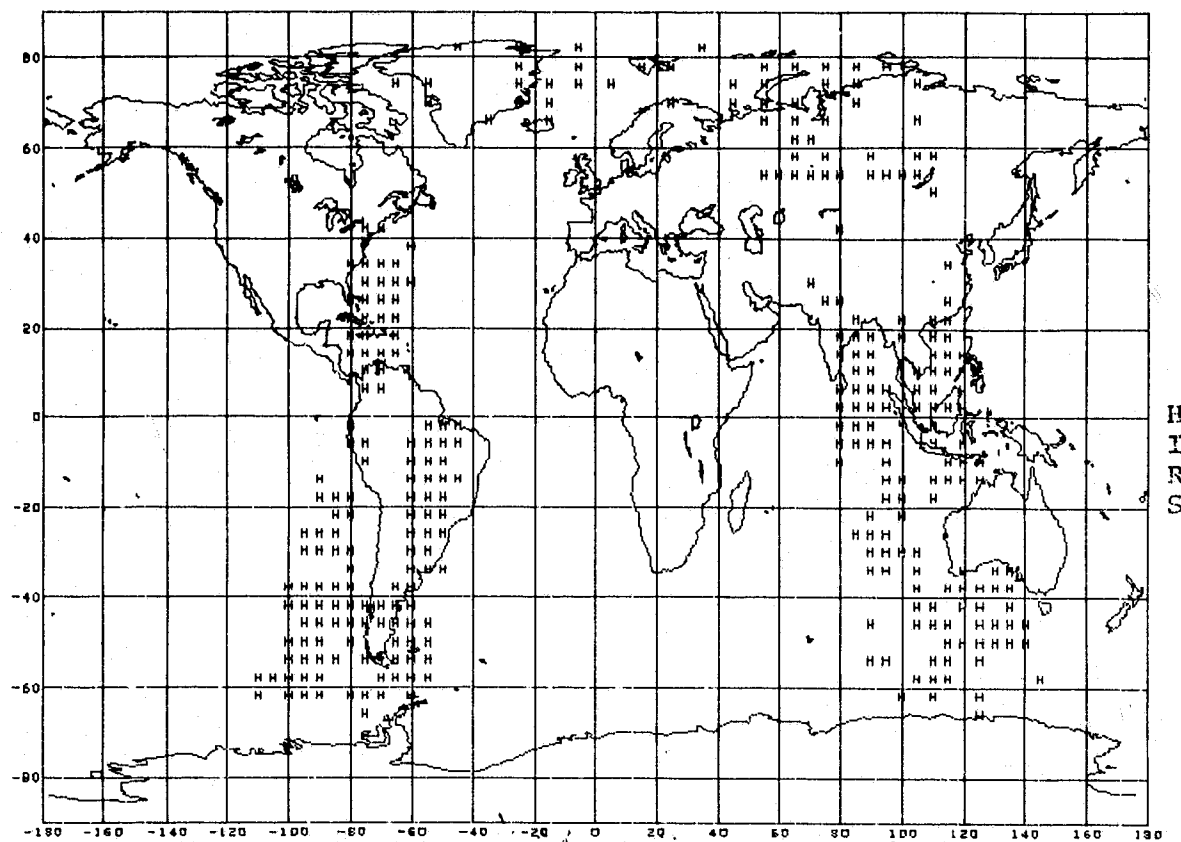
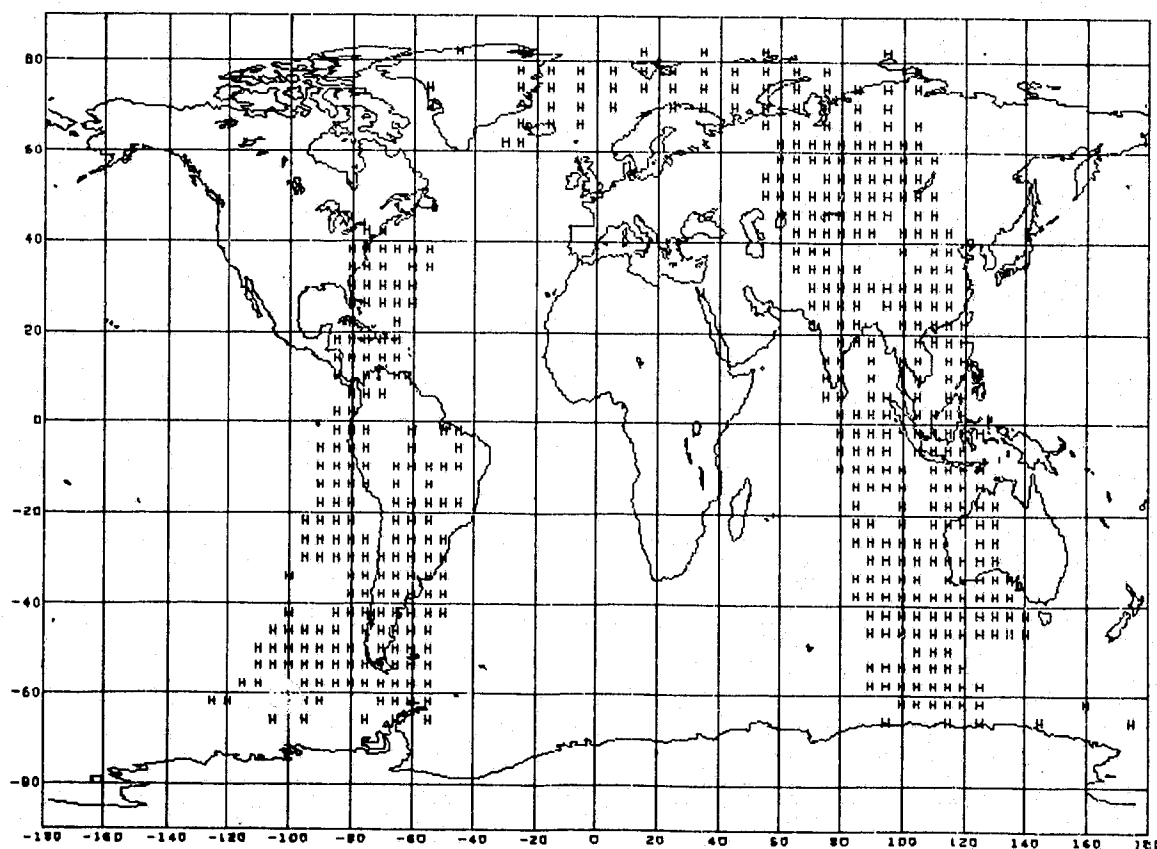


Figure 15. Acceptable HIRS and SCAMS Retrievals for  
Aug. 21 0Z - Aug. 21 03Z



H  
I  
R  
S

ORIGINAL PAGE IS  
OF POOR QUALITY



S  
C  
A  
M  
S

Figure 16. Acceptable HIRS and SCAMS Retrievals for  
Aug. 21 03Z - Aug. 21 06Z

passed all the quality tests described) satellite retrievals for three orbits. Successful retrievals represent about 80 percent of all possible retrievals for SCAMS and about 55 percent for HIRS. A majority of the unsuccessful HIRS retrievals occur over land during the day where reflected solar radiation and/or hot surfaces cause errors.

The quality of retrieved temperature profiles can be judged by comparison of retrieved temperatures with radiosonde colocated in a space time window. Table 7 shows the results of comparing the retrievals over water with radiosonde colocated within  $\pm 110$  km,  $\pm 6$  hours during the period August 18 to September 1. The large time window was chosen so as to minimize overlap in time between satellite and radiosonde coverage. The chart shows, for each pressure level, the RMS error of retrieved temperature compared to radiosonde, the RMS error of the initial guess compared to radiosonde, and the correlation coefficient of guess and retrieval errors. Also shown are the total number of colocated retrievals included in the statistic. Results are shown for two sets of retrievals for each instrument, using either a 12-hour forecast or a zonally averaged climatology initial guess.

The quality of the forecast in the lower troposphere in the vicinity of radiosondes is seen to be much better than climatology. The forecast is of unknown quality in the data-sparse regions where satellite retrievals are most significant and probably no better than climatology. The results of the two retrievals give an idea of the accuracies of retrievals near radiosondes and away from radiosondes where, presemably, zonally averaged climatology is as good a guess as near radiosondes.

Table 7. Temperature RMS Errors and Correlation Coefficients vs. Height  
Water,  $\pm 6$  hrs,  $\pm 110$  km,  $18^{\circ}\text{N} - 70^{\circ}\text{N}$ , DST Summer (Aug 18-Sept 1)

Pressure (mb)	SCAMS		HIRS		HIRS/SCAMS	
	Fore.	Clim.	Fore.	Clim.	Fore.	Clim.
1000	2.77	3.06	2.73	2.73	2.68	2.78
	2.13	3.72	1.99	3.37	2.07	3.82
	.48	.33	.38	.19	.46	.36
850	2.42	2.50	2.39	2.53	2.26	2.36
	1.82	3.65	1.67	3.27	1.78	3.63
	.55	.36	.50	.48	.59	.44
700	1.92	1.87	1.99	2.05	1.84	1.82
	1.71	2.95	1.54	2.66	1.71	2.92
	.63	.33	.39	.26	.62	.35
500	1.80	1.85	2.04	1.93	1.88	1.85
	1.79	3.08	1.67	2.70	1.78	3.08
	.69	.42	.46	.36	.64	.38
400	2.13	2.24	2.05	2.13	2.20	2.25
	2.19	3.56	2.07	2.19	2.20	3.52
	.87	.74	.70	.76	.84	.73
300	2.08	2.97	2.40	3.01	2.19	2.96
	3.01	3.77	2.81	3.44	2.93	3.76
	.80	.91	.74	.88	.75	.90
250	2.32	3.01	2.56	2.88	2.41	2.95
	2.49	4.95	2.33	4.27	2.44	3.71
	.87	.85	.73	.82	.80	.84
200	2.94	3.32	3.09	3.15	3.02	3.22
	3.71	4.39	3.61	4.58	3.73	4.45
	.91	.93	.75	.84	.83	.90
150	2.66	2.87	2.75	2.81	2.66	2.78
	3.70	4.65	4.02	4.77	3.70	4.72
	.77	.78	.65	.66	.71	.73
100	2.36	2.54	2.41	2.50	2.37	2.57
	3.19	4.43	3.44	4.27	3.19	4.59
	.73	.75	.76	.74	.75	.76
70	2.06	2.27	2.12	2.22	2.05	2.23
	3.36	3.13	3.79	3.04	3.50	3.25
	.71	.70	.70	.78	.69	.73
50	2.18	2.09	2.01	2.03	2.06	1.95
	2.80	3.04	2.82	3.29	2.89	3.14
	.83	.68	.75	.75	.77	.68
Colocations	505	493	316	280	548	536

The quality of retrievals between 1000 and 400 mb, using a climatology guess, is only slightly degraded over that with the forecast guess indicating that retrievals are essentially guess-independent. The errors are also shown to be only slightly correlated with the guess. HIRS only retrievals are somewhat better than SCAMS retrievals at the surface, especially with a poor guess, and somewhat worse at 500 to 700 mb. The surface errors in SCAMS retrievals are partly due to errors in surface emissivity and partly due to errors in the shape of the initial guess between 1000 and 500 mb, especially with regard to the 850-mb temperature. The errors in HIRS come in part from cloud problems, errors in physics (i.e., transmission functions, effects of water vapor, surface emissivity and reflectivity), and also from the fact that three channels are being used to determine structure in the lower troposphere, when, in general, the solution in the upper troposphere (whose temperatures effect the radiances of the HIRS 4.5  $\mu$ m channels as much as detailed structure in the lower troposphere) is not known very well.

As observed from Table 7, the retrieved temperatures in the range 300 to 200 mb are considerably poorer than elsewhere and are marked by high correlations with the guess errors. This is because there is little direct information about this portion of the atmosphere in the radiances. The major difference in the quality of forecast and climatology guess retrievals also occurs in this region, because the poor climatology guess cannot be corrected adequately. From 150 to 50 mb, the retrievals are again good and comparable because of the channels sounding roughly 150 mb and 50 mb.

## 2.5.4 COMBINED HIRS-SCAMS RETRIEVALS

Combining the HIRS and SCAMS observations into one sounding helps to alleviate some of the problems of either instrument. The HIRS retrieval is somewhat guess-dependent in its calculation of  $\eta$ . Therefore, a microwave retrieval is performed first to give a reasonable temperature profile to be used as the initial guess for the HIRS retrieval. This guess is used to calculate the HIRS transmission functions, which are fairly temperature-dependent; as a first guess to give apparent temperature profiles, and to compute  $\eta_6$  and  $\eta_7$ . The apparent temperature profiles are constructed as in the HIRS alone case with characteristic pressures nominally 1000, 800, and 600 mb in the troposphere. While, as in the HIRS, there is little information in the upper stratosphere, this region has already been significantly improved over the initial guess by the microwave retrieval using the 500-mb channel. Thus, structure determined by the HIRS channels in the lower troposphere will be less effected by temperature errors in the upper troposphere and tend to be more accurate. Some of the inaccuracy in retrieved surface temperatures from SCAMS, due to errors in microwave emissivity, is removed by using the 15  $\mu\text{m}$  channels to determine  $\eta$ . In this case, only one iteration on  $\eta$  is performed to minimize the effects of noise (observational and computational) on the 15  $\mu\text{m}$  channels. This returns a surface temperature somewhat correlated to (but not identical to) the microwave temperature. Improvements are often of the order of 3° to 4° in cases of poorly determined surface emissivity. A second iteration on  $\eta$  is done to check the consistency of the infrared and microwave channels.

If the second iteration on  $\eta$  produces a surface temperature that does not pass the basic guess consistency check, i.e., differs from the guess temperature by more than 6°, the combined retrieval is rejected. The combined retrieval is also rejected for any of the reasons that pertain to HIRS alone soundings. In case the combined retrieval is rejected, the SCAMS alone retrieval is used provided it, too, does not fail the basic test.

Statistics for the combined retrievals are also shown in Table 7. The basic error structure of the retrievals is similar to HIRS or SCAMS alone but the results indicate the best qualities of each in that the yield is even larger than that of the microwave alone sounder, the 1000 mb and 850 mb temperatures are more accurate, especially with a poor guess, and the 700 mb and 500 mb retain the accuracy of the SCAMS measurements.

### 2.5.5 COMPARISON OF VTPR AND NIMBUS SOUNDINGS

Table 8 shows a set of similar statistics for the VTPR soundings. Figures 17 and 18 show the results of Table 8 along with those of the combined NIMBUS sounders. Unlike the NIMBUS soundings, the quality of the retrievals is closely tied to that of the guess from 700 mb to 1000 mb with error correlation coefficients close to 1. This is because the instrument has no capability of measuring lower tropospheric temperatures independent of outside information. Only in the region 300 mb to 200 mb, where NIMBUS has very little information, does VTPR show an improvement over NIMBUS results. Because real sounding ability is absent in the lower troposphere, the VTPR sounder alone is not a practical instrument.

Table 8. Temperature RMS Errors and Correlation Coefficients  
Versus Height: Water, +6 hrs, +110 km, 18°N - 70°N  
Summer DST (Aug 18-25)  
EXPERIMENT

VTPR

Height (mb)	Frcst Guess	Clim Guess
1000	2.07	3.07
	2.07	3.26
	.79	.87
850	1.90	2.65
	1.82	2.68
	.96	.96
700	2.06	2.71
	1.75	2.59
	.85	.86
500	1.77	2.36
	1.74	3.16
	.72	.75
400	2.15	2.35
	2.21	3.58
	.74	.66
300	2.15	2.53
	2.96	3.55
	.57	.68
250	2.65	2.60
	2.61	4.04
	.80	.69
200	2.54	2.85
	3.29	3.77
	.88	.91
150	2.35	2.25
	2.91	3.52
	.71	.73
100	2.47	2.41
	2.73	3.34
	.76	.74
70	2.17	2.33
	3.27	2.93
	.65	.81
50	2.20	2.47
	2.68	2.81
	.69	.73

Note: first line at each height = retrieval error; second line =  
guess error; third line = correlation.



ORIGINAL PAGE IS  
OF POOR QUALITY

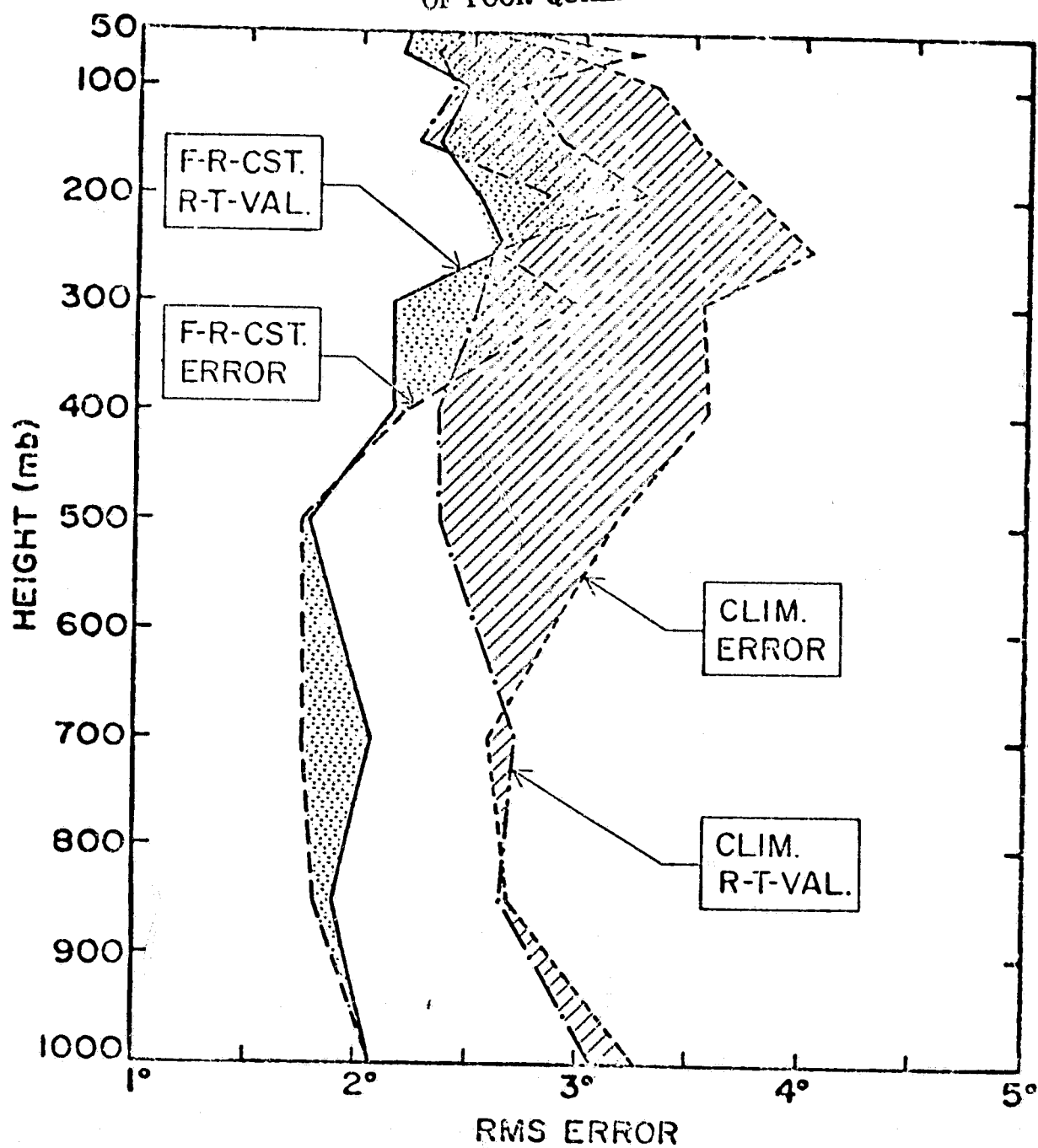


Figure 17. VTPR Temperature Errors Versus Height -  
Water,  $\pm 6$  hrs,  $\pm 110$  km,  $18^{\circ}\text{N}$  -  $70^{\circ}\text{N}$   
Aug 18 - Aug 25

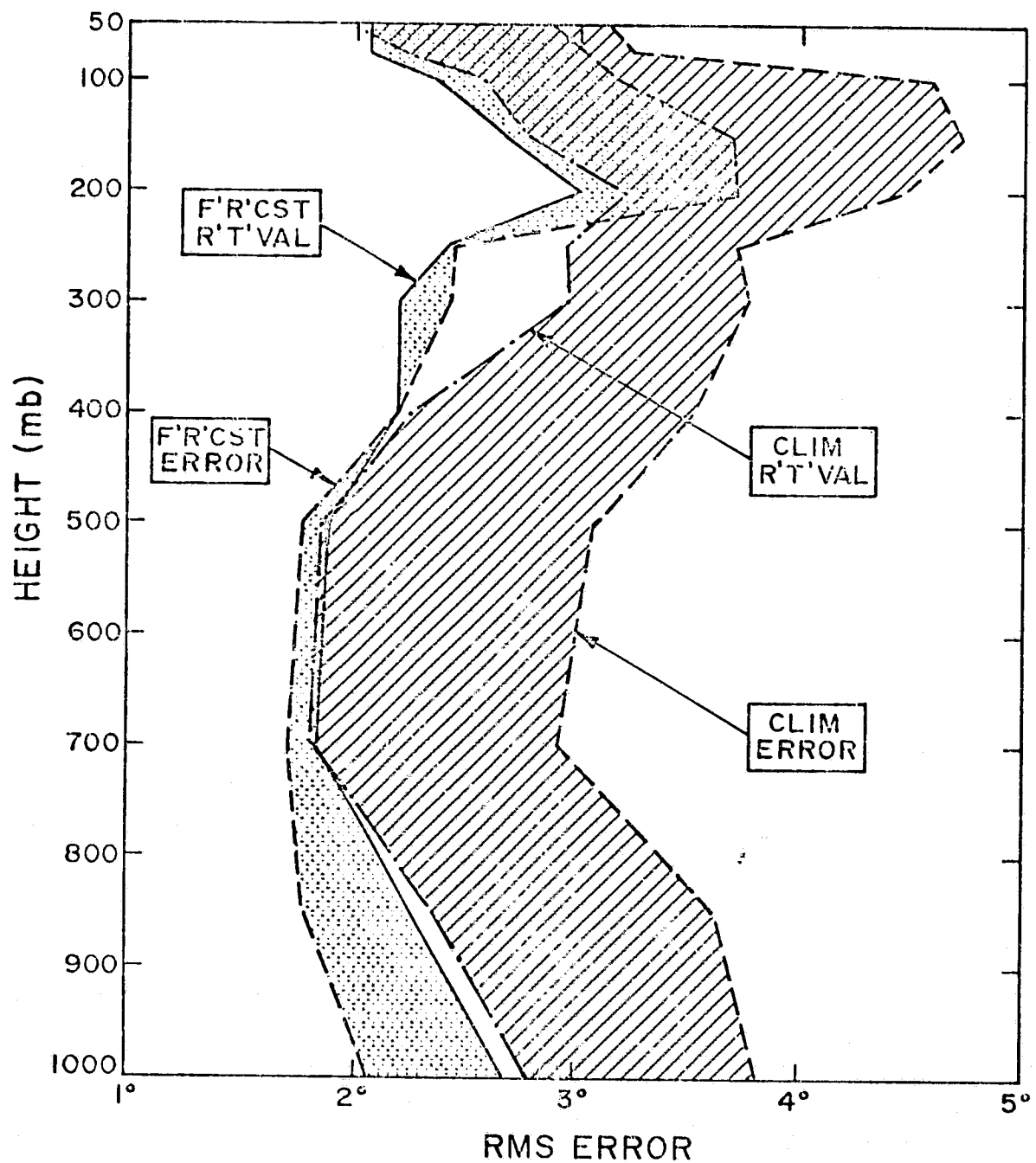


Figure 18. HIRS/SCAMS Temperature Errors Versus Height,  
Water,  $\pm 6$  hrs,  $\pm 110$  km,  $18^{\circ}\text{N} - 70^{\circ}\text{N}$ ,  
Aug 18 - Sept 1

## 2.5.6 NIMBUS 6 SOUNDINGS IN THE WINTER DST PERIOD

During the winter DST period, the 15  $\mu\text{m}$  channels of the HIRS instrument became too noisy for use. Therefore, procedures had to be modified so as to use only the 4.3  $\mu\text{m}$  HIRS channels and the SCAMS channels. The major consequence of this is that HIRS alone retrievals become impossible because of lack of cloud filtering ability. A secondary consequence is that no analogue of the combined summer retrieval procedure is possible in the winter.

### 2.5.6.1 WINTER RETRIEVAL PROCEDURES

The winter retrieval procedures used are basically similar to those in the summer. The 4.3  $\mu\text{m}$  channel 12 sounding at 2 mb was used in place of the 15  $\mu\text{m}$  channel 2 for sounding the upper stratosphere. Microwave retrievals were run just as in the summer but using the channels 12, 17, 16, and 15. Combined microwave-infrared retrievals were run with channels 12, 17, 10, 9, and 8 for construction of apparent temperature profiles. Channels 16 and 15 were used for determination of  $\eta$  as described in Section 2.3.2.1.6. The infrared apparent temperature profiles are modified in a manner similar to that using the 15  $\mu\text{m}$  channels for  $\eta$ . The appropriate  $\eta$ 's to be substituted into Equation (9) for channels 10, 9, and 8 are:

$$\eta_8 = .75\eta_{15} + .25\eta_{16}, \quad \eta_9 = .5(\eta_{15} + \eta_{16}), \quad \text{and} \quad \eta_{10} = .25\eta_{15} + .75\eta_{16}.$$

In the winter runs, the characteristic pressures of channels 8, 9, and 10 were taken to be 1000 mb, 700 mb, and 400 mb, independent of temperature profile. Using the summer procedure of putting the characteristic pressures at the peak of the Planck-weighted weighting function, nominally 1000, 800, and 600 mb, produced substantially worse retrievals. The summer procedure

has the advantage of giving potential increased resolution in the lower troposphere, but has the disadvantage of producing spurious structure as a result of noise in the measurements or errors in the upper tropospheric initial guess. Probably a combination of increased problems in the winter due to larger errors from both sources made the technique impractical.

#### 2.5.6.2 RESULTS OF WINTER RETRIEVAL

Table 9 gives statistics for temperature retrievals over water for the winter period compared to radiosondes colocated within 110 km and 6 hours. Statistics for the SCAMS alone and combined HIRS/SCAMS retrievals are similar to each other. As in the summer, the quality of the retrievals is not highly dependent on that of the initial guess. The .5° degradation in the quality of retrieved temperatures at 850 and 700 mb using a climatology guess should be gauged against the 4.5° degradation in RMS error in the guess temperatures.

A different indication of the quality of the soundings is given in Table 10. Here detailed results are presented for two HIRS/SCAMS soundings colocated with radiosondes  $\pm 1$  hr,  $\pm .75^\circ$  latitude, longitude. The column labeled ADP gives the radiosonde temperature report at a pressure level. The columns labeled T Sol and Diff give the retrieved temperature profile and the error compared to radiosonde. The columns labeled T Guess and Diff give the initial (climatology) guess and its error compared to radiosonde. The highest pressure shown is the radiosonde surface pressure. Also shown are the apparent 4.3- $\mu$ m temperatures in each field of view

Table 9. Temperature Errors and Correlation Coefficients  
vs. Height, Water, +6 hrs, +110 km, 18°N-70°N  
Winter DST (Jan 29 - Feb 12)

Height (mb)	4.3μ, Microwave		Microwave	
	Frcast Guess	Clim. Guess	Frcast Guess	Clim. Guess
1000	2.80	2.78	3.03	3.13
	2.55	7.28	2.72	8.34
	.63	.22	.51	.24
850	2.50	2.94	2.70	2.83
	1.90	6.57	2.12	7.22
	.70	.16	.63	.30
700	2.17	2.70	2.18	2.54
	1.91	6.00	2.06	6.66
	.65	.12	.65	.26
500	2.14	2.13	2.12	2.31
	1.96	4.97	1.90	5.71
	.50	.18	.62	.32
400	2.40	2.39	2.19	2.53
	2.10	4.59	2.26	5.07
	.58	.33	.80	.64
300	2.55	2.78	2.46	2.79
	2.78	3.91	2.97	3.84
	.79	.66	.88	.70
250	2.62	3.22	2.50	3.24
	2.68	4.01	2.63	4.24
	.90	.82	.91	.69
200	2.89	3.08	2.95	3.18
	3.49	5.16	3.66	5.75
	.85	.75	.85	.65
150	3.00	2.80	2.93	2.88
	3.79	4.34	3.48	5.34
	.76	.21	.79	.18
100	2.98	3.04	2.53	2.56
	3.57	4.02	3.28	5.20
	.73	.33	.76	.28
70	2.69	2.87	2.62	2.94
	3.59	4.53	3.28	6.14
	.72	.41	.74	.54
50	2.90	2.87	3.05	2.89
	4.17	4.62	4.20	5.81
	.79	.56	.78	.65

Note: First line at each height = retrieval error;  
second line = guess error; third line = correlation.

Table 10  
SELECT WINTER HIRS/SCAMS RETRIEVALS

STATION NO. 03026					
LATITUDE 58.		REGION 1		LONGITUDE 6.	
PRES	ADP	T SOL	DIFF	T GUESS	DIFF
50.0	202.9	204.6	1.7	214.0	11.1
70.0	202.7	204.9	2.2	214.8	12.1
100.0	204.1	205.0	0.9	215.4	11.3
150.0	207.9	205.8	-2.1	217.0	9.1
200.0	204.1	208.6	4.5	215.9	11.8
250.0	208.1	211.5	3.4	214.8	6.7
300.0	217.1	216.8	-0.3	217.0	-0.1
400.0	232.1	232.7	0.6	227.9	-4.2
500.0	243.7	246.7	3.0	238.1	-5.6
700.0	263.7	266.1	2.4	253.0	-10.7
850.0	269.7	272.6	2.9	257.7	-12.0
991.0					

STA. RMS 2.50  
AVE. RMS 2.50

STA. RMS 9.39  
AVE. RMS 9.39

$\eta_{15}=2.02$   
 $\eta_{16}=1.06$   
 $T_1(850)=262.3$   
 $T_2(850)=253.0$

STATION NO. 03920					
LATITUDE 54.		REGION 1		LONGITUDE 6.	
	ADP	T SOL	DIFF	T GUESS	DIFF
20.0	214.5	209.4	0.0	214.7	0.0
30.0	211.5	209.4	0.0	215.2	0.0
50.0	208.1	209.1	1.0	215.4	7.3
70.0	210.5	209.5	-1.0	216.3	5.8
100.0	208.9	209.8	0.0	216.9	8.0
150.0	210.9	210.7	-0.2	218.3	7.4
200.0	208.5	212.2	3.7	217.1	8.6
250.0	211.5	213.2	1.7	215.3	3.8
300.0	220.5	217.2	-3.3	217.1	-3.4
400.0	234.9	231.6	-3.3	227.9	-7.0
500.0	244.7	244.5	-0.2	238.5	-6.2
700.0	262.1	263.6	1.5	253.4	-8.7
850.0	270.7	271.4	0.7	258.7	-12.0
985.3					

STA. RMS 2.00  
AVE. RMS 2.25

STA. RMS 7.47  
AVE. RMS 8.43

$\eta_{15}=.86$   
 $\eta_{16}=.16$   
 $T_1(850)=268.2$   
 $T_2(850)=265.3$

at the first radiosonde level above the surface (in both cases 850 mb) and  $\eta$  determined from each microwave channel.

The first case represents a highly overcast situation in that the apparent 850-mb temperatures in each field of view are considerably colder than the actual temperature. The retrieved lower tropospheric temperatures, using  $\eta$  determined from the microwave observations, gave good, but slightly too warm, retrievals, indicating  $\eta_8$  being too large. Evidently,  $\eta_{15}$  was too large, most likely due to surface emissivity errors. A microwave only retrieval would then have given even larger positive errors in retrieved surface temperature. Mixing  $\eta_{16}$  into  $\eta_8$  improved the quality of the retrieval.

The second case is clearer as the apparent temperatures in the two fields of view are closer to each other and to the true value. Again  $\eta$  determined from the microwave gave very good lower tropospheric temperatures. Stratospheric temperatures are also very good. The improvement over the bad guess in the region 200-300 mb is smaller, however, because of lack of specific information in the soundings for this region.

## 2.5.7 COMPARISON OF QUALITY OF WINTER AND SUMMER SOUNDINGS

A comparison of Tables 7 and 9 appears to indicate significant differences in the quality of winter and summer retrievals with a general degradation of about .3°. The quality of the 12-hour forecast guess compared to radiosondes appears also to be significantly poorer in the winter from 500 mb to the surface. This may be due

either to an actually poorer forecast near radiosondes or alternatively to larger spatial and temporal variability in the winter within the space-time window, causing a degradation in the intercomparison between forecast and radiosonde values. The latter possibility applies equally well to comparisons of retrieved temperatures with radiosonde measurements in the lower troposphere. Therefore, the degradation in quality of winter retrievals may in fact be less than is apparent from Tables 7 and 9, at least with regard to SCAMS alone retrievals. In the summer, an additional significant improvement in lower tropospheric retrievals was obtained by combined use of HIRS/SCAMS channels, which was not possible in the winter.

## 2.6 ASSESSMENT OF RETRIEVALS IN THE ARCTIC

Satellite temperature retrievals over the Arctic Ocean are very important because there is a general lack of conventional data in this region. There has been some question on the quality of satellite retrievals over the Arctic Ocean, especially during the summer, because during that period this region is generally covered by low-lying stratus clouds, which would potentially degrade (or worse yet prevent one from doing) infrared temperature soundings. The quality of microwave soundings was also questioned because the ocean is covered by broken sea-ice whose surface emissivity in the microwave is extremely variable. As described in the theory and implementation sections, the effects of clouds and surface emissivity can, in principle, be determined from the observations, provided the field of



view is not completely overcast (over a 400-km grid). We have conducted a special study over the Arctic, both because of the significance of retrieved temperatures there for Arctic studies and to determine the adequacy of the algorithms developed for cloud filtering and surface emissivity under trying conditions.

Because of the general lack of conventional data, it is difficult to assess the quality of the temperature soundings. We have taken the approach of comparing surface temperatures retrieved by infrared alone and microwave alone to determine if either of these problems is in fact degrading the quality of our results since each problem would have its largest effect on the retrieved surface temperature, but in a different way.

The RMS difference for the colocated retrieved HIRS and SCAMS surface temperature over ocean between 65°N and 85°N is roughly 3°. This result is independent of the use of a forecast or climatology guess. Since RMS differences between 1000 mb retrieved temperatures and radiosonde reports is of the same order of magnitude globally, it is considered that Arctic retrievals are of comparable quality to those elsewhere.

Another assessment was made by looking at the 2-week averaged retrieved surface temperatures in the 65°N to 85°N region for both the HIRS and SCAMS retrievals. These are shown in Tables 11 and 12, which have for each grid point the average 2-week surface temperature, its standard deviation, and the number of observations entering into the statistic. The area enclosed by the line indicates land. The remaining area is water. The grid index going from 39 to 44 repre-

Table 11. SCAMS Surface Temperatures

DISPLAY OF AVERAGES AND STANDARD DEVIATIONS OF SURFACE TEMPERATURES FOR SUCCESSFUL MICROWAVE RETRIEVALS

	2	4	6	8	10	12	14	16	18	20	22	24	26	28	30	32	34	36
39	283.5 1.8 12	284.1 3.3 6	278.1 0.0 1	279.2 0.0 1	279.1 1.4 6	283.7 2.4 17	285.6 3.7 26	285.3 4.0 38	285.2 3.8 45	282.5 2.6 47	283.2 3.6 38	283.6 3.8 38	279.6 3.6 36	274.1 2.9 12	286.1 2.2 35	285.6 2.1 41	286.8 2.2 38	286.9 2.3 24
40	281.1 3.7 18	280.0 3.6 7	280.1 3.4 6	282.1 2.9 7	283.1 3.7 12	282.3 3.9 26	282.2 3.9 42	282.2 4.2 53	281.5 4.0 58	279.7 4.2 65	280.9 3.8 59	279.9 4.0 57	278.8 2.0 54	263.4 0.0 2	274.4 1.3 3	281.2 2.7 56	283.8 1.9 51	285.2 1.8 44
41	277.5 3.3 42	278.2 2.8 24	279.2 3.3 14	277.6 4.5 17	277.5 2.2 28	275.9 4.0 38	278.0 5.3 62	277.9 4.3 69	277.2 4.5 79	274.7 4.9 81	276.1 3.9 84	280.6 3.8 76	275.1 2.3 29	269.1 0.0 1	263.9 0.0 1	274.5 2.8 28	278.9 2.1 75	282.1 2.4 64
42	274.9 2.9 39	275.9 2.2 38	276.2 2.2 29	276.2 2.3 33	274.7 2.4 35	274.6 2.3 47	273.6 3.2 59	274.8 2.2 70	271.8 3.8 64	272.6 3.9 38	276.7 2.3 77	273.5 6.3 57	270.9 2.9 8	0.0 0	0.0 0	261.8 3.9 44	276.6 2.2 70	280.2 2.4 64
43	275.3 2.9 35	271.9 2.4 38	273.2 2.0 43	274.7 2.8 40	271.9 2.9 44	272.8 2.7 50	271.1 2.3 51	269.0 2.4 52	271.8 2.2 60	268.1 3.5 22	270.2 1.4 38	262.2 3.6 53	261.6 3.1 5	258.8 1.0 2	264.9 5.0 19	266.5 2.9 50	275.7 2.3 61	276.8 1.9 55
44	280.0 0.0 0	271.5 3.5 44	0.0 0.0 0	272.5 2.7 50	0.0 0.0 0	270.8 3.3 51	0.0 0.0 0	269.0 2.3 53	0.0 0.0 0	271.4 2.0 53	0.0 0.0 0	270.4 2.3 70	0.0 0.0 0	267.9 3.8 55	0.0 0.0 0	268.8 2.4 40	0.0 0.0 0	273.9 2.9 60
	38	40	42	44	46	48	50	52	54	56	58	60	62	64	66	68	70	72
39	286.3 2.5 38	285.1 3.9 38	283.8 3.0 34	283.2 3.0 37	280.5 3.2 40	279.6 2.9 42	281.1 3.0 44	282.1 2.3 41	280.4 3.0 38	278.0 3.1 38	277.4 4.1 38	277.1 3.5 38	277.8 3.2 34	275.1 3.0 34	277.4 3.3 41	279.6 2.5 33	278.9 2.4 29	284.9 3.1 24
40	286.6 2.1 41	282.9 3.1 49	279.7 2.4 41	280.7 3.2 52	282.1 2.6 55	280.4 3.3 53	278.4 2.9 56	281.2 2.7 55	280.7 3.0 53	278.4 2.7 52	276.8 4.4 56	275.9 3.8 46	275.5 3.4 51	273.7 2.9 53	276.7 2.3 50	277.5 3.6 54	279.3 3.5 48	279.7 3.1 33
41	282.0 2.5 62	283.3 2.8 61	281.8 2.8 49	283.3 2.0 54	282.4 2.1 47	279.9 1.7 59	278.9 1.5 51	280.7 3.7 60	279.8 3.4 64	278.6 3.1 64	276.6 3.8 65	275.6 2.5 63	275.8 2.6 66	276.5 2.7 54	275.3 2.9 69	276.3 2.2 68	276.4 3.9 59	276.8 3.7 52
42	281.4 1.7 46	281.9 1.8 57	281.4 2.0 50	282.4 1.4 42	281.4 1.7 46	276.5 2.4 47	279.3 1.7 55	280.1 1.8 37	277.7 3.6 58	273.4 3.0 48	273.8 4.2 63	275.2 3.0 59	275.0 2.5 55	274.2 1.6 60	273.4 1.1 63	273.0 2.5 60	273.5 3.2 43	274.2 3.2 41
43	278.8 1.4 52	276.3 2.2 56	277.0 1.9 54	278.6 1.9 52	278.0 2.6 42	277.8 1.6 49	275.4 2.2 42	276.4 2.3 49	276.4 2.5 51	275.3 1.9 50	274.7 2.0 51	276.2 2.2 58	274.6 1.7 54	273.7 2.1 57	274.0 2.5 54	271.5 1.9 50	275.0 2.5 47	274.5 3.3 41
44	0.0 0.0 0	274.7 1.9 44	0.0 0.0 0	272.5 2.7 50	0.0 0.0 0	271.8 2.2 51	0.0 0.0 0	271.5 1.3 53	0.0 0.0 0	271.5 2.0 53	0.0 0.0 0	271.9 2.1 70	0.0 0.0 0	272.4 2.2 53	0.0 0.0 0	273.3 2.0 40	0.0 0.0 0	272.2 2.5 45

2-66

ORIGINAL PAGE IS  
OF POOR QUALITY

Table 12. HIRS Surface Temperatures

DISPLAY OF AVERAGES AND STANDARD DEVIATIONS OF SURFACE TEMPERATURES FOR SUCCESSFUL INFRARED RETRIEVALS

	2	4	6	8	10	12	14	16	18	20	22	24	26	28	30	32	34	36
39	281.2 2.2 8	0.0 0.0 0	278.2 0.0 2	278.3 0.0 1	278.1 2.0 3	283.7 4.1 3	285.5 5.8 11	287.0 6.3 21	284.9 3.8 25	282.4 2.8 35	282.2 3.9 26	281.8 2.3 23	279.3 1.8 22	277.7 2.6 24	281.1 2.0 30	282.5 2.5 26	282.8 2.1 33	282.2 1.8 24
40	284.4 4.7 11	283.0 4.2 8	278.1 0.7 7	276.1 2.5 6	279.2 5.4 11	282.1 4.8 18	284.3 6.0 32	283.2 6.5 38	282.8 5.2 47	280.7 5.3 29	281.5 4.3 43	279.3 3.6 46	278.6 2.1 42	270.0 3.1 53	277.8 1.9 34	278.7 1.7 43	280.0 1.3 37	281.0 2.2 41
41	277.2 3.2 38	279.2 3.5 15	274.7 3.1 15	271.3 2.5 13	276.6 2.5 24	276.0 5.6 48	278.6 5.6 61	277.7 4.5 71	276.8 4.2 77	276.9 4.8 65	276.4 4.7 79	279.2 2.9 62	279.6 1.6 57	266.2 2.5 63	265.5 4.6 60	279.1 2.7 72	277.4 1.6 72	278.9 1.9 56
42	275.0 3.8 40	275.9 2.6 30	276.2 2.7 27	275.9 2.8 26	274.9 3.5 35	275.0 2.5 41	273.7 3.5 55	275.3 3.2 53	271.0 3.0 56	270.0 2.8 52	276.6 2.1 78	276.9 5.7 53	271.6 2.4 43	266.2 2.6 43	264.6 3.7 38	270.8 5.6 51	275.8 1.9 68	276.7 2.0 64
43	274.7 3.0 32	273.7 2.0 42	272.3 2.5 49	273.6 2.3 33	270.1 2.2 40	270.5 2.3 46	269.8 2.1 51	269.7 3.4 53	272.5 2.3 57	264.1 4.1 44	274.1 2.5 55	265.7 3.6 56	266.5 3.3 39	265.5 3.7 48	268.5 3.5 45	267.3 1.9 55	275.2 2.1 56	274.1 1.6 54
44	0.0 0.0 0	269.5 3.2 35	0.0 0.0 0	269.9 2.3 45	0.0 0.0 0	268.2 3.6 44	0.0 0.0 0	268.3 2.6 48	0.0 0.0 0	268.0 2.2 62	0.0 0.0 0	270.3 2.1 63	0.0 0.0 0	267.4 2.4 52	0.0 0.0 0	267.4 1.6 56	0.0 0.0 0	273.6 2.1 47
	38	40	42	44	46	48	50	52	54	56	58	60	62	64	66	68	70	72
39	285.5 2.1 32	286.8 4.0 29	286.7 4.0 25	283.8 4.4 29	282.0 3.7 32	281.5 3.5 27	282.2 3.8 33	282.3 3.5 29	281.6 3.9 29	278.7 4.5 21	277.4 4.8 29	277.7 5.5 29	278.2 4.5 32	276.3 3.7 27	278.1 3.8 13	280.0 3.9 26	280.1 3.7 21	284.7 4.0 21
40	282.4 2.3 37	282.0 2.9 46	281.8 4.5 39	280.5 4.4 43	280.6 3.5 50	278.7 3.4 45	277.4 3.7 48	280.2 3.2 49	280.8 4.3 42	279.2 4.3 39	277.1 5.4 35	276.4 5.9 30	276.0 4.0 43	275.4 4.1 38	277.9 3.1 47	278.3 3.4 49	279.5 3.9 34	282.1 5.0 13
41	280.0 2.4 52	281.4 2.4 55	279.2 3.4 68	277.9 2.1 64	276.9 2.3 63	276.4 1.9 66	278.5 1.4 69	279.4 3.5 60	278.1 4.4 66	277.5 5.0 71	275.4 5.2 72	275.8 3.1 68	274.3 3.3 71	274.6 2.6 67	274.8 3.1 80	276.0 3.8 73	276.0 3.9 59	276.4 3.1 50
42	276.9 1.7 60	278.5 2.0 60	277.3 2.5 55	277.3 2.0 49	276.6 1.8 53	273.5 2.6 66	276.3 1.9 73	277.3 1.7 72	276.3 4.6 68	270.3 4.8 46	272.6 5.9 67	273.2 3.0 72	272.8 2.6 72	273.4 1.3 71	273.6 1.6 67	271.8 3.3 67	273.2 4.2 50	274.8 4.5 50
43	276.4 2.0 50	275.0 2.1 50	275.7 1.7 56	274.8 2.0 43	274.0 2.4 52	274.8 1.8 54	273.2 2.3 60	273.5 2.9 56	274.4 3.4 50	272.9 2.3 55	271.2 2.9 47	273.2 2.4 51	272.2 1.9 63	271.6 2.1 67	272.4 1.7 65	270.2 2.1 61	273.7 2.8 43	274.3 3.2 39
44	0.0 0.0 0	274.5 1.5 33	0.0 0.0 0	272.1 2.3 44	0.0 0.0 0	270.8 1.9 44	0.0 0.0 0	270.5 2.1 43	0.0 0.0 0	270.3 2.3 48	0.0 0.0 0	271.3 2.1 43	0.0 0.0 0	270.4 2.6 58	0.0 0.0 0	271.1 2.7 45	0.0 0.0 0	270.0 2.7 38

2-67

ORIGINAL PAGE IS  
OF POOR QUALITY

sents latitude from 62°N to 82°N. The index from 2 to 36 to 72 represents longitude from 170°W to 0 to 180°E. A comparison of the two maps shows good agreement in general, but in some areas the microwave retrievals are systematically 3° to 4° warmer. This could be due to cloud or emissivity (or other) problems. It is also apparent that the microwave retrievals are too cold over Greenland [roughly (40-43), (28-30)], causing most retrievals to be rejected. The source of this problem is being investigated.

Nevertheless, except for some special cases, the agreement between HIRS and SCAMS surface temperatures indicates that retrievals are of generally good quality over the Arctic.

## 2.7 CLOUD HEIGHT RETRIEVALS

Equations 17 and 18 indicate the procedures developed for cloud height determination. Cloud heights and fractions were retrieved using first the 15- $\mu$ m channels 6 and 7 and then the 4.3- $\mu$ m channels 8 and 10 [8 and 9 produced redundant curves of  $\alpha(P_c)$ ]. Each determination is essentially independent of the other.

Table 13 shows a comparison of  $P_c$  determined from the 4.3- $\mu$ m channels versus  $P_c$  determined from the 15- $\mu$ m channels. In the calculations,  $P_c$  was not allowed to be less than 200 mb or greater than 700 mb. Most cases lie between the lines indicating agreement to better than 50 mb. Table 14 shows a comparison of  $\alpha$  determined from the 15- $\mu$ m channels compared with that from the 4.3- $\mu$ m channels, both computed using the average cloud pressure determined from the 15- $\mu$ m and 4.3- $\mu$ m channels. In this case, there is a clear bias toward slightly lower cloud fractions determined from the 4.3- $\mu$ m channels.

This is consistent with the fact that black clouds were assumed in the determination of  $\alpha$ . This assumption is valid in the 15- $\mu$ m region, but clouds in the 4.3- $\mu$ m region have transmissivities greater than zero (emissivity less than 1), and the apparent cloud fraction (assuming emissivity equals 1) is less than the true value.

Table 13

DISTRIBUTION OF CLOUD HEIGHTS FOR 4.3 MICRON CHANNELS VS. CLOUD HEIGHTS FOR 15  
MICRON CHANNELS

4.3 MICRON RESULTS DISPLAYED ON HORIZONTAL SCALE, 15 MICRON RESULTS DISPLAYED ON VERTICAL SCALE

	200.	220.	240.	260.	280.	300.	320.	340.	360.	380.	400.	425.	450.	475.	500.	525.	550.	575.	600.	625.	650.	675.	700.
200.	12	2	7	3	2	1	2	1	1	1	3	2	0	4	1	2	2	1	1	1	1	0	3
220.	1	3	0	0	0	0	0	0	0	0	1	1	0	0	0	0	0	0	0	0	0	0	0
240.	0	0	2	2	3	0	0	0	1	0	0	0	0	0	0	0	0	0	0	0	0	0	0
260.	2	1	2	3	1	1	1	2	0	1	0	1	0	0	0	0	0	0	0	0	0	0	1
280.	0	1	0	0	1	1	2	1	2	1	0	0	0	0	0	0	0	0	0	0	0	0	0
300.	0	0	0	1	1	1	2	2	2	1	2	0	0	0	0	1	0	0	0	0	0	0	0
320.	0	0	0	0	1	0	3	6	2	2	1	0	0	0	0	0	0	0	0	0	0	0	0
340.	0	0	0	0	0	0	3	3	5	0	1	0	0	0	1	0	0	0	0	0	0	0	0
360.	0	0	0	0	0	1	4	2	5	1	2	1	0	1	0	0	0	0	0	0	0	0	0
380.	0	0	0	0	0	2	2	1	4	9	3	3	2	0	1	0	0	1	0	0	0	0	1
400.	1	1	0	0	0	1	0	0	1	3	7	2	3	1	1	0	0	0	0	0	0	0	0
425.	1	0	0	0	0	0	2	0	3	5	3	1	5	4	2	3	2	0	1	0	0	1	1
450.	0	0	0	0	0	1	0	1	0	1	4	1	6	3	1	3	0	0	0	0	0	0	1
475.	0	0	0	0	0	1	0	1	1	1	2	2	5	3	3	2	2	0	0	0	0	0	0
500.	0	0	0	0	0	0	0	1	0	0	0	0	1	3	4	2	2	1	1	0	0	0	2
525.	1	0	0	0	0	0	0	0	0	0	0	4	2	1	2	4	3	1	1	0	0	0	0
550.	0	0	0	0	0	0	2	0	0	0	1	1	1	4	0	1	4	4	2	0	0	1	1
575.	0	0	0	0	0	0	0	0	0	0	3	0	1	1	4	1	0	1	3	3	1	0	1
600.	0	0	0	0	0	0	0	0	0	0	0	2	2	0	2	2	4	1	1	3	1	2	1
625.	1	0	0	0	0	0	0	0	1	0	0	0	0	0	0	0	0	0	3	0	1	2	1
650.	0	0	0	0	0	0	0	0	0	0	0	0	0	0	1	1	0	0	0	2	0	3	2
675.	0	0	0	0	0	0	0	1	2	0	0	0	0	0	0	0	1	0	2	3	2	1	7
700.	3	1	0	0	0	0	0	0	1	1	1	0	1	1	2	3	2	1	5	3	2	3	42

Table 14

DISTRIBUTION OF ALPHAS COMPUTED FOR 4.3 MICRON CHANNELS VS. ALPHAS FROM 15 MICRON CHANNELS

ALPHAS FROM 4.3 ON HORIZONTAL SCALE. ALPHAS FROM 15 ON VERTICAL SCALE.

2-71

	0.0 to 0.1	0.1 to 0.2	0.2 to 0.3	0.3 to 0.4	0.4 to 0.5	0.5 to 0.6	0.6 to 0.7	0.7 to 0.8	0.8 to 0.9	0.9 to 1.0
0 to 0.1	43	14	1	0	0	0	0	0	0	0
1 to 0.2	7	28	4	0	0	0	0	0	0	0
2 to 0.3	11	18	19	4	2	0	0	0	0	0
3 to 0.4	3	11	18	17	2	0	0	0	0	0
4 to 0.5	3	1	9	26	17	1	0	0	0	0
5 to 0.6	2	0	2	13	24	13	3	0	0	0
6 to 0.7	0	1	2	4	9	13	17	1	0	0
7 to 0.8	0	0	1	2	2	11	17	14	2	0
8 to 0.9	2	0	1	1	1	5	4	14	2	0
9 to 1.0	6	0	1	2	3	8	5	8	9	2

## 2.8 COMPARISON OF GISS AND NESS NIMBUS 6 RETRIEVALS

A detailed study of the relative characteristics of GISS and NESS retrievals with regard to yield, accuracy, and ability to retrieve features of meteorological interest has not been made at this time. This section will present some rough statistics to indicate the general comparable quality of retrievals using both methods.

### 2.8.1 YIELD

When making comparisons of yield of both retrieval schemes, it must be borne in mind that NESS retrievals are done globally over a 300 km grid, corresponding to roughly  $2.5^\circ \times 2.5^\circ$  at the equator, while GISS retrievals are done at a  $4^\circ$  latitude  $\times$   $5^\circ$  longitude grid globally (above  $66^\circ$ , the grid is  $4^\circ \times 10^\circ$ ). As a result of this, global coverage gives a potential of roughly 3 times as many soundings on the NESS grid than on the GISS grid. Tables 2 and 3 show typical NESS yield to be 5700 retrievals per day. The typical yield of GISS soundings is 4800 retrievals per day, or roughly 85% of grid points observed by the satellite.

Tables 15 and 16 give the latitudinal breakdown of GISS and NESS retrievals colocated with radiosondes,  $\pm 6$  hours, over land and water, and over water alone, for the DST 5 and DST 6 periods. The ratio of all GISS/NESS retrievals in a latitude band is most likely similar to the ratio of those colocated with radiosondes as shown in the tables. The relative distribution of



Table 15. DST-5 Zonal Colocations of GISS and NESS Retrievals to Radiosondes  
August 18 to September 1  
±6 Hours, Land/Water and Water Only

	Method	North						South						Total
		70/60	60/50	50/40	40/30	30/18	18/18	18/30	30/40	40/50	50/60	60/70		
Land/Water	GISS	498	1447	656	472	237	150	45	57	0	4	13	3579	
	NESS	501	994	630	561	366	270	61	48	38	2	28	3499	
Water	GISS	28	165	78	144	133	70	23	26	0	4	0	671	
	NESS	67	121	135	152	193	125	29	22	33	2	0	879	

Table 16. DST-6 Zonal Colocations of GISS and NESS Retrievals to Radiosondes  
January 29 to February 12  
±6 Hours, Land/Water and Water Only

	Method	North							South				Total
		70/60	60/50	50/40	40/30	30/18	18/18	18/30	30/40	40/50	50/60	60/70	
Land/Water	GISS	421	1369	579	518	264	100	38	42	1	6	11	3349
	NESS	579	1006	918	600	438	205	58	46	29	13	15	3907
Water	GISS	34	117	57	148	138	65	22	22	1	6	9	619
	NESS	36	139	167	200	211	148	25	23	23	13	3	988

colocations, as seen from the tables, corresponds roughly with what one would expect from the difference in grid sizes as a function of latitude.

## 2.8.2 ACCURACY OF RETRIEVALS

A comparison of Tables 7 and 9 and Figure 18 with Figures 7 and 8 indicate the GISS and NESS retrievals to be of comparable quality near radiosondes, the GISS retrievals being slightly worse in the summer and better in the winter. Table 17 gives the latitudinal breakdown of total profile RMS errors of GISS and NESS retrievals over water vs. radiosonde colocated to  $\pm 3$  hours for both the DST 5 and DST 6 period. In general, the latitudinal breakdown is fairly homogeneous. The summer retrievals are roughly comparable overall, with the exception of the zone  $50^{\circ}/40^{\circ}\text{N}$ , where, in fact, the lower tropospheric retrievals are comparable to elsewhere, but upper tropospheric and stratospheric temperatures are poor. The GISS winter retrievals are significantly better in all zones from  $18^{\circ}\text{N}$  -  $70^{\circ}\text{N}$ . The loss of the  $15\text{ }\mu\text{m}$  channels appears to have degraded the quality of NESS retrievals more than the GISS retrievals.

## 2.8.3 DEPENDENCE OF RETRIEVALS ON THE INITIAL GUESS

The potential impact of assimilating satellite retrievals into a forecast model is maximized if the satellite temperature errors and forecast temperature errors are uncorrelated to each other. Tables 7 and 9 include the correlations of errors of retrievals vs. both forecast and climatology guess errors. While we have demonstrated

Table 17. Zonal Accuracies of GISS and NESS Retrievals  
 DST-5: August 18 - September 1  
 DST-6: January 29 - February 12  
 +3 Hours, 110 Km, Water

	Method	North						South					
		70/60	60/50	50/40	40/30	30/18	18/18	18/30	30/40	40/50	50/60	60/70	
DST-5	GISS	2.30	2.40	2.82	2.14	2.22	2.05	2.47	2.48	0	2.74	0	
	NESS	2.27	2.39	2.36	2.20	2.02	1.99	2.52	2.90	2.39	1.75	0	
DST-6	GISS	2.38	2.71	2.58	2.72	2.55	2.13	1.91	2.30	0	2.51	3.08	
	NESS	3.01	3.06	3.01	2.94	2.85	1.88	2.07	2.84	3.01	2.44	0	

that the retrieved temperatures from 500 mb to the surface are fairly guess independent, the correlation of retrieval errors to forecast errors appears to be moderate, roughly .5. This is in fact an example of "spurious correlation" arising because correlations are being made of two quantities with a common quantity (the radiosonde temperature) subtracted from them.

Table 18 gives the correlation coefficients vs. height of GISS retrieval errors vs. GISS forecast errors and NESS retrieval errors vs. GISS forecast errors. The NESS retrievals ought to be completely uncorrelated with the GISS forecast because the GISS forecast in no way entered into the calculation of NESS temperature profiles. The correlations are in fact .3-.4 on the whole. The GISS retrievals are only slightly more correlated from 500 mb to 1000 mb. This indicates that the errors are to a good extent uncorrelated with the forecast guess. The region from 300 mb to 200 mb, on the other hand, is highly correlated, as discussed previously, because the soundings contain less detailed information in this region.

## 2.9 CONCLUSIONS

This chapter has shown that an alternate scheme for processing HIRS/SCAMS data to retrieve temperature profiles has been developed at GISS, which is fundamentally different from the approach used to create the operational NIMBUS 6 DST temperatures developed at NOAA/NESS, in that unlike the operational approach, the GISS approach makes no use of a priori statistics.

Table 18. Correlation Coefficients for GISS  
and NESS Retrievals Versus Forecast, Winter DST  
±3 hours, 110 km, Water, 18°N-70°N Latitude

Pressure (mb)	Method	
	GISS	NESS
1000	.46	.31
850	.60	.31
700	.45	.39
500	.44	.40
400	.57	.48
300	.85	.48
250	.87	.65
200	.81	.55
150	.61	.39
100	.65	.66
70	.62	.47
50	.69	--
Total	.63	.46

Use of statistics tends to bias the solution towards the expected, with a decrease in probability of finding less common meteorological situations. The GISS approach, on the other hand, is not biased towards the expected, but does put a great emphasis on the ability to theoretically reproduce and account for the atmospheric and surface physics. Systematic errors in retrieved temperatures will occur in situations where the physics is not adequately accounted for. Therefore the retrieved temperature fields should have greater variability than with a statistical approach, though some of it may be spurious. Techniques are presently being developed to distinguish the spurious from the real (or at least realistic) meteorological situation.

Specific findings in the chapter are summarized below:

- GISS HIRS alone and SCAMS alone retrievals are of comparable quality in the summer DST 5 period. A combination HIRS/SCAMS retrieval system gives a significant improvement in the lower tropospheric results.
- HIRS alone retrievals are impossible during the winter DST 6 period because of loss of the 15  $\mu\text{m}$  channels. GISS HIRS/SCAMS retrievals are slightly better than SCAMS alone. Most information in the HIRS/SCAMS sounder comes from SCAMS.
- GISS temperature retrievals in the lower troposphere are essentially independent of the initial guess. They should therefore be of comparable quality in data sparse regions as

near radiosondes. The RMS errors over the lowest 500 mb, using a climatology guess, are 2.2° for the summer and 2.6° for the winter. Part of this increase is due to the greater spatial and temporal variability of temperatures in the winter; part is due to loss of the 15  $\mu$ m channels.

- GISS retrievals in the Arctic for both summer and winter periods are of comparable quality to those elsewhere.
- The yield of GISS retrievals is about 85% of all satellite collocations for both winter and summer. The number of retrievals per day is slightly less than NESS due primarily to a larger grid size.
- The accuracies of GISS and NESS retrievals are comparable in summer. GISS retrievals appear to be better in winter.
- Cloud heights determined by GISS retrievals by two sets of measurements differ on the whole by between 0-50 mb. This indicates the accuracy of cloud height determination to be about 25 mb.

### 2.9.1 EXPECTATIONS FOR FGGE

The temperature sounding system on TIROS-N to be used in FGGE is basically similar to that on NIMBUS 6. SCAMS is to be replaced by MSU, which is basically similar but contains an additional stratospheric sounding channel and slightly lower noise levels. HIRS is to be replaced by TSU, again basically similar, but with substantially improved noise levels and a very important correction in that both



the 15  $\mu\text{m}$  and the 4.3  $\mu\text{m}$  channels will be seeing the same field of view at the same time. Slight differences in the fields of view of the two sets of channels on the HIRS, coupled with relatively high noise levels, seriously degraded the cloud filtering ability and general overall quality of the HIRS retrievals. These contributed to the relatively large (2.7°) surface temperature RMS errors. TSU will also have an additional 3.7  $\mu\text{m}$  window channel, thus allowing one to retrieve ground temperature independent of surface (air) temperature during the day. On HIRS, retrievals over land during the day, especially arid land, could not be done because of large differences in ground and surface temperatures.

These changes should make significant improvement in the quality of TIROS-N temperatures over NIMBUS 6, perhaps of the order of a few tenths of a degree at the surface. The limiting factor in the accuracy of the retrieved temperatures will still be the lack of sufficient vertical resolution to measure significant meteorological features. The sounders on TIROS-N will be no better in this regard than those on NIMBUS 6.

## REFERENCES

- Chahine, M. T. (1970). Inverse problems in radiative transfer: determination of atmospheric parameters. J. Atmos. Sci., 27, 960-967.
- \_\_\_\_\_ (1974). Remote sounding of cloudy atmospheres. I. The single cloud layer. J. Atmos. Sci., 31, 233-243.
- \_\_\_\_\_ (1975). An analytical transformation for remote sensing of clear column atmospheric temperature profiles. J. Atmos. Sci., 32, 1946-1952.
- Susskind, J., M. Halem, D. Edelman, E. Tobenfeld, J. Searl, R. Karn, R. Dilling, D. Sakal, C. Y. Tung, H. Carus, N. Rushfield and L. Tsang (1977). GISS VTPR Processing Manual, Goddard Institute for Space Studies, 2880 Broadway, New York, N. Y. 10025.
- Waters, J. W., K. F. Kunzi, R. L. Pettyjohn, R. K. L. Poon, and D. H. Staelin (1975). Remote Sensing of atmospheric temperature profiles with the Nimbus 5 microwave spectrometer. J. Atmos. Sci., 32, 1953-1969.

**Appendix A**  
**(Chapter 2: STS)**

ORBITS 3150  
3151

February 2 0708-0855

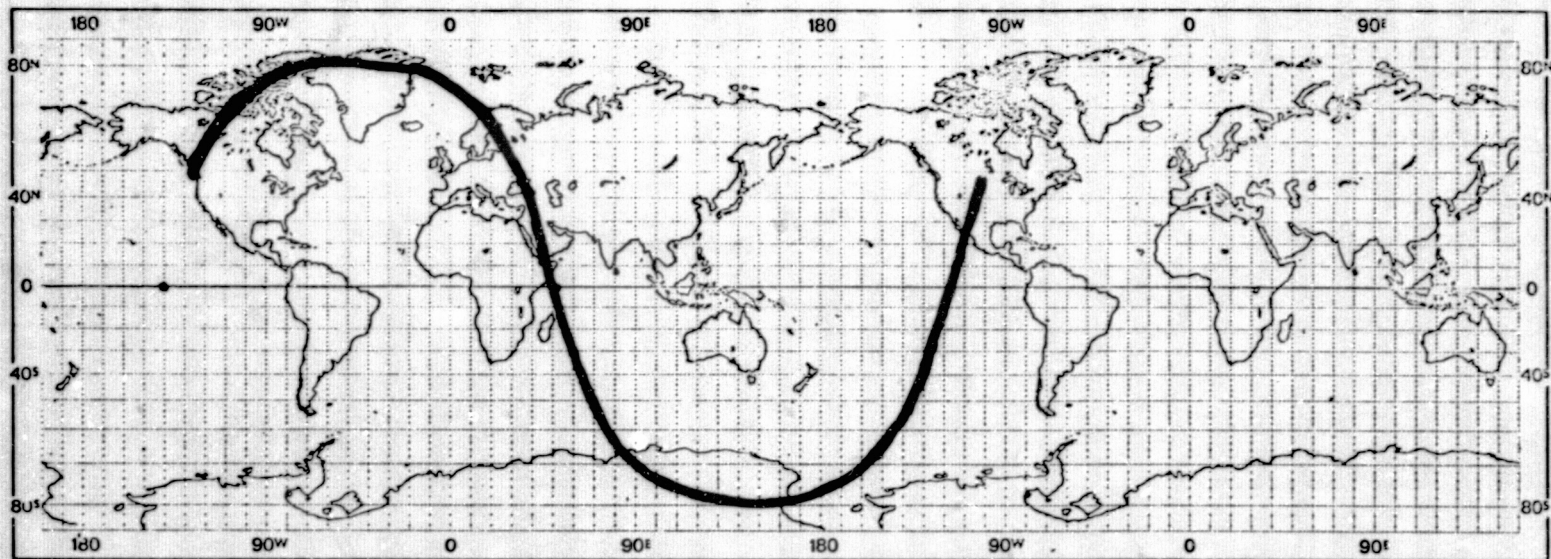


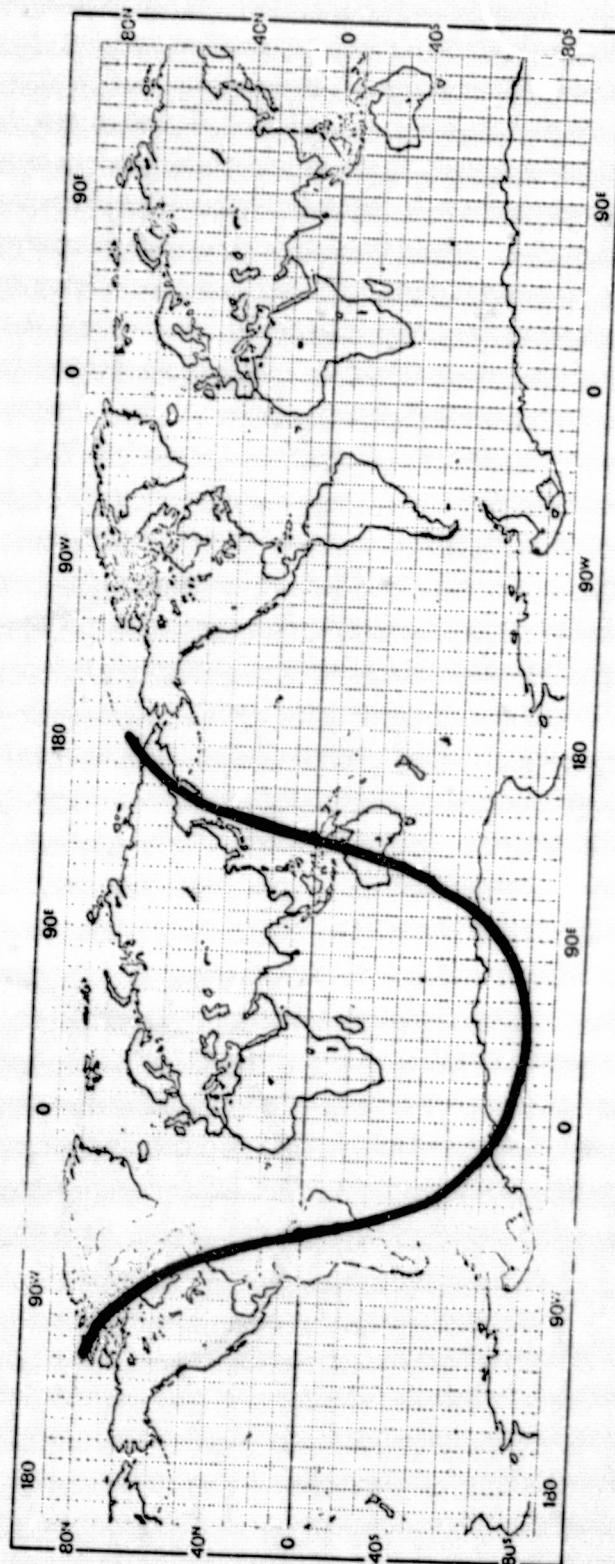
Figure 1A. DST-6 Subsattellite Tracks of Missing Orbits

A-1

ORIGINAL PAGE IS  
OF POOR QUALITY

ORBIT 3155A

February 2 1406-1558

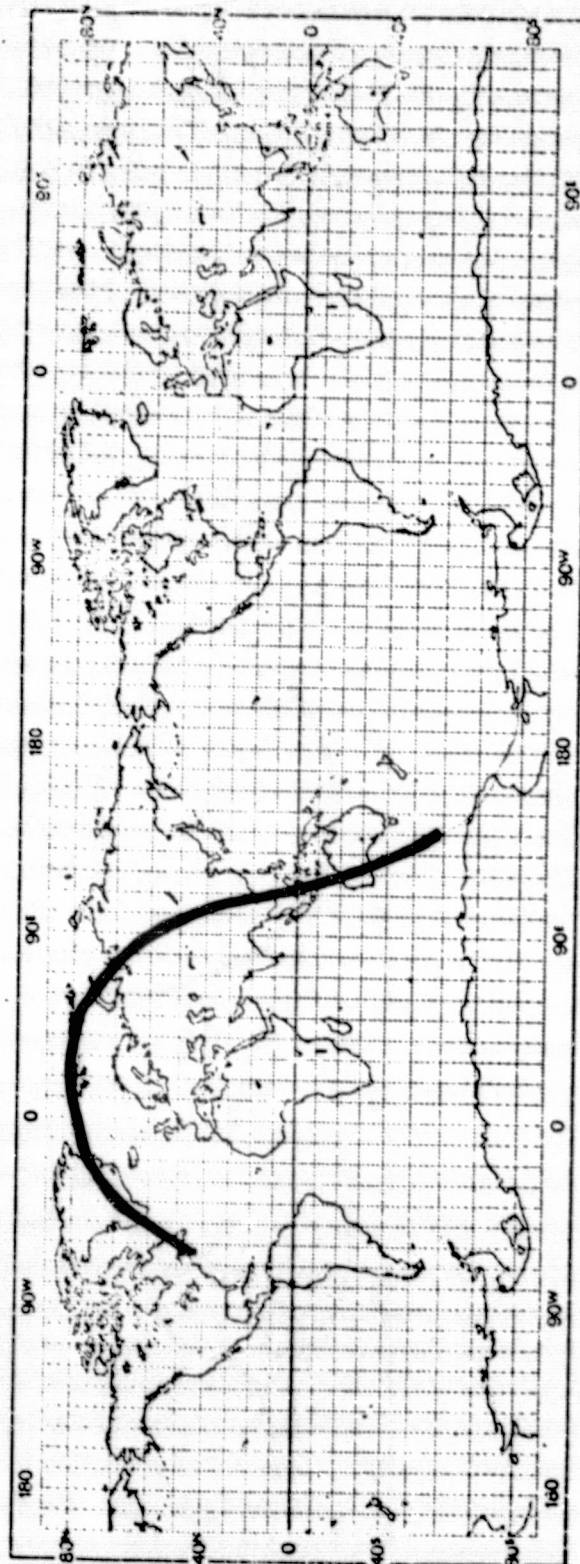




ORIGINAL PAGE IS  
OF POOR QUALITY

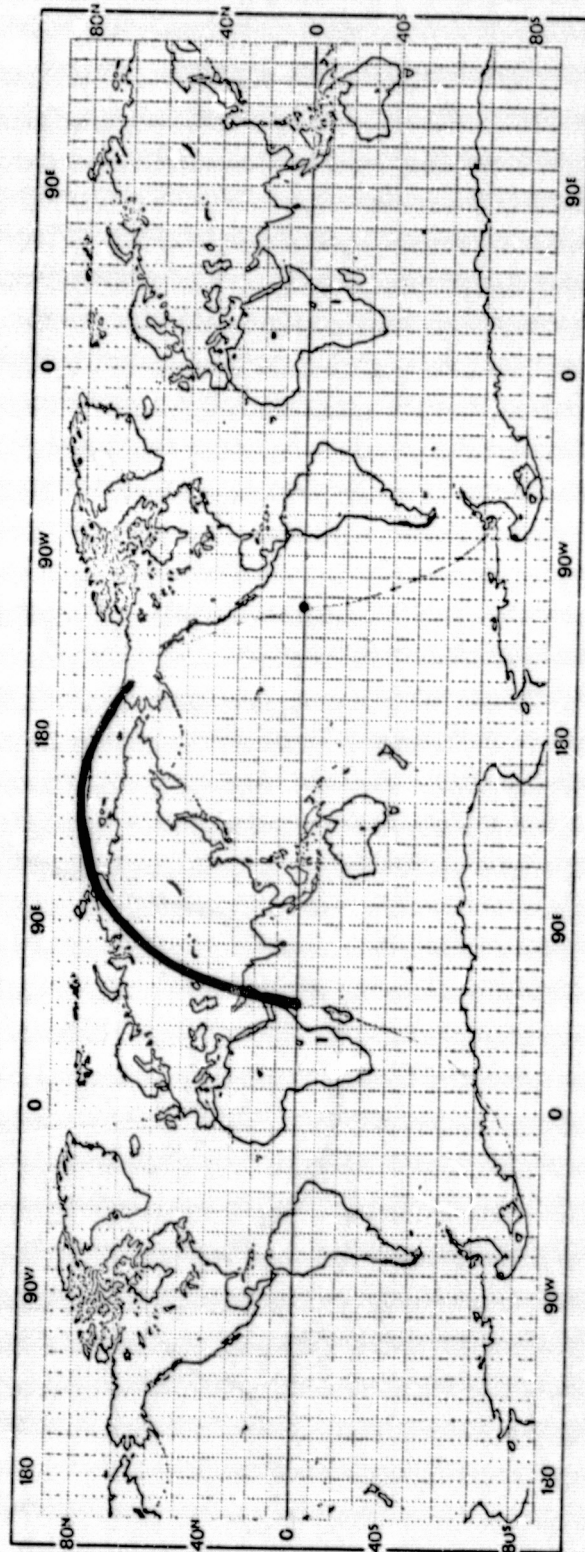
ORBIT 3162R

February 3 0342-0440



ORBIT 3185A

February 4 1945-2018

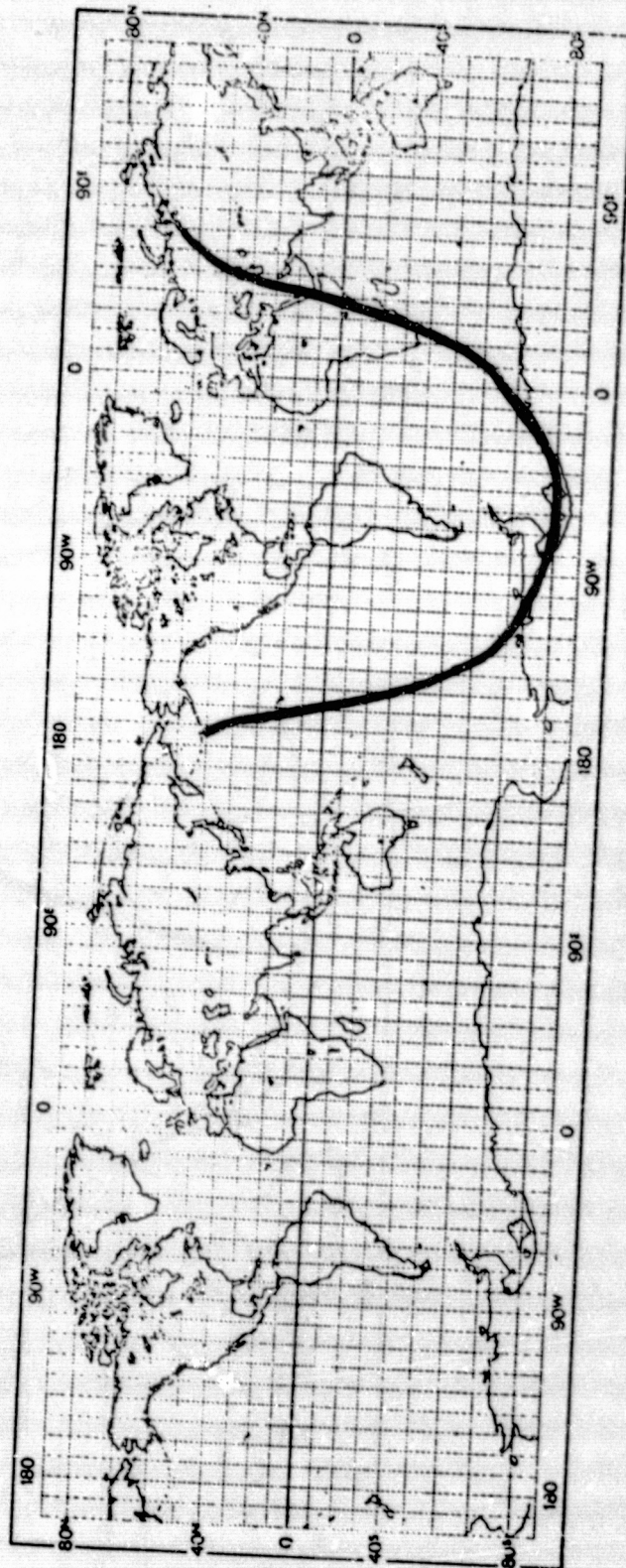




ORIGINAL PAGE IS  
OF POOR QUALITY

ORBIT 3199A

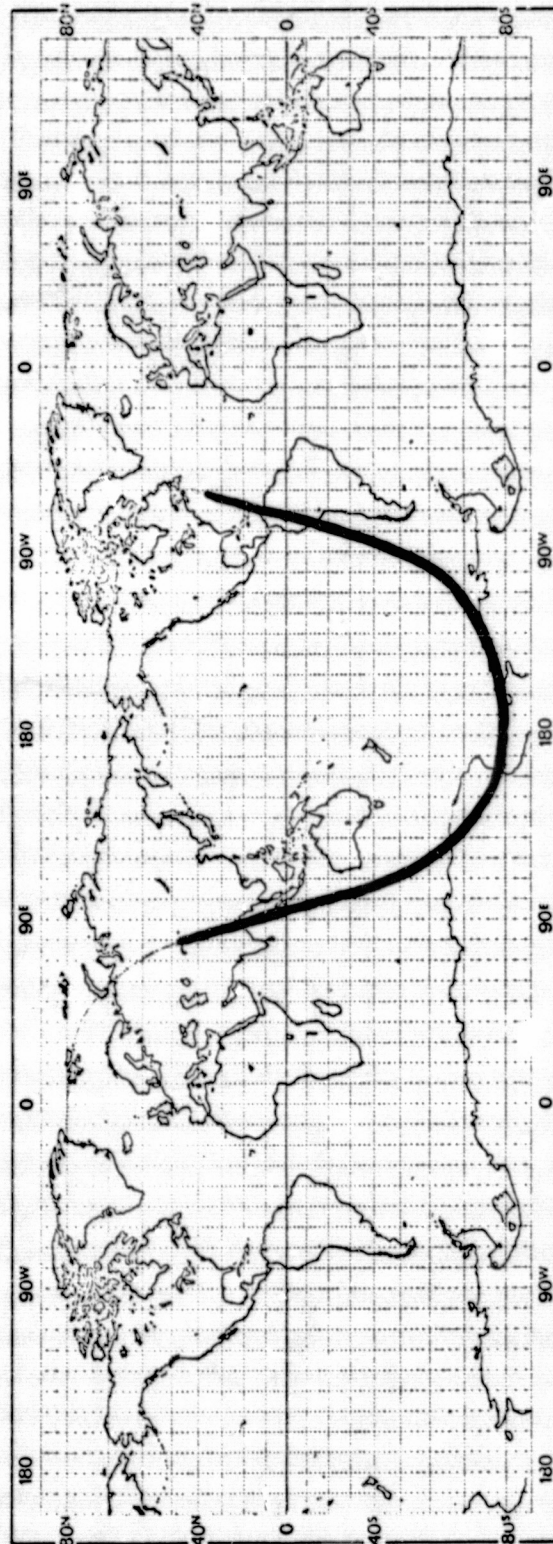
February 5 2103-2233





ORBIT 3203R

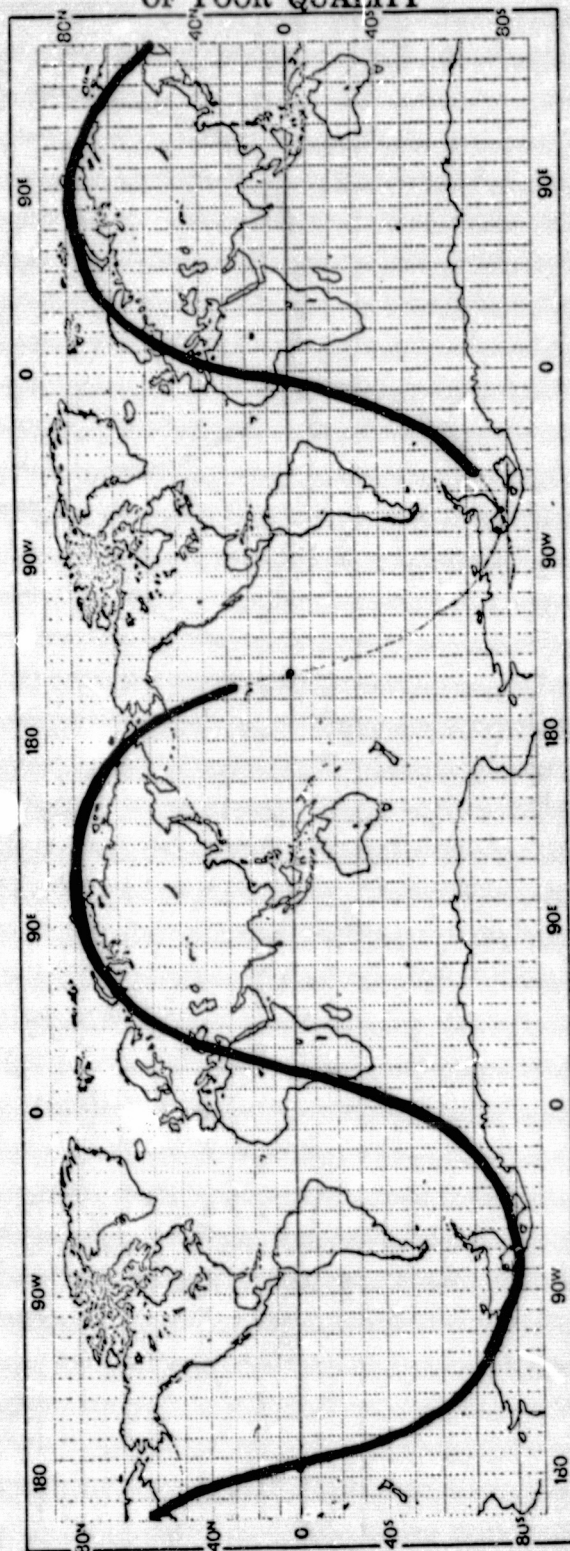
February 6 0422-0542



ORBITS 3212A  
3213A  
3213O

February 6 2142 - February 7 0044

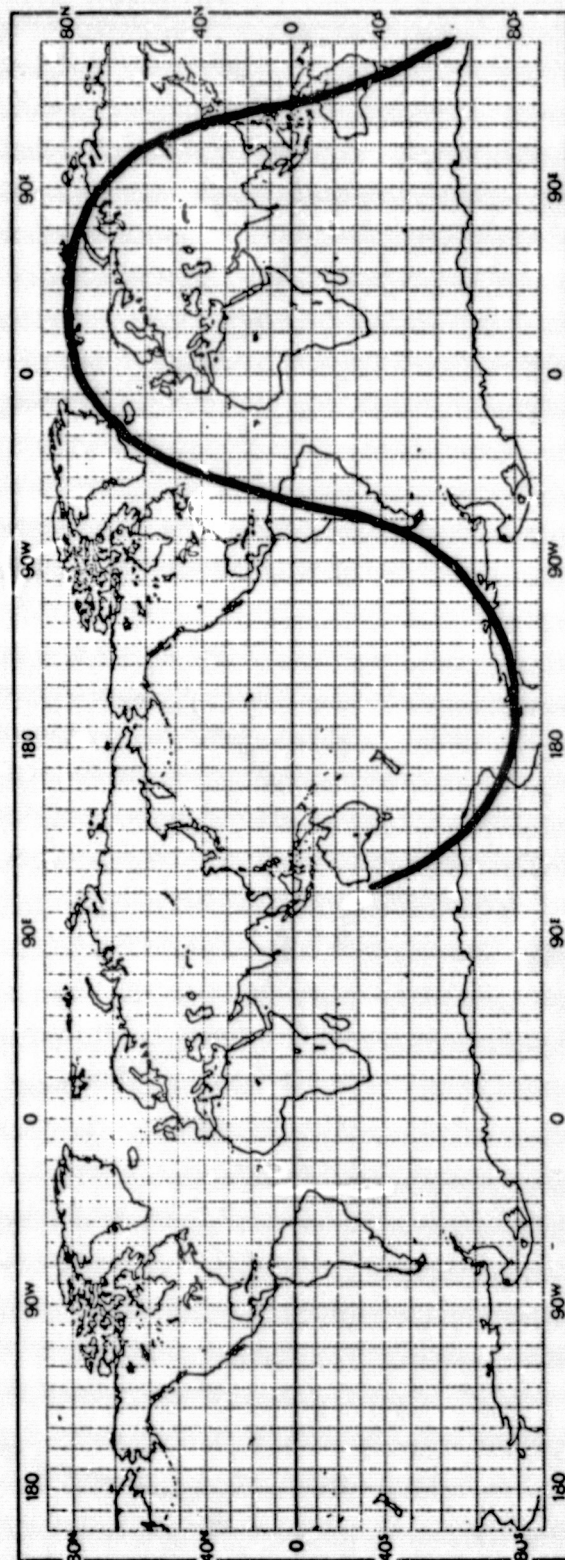
ORIGINAL PAGE IS  
OF POOR QUALITY





ORBITS 3216R  
3218A

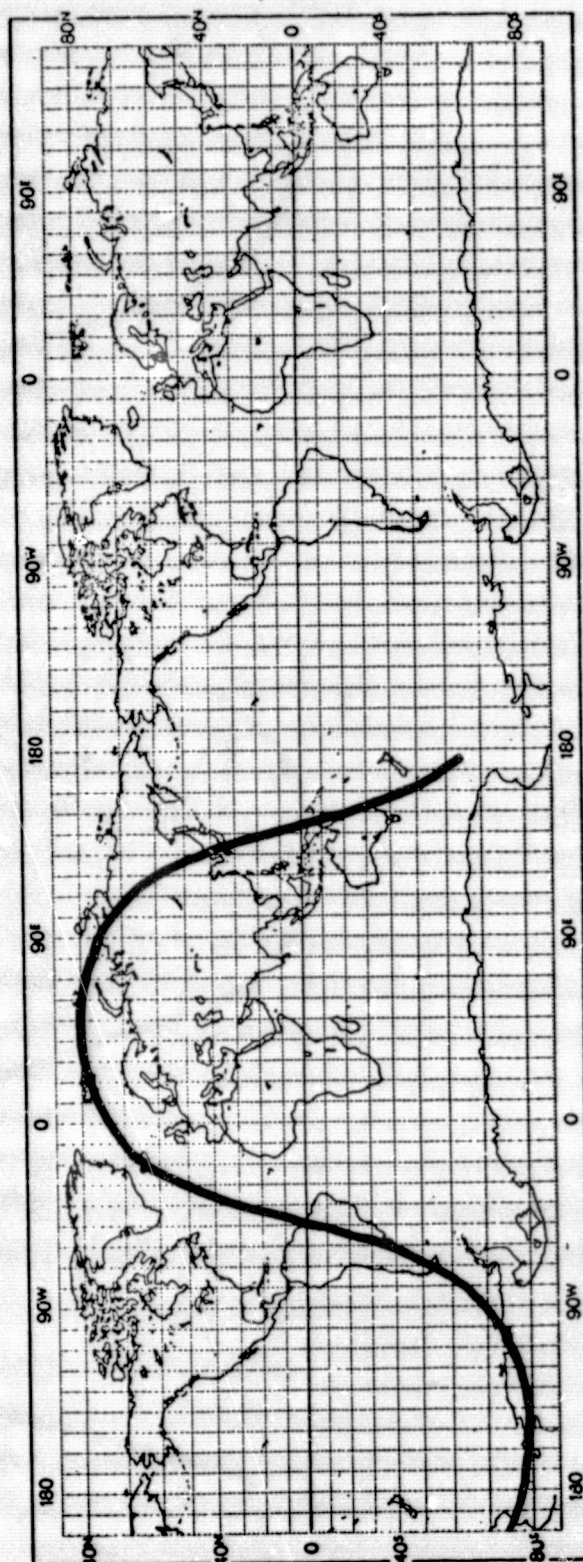
7 February 0233-0434



ORBITS 3229R

8 February 0157-0351

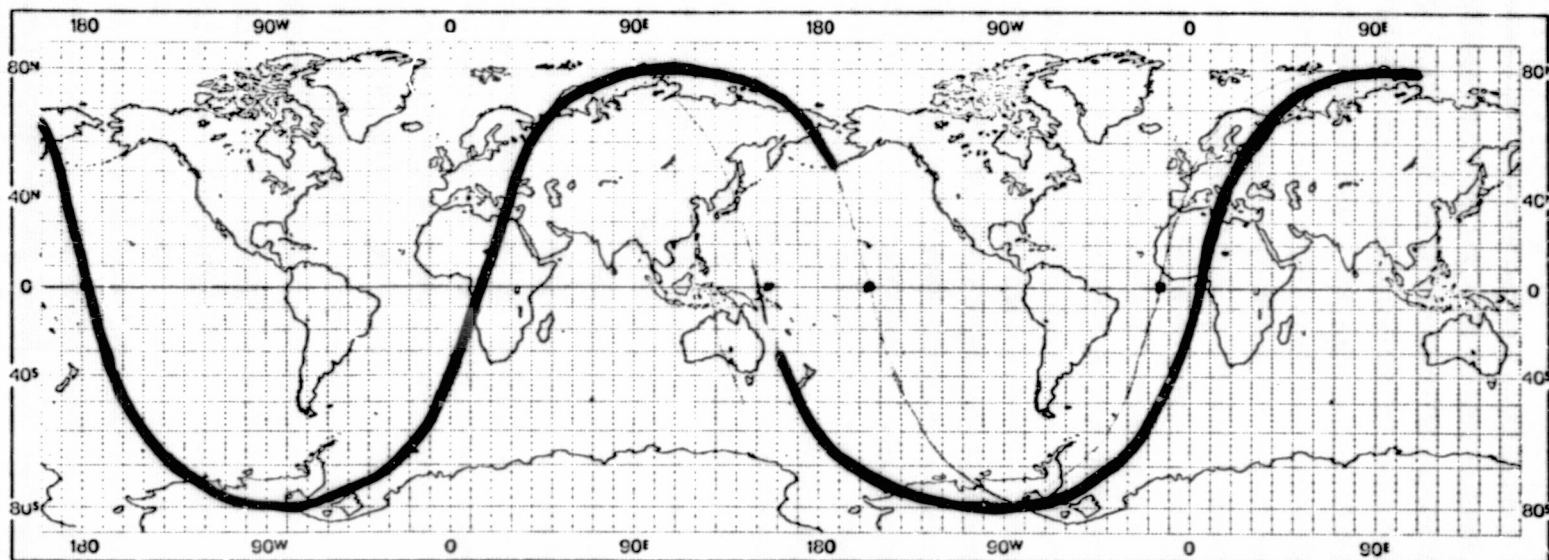
ORIGINAL PAGE IS  
OF POOR QUALITY





ORBITS 3239A  
32400

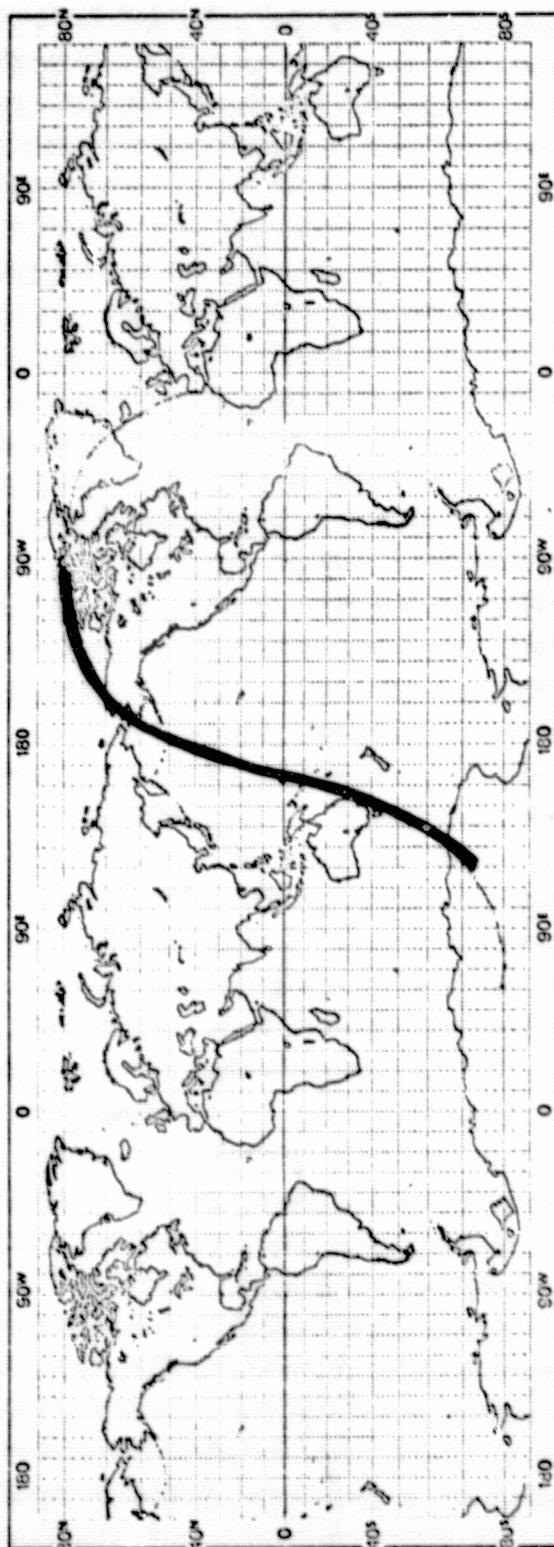
February 8 2213 - February 9 0123



ORBIT 3268A

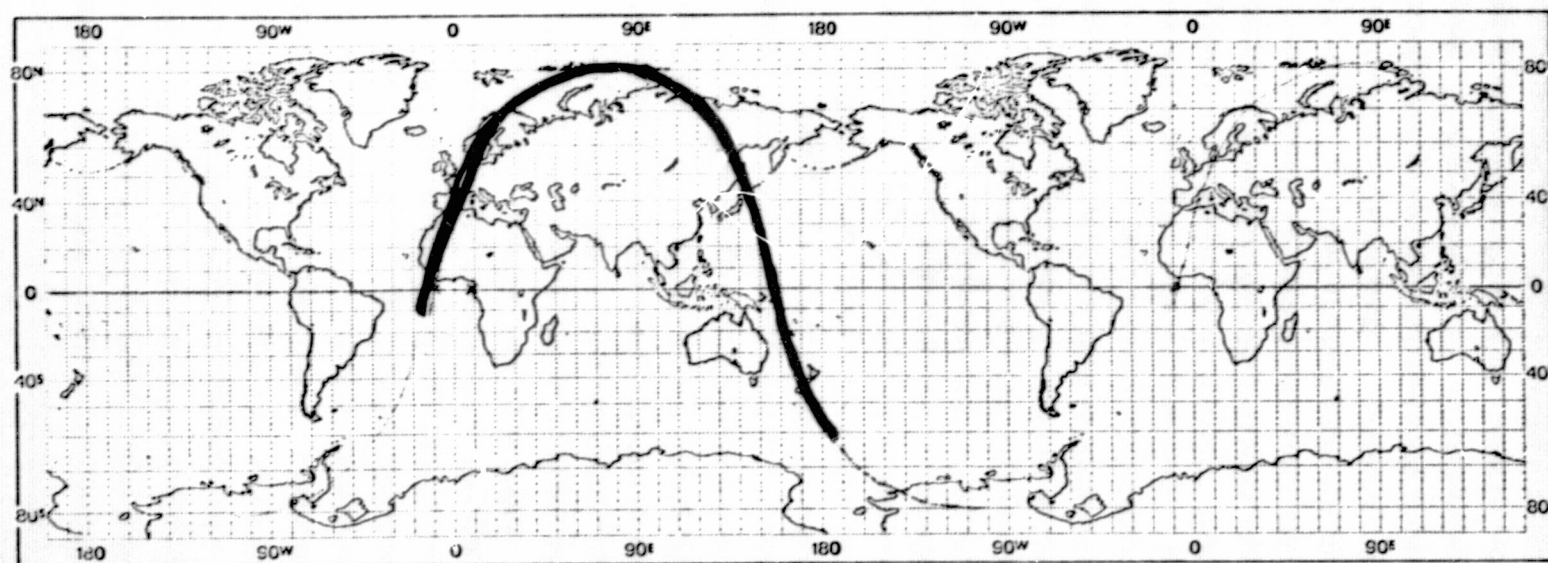
February 10 1202-1257

ORIGINAL PAGE IS  
OF POOR QUALITY



ORBITS 32800  
32810

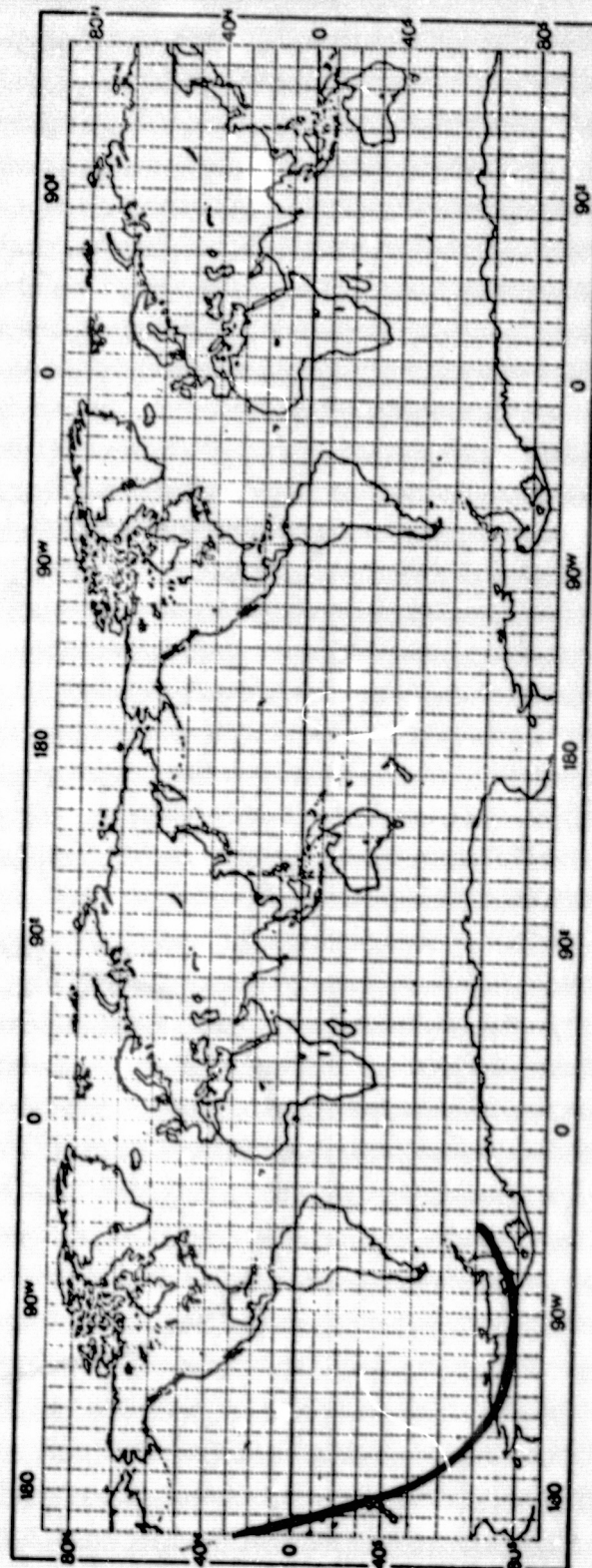
February 12 0015-0052





ORBITS 3293A  
3294O

February 12 2359 - February 13 0044

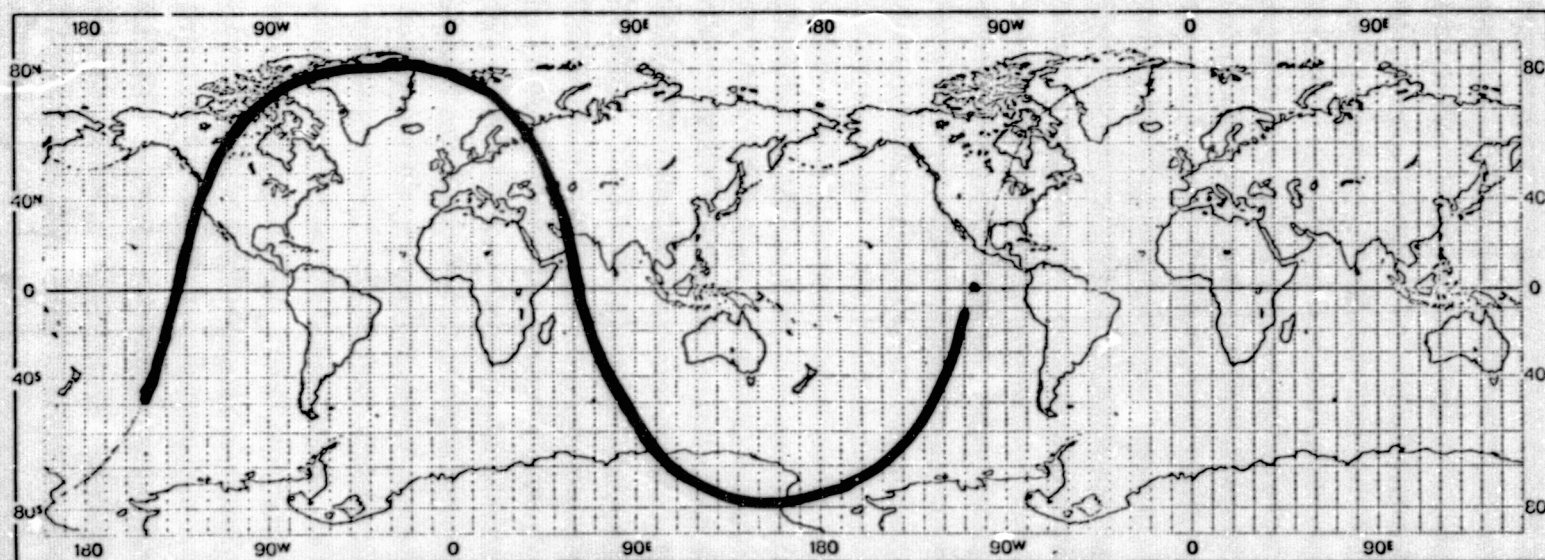


ORIGINAL PAGE IS  
OF POOR QUALITY



ORBITS 3297R  
3298A

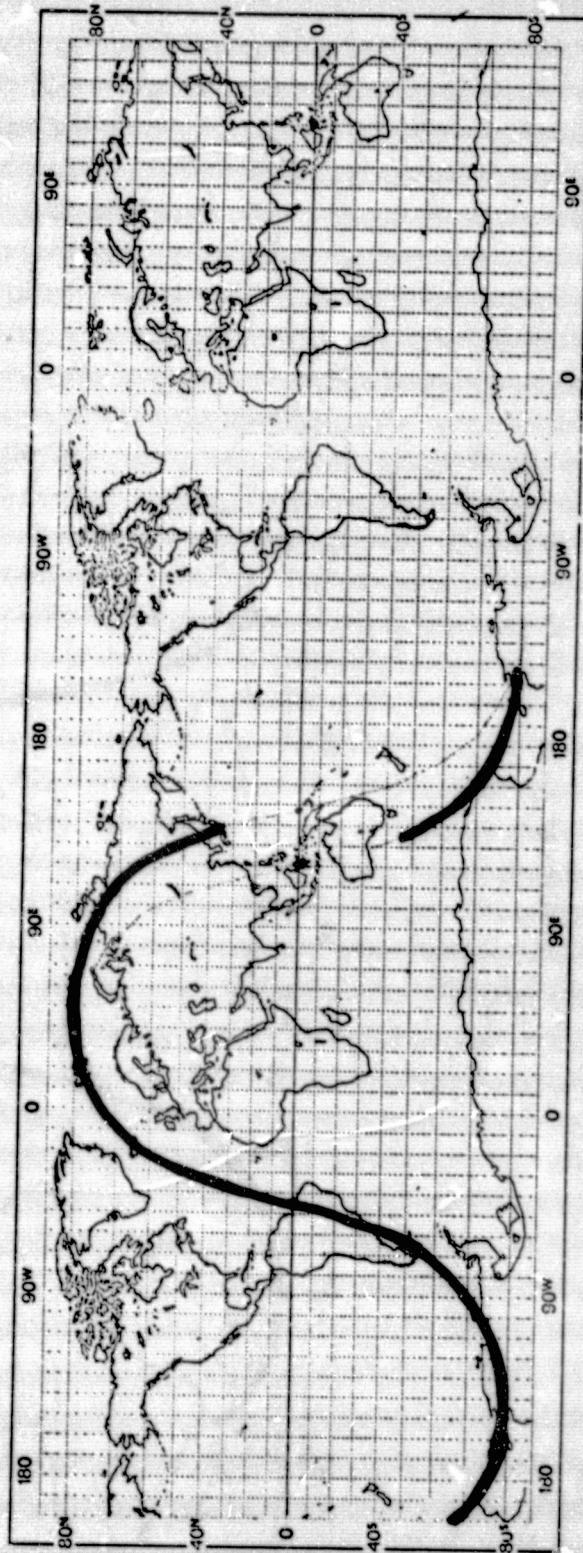
February 13 0646-0817



ORIGINAL PAGE IS  
OF POOR QUALITY

ORBITS 33350  
3336R

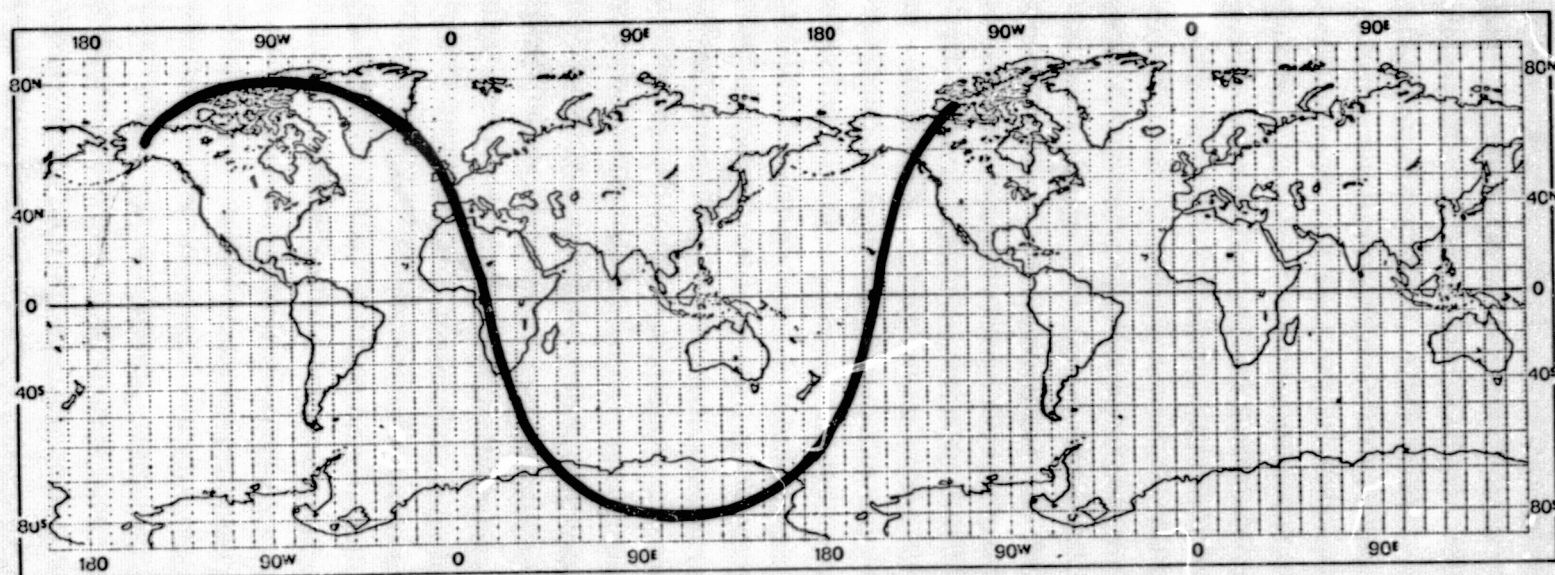
February 16 0270-0328





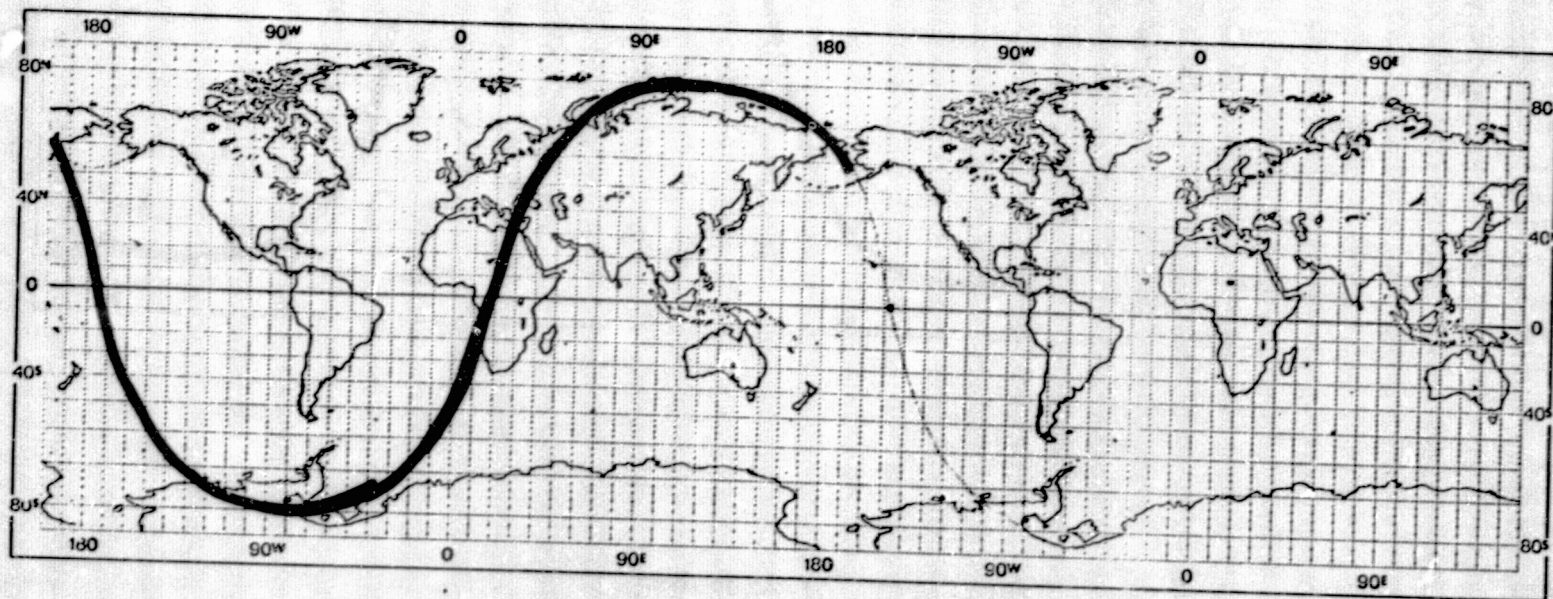
ORBITS 3339A  
3340A

February 16 0937-1128



ORBITS 3346A  
3347A

February 16 2155-2343

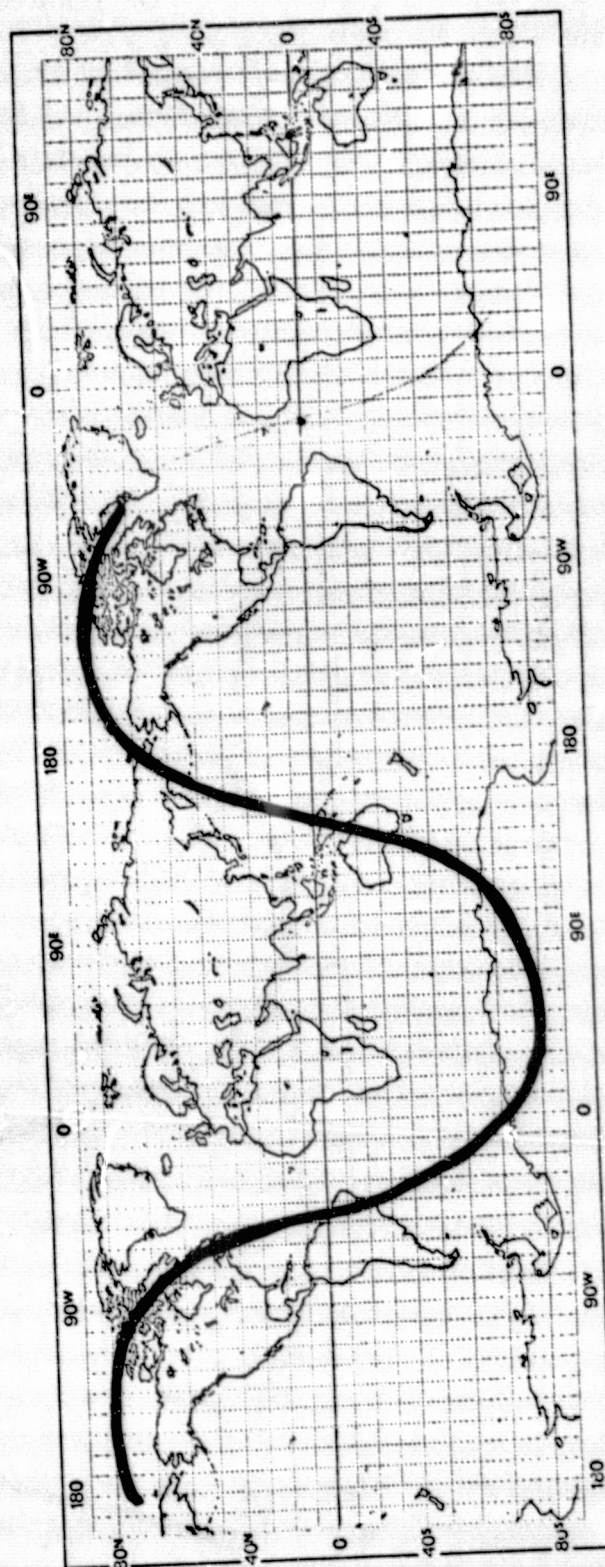


ORIGINAL PAGE IS  
OF POOR QUALITY



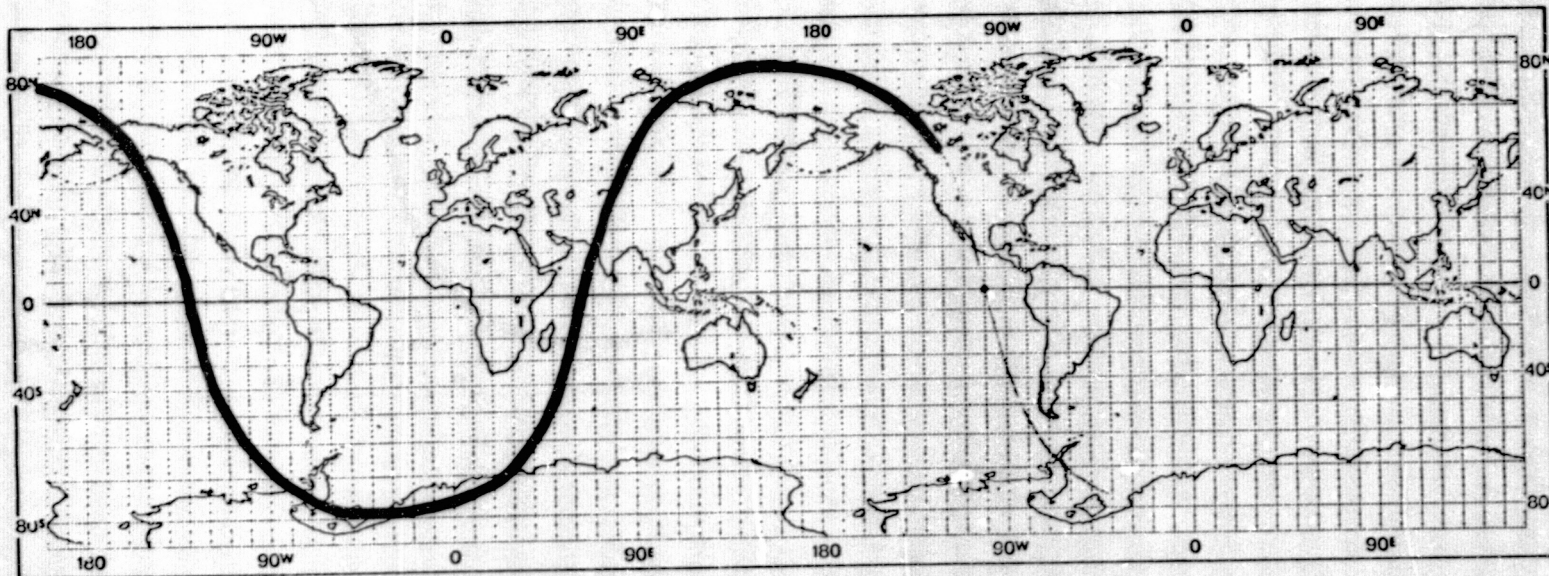
ORBITS 3368A  
3369A

February 18 1329-1521



ORBITS 3371A  
3372A

February 18 1844-2042

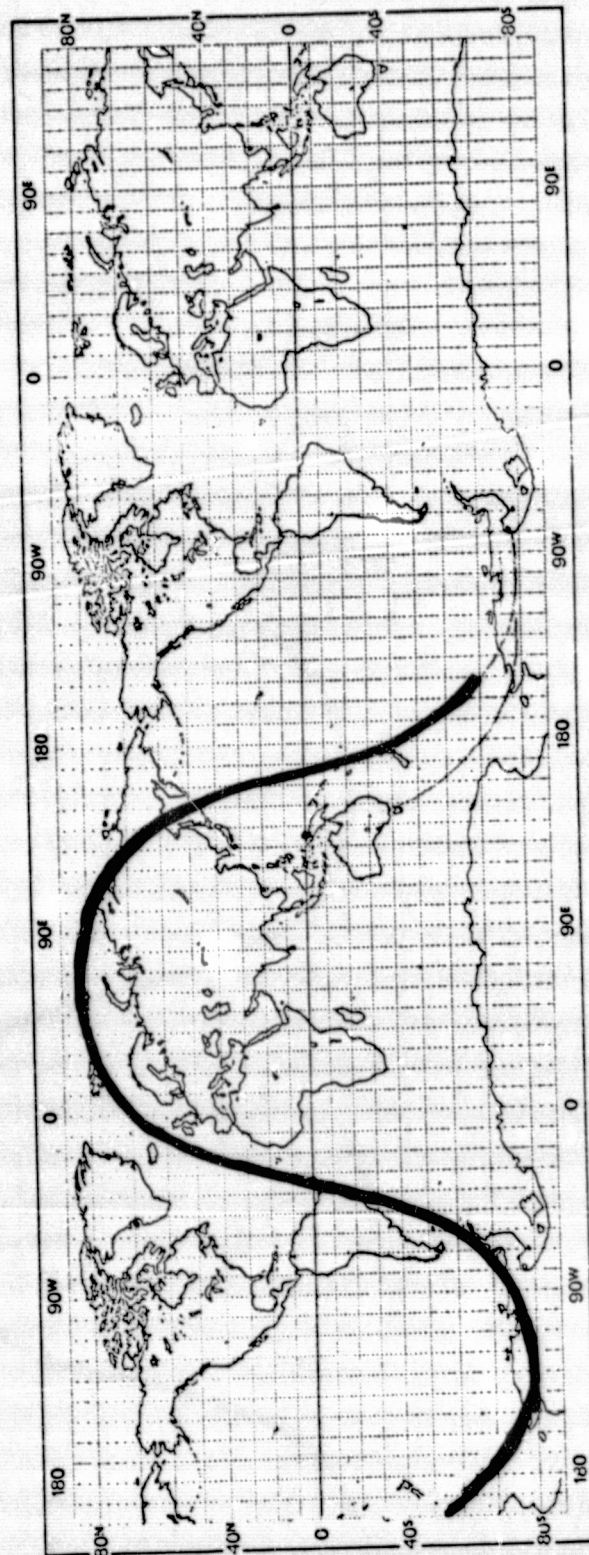


ORIGINAL PAGE IS  
OF POOR QUALITY



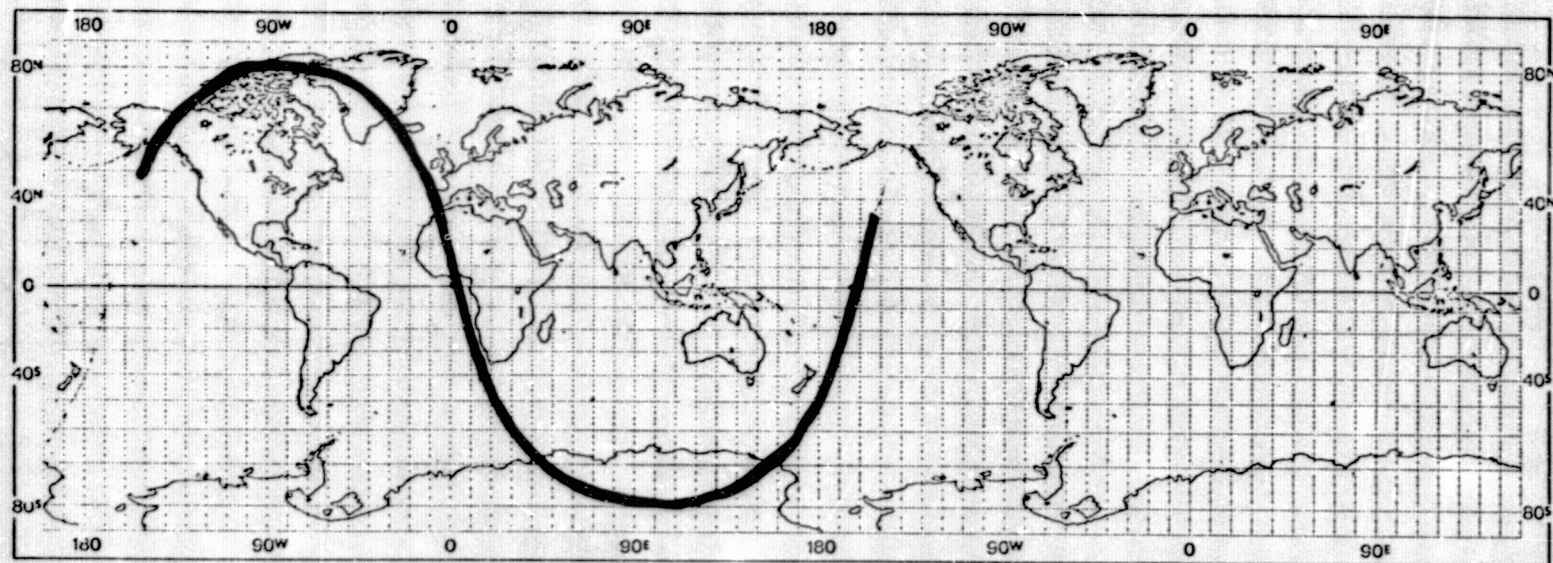
ORBITS 33880  
3390R

February 20 0023-0230



ORBITS 3393A  
3394A

February 20 1023-1215

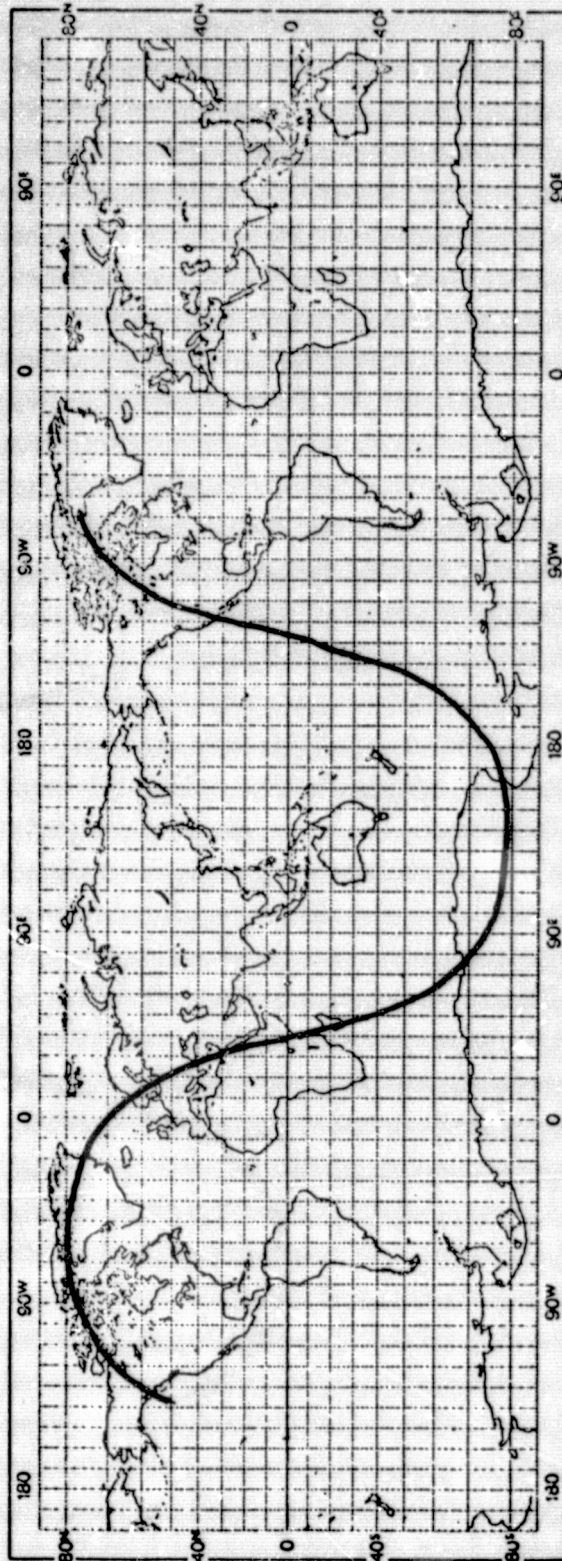


ORIGINAL PAGE IS  
OF POOR QUALITY



ORBITS 3405  
3406

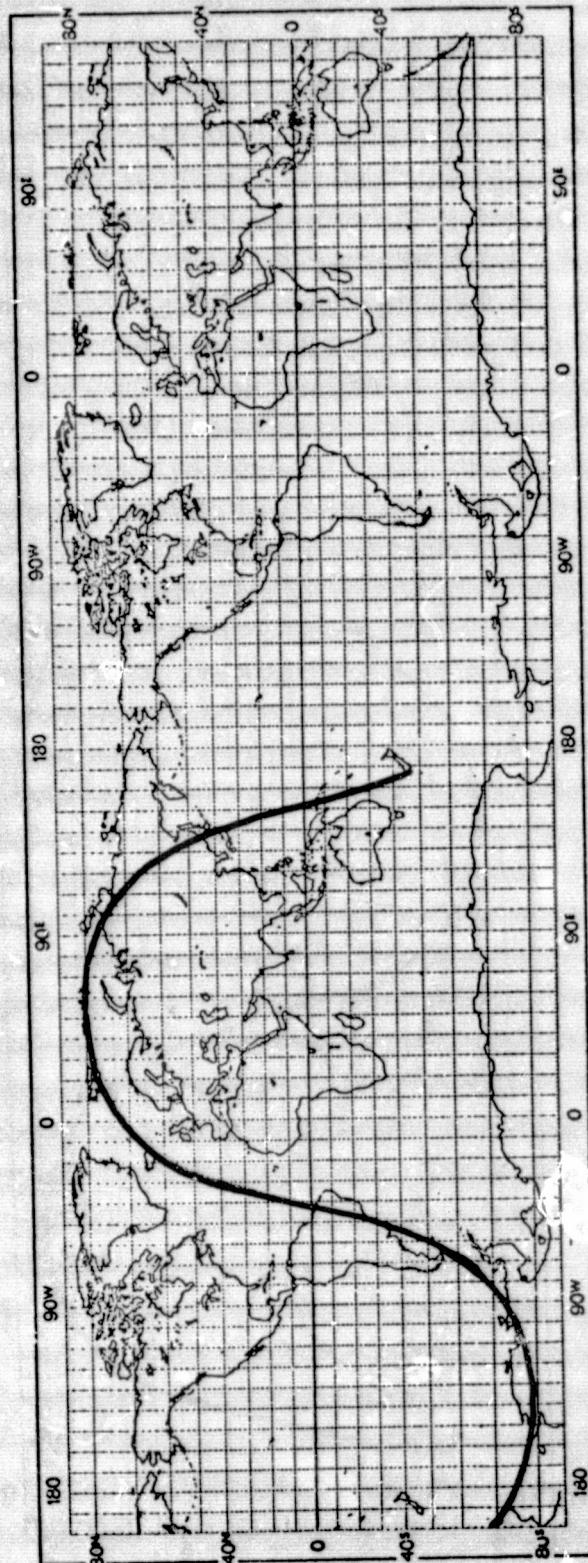
February 21 0752-0946



ORIGINAL PAGE IS  
OF POOR QUALITY

ORBITS 3442  
3443

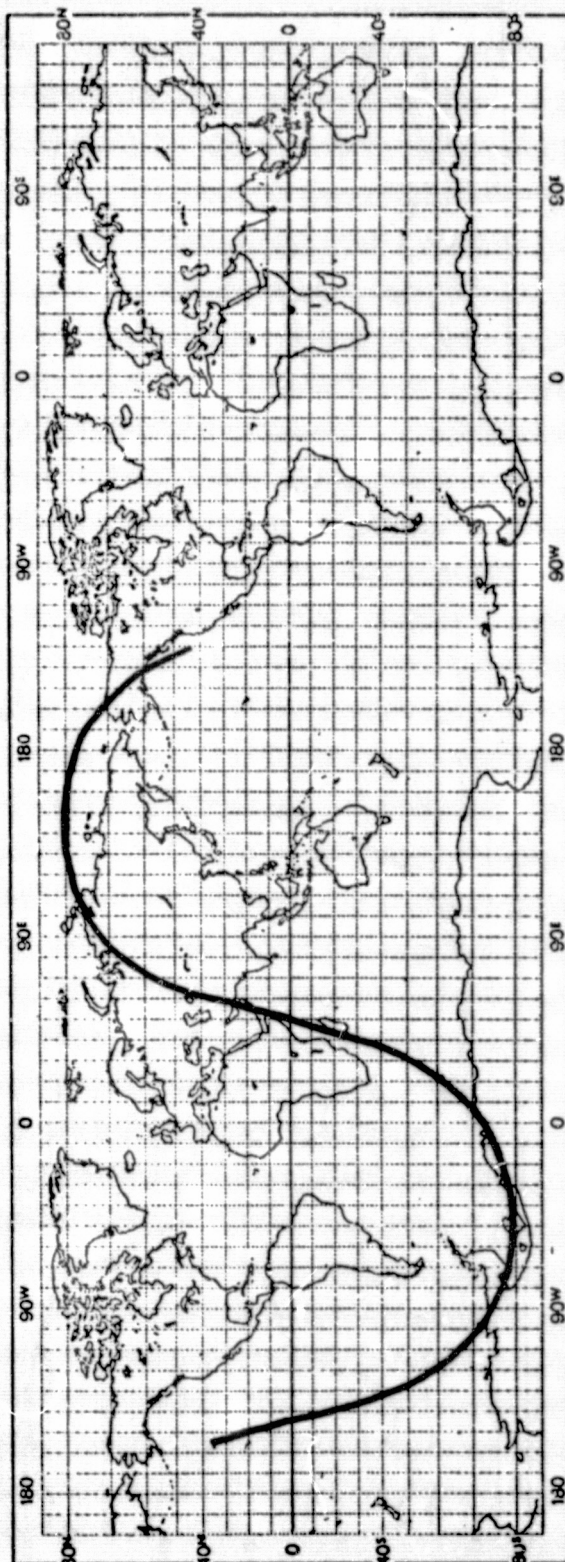
February 24 0118-0310





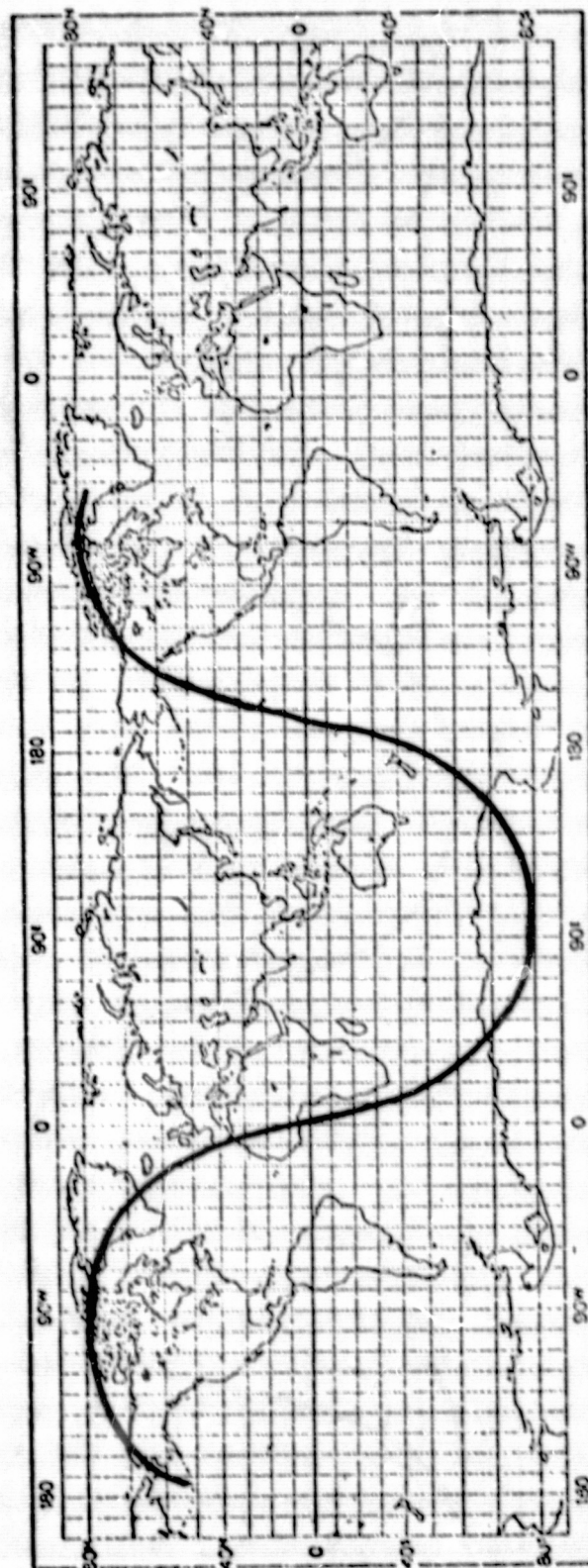
ORBITS 3452  
3453

February 24 1946-2031



ORBITS 3460  
3461

February 25 1021-1271

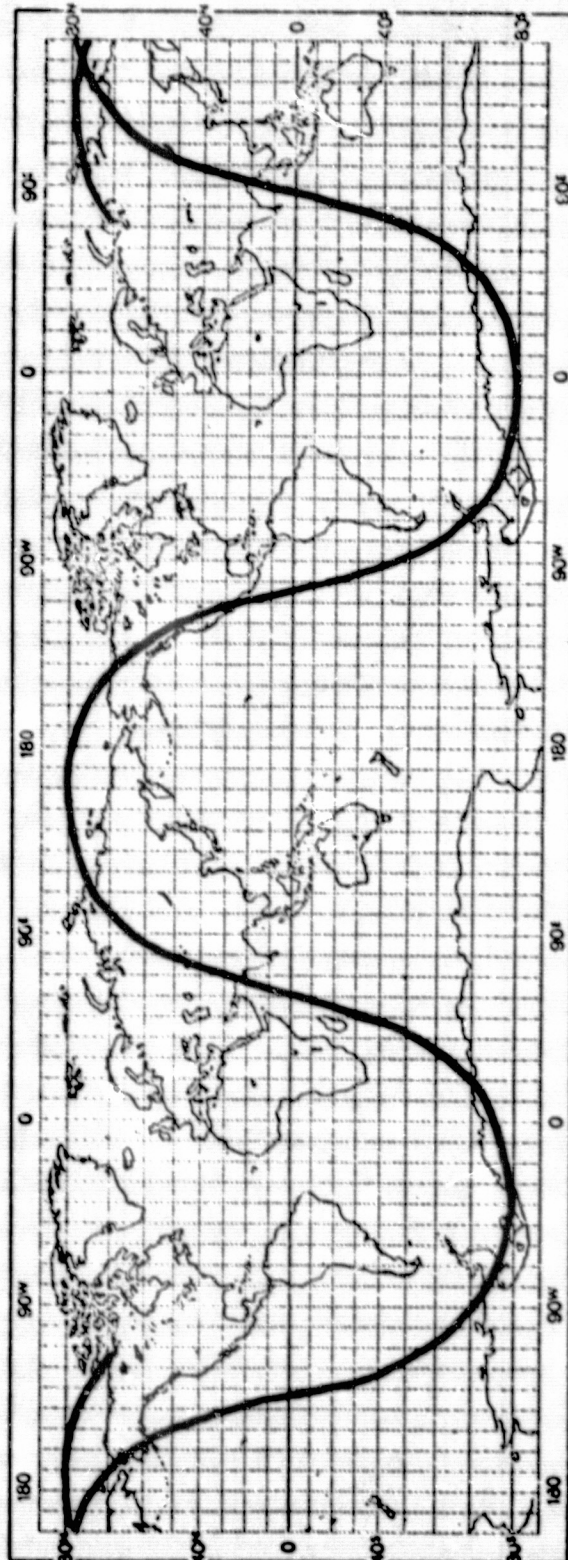


ORIGINAL PAGE IS  
OF POOR QUALITY



ORBITS 3464  
3465  
3466

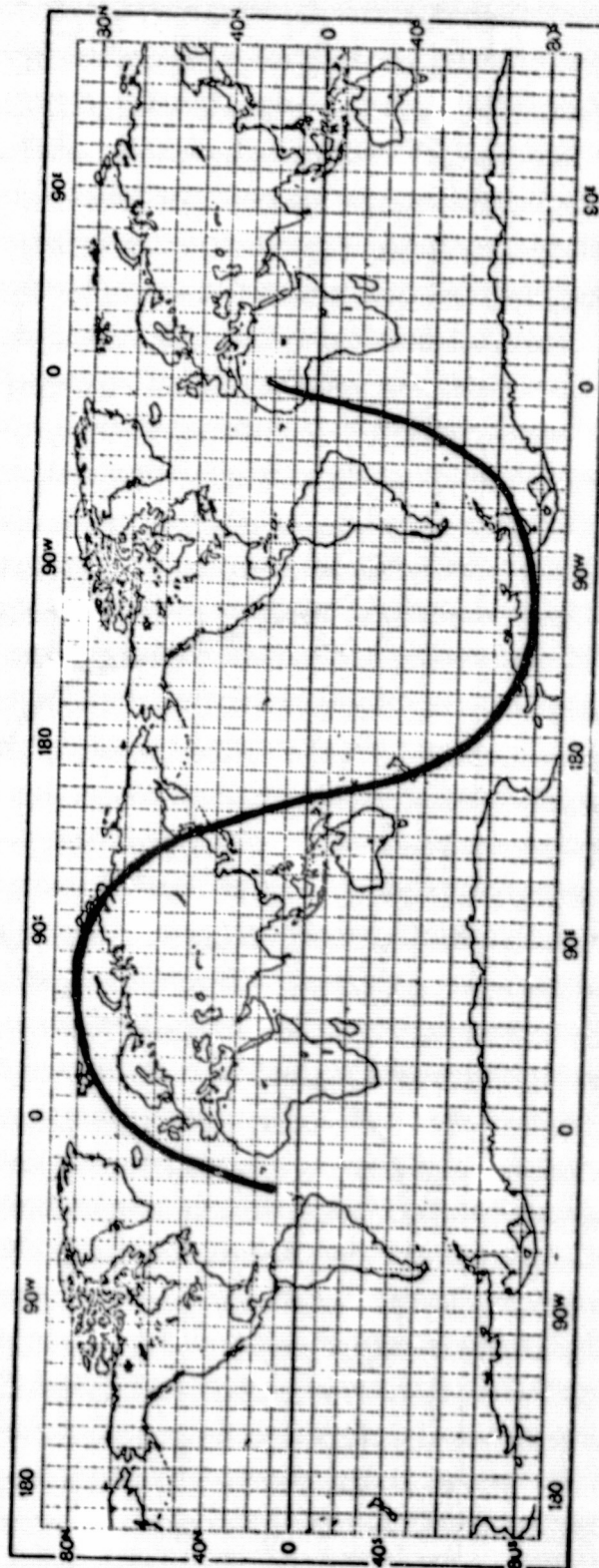
February 25 1723-2103



ORIGINAL PAGE IS  
OF POOR QUALITY

ORBITS 3481  
3482

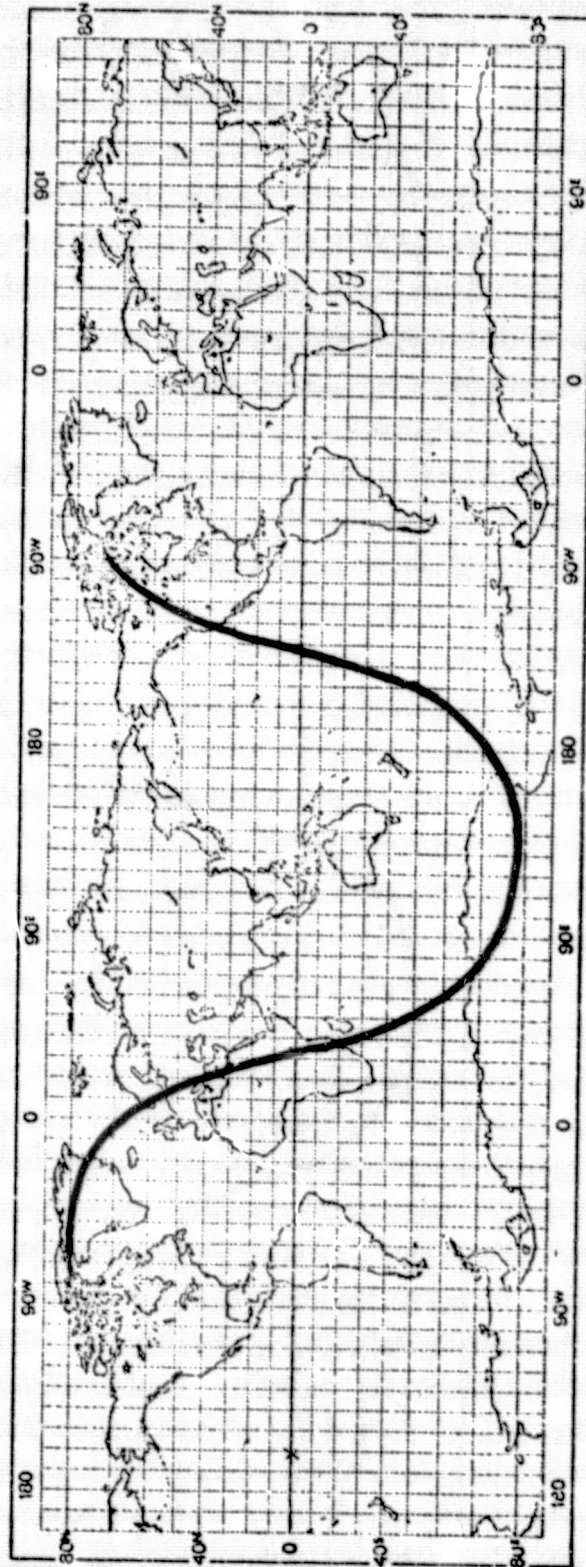
February 26-27 2346-0207





ORBITS 3499  
3500

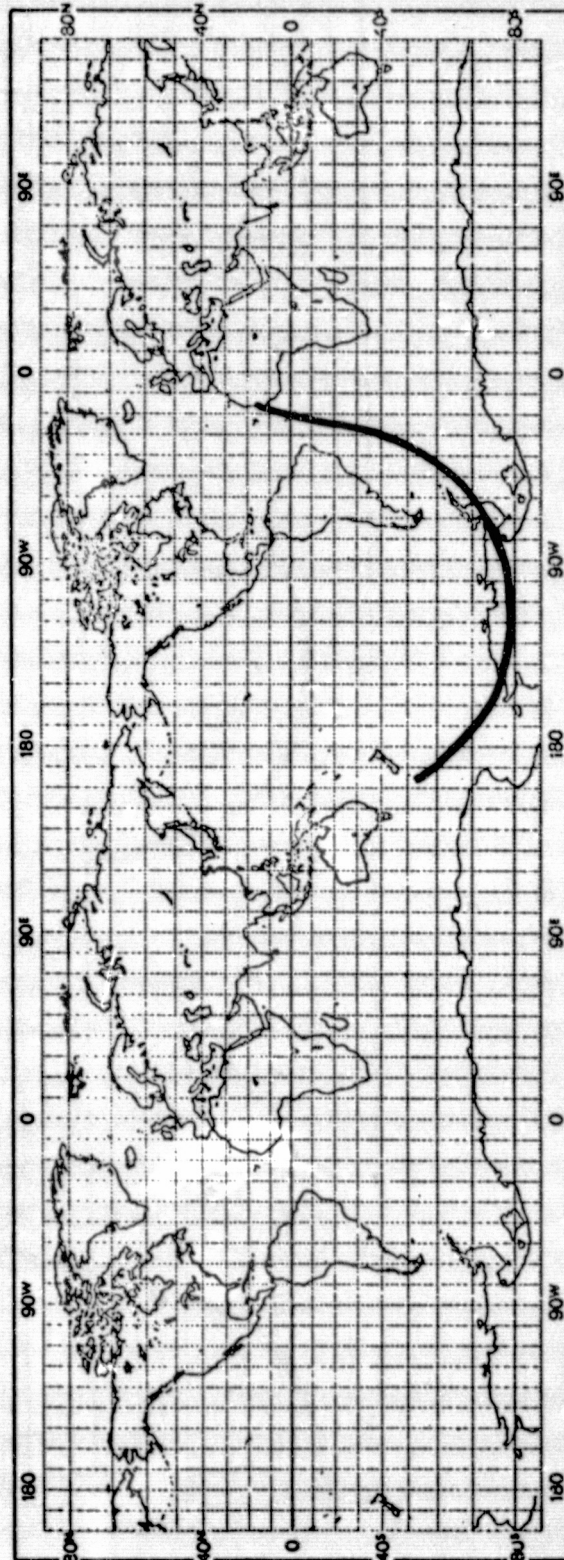
February 28 0816-1002



ORIGINAL PAGE IS  
OF POOR QUALITY

ORBIT 3502

February 28 1302-1345





ORBITS 3504  
3505  
February 28 1703-1858

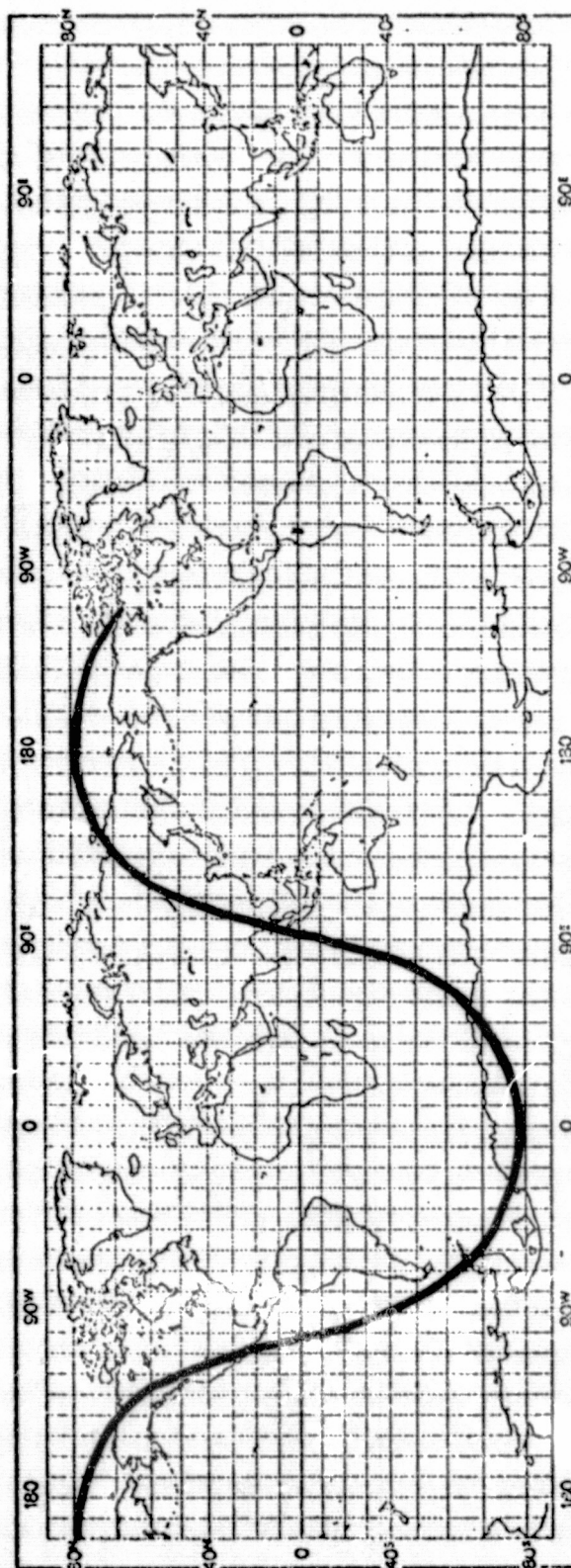


Table 1A. Missing NIMBUS DST-6 Temperature Data by Date/Time

LENGTH OF GAP (HOURS)	TAU	DATE	TIME
6.30	28538.24 28544.54	76/ 1/31 76/ 1/31	2.14.17 8.32.20
1.99	28547.98 28549.57	76/ 1/31 76/ 1/31	11.58.35 13.58.7
1.79	28591.15 28592.94	76/ 2/ 2 76/ 2/ 2	7. 8.54 8.56.15
1.89	28598.11 28600.00	76/ 2/ 2 76/ 2/ 2	14. 6.33 15.59.45
0.58	28611.71 28612.69	76/ 2/ 3 76/ 2/ 3	3.42.25 4.41.15
0.55	28651.76 28652.31	76/ 2/ 4 76/ 2/ 4	19.45.28 20.18.30
1.49	28677.07 28678.56	76/ 2/ 5 76/ 2/ 5	21. 3.59 22.33.30
1.33	28684.35 28685.72	76/ 2/ 6 76/ 2/ 6	4.23.12 5.43.7
3.05	28701.70 28704.75	76/ 2/ 6 76/ 2/ 7	21.41.57 0.44.45
2.02	28706.56 28708.55	76/ 2/ 7 76/ 2/ 7	2.33.30 4.34.41
1.90	28729.50 28731.86	76/ 2/ 8 76/ 2/ 8	1.57.25 3.51.33
3.17	28750.23 28753.40	76/ 2/ 8 76/ 2/ 9	22.13.35 1.23.54
0.91	28788.05 28788.96	76/ 2/10 76/ 2/10	12. 2.48 12.57.25
0.62	28824.26 28824.88	76/ 2/12 76/ 2/12	0.15.28 0.52.44
0.75	28847.99 28848.74	76/ 2/12 76/ 2/13	23.59.17 0.44.17
1.51	28854.78 28856.29	76/ 2/13 76/ 2/13	6.46.38 8.17.20

A-31

ORIGINAL PAGE IS  
OF POOR QUALITY

Table 1A. (Concluded)

LENGTH OF GAP(HOURS)	TAU	DATE	TIME
1.34	28922.13 28923.47	76/ 2/16 76/ 2/16	2. 7.44 3.28. 7
1.25	28929.63 28931.48	76/ 2/16 76/ 2/16	9.37.44 11.28.35
1.81	28941.92 28943.73	76/ 2/16 76/ 2/16	21.55. 4 23.43.35
1.81	28981.50 28983.37	76/ 2/18 76/ 2/18	13.29.45 15.22. 1
1.96	28986.75 28988.71	76/ 2/18 76/ 2/18	18.44.45 20.42.25
2.16	29016.40 29018.56	76/ 2/20 76/ 2/20	0.23.54 2.33.30
1.87	29026.38 29028.25	76/ 2/20 76/ 2/20	10.22.44 12.14.45
1.76	29216.28 29218.04	76/ 2/28 76/ 2/28	8.16.38 10. 2.20
0.72	29221.04 29221.76	76/ 2/28 76/ 2/28	13. 2.20 13.45.28
1.91	29225.06 29226.97	76/ 2/28 76/ 2/28	17. 3.30 18.58. 7
1.86	29264.67 29266.55	76/ 3/ 1 76/ 3/ 1	8.40. 4 10.32.48
1.81	29295.02 29296.55	76/ 3/ 2 76/ 3/ 2	15. 1.10 16.50.51

Table 1A. (Concluded)

LENGTH OF GAP(HOURS)	TAU	DATE	TIME
1.34	28922.13 28923.47	76/ 2/16 76/ 2/16	2. 7.44 3.28. 7
1.85	28929.63 28931.48	76/ 2/16 76/ 2/16	9.37.44 11.28.35
1.81	28941.92 28943.73	76/ 2/16 76/ 2/16	21.55. 4 23.43.35
1.81	28981.50 28983.37	76/ 2/18 76/ 2/18	13.29.45 15.22. 1
1.96	28986.75 28988.71	76/ 2/18 76/ 2/18	18.44.45 20.42.25
2.10	29016.40 29018.56	76/ 2/20 76/ 2/20	0.23.54 2.33.30
1.87	29026.38 29028.25	76/ 2/20 76/ 2/20	10.22.44 12.14.45
1.76	29216.28 29218.04	76/ 2/28 76/ 2/28	8.16.38 10. 2.20
0.72	29221.04 29221.76	76/ 2/28 76/ 2/28	13. 2.20 13.45.28
1.91	29225.06 29226.97	76/ 2/28 76/ 2/28	17. 3.30 18.58. 7
1.86	29264.67 29266.55	76/ 3/ 1 76/ 3/ 1	8.40. 4 10.32.46
1.83	29295.02 29296.15	76/ 3/ 2 76/ 3/ 2	15. 1.10 16.50.51

Table 2A. DST-6 Retrieved Profile Count  
by Date and Bin Number

ORIGINAL PAGE IS  
OF POOR QUALITY

1/31/76--0	(28536)	NIMB06*1	1079 STATIONS--	250366 BYTES
1/31/76--6	(28542)	NIMB06*1	166 STATIONS--	38550 BYTES
1/31/76--12	(28548)	NIMB06*1	1018 STATIONS--	236214 BYTES
1/31/76--18	(28554)	NIMB06*1	1541 STATIONS--	357550 BYTES
2/ 1/76--0	(28560)	NIMB06*1	1227 STATIONS--	284702 BYTES
2/ 1/76--6	(28566)	NIMB06*1	1452 STATIONS--	336902 BYTES
2/ 1/76--12	(28572)	NIMB06*1	1513 STATIONS--	351054 BYTES
2/ 1/76--18	(28578)	NIMB06*1	1563 STATIONS--	362654 BYTES
2/ 2/76--0	(28584)	NIMB06*1	1382 STATIONS--	320662 BYTES
2/ 2/76--6	(28590)	NIMB06*1	1141 STATIONS--	264750 BYTES
2/ 2/76--12	(28596)	NIMB06*1	1379 STATIONS--	319966 BYTES
2/ 2/76--18	(28602)	NIMB06*1	1318 STATIONS--	305814 BYTES
2/ 3/76--0	(28608)	NIMB06*1	1221 STATIONS--	283310 BYTES
2/ 3/76--6	(28614)	NIMB06*1	1252 STATIONS--	290502 BYTES
2/ 3/76--12	(28620)	NIMB06*1	1613 STATIONS--	374254 BYTES
2/ 3/76--18	(28626)	NIMB06*1	1415 STATIONS--	325318 BYTES
2/ 4/76--0	(28632)	NIMB06*1	1036 STATIONS--	240390 BYTES
2/ 4/76--6	(28638)	NIMB06*1	1582 STATIONS--	367062 BYTES
2/ 4/76--12	(28644)	NIMB06*1	1410 STATIONS--	327158 BYTES
2/ 4/76--18	(28650)	NIMB06*1	1497 STATIONS--	347342 BYTES
2/ 5/76--0	(28656)	NIMB06*1	1226 STATIONS--	284470 BYTES
2/ 5/76--6	(28662)	NIMB06*1	1616 STATIONS--	374950 BYTES
2/ 5/76--12	(28668)	NIMB06*1	1489 STATIONS--	345486 BYTES
2/ 5/76--18	(28674)	NIMB06*1	1541 STATIONS--	357550 BYTES
2/ 6/76--0	(28680)	NIMB06*1	1038 STATIONS--	240354 BYTES
2/ 6/76--6	(28686)	NIMB06*1	1098 STATIONS--	254774 BYTES
2/ 6/76--12	(28692)	NIMB06*1	1465 STATIONS--	339918 BYTES
2/ 6/76--18	(28698)	NIMB06*1	1545 STATIONS--	358478 BYTES
2/ 7/76--0	(28704)	NIMB06*1	524 STATIONS--	121606 BYTES
2/ 7/76--6	(28710)	NIMB06*1	1157 STATIONS--	268462 BYTES
2/ 7/76--12	(28716)	NIMB06*1	1522 STATIONS--	353142 BYTES
2/ 7/76--18	(28722)	NIMB06*1	1594 STATIONS--	369846 BYTES
2/ 8/76--0	(28728)	NIMB06*1	1337 STATIONS--	310222 BYTES
2/ 8/76--6	(28734)	NIMB06*1	1226 STATIONS--	284470 BYTES
2/ 8/76--12	(28740)	NIMB06*1	1532 STATIONS--	355462 BYTES
2/ 8/76--18	(28746)	NIMB06*1	1486 STATIONS--	344790 BYTES
2/ 9/76--0	(28752)	NIMB06*1	661 STATIONS--	153390 BYTES
2/ 9/76--6	(28758)	NIMB06*1	1539 STATIONS--	357066 BYTES
2/ 9/76--12	(28764)	NIMB06*1	1506 STATIONS--	349430 BYTES
2/ 9/76--18	(28770)	NIMB06*1	1555 STATIONS--	361726 BYTES
2/ 10/76--0	(28776)	NIMB06*1	1532 STATIONS--	355462 BYTES
2/ 10/76--6	(28782)	NIMB06*1	1326 STATIONS--	308134 BYTES
2/ 10/76--12	(28788)	NIMB06*1	1624 STATIONS--	376806 BYTES
2/ 10/76--18	(28794)	NIMB06*1	1536 STATIONS--	356390 BYTES
2/ 11/76--0	(28800)	NIMB06*1	1517 STATIONS--	351982 BYTES
2/ 11/76--6	(28806)	NIMB06*1	1507 STATIONS--	349662 BYTES
2/ 11/76--12	(28812)	NIMB06*1	1523 STATIONS--	353374 BYTES
2/ 11/76--18	(28818)	NIMB06*1	1544 STATIONS--	358246 BYTES
2/ 12/76--0	(28824)	NIMB06*1	1540 STATIONS--	357318 BYTES
2/ 12/76--6	(28830)	NIMB06*1	1522 STATIONS--	353142 BYTES
2/ 12/76--12	(28836)	NIMB06*1	1495 STATIONS--	346878 BYTES
2/ 12/76--18	(28842)	NIMB06*1	1553 STATIONS--	360334 BYTES
2/ 13/76--0	(28848)	NIMB06*1	1347 STATIONS--	312542 BYTES
2/ 13/76--6	(28854)	NIMB06*1	1215 STATIONS--	281918 BYTES
2/ 13/76--12	(28860)	NIMB06*1	1534 STATIONS--	355926 BYTES
2/ 13/76--18	(28866)	NIMB06*1	1422 STATIONS--	329942 BYTES
2/ 14/76--0	(28872)	NIMB06*1	1193 STATIONS--	276814 BYTES
2/ 14/76--6	(28878)	NIMB06*1	1145 STATIONS--	265678 BYTES
2/ 14/76--12	(28884)	NIMB06*1	1202 STATIONS--	278902 BYTES
2/ 14/76--18	(28890)	NIMB06*1	1568 STATIONS--	363814 BYTES
2/ 15/76--0	(28896)	NIMB06*1	1377 STATIONS--	319502 BYTES
2/ 15/76--6	(28902)	NIMB06*1	1455 STATIONS--	346878 BYTES
2/ 15/76--12	(28908)	NIMB06*1	1469 STATIONS--	345486 BYTES
2/ 15/76--18	(28914)	NIMB06*1	1566 STATIONS--	363814 BYTES



Table 2A. (Concluded)

2/16/76--	0 (28920)	NIMB06*1	922 STATIONS--	213942 BYTES
2/16/76--	6 (28926)	NIMB06*1	1477 STATIONS--	342702 BYTES
2/16/76--	12 (28932)	NIMB06*1	817 STATIONS--	189582 BYTES
2/16/76--	18 (28938)	NIMB06*1	1597 STATIONS--	370542 BYTES
2/17/76--	0 (28944)	NIMB06*1	974 STATIONS--	226006 BYTES
2/17/76--	6 (28950)	NIMB06*1	1438 STATIONS--	333654 BYTES
2/17/76--	12 (28956)	NIMB06*1	1517 STATIONS--	351982 BYTES
2/17/76--	18 (28962)	NIMB06*1	1622 STATIONS--	376342 BYTES
2/18/76--	0 (28968)	NIMB06*1	1251 STATIONS--	290270 BYTES
2/18/76--	6 (28974)	NIMB06*1	1469 STATIONS--	340846 BYTES
2/18/76--	12 (28980)	NIMB06*1	972 STATIONS--	225542 BYTES
2/18/76--	18 (28986)	NIMB06*1	965 STATIONS--	224150 BYTES
2/19/76--	0 (28992)	NIMB06*1	1275 STATIONS--	295238 BYTES
2/19/76--	6 (28998)	NIMB06*1	1577 STATIONS--	365902 BYTES
2/19/76--	12 (29004)	NIMB06*1	1458 STATIONS--	338294 BYTES
2/19/76--	18 (29010)	NIMB06*1	1613 STATIONS--	374254 BYTES
2/20/76--	0 (29016)	NIMB06*1	993 STATIONS--	230414 BYTES
2/20/76--	6 (29022)	NIMB06*1	1361 STATIONS--	315790 BYTES
2/20/76--	12 (29028)	NIMB06*1	1059 STATIONS--	245720 BYTES
2/20/76--	18 (29034)	NIMB06*1	1690 STATIONS--	392118 BYTES
2/21/76--	0 (29040)	NIMB06*1	595 STATIONS--	138078 BYTES
2/21/76--	6 (29046)	NIMB06*1	1214 STATIONS--	281686 BYTES
2/21/76--	12 (29052)	NIMB06*1	1277 STATIONS--	296302 BYTES
2/21/76--	18 (29058)	NIMB06*1	1642 STATIONS--	380582 BYTES
2/22/76--	0 (29064)	NIMB06*1	1504 STATIONS--	348966 BYTES
2/22/76--	6 (29070)	NIMB06*1	1642 STATIONS--	380582 BYTES
2/22/76--	12 (29076)	NIMB06*1	1614 STATIONS--	374466 BYTES
2/22/76--	18 (29082)	NIMB06*1	1574 STATIONS--	355206 BYTES
2/23/76--	0 (29088)	NIMB06*1	1556 STATIONS--	367590 BYTES
2/23/76--	6 (29094)	NIMB06*1	1665 STATIONS--	386318 BYTES
2/23/76--	12 (29100)	NIMB06*1	1560 STATIONS--	361958 BYTES
2/23/76--	18 (29106)	NIMB06*1	1550 STATIONS--	359638 BYTES
2/24/76--	0 (29112)	NIMB06*1	1188 STATIONS--	275684 BYTES
2/24/76--	6 (29118)	NIMB06*1	1478 STATIONS--	342934 BYTES
2/24/76--	12 (29124)	NIMB06*1	1605 STATIONS--	373326 BYTES
2/24/76--	18 (29130)	NIMB06*1	1441 STATIONS--	334350 BYTES
2/25/76--	0 (29136)	NIMB06*1	1511 STATIONS--	350590 BYTES
2/25/76--	6 (29142)	NIMB06*1	1568 STATIONS--	363814 BYTES
2/25/76--	12 (29148)	NIMB06*1	1100 STATIONS--	255238 BYTES
2/25/76--	18 (29154)	NIMB06*1	666 STATIONS--	154550 BYTES
2/26/76--	0 (29160)	NIMB06*1	1406 STATIONS--	326230 BYTES
2/26/76--	6 (29166)	NIMB06*1	1572 STATIONS--	364742 BYTES
2/26/76--	12 (29172)	NIMB06*1	1611 STATIONS--	373790 BYTES
2/26/76--	18 (29178)	NIMB06*1	1586 STATIONS--	368454 BYTES
2/27/76--	0 (29184)	NIMB06*1	963 STATIONS--	223454 BYTES
2/27/76--	6 (29190)	NIMB06*1	1482 STATIONS--	343662 BYTES
2/27/76--	12 (29196)	NIMB06*1	1555 STATIONS--	370078 BYTES
2/27/76--	18 (29202)	NIMB06*1	1634 STATIONS--	379126 BYTES
2/28/76--	0 (29208)	NIMB06*1	1367 STATIONS--	317182 BYTES
2/28/76--	6 (29214)	NIMB06*1	1333 STATIONS--	309294 BYTES
2/28/76--	12 (29220)	NIMB06*1	851 STATIONS--	197470 BYTES
2/28/76--	18 (29226)	NIMB06*1	1051 STATIONS--	243870 BYTES
2/29/76--	0 (29232)	NIMB06*1	1565 STATIONS--	363118 BYTES
2/29/76--	6 (29238)	NIMB06*1	1548 STATIONS--	359174 BYTES
2/29/76--	12 (29244)	NIMB06*1	1234 STATIONS--	286326 BYTES
2/29/76--	18 (29250)	NIMB06*1	1596 STATIONS--	370310 BYTES
3/ 1/76--	0 (29256)	NIMB06*1	1442 STATIONS--	334582 BYTES
3/ 1/76--	6 (29262)	NIMB06*1	1532 STATIONS--	355462 BYTES
3/ 1/76--	12 (29268)	NIMB06*1	1171 STATIONS--	271710 BYTES
3/ 1/76--	18 (29274)	NIMB06*1	1674 STATIONS--	388406 BYTES
3/ 2/76--	0 (29280)	NIMB06*1	1609 STATIONS--	373326 BYTES
3/ 2/76--	6 (29286)	NIMB06*1	1535 STATIONS--	356166 BYTES
3/ 2/76--	12 (29292)	NIMB06*1	1523 STATIONS--	353374 BYTES
3/ 2/76--	18 (29298)	NIMB06*1	1085 STATIONS--	252454 BYTES
3/ 3/76--	0 (29304)	NIMB06*1	1612 STATIONS--	374022 BYTES
3/ 3/76--	6 (29310)	NIMB06*1	1565 STATIONS--	363118 BYTES
3/ 3/76--	12 (29316)	NIMB06*1	1306 STATIONS--	303030 BYTES
3/ 3/76--	18 (29322)	NIMB06*1	1472 STATIONS--	341542 BYTES
3/ 4/76--	0 (29328)	NIMB06*1	1566 STATIONS--	363350 BYTES
3/ 4/76--	6 (29334)	NIMB06*1	1581 STATIONS--	366830 BYTES
3/ 4/76--	12 (29340)	NIMB06*1	1409 STATIONS--	326926 BYTES
3/ 4/76--	18 (29346)	NIMB06*1	1603 STATIONS--	371534 BYTES
3/ 5/76--	0 (29352)	NIMB06*1	1230 STATIONS--	265358 BYTES

### CHAPTER III

### 3. ANALYSIS AND ASSIMILATION

(M. Ghil, Scientist; R. Dilling, Manager)

ORIGINAL PAGE IS  
OF POOR QUALITY

#### 3.1. INTRODUCTION

To achieve the goal of improved 2 to 5 day numerical weather forecasts we need a better knowledge of the state of the atmosphere at the beginning of the forecast -- the initial state. During the 1976 Impact Test Project the main thrust of the work done by the Analysis and Assimilation Group at GISS was the attempt to optimize the use of satellite-derived temperature data in the approximation of initial states.

The GISS approach to satellite-data utilization has been that of assimilating the data continuously into a model integration running from 48 hours before initial forecast time and up to the initial time (Jastrow and Halem, 1973). In the past, the assimilation was done by direct insertion (Bengtsson, 1975, p. 24) of the data at adjacent model grid points. It seemed desirable to try to improve upon this procedure by other techniques that take into account observed data, as well as forecast values, according to certain meteorological criteria of dynamical and statistical nature.

The Analysis and Assimilation Group set out for the Impact Test Project to develop, test and evaluate a number of techniques and apply the more successful ones to DST-5 (Aug.-Sept. 1975) and DST-6 (Jan.-March 1976) data. The techniques considered were:

(a) different variants and improvements of the GISS direct insertion analysis and assimilation scheme, (b) variational methods,



(c) utilization of a filtered equations model for initialization and assimilation purposes, and (d) statistical assimilation methods.

The basic assimilation procedure in all the tests reported herein was essentially time-continuous, four-dimensional assimilation of satellite-derived temperature data into a 48-hour model integration. For instance, in order to obtain the initial state at 00Z February 1, 1976, an integration, or run, of the current GISS model (see Chapter 4: Forecast Model Development) was started at 00Z January 30, from a conventional objective analysis. Then forecast values were modified taking into account the additional information obtained from satellites during the 48 hours till initial forecast time on February 1.

Modifications of grid point values of meteorological variables were made at every model time step during the assimilation run. The modifications were based on the satellite-derived temperature values obtained during the time step in question. The algorithm which yields modified values of grid variables by using observed temperature values constitutes the specific assimilation method or technique. The methods and techniques we studied are in different stages of development and assessment at the writing of this Report.

In the area of changes and improvements in insertion methods previously used at GISS, progress has been made in two directions: (1) development, testing and application of a successive correction method to the analysis of conventional synoptic data,

as well as to the assimilation of satellite-derived temperature data, and (2) development, testing, and evaluation of an automated consistency check of synoptic and asynoptic data.

The development and testing of a variational method are in progress. The method attempts to minimize in a root-mean-square sense the difference between the meteorological variable values inserted into the model and the observed values of these variables, while at the same time forcing the inserted values to satisfy certain smoothness and compatibility constraints derived from model dynamics. The method concentrates on asynoptic data and uses a direct minimization technique.

A partial evaluation of the GISS Filtered Equations Model (FEM) for initialization and assimilation purposes resulted in the assignment of a low priority to the continuation of this effort, and work on this approach has been discontinued.

The statistical methods were easiest to develop within the short time span of the Impact Test Project and proved particularly successful in obtaining consistent forecast improvements from the use of sounding temperatures. This is the first time that such methods have been applied to a truly four-dimensional assimilation procedure using large sets of real data, and we believe that the modest, but statistically significant success of our impact tests is due to a large extent to this assimilation method.

## 3.2 METHODS

### 3.2.1 DIRECT INSERTION METHOD (DIM) (R. Dilling and M. Ghil)

#### 3.2.1.1 INTRODUCTION

A direct insertion method of four-dimensional data assimilation has been used at GISS for a number of years. The method used for conventional synoptic data was described by Russell (1975). Asynoptic data, such as temperature profiles derived from given satellite-measured radiances were first inserted directly into the model: indeed, these profiles were obtained in the past by GISS processing methods at GISS model grid points in the horizontal, and at model sigma levels in the vertical. More recently, temperature profiles derived by different methods at NESS from satellite radiances have been inserted at each model time step using an adaptation of the direct insertion method. This adaptation was also described by Russell (1975).

The purpose of this section is to briefly describe the direct insertion method, the quality control of insertion data, and the results of the method for two winter experiments. The quality control methods described here should be compared with the automated consistency check (ACC) described in Subsection 3.2.2. The DIM experiment results are to be compared with the results of experiments using the successive correction method (SCM, Subsection 3.2.4) and the statistical assimilation method (SAM, Subsection 3.2.7). Such a comparison appears in Subsection 3.3.2.

#### 3.2.1.2 QUALITY CONTROL OF INSERTION DATA

The two numerical experiments we discuss used different quality controls for satellite data. In this section we define

the rejection criteria used for both conventional and satellite data. The basic idea of the quality controls here is to eliminate totally erroneous observations by comparing them with model forecast values; the latter have the advantage of always being "reasonable," even when not entirely correct.

The comparison between model forecast values and observed data is made at observation points. Thus, model data are first interpolated vertically to the mandatory pressure levels and then horizontally to the latitude and longitude of the observation. For each variable  $Q$ , the acceptance test is

$$|Q_{fcst.}^k - Q_{obs.}^k| \leq L_Q^k,$$

where  $L_Q^k$  is the maximum acceptable absolute difference for quantity  $Q$  at mandatory pressure level  $k$ . The quantities subject to quality checks are the horizontal velocity components  $u, v$ , the temperature  $T$ , the relative humidity  $q$ , and the surface pressure  $p_s$ . The standard rejection criteria used for synoptic and asynoptic data are given in Table 1.

Table 1  
Standard Rejection Criteria  $L_Q^k$

Quantity	Synoptic	Asynoptic
$Q_{(k=1,11)}^k$		
$u$	30 m/sec	n.a.
$v$	30 m/sec	n.a.
$T$	7°C	7°C
$q$	0.25	n.a.
$p_s$	20 mb	n.a.

For asynoptic satellite-derived temperature profiles a special set of rejection criteria have been defined and used in one of the two numerical experiments we describe. This set consists of the following tests, all of which must be satisfied for the temperature data at a given location and level to be inserted:

- a. The "weighted profile RMS error" must not exceed 5°C. This weighted RMS error is defined as

$$\frac{\sum_k \frac{1}{(L_T^k)^2} (T_{fcst.}^k - T_{sat.}^k)^2}{\sum_k \frac{1}{(L_T^k)^2}} ;$$

here the sums are over mandatory pressure levels and the weights  $L_T^k$  are given in Table 2. If this criterion is not satisfied, all the temperature data at that location,  $1 \leq k \leq 11$ , are discarded.

Table 2  
Special Satellite-Temperature Rejection Criteria  $L_T^k$

k	Pressure level	$L_T^k$
1	1000 mb	3°C
2	850	3.5°C
3	700	4°C
4	500	4.5°C
5	400	5°C
6	300	5.5°C
7	250	6°C
8	200	6.5°C
9	150	7°C
10	100	7.5°C
11	70	8°C

- b. If test a. is satisfied then each level  $k$  is individually tested for acceptance:

$$|T_{fcst.}^k - T_{sat.}^k| \leq L_T^k$$

- c. Finally, if the time of the satellite observation from which the temperature is derived is within 6 hours after synoptic time (00Z or 12Z), then a weight factor  $F$  is used:

$$F(\tau) = 1, \quad 6 \leq \tau < 12,$$

$$F(\tau) = \frac{\tau}{6}, \quad 0 \leq \tau < 6;$$

here  $\tau$  is the difference expressed in hours between the time of the satellite observation and the closest preceding synoptic time. The difference between the satellite-derived value and the model value is multiplied by the factor  $F$ , and it is this modified correction which is added to the model value; this factor reflects in a crude way the relative confidence in forecast and observation as time elapses from synoptic analysis time.

### 3.2.1.3 DESCRIPTION OF DIM EXPERIMENTS

The two DIM experiments we discuss in this section are denoted by numbers 8186 and 8240. Each numerical experiment assimilated conventional synoptic data using a 12-hour cycle beginning 00Z, Jan. 29, 1976 and ending 03Z Feb. 21, 1976.

In experiment 8240 only NESS-processed NIMBUS temperature data were inserted, whereas in 8186 NESS-processed VTPR, as well as NIMBUS temperature data, were inserted. The quality controls for 8186 were the standard rejection criteria for both synoptic and asynoptic data. For 8240 the standard rejection criteria were used for conventional data, and the special rejection criteria were used

for the satellite data. The forecast model used in the four-dimensional assimilations was the current standard 4° by 5° GISS GCM (see Chapter 4). A geostrophic correction based on satellite-derived temperature data was made to the winds near temperature insertion points (cf. Stone et al., 1973; see also Kistler and McPherson, 1975). The impact tests consisted of studying 11 forecasts from 03Z February n, where n = 1,3,5,7...11. Each forecast from an initial state obtained by four-dimensional assimilation of satellite data was compared with a forecast from a control initial state at the same time; the control, or NOSAT, initial state obtains by a four-dimensional assimilation in which no satellite data are actually inserted.

Table 3

Experiment 8136  
Average Impact over North America

	48 hour		72 hour	
	RMS	Skill Score	RMS	Skill Score
SLP	.21±.40	-1.55±1.86	-.48±.27	-3.96±2.16
Z500	.43±3.54	-1.42±1.28	-3.34±2.96	-.69±1.19

Table 4

Experiment 8240  
Average Impact over North America

	48 hour		72 hour	
	RMS	Skill Score	RMS	Skill Score
SLP	.25±.18	.06±1.12	.27±.32	.76±1.90
Z500	2.46±1.97	.25±.79	-.41±3.41	-.52±.89

### 3.2.1.4 RESULTS OF DIM EXPERIMENTS

RMS errors and S1 skill scores of sea-level pressures (SLP) and of 500 mb geopotential heights (Z500) were calculated at 48 and 72 hours after initial time for each forecast, based on the difference between forecast values and the corresponding values provided by the NMC analysis at the same synoptic times. These error measures were computed for both the control forecasts which were started from NO SAT initial states, and the experimental forecasts 8186 and 8240.

Tables 3 through 6 summarize the impact results for the 11 individual forecasts. Differences  $d_i$ ,  $1 \leq i \leq 11$ , between the error measures (RMS or S1) for the experimental forecasts and the corresponding error measure for the NO SAT forecast with the same initial time were computed. The entries in the tables are the average  $\bar{d}$ ,  $\bar{d} = \sum_1^{11} d_i / 11$ , and the standard deviation  $\sigma$ ,  $\sigma^2 = \sum_1^{11} (d_i - \bar{d})^2 / 11$ , of RMS error differences, and of the S1 skill-score differences over the 11 cases, respectively. They are given in the form  $\bar{d} \pm \sigma$ . We consider a result statistically significant if  $\bar{d} > \sigma$ . Results for verification over North America ( $30^\circ\text{N}$  to  $70^\circ\text{N}$  and  $75^\circ\text{W}$  to  $130^\circ\text{W}$ ) are given in Tables 3 and 4 for run 8186 and run 8240, respectively. Similar results for verification over Europe ( $30^\circ\text{N}$  to  $86^\circ\text{N}$  and  $10^\circ\text{W}$  to  $40^\circ\text{E}$ ) are given in Tables 5 and 6.

A statistically significant ( $\bar{d} \approx 2\sigma$ ) positive impact occurs for experiment 8186 in the S1 score of the 72-hour sea-level pressure over Europe (Table 5), and marginal ( $\bar{d} \approx \sigma$ ) positive impact obtains for the 48-hour skill of sea-level pressure over Europe; even these impacts are not consistent with the results for RMS errors or for the the 500-mb heights. A marginally significant ( $\bar{d} \approx \sigma$ ) positive impact



occurs also in the RMS error of the 500-mb heights at 48 hours over Europe in both experiments (Tables 5 and 6). All other impacts are negative and/or statistically insignificant.

Table 5

Experiment 8186  
Average Impact over Europe

	48 hour		72 hour	
	RMS	Skill Score	RMS	Skill Score
SLP	0.38±.32	1.65±1.31	0.15±.43	2.31±1.37
Z500	3.5±3.23	1.36±1.69	0±3.17	-1.46±1.48

Table 6

Experiment 8240  
Average Impact over Europe

	48 hour		72 hour	
	RMS	Skill Score	RMS	Skill Score
SLP	.25±.19	.28±.53	.39±.23	.66±1.21
Z500	1.46±2.35	.19±.98	1.40±2.68	-.39±.95

The results for experiment 8240 are also summarized in Subsection 3.3.2.3.

### 3.2.1.5 CONCLUSION

We see that assimilation of DST-6 asynoptic data by the Direct Insertion Method failed to exhibit a positive statistically significant impact of the satellite observations. This method has been presented primarily for comparison with the results of the new techniques developed and tested by the Analysis and Assimilation Group.

## 3.2.2 AUTOMATED CONSISTENCY CHECK (ACC) (K.K. Wong, P. Suchanick, and M. Ghil)

### 3.2.2.1 INTRODUCTION

One of the problems encountered in assimilating observational data into numerical forecasting models is that of determining whether the data inserted are of a reliable nature (e.g., Gandin, 1963, pp. 158-166). The method previously used at GISS was to compare the observed value with the model forecast values at adjacent grid points and reject the data if the difference exceeded a specified value.

The above procedure is described in Subsection 3.2.1.2 and referred to throughout the rest of this report as quality control; it had the considerable advantage of being very easy to implement. Its drawback is that it only allows for the use of very large error tolerances, and thus rejects only observations which had highly unreasonable values. It does not use the error structure of the data themselves and would in fact reject useful data when the forecast model happened to differ considerably from the actual state of the atmosphere. To eliminate the obvious shortcomings of this type of method, a procedure was developed that uses as rejection criterion a comparison of a given observation with the observations surrounding it.

### 3.2.2.2 PROCEDURE

Since in most cases the data are not received in a strict geographical order, the first step in the procedure is to order the data according to latitude and longitude. Surface quantities,

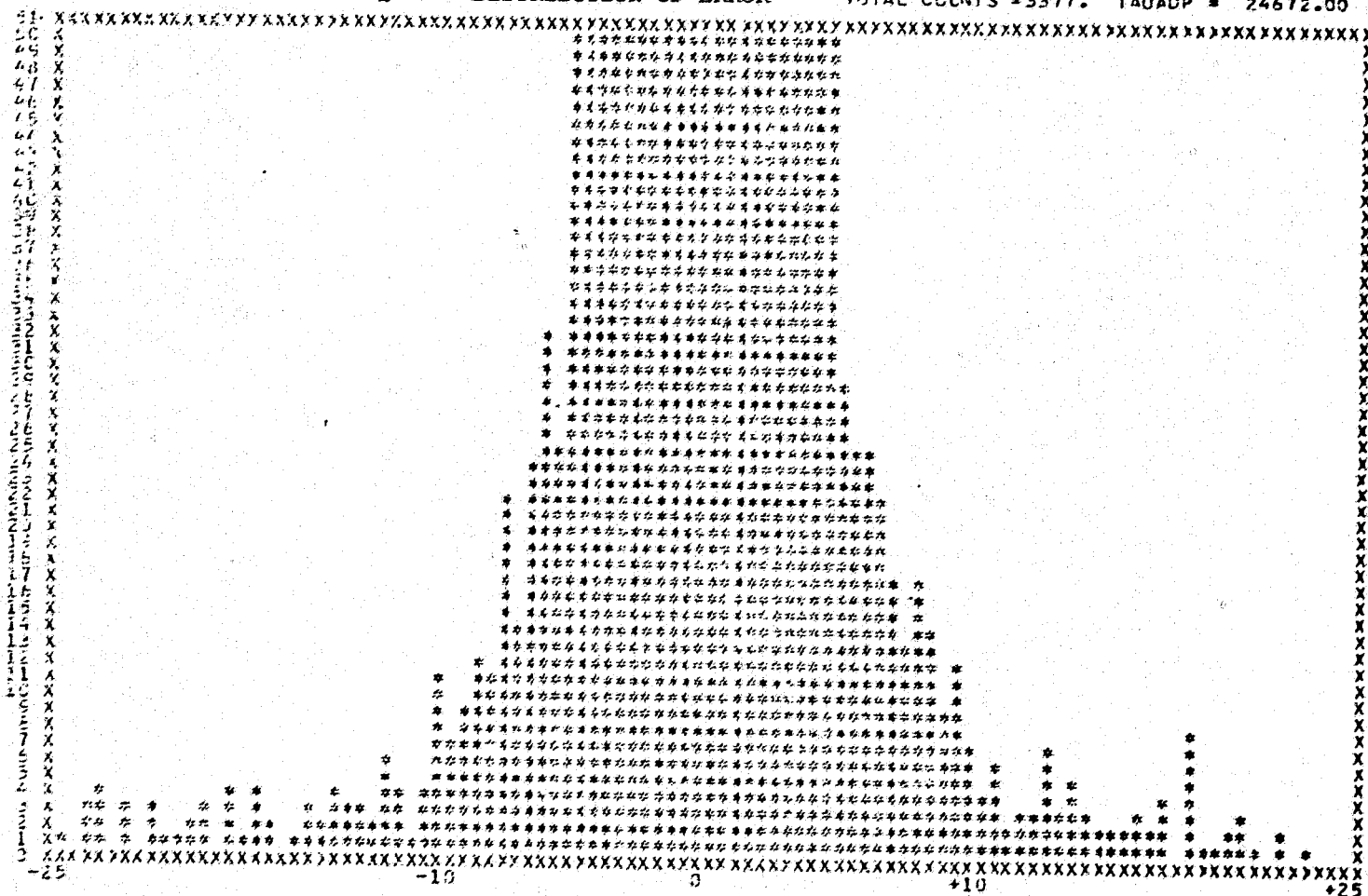
pressure and temperature, are reduced to sea level.

For each observation point all the observations within a given radius are then stored and sorted according to distance from the selected observation point. Next, the sorted data points are scanned according to increasing distance, until three points are found which form a triangle having the observation in question in its interior.

The quantities at the three points forming the triangle are then linearly interpolated to the interior observation point, and the difference between the interpolated value and the observation is calculated. Histograms of the computed differences are shown in Figures 1 to 3. If a triangle cannot be formed about a selected observation, or if the observation is missing, or if it is obviously in error, it will be ignored in further computations.

The standard deviation  $\sigma$  of the difference for all observations is computed and it serves as the basis for the rejection criterion. The computed values of  $\sigma$  for the different quantities are as given in the first row of entries in Table 7. If the difference between an observation and the interpolated value of its three selected neighbors is less than  $2\sigma$  the observation is considered reliable and is used in the assimilation without further modification. If the difference lies between  $2\sigma$  and  $3\sigma$ , it is assumed that the observation is partially correct; the observed value is then modified to a value equal to the interpolated one plus or minus  $2\sigma$ , depending on whether it exceeds  $2\sigma$  in the positive or negative direction. Finally, if the difference is greater than  $3\sigma$ , the observation is considered to be in error and will be rejected.

SEA-LEVEL PRESSURE \* FREQUENCY DISTRIBUTION OF ERROR \* TOTAL COUNTS = 3377. TAUADP = 24672.00



NUMBER OF COUNTS = 3256.

MEAN VALUE = 0.006143

STANDARD DEVIATION = 4.68938

Figure 1. Histogram of the distribution of differences between the observed values of sea-level pressure,  $p_s$ , at a given point, and the values obtained by linear interpolation from observed values at the 3 observation points which are the nearest neighbors of the point under consideration;  $\mu=0.006$  mb,  $\sigma=4.689$  mb.

ORIGINAL PAGE IS  
OF POOR QUALITY

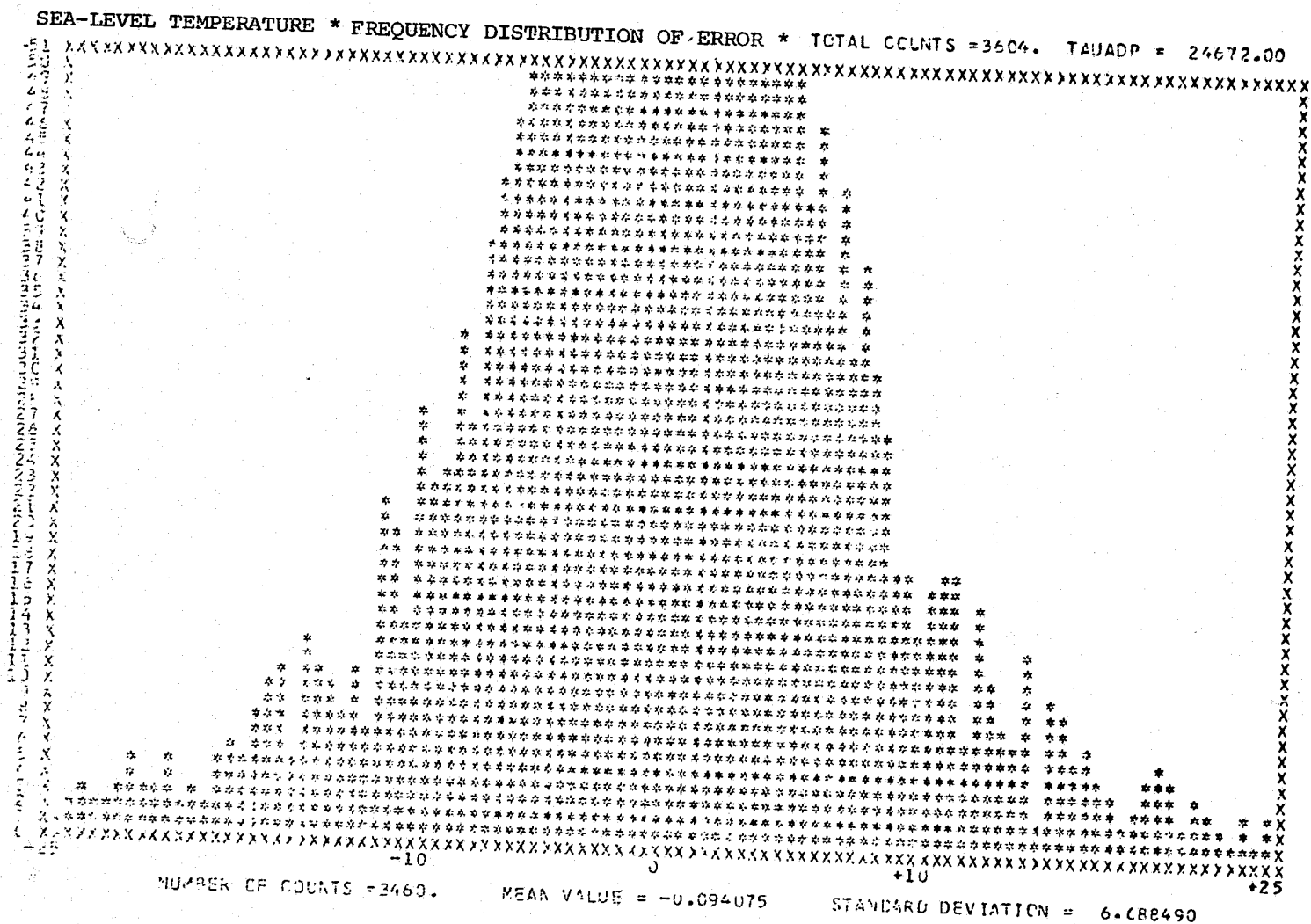


Figure 2. Same as Fig. 1: histogram corresponding to  $T_s$  (sea-level temperature);  $\mu = -0.094^\circ\text{C}$ ,  $\sigma = 6.688^\circ\text{C}$ . Notice that  $\mu/\sigma$  again does not differ significantly from zero.

TEMPERATURE LEVEL 4 (500 MB) \*\*\* FREQ. DISTRIBUTION OF ERROR \* TOTAL COUNTS = 471. TAUADP = 24672.00

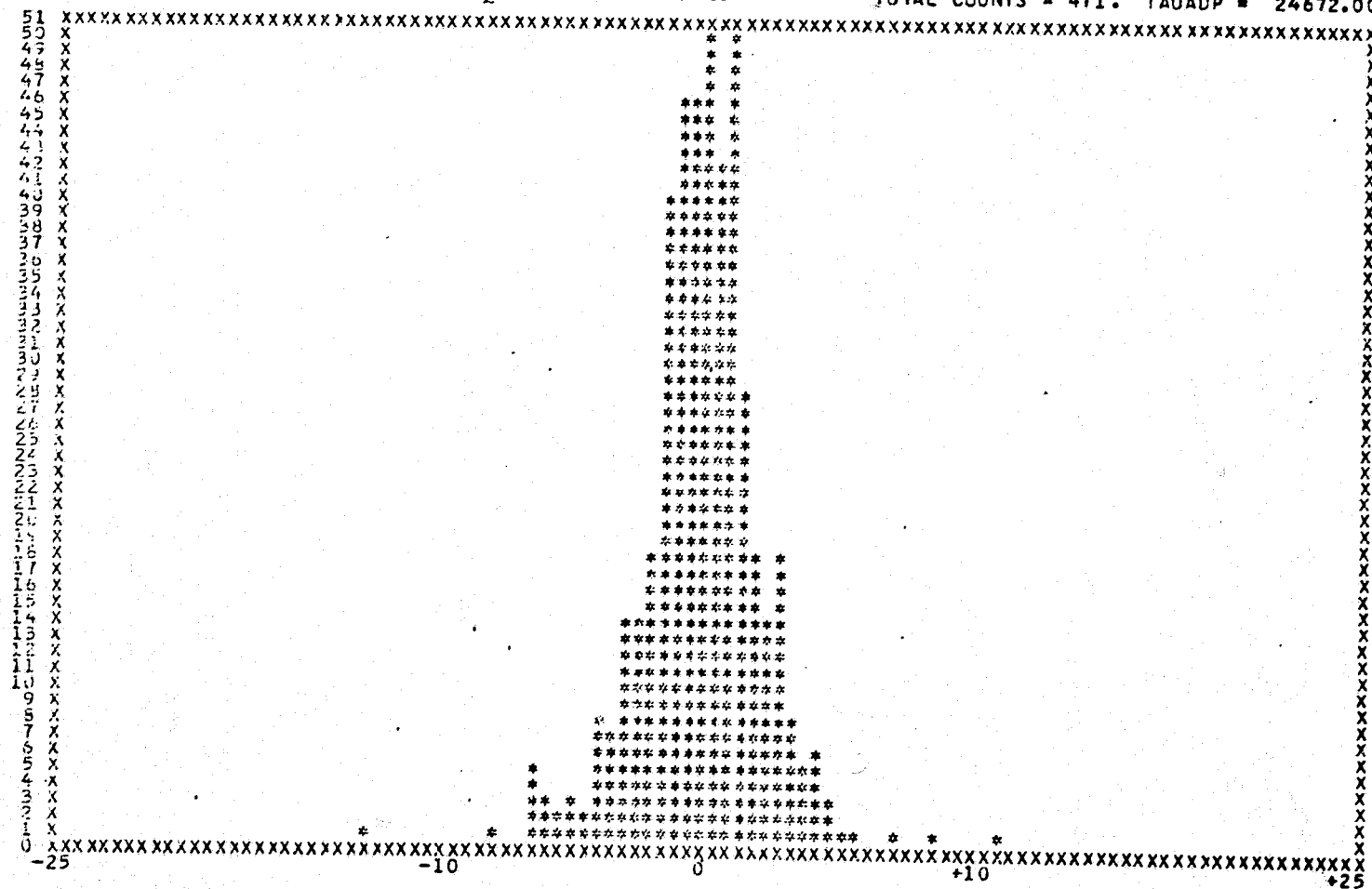


Figure 3. Same as Figs. 1 and 2: histogram corresponding to the temperature  $T_4 = T(p_4)$ , at the mandatory pressure level  $p_4 = 500$  mb;  $\mu = -0.076^\circ\text{C}$ ,  $\sigma = 2.335^\circ\text{C}$ . Notice that  $\sigma$  here is considerably smaller than for  $T_s$ .

### 3.2.2.3 RESULTS

A test analysis was performed on surface pressure, surface temperature and upper air temperature at mandatory levels. The test compares the number of observations accepted and rejected using the above criteria with the corresponding quantities when using "quality control", i.e., the differences between the model forecast value and the observation. The rejection criteria currently used in quality control are 20 mb for surface pressure and 7°C for surface and upper air temperatures. Results of this comparison are shown in Table 7. The three categories in Table 7 refer to the observations accepted, modified, or rejected by the ACC criteria. The subdivisions labeled "accepted" and "rejected" refer to the number accepted or rejected by the quality control procedure based on the difference between forecast and observational values.

Table 7

σ Value	P <sub>s</sub>	T <sub>s</sub>	Temperature at Mandatory Levels (mb)									
			850	700	500	400	300	250	200	150	100	70
A	4.7	6.7	3.8	3.5	2.3	3.4	3.6	5.8	3.3	3.5	2.4	3.3
C accepted	3199	3067	259	376	396	382	375	293	268	255	204	230
P rejected	1	207	5	1	0	0	5	20	13	28	48	3
M												
O accepted	90	131	3	8	13	6	7	6	7	4	6	6
D rejected	0	29	0	1	1	0	1	9	8	1	2	1
R												
E accepted	166	218	19	11	9	9	8	6	7	7	0	11
J rejected	18	73	6	7	0	1	1	5	1	2	1	3

In general, it can be seen that a significant difference between the two methods appears in the numbers for surface pressure and temperature. A significant number of surface temperature observations (207), which under "quality control" would have been rejected, are accepted under ACC. Conversely, a sizeable number of surface pressure and temperature quantities that were accepted under quality control standards are either modified or rejected with ACC. Another significant difference appears in the 250- to 70-mb temperature observations where a large number of observations are rejected by quality control and are acceptable under ACC. This is probably due to the inaccurate representation of the temperature inversions in the tropopause region by the forecast model.

#### 3.2.2.4 CONCLUSIONS AND RECOMMENDATIONS

An inherent drawback in this procedure is accounting for observations in data-sparse regions. With conventional synoptic data, a significant number of reports cannot be evaluated with this procedure; "quality control" procedures have to be used for such observations.

The ACC method is currently being modified to apply to asynoptic satellite data. Considerable improvement over present quality control procedures is expected in this application, where no data sparsity problem exists. For asynoptic data, ACC can be combined with the local interpolation procedure (LIP, Subsection 3.2.3) to provide a simple, effective filter of observational errors.

Assimilation runs remain to be made and results analyzed to test the effect of synoptic and asynoptic data verified by the ACC method on forecast accuracy.



### 3.2.3 LOCAL INTERPOLATION PROCEDURE (LIP) (H. Carus, M. Ghil, and R. Dilling)

#### 3.2.3.1 INTRODUCTION

Satellite-derived temperature data, as well as conventional synoptic data, are obtained in general at locations that do not coincide with grid points of a computational grid. Values of the observed fields at grid points have therefore to be computed from the values at the observation points. Subsections 3.2.1 (DIM) and 3.2.4 (SCM) describe two simple procedures for such a computation.

In addition to the problem of the difference in location, we also have to deal with the fact that the observations contain measurement errors, and also errors because of the difference between the length scale of which a measurement is representative and the scale of the model's grid size. A certain filtering of these observational errors is contained in each of the methods presented in Subsections 3.2.2 (ACC), 3.2.4 (SCM), 3.2.5 (AVM) and 3.2.7 (SAM). The method we present here obtains values of the observed fields at grid points and also contributes to filtering out the errors. It has been developed mainly as a preliminary data handling procedure for the statistical assimilation method (SAM).

#### 3.2.3.2 THE METHOD

The method is based on least-square-fitting of low-degree polynomials to the data. The value of the fitted polynomial at a

grid point in the vicinity of observations is accepted as the value of the pre-filtered observed field at that point. The filtering obtains because of the least-square fit. The polynomials depend on a number of parameters which is smaller than the number of observations; the parameters are simply the coefficients of the polynomial. Thus we can place higher confidence, in a statistical sense, on the values of the coefficients than on the individual observations. Furthermore, low-degree polynomials are considerably smoother than a high-degree interpolation polynomial which would actually pass through all the observations. A good rule of thumb for least-square polynomial fitting is that the number of coefficients should be comparable to the square-root of the number of observations fitted (cf. Isaacson and Keller, 1966).

In its present form, the method has been formulated for satellite-derived temperature data obtained in 10-minute time intervals. (compare Subsection 3.2.7.2). Such an interval is sufficiently small so that time itself need not be considered as a variable, and the data are assumed to be simultaneous. We found in general that a sufficiently large number of temperature retrievals obtain within an interval so as to expect a large part of the noise to be filtered out by the least-square fit of polynomials up to the third degree. The independent variables in our polynomials are latitude  $\phi$  and longitude  $\lambda$ . The fit occurs on fixed mandatory pressure levels, so that no vertical variable is necessary.

We regard a gridpoint as lying in the vicinity of an observation point, or retrieval, if it is a corner of a grid rectangle containing one or more retrievals. Such a restriction is required

to avoid using the fitted polynomial in an extrapolatory mode. The value of the observed temperature field at a grid point, or hypothetical retrieval at the gridpoint, is assigned the time of the earliest retrieval in any of the four grid rectangles surrounding the gridpoint; the assignment of time is necessary since the hypothetical retrievals are computed "off-line", before their use for assimilation purposes. The hypothetical retrievals at grid points become observed temperatures for an assimilation run, replacing the raw observations at their off-grid locations.

Since the data are provided and fitted in discontinuous patches, the question of the continuity of the prefiltered observation field arises. This question was confronted in an ad hoc manner, which reduces discontinuities without eliminating them altogether. Each 10-minute patch was subdivided into three equal subpatches. The least-square polynomial is calculated for the whole patch, but the hypothetical retrievals are computed and assigned only for the middle third of the patch. To provide for geographical continuity of the hypothetical retrievals, therefore, the 10-minute intervals used have a two-thirds overlap, so that the middle thirds of successively used intervals are chronologically contiguous.

### 3.2.3.3 PRELIMINARY RESULTS

The effect that the degree of the least-square polynomial used has on the fit and on the continuity was investigated in a preliminary empirical study. We limited ourselves to linear, quadratic and cubic fits; experience has shown that polynomials of higher degree are unreliable for smooth data fitting due to their oscillatory nature. The degree of the polynomial was further limited by the number of

retrievals available for the fitting since a fit based on insufficient data cannot be relied on. The actual criterion used was that the number of data must be no less than one-third of the square of the number of coefficients to be determined by the fitting. Table 8 shows the minimum number of retrievals required by this criterion.

Table 8. Characteristics of the Polynomial Fit

<u>Degree</u>	<u>No. of Coefficients</u>	<u>No. of Retrievals Required</u>
1	3	3
2	6	12
3	10	33

The preliminary empirical study to determine the appropriate degree of the fitting polynomial was applied to four sets of temperature data processed by NESS from NIMBUS-6 radiance data, each being subjected to 12 minutes of processing on an AMDAHL 470V/6 computer. These sets are described in Table 9.

Table 9. Data Used in the Preliminary Study

<u>Reference Description</u>	<u>Initial Time Index</u>	<u>Final Time Index</u>	<u>Duration (Simulated Time in Hours)</u>
Winter 1	28480	28505	25
Winter 2	28685	28698	13
Summer 1	24738	24750	12
Summer 2	24548	24568	20

The durations vary between data sets because of missing retrievals.

The goodness of fit of the three types of polynomials for the data described above is shown in Table 10.

Table 10. Goodness of Fit (0°C)

<u>Degree</u>	<u>1</u>	<u>2</u>	<u>3</u>
Winter 1	1.67	1.20	0.94
Winter 2	1.40	0.94	0.68
Summer 1	1.24	0.83	0.58
Summer 2	1.15	0.75	0.55

The goodness of fit is measured by the root-mean-square (RMS) error of the polynomial values versus the actual retrieval values at the observation points; the rms error shown is averaged over all mandatory pressure levels. The best fit is given by the third-degree polynomials. This is to be expected, since the fit will improve with the number of parameters available, and the error will be zero in particular for a polynomial of interpolation. However, the improvement in fit shown in Table 10 is larger from first degree to second, than from second to third; this was the case for all data sets tested.

A problem arises when a hypothetical retrieval at a grid point can be evaluated in two different ways because the gridpoint is in the vicinity of two different but proximate sets of retrievals. This is the continuity problem mentioned earlier. We call the differences between the two values salti; for the data sets in Table 9, we also computed the RMS values of the salti. These RMS values are shown in Table 11, again averaged over all levels.

Table 11. RMS of Salti (°C)

The numbers in parentheses show the number of gridpoints for which salti were observed.

	1st Degree	2nd Degree	3rd Degree
Winter 1	2.35 (1062)	1.93 (998)	2.67 (603)
Winter 2	2.42 (1036)	1.86 (993)	1.82 (454)
Summer 1	1.98 (1102)	1.62 (1073)	1.72 (582)
Summer 2	1.96 ( 936)	1.47 (884)	1.65 (480)

The magnitude of the salti are a measure of the smoothness of the fit as the intervals change. Table 11 shows clearly that polynomials of the second degree afford, in general, a smoother transition between intervals than those of first or third degree. When salti occur, our procedure is to average the two hypothetical

retrievals and to assign to the obtaining hypothetical retrieval the earlier of the two discrete times.

Examination of Tables 10 and 11 shows that polynomials of the second degree appear to be the most suitable compromise between goodness of fit and smoothness of fit.

### 3.2.3.4 CONCLUSION

The computation of hypothetical retrievals using second-degree polynomials is currently being implemented. We shall use the prefiltered asynoptic temperature data provided by this procedure as observational data for future assimilation runs based on SAM. The effect of prefiltering on initial states obtained with SAM and on the quality of forecasts from these initial states will be assessed.

## 3.2.4 SUCCESSIVE CORRECTION METHOD (SCM) (P. Suchanick and M. Ghil)

### 3.2.4.1 INTRODUCTION

A successive correction technique has been applied to the objective analysis of conventional synoptic data, as well as to the time-continuous, four-dimensional (4-D) assimilation of satellite-derived asynoptic data. It is based on a simplified version of the method proposed by Begthorsson and Döös (1955) and implemented operationally for the purposes of synoptic objective analysis by Cressman (1959). To the best of our knowledge, the application of this method to asynoptic satellite data is new.

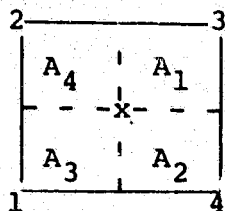
### 3.2.4.2 THE ANALYSIS METHOD

The analysis method is essentially one of applying successive corrections to a first guess field. The first guess field is the model forecast field in all our applications. Corrections are determined as the difference between the observed data and the first guess field which is interpolated to the observation point. Linear interpolation is used to evaluate the first guess field at observation points from the four grid points surrounding the observation (cf. Russell, 1975). Moreover, forecast values are computed at sigma levels, while the observations are given at mandatory pressure levels; hence an interpolation procedure, linear in  $\log p$ , is performed with respect to the vertical to obtain model values at mandatory levels.

The model forecast value at the observation point,  $\phi^{\circ}_f$ , is thus given by:

$$\phi^{\circ}_f = \sum_{j=1}^4 \alpha_j \frac{\phi_{j,1} \ln \frac{p_2}{p_l} + \phi_{j,2} \ln \frac{p_l}{p_1}}{\ln p_2 - \ln p_1} ; \quad (1)$$

here the subscripts 1 and 2 refer to the sigma level above and below a given mandatory level ( $l$ ) respectively, while  $\alpha_j$  are the horizontal weights proportional to the area  $A_j$  of the opposite rectangle of a grid box, as in the diagram below.



$$\alpha_j = \frac{A_j}{\sum_{j=1}^4 A_j} \quad (2)$$

The observations are taken one at a time and the difference  $\delta$  between the observation and the forecast at mandatory levels,

$$\delta = \phi^o - \phi_f^o \quad (3)$$

is computed. If the lowest sigma level of a particular grid point has a pressure which is lower than that of the lowest mandatory level at that point, the model quantity is extrapolated to the mandatory level. In the case of temperature, the surface temperature is used as the lowest level. If the model surface pressure is lower than the lowest mandatory-level pressure at that point, then the temperature is reduced hydrostatically to the value at the mandatory level.

At this point, a quality check is made (see Subsection 3.2.1): if  $\delta$  exceeds a specified value, it will be ignored in further computation.

The actual analysis is performed on the mandatory pressure levels, separately for each point. It consists of a number of successive scans. Each scan, indexed  $k$ , takes into consideration the observations that are within the scanning radius  $D_k$  of the given grid point. The difference  $\delta_i^{(k)}$  at observation point  $i$  is multiplied by a weighting function given by Cressman (1959) as

$$w_i^{(k)} = \frac{D_k^2 - d_i^2}{D_k^2 + d_i^2} \quad (4)$$

where  $d_i$  is the distance between observation point  $i$  and the grid point we consider, and  $d_i < D_k$ ; clearly  $w_i^{(k)} = 0$  if  $d_i > D_k$ .



The total correction  $C_k$  applied to a given grid point during scan  $k$  is given by

$$C_k = \frac{\sum_{i=1}^{N_k} w_i \delta_i^{(k)}}{N_k} \quad (5)$$

where  $N_k$  is the total number of observations within radius  $D_k$  of the given grid point.

Note: Tests were made with

$$C_k = \frac{\sum_{i=1}^{N_k} w_i \delta_i^{(k)}}{\sum_{i=1}^{N_k} w_i} \quad (5')$$

as suggested by Stephens and Stitt (1970). Theoretical considerations suggest that division by  $N$  is preferable, and this was borne out by test results.

A number of scans is performed with successively smaller radii for each type of analysis. Preliminary testing was carried out to determine an optimal number of scans as well as optimal scanning radii.

### 3.2.4.3 APPLICATIONS AND RESULTS

The above scheme was implemented for the insertion of satellite data in GISS assimilation runs. The data consist solely of temperature profiles given at 11 mandatory pressure levels and are inserted in 10-minute intervals. Four scans are made with scan sizes of 700, 600, 500, and 400 km. Runs were made covering the period from January 29, 1976 to February 21, 1976 with 72-hour

forecast runs made from 03Z on the days February 1,3,5,7,9,11,13,15, 17, and 21. Sea level pressure and 500mb-height skill score and RMS error impacts over the NO SAT control run are shown for 48 and 72 hours in Tables 12 to 15. These error measures and the corresponding impacts were computed as described in Subsection 3.2.1 (DIM).

Experiment number 8310 consists of the insertion of conventional synoptic data by the direction insertion method (DIM), and of the insertion of vertical temperature profiles provided by NESS, using radiance data from NOAA-4 (VTPR) and NIMBUS-6 satellites, by the SCM method; in the insertion of asynoptic data we also used the standard rejection criteria explained in Subsection 3.2.1.2 (Table 1). A geostrophic wind correction as in 3.2.1.3 is also made. Experiment 8310 is thus comparable to DIM experiment 8186. Experiment number 8352 is similar to 8310, except for the use of special "quality" rejection criteria described in Subsection 3.2.1.2. It is thus comparable to DIM experiment 8240, plus the utilization of VTPR data. The plots of the differences between 500 mb geopotential heights in experiment 8310 and in the NO SAT control run are shown in Figures 4a and 4b.

A considerable net improvement in both skill score impact and RMS impact of satellite data over DIM results seems to be obtained when using SCM for the assimilation of the data. This can be seen from a comparison of Tables 12 and 14 with Tables 3 and 5 in Subsection 3.2.1. A similar improvement can be observed by comparing in turn Table 13 and 15 with Tables 4 and 6 of Subsection 3.2.1. This improvement is observed consistently in the algebraic amount of the impact (sign and magnitude), as well as in the statistical significance (ratio of the mean impact to its variance); it is observed in all the verified quantities, with the possible exception

Table 12  
Experiment 8310  
Average Impact Over North America

	48-hour		72-hour	
	RMS	Skill Score	RMS	Skill Score
SLP	0.54±0.38	1.75±1.96	0.71±0.51	1.57±3.19
Z500	6.65±3.33	1.53±1.19	5.63±3.52	2.41±1.34

Table 13  
Experiment 8352  
Average Impact Over North America

	48-hour		72-hour	
	RMS	Skill Score	RMS	Skill Score
SLP	0.72±0.31	2.25±1.60	0.57±0.46	0.91±2.50
Z500	0.26±2.50	1.58±0.69	3.25±3.16	1.04±0.78

Table 14  
Experiment 8310  
Average Impact Over Europe

	48-hour		72-hour	
	RMS	Skill Score	RMS	Skill Score
SLP	0.58±0.35	2.48±1.44	-0.58±0.49	3.11±2.49
Z500	7.16±3.72	0.93±1.96	0.49±4.85	-0.96±3.51

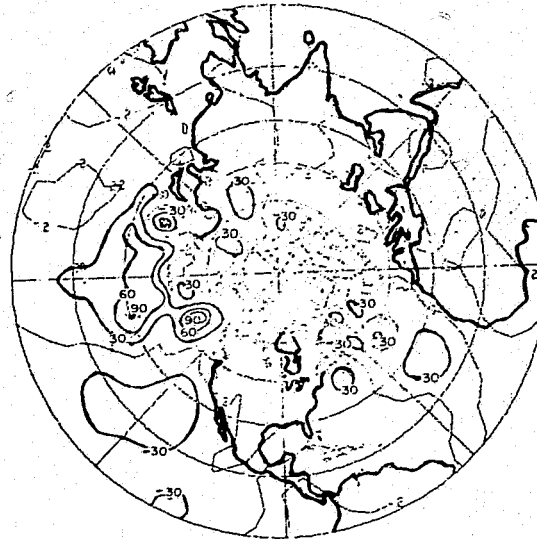
Table 15  
Experiment 8352  
Average Impact Over Europe

	48-hour		72-hour	
	RMS	Skill Score	RMS	Skill Score
SLP	0.36±0.21	1.04±0.78	0.40±0.42	1.84±1.16
Z500	4.82±2.88	0.58±1.10	5.68±2.45	0.68±1.49

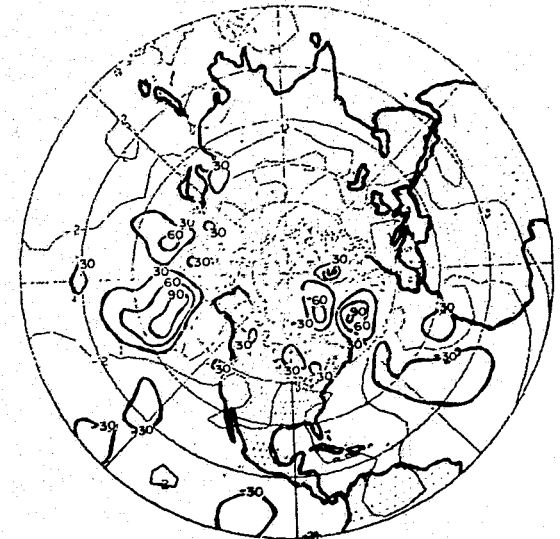
2 SAT



FEB 1



FEB 3



FEB 5



FEB 7



FEB 9



FEB 11

Figure 4a. Plot of the difference between the heights of the 500 mb geopotential surface in the initial states produced at 03Z on the given dates (Feb. 1, 3, 5, 7, 9, 11) by experiment 8310, using SCM, and by the control run.

ORIGINAL PAGE IS  
OF POOR QUALITY

2 SAT



FEB 13

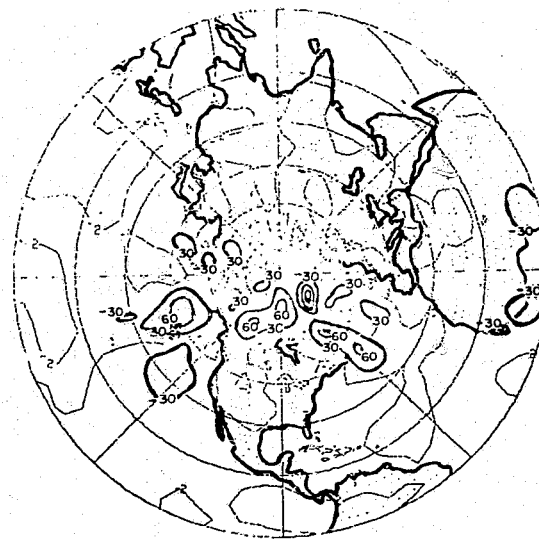


FEB 17

FEB 15



FEB 19



FEB 21

Figure 4b. Plot of the difference between the heights of the 500 mb geopotential surface in the initial states produced at 03Z on the given dates (February 13, 15, 17, 19, 21) by experiment 8310, using SCM, and by the control run.

of the RMS error in the 500mb height verified at 48h over North America (Table 13 vs. Table 4), and of the S1 score of 500mb heights verified at 72h over Europe (Table 14 vs. Table 5). The improvement cannot be explained either by the slight differences in quality control procedures between experiments 8310 (SCM) and 8186 (DIM), or in the satellite data quantity between 8352 (SCM) and 8240 (DIM); it has to be attributed mostly to the different assimilation methods. The results for experiments 8310 and 8352 are summarized also in Subsection 3.3.2.3, as well as those for experiment 8240. The more general comparisons there support our conclusions here.

The SCM procedure was also used for the insertion of conventional synoptic data in the GISS model with an ultrafine grid ( $2.5^\circ \times 3^\circ$ , see Chapter 4). The data consist of surface pressure and temperature, upper air reports of temperature, wind and relative humidity, and aircraft reports of temperature and winds. Assimilation and forecast runs were made covering the same period as above. Sea level pressure and 500mb height skill scores after 48 and 72 hours are shown in Table 16. No control run using DIM was available for the ultrafine GISS model, but some indirect comparisons are made in Chapter 4.

Table 16

Average Skill Scores of Ultra-Fine NO SAT Assimilation

	AVG	SD	SE
48 HR SLP N.A.	67.06	9.05	2.73
72 HR SLP N.A.	74.25	11.20	3.38
48 HR Z500 N.A.	35.99	4.87	1.47
72 HR Z500 N.A.	42.57	6.51	1.96
48 HR SLP N.A.	58.99	5.29	1.60
72 HR SLP EUR.	68.14	7.63	2.30
48 HR Z500 EUR.	54.07	6.29	1.90
72 HR Z500 EUR.	61.66	7.20	2.17

#### 3.2.4.4 CONCLUSIONS AND RECOMMENDATIONS

Analysis of skill score and RMS results suggests a modest but consistent improvement achieved with the SCM method over the direct insertion technique when applied to the time continuous, 4-D assimilation of asynoptic satellite temperature data.

The effect of the SCM method on the insertion of conventional synoptic data has yet to be fully analyzed. Analysis of sea-level pressure and 500 mb height charts suggest that at the least, the SCM analysis is somewhat smoother than that produced by the direct insertion approach.

Further analysis is needed specifically to determine optimal scanning radii and number of scans; such optimization may further improve results.

#### 3.2.5 ASYNOPTIC VARIATIONAL METHOD FOR SATELLITE DATA ASSMILATION (M. Ghil and R. Mosebach)

##### 3.2.5.1 INTRODUCTION

One of the most promising approaches in the objective analysis of synoptic data has been the variational method proposed by Sasaki (1958). This method has been further developed and applied to more and more realistic problems and to real-data studies by Sasaki (1969, 1970a, b, c), Stephens (1970), Lewis (1972), Lewis and Grayson (1972), and Achtemeier (1975), among others.

The main idea of the approach is to obtain an analyzed field which is as close as possible to the observations, while at the same time satisfying exactly or approximately certain dynamic relationships which are believed to hold for the true fields. When it is required that these relationships be satisfied exactly, these relationships are called strong constraints, when satisfied only in an approximate sense, by minimization, they are called weak constraints. The most common relations or constraints chosen thus far have been those aimed at preparing the initial state in such a way as to prevent inertia-gravity waves from developing unrealistic amplitudes and cause serious and rapid deterioration in the forecast from this initial state.

We decided to attempt the adaptation of this method to the time-continuous, four-dimensional assimilation of satellite-derived temperature data. For this purpose it seemed reasonable to apply the variational method to grid point values surrounding a limited area of observational data. Satellite sounding data obtained during a short time interval comparable to the forecast model integration time step extend over such a limited area. The method provides a rational procedure for inferring from temperature data the values of other meteorological variables, such as the winds, at adjacent grid points. This inference is based on the natural coupling between variables given by the variational constraints.



The variational method also provides in this context a dynamically consistent way of obtaining a smooth transition between the values of the variables in the limited area in which they have been corrected by the instantaneously available observations, and their values in the surrounding domain.

The limited-area approach dictated by the nature of the application also influenced the choice of minimization technique to be used. The variational method essentially consists of minimizing a functional of the functions to be determined; in our case these functions are the meteorological variables, regarded as functions of position at given, fixed time. This minimization must be performed in the presence of constraints, the latter being usually included in the functional itself by the use of Lagrange multipliers.

The minimization technique which has been widely used in meteorological applications is based on the derivation and solution of the Euler-Lagrange equations corresponding to the functional which is to be minimized. The solutions of the Euler-Lagrange equations yield extrema, in particular the desired minima, of the functional. These equations, however, turn out in general to be rather complicated partial differential equations, and in meteorological applications they are often of mixed elliptic-hyperbolic type. The latter fact creates a difficulty in their numerical solution. This difficulty has been circumvented in some of the quoted literature by modifying the equations or the data, so that the equations after modification become elliptic everywhere and thus solvable by standard numerical methods. The shortcomings of such

an approach have been pointed out by Ghil (1975) in a slightly different context; numerical solutions for a meteorologically significant problem of mixed type have been given by Ghil and Shkoller (1976), and by Ghil et al. (1977).

For the immediate needs of the Impact Test Project, instead of developing numerical methods for the solution of the relevant Euler-Lagrange equations, it seemed more expedient to use a direct minimization technique. The use of such a technique was also facilitated and made rather natural by the relatively small number of points involved in the limited-area application.

### 3.2.5.2 THE METHOD

The meteorological variables which we wish to adjust in the neighborhood of satellite temperature retrievals are the horizontal velocity field  $\underline{V} = \underline{V}(\lambda, \theta, \sigma)$ , the surface pressure  $\pi = \pi(\lambda, \theta)$ , and the model temperature field itself,  $T = T(\lambda, \theta, \sigma)$ . Unsubscripted symbols shall denote the values of the variables which are used by the model in the next time step of the data assimilation process. The superscript  $( )^\circ$  shall denote the values of the variables which we desire to approximate as closely as possible while still satisfying the selected constraints. Thus  $T^\circ$  is the temperature given by satellite observations,  $\pi^\circ$  is the surface pressure forecasted by the model during the assimilation process for the time in question; and  $\underline{V}^\circ$  is obtained from  $T^\circ$  and forecast values of  $\underline{V}$  by the geostrophic correction formula mentioned in Subsection 3.2.1.

The functional we wish to minimize is

$$F(T, \pi, \underline{V}) \equiv \int \alpha |\underline{V} - \underline{V}^0|^2 + \beta (\pi - \pi^0)^2 + \gamma \pi_t^2 + \delta (T - T^0)^2 ; \quad (1)$$

here  $\alpha, \beta, \gamma$ , and  $\delta$  are positive constant weights. The constraint chosen is that  $\pi_t$  be as small as possible, i.e., that spurious pressure tendencies be eliminated. The expression used for  $\pi_t$  in the evaluation of (1) is

$$\pi_t = -\underline{V} \cdot \int_0^1 \underline{\nabla} \pi d\sigma \quad (2)$$

We notice that the weak constraint (2) couples  $\pi$  and  $\underline{V}$ , but not  $T$ . Therefore  $F$  will be decreased by as much as possible with respect to  $T$  by simply setting  $T = T^0$ . However  $T^0$  enters, as mentioned previously, into the definition of  $\underline{V}^0$ .

In actual computations the continuous functions  $T$ ,  $\pi$ , and  $\underline{V}$  are approximated by discrete functions defined on a fixed grid, and the integral in (1) is approximated by a sum. For instance, with  $a$  the radius of the Earth, and  $\Delta S$  a discrete area element,

$$\int \beta (\pi - \pi^0)^2 (\lambda, \theta, \sigma) a \cos \theta d\lambda d\theta d\sigma \sim \sum_{i,j,k} \{ (\pi - \pi^0)^2 \Delta S \Delta \sigma \}_{i,j,k} ; \quad (3)$$

similar approximations are made for the other two terms in the integrand. Both  $\pi_t$  and  $|\underline{V} - \underline{V}^0|^2$  are evaluated in a way consistent with the finite-difference formulation of the GISS General Circulation Model (GCM) (Arakawa, 1972; Tsang and Karn, 1973; Ghil and Mosebach, 1976).

After discretization,  $F$  becomes just a simple quadratic function of the individual grid-point variables  $\pi_{ijk}, \underline{V}_{ijk}$ . A large number of methods exist for minimizing such quadratic functions of a large number of variables. The technique we chose is

an adaptation of the conjugate-gradient method of Powell (1964); this method does not require the computation of derivatives, which is expensive. The basic program which was adapted to our application is a Fortran program due to N. Rushfield (1970, personal communication). Its flowchart is given as Figure 5.

*Choosing Conjugate Directions.* The method essentially consists of successive searches for the minimum along  $n$  linearly independent directions, where  $n$  is the total number of variables. The search occurs first along the coordinate axes corresponding to the  $n$  variables. These  $n$  searches constitute the first iteration. At the end of the first and of each following iteration, one direction of search is changed, according to a certain algorithm. In principle, the method needs  $n$  iterations to determine the  $n$  directions which are mutually conjugate, in a well-defined sense, with respect to the particular quadratic to be minimized; at the end of these  $n$  iterations the location and value of the minimum are found. Thus, only a number of function evaluations of the order of  $n^2$  should be needed to find the minimum.

In practice, new directions found according to the basic algorithm can be close to being linearly dependent. To avoid this and ensure a reasonable converge rate, changes in the algorithm are necessary and have been implemented in the program (cf. Powell, 1964; Rushfield, 1970).

*The Linear Search.* The search along each direction is performed independently of the other directions. The crucial fact about mutually conjugate directions is that for such directions,

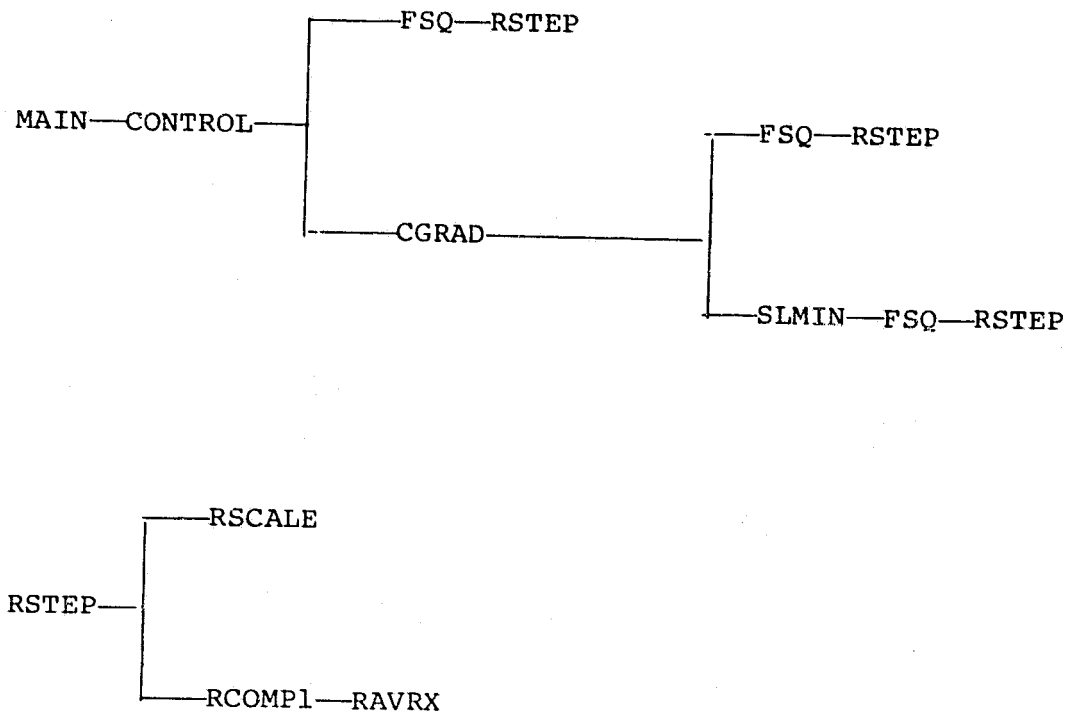


Figure 5. Variational Method Flowchart

Function FSQ computes the value of the function F, SLMIN performs the linear search along one direction, CGRAD chooses a new direction to replace an old one; RSTEP, RSCALE, RCOMPl, and RAVRX are subroutines used in the function evaluation and consistent with the GISS GCM.

and only for them,  $n$  independent searches will yield the minimum of the given quadratic. The search is basically done by determining triplets of points along the direction searched and fitting parabolas through them. The idea is that the turning point of such a parabola is an approximation to the minimum along the given direction. The detailed linear-search algorithm is given in Table 17.

*Convergence Criterion.* Convergence is assumed if after any iteration none of the variables have changed by more than a prescribed small quantity  $\epsilon$ . The more complicated criterion proposed by Powell (1964) does not seem to be necessary in the case of a quadratic function like the one we attempt to minimize.

### 3.2.5.3 PRELIMINARY RESULTS

*Analytic Test Cases.* The program was tested by attempting the minimization of a number of analytically prescribed quadratic functions of up to 100 variables. The convergence criterion was taken to be a change of not more than  $\epsilon = .02$  in any variable. Sample cases are presented in Table 18. All computations were carried out with a Fortran H compiler and an optimization level  $OPT = 2$ . The computer used was either an AMDAHL 470V/6 or an IBM 360/95 machine. Computing times on both are quite similar, and the ones listed correspond to the AMDAHL computer, which are in general slightly larger. We notice that for all test cases in Table 18, convergence was achieved within a few iterations.

*Real Data Tests.* The method was tested for a nine-level

Table 17. Description of the Linear Search Algorithm

- (1) Start with the initial value of the function,  $F$ .
- (2) Move along a specified direction by a specified amount, changing one (for the first iteration) or more (for successive iterations) of the variables and get a new value of the function,  $F'$ .
- (3) Continue until at point C the value of the function is greater than at a previous point B. Call point reached before B, point A.
- (4) Three points are now defined. Fit a quadratic form to these points and find the turning point of the quadratic (point D). If the turning point is a minimum and if D is sufficiently close to A, B, or C, then choose point D as the minimum. Otherwise, take point D and the two points A, B and C and repeat Step 4.

ORIGINAL PAGE IS  
OF POOR QUALITY

Table 18. Test Cases for Variational Technique

Function F	Initial Guess	No. of Iterations	Time for Computation*
$F = \sum_{i=1}^{10} (x_i)^2$	$x_i = 1.5$ for all $i$	4	.15 min.
$F = \sum_{i=1}^{10} (x-i)^2$	$x_i = 1.5$ for all $i$	2	.13 min.
$F = \sum_{i=1}^{100} (x-i)^2$	$x_i = 1.5 \quad i \leq 10$ $x_i = 0 \quad i > 10$	3	.19 min.
$F = \sum_{i=1}^{10} \sin^2(x_i)$	$x_i = a_i \frac{\pi}{4}$ $a =$ random variable with normal distribution about 0, range: $[-1,1]$	3	.16 min.
$F = x_1^2 - 2x_1x_2 + x_2^2$	$x_1 = -4$ $x_2 = 2$	2	.13 min.
$F = \sum_{i=1}^{10} \sin^2(2x_i + 3x_{i+1})$	$x_i = a_i \frac{\pi}{4}$ $a =$ random variable with normal distribution about 0, range: $[-1,1]$	11	.12 min.
$F = \sum_{i=1}^{10} (2x_i + 3x_{i+1})^2$	$x_i = a_i \frac{\pi}{4}$ $a =$ random variable with normal distribution about 0, range: $[-1,1]$	10	.78 min.

\*Computations were performed on an Amdahl 470V/6 with compiler optimization level OPT=2.



2 x 2 square of the GISS GCM computational grid corresponding to the indices J=10,11, I=10,11 (cf. Tsang and Karn, 1973; see also Fig. 8). This means that 76 variables were involved (72=9x4x2 horizontal wind component values + 4 surface pressure values). The observed values for this test were taken from the NMC analysis at 00Z August 23, 1976. The results are shown in Table 19. After the first iteration the variables do not change appreciably. In fact, the convergence is assumed after only two iterations, with the convergence criterion of  $\epsilon = .02$  (i.e., less than a 2 percent change in all of the variables.) Figures 6 and 7 show the percentage change in the zonal wind for each level at particular grid points.

The basic problem in the implementation of this approach is that the time necessary to calculate the function is large. Since each linear search requires that the function be computed several times, and since each iteration requires a linear search over as many directions as there are variables, reducing this computation time is crucial.






Referring again to Table 19, we see that 13.3 seconds are required for one iteration. The problem arises when we realize that we are only dealing with 76 variables and that the computation time is quadratically proportional to the number of quantities. Thus, if we were to deal with a patch of 5 x 5 grid points, we would increase the time for one iteration to:

$$\frac{25 \times 25}{4 \times 4} \times 13.3 \frac{\text{sec}}{\text{iter.}} = 8.66 \frac{\text{min}}{\text{iter.}}$$

This number of grid points is typical of the patch size involved in some other assimilation methods discussed in this report for

Table 19. Results for a real date test of AVM (see text). The time required per iteration was 13.3 sec.

ORIGINAL PAGE IS  
OF POOR QUALITY

QUANTITY DESCRIPTION	QUANT. #	INITIAL VALUE	VALUE AFTER ITER. 1	VALUE AFTER ITER. 2
 U WINDS J=10,11 I=10,11 L=1,9	PZ( 1) =	34.84640	37.97737	37.943
	PZ( 2) =	30.81660	31.15787	31.1751
	PZ( 3) =	34.83800	31.15448	31.1361
	PZ( 4) =	32.78798	31.09621	31.0996
	PZ( 5) =	28.12766	24.83625	24.682
	PZ( 6) =	15.77712	15.82830	15.827
	PZ( 7) =	25.16211	25.41980	25.444
	PZ( 8) =	26.19737	25.56117	25.536
	PZ( 9) =	25.72203	24.37114	24.375
	PZ(10) =	30.81445	30.35106	30.350
	PZ(11) =	25.46675	27.74612	27.747
	PZ(12) =	29.40257	28.55556	28.555
	PZ(13) =	20.07941	19.66182	19.635
	PZ(14) =	-1.73259	-1.15499	-1.1951
	PZ(15) =	21.56432	21.61255	21.402
	PZ(16) =	3.37877	3.01574	3.015
	PZ(17) =	15.28450	15.22234	15.223
	PZ(18) =	-1.65081	-1.65039	-1.650
	PZ(19) =	16.56130	16.58069	16.572
 V WINDS J=10,11 I=10,11 L=1,9	PZ(20) =	1.27659	0.95472	0.999
	PZ(21) =	12.23668	12.45430	12.444
	PZ(22) =	-1.64333	-1.61375	-1.615
	PZ(23) =	13.62582	13.65375	13.648
	PZ(24) =	1.25727	1.07073	1.066
	PZ(25) =	6.06679	10.06787	10.065
	PZ(26) =	-1.27746	-1.41971	-1.421
	PZ(27) =	11.21120	11.56654	11.564
	PZ(28) =	1.42249	1.23781	1.236
	PZ(29) =	7.85055	8.02812	8.027
	PZ(30) =	-1.22626	-1.34382	-1.345
	PZ(31) =	9.42155	9.28642	9.286
	PZ(32) =	1.75892	1.60777	1.606
	PZ(33) =	6.12418	6.25849	6.298
	PZ(34) =	-1.66674	-1.66354	-1.664
	PZ(35) =	7.67974	7.69865	7.699
	PZ(36) =	1.42357	1.25941	1.298
	PZ(37) =	16.68805	16.50269	16.500
	PZ(38) =	12.98461	13.17152	13.174
	PZ(39) =	22.58107	22.55549	22.555
 PRESSURE J=10,11 I=10,11	PZ(40) =	20.57036	20.55832	20.558
	PZ(41) =	-3.78887	-3.75759	-3.798
	PZ(42) =	-10.66999	-10.57439	-10.573
	PZ(43) =	1.77224	1.87376	1.874
	PZ(44) =	-8.94705	-9.00049	-9.001
	PZ(45) =	-6.70700	-6.68185	-6.681
	PZ(46) =	-10.82803	-10.77687	-10.776
	PZ(47) =	5.64361	5.52761	5.528
	PZ(48) =	-3.54700	-3.60386	-3.604
	PZ(49) =	-6.25711	-6.21324	-6.212
	PZ(50) =	-8.04783	-8.00304	-8.002
	PZ(51) =	4.81805	4.76107	4.761
	PZ(52) =	-0.55705	-0.60774	-0.608
	PZ(53) =	-6.11233	-6.06247	-6.062
	PZ(54) =	-6.66654	-6.63145	-6.631
	PZ(55) =	2.26948	2.20247	2.202
	PZ(56) =	-0.62122	-0.66409	-0.664
	PZ(57) =	-5.15261	-5.54206	-5.543
	PZ(58) =	-6.72111	-6.69280	-6.692
	PZ(59) =	0.52244	0.47782	0.477
 PRESSURE J=10,11 I=10,11	PZ(60) =	-2.84487	-2.58047	-2.581
	PZ(61) =	-5.04040	-4.99556	-4.996
	PZ(62) =	-6.52018	-6.49707	-6.497
	PZ(63) =	-0.71935	-0.97706	-0.978
	PZ(64) =	-3.97810	-4.00746	-4.008
	PZ(65) =	-4.71105	-4.72855	-4.727
	PZ(66) =	-6.25654	-6.23760	-6.237
	PZ(67) =	-2.52236	-2.08210	-2.083
	PZ(68) =	-5.37243	-5.39700	-5.397
	PZ(69) =	-3.17170	-3.13927	-3.139
 PRESSURE J=10,11 I=10,11	PZ(70) =	-5.15082	-5.66026	-5.660
	PZ(71) =	-2.25481	-2.29976	-2.299
	PZ(72) =	-1.57833	-1.77219	-1.772
	PZ(73) =	1001.15455	1001.45117	1001.413
	PZ(74) =	1000.83750	1000.18028	1000.138
	PZ(75) =	1002.03252	1002.97144	1002.126
	PZ(76) =	1000.25456	1001.93579	1002.154
FUNCTION		.5242 E+21	.3809 E+19	.3754 E+19

# Change in "U" winds after variational corrections

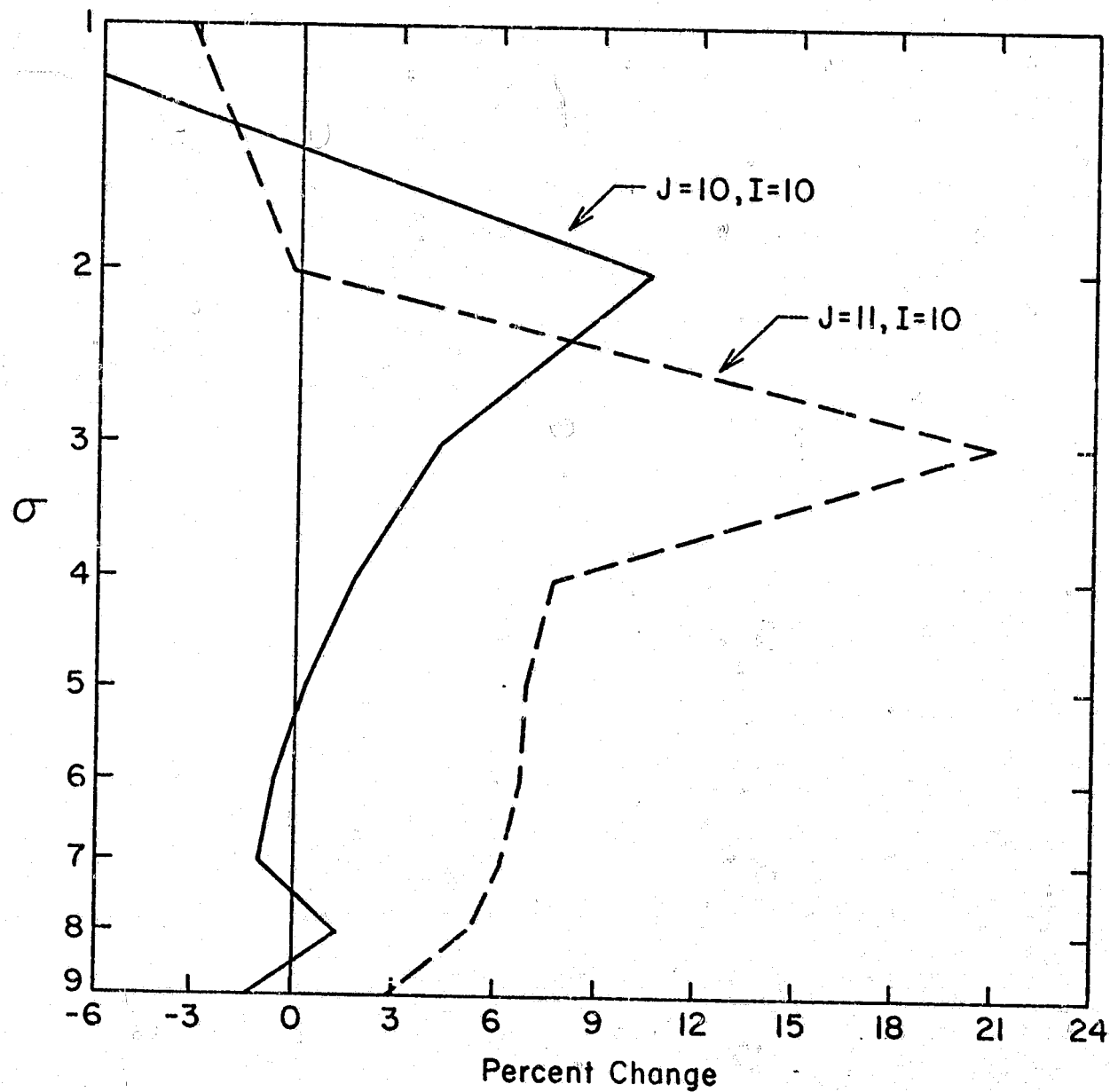


Figure 6.

# Change in "U" winds after variational corrections

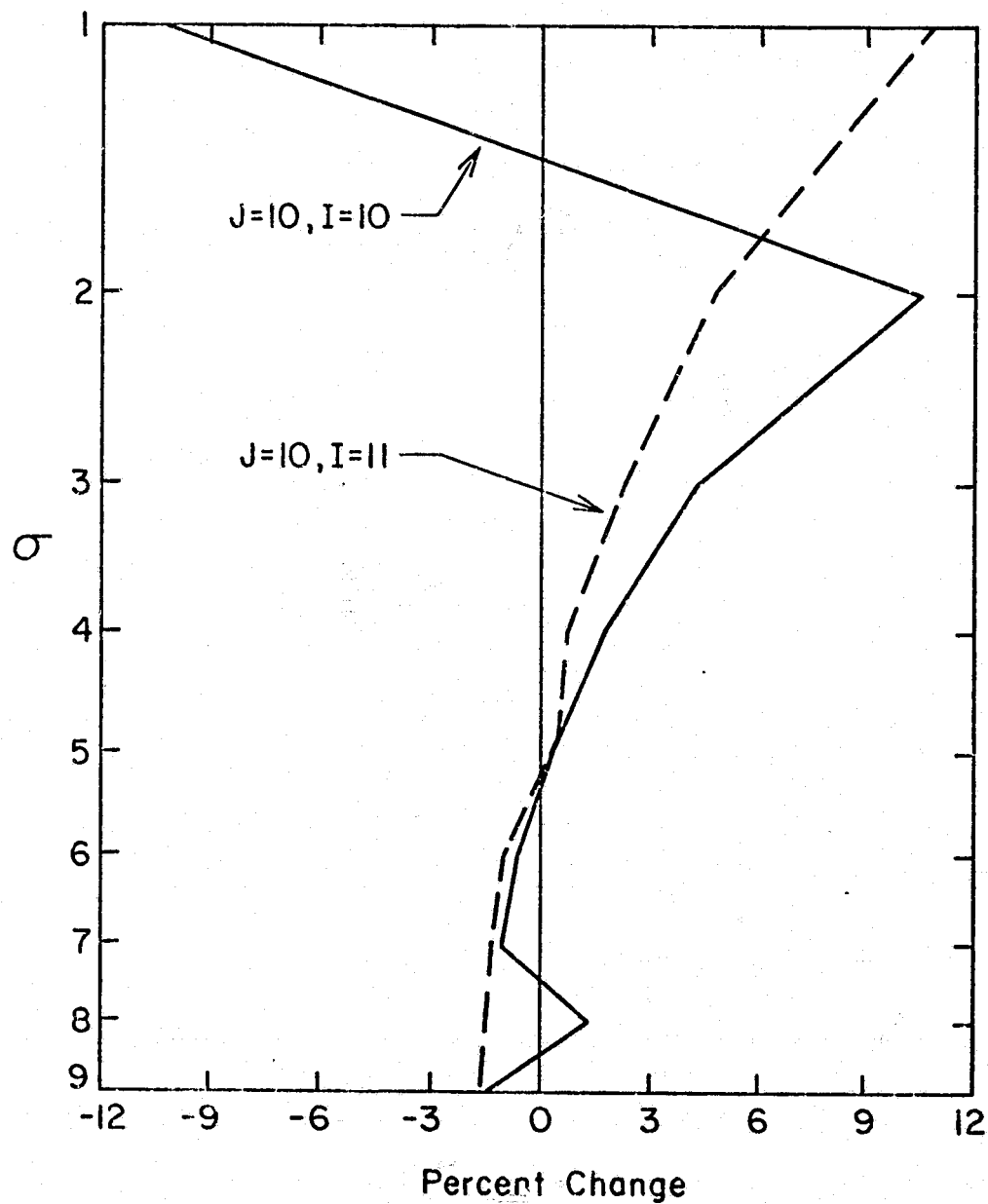


Figure 7.

C-3

dealing with satellite-derived temperature data obtained over a 10-minute time interval.

The hope is that the time will increase less than quadratically or that some other way will be envisioned to reduce this time estimate. One way would be not to perform the three-point zonal averaging (AVRX) usually done in the GISS GCM differencing scheme every time we calculate the function. Results for this latter procedure are given in Table 20. A 15 percent time savings is achieved, and variable values after the variational corrections equal the previous ones to at least three significant digits.

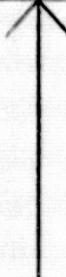
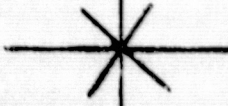

#### 3.2.5.4 APPLICATION TO LARGE REGIONS

Ignoring, for the moment, the time problems, experiments are being conducted to apply the method to the full neighborhood of a satellite retrieval patch. Figure 8 shows one such patch. The H's denote the grid points where satellite temperature data were obtained. Geostrophic corrections were made to winds at these points, in addition to those marked with +'s. We shall attempt to apply the variational method to the entire region including the shaded area. The size of this region is taken to be twice that of the geostrophically corrected area. The values of the observed variables in the AVM function  $F$  are chosen to be the current model values for the shaded area. That is, in the shaded area the values are the same as before the insertion; the grid points marked with H's or +'s now have geostrophically corrected values.

An immediate problem to be faced is the size of the matrix

ORIGINAL PAGE IS  
OF POOR QUALITY

Table 20. Same as Table 19, but with ARVX computation omitted (see text and Figure 5). The computation time was reduced to 11.3 sec. per iteration. Results are the same to within the required accuracy.

QUANTITY DESCRIPTION	QUANT. #	INITIAL VALUE	VALUE AFTER ITER. 1	VALUE AFTER ITER. 2
 U WINDS J=10,11 I=10,11 L=1,9	PZ( 1 )	34.24640	37.66510	37.9335
	PZ( 2 )	20.51560	21.00562	21.5022
	PZ( 3 )	24.82800	21.00856	21.0226
	PZ( 4 )	22.78798	21.65221	21.6552
	PZ( 5 )	25.12756	25.12703	25.171
	PZ( 6 )	15.77712	15.61915	15.820
	PZ( 7 )	15.16211	15.61066	15.9322
	PZ( 8 )	26.15737	25.67249	25.671
	PZ( 9 )	25.73203	24.61515	24.636
	PZ( 10 )	0.63145	0.41915	0.415
	PZ( 11 )	28.66675	27.63859	27.828
	PZ( 12 )	9.46257	6.15350	5.1535
	PZ( 13 )	20.07941	19.74416	19.735
	PZ( 14 )	-1.73249	-1.66471	-1.665
	PZ( 15 )	21.66432	21.66673	21.413
	PZ( 16 )	3.7877	3.16465	1.164
	PZ( 17 )	15.88450	15.64803	1.244
	PZ( 18 )	-1.65031	-1.60751	-1.808
	PZ( 19 )	16.46140	16.52937	16.515
 V WINDS J=10,11 I=10,11 L=1,9	PZ( 20 )	1.27759	1.11513	1.114
	PZ( 21 )	12.22668	12.40851	12.402
	PZ( 22 )	-1.64333	-1.63597	-1.540
	PZ( 23 )	13.68855	13.76255	13.757
	PZ( 24 )	1.65727	1.17120	1.170
	PZ( 25 )	6.56729	9.55871	5.996
	PZ( 26 )	-1.65774	-1.35566	-1.356
	PZ( 27 )	11.41100	11.45254	11.457
	PZ( 28 )	2.67246	1.32276	1.322
	PZ( 29 )	7.85055	7.55182	7.551
	PZ( 30 )	-1.63636	-1.28888	-1.289
	PZ( 31 )	9.44145	9.78255	9.577
	PZ( 32 )	1.58453	1.67558	1.675
	PZ( 33 )	6.12416	6.63321	6.224
	PZ( 34 )	-1.66674	-1.6673	-1.317
	PZ( 35 )	-7.67974	7.79671	7.797
	PZ( 36 )	1.63257	1.26046	1.260
	PZ( 37 )	16.68805	16.52807	16.527
	PZ( 38 )	12.64651	13.06048	12.066
	PZ( 39 )	22.78107	22.7572	22.755
 PRESSURE J=10,11 I=10,11	PZ( 40 )	20.57036	20.56256	20.562
	PZ( 41 )	-3.68837	-3.79847	-3.799
	PZ( 42 )	-10.68589	-10.68037	-10.630
	PZ( 43 )	1.77224	1.81822	1.818
	PZ( 44 )	-8.54705	-8.57048	-8.971
	PZ( 45 )	-6.63700	-6.69904	-6.699
	PZ( 46 )	-10.88803	-10.81241	-10.816
	PZ( 47 )	5.64261	5.58233	5.538
	PZ( 48 )	-3.54700	-3.57138	-3.572
	PZ( 49 )	-6.63711	-6.63977	-6.639
	PZ( 50 )	-8.64783	-8.68894	-8.688
	PZ( 51 )	4.61805	4.75472	4.755
	PZ( 52 )	-0.57705	-0.57865	-0.575
	PZ( 53 )	-6.11233	-6.09179	-6.091
	PZ( 54 )	-6.66554	-6.55170	-6.552
	PZ( 55 )	2.26548	2.24151	2.341
	PZ( 56 )	-0.52122	-0.53543	-0.540
	PZ( 57 )	-5.57051	-5.57030	-5.570
	PZ( 58 )	-6.21111	-6.70912	-6.709
	PZ( 59 )	0.54244	0.51527	0.515
	PZ( 60 )	-2.54487	-2.55558	-2.556
	PZ( 61 )	-3.64049	-3.62200	-3.622
	PZ( 62 )	-6.52018	-6.51038	-6.510
	PZ( 63 )	-0.51835	-0.54369	-0.544
	PZ( 64 )	-3.57810	-3.55056	-3.551
	PZ( 65 )	-4.21105	-4.25492	-4.255
	PZ( 66 )	-6.35654	-6.34850	-6.348
	PZ( 67 )	-2.53235	-2.53342	-2.534
	PZ( 68 )	-3.57283	-3.58309	-3.583
	PZ( 69 )	-3.17172	-3.15758	-3.158
	PZ( 70 )	-5.65982	-5.66572	-5.666
	PZ( 71 )	-2.25481	-2.27258	-2.273
	PZ( 72 )	-5.55233	-5.70076	-5.701
	PZ( 73 )	1001.83544	1001.65356	1001.630
	PZ( 74 )	558.45730	558.41971	558.407
	PZ( 75 )	1002.54352	1002.54336	1002.543
	PZ( 76 )	1000.25456	1001.14697	1001.360
FUNCTION		.2103 E+21	.2449 E+19	.2416 E+19



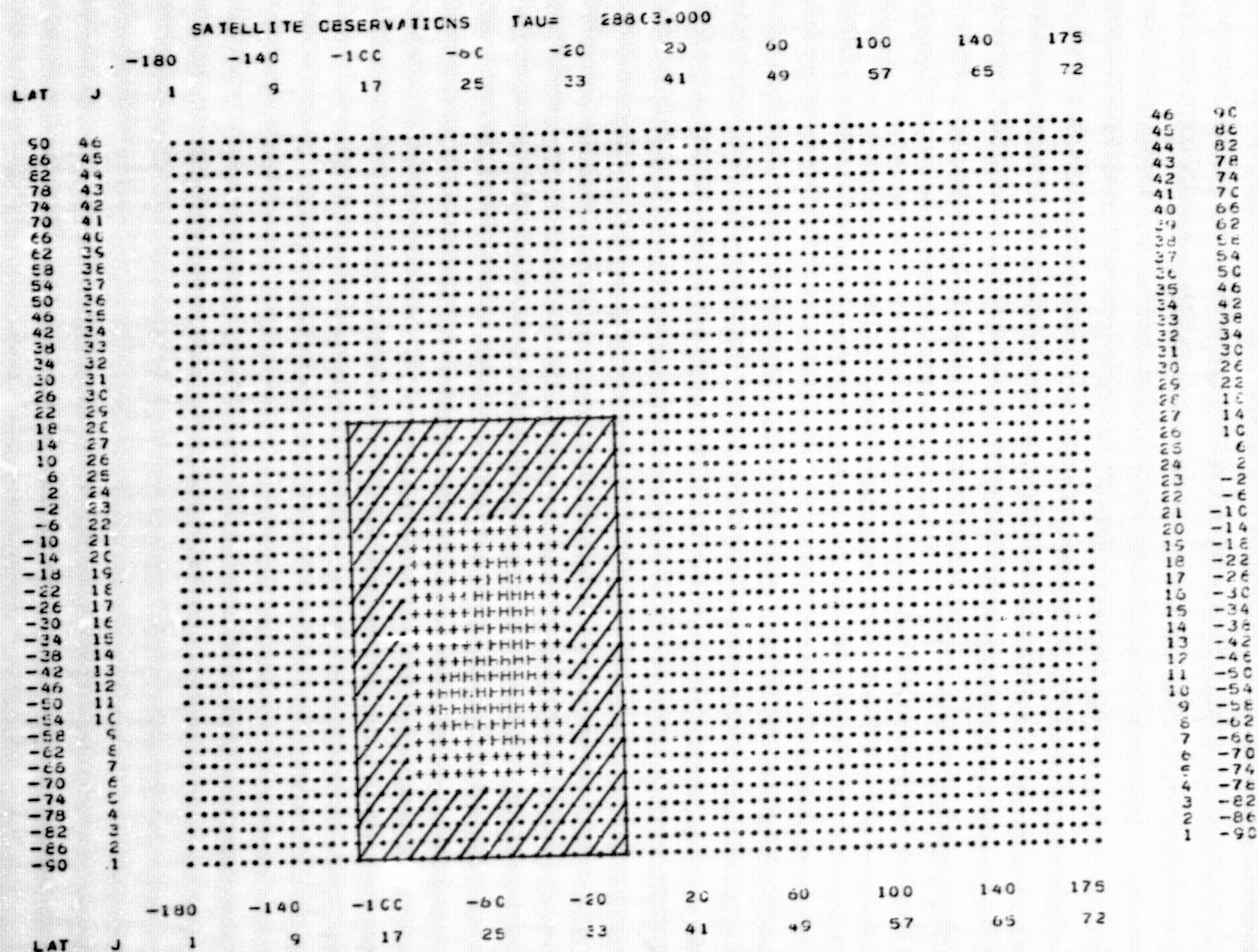


Figure 8. Plot of data used in the application of the variational method to satellite observations obtained within a 10-minute interval. The dots are GISS GCM grid points. Grid points marked "H" are in the immediate vicinity of satellite observations; both temperature and wind corrections applied at these points are used as observational data by the AVM. At grid points marked "+" only geostrophic wind corrections, and no temperature corrections are applied previous to AVM. The total area to which AVM corrections are made includes the shaded area, as well as points marked "H" and "+".

U which determines the directions chosen for each linear search (see Powell, 1964). For a  $25 \times 25$  patch this matrix would have dimensions of  $11825 \times 11825$  or use 559 megabytes of storage. It may be possible to write the matrix U to disk one line at a time. For testing, we set U equal to the identity matrix, which is equivalent to choosing the directions as the variables themselves (i.e., always varying only one at a time and never a linear combination thereof). If convergence is fast as in the  $2 \times 2$  case this seems to be the best idea anyway, since the matrix only changes after the first iteration. As of now, there are no results for using the AVM on this expanded region.

### 3.2.5.5 CONCLUDING REMARKS

The asynoptic variational method (AVM) formulated herein seems to be promising, both dynamically and computationally. We expect that only one or two iterations of the conjugate-gradient algorithm used are needed in real-data applications; this will achieve the adjustment of meteorological variables to values which are within observational error of the satellite-derived values, and which also satisfy the dynamical constraints we impose. A number of approaches are being pursued to reduce the computational time required.



### 3.2.6 FILTERED EQUATIONS METHOD (FEM) (L. Peng and B. Shkoller)

#### 3.2.6.1 FILTERED EQUATIONS METHOD, I: PRELIMINARY TESTS OF A GLOBAL BALANCE-EQUATION MODEL

##### 3.2.6.1.1 INTRODUCTION

Since four-dimensional data assimilation was first proposed by the GARP Study Conference at Stockholm in 1967 as a technique to obtain a better representation of atmospheric synoptic states, a large number of assimilation experiments have been carried out using primitive-equation models (see the reviews by Bengtsson, 1975, and by McPherson, 1975). One of the major objectives of these experiments was to reduce or damp the spurious onset of large inertia-gravity waves, often referred to as "initialization shock"; these "shocks" were excited by the insertion of data, particularly when real data were used, and have to be considered meteorologically as "noise". It has been found that requiring local balance between corrections of the mass field and the wind corrections can reduce the excitation of inertia-gravity waves and hence accelerate the assimilation process (Rutherford, 1973; Stone et al., 1973; Kistler and McPherson, 1975). A more far-reaching solution of the noise problem seems to be the use of a filtered model. It is expected that in a filtered model the inserted information will be effectively absorbed without contamination by excited gravity waves and that the impact of insertion will be enhanced. The crucial question is then: How accurate can the evolution of atmospheric synoptic states be described by a filtered model?

The most complete and accurate system of equations which does not admit high-frequency oscillations is the system of balance

equations (Bolin, 1955, 1956; Charney, 1955; Monin, 1952, 1958; Thompson, 1956). The major way in which this system differs from the full baroclinic primitive-equation of large-scale atmospheric flow model is the omission of the terms in the divergence equation which are related to the irrotational component of the horizontal wind. Charney (1962) has shown that this system can be obtained as a second-order approximation in the expansion of the primitive equations in terms of the Rossby number,  $R_0$ ; in addition, a term arising from the beta effect on the irrotational wind appears in the balance equation in the case of planetary scales. According to Charney (1973), the expansion holds even for  $R_0 = O(1)$ , provided the Richardson number,  $R_i$ , is sufficiently large for  $(R_i R_0)^{-1}$ , to be small. Most recently, Moura (1976) examined the accuracy of the balance system for describing slow, large-scale motions in the atmosphere; he considered solutions of a linearized form of the system and compared them with solutions of the linearized Laplace tidal equations, as obtained by Longuet-Higgins (1968). The results show that the balance system describes well the slow, large-scale atmospheric motions, except the Kelvin wave which is not a solution of the system. The previously mentioned additional term in Charney's balance equation corrects this deficiency, but introduces additional unrealistic high-frequency modes. Despite this Kelvin wave deficiency and possible inadequacies in the case of rapid synoptic development (as mentioned by Bolin, 1956), or in the presence of strong heating (Charney, 1963; Murakami, 1972), the use of a filtered global weather prediction model based on the balance system seems feasible. At least, it is worth the effort to test it.

Aside from the question of its physical applicability, the balance system presents a serious mathematical problem in

solving it. The complicated nonlinear balance constraint between mass distribution and motion makes it very difficult to obtain a single diagnostic equation which could be solved for the irrotational wind or for the vertical velocity; it is even more difficult to obtain a mathematical condition guaranteeing the existence of a solution for such a diagnostic equation. Because of these difficulties, all the reported methods of solving the balance system are iterative and not known a priori to converge. Charney (1962) has found, in integrating the system over North America, that the iterative method he proposes will converge only if the potential vorticity is positive and he suggests to impose this constraint on the flow. The implication of such a constraint is, however, not clear in the case of cross-equator flow. Masuda (1971) reports some test results of a pseudo-hemispheric balance model in which the values of the Coriolis parameter  $\underline{f}$  used by the model between  $30^{\circ}\text{N}$  and the equator are modified so that the modified  $\underline{f}$  decreases linearly toward a non-zero value,  $2\Omega\sin(\pi/6)$ , at the equator. All these considerations indicate the kind of difficulties one would encounter in working with a global balance-equation model.

The purpose of this work is to formulate a global balance-equation model for numerical weather prediction, to test its forecasting skill, and to assess its potential as a tool for data assimilation. The model equations are given in Subsection 3.2.6.1.2. The method of solution is described in Subsection 3.2.6.1.3. The results of forecast tests and their discussion follow in Subsections 3.2.6.1.4 and 3.2.6.1.5.

The potential of the balance system as a data assimilation tool is discussed in the next Section, 3.2.6.2.

### 3.2.6.1.2 THE MODEL

For the convenience of handling boundary conditions at the Earth's surface our filtered model uses the so-called sigma coordinate system; this has the added advantage of facilitating comparisons with the existing GISS Primitive Equation Model. In  $\sigma$  coordinates, the basic equations governing atmospheric large-scale, quasi-horizontal motions may be written as follows:

$$\frac{\partial \underline{V}}{\partial t} = -(\underline{V} \cdot \nabla) \underline{V} - \dot{\sigma} \frac{\partial \underline{V}}{\partial \sigma} - \frac{\sigma R T}{P} \nabla \pi - \nabla \phi - f \underline{k} \times \underline{V} + \underline{F} \quad (2.1)$$

$$\frac{\partial \phi}{\partial \sigma} = - \frac{R T}{P} \pi \quad (2.2)$$

$$\frac{\partial \pi}{\partial t} = - \nabla \cdot (\pi \underline{V}) - \frac{\partial}{\partial \sigma} (\pi \dot{\sigma}) \quad (2.3)$$

$$\frac{\partial}{\partial t} (\pi T) = - \nabla \cdot (\pi T \underline{V}) - \frac{\partial}{\partial \sigma} (\pi T \dot{\sigma}) - \frac{\sigma R \pi^2 T}{P C} (\nabla^2 \chi + \frac{\partial \dot{\sigma}}{\partial \sigma} - \frac{\dot{\sigma}}{\sigma}) + \frac{\pi Q}{C_P} \quad (2.4)$$

$$\frac{\partial}{\partial t} (\pi q) = - \nabla \cdot (\pi q \underline{V}) - \frac{\partial}{\partial \sigma} (\pi q \dot{\sigma}) + \pi (E - C). \quad (2.5)$$

Here

$t$  = time,

$\sigma$  = the vertical coordinate,  $(p - p_t) / (p_s - p_t)$ ,

$p$  = pressure,

$p_t$  = pressure at the top of model atmosphere, assumed constant,

$p_s$  = pressure at bottom of model atmosphere,

$\pi = p_s - p_t$ ,

$\underline{V}$  = horizontal velocity,

$\underline{\nabla}$  = gradient operator on constant  $\sigma$  - surface,

$\dot{\sigma} = d\sigma/dt$ ,

$\underline{k}$  = vertical unit vector,

$f$  = Coriolis parameter,

$R$  = gas constant,

$c_p$  = specific heat at constant pressure,

$Q$  = heating rate per unit mass,

$q$  = specific humidity ,

$E$  = evaporation rate ,

$C$  = condensation rate ,

$\Phi$  = geopotential ,

$t$  = temperature ,

$\underline{F}$  = horizontal friction force .

Let us write

$$\underline{V} = \underline{V}_\psi + \underline{V}_\chi \quad (2.6)$$

$$\underline{V}_\psi = \underline{k} \times \underline{\nabla}\psi \quad (2.7)$$

$$\underline{V}_\chi = \underline{\nabla}\chi . \quad (2.8)$$

We apply the curl operator  $\underline{\nabla} \times$  to Equation (2.1): the vertical component of the resultant gives:

$$\left( \frac{\partial}{\partial t} + \underline{V} \cdot \underline{\nabla} + \dot{\sigma} \frac{\partial}{\partial \sigma} \right) (\nabla^2 \psi + f) + \left[ (\nabla^2 \psi + f) \nabla^2 \chi + \left( \underline{\nabla} \dot{\sigma} \times \frac{\partial \underline{V}}{\partial \sigma} \right) \cdot \underline{k} \right] + R \underline{k} \cdot (\underline{\nabla} T \times \underline{\nabla} \pi \frac{\sigma}{p}) = \underline{k} \cdot (\underline{\nabla} \times \underline{F}) . \quad (2.9)$$

The dot-differentiation  $\underline{\nabla} \cdot$ , of (2.1) gives:

$$\left[ \left( \frac{\partial}{\partial t} + \dot{\sigma} \frac{\partial}{\partial \sigma} \right) \nabla^2 \chi + (\nabla^2 \chi)^2 + \underline{\nabla} \dot{\sigma} \cdot \frac{\partial \underline{V}}{\partial \sigma} \right] + \nabla^2 \Phi + R \underline{\nabla} \cdot (T \underline{\nabla} \pi \frac{\sigma}{p}) - f \nabla^2 \psi - \underline{\nabla} f \cdot \underline{\nabla} \psi - \underline{\nabla} (\underline{V} \cdot \underline{\nabla} \psi) = \underline{\nabla} \cdot \underline{F} \quad (2.10)$$

Equations (2.9) and (2.10) are respectively analogous to the vorticity equation and the divergence equation in the p- or z- coordinate systems. We neglect the terms quadratic in  $\chi$  and  $\dot{\sigma}$  in the vorticity equation, and all the terms involving either  $\chi$  or  $\dot{\sigma}$  in the divergence equation; this yields

$$\frac{\partial}{\partial t} \nabla^2 \psi = -\underline{\nabla} \cdot \{ (\nabla^2 \psi + f) \underline{V} \} - \underline{\nabla} \cdot (\dot{\sigma} \underline{\nabla} \frac{\partial}{\partial \sigma} \psi) - \underline{k} \cdot (\frac{\sigma R}{p} \underline{\nabla} T \times \underline{\nabla} \pi) + \underline{k} \cdot (\underline{\nabla} \times \underline{F}) \quad (2.11)$$

$$\nabla^2 \phi + \sigma R \underline{\nabla} \cdot (\frac{T}{p} \underline{\nabla} \pi) - \underline{\nabla} \cdot (f \underline{\nabla} \psi) + \frac{1}{2} \nabla^2 (\underline{\nabla} \psi \cdot \underline{\nabla} \psi) - \underline{\nabla} \cdot \{ (\nabla^2 \psi) \underline{\nabla} \psi \} = 0. \quad (2.12)$$

The second equation is the so-called balance equation, which expresses the balance constraint between mass distribution and motion and, according to Thompson (1956) and Bolin (1956), filters out gravity waves.

Equations (2.11) and (2.12) may replace (2.1) and form a complete system of equations with Eqs. (2.2) to (2.8). The complete system obtained by this replacement is the system of balance equations in  $\sigma$  coordinates; they are the equations governing our model. This balance system can be justified by a scale analysis, similar to the analysis of Charney (1962); such an analysis is beyond the scope of the present report.

The top and bottom boundary conditions are:

$$\dot{\sigma} = 0 \quad \text{at} \quad \sigma = 0, \quad \text{and} \quad \dot{\sigma} = 0 \quad \text{at} \quad \sigma = 1.$$

With these boundary conditions, (2.3) determines sea-level pressure tendency, namely,

$$\frac{\partial}{\partial t} \pi = - \int_0^1 \underline{\nabla} \cdot (\pi \underline{V}) d\sigma.$$

There is no need for lateral boundary conditions in a global model.

### 3.2.6.1.3 METHOD OF SOLUTION.

Since it is not possible to determine the fields of  $\chi$  and  $\dot{\sigma}$  diagnostically from the other fields, we seek  $\chi$  and  $\dot{\sigma}$  simultaneously with the other unknowns. To do so, we replace Equations (2.2) and (2.12) by their local time derivatives and treat  $\partial\psi/\partial t$ ,  $\partial T/\partial t$ ,  $\partial\pi/\partial t$ ,  $\partial\phi/\partial t$ ,  $\partial q/\partial t$ ,  $\chi$ , and  $\dot{\sigma}$  as unknowns of the new system of the equations. After substitution and rearranging terms, the new system of equations may be rewritten as follows:

$$\begin{aligned} \frac{\partial}{\partial t} \nabla^2 \psi = & -(\underline{k} \times \underline{\nabla} \psi) \cdot \underline{\nabla} (\nabla^2 \psi + f) - \underline{\nabla} \cdot \{ (\nabla^2 \psi + f) \underline{\nabla} \chi \} \\ & - \underline{\nabla} \cdot (\dot{\sigma} \frac{\partial}{\partial \sigma} \underline{\nabla} \psi) - \left( \frac{\sigma R}{p} \underline{\nabla} T \times \underline{\nabla} \pi \right) \cdot \underline{k} + \underline{k} \cdot (\underline{\nabla} \times \underline{F}) \end{aligned} \quad (3.1)$$

$$\begin{aligned} \frac{\partial}{\partial t} \left\{ R \nabla^2 \int_0^1 \frac{\pi T}{p} d\sigma + R \sigma \underline{\nabla} \cdot \left( \frac{T}{p} \underline{\nabla} \pi \right) - \underline{\nabla} \cdot (f \underline{\nabla} \psi) + \frac{1}{2} \nabla^2 (\underline{\nabla} \psi \cdot \underline{\nabla} \psi) \right. \\ \left. - \underline{\nabla} \cdot (\nabla^2 \psi \underline{\nabla} \psi) \right\} = 0 \end{aligned} \quad (3.2)$$

$$\begin{aligned} \frac{\partial}{\partial t} (\pi T) = & -(\underline{k} \times \underline{\nabla} \psi) \cdot \underline{\nabla} (\pi T) - \underline{\nabla} \cdot (\pi T \underline{\nabla} \chi) - \frac{\partial}{\partial \sigma} (\pi T \dot{\sigma}) \\ & - \frac{\sigma R \pi^2 T}{p C_p} (\nabla^2 \chi + \frac{\partial \dot{\sigma}}{\partial \sigma} - \frac{\dot{\sigma}}{\sigma}) + \frac{\pi}{C_p} Q \end{aligned} \quad (3.3)$$

$$\frac{\partial}{\partial t} \pi = -(\underline{k} \times \underline{\nabla} \psi) \cdot \underline{\nabla} \pi - \underline{\nabla} \cdot (\pi \underline{\nabla} \chi) - \frac{\partial}{\partial \sigma} (\pi \dot{\sigma}) \quad (3.4)$$

$$\frac{\partial}{\partial t} (\pi q) = -(\underline{k} \times \underline{\nabla} \psi) \cdot \underline{\nabla} (\pi q) - \underline{\nabla} \cdot (\pi q \underline{\nabla} \chi) - \frac{\partial}{\partial \sigma} (\pi q \dot{\sigma}) + \pi (E - C) \quad (3.5)$$

Equations (3.1) to (3.5) are solved for  $\partial\psi/\partial t$ ,  $\partial T/\partial t$ ,  $\partial\pi/\partial t$ ,  $\partial q/\partial t$ ,  $\chi$ , and  $\dot{\sigma}$  with the top and bottom boundary conditions,

$$\dot{\sigma} = 0 \quad \text{at} \quad \sigma = 0 \quad \text{and} \quad \sigma = 1. \quad (3.6)$$

Our model atmosphere is global and hence no physical lateral boundaries are present. This is an important advantage, since fictitious boundaries cause errors that eventually propagate throughout the computational domain. Because of the lack of a suitable global plane projection which does not seriously distort some areas, however, the difficulties associated with lateral boundary conditions do not completely vanish in a global model. If two or more plane projections are "patched" together to represent the globe, difficulties arise in the patching area. If a spherical coordinate system is employed, care must be taken to avoid singularities at the poles while asymmetry will still be allowed there. The use of the scalars  $\psi$ ,  $\chi$  instead of the two-vector  $\underline{V}$  is an important advantage in this respect.

Our model uses a multi-level latitude-longitude grid system. Both poles are grid points. At each pole, we treat each discrete variable as the average over the area bounded by the latitude circle half-way between the pole and its neighboring grid points, and Equations (3.1) to (3.5) are averaged over this area. The areal integration of the divergence or the curl of a horizontal vector is respectively reduced to meridional fluxes across or zonal circulation along the previously mentioned latitude circle.

The numerical procedure of our solution method is primarily a block relaxation method. It is described below. We start from a certain first guess of the dependent variables, and then successively adjust the variables block by block until the solution is



reached within a certain error. Each block consists of all the discrete dependent variables along a vertical line of fixed latitude and longitude.

In our multi-level latitude-longitude grid system, the discrete dependent variables are only staggered in the vertical direction;  $\delta$  is represented at the mid-point between the levels, while all the other variables are represented at each level. The Jacobian representing advection in the vorticity equation is approximated by Arakawa's (1972) scheme. Other nonlinear transport and divergence terms in the system of equations are approximated by the box method, and the usual centered difference scheme is employed in the remaining terms. In terms of the discrete variables in the grid, Equations (3.1) to (3.4) may be written for an N-level model as follows:

$$\sum_{m=1}^{4N} A_{p,m}(i,j) X_m(i,j) = B_p(i,j), \quad \begin{array}{l} p = 1, 2, \dots, 4N, \\ i = 1, 2, \dots, I, \\ j = 1, 2, \dots, J; \end{array} \quad (3.7)$$

where, for each horizontal grid point  $(i,j)$ , the 4N-dimensional vector  $X_m(i,j)$ , is the transpose of

$$\left\{ \left( \frac{\partial \psi}{\partial t} \right)_{ij1}, \dots, \left( \frac{\partial \psi}{\partial t} \right)_{ijN}, \left( \frac{\partial T}{\partial t} \right)_{ij1}, \dots, \left( \frac{\partial T}{\partial t} \right)_{ijN}, x_{ij1}, \dots, x_{ijN}, \right. \\ \left. \delta_{ij, \frac{1}{2}}, \dots, \delta_{ij, N - \frac{1}{2}}, \left( \frac{\partial \pi}{\partial t} \right)_{ij} \right\}.$$

The  $4N \times 4N$  matrix,  $A_{pm}(i,j)$ , is a function of  $\pi$ ,  $\psi$ , and  $T$  only, while the  $4N$ -dimensional vector,  $B_p(i,j)$ , is not only a function of  $\pi$ ,  $\psi$ , and  $T$ , but also a function of  $X_m(i',j')$ ,  $(i',j') \neq (i,j)$ .

For given initial conditions,  $T$ ,  $q$ ,  $\pi$ , and  $\underline{v}$  at  $t = t_0$ , the equation

$$\nabla^2 \psi = \underline{k} \cdot (\underline{v} \times \underline{v})$$

is solved for  $\psi$ . The first guess for  $X_m(i,j)$  is then obtained follows:  $\chi$  is set equal to zero everywhere;  $\sigma$  and  $\partial\pi/\partial t$  are computed from the continuity equation and the boundary condition (3.6); finally,  $\partial\psi/\partial t$  and  $\partial T/\partial t$  are computed from the vorticity equation and the first law of thermodynamics, respectively. For  $t$  greater than  $t_0$ , the first guess of  $X_m(i,j)$  takes the final value of  $X_m(i,j)$  at the previous time step.

The integration of Equations (3.1) to (3.6) consists simply in the following algorithm:

(a) Given  $\psi$ ,  $\pi$ ,  $T$ ,  $q$ , and a first guess of  $X_m(i,j)$  at time  $t$ , compute the forcing functions  $\underline{F}$ ,  $Q$ ,  $E-C$ , and the coefficient matrices  $A_{pm}(i,j)$ .

(b) Perform block relaxation; i.e., for fixed  $(i,j)$  compute  $B_p(i,j)$  for all  $p$ , using the current  $X_m(i',j') \neq (i,j)$ ; then solve (3.7) for new  $X_m(i,j)$ ,  $m = 1, 2, \dots, 4N$ ; do this for all  $(i,j)$

successively. Repeat the process until for each  $m$  the differences between the corresponding vectors  $X_m(i,j)$  of two consecutive iterations become less than  $\epsilon \cdot \text{Max}(X_m)$ , for all  $(i,j)$ , where  $\epsilon$  is a small prescribed constant.

(c) Calculate  $\psi$ ,  $\pi$ , and  $T$  at  $t+\Delta t$  from the final  $x_m(i,j)$  of (b) by a leap-frog scheme (use forward extrapolation for the first time step).

(d) Make a convective adjustment if the temperature lapse rate becomes superadiabatic.

(e) Calculate  $q$  at  $t + \Delta t$  directly from (3.5).

Steps (a) through (e) are performed first for  $t = t_0$ , then for  $t = t_0 + \Delta t$ ,  $t_0 + 2\Delta t$  and so on, until  $t$  equals the time up to which we wish to forecast.

In closing this section, we wish to point out that the replacement of the original diagnostic balance equation by its prognostic form relaxes the balance requirement while still preserving the filtering property. In other words, because the model uses the balance relation between the time change of the wind field and that of the mass field, the initial wind and mass fields need not be balanced, and accordingly, the predicted wind and mass fields are not necessarily in balance. However, the amount of imbalance in the initial data is preserved throughout the integration, and not increased.

### 3.2.6.1.4 SOME PRELIMINARY TESTS.

The version of the balance-equation model that was tested has three levels and a horizontal grid-spacing of  $4^{\circ}$  latitude and  $5^{\circ}$  longitude. The ground surface height at each grid point is the same as in the GISS primitive-equation (PE) model (Somerville et al., 1974). Friction and non-adiabatic heating were not included. The data sets used for the initial conditions were horizontal wind, temperature, and surface pressure spatially interpolated to the GISS grid from the National Meteorological Center's objective analysis. The predicted sea-level pressure and 500-mb geopotential height fields after every 12-hour interval following the initial conditions were compared with the corresponding NMC analysis, and the  $S_1$  skill-scores (see, for instance, Druyan, 1974, for definition) and root-mean-square errors were computed.

In a few tests, our model forecasts were also compared with the forecasts made by the three-level, adiabatic and frictionless version of the GISS PE model (A. Bayliss, personal communication, 1976) using the same initial conditions. In one case, further comparison was made with a 24-hour forecast by the nine-level, adiabatic and frictionless version of the GISS PE model.

The length of the time step  $\Delta t$  was 0.5 hour for some tests and 1 hour for the others. When  $\Delta t = 1h$  was used, smoothing was performed near the poles. For the initial time step the convergence

of our iterative method is slow, because we started with  $\chi = 0$  everywhere. It needed about 65 iterations to satisfy the convergence test with  $\epsilon = .005$ . Afterwards, convergence was reached in 5 to 10 iterations for  $\epsilon = .01$ .

Each test was terminated after 48 or after 60 hours depending on the quality of the forecast. We focused our attention particularly on the quality of the forecasts over the United States and neighboring areas, because the verification of the forecasts is more reliable over this region.

The quality of the model forecast varied considerably from one test to another. The worst and the best test cases, respectively, are the forecasts made from initial conditions at 00Z January 1, 1975 and 00Z August 18, 1975, respectively. Tables 21 and 22 show the  $S_1$  skill scores and rms errors in the predicted sea-level pressure and 500-mb geopotential height fields in the former and the latter cases, respectively. For comparison, we also show in the tables skill scores and rms errors for the corresponding forecasts made by the three-level, frictionless and adiabatic version of the GISS model. It is clear from the tables that at least for the three-level frictionless and adiabatic version of the models, the balance-equation (BE) model, even at its worst, is equal to or better than the PE model.

In the remainder of this section we discuss four test cases in some detail. The first one is the worst case mentioned above. Figure 9 shows: (a) the initial sea-level pressure (SLP)

Table 21.  $S_1$  skill scores and rms errors of the forecasts made with the 3-level, adiabatic frictionless versions of the balance-equation (BE) and primitive-equation (PE) models with initial data as of 00Z January 1, 1975.

Elapsed Time	Region	Sea-Level Pressure Error				500 mb Height Error			
		$S_1$ (%)		rms(mb)		$S_1$ (%)		rms(m)	
		BE	PE	BE	PE	BE	PE	BE	PE
12 hours	A	51.3	57.6	4.0	5.9	28.7	35.7	47.2	54.8
	B	49.8	74.2	1.8	3.6	49.3	61.4	14.8	21.2
	C	50.1	56.8	5.3	6.1	32.0	36.7	55.8	59.7
	D	52.8	61.9	4.6	5.9	40.7	44.7	55.3	61.0
24 hours	A	69.9	73.6	7.2	8.1	48.6	51.5	73.8	74.5
	B	59.5	82.0	2.7	2.9	62.9	65.8	31.0	25.1
	C	67.1	71.9	6.9	7.3	43.7	44.8	64.5	64.9
	D	66.0	72.3	6.4	6.9	49.5	49.9	61.7	62.5

Region A: 22°N - 62°N and 40°W - 140°W  
 B: 22°S - 22°N  
 C: North of 22°  
 D: Global

Table 22. Same as Table 21, but for initial conditions as of  
00Z August 18, 1975

Elapsed Time	Region	Sea-Level Pressure Error				500 mb Height Error			
		S <sub>1</sub> (%)		rms (mb)		S <sub>1</sub> (%)		rms (m)	
		BE	PE	BE	PE	BE	PE	BE	PE
12 hours	A	40.4	71.4*	2.1	4.3*	32.9	34.4	25.0	41.6
	B	42.5	77.8	1.5	3.4	52.1	67.7	12.6	22.5
	C	41.1	55.9	2.3	3.7	35.5	36.8	25.6	30.7
	D	44.4	57.6	3.9	4.5	40.3	41.8	37.8	37.6
24 hours	A	56.8		3.4		39.6		31.4	
	B	53.1		2.3		59.0		16.8	
	C	56.0		4.1		42.7		39.9	
	D	60.7		7.0		48.8		66.0	

Region A: 26°N - 78°N and 40°N - 140°N

B: 22°S - 22°N

C: North of 22°N

D: Global

\*Computed for a region somewhat smaller than region A.

distribution over North America and the neighboring oceans at 00Z January 1, 1975, (c) the observed SLP distribution at 00Z January 2, 1975, (b) and (d), the 24-hour forecasts by the three-level BE model and by the three-level PE model, respectively.

The observed significant synoptic developments in this area during the 24-hour period from 00Z January 1 to 00Z January 2 were as follows. The high pressure near the west coast moved eastward across the United States. A cyclone deepened rapidly on the Atlantic coast. A deep extensive low in the high latitudes moved eastward. The high pressure over the eastern Pacific pushed nearly northward. On the northwest side of the high pressure a low pressure moved northeastward as it deepened rather quickly. Both models did not predict these developments satisfactorily.

The intensity of the East Coast cyclone is accurately predicted by both models, but the forecast center position is far inland, and the PE forecast is slightly worse. The movement of the high-latitude low is well predicted by both models, but false intensification is apparent and strong in both model predictions. Again, the PE prediction is slightly worse. The deepening of the Pacific low is not predicted by either model, and in this respect our model makes a poorer prediction. In both model predictions the movements of the low are too slow.

The northward movement of the eastern Pacific high is well predicted by both models; the predicted center pressures, however, are much too high, and the PE forecast appears worse. Our model's prediction of the movement of the high pressure system over the Central part of the United States is much too slow, and the predicted center pressure is again much too high. The PE model prediction is even worse. Over the western part of the United States, both model predictions are



disastrous. In general, the overall sea-level pressure gradients in Figures 9b and 9d are obviously stronger than in Figure 9c.

Figure 10 shows: (a) the initial 500-mb geopotential height distribution at 00Z January 1, 1975, (b) the 24-hour forecast by our model, (c) the observed distribution at 00Z January 2, 1975, and (d) the 24-hour forecast by the three-level, frictionless and adiabatic version of the GISS model. It is clear that the predicted movements of the low troughs and high ridges are too slow in both models.

Both models failed in predicting the following important developments: (1) the developing of a ridge over the central part of the United States, (2) the relative decrease in height over the Rocky Mountains, and (3) the developing of a shallow trough along  $155^{\circ}$  W.

The next test case we discuss started with the initial conditions at 00Z January 2, 1975. The initial sea-level pressure and 500-mb geopotential height fields are shown in Figures 9c and 10c, respectively. Figure 11 shows: (a) the 24-hour forecast of sea-level pressure for 00Z January 3, 1975, made by our three-level model, (b) the observed sea-level pressure at 00Z January 3, (c) and (d) the 24-hour forecasts of sea-level pressure made by the three- and nine-level frictionless adiabatic versions of the GISS PE model, respectively. Clearly, all model predictions of sea-level pressure have much stronger gradients than the observed. This must be due to the exclusion of friction and nonadiabatic heating, since the skill of the nine-level GISS PE model (with friction and non-adiabatic heating included) has been well demonstrated (Somerville, et al., 1974; Druyan, 1974). It is quite surprising that the sea-level pressure forecast by our

three-level model (Fig. 11a) is as accurate as the forecast by the nine-level no-forcing version of the GISS model (Fig. 11d), and even somewhat better than it. The skill of the three-level PE forecast (Fig. 11c) is obviously the worst.

The forecasts of 500-mb geopotential height made by the three models and the observed height distribution at 00Z January 3, 1975, are shown in Fig. 12. The forecast by our three-level model (Fig. 12a) looks almost like a copy of the nine-level PE model (Fig. 12d). Both forecasts miss the closed isolines over the Gulf of St. Lawrence and the Gulf of Mexico. The predicted trough over Nebraska is weaker, and the predicted low over Greenland is deeper than the corresponding observed features in both forecasts. There is no observed trough or ridge over the northeast Pacific like there is both forecasts. Clearly, the forecast by the three-level PE model is again much worse than the forecast by our three-level model.

The third test case we discuss started with initial conditions at 00Z August 18, 1975. Fig. 13 shows: (a) the initial sea-level pressure, (b) the 24-hour forecast by our model, and (c) the observed sea-level pressure at 00Z August 19, 1975. During this 24-hour period the observed features of the circulation developed as follows: the Arctic high pressure moved eastward; the pressure systems over the northeastern Pacific were stationary, while the Aleutian low deepened slightly; the pressure systems over North America were also stationary, but the low pressure near the Rocky Mountains deepened; the low pressure over the Atlantic moved slowly northeastward; the high

center behind it was about to combine with the Atlantic high. All these features are predicted quite well, except that the predicted Atlantic low moved slower and the low pressure, which was originally centered near the Rocky Mountains, was predicted to shift into a wrong position.

Fig. 14 shows: (a) the initial 500-mb geopotential height distribution, (b) the 24-hour forecast by the model, and (c) the observed distribution at 00Z August 19, 1975. The intensity of the centers and the positions of the troughs and ridges are well predicted, except that the predicted geopotential heights over the east Atlantic near the African coast are too high. The computed skill scores and rms errors (Table 22) also indicate good agreement between forecast values and observed values.

The last test case was started with initial conditions at 00Z August 19, 1975; the initial sea-level pressure and the 500-mb geopotential are shown in Figures 13c and 14c. Figures 15a and 15b show the 24-hour forecasts of sea-level pressure and 500-mb geopotential height, respectively. Figures 15c and 15d show the observed sea-level pressure and the 500-mb geopotential height at 00Z August 20, 1975, respectively. During the 24-hour period, the center of the eastern Pacific high moved northeastward. The Aleutian low weakened. The Arctic high moved eastward and weakened. The low pressure over the western

part of the United States was almost stationary, but weakened. The cyclone over the eastern part of Canada moved eastward to the sea and intensified. The high pressures over the east and west Atlantic combined into one with greater intensity. The Atlantic low moved northeastward and intensified. These features are rather well predicted by the model, except that the weakening of the low pressure over the western part of the United States is not predicted and that the predicted center position of the low is incorrect. The positions and intensities of the 500-mb lows, troughs and ridges are also predicted rather well. However, the predicted geopotential heights over the region southwest from the west coast of the United States are slightly higher, and the predicted gradients along the Atlantic trough are somewhat stronger than the observed.

It has been mentioned in the above discussion that the pressure systems of the 24-hour forecast in the January cases are too strong. In the August cases, the same kind of error becomes apparent in the 48-hour forecasts. Figures 16a and 16c show the 48-hour forecasts of sea-level pressure and 500-mb height (24 hours after Figures 15a and 15b), respectively. As compared with the corresponding plots of observed quantities (Figures 16b and 16d), the false intensifications are clearly seen. We expect, according to our experience with the PE model, that the over-predicted pressure gradients will disappear or be largely

reduced when frictional dissipation and nonadiabatic heating and cooling are included in the model in an adequate form. When these physical mechanisms are included in the model, it will be meaningful to test the model further beyond one day.

### 3.2.6.1.5 SUMMARY AND CONCLUDING REMARKS

A multi-level balance-equation model of the global atmosphere is developed in a spherical sigma coordinate system. The model equations are the vorticity equation, the balance equation, and the laws of conservation of thermal energy, of mass and of moisture. An iterative numerical method is used for the time integration of this highly implicit system of equations. Some test forecasts have been made with a three-level adiabatic and frictionless version of the model, using a latitude-longitude grid with  $4^{\circ}$  spacing in latitude and  $5^{\circ}$  in longitude. Global objective analyses made available by the National Meteorological Center, NOAA, were used to obtain the initial conditions and also to verify the forecasts. Some forecast examples are shown and compared with predictions by two versions of a primitive-equation (PE) model.

The results demonstrate: (a) that it is feasible to construct a global filtered model on the basis of the balance equations, (b) that a limited number of forecasts made with such a model compare favorably to forecasts made with an analogous version of a PE model, and (c) that, even for short-range weather predictions, the complete success of a balance equation model will depend

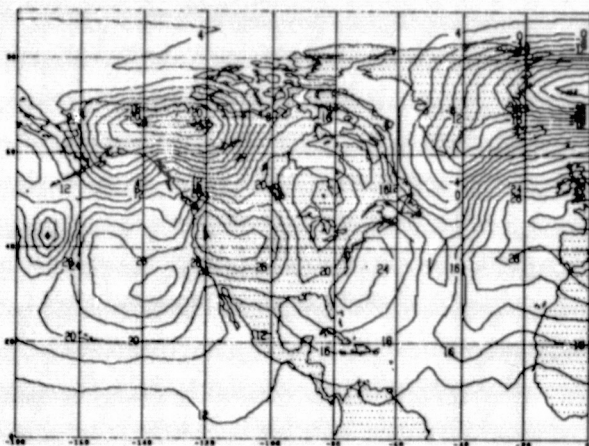


Fig. 9a. Initial sea-level pressure (mb-1000), valid 0000 GMT 1 January 1975.

ORIGINAL PAGE IS  
OF POOR QUALITY

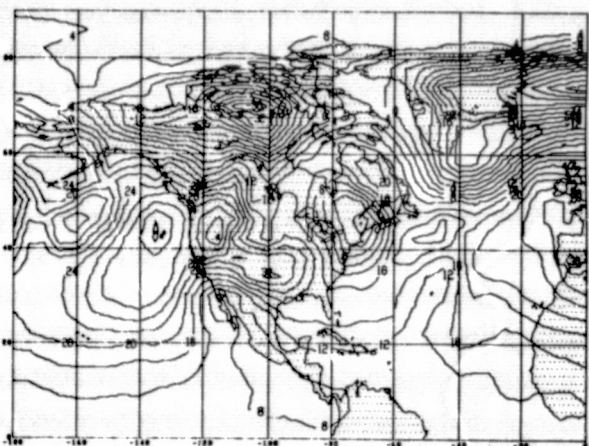


Fig. 9b. The 24-hr forecast sea-level pressure (mb-1000) by 3-level PE model, valid 0000 GMT 2 January 1975.

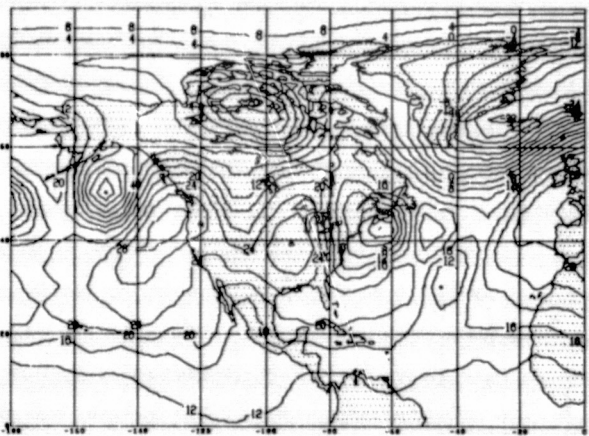


Fig. 9c. The observed sea-level pressure (mb-1000) valid 0000 GMT 2 January 1975.

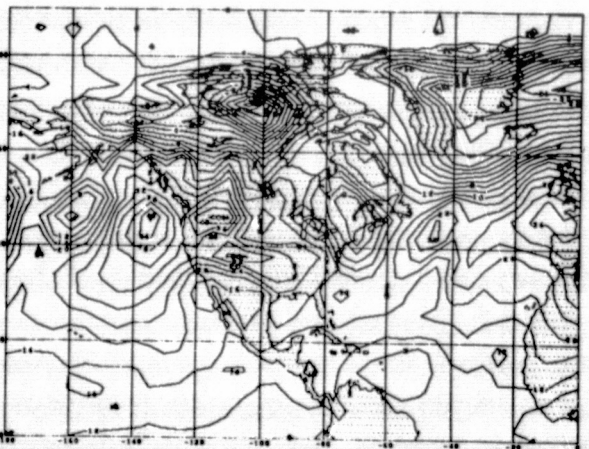


Fig. 9d. The 24-hr forecast sea-level pressure (mb-1000) by 3-level PE model, valid 0000 GMT 2 January 1975.

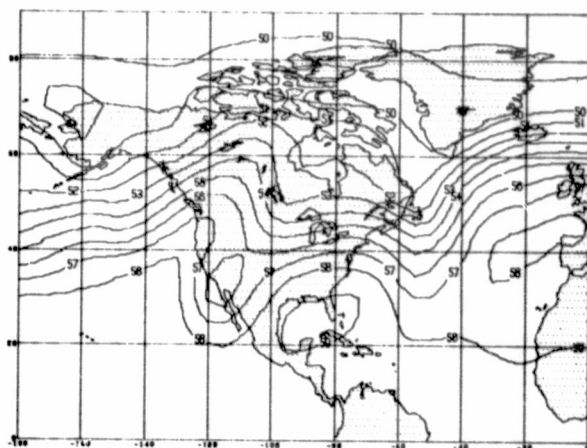


Fig. 10a. Initial 500mb heights (100m), valid 0000 GMT 1 January 1975.

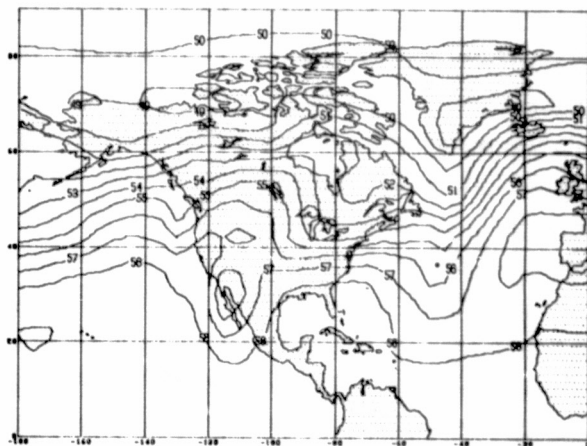


Fig. 10b. The 24-hr forecast by 3-level BE model, 500mb heights (100m), valid 0000 GMT 2 January 1975.

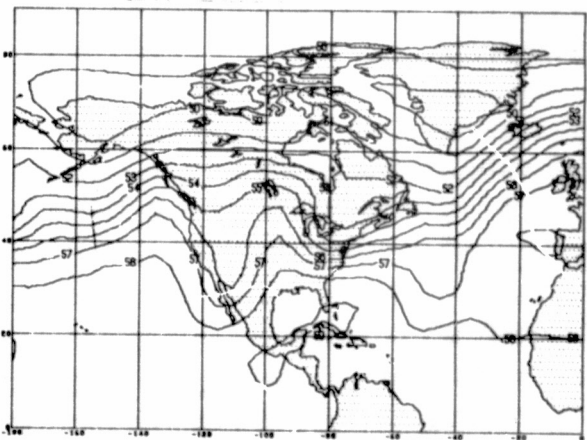


Fig. 10c. The observed 500mb heights (100m), valid 0000 GMT 2 January 1975.

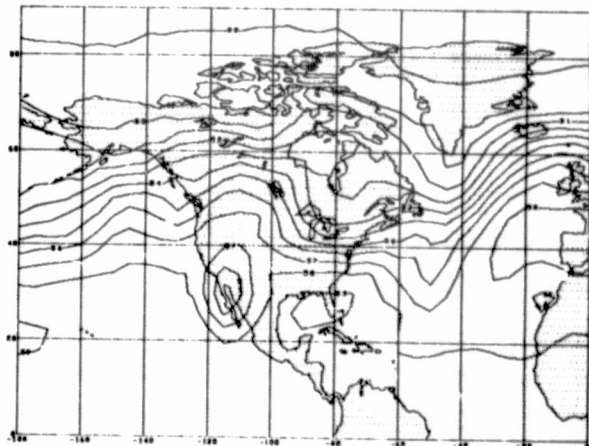


Fig. 10d. The 24-hr forecast 500mb heights (100m) by 3-level PE model, valid 0000 GMT 2 January 1975.



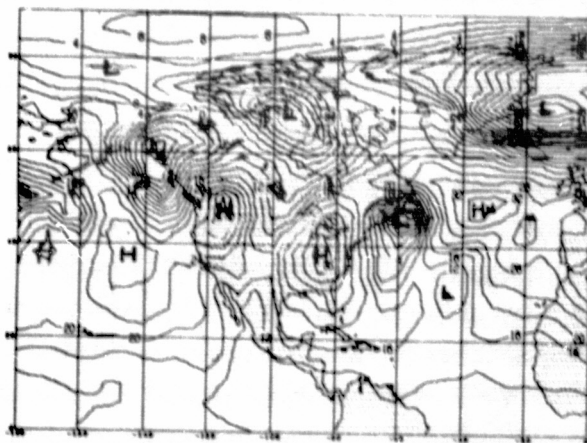


Fig. 11a. The 24-hr forecast sea-level pressure (mb-1000) by 3-level BE model, valid 0000 GMT 3 January 1975.

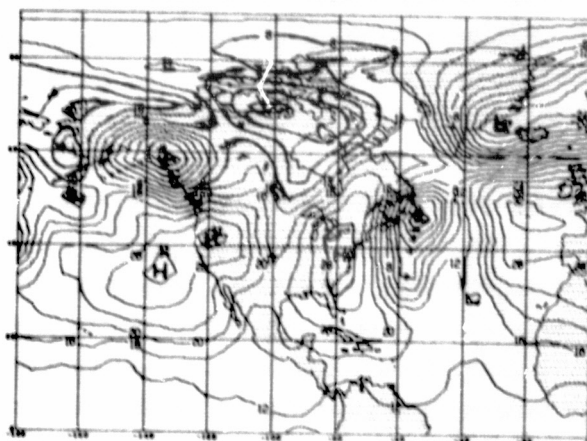


Fig. 11b. The observed sea-level pressure (mb-1000), valid 0000 GMT 3 January 1975.

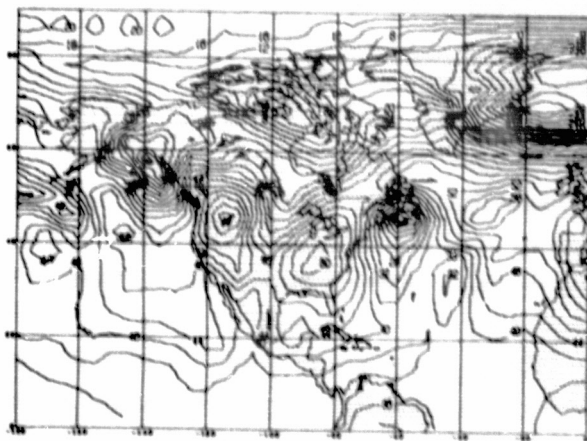


Fig. 11c. The 24-hr forecast sea-level pressure (mb-1000) by 3-level PE model, valid 0000 GMT 3 January 1975.

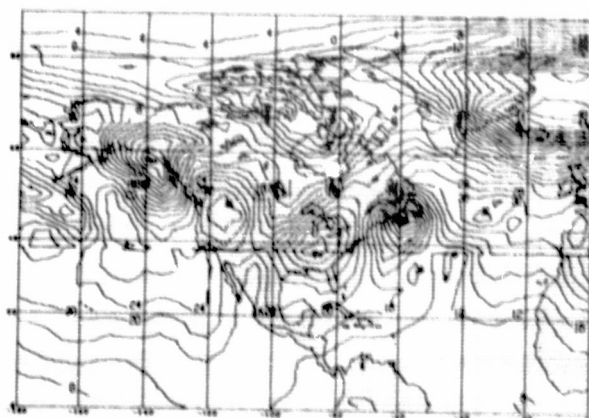


Fig. 11d. The 24-hr forecast sea-level pressure (mb-1000) by level P6 model, valid 0000 GMT 3 January 1975.

ORIGINAL PAGE IS  
OF POOR QUALITY



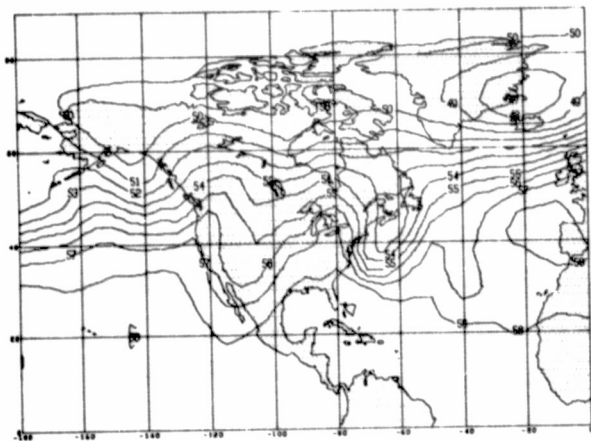


Fig. 12a. The 24-hr forecast 500mb heights (100m) by 3-level BE model, valid 0000 GMT 3 January 1975.

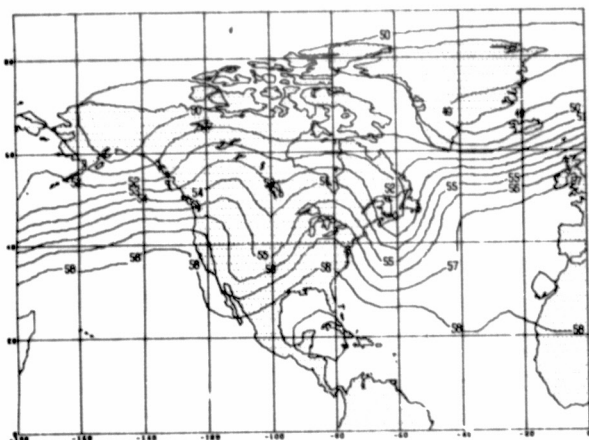


Fig. 12b. The observed 500mb heights (100m), valid 0000 GMT 3 January 1975.

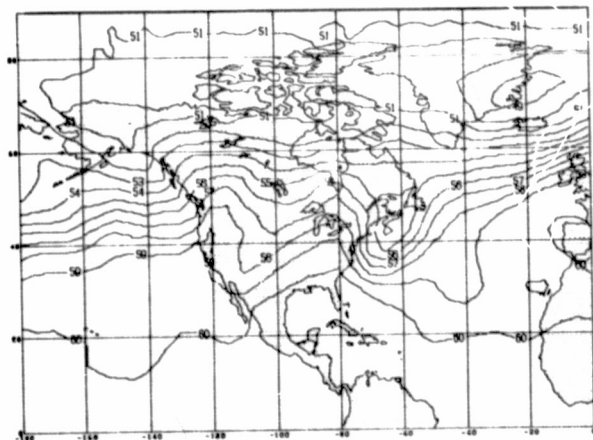


Fig. 12c. The 24-hr forecast 500mb heights (100m) by 3-level PE model, valid 0000 GMT 3 January 1975.

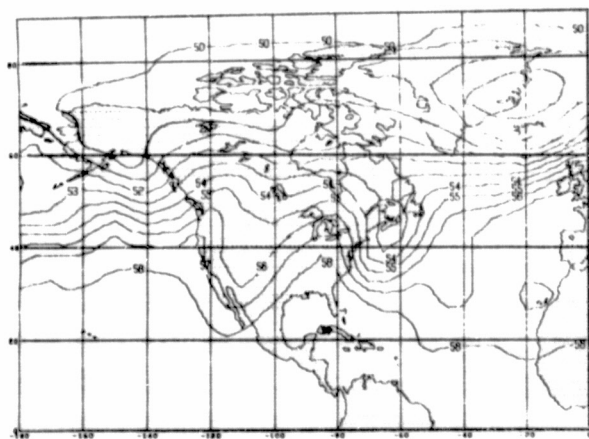


Fig. 12d. The 24-hr forecast 500mb heights (100m) by 9-level PE model, valid 0000 GMT 3 January 1975.

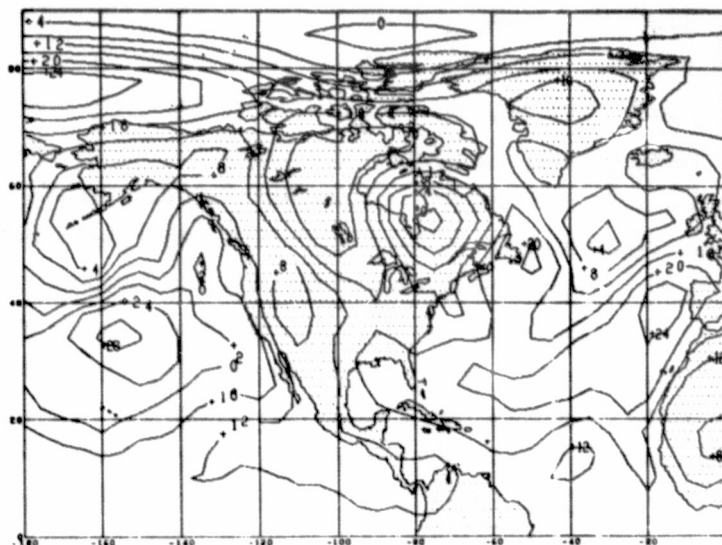


Fig. 13a. Initial sea-level pressure (mb-1000), valid 0000 GMT 18 August 1975.

ORIGINAL PAGE IS  
OF POOR QUALITY

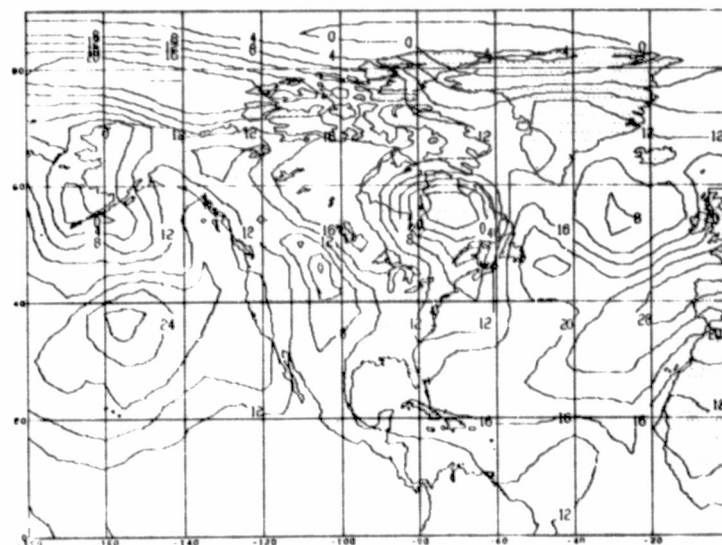


Fig. 13b. The 24-hr forecast sea-level pressure (mb-1000) by 3-level BE model, valid 0000 GMT 19 August 1975.

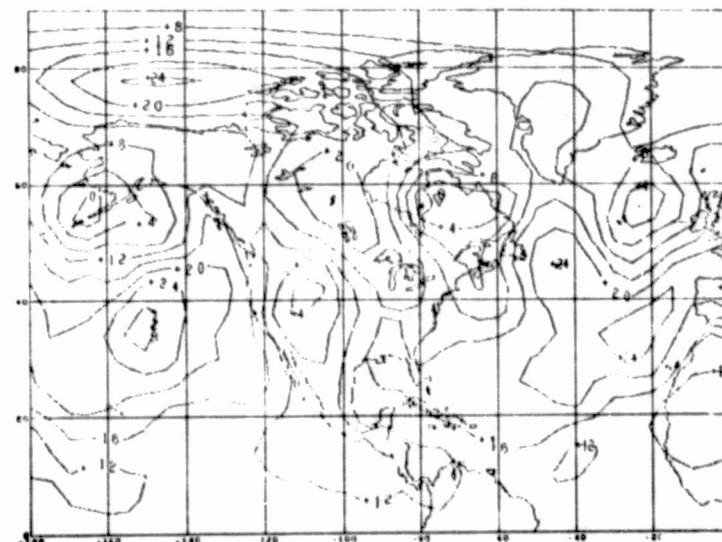


Fig. 13c. The observed sea-level pressure (mb-1000), valid 0000 GMT 19 August 1975.

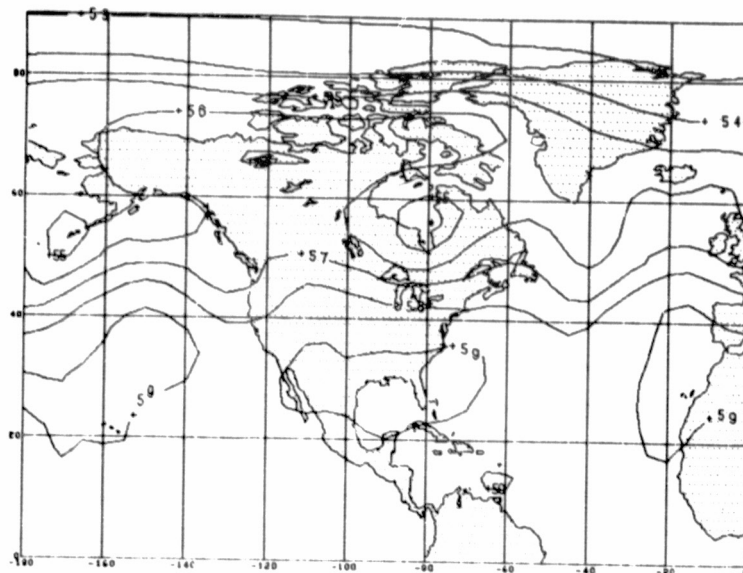


Fig. 14a. Initial 500mb heights (100m), valid 0000 GMT 18 August 1975.

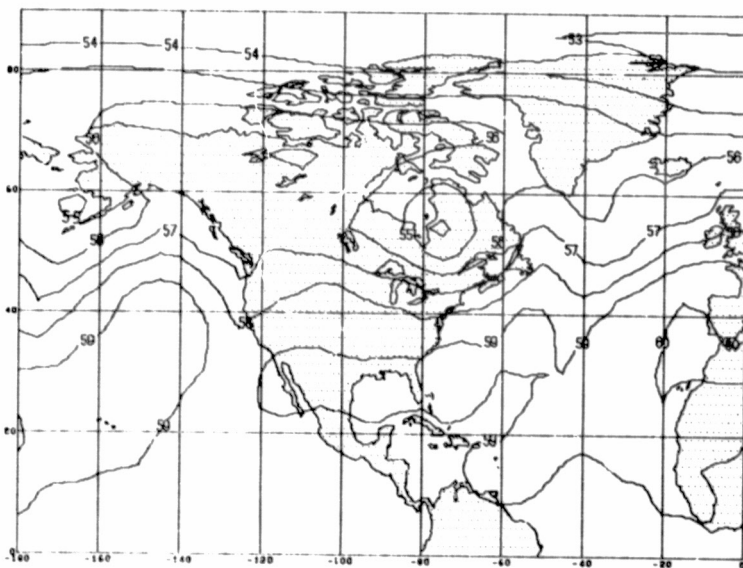


Fig. 14b. The 24-hr forecast 500mb heights (100m) by 3-level BE model, valid 0000 GMT August 1975.

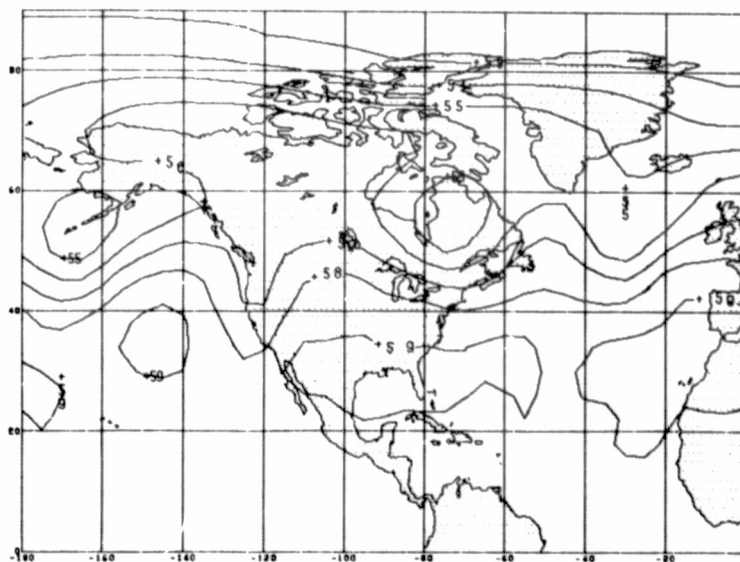


Fig. 14c. The observed 500mb heights (100m), valid 0000 GMT 19 August 1975.

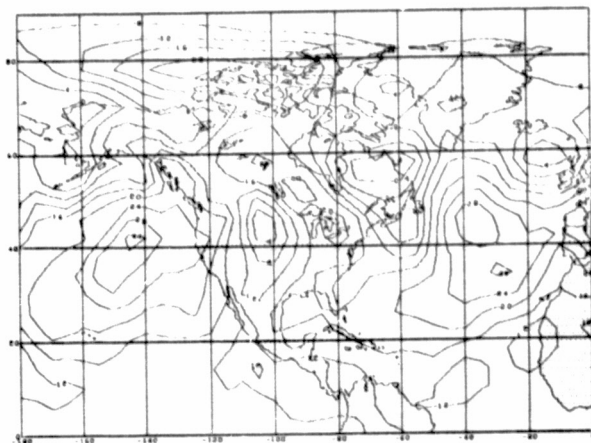


Fig. 15a. The 24-hr forecast sea-level pressure (mb-1000) by 3-level BE model, valid 0000 GMT 20 August 1975.

ORIGINAL PAGE IS  
OF POOR QUALITY

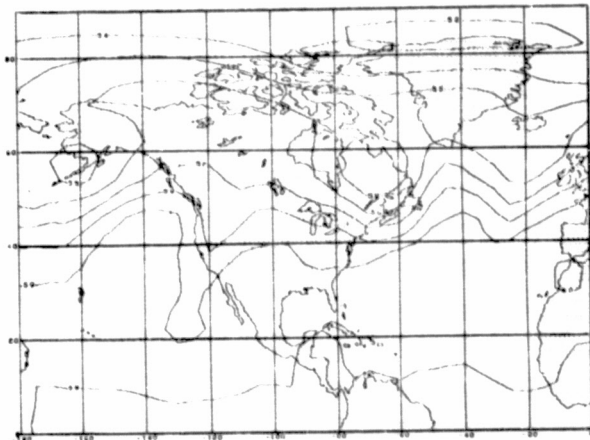


Fig. 15b. The 24-hr forecast 500mb heights (100m) by 3-level BE model.

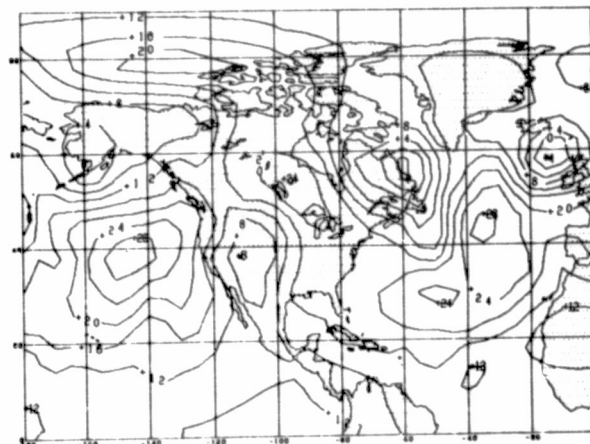


Fig. 15c. The observed sea-level pressure (mb-1000), valid 0000 GMT 20 August 1975.

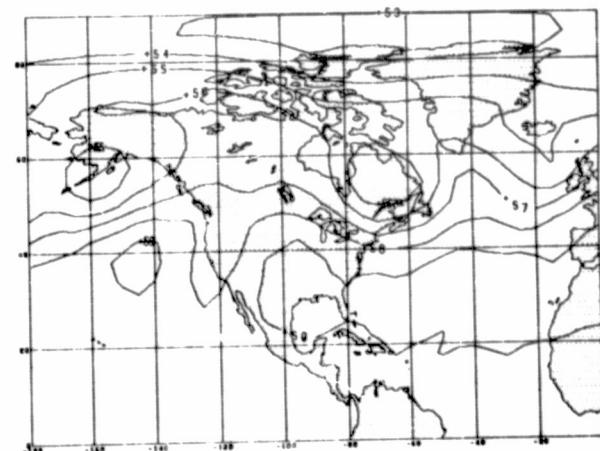


Fig. 15d. The observed 500mb heights (100m), valid 0000 GMT 20 August 1975.

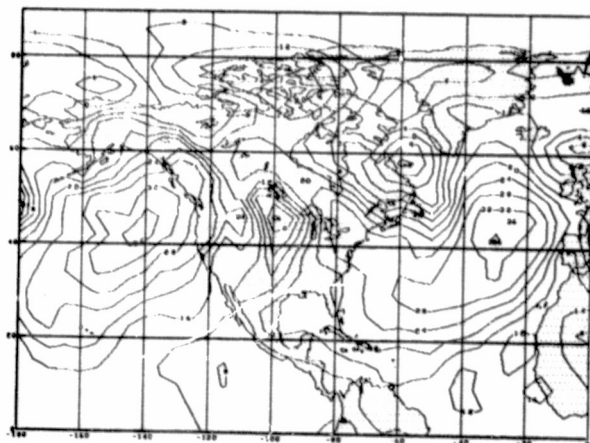


Fig. 16a. The 48-hr forecast sea-level pressure (mb-1000) by 3-level BE model, valid 0000 GMT 21 August 1975.

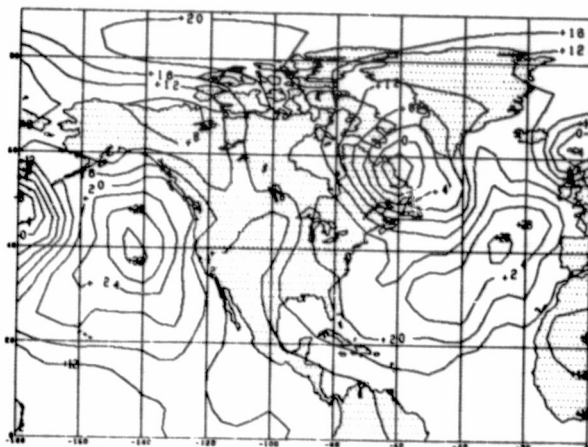


Fig. 16b. The observed sea-level pressure (mb-1000), valid 0000 GMT 21 August 1975.

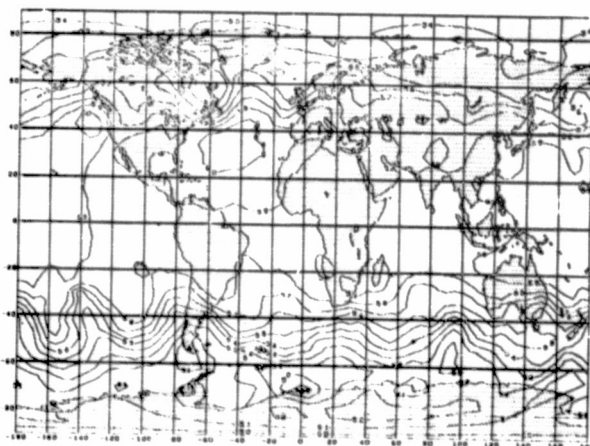


Fig. 16c. The 48-hr forecast 500mb heights (100m) by 3-level BE model, valid 0000 GMT 21 August 1975.

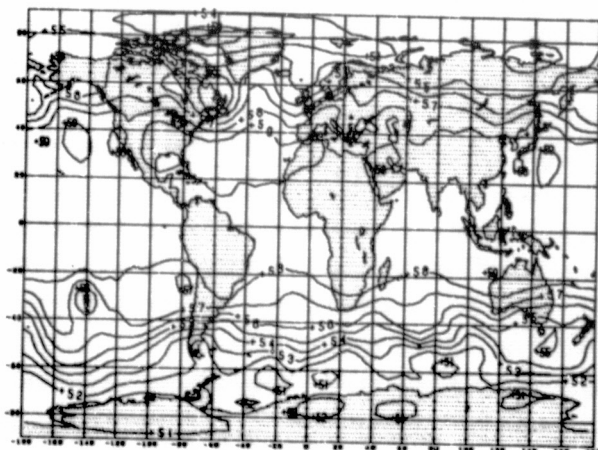


Fig. 16d. The observed 500mb heights (100m) valid 0000 GMT 21 August 1975.

crucially upon the careful parameterization of the diabatic heating (or cooling) and frictional dissipation processes. One must realize that the task of parameterizing various subscale forcing processes in a balanced equation model is even more difficult than the corresponding task in a PE model: in addition to all the parameterization difficulties confronting us in a PE model, we must successfully parameterize the dispersive effect of gravity waves on heat and momentum transports, particularly when the forcing on any scale exceeds the bound that limits the validity of the balance equations.

Besides the task of including forcing in the balance equation model more work needs to be done in order to make the method of solution more efficient and to improve the model in the region of steep mountains where forecast errors are generally larger.

### 3.2.6.2 FILTERED EQUATIONS METHOD, II: THE BALANCE-EQUATION MODEL AS A DATA ASSIMILATION TOOL

#### 3.2.6.2.1 INTRODUCTION

In Section 3.2.6.1 we described a balance-equation (BE) model. One of the main reasons for developing this model was to eventually use it as a data assimilation tool. In this section we describe some preliminary tests of using the BE model to help assimilate satellite-derived temperature data, in combination with the GISS 9-level primitive-equation (PE) model.

The nine-level version of the balance-equation model is still too time consuming and needs further evaluation and improvement. Hence, a successful test of using it exclusively to carry out data assimilation was not deemed useful at this stage. Instead, tests have been made to assess the potential of the BE model as a partial-balancing device in PE-model data assimilation.

### 3.2.6.2.2 THE METHOD

The basic idea of partial balancing can easily be described as follows. Define an atmospheric function,  $F$ , by

$$F(\psi, \phi, T, \pi) \equiv \underline{\nabla} \cdot (\underline{\nabla}\phi + \sigma\alpha \underline{\nabla}\pi) - \underline{\nabla} \cdot [(\underline{f} + \underline{\nabla}^2\psi)\underline{\nabla}\psi] + \frac{1}{2}\underline{\nabla}^2 (\underline{\nabla}\psi \cdot \underline{\nabla}\psi); \quad (2.1)$$

here  $\underline{\nabla}$  is the gradient operator in the  $\sigma$ -coordinate system,  $\psi$  is the stream function defined by  $\underline{\nabla}^2\psi = \underline{k} \cdot (\underline{\nabla} \times \underline{V})$ , and the other notations are conventional. Denote the local value of  $F$  by  $R$ , so that

$$F(\psi, \phi, T, \pi) = R; \quad (2.2)$$

this reduces to the well-known balance equation in the  $\sigma$ -coordinate system for  $R = 0$ . For nonzero  $R$ , we say that there exists inertial-gravitational imbalance in the atmosphere. In case of four-dimensional (4-D) data assimilation, excessive imbalance is generated as a result of the updating process. (See, for instance, Appendix

B.) Therefore, it is desirable at a certain stage of the assimilation to reduce the imbalance artificially, i.e., to find corrections  $\Delta\psi$ ,  $\Delta\phi$ ,  $\Delta T$  and  $\Delta\pi$  such that

$$F(\psi + \Delta\psi, \phi + \Delta\phi, T + \Delta T, \pi + \Delta\pi) = (1-\alpha)R$$

or,

$$F(\psi + \Delta\psi, \phi + \Delta\phi, T + \Delta T, \pi + \Delta\pi) - F(\psi, \phi, T, \pi) = -\alpha F(\psi, \phi, T, \pi),$$

where  $0 < \alpha < 1$ , and  $\alpha$  may be a function of space and time if desired. One way to find such increments is the following: regard the increments in the above equation as temporal changes, and substitute the above equation, instead of the balance equation proper, in the BE model; then solve for the required increments by integrating the model forward and backward about the current time  $t$ .

In the experiments we describe herein, the above partial-balancing procedure (PBP) was applied intermittently every 12 hours during the assimilation process. The total reduction of imbalance in each application of the procedure depends upon the number (ISTEP) of forward and backward time steps performed, on the length of the time interval ( $\Delta t$ ) used, and on the number of iterations (ITER) in each time step, since the balance-equation model uses an iterative method for time integration.



### 3.2.6.2.3 PRELIMINARY RESULTS

Nineteen assimilation experiments were run with DST-5 data, starting from 00Z August 18, 1975, and using different values of the parameters ISTEP, ITER and  $\Delta t$ , as well as different smoothing procedures when necessary. We were interested in the impact of the above-described PBP on the accuracy of forecasts started from initial conditions obtained with the aid of PBP. A number of 72- to 84-hour forecasts were made from such initial conditions with the GISS PE model. These forecasts were then compared with the corresponding forecasts of control experiments which were started from initial conditions obtained by using the same data assimilated by the direct insertion method, with geostrophic wind corrections (DIM, Subsection 3.2.1).  $S_1$  skill score and rms errors were computed for each forecast against the corresponding NMC objective analyses. Both the computed skill scores and rms errors seem to indicate that forecasts made from initial conditions assimilated with the aid of the PBP have generally no better skill than of forecasts made from the control initial conditions. Two typical examples are given below.

Table 23 shows the evaluation, over North America, of forecast run 7937 in which the initial conditions were taken from assimilation experiment 7936 after a two-day assimilation. In experiment 7936, ISTEP in each application of PBP is 2, i.e., marching forward and backward once, while  $\Delta t = 10$  min., and ITER = 6; the local time derivatives of  $\psi$ ,  $\phi$ , T and  $\pi$ , as well as  $\chi$  and  $\delta$  were smoothed

Table 23. The RMS errors and skill scores ( $S_1$ ) over North America of the forecast run 7937, as compared with the control forecast 7819. (In parentheses is the difference between the two forecasts. Positive sign means worse, negative sign means better.)

		Elapsed Time (hrs.)					
		12	24	36	48	60	72
Sea-level pressure	$S_1$ (%)	42.4 (+.5)	49.4 (+.4)	68.0 (+.5)	81.8 (+2.6)	96.2 (+3.6)	98.6 (+4.2)
	rms (mb)	1.57 (-.38)	2.07 (-.02)	3.04 (+.19)	3.97 (+.21)	5.64 (+.43)	6.67 (+.63)
500 mb heights	$S_1$ (%)	25.8 (+.7)	30.5 (-.6)	33.6 (+1.0)	41.5 (+1.0)	47.9 (-.6)	54.5 (-1.8)
	rms (m)	18.2 (+.9)	22.1 (-.5)	27.0 (+3.9)	33.6 (+2.9)	42.3 (+1.4)	58.0 (+.2)

Table 24. The RMS and skill scores ( $S_1$ ) over North America of the forecast run 7927, as compared with the control forecast 7819. (In parentheses is the difference between the two forecasts. Positive sign means worse, negative sign means better.)

		Elapsed Time (hrs.)					
		12	24	36	48	60	72
Sea-level pressure	$S_1$ (%)	49.2 (+7.3)	52.6 (+3.6)	69.0 (+1.5)	76.8 (-2.4)	90.2 (-2.4)	89.5 (-4.9)
	rms (mb)	2.43 (+.48)	2.21 (+.12)	3.36 (+.51)	4.10 (+.34)	5.38 (+.17)	58.5 (-1.0)
500 mb heights	$S_1$ (%)	35.0 (+9.9)	37.1 (+6.0)	36.5 (+3.9)	41.7 (+1.2)	47.0 (-.5)	51.6 (-4.7)
	rms (m)	27.6 (+10.3)	31.5 (+8.9)	36.3 (+3.2)	45.8 (+15.1)	44.6 (+3.7)	58.4 (+.6)

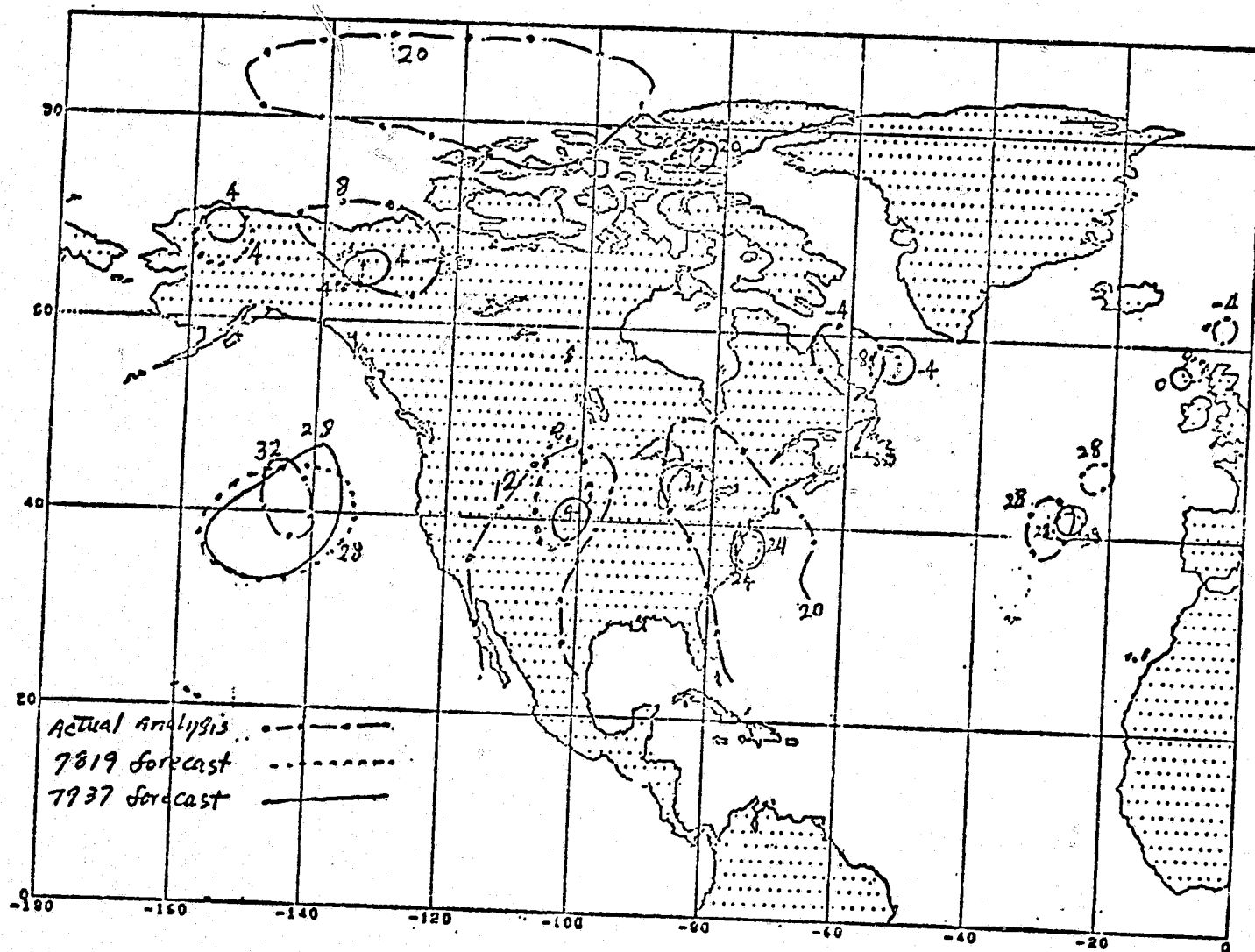


Figure 17. Sea-level pressure centers at 00Z August 21 forecast in experiments 7819 and 7927, as compared with actual analysis.

horizontally in each iteration by a 5-point averaging formula with equal weights for all points, including the center point. Table 23 indicates that forecast 7937 seems slightly better than the forecast of the control experiment 7819 at 24 h, but slightly worse thereafter. The slight skill improvement relative to the control in the 24-hour forecast is, however, not synoptically significant. Figure 17 shows a comparison of the forecast sea-level pressure centers plotted with their inner closed isobars.

Table 24 shows the evaluation, over North America, of forecast run 7927 in which the initial conditions were taken from assimilation experiment 7926 after a two-day assimilation. In 7926,  $ISTEP = 2$ ,  $\Delta t = 30$  min.,  $ITER = 4$ , and whenever the iterative method exhibited an instability, the temperature and vorticity fields were smoothed horizontally using a 5-point averaging formula with the center point weighted by 4, and the other four points weighted by 1. Table 24 reveals that the forecast skill of run 7927 is worse than that of control run 7819. After 60 hours the skill scores of 7927 show some improvement compared with those of 7819, but this statistical improvement has no synoptic significance at all. The sea-level pressure (SLP) fields for forecasts started from 03Z August 20 both in experiment 7927 and in experiment 7819, as well as the actual SLP analysis for 00Z August 23 are plotted in Figures 18 through 20, respectively. It is very clear that both forecasts miss completely the low pressure system, centered near ( $50^{\circ}N$ ,  $80^{\circ}W$ ), and the secondary low center close to Nova Scotia. The forecast fields for experiment 7927 are no better than those for control run 7819, except that the

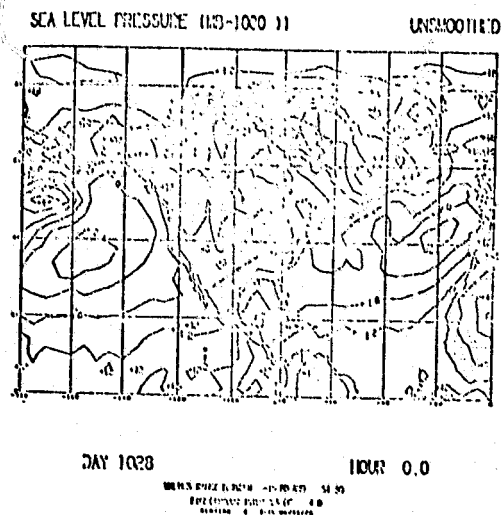


Figure 18. Sea-level pressure forecast for 00Z August 23 by run 7927.

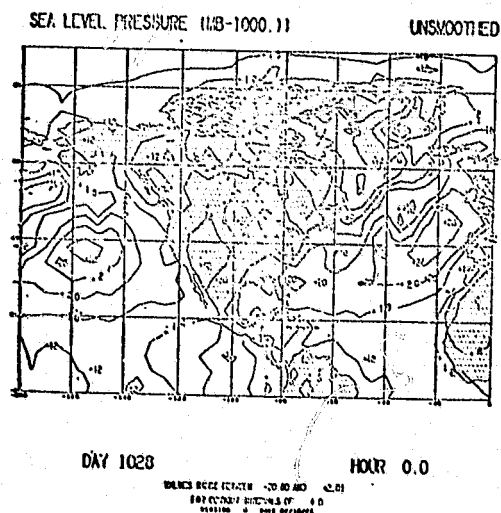


Figure 19. Sea-level pressure forecast for 00Z August 23 by run 7819.

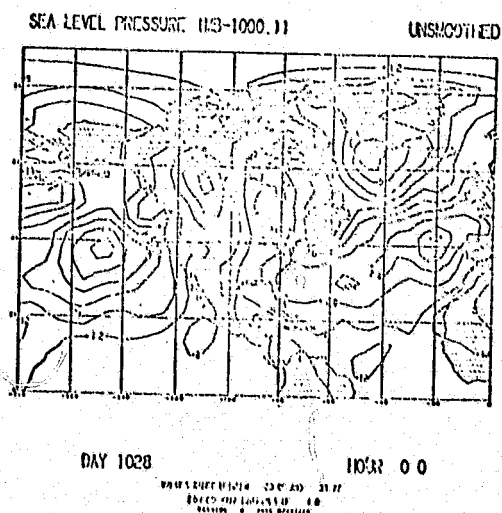


Figure 20. Actual analysis of sea-level pressure for 00Z August 23.

number of very small eddies are reduced. Furthermore, forecast 7927 weakens the two maritime semi-stationary high pressure centers in the verification region by a 4 mb more than the control forecast.

The above two examples indicate that, relatively speaking, the assimilation which averages horizontally the local time derivatives in each iteration is better than the assimilation which smoothes the temperature and vorticity fields themselves. There is an excess of smoothing in either case. It may be possible to find ways to reduce the excess smoothing.

#### 3.2.6.2.4 CONCLUDING REMARKS

The results of the experiments tend to indicate that the partial-balancing procedure described above does not provide a significant improvement in data assimilation over the straight forward procedure used for the control case. We note, however,

(a) that all the assimilation experiments were carried out only for a short period - mostly 2 days, and

(b) that during the assimilation period, most of the synoptic systems were semi-stationary and rather weak (see Figure 21).

Under these unfavorable circumstances, one hardly expects much benefit from assimilation. Since all the experiments were done within this single unfavorable period, it is proper to say that the test is inconclusive.

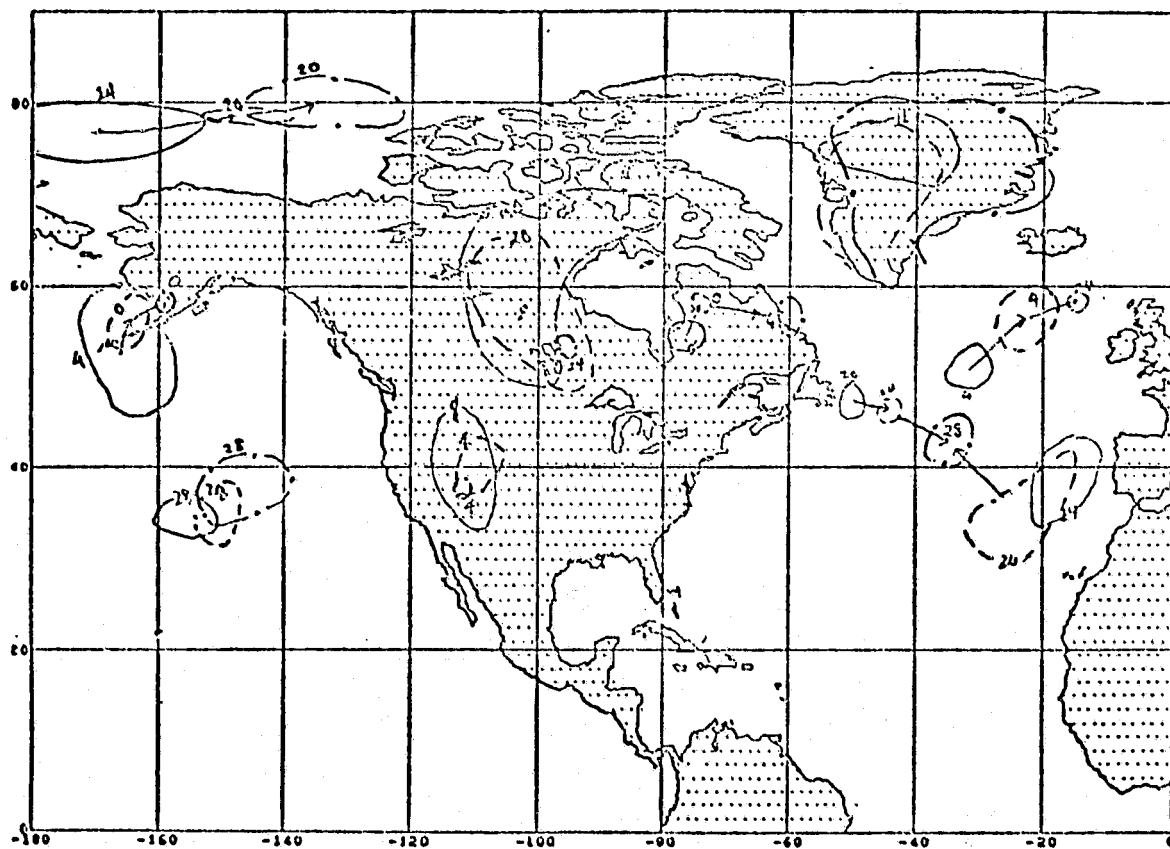


Figure 21. The Intensities and Trajectories of Sea Level Pressure Centers During the Period of the Assimilation Experiments.

### 3.2.7 STATISTICAL ASSIMILATION METHOD (M. Ghil, R. Dilling and H. Carus)

#### 3.2.7.1 INTRODUCTION

It is well known that observational systems do not provide values of the atmospheric variables which are entirely exact and accurate at any given time. Numerical weather prediction models attempt to give as close an approximation to future states of the atmosphere as possible, say 2 to 5 days in advance. For an accurate approximation of future values to be possible, it is necessary to start the prediction with the best possible approximation of the meteorological variables at the present, i.e., at the initial time of a numerical forecast.

In principle, information from observations at some initial time should be sufficient, at least in quantity if not in quality to determine the complete initial atmospheric state at that time. In practice, the observational network is not sufficiently dense and uniform to provide the amount of information needed. In particular, over large areas on the surface of the earth, observational data are completely missing at synoptic times (00Z and 12Z).

It is natural therefore to attempt to fill the void and include in the specification of an initial state, in addition to observations at the initial time, information provided from a model forecast, as well as by the available observations, before initial time. The forecast model, of course, provides information based on a previous initial state, and hence also on observations at previous times. Furthermore, it should be possible to improve the approximation of the initial state by utilizing a priori information on the cumulative statistical structure of both model errors and observational errors.



The idea of using cumulative statistical information about observational errors in order to compensate for the deficiencies in the amount and accuracy of the observations at a given synoptic time was proposed by Eliassen (1954). Gandin (1963) applied extensively statistical methods to the objective analysis of conventional synoptic data. This approach to objective analysis has come to be known in the meteorological literature as "optimal interpolation."

The inclusion of forecast information into the specification of an initial state by statistical methods leads to "optimal interpolation" of the differences between observations and forecast values, rather than of the synoptic observations themselves. This approach has been advocated and implemented by Rutherford (1972, 1973).

The application of statistical methods not only to the objective analysis of conventional synoptic observations, but also to the time-continuous assimilation of asynoptic satellite-derived data, was first carried out with SIRS data for a non-divergent barotropic model by Bengtsson and Gustavsson (1971, 1972). Our procedure of local "optimal interpolation" based on differences between satellite observations and forecast values combines the above ideas for blending of satellite data in a time-continuous manner into assimilation runs of the GISS GCM. The statistically determined corrections are then added at each model time step of the assimilation cycle to the forecast values. We have been further encouraged in the vigorous pursuit of this particular approach by the conclusions of Phillips (1976), to wit that only an explicit consideration of the statistical error structure of satellite temperature data will enhance their impact on numerical weather forecasts.

In Subsection 3.2.7.2 the four-dimensional time-continuous statistical assimilation method (SAM) we developed is described. The application of the method to DST-5 and DST-6 data is described in Subsection 3.3.1 of the Results Section of this Chapter. The results of this method are then compared with those of the direct insertion (DIM) and asynoptic successive correction method (SCM) in Subsection 3.3.2. Finally, our conclusions concerning the effect of the assimilation method and of the quantity and quality of satellite data on forecast improvement are drawn in Section 3.4.

### 3.2.7.2 THE METHOD

The theoretical considerations in developing a statistical assimilation method are presented in any one of the references mentioned in the Introduction (Subsection 3.2.7.1). We shall not dwell upon them here and only present the actual procedure used in the numerical experiments we discuss in Section 3.3.

The vertical temperature profiles obtained from satellite-based radiance measurements are grouped by 10-minute time intervals. This is the length of the time step  $\Delta t$  for the GISS GCM (see Chapter 4), and there was no reason to use smaller groups of data. Certainly  $\Delta t$  is very short compared to the characteristic time scale of synoptic motions (6-12h) and therefore the assimilation using such groups of data can be termed time-continuous in the context of global and of large-scale forecasts. A plot of a typical group of temperature data obtained in a 10-minute time interval is shown in

Figure 22. In the sequel we shall refer for the sake of brevity to satellite-derived temperatures as observed temperatures.

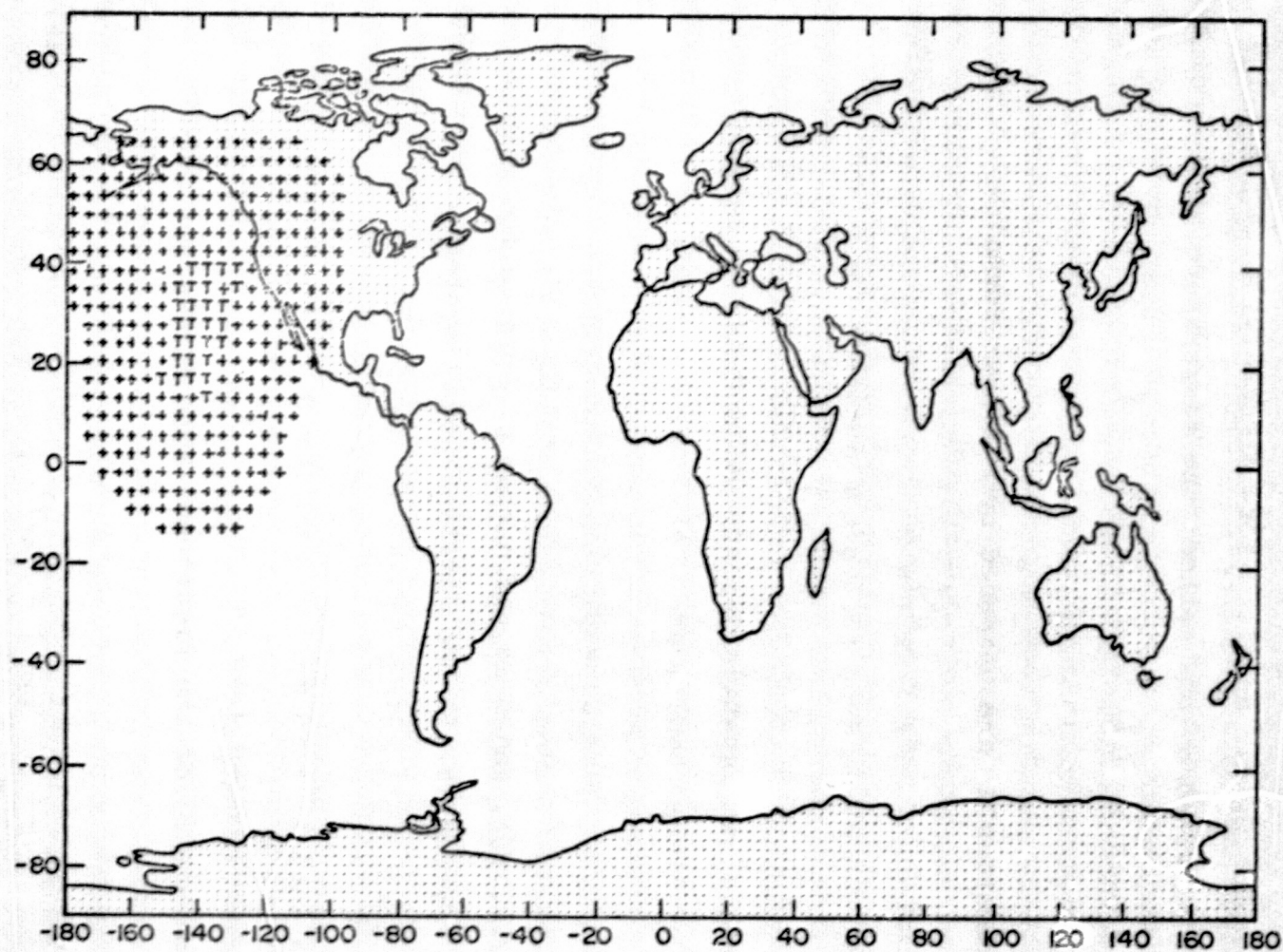
The basic idea of the method is that these temperature data, which differ from the model forecast values at the same time and location, should be used in order to improve the estimate of the true atmospheric temperature in a neighborhood of the observations. The weight to be given to forecast values and to observed values in an averaging process is determined from previously available information on the error structure of both model forecasts and satellite observations.

In the present implementation of the method, only information at the same mandatory pressure level is used, i.e., the "optimal interpolation" is two-dimensional. The formula used for the interpolation of forecast values from grid points to observation points is given in Subsection 3.2.4 (SCM).

To simplify notation, we shall use a single subscript to indicate location, thus:  $\tilde{k} = (i, j)$ , where  $i$  stands for discretized longitude and  $j$  for discretized latitude. Let  $\tilde{k}$  be an observation point (on a fixed mandatory pressure level),  $T_{\tilde{k}}^o$  the observed temperature, and  $T_{\tilde{k}}^f$  the (interpolated) model temperature at the observation point  $\tilde{k}$ . Let  $\gamma_{\tilde{k}}$  be the difference between the observed and the forecast temperatures at  $\tilde{k}$ ,

$$\gamma_{\tilde{k}} = T_{\tilde{k}}^o - T_{\tilde{k}}^f \quad (1)$$

We wish to compute corrections  $\delta_{\tilde{l}}$  to forecast values at grid points  $\tilde{l} = (m, n)$  near the observation points  $\tilde{k}$ , where  $\tilde{k}$  ranges



ORIGINAL PAGE IS  
OF POOR QUALITY

Fig. 22. Domain of influence of satellite temperature retrievals in 10 min. time intervals. The T's stand for grid points in the immediate neighborhood of satellite retrievals, the +'s for points affected by the retrievals in the statistical assimilation method.

over a group, or "patch", of observations such as the one shown in Figure 22. In the figure, observation points  $\underline{k}$  are marked by T's; grid points  $\underline{l}$  which are affected by the observations after corrections are made appear as +'s. More precisely, after applying the corrections provided by our method, the temperature at  $+$  - points, as well as at T-points, will be different from the forecast value, i.e.,

$$T_{\underline{l}} = T_{\underline{l}}^f + \delta_{\underline{l}}.$$

The corrections  $\delta_{\underline{l}}$  are computed by a linear formula,

$$\delta_{\underline{l}} = \sum_k \alpha_{\underline{l}}^k \gamma_k ; \quad (2)$$

here and in the sequel we drop the vector notation for  $\underline{k}$  and  $\underline{l}$ , the multi-index character of  $k$  and  $l$  being tacitly understood.

The coefficients  $\alpha_{\underline{l}}^k$  in Equation (2) are defined as the solution of the system of linear equations

$$A_{\underline{l}} \alpha_{\underline{l}} = \beta_{\underline{l}} \quad (3)$$

where  $\alpha_{\underline{l}} = (\alpha_{\underline{l}}^1, \dots, \alpha_{\underline{l}}^N)$ , and  $N$  is the number of observation points in the patch. System (3) is the familiar normal system which arises in all statistical applications based on a least-squares approach.

The statistical information accumulated on observations and forecasts is incorporated into the entries  $a_{kk'}^{\underline{l}}$  of the matrix  $A_{\underline{l}}$  and into the components  $\beta_{\underline{l}}^k$  of the right-hand side vector  $\beta_{\underline{l}}$ . These are given by

$$a_{kk'}^{\underline{l}} = \phi(s_{kk'}) , \quad (4a)$$

$$\beta_{\underline{l}}^k = \phi(s_{k\underline{l}}) ; \quad (4b)$$

here  $s_{kk'}$  is the (spherical) distance between the two observation points  $k$  and  $k'$ , and  $s_{k\ell}$  is the distance between the observation point  $k$  and the grid point  $\ell$ , at which we wish to make the correction. Notice that  $\tilde{A}$  depends on observation points only, and we can drop the subscript  $\ell$ , while  $\tilde{\beta}_{\ell}$  depends on both observation points and the correction point we consider.

The function  $\phi(s)$  is a correlation function. The fact that it depends only on the distance  $s$  reflects the assumptions of homogeneity and of isotropy we made at the outset concerning the error structure. We shall comment on the effect of these assumptions and on related questions in Sections 3.3 and 3.4, as the occasion arises.

A preliminary correlation function  $\psi(s)$  was computed for DST-5 and for DST-6 separately, based in each case on all the pairs of differences  $(\gamma_k, \gamma_{k'})$  available within the same DST period. The observations within the same interval  $\Delta t$  were considered as simultaneous and classified according to the distance  $s$  between them. Thus, letting  $\tau$  index the successive time intervals  $\Delta t$ , we have

$$\psi(s) = \frac{\sum_{\tau} \sum s_{kk'} = s \gamma_k(\tau) \gamma_{k'}(\tau)}{[\sum \gamma_k^2(\tau) \sum \gamma_{k'}^2(\tau)]^{1/2}} ; \quad (5)$$

here  $\tau$  runs over all the time intervals of  $\Delta t = 10$  minutes within a DST period, and the sums in the denominator run over all the points,  $k$  as well as  $k'$ , present in the pairs  $\gamma_k \gamma_{k'}$  of the numerator. Fur-

ther details on the computation of  $\psi(s)$  are given in Ghil et al. (1976a) for DST-5. The computation for DST-6 was entirely analogous. It is important to notice that the forecast values which enter into Equations (1) and (5) are based on 12-hour forecasts between synoptic times. The effect of forecast deterioration over 12 hours is not explicitly taken into account in the present implementation of the method any more than anisotropy is.

The function  $\psi(s)$  was computed for discrete values of  $s$ ,  $s_1 = 100\text{km}$ ,  $s_2 = 300\text{km}$ , ...,  $s_p = (2p-1) \times 100\text{km}$ . This means in particular that the sums in Equation (5) extend over  $(s_{p-1} + s_p)/2 \leq s < (s_p + s_{p+1})/2$ , rather than over  $s = s_p$ . The continuous function  $\phi(s)$  used in (4) was obtained in some cases from the discrete values  $\psi_p = \psi(s_p)$  by extending  $\psi(s)$  to the other values of  $s$  using linear interpolation. In fact the procedure was somewhat more complicated, and is described in detail in Subsection 3.3.1.2. In other cases we fitted an analytic function  $\phi = \phi(s; s_0, c)$ , depending on the parameters  $s_0$  and  $c$ , to the values  $\psi_p = \psi(s_p)$ , by a least-squares fit. In other words, we obtained the values of  $s_0$  and of  $c$  for which  $\phi(s; s_0, c)$  satisfied

$$\sum_p [\phi(s_p; s_0, c) - \psi_p]^2 = \text{minimum} . \quad (6)$$

Further details on the analytic expressions we used for  $\phi$  and on the determination of  $s_0$  and of  $c$  are given in Section 3.3 and in Appendix A.

Having described the computation of the correlation function  $\phi(s)$  in (4), we return now to the algorithm given by Equations (1)

to (4) for obtaining the corrections  $\delta_{\ell}$ . It is clear that  $\tilde{A}$  is determined exclusively by the geometry of an observation patch. But the weights  $\alpha_{\ell}$  depend on the correction point  $\ell$ , because  $\tilde{\beta}_{\ell}$  in Equation (3) does. This would seem to imply that for every correction point  $\ell$  we need to solve Equation (3) for the weights  $\alpha_{\ell}$ ; such an approach would be computationally rather expensive. The number  $N$  of observation points in a patch is typically 50, so that a few thousand algebraic operations might be involved in making the correction at just one point. Fortunately, it is rather easy to circumvent this difficulty.

Let  $\tilde{\gamma} = (\gamma_1, \dots, \gamma_N)$  stand for the vector of differences  $\gamma_k$ . Combining Equations (2) and (3), the correction  $\delta_{\ell}$  is given by

$$\delta_{\ell} = \alpha_{\ell}^T \tilde{\gamma} = (\tilde{A}^{-1} \tilde{\beta}_{\ell})^T \tilde{\gamma}; \quad (7)$$

$( )^T$  denotes the transpose of a vector or a matrix,  $\tilde{x}^T \tilde{y}$  is the inner or scalar product of the column vectors  $\tilde{x}$  and  $\tilde{y}$ , and  $\tilde{A}^{-1}$  is the inverse of the matrix  $\tilde{A}$ . The matrix  $\tilde{A}$ , however, is symmetric,  $\tilde{A}^T = \tilde{A}$ , since  $a_{kk'} = \phi(s_{kk'}) = \phi(s_{k'k}) = a_{k'k}$ . This allows us to write Equation (7) as

$$\delta_{\ell} = \tilde{\beta}_{\ell}^T \tilde{A}^{-1} \tilde{\gamma}, \quad (8)$$

where we used the rules for the transpose of a product and of an inverse. Equation (8) makes it evident that we only need to compute the vector  $\tilde{\eta} = \tilde{A}^{-1} \tilde{\gamma}$  for an observation patch once; all the corrections  $\delta_{\ell}$  are then computed as inner products  $\tilde{\beta}_{\ell}^T \tilde{\eta}$ . Thus, the total number



of operations per patch is reduced to a few thousand, rather than a hundred times as much. Computer time estimates for the implementation of SAM will be given in Section 3.3. In the present version of the method, a general-purpose linear equation solver is used to solve the system

$$\tilde{A}\tilde{\eta} = \tilde{\gamma} \quad ; \quad (9)$$

the solver is based on Gaussian elimination with partial pivoting.

This concludes the description of the method. We proceed with a description of the numerical experiments and their results in the next section.

### 3.3 RESULTS (M. Ghil, M. Halem and R. Dilling)

#### 3.3.1 DESCRIPTION OF THE EXPERIMENTS

##### 3.3.2.2 INTRODUCTION

The purpose of our experiments was to study the effect of satellite data on the quality of initial states obtained with the aid of such data, and on the accuracy of forecasts starting from such initial states. Specifically we studied the effect of the quantity and accuracy of the satellite data themselves on the one hand, and of the assimilation methods used to extract the information from the data, on the other.

Experiments were carried out for the DST-5 (August 18 to September 2) and DST-6 (January 29 to February 21) periods. The temperature data used were based on radiance measurements obtained from the VTPR instrument on board the NOAA-4 satellite and from the HIRS and SCAMS instruments on board the NIMBUS-6 satellite. We used in separate experiments temperature data derived from the measured radiances by the

processing methods developed by NESS (Smith and Woolf, 1976), as well as those derived by GISS (Chapter 2 of this Report).

All the experiments consisted basically of a continuous assimilation run, extending over the entire DST period, and of forecasts started from selected initial states produced by the assimilation run. The assimilation methods used for the satellite data were direct insertion (DIM, Subsection 3.2.1), asynoptic successive correction (SCM, Subsection 3.2.4), and time-continuous local statistical assimilation (SAM, Subsection 3.2.7).

The assimilation run of every experiment was started at 00Z on the first day of the DST period (August 18 for DST-5 and January 30 for DST-6) from an initial state given by a GISS objective analysis of conventional synoptic data available at that time (cf. Subsection 3.2.1). At every model time step, i.e., every 10 minutes thereafter, corrections were made to the model temperatures, using satellite-derived temperature data which had become available during those 10 minutes. The assimilation method used determines the way in which the corrections were obtained from the data. In the control run, or NOSAT run, no temperature corrections were made at asynoptic times. In some runs, wind corrections based on a geostrophic formula (cf. Subsection 3.2.1) were also made at grid points where a temperature correction was made and at immediately adjacent grid points.

The forecasts based on a given assimilation run were started at 03Z on selected days during the DST period, beginning 2 days after the

start of the period, i.e., August 20 for DST-5 and February 1 for DST-6. The reason to start the forecasts at 03Z and not at 00Z was to achieve as close a parallel as possible with operational practice at NMC, because NMC uses intermittent assimilation with a +3h "window" for satellite data. Thus, an operational NMC forecast started at 00Z uses all asynoptic information up to 03Z; so do our experimental runs started at 03Z as we rely on time-continuous assimilation. Starting 3h after the insertion of asynoptic data also has the effect of letting the model smooth out the initialization shock occurring at synoptic time (see Appendix B; Ghil, 1975; and Ghil et al., 1977).

Because of the short duration of the Impact Test Project, methods were still being developed while some experiments were carried out or had been completed. The summer experiments (DST-5) were carried out first, and more refined methods became available for the winter experiments (DST-6). We expect to be able to perform in the near future on DST-5 data some of the experiments we have carried out with DST-6 data. The only methods which have been extensively tested, and on the results of which we report here, are direct insertion (DIM, Subsection 3.2.1), asynoptic successive correction (SCM, Subsection 3.2.4), and statistical assimilation (SAM, Subsection 3.2.7).

### 3.3.1.2 SUMMER EXPERIMENTS

A summary description of DST-5 experiments is given in Table 25. The number of parameters which influence the assimilation process is large, and the computational effort to carry out a full-length experiment for the entire DST period is considerable. Therefore, it was not possible to perform experiments for all the possible combinations of parameter values. Even so, experiments were performed for a representative number of combinations.

The major parameters which were varied from experiment to experiment were: (1) the use of data from one or two satellites, (2) the use of temperature data processed by NESS methods or by GISS methods, and (3) the assimilation method of the data. As we can see from the table, experiments were carried out with data from one satellite only, the NIMBUS-6, as well as with data from both NOAA-4 and NIMBUS-6; with NESS-processed data as well as with GISS-processed data; with the methods of direct insertion (DIM), successive corrections (SCM), and statistical assimilation (SAM).

A few more comments are in order concerning details of the SAM experiments. In two of them, Numbers 8119 and 8130, the correlation curve  $\phi(s)$  was not obtained by a least-squares fit of a two-parameter analytic function  $\phi(s; s_0, c)$  to the global data  $\psi(s)$  as described in Subsection 3.2.7.2. At the time of preparation for these DST-5 experiments, we considered separate data curves  $\phi_{k\ell}(s)$  for different latitude bands  $k$  and mandatory pressure levels  $\ell$ , as described in Ghil et al. (1976a). The curve  $\phi(s)$  for these two experiments was then obtained by a least-squares fit of a piecewise-linear function to all the data curves  $\psi_{k\ell}(s)$  jointly; this least-squares fit is described in Ghil and Economedes (1976). The reasons for using  $\phi$  of the form

$$\phi(s; s_0, c) = (1-c)e^{-s/s_0} + c \quad , \quad (2.1)$$

with certain non-zero values of  $c$ , will be discussed in the next Subsection, in connection with the winter experiments. The main

Table 25. Summary of DST-5 satellite-data assimilation experiments.

Experiments.

Experiment No.	Satellite Data				Assimilation Method	Correlation Curve		Bias Removed	
	NESS		GISS			$(1-c)e^{-s/s_o} + c$	at observation	at grid point	
	VTPR	NIMB	VTPR	NIMB					$s_o$ (km)
7336					NO SAT				
7854	X	X			DIM				
7970		X			DIM				
8036			X	X	SCM				
8119		X			SAM	piece-wise linear		X	
8130		X			SAM	piece-wise linear			
8637	X	X			SAM	4290	-.406		
8645	X	X			SAM	2717	0		
8656	X	X			SAM	4290	-.406	X	
8662	X	X			SAM	4290	-.406		X=bias prop. to sum of weights
8692	X	X			SAM	4329	-.416		
					NIMBUS and	3093	-.098		
					VTPR	4290	-.406		
8708	X	X			COMBINED	2717	0	X	

The use of data from the VTPR instrument on board the NOAA-4 satellite is denoted by VTPR, the use of the data from the HIRS and SCAMS instruments on board the NIMBUS-6 satellite by NIMB. The processing method of the data is indicated by the acronyms introduced throughout this Chapter as DIM, SCM or SAM, with the control run appearing as NO SAT. Additional remarks concerning the method are explained in the text.

reason has to do with the problem of the systematic warm bias in satellite-derived temperatures (Phillips, 1976; Tracton and McPherson, 1977).

A first approach in attempting to deal with the bias problem consisted in simply computing the average difference between observations and interpolated forecast values over a satellite-data "patch" (see Subsection 3.2.7.2) at time  $\tau$ ,

$$\bar{\gamma}(\tau) = \sum_{k=1}^{N_{\tau}} \gamma_k(\tau) / N_{\tau} \quad , \quad (2.2a)$$

and multiplying it by a coefficient  $p$ ; here  $N_{\tau}$  is the number of observations at time  $\tau$ . The corrections  $\delta_{\theta}$  are then made using the modified differences

$$\gamma'_k = \gamma_k - p\bar{\gamma} \quad , \quad 0 < p < 1; \quad (2.2b)$$

thus  $p = 0$  means no modification of the procedure described in Subsection 3.2.7.2, while  $p = 1$  means that  $\bar{\gamma}' = 0$ . In practice only  $p = 0$ ,  $p = 1$  were used, and no experiments with intermediate values were carried out. An experiment with  $p = 1$  is marked as "bias removed at observation point" in Table 25.

Another straightforward attempt to deal with the bias problem, along the same lines as the first, was to "remove the bias at grid

points" (experiment Number 8662). In this approach, the weighted average  $\bar{\delta}$  of the corrections is computed first,

$$\bar{\delta} = \frac{\sum_{\ell'} \alpha^{(\ell')} \delta_{\ell'}}{\sum_{\ell''} \alpha^{(\ell'')}} ; \quad (2.3a)$$

here  $\alpha^{(\ell'')}$  is the sum of the weights at correction point  $\ell''$ ,

$$\alpha^{(\ell'')} = \sum_{k=1}^{N_T} \alpha_{\ell''}^k \quad (2.3b)$$

(see Subsection 3.2.7.2 for the definition of the weights  $\alpha_{\ell}^k$ ). The modified corrections are

$$\delta_{\ell}' = \delta_{\ell} - \bar{\delta} ; \quad (2.3c)$$

this modification is denoted as "bias removed at grid point" in Table 26 of the next Subsection with the remark that "bias at grid point is constant." It was not actually used for an experiment with DST-5 data.

A slightly different form of the above modification was used in a summer experiment (Number 8662), and is denoted in the same way in the "bias removal" column of Table 25. The remark it bears is "bias proportional to sum of weights." The formula for this modification is

$$\delta_{\ell}' = \delta_{\ell} - \alpha^{(\ell)} \bar{\delta} , \quad (2.4a)$$

with  $\bar{\delta}$  now defined as

$$\bar{\delta} = \frac{\sum_{\ell'} \delta_{\ell}'}{\sum_{\ell''} \alpha^{(\ell'')}} . \quad (2.4b)$$

The different curves  $\psi_{k\ell}(s)$  mentioned before (Ghil et al., 1976a; Ghil and Economedes, 1976) exhibited the striking property of a much faster decay at high latitudes than at lower latitudes: a function  $\psi_{k_1\ell}(s)$  attained any given threshold value  $\varepsilon, 0 < \varepsilon < 1$ , faster, that is for smaller  $s$ , than the function  $\psi_{k_2\ell}(s)$ , whenever  $k_1$  corresponded to a higher latitude band than  $k_2$  (for fixed level  $\ell$  and in the same hemisphere). This is in agreement with the well-known influence of latitude on the value of the Coriolis parameter, on the Rossby radius of deformation and hence on geostrophic adjustment. The dependence of curves  $\psi_{k\ell}$  on the level  $\ell$  seemed much smaller and less systematic.

The latitude dependence of the correlation functions for the observed-minus-forecast temperature field clearly points to the fact that the homogeneity assumption made at the beginning of Subsection 3.2.7.2 is not supported by the data. Without modifying the general form of the algorithm, described there, we decided to allow for latitude dependence by using instead of  $\phi(s)$  described in Subsection 3.2.7.2 and in Appendix A, a modified  $\phi'(s; i, j)$ ,

$$\phi'(s; i, j) = \phi(s_{ij}) \cos \theta_{ij} \quad ; \quad (2.5)$$

here  $s=s_{ij}$  is still the spherical distance between points  $i$  and  $j$ , but  $\theta_{ij}$  depends on the latitude band in which those points lie. Further details are provided in Appendix A.

The use of such a modified, or latitude-scaled correlation function has the added advantage that polar regions, over which the



earth-orbiting satellites pass more frequently, are not completely "swamped" by satellite-derived data which would cancel completely the stabilizing influence of model forecast values. This modification was used in all the SAM experiments of Table 25 starting with 8637.

A certain well-known difficulty in solving system (9) of Subsection 3.2.7.2 arises from the fact that such a system appearing in statistical computations is typically ill-conditioned. In other words, as the number  $N$  of observations  $\gamma_1, \dots, \gamma_N$  increases, the "weighted corrections"  $\eta$  become more and more sensitive to errors in the data, in  $A$ , as well as in  $\gamma$ .

Because of the ill-conditioning of this system, and in order to presmooth observational errors, the NESS-processed observations were first averaged to the GISS GCM grid points. This averaging was also performed in all SAM experiments in which the modified  $\phi'(s)$  was used. It had the additional advantage of further reducing computation time. In the future we plan to use for this purpose the more elaborate form of smoothing described in Subsection 3.2.3 (LIP), instead of this simple averaging procedure. One further comment which is in order at this point is that after the statistical temperature corrections were carried out in experiments 8119 through 8708, a geostrophic wind correction as mentioned in Subsection 3.2.1

was also performed. This was also the case with the DIM and SCM experiments (7854 through 8036). Experiment 8692 was not completed and we shall not dwell on the modification of SAM it contains.

We turn now to the description of experiments performed with DST-6 data.

### 3.3.1.3 WINTER EXPERIMENTS

A summary description of DST-6 experiments is given in Table 26. Most experiment descriptions in the Table are self-explanatory after referring back to the previous subsection.

A latitude-scaled correlation function [cf., Equation (2.5) above], averaging to GISS grid points, and geostrophic wind corrections were also used in all DST-6 SAM experiments, except 8497, where neither one of these modifications of the algorithm in Subsection 3.2.7.2 was used. Geostrophic wind correction was used in the DIM and SCM experiments (8210 through 8447) as well.

Experiment 8497 did not necessitate averaging to GISS grid points, since the GISS processing of satellite radiances provides temperature profiles only at GISS grid points in the first place. The remark "RAG" for experiment 8497 refers to the acronym "retrieve as you go"; the meaning of this was that the radiance observations were processed concomitantly with the assimilation:

Table 26. Summary of DST-6 satellite-data assimilation experiments.

Experiment No.	Satellite Data				Assimilation Method	Correlation Curve		Bias Removed	
	NESS		GISS			$(1-c)e^{-s/s_o} + c$	at observa- tion	at grid point	
	VTPR	NIMB	VTPR	NIMB					$s_o$ (km)
7578					NO SAT				
8240		X			DIM				
8310	X	X			SCM				
8352		X			SCM				
8405		*			SCM				
8447		X			SCM over land				
8472		X			SAM	1831	.018	X	
8497				X	RAG (DIM)				
8545	X	X			SAM	1842	.015		
8566	X	X			SAM	1842	.015	X	
8574	X				SAM	2293	-.124		
8581	X	X			SAM	1842	.015	X	X=Bias at grid point is constant
8593	X	X			SAM	1842	.015		X=Bias prop. to sum of weights
8695				**	SAM	1226	.129		

\*simulated NESS NIMBUS based on NO SAT 12-hour forecast

\*\*NIMBUS microwave (SCMS) data only

The same notation is used as in Table 25. In addition, the acronym RAG stands for Retrieve-as-you-go; this means that, in the GISS processing of satellite data, an updated temperature which uses previously assimilated information was employed as a first guess for the retrieval or derivation of a temperature profile from radiometric measurements.

Table 26. Summary of DST-6 satellite-data assimilation experiments.

Experiment No.	Satellite Data				Assimilation Method	Correlation Curve		Bias Removed	
	NESS		GISS			$(1-c)e^{-s/s_o} + c$	at observa- tion	at grid point	
	VTPR	NIMB	VTPR	NIMB					$s_o$ (km)
7578					NO SAT				
8240		X			DIM				
8310	X	X			SCM				
8352		X			SCM				
8405		*			SCM				
8447		X			SCM over land				
8472		X			SAM	1831	.018	X	
8497				X	RAG (DIM)				
8545	X	X			SAM	1842	.015		
8566	X	X			SAM	1842	.015	X	
8574	X				SAM	2293	-.124		
8581	X	X			SAM	1842	.015	X	X=Bias at grid point is constant
8593	X	X			SAM	1842	.015		X=Bias prop. to sum of weights
8695				**	SAM	1226	.129		

\*simulated NESS NIMBUS based on NO SAT 12-hour forecast

\*\*NIMBUS microwave (SCAMS) data only

The same notation is used as in Table 25. In addition, the acronym RAG stands for Retrieve-as-you-go; this means that, in the GISS processing of satellite data, an updated temperature which uses previously assimilated information was employed as a first guess for the retrieval or derivation of a temperature profile from radiometric measurements.

the temperature processing, or retrieval, in the experiment was done using as a first guess the temperature at the previous time step of the assimilation process. Unfortunately the experiment is not complete at the time of this writing, and we shall not be able to report on its results.

Experiment 8405 was set up as a control experiment to check the information content of satellite data, and to study the possible smoothing effect of SCM or SAM on variable values produced by assimilation runs. In it the temperature data used as "observations" were model values produced from a NOSAT 12h-forecast, to which simulated observed-minus-forecast differences were added; these differences were computed at the true NIMBUS observation locations, by using a random-number generator function with the statistical properties determined from actual data.

There only remains to discuss the form (2.1) (see Subsection 3.3.1.2 above) of the correlation function  $\phi(s)$ . It was clear from the aspect of the latitude-and-height dependent curves  $\psi_{k\ell}(s)$  (Ghil et al., 1976a), as well as from the aspect of the globally-averaged curve  $\psi(s)$  (Ghil et al., 1976b) that an exponential would be best suited for an analytic function  $\phi(s)$  which approximated well  $\psi(s)$ .

Both normal functions  $\exp(-s^2/s_0^2)$  and simple exponentials  $\exp(-s/s_0)$  were tested. The simple exponential provided better least-squares fits to  $\psi(s)$  in all cases (summer or winter data, as well as data from one or two satellites).

The idea of using a second parameter  $c$ , besides  $s_0$ , was based on the following concept (Phillips, private communication, 1976): Let  $x$  and  $y$  be random variables with mean  $\bar{x}$  and  $\bar{y}$ , respectively. They can be written then as

$$x = \bar{x} + \xi, y = \bar{y} + \eta \quad , \quad (3.1)$$

where  $\xi$  and  $\eta$  are random variables with mean zero,  $\bar{\xi} = \bar{\eta} = 0$ , and with the same standard deviation as  $x$  and  $y$  respectively. The covariance of  $x$  and  $y$  is then,

$$\overline{xy} = \bar{x}\bar{y} + \bar{\xi}\bar{\eta} \quad . \quad (3.2)$$

Now let  $x$  and  $y$  stand for  $\gamma_k$  and  $\gamma_{k'}$  of Subsection 3.2.7.2. Assume that the satellite measurements have indeed a warm bias, i.e.,  $\bar{\gamma}_k = \bar{\gamma}_{k'} = \bar{\gamma} > 0$ ; then the assumption of lack of correlation over large distances between observation-minus-forecast differences would result in

$$\overline{\gamma_k \gamma_{k'}} \rightarrow \bar{\gamma}^2 > 0 \quad , \quad (3.3a)$$

$$\overline{(\gamma_k - \bar{\gamma})(\gamma_{k'} - \bar{\gamma})} \rightarrow 0 \quad , \quad (3.3b)$$

as  $s_{kk'} \rightarrow \infty$ . Thus a warm bias would seem to imply a positive asymptotic value for  $\phi(s)$ , and one should have  $c \cong \bar{\gamma}^2$  in (2.1).

This idea was applied first to experiments with DST-6 data; from Table 26 we see that the values of  $c$  given by the best two-parameter least-squares fit were positive and small. A small negative value of  $c$  obtained for experiment 8574, which was actually performed later than most of the other winter experiments; large negative values of  $c$  obtained also for the DST-5 data when we attempted to apply

this concept to them. The meaning of a negative  $c$  is not entirely clear (see, however, Gandin, 1963, Figs. 10 and 14; Phillips, 1976, Figs. 5 and 7); indeed,  $\bar{\gamma} < 0$  would still give a positive  $c = \bar{\gamma}^2$ . A more careful study of the effect of very long waves on statistical structures of meteorological fields remains to be done. At this stage, functions  $\phi(s; s_0, c)$  with  $c < 0$  were only used for reasons of consistency.

In the experiments with data for which a least-squares fit of  $\phi(s; s_0, c) = (1-c)e^{-s/s_0} + c$  yielded  $c \neq 0$ , we actually used a modified  $\phi''(s)$ ,  $\phi'' = e^{-s/s_0}$ , with  $s_0$  provided by the two-parameter fit  $(s_0, c)$ . This was done in accordance with an attempt at removing the bias which seems somewhat more sophisticated than the ones described in the previous Subsection.

Before proceeding to a presentation and discussion of results, we shall stop briefly to comment on the present status of computer implementation of the different methods.

#### 3.3.1.4 COMPUTATIONAL ASPECTS OF EXPERIMENTS

It is clear that more sophisticated assimilation methods require more computer time; it is important that improvements in results not be obtained at excessive cost. The discussion in this subsection, in conjunction with the results we present in 3.3.2, will show that the computer time necessary to implement the more successful ones among our methods is quite reasonable.

The only additional computer time spent in applying our assimilation methods is in the assimilation run itself: forecasts require

the same time as if they were started from an initial state determined by conventional synoptic analysis. The time to carry out a 24h forecast is essentially the unit of time required to make the comparisons that follow and are independent, to a certain extent, of the computer installation; there will still be a certain dependence which comes from the ratio of time spent in data transmission to and from peripheral equipment to that of computing time proper. The timing at other installations will also depend somewhat on the forecast model itself; this dependence can be eliminated by studying the number of arithmetic operations per 24h in each model, and comparing it with the corresponding number for the GISS GCM.

The timing estimates we give are for the present version of the GISS GCM (v. Chapter 4), the present status of our assimilation methods and for an Amdahl 470/6 computer with 2 megabytes of core. A 24h forecast runs in 40 minutes; a 24h NO SAT assimilation run, in 48 minutes; a 24h SCM assimilation run in 58 minutes; and a 24h SAM run in 96 minutes.

The differences in time between the NO SAT assimilation and the forecast is accounted for by the time necessary to make two synoptic analyses; this time is very short since the present GISS method of objective analysis is very simple (Subsection 3.2.1). We notice that the SCM assimilation requires only an amount of time which is negligibly larger than the NO SAT run.

The time necessitated by the SAM method as measured here is only about 60 percent longer than that for SCM. We hope to reduce this time even further. The present length of time is due to two factors. The first and most important is that the present version of SAM is still experimental: a number of diagnostic quantities are computed



and printed which would not be required in an operational version of the code. The second vector is that the solution algorithm for system (9) of Subsection 3.2.7.2 is very inefficient: it does not take advantage of the symmetry of  $A$  and of its relative sparsity.

We plan to implement a more efficient linear equation solver within the SAM method in the near future. We expect that an operational version of the code, without diagnostic quantities being computed and printed, will then run in a time much closer to that necessitated at present by SCM; say in not more than 75 minutes, or 50 percent over a NO SAT run.

Herewith the description of experiments performed with both DST-5 and DST-6 data is complete; we are ready to present and discuss the results of these experiments.

### 3.3.2 COMPARISON OF RESULTS

#### 3.3.2.1 INTRODUCTION

In this subsection we shall only discuss statistical measures of satellite-data impact on forecast accuracy. A more detailed study of the differences in initial states produced by the assimilation of satellite-derived temperature data, from a synoptic point of view, appears in Chapter 5, Evaluation and Verification Tests. Chapter 5 also contains a study of the effect of differences in the model-predicted large scale fields on local weather forecasts.

The statistical measures of impact we used were  $S_1$  skill scores and root-mean-square (rms) differences. The meteorological fields we studied in particular were the sea-level pressure  $p_s$  and the height  $\phi$  of the 500-mb geopotential surface. First the difference between values of the field produced by a model forecast and the field values of the NMC objective analysis at the same synoptic time were computed. These differences were computed for the synoptic time 2 days and 3 days after the initial time of the forecast. They will be referred to in the sequel as differences at 48 h and 72 h after initial time, although they actually correspond to 45 h and 69 h (see Subsection 3.3.1.1), respectively.

The next step was to compute the rms value of the difference. The actual impact measure consisted in subtracting the rms difference for the control, or NO SAT, forecast from the rms difference for the experimental forecast. A positive value of this difference then means positive impact of, or improvement due to satellite data for the given experiment and quantity, while a negative value means negative impact. The computations for skill score impacts were done in analogous fashion. To preserve the simple connection above between positive difference and positive impact, the  $S_1$  skill scores were defined so that higher score means poorer skill, i.e., zero corresponds to perfect skill and 100 to no skill.

The verification regions over which the impact was measured were North America, or NA, and Europe, or EU. The verification

region labelled NA was a latitude-longitude rectangle extending from 30°N to 70°N and 75°W to 130°W, while EU extended from 30°N to 86°N and from 10°W to 40°E. These regions were selected because the operational NMC analyses for them are reliable, and because they are situated downstream from large areas over which conventional data coverage is sparse, i.e., the North Pacific and the North Atlantic basins respectively; moreover, being densely populated, the importance of good 2 to 3 day forecasts for these regions is particularly great. The downstream effect of good satellite data coverage over the ocean basins to the west of the verification areas should be noticeable at 48 to 72h after initial forecast time, provided (1) the forecast model is sufficiently skillful, (2) the asynoptic data are sufficiently accurate, and (3) their assimilation was done in a way which extracts the information from the data without harming model performance.

### 3.3.2.2 DST-5 RESULTS

Due to the very limited duration of the DST-5 period, forecasts were performed for every day of the period, starting with August 20, 1975 at 03Z. Tables 27 through 34 present daily values of  $S_1$  skill score impacts and  $\sigma_1$  RMS impacts for  $p_s$  (SLP) and  $\phi$  (2500), at 48h and 72h, over North America (NA) and Europe (EU); Tables 27a, 28a, 29a, 30a, 31a, 32a, 33a, 34a give the  $S_1$  impacts, while Tables 27b, 28b, 29b, 30b, 31b, 32b, 33b, 34b give the corresponding RMS impacts. Experiments 7336 through 8130 were completed, experiments 8637 through 8708 are still being performed (compare Table 25 of Subsection 3.3.1 for a description of the experiments). The columns labelled 8/20 through 9/2 contain the results for the forecasts started on the

Table 27a. 48 HR. SLP SKILL SCORE IMPACT ON NORTH AMERICA

EXP	8/20	8/21	8/22	8/23	8/24	8/25	8/26	8/27	8/28	8/29	8/30	8/31	9/1	9/2	*****EXPERIMENT*****	*****DIFF.FROM(7336)*****				
															AVE	SD	SE	AVE	SD	SE
7336	75.8	79.1	78.5	69.6	64.4	63.3	67.6	65.4	61.7	66.0	67.5	75.2	83.1	68.4	70.74	7.05	1.22	0.0	0.0	0.0
7854	1.2	-3.0	6.1	7.1	-1.6	0.0	5.9	1.9	3.8	-1.4	-0.6	5.7	2.6	-3.0	68.98	7.37	1.97	1.76	3.51	0.94
7979	2.0	-1.7	7.9	3.2	-3.4	3.0	5.6	4.3	4.5	-0.9	1.8	7.3	5.9	-4.2	68.01	7.12	1.90	2.74	3.96	1.06
8026	1.3	0.9	4.6	6.5	-0.7	1.0	1.7	1.6	1.1	1.4	-1.1	5.0	-1.8	-3.2	69.44	7.22	1.93	1.31	2.66	0.71
8119	6.7	3.9	6.6	2.1	-6.9	-3.3	-2.0	-5.1	2.6	-5.4	-0.7	1.3	-0.5	-8.8	71.42	5.63	1.50	-0.68	4.85	1.30
8130	4.5	0.6	8.6	7.4	-9.5	-0.7	-0.3	-0.9	5.2	-5.0	2.0	1.5	9.1	-8.7	69.76	6.29	1.68	0.99	5.85	1.56
8637****	4.9****		4.1****	-0.5****		1.24****	-6.9****		5.3****	-5.7					69.37	4.68	1.77	0.32	5.01	1.89
8845****	1.0	5.6	6.9	-3.6	-1.9	2.0	1.5****	-5.0	-3.7	6.5	3.2	-3.0			69.95	5.31	1.53	0.79	4.23	1.22
8856****	-2.5****	-11.5****	-3.7****	-4.8****											75.03	7.53	3.77	-5.63	4.00	2.00
8862****	4.6****	6.5****	-2.0****	-2.0****	-5.2****	0.7****	-7.4								70.37	5.06	1.91	-0.69	5.62	1.90
8892****	2.2****	5.7****	9.2****	5.1****	-4.9****										67.06	6.72	3.01	1.66	4.28	1.92
8708****	2.8****	-1.2****	4.0****												68.86	8.67	5.01	1.87	2.69	1.55

Table 27b. 48 HR. SLP RMS IMPACT CA NORTH AMERICA

EXP	8/20	8/21	8/22	8/23	8/24	8/25	8/26	8/27	8/28	8/29	8/30	8/31	9/1	9/2	*****EXPERIMENT*****			****DIFF. FROM (7336)****		
															AVE	SC	SE	AVE	SC	SE
7336	3.8	5.6	6.0	5.6	4.1	4.1	5.4	6.5	4.3	4.2	4.7	4.9	4.1	3.2	4.79	0.53	0.25	0.0	0.0	0.0
7854	0.1	-0.4	0.8	0.8	-0.1	-0.1	1.3	1.1	0.4	0.1	-0.1	0.4	-0.2	-0.1	4.49	0.72	0.19	0.29	0.51	0.14
7970	0.1	-0.2	1.0	0.7	-0.4	-0.6	0.7	0.6	0.1	0.1	0.2	0.2	-0.1	-0.0	4.62	0.70	0.19	0.17	0.46	0.12
8036	0.1	0.1	0.8	0.6	-0.0	0.2	0.0	0.0	-0.4	0.2	-0.0	0.0	-0.5	-0.3	4.72	0.79	0.21	0.66	0.35	0.09
E119	0.6	-0.1	-0.0	0.6	-0.4	0.4	0.6	0.5	0.0	-0.4	0.1	0.1	-0.0	*****	4.76	0.83	0.23	0.15	0.35	0.10
E130	0.3	-0.1	1.2	1.0	-0.6	0.1	0.3	1.1	0.7	-1.8	0.4	-0.0	0.9	-0.3	4.56	0.96	0.26	0.22	0.21	0.22
E637*****	0.2*****	0.8*****	-0.24*****	-0.84*****	-0.7*****	0.2*****	0.3								4.97	1.34	0.51	-0.02	0.57	0.22
E645	-0.1	-0.0	1.2	1.1	-0.6	-0.1	0.6	-0.0	-0.2	-0.4	-0.4	0.5	-1.1	-0.2	4.78	0.77	0.21	0.01	0.64	0.17
E656*****	-0.4*****	-0.9*****	-0.9*****	0.24*****	*****	*****	*****	*****	*****	*****	*****	*****	*****	*****	5.96	0.66	0.33	-0.52	0.22	0.26
E662*****	-0.1*****	0.3*****	-0.2*****	-0.9*****	-0.3*****	-2.8*****	-0.3								5.56	1.56	0.55	-0.61	1.04	0.39
E692*****	0.3*****	0.9*****	0.0*****	0.5*****	-0.4*****	0.3*****	-0.2								4.74	0.87	0.33	0.21	0.42	0.16
E708*****	-0.24*****	0.2*****	-0.0*****	0.24*****	-0.6*****	0.3*****	-0.2								4.92	0.91	0.34	0.03	0.45	0.17

ORIGINAL PAGE IS  
OF POOR QUALITY

Table 28a. 72 HR. SLP SKILL SCORE IMPACT ON NORTH AMERICA

EXP	8/20	8/21	8/22	8/23	8/24	8/25	8/26	8/27	8/28	8/29	8/30	8/31	9/1	9/2	*****EXPERIMENT*****	SD	SE	*****DIFF. FROM (7336)*****	SD	SE
	AVE																			
7336	54.1	90.3	77.2	76.0	67.8	78.8	75.2	77.4	72.4	80.7	82.3	91.7	77.0	72.9	79.56	7.68	2.05	0.0	0.0	0.0
7854	2.7	-1.3	6.5	6.6	-3.6	-0.3	5.0	2.8	0.6	4.2	-1.9	12.3	-1.7	-3.3	77.55	7.30	1.95	2.01	4.57	1.22
7970	2.5	5.2	3.7	3.7	-2.6	1.3	7.9	6.4	-1.2	4.6	2.5	16.4	-0.1	-5.0	76.32	6.23	1.66	3.24	5.18	1.38
8036	2.4	4.2	9.4	5.4	2.3	2.7	3.0	3.3	-2.5	1.4	1.5	8.3	-4.9	2.3	76.79	7.43	1.95	2.77	3.66	0.93
8119	12.3	1.0	4.1	6.3	-3.1	-2.9	-6.0	-3.5	-7.2	-2.6	2.0	7.5	-2.5	-6.5	79.63	5.25	1.40	-0.08	5.83	1.56
8130	7.3	10.6	5.5	10.8	-11.5	-5.9	-4.1	4.1	-4.1	1.2	4.5	3.3	-3.6	-7.6	78.81	6.02	1.61	0.75	6.94	1.85
8637****	6.6****	10.2****	-2.9****	-2.8****	-2.5****	9.8****	-7.8	79.60	6.22	2.35	1.51	7.19	2.72							
8645****	8.2	6.3	9.9	-9.2	-4.3	3.9	8.5****	0.4	3.2	7.3	-2.0	-3.0	76.51	5.96	1.72	2.44	6.04	1.74		
8656****	3.5****	-4.4****	-5.8****	-2.8*****	*****	*****	*****	82.98	3.23	1.61	-2.36	4.12	2.06							
8662****	5.5****	8.8****	-1.7****	5.9****	-2.1****	0.3****	-8.6	79.96	8.15	3.08	1.15	5.97	2.26							
8692****	6.3****	9.1****	-2.0****	2.5****	-1.9*****	*****	*****	77.85	7.03	3.14	2.79	4.51	2.19							
8708****	5.6****	5.2****	0.4*****	*****	*****	*****	*****	77.96	6.95	4.01	3.74	2.87	1.66							

Table 28b. 72 HR. SLP RMS IMPACT ON NCRTH AMERICA

EXP	8/20	8/21	8/22	8/23	8/24	8/25	8/26	8/27	8/28	8/29	8/30	8/31	9/1	9/2	*****EXPERIMENT*****			*****DIFF. FROM (7336)*****		
															AVE	SD	SE	AVE	SD	SE
7336	6.4	6.7	6.0	4.6	4.7	6.8	6.9	6.5	5.5	5.7	5.6	4.5	4.0	4.3	5.59	1.01	0.27	C.0	0.0	0.0
7854	0.5	-0.6	0.5	0.1	-0.3	1.0	1.6	1.3	0.3	0.5	-0.3	0.6	-0.1	0.5	5.20	0.93	0.25	C.39	0.62	0.16
7970	0.4	0.4	0.5	-0.3	-0.8	1.2	1.4	0.7	C.0	0.4	-0.1	0.3	-0.2	0.3	5.30	0.70	0.19	C.30	0.57	0.15
8036	0.5	0.5	0.9	0.2	0.2	0.6	0.2	-0.4	-0.2	-0.0	-0.6	0.3	-0.2	0.5	5.42	1.02	0.27	C.18	0.42	0.11
8119	1.1	-0.9	0.6	0.1	0.1	0.2	0.6	0.1	-0.2	0.1	0.5	0.4	-0.5	*****	5.53	0.99	0.27	C.17	0.52	0.14
8130	0.9	1.0	0.3	0.2	-0.7	0.6	0.9	0.8	-0.6	-0.2	0.7	0.1	0.1	-0.6	5.34	0.71	0.19	0.25	0.61	0.16
8637	*****	1.0	*****	0.5	*****	0.7	*****	0.2	*****	-0.4	*****	0.7	*****	-0.1	5.22	1.08	0.41	0.37	0.48	0.18
8645	0.3	1.2	0.8	0.2	-1.2	0.4	0.9	1.1	-1.0	-0.4	-0.5	0.0	-0.4	0.2	5.47	0.81	0.22	C.13	0.74	0.20
8656	*****	-0.1	*****	-0.7	*****	-0.1	*****	1.3	*****	*****	*****	*****	*****	*****	6.06	0.92	0.46	0.10	0.84	0.42
8662	*****	0.7	*****	0.5	*****	0.9	*****	1.1	*****	-0.3	*****	-1.8	*****	-0.2	5.45	0.83	0.31	C.14	1.00	0.38
8692	*****	0.9	*****	-0.1	*****	1.0	*****	0.8	*****	-0.5	*****	-0.3	*****	0.0	5.35	0.74	0.28	C.24	0.62	0.24
8708	*****	0.6	*****	0.1	*****	0.9	*****	1.4	*****	0.3	*****	-0.2	*****	-0.1	5.17	0.69	0.26	0.42	0.57	0.22

ORIGINAL PAGE IS  
OF POOR QUALITY

Table 29a. 48 HR. Z500 SKILL SCORE IMPACT ON NORTH AMERICA

EXP	8/20	8/21	8/22	8/23	8/24	8/25	8/26	8/27	8/28	8/29	8/30	8/31	9/1	9/2	*****EXPERIMENT*****			****DIFF. FROM (7336)****		
															AVE	SD	SE	AVE	SD	SE
7336	40.0	47.3	52.7	51.5	54.3	44.9	42.7	47.4	40.7	49.5	43.1	54.9	55.5	38.0	47.32	5.91	1.58	0.0	0.0	0.0
7854	-1.0	-1.9	5.4	6.0	-1.3	-4.4	2.0	0.8	0.3	-0.8	-1.6	5.5	-3.8	-2.4	47.12	5.70	1.52	0.20	3.38	0.90
7970	0.2	-0.6	5.1	6.1	-3.2	-2.3	2.5	3.0	-3.0	-1.2	-2.1	6.8	0.1	-4.8	46.85	5.08	1.36	0.47	3.67	0.98
8036	-0.6	-0.1	4.2	6.4	-2.0	0.5	-1.5	-3.1	-3.4	-0.3	-0.2	2.7	-2.2	-2.2	47.45	5.37	1.44	-0.13	2.82	0.75
8119	-2.1	-2.4	7.2	9.3	-1.7	-1.7	2.1	0.8	2.8	-0.2	-0.7	7.2	-2.8	-13.4	47.00	5.73	1.53	0.32	5.58	1.49
8130	-2.9	-0.9	6.1	9.5	-2.2	-1.4	-0.7	2.2	1.1	-1.7	-3.9	6.4	1.6	-9.1	47.03	4.58	1.22	0.29	4.75	1.27
8037*****	-4.1*****			5.9*****	-1.8*****			0.9*****	-1.7*****			2.5*****	-8.5		48.59	2.91	1.10	-0.95	4.66	1.76
8645*****	-3.2	4.4		6.7	2.3	-0.3	0.6	1.5*****	-2.9	-1.8	3.5	0.1	-7.8		48.22	4.04	1.17	0.26	3.88	1.12
8650*****	-4.0*****			3.1*****	-3.4*****			-4.0*****	*****	*****	*****	*****	*****		49.86	1.74	0.87	-2.09	3.48	1.74
8662*****	-1.7*****			6.7*****	-1.7*****			0.4*****	-2.4*****			0.1*****	-7.3		48.48	3.68	1.39	-0.84	4.19	1.58
8692*****	-2.9*****			7.5*****	-0.4*****			2.7*****	-1.1*****	*****	*****	*****	*****		46.95	3.17	1.42	1.17	4.06	1.82
8708*****	-2.5*****			5.1*****	2.6*****	*****	*****	*****	*****	*****	*****	*****	*****		46.16	3.78	2.18	1.74	3.91	2.26



Table 29b. 48 HR. Z500 RMS IMPACT ON NORTH AMERICA

EXP																*****EXPERIMENT*****			*****DIFF. FROM (7336)*****		
	8/20	8/21	8/22	8/23	8/24	8/25	8/26	8/27	8/28	8/29	8/30	8/31	9/1	9/2		AVE	SD	SE	AVE	SD	SE
7336	29.1	48.7	59.1	52.1	57.8	51.2	51.9	43.9	46.9	56.4	36.4	57.8	52.8	37.4		49.73	10.08	2.69	0.0	0.0	0.0
7854	-1.8	-0.5	4.7	9.8	-3.3	-3.7	8.1	14.0	2.5	-0.4	-4.2	12.0	-2.2	-1.2		47.31	8.66	2.32	2.42	6.20	1.66
7970	-1.7	-2.3	7.1	5.7	-6.7	-3.2	0.4	9.2	-2.8	-1.0	-6.2	9.0	-2.2	-5.7		49.75	8.17	2.18	-0.02	5.52	1.47
8036	-1.4	-0.0	4.5	9.7	-3.7	1.1	-0.2	-4.6	-7.6	-3.6	-4.8	3.5	-5.2	-2.8		50.81	9.96	2.66	-1.08	4.61	1.23
8119	-0.2	-2.8	9.0	14.6	-3.7	-1.4	7.2	5.6	0.7	-4.2	-4.6	7.0	0.8	*****		48.53	9.53	2.64	2.14	6.00	1.66
8130	-1.1	-2.3	9.1	13.7	-5.0	2.1	2.3	14.1	1.8	-10.3	-6.4	6.8	2.7	-9.3		48.43	9.28	2.48	1.30	7.73	2.07
8637	*****	-8.4	*****	12.3	*****	-3.4	*****	3.2	*****	-4.4	*****	6.4	*****	-5.5		52.57	8.36	3.16	0.02	7.48	2.83
8645	-3.4	-7.8	5.6	12.9	4.0	2.6	2.2	8.6	3.5	-3.8	-7.4	7.1	-1.6	-11.1		48.92	7.98	2.13	0.80	6.50	1.84
8656	*****	-7.1	*****	-19.7	*****	-15.5	*****	-4.6	*****	*****	*****	*****	*****	*****		65.86	6.99	3.50	-11.72	7.09	3.54
8662	*****	-3.8	*****	11.3	*****	-1.8	*****	-0.6	*****	-5.3	*****	-13.3	*****	-5.0		55.22	11.26	4.26	-2.63	7.38	2.79
8692	*****	-4.2	*****	13.2	*****	-1.8	*****	13.7	*****	-1.5	*****	8.9	*****	-5.4		49.32	6.53	2.47	3.27	8.35	3.16
8708	*****	-6.3	*****	10.4	*****	-5.3	*****	14.6	*****	-11.2	*****	2.0	*****	-10.6		53.51	8.24	3.12	-0.92	10.22	3.86

ORIGINAL PAGE IS  
OF POOR QUALITY

Table 30a. 72 HR. 2500 SKILL SCORE IMPACT ON NORTH AMERICA

EXP	8/20	8/21	8/22	8/23	8/24	8/25	8/26	8/27	8/28	8/29	8/30	8/31	9/1	9/2	*****EXPERIMENT*****			*****DIFF. FROM (7336)*****		
															AVE	SD	SE	AVE	SD	SE
7336	51.9	57.3	62.6	59.8	53.9	45.7	54.5	55.5	51.5	53.6	57.0	60.4	50.0	48.7	54.46	4.74	1.27	0.0	0.0	0.0
7854	-1.5	-3.2	4.6	4.4-10.4	-5.3	3.6	1.7	0.3	-1.0	-1.5	4.5	-3.8	-1.0		55.07	4.11	1.10	-0.61	4.29	1.15
7970	2.2	1.5	1.6	3.9-10.3	-3.3	4.2	-0.2	-2.9	0.2	-0.3	4.8	-4.1	-2.7		54.84	4.21	1.13	-0.39	4.05	1.08
8036	-1.3	1.5	7.2	6.8	-1.3	-0.6	0.3	-9.8	-5.9	-1.0	7.5	1.4	-3.2	-0.4	54.37	4.60	1.23	0.09	4.84	1.29
8119	0.7	-1.1	9.9	10.6	-5.3	-4.1	1.0	0.2	-2.1	0.1	3.5	7.8	-8.0	-11.4	54.33	3.43	0.92	0.13	6.38	1.70
8130	-1.4	3.1	8.6	8.4-11.2	-2.8	-2.0	-2.9	-3.4	-1.9	4.9	3.8	-4.4	-12.0		55.40	4.09	1.09	-0.94	6.24	1.67
8637	*****	-2.4	*****	2.8	*****	-3.1	*****	-3.1	*****	-5.6	*****	1.0	*****	-6.4	56.85	3.83	1.45	-2.42	3.30	1.25
8645	*****	-0.7	6.6	3.9	-1.1	-4.4	1.5	0.2	*****	-7.3	2.6	1.9	-2.4	-6.1	55.37	2.87	0.83	-0.45	4.13	1.19
8656	*****	0.1	*****	2.6	*****	-2.2	*****	-7.9	*****	*****	*****	*****	*****	*****	56.44	6.42	3.21	-1.87	4.49	2.24
8662	*****	-0.8	*****	2.9	*****	-4.7	*****	-1.6	*****	-4.1	*****	0.7	*****	-0.5	55.57	4.06	1.53	-1.14	2.64	1.00
8692	*****	-1.0	*****	3.8	*****	-2.1	*****	-1.1	*****	-4.7	*****	*****	*****	*****	55.59	3.94	1.76	-1.21	3.20	1.43
8708	*****	0.8	*****	2.6	*****	-0.2	*****	*****	*****	*****	*****	*****	*****	*****	53.16	6.32	3.65	1.11	1.42	0.82

Table 30b. 72 HR. 2500 RMS IMPACT CN NORTH AMERICA

EXP	8/20	8/21	8/22	8/23	8/24	8/25	8/26	8/27	8/28	8/29	8/30	8/31	9/1	9/2	*****EXPERIMENT*****	*****DIFF. FROM (7336)*****				
															AVE	SD	SE	AVE	SD	SE
7336	53.9	70.1	68.0	65.8	61.0	49.7	75.8	61.9	52.7	56.5	58.1	58.8	42.1	42.3	52.76	9.72	2.60	6.0	6.0	0.0
7854	-1.9	9.6	7.8	7.7	-9.3	1.2	23.4	15.6	3.9	-0.3	-0.7	7.4	-7.4	-3.4	54.93	6.65	1.78	3.83	6.28	2.37
7970	5.2	1.9	9.3	3.9	-10.6	-5.5	15.4	6.5	-3.5	-0.7	-4.9	5.5	-10.7	-7.4	58.45	6.62	1.77	6.31	7.79	2.08
8036	-1.3	4.2	11.0	12.6	-1.4	1.1	1.7	-19.7	-11.8	-6.8	6.6	0.2	-4.6	-2.3	59.51	10.81	2.89	-6.75	8.50	2.27
8119	1.8	-1.2	16.6	18.0	-5.4	-2.8	16.3	3.0	-0.3	-3.8	0.4	7.4	-14.4	*****	57.29	6.51	1.81	2.74	5.55	2.65
8130	1.5	5.5	12.5	12.8	-11.9	-5.7	13.6	1.3	-7.4	-41.8	4.1	2.5	-15.0	-13.9	61.75	12.01	3.21	-2.99	14.75	3.94
8637	*****	-5.5	*****	8.7	*****	-10.7	*****	12.0	*****	-13.4	*****	0.2	*****	-14.3	61.15	8.72	3.29	-3.28	16.60	4.00
8645	-0.3	-4.2	13.2	8.6	-4.3	-8.3	10.0	9.3	-12.7	-13.6	-0.7	2.2	-7.6	-14.5	60.41	7.62	2.04	-1.65	9.29	2.48
8656	*****	-1.4	*****	-30.1	*****	9.4	*****	-3.3	*****	*****	*****	*****	*****	*****	68.20	22.83	11.42	-6.32	16.78	8.39
8662	*****	-0.9	*****	6.6	*****	-23.9	*****	10.8	*****	-6.5	*****	-5.9	*****	-5.6	61.49	9.55	3.61	-3.62	11.17	4.22
8692	*****	-1.3	*****	8.3	*****	-8.5	*****	9.8	*****	-7.1	*****	-0.2	*****	-10.9	59.27	6.58	2.49	-1.40	6.11	3.07
8708	*****	-0.9	*****	2.1	*****	13.0	*****	12.5	*****	-8.4	*****	2.6	*****	-21.1	57.88	11.63	4.39	-0.01	11.93	4.51

OF POOR QUALITY

ORIGINAL PAGE IS  
OF POOR QUALITY

Table 31a. 48 HR. SLP SKILL SCORE IMPACT ON EUROPE

EXP	8/20	8/21	8/22	8/23	8/24	8/25	8/26	8/27	8/28	8/29	8/30	8/31	9/1	9/2	*****EXPERIMENT*****			*****DIFF.FROM(7336)*****			
															AVE	SD	SE	AVE	SD	SE	
7336	73.4	64.6	67.8	66.2	66.6	69.6	82.5	64.1	60.0	68.2	66.5	55.0	61.3	70.3	66.86	6.45	1.72	0.0	0.0	0.0	
7854	3.6	1.2	-0.2	-1.3	0.8	5.3	8.5	-0.6	0.6	1.8	3.4	-2.6	2.1	-0.9	65.31	4.69	1.25	1.55	2.92	0.78	
7970	0.1	-1.0	-2.2	-1.4	3.0	4.4	5.9	0.7	1.1	2.0	3.1	-1.6	3.9	5.4	65.19	5.61	1.50	1.67	2.69	0.72	
8036	2.3	-2.1	1.5	-3.3	-1.5	-1.0	5.2	1.3	1.3	5.9	6.7	0.8	-0.2	0.2	65.64	6.09	1.63	1.22	2.99	0.80	
8119	-2.1	-3.8	3.2	-6.6	-0.5	-1.0	7.6	-1.7	-6.9	2.0	-0.6	-4.7	-5.8	-11.3	69.16	5.45	1.47	-2.30	4.77	1.27	
8130	0.5	-1.0	-1.6	-8.7	-4.1	8.3	13.7	-4.0	-14.7	-4.7	-5.3	-2.8	3.0	-9.1	69.04	6.38	1.70	-2.18	7.17	1.92	
8637*****	2.8*****	1.8*****	-1.5*****	2.0*****	-2.0*****	-6.8*****	-0.4								66.01	4.43	1.68	-0.58	3.31	1.25	
8645*****	2.1	-2.5	-2.1	-1.9	-4.4	3.7	4.3*****	-1.0	0.2	-3.9	0.5	0.7				67.24	5.95	1.72	-0.35	2.80	0.81
8656*****	-0.3*****	-6.6*****	-3.4*****	5.7*****											67.26	7.02	3.51	-1.14	5.24	2.62	
8662*****	1.6*****	1.8*****	-0.5*****	-0.5*****	-0.2*****	-5.1*****	2.3								65.52	3.51	1.33	-0.09	2.48	0.94	
8692*****	2.3*****	0.3*****	-0.5*****	0.7*****	-3.1*****											66.68	4.06	1.81	-0.14	2.00	0.89
8708*****	-0.7*****	-4.0*****	-0.3*****												70.45	5.30	3.06	-3.65	2.80	1.62	

Table 31b. 48 HR. SLP RMS IMPACT ON EUROPE

EXP	8/20	8/21	8/22	8/23	8/24	8/25	8/26	8/27	8/28	8/29	8/30	8/31	9/1	9/2	*****EXPERIMENT*****			*****DIFF. FROM (7336)*****		
															AVE	SD	SE	AVE	SD	SE
7336	3.3	5.1	4.0	3.7	5.5	7.7	6.7	4.1	3.2	5.1	6.8	5.7	3.6	4.0	4.89	1.43	0.36	0.0	0.0	0.0
7854	0.0	0.7	0.6	0.5	0.9	1.2	0.8	0.2	0.9	1.1	1.1	0.5	0.6	0.5	4.20	1.24	0.33	0.69	0.35	0.09
7970	0.0	0.6	0.6	0.4	0.9	0.9	0.9	0.6	0.9	0.5	-0.0	0.2	0.5	0.7	4.34	1.43	0.38	0.55	0.31	0.08
8036	0.1	0.3	0.6	0.4	0.3	0.2	0.7	0.5	0.1	2.8	0.9	-0.2	0.1	0.3	4.39	1.50	0.40	0.50	0.73	0.19
8119	-0.4	0.2	-0.7	0.4	0.8	1.2	1.2	0.6	-0.7	1.6	0.5*****	-0.9*****			4.60	1.08	0.31	0.30	0.83	0.24
8130	-0.9	0.7	-0.6	0.0	0.9	1.7	2.4	0.1	-0.6	1.9	0.0	2.3	1.1	-0.5	4.28	1.08	0.29	0.61	1.13	0.30
8637*****	-1.0*****	-0.9*****	-1.4*****					0.7*****		1.1*****	0.7*****	-0.0			5.18	1.91	0.72	-0.12	0.98	0.37
8645	-0.5	-0.3	0.2	-0.5	0.4	-0.6	0.0	0.7	0.3	1.4	0.9	1.0	0.2	0.4	4.64	1.51	0.40	0.26	0.61	0.16
8656*****	0.3*****	-0.4*****	-1.9*****					1.1*****							5.38	2.87	1.44	-0.23	1.26	0.63
8662*****	0.7*****	-0.6*****	-0.9*****					0.3*****		0.6*****	1.1*****	-0.5			4.97	1.61	0.61	0.09	0.76	0.29
8692*****	-0.4*****	-1.1*****	-0.7*****					0.4*****		0.2*****	0.3*****	0.1			5.16	1.57	0.55	-0.10	0.67	0.25
8708*****	0.1*****	-0.3*****	-1.3*****					0.8*****		0.3*****	1.8*****	0.2			4.84	1.91	0.72	0.22	0.94	0.36

ORIGINAL PAGE IS  
OF POOR QUALITY

Table 32a. 72 HR. SLP ERROR IMPACT ON EUROPE

EXP	8/20	8/21	8/22	8/23	8/24	8/25	8/26	8/27	8/28	8/29	8/30	8/31	9/1	9/2	*****EXPERIMENT*****			****DIFF.FROM(7335)****		
															AVE	SD	SE	AVE	SD	SE
7336	74.8	76.6	77.6	73.5	73.3	102.0	92.2	70.6	80.8	71.0	72.7	67.2	74.5	82.2	77.79	9.27	2.46	0.0	0.0	0.0
7654	6.9	3.0	-2.7	6.0	3.9	11.0	10.4	-5.8	2.1	1.9	-1.6	-1.2	2.2	3.2	74.98	6.73	1.80	2.81	4.76	1.27
7970	1.8	-1.0	-3.0	6.1	5.8	8.9	5.3	1.9	0.7	3.6	-2.3	-3.1	8.9	4.4	75.07	8.17	2.18	2.71	4.10	1.10
8036	2.0	-1.8	3.9	4.0	1.1	6.0	12.5	3.6	5.9	4.9	6.0	-4.8	-3.3	2.1	74.78	7.71	2.06	3.01	4.40	1.18
8119	-3.7	2.5	1.8	2.6	-0.4	15.0	0.4	-15.8	12.4	3.2	-6.3	-9.2	-4.8	-11.9	78.80	8.25	2.20	-1.02	8.52	2.28
8130	5.6	5.6	-3.4	-3.5	-3.4	17.9	7.7	-18.6	0.0	-6.3	-8.6	-1.6	-6.8	-0.3	78.91	5.99	1.60	-1.12	8.63	2.31
8637*****	2.9*****	7.8*****	-0.5*****	4.7*****	1.5*****	-7.7*****	-0.8								76.44	12.97	4.90	1.14	4.92	1.86
8645*****	4.1	-5.8	1.8	-3.8	-3.3	3.5	1.6*****	-1.0	-0.4	-5.7	5.3	0.5			78.04	10.52	3.04	-0.26	3.75	1.08
8656*****	-0.8*****	-2.4*****	-3.2*****	3.3*****											81.42	16.44	8.22	-0.74	2.88	1.44
8662*****	7.4*****	7.5*****	-1.8*****	-2.8*****	-1.7*****	-6.3*****	1.6								77.01	12.62	4.77	0.58	5.21	1.97
8692*****	3.2*****	4.2*****	-2.1*****	-4.9*****	-1.0*****										78.87	14.31	6.40	-0.13	3.79	1.70
8708*****	-0.1*****	2.9*****	-3.6*****												84.31	18.72	10.81	-0.27	3.27	1.89

Table 32b. 72 HR. SLP RMS IMPACT ON EUROPE

EXP	8/20	8/21	8/22	8/23	8/24	8/25	8/26	8/27	8/28	8/29	8/30	8/31	9/1	9/2	*****EXPERIMENT*****			*****DIFF. FROM (7336)*****		
															AVE	SD	SE	AVE	SD	SE
7336	4.9	4.8	4.2	6.1	7.6	11.2	8.3	3.9	5.7	6.8	7.6	4.6	4.4	5.4	6.11	2.02	0.54	6.0	6.0	0.0
7854	0.7	0.2	0.2	1.2	0.5	1.4	1.0	0.2	0.6	1.2	0.2	-0.5	0.4	0.4	5.56	1.74	0.46	0.55	6.51	0.14
7970	0.3	0.4	0.3	1.2	1.4	1.8	1.1	0.9	0.1	-0.3	-0.3	-0.1	0.7	0.3	5.55	1.78	0.48	0.56	6.64	0.17
8036	-0.2	0.1	0.7	0.8	0.6	1.2	2.1	0.8	0.3	0.9	0.6	-0.2	0.0	0.7	5.52	1.71	0.46	0.60	6.60	0.16
8119	0.7	-0.0	-0.3	1.1	1.7	2.2	2.0	-0.4	2.7	1.6	-0.6*****	-0.4*****			5.43	1.70	0.49	0.87	1.18	0.34
8130	0.5	0.8	-1.0	0.6	1.6	3.8	2.9	-0.8	2.4	0.6	-1.4	0.5	-0.3	0.2	5.37	1.46	0.39	0.74	1.56	0.40
8637*****	-0.8*****	-0.3*****	-1.0*****					0.4*****	-0.5*****	-1.4*****					6.58	2.72	1.03	-0.46	0.68	0.26
8645	-0.2	0.2	-0.4	-0.9	0.6	-0.3	0.9	0.2	0.6	0.8	0.5	-0.4	0.5	0.7	5.92	2.02	0.50	0.19	0.54	0.14
8656*****	0.4*****	-2.6*****	-1.4*****					0.1*****							7.38	4.10	2.05	-0.88	1.42	0.71
8662*****	0.7*****	0.4*****	-0.0*****					0.5*****	-0.2*****	-0.2*****					5.93	2.89	0.98	0.18	0.35	0.13
8692*****	-0.4*****	-0.5*****	-0.0*****					-1.1*****	0.1*****	-0.9*****					6.47	2.20	0.83	-0.35	0.56	0.21
8708*****	0.7*****	-0.5*****	-98.2*****					1.7*****	-0.1*****	-0.1*****					19.76	39.54	14.94	-13.64	37.28	14.09

3-127

ORIGINAL PAGE IS  
OF POOR QUALITY

Table 33a. 48 HR. Z500 SKILL SCORE IMPACT ON EUROPE

EXP	8/20	8/21	8/22	8/23	8/24	8/25	8/26	8/27	8/28	8/29	8/30	8/31	9/1	9/2	*****EXPERIMENT*****	*****DIFF. FROM(7336)*****				
															AVE	SD	SE	AVE	SD	SE
7336	57.3	57.8	56.5	53.3	51.1	59.4	58.4	46.3	40.2	48.5	51.5	44.9	46.2	50.7	51.58	5.67	1.57	0.0	0.0	0.0
7854	7.7	2.0	-4.2	1.5	0.6	9.1	9.3	-1.5	-1.3	-1.2	5.4	-4.4	-2.4	-2.5	50.29	4.44	1.19	1.29	4.77	1.27
7970	4.6	1.6	-1.6	-0.3	2.1	6.2	7.5	0.9	-0.2	-1.1	3.6	-2.3	-2.3	2.2	50.09	4.53	1.21	1.49	3.10	0.83
8036	5.4	-1.0	-0.2	-0.1	1.1	4.2	7.0	2.8	-0.3	-1.5	1.4	-5.1	-5.2	-5.1	51.34	4.88	1.30	0.24	3.81	1.02
8119	5.0	0.7	2.0	-1.6	-8.1	3.3	-3.7	-2.9	-17.2	-3.1	-5.3	-13.3	-10.2	-8.0	56.03	3.35	0.90	-4.46	6.39	1.71
8140	4.3	-1.3	5.8	-3.3	-4.0	10.0	3.4	-2.8	-14.5	-5.1	-7.9	-10.0	1.2	-7.7	53.90	4.20	1.12	-2.32	6.71	1.79
8637*****	5.9*****	2.6*****	-2.9*****	4.3*****	-5.6*****	-4.9*****	-0.3	51.69	5.99	2.26	-0.13	4.53	1.71							
8645*****	5.0	7.4	3.6	-1.2	-0.7	5.1	3.3*****	-2.9	-0.6	-3.8	-0.9	-1.1	50.69	4.08	1.18	1.16	3.65	1.05		
8656*****	5.4*****	-3.5*****	-2.6*****	1.6*****	*****	*****	*****	*****	*****	*****	*****	*****	53.78	7.33	3.66	0.22	4.12	2.06		
8662*****	5.6*****	4.1*****	-0.8*****	3.1*****	-3.2*****	-4.2*****	0.4	50.83	5.07	1.92	0.73	3.71	1.40							
8692*****	4.5*****	3.0*****	-1.0*****	5.8*****	-4.2*****	*****	*****	*****	*****	*****	*****	*****	51.43	7.15	3.20	1.63	4.13	1.85		
8703*****	3.1*****	3.5*****	-0.6*****	*****	*****	*****	*****	*****	*****	*****	*****	*****	54.85	5.11	2.95	1.98	2.28	1.32		



Table 33b. 48 HR. 2500 RMS IMPACT ON EUROPE

EXP	*****EXPERIMENT*****														*****DIFF. FROM (7336)*****					
	8/20	8/21	8/22	8/23	8/24	8/25	8/26	8/27	8/28	8/29	8/30	8/31	9/1	9/2	AVE	SD	SE	AVE	SD	SE
7336	41.9	64.6	53.8	44.4	67.1	94.5	73.7	60.8	52.9	63.6	77.9	59.7	55.2	67.5	61.97	13.65	3.65	6.0	6.0	0.0
7854	6.1	9.5	4.1	5.5	11.5	18.6	11.9	-4.1	4.8	9.3	9.1	-3.1	1.1	2.9	55.74	10.25	2.90	6.23	6.08	1.62
7970	2.3	6.6	4.9	1.0	14.9	13.4	10.9	1.3	8.1	4.1	-1.5	-3.9	25.9	7.9	55.05	14.42	3.83	6.92	7.67	2.05
8026	20.1	41.5	8.1	4.6	7.6	8.0	10.2	2.4	5.1	5.4	4.7	-7.5	-4.2	1.2	54.67	17.65	4.72	7.30	11.84	3.17
8119	1.3	5.9	0.1	6.4	3.8	4.9	-2.0	2.8-10.0	-8.7-16.4	*****	-22.9	*****			65.43	17.45	5.04	-2.90	9.51	2.75
8120	-3.0	16.4	-1.8	-0.4	6.3	20.4	14.8	5.1	-3.3	-3.1-23.1	2.9	7.3	9.4		58.55	14.80	3.95	3.42	10.83	2.89
8637	*****	-0.8	*****	9.4	*****	-1.8	*****	16.3	*****	14.4	*****	-5.7	*****	6.4	58.13	20.08	7.59	5.46	6.48	3.21
8645	1.4	2.7	8.5	12.6	5.7	9.8	14.3	19.4	2.5	6.5	3.0	-2.4	-2.5	14.1	54.86	14.14	3.78	7.11	6.62	1.77
8656	*****	13.5	*****	-4.4	*****	3.0	*****	11.9	*****	*****	*****	*****	*****	*****	60.07	21.01	10.51	6.00	6.33	4.16
8662	*****	14.6	*****	6.1	*****	-8.1	*****	5.0	*****	-7.5	*****	-8.5	*****	-3.0	63.79	20.39	7.71	-0.20	6.92	3.37
8652	*****	8.3	*****	7.1	*****	7.7	*****	20.9	*****	5.2	*****	-12.6	*****	15.2	56.18	18.35	6.94	7.40	10.39	3.93
8708	*****	2.1	*****	8.1	*****	20.1	*****	13.0	*****	5.8	*****	-5.8	*****	5.0	56.69	12.52	4.73	6.91	6.20	3.10

Table 34 a. 72 HR. Z500 SKILL SCORE IMPACT ON EUROPE

EXP	8/20	8/21	8/22	8/23	8/24	8/25	8/26	8/27	8/28	8/29	8/30	8/31	9/1	9/2	*****EXPERIMENT*****			*****DIFF. FROM (7336)*****		
															AVE	SD	SE	AVE	SD	SE
7336	70.6	72.4	66.6	67.4	57.8	61.6	69.8	57.7	51.3	60.9	56.4	50.1	58.3	53.6	62.49	9.18	2.45	0.0	0.0	0.0
7854	4.3	-0.4	-3.9	4.5	1.6	12.3	1.8	-1.7	1.5	3.9	-3.8	-7.1	-0.9	-5.4	62.01	6.56	1.75	0.48	4.99	1.33
7970	0.1	-3.5	-2.1	4.0	2.0	12.1	7.5	3.0	1.4	5.4	-3.9	-7.2	1.1	-1.9	61.20	7.52	2.01	1.29	5.02	1.34
8036	0.9	-1.5	0.1	6.8	3.2	6.8	6.4	2.5	1.8	2.1	1.5	-8.5	-2.9	-4.0	61.40	7.55	2.02	1.09	4.32	1.16
8119	2.8	-1.0	7.4	0.3	-6.9	10.8	-5.5	-3.3	-8.7	2.8	-12.8	-16.3	-4.8	-8.0	65.57	5.40	1.44	-3.09	7.52	2.01
8130	5.4	0.8	12.6	0.0	-3.3	16.4	6.5	-7.4	-8.5	4.3	-16.3	-8.8	1.1	-7.0	62.79	5.51	1.47	-0.30	8.98	2.40
8637*****	9.5*****	4.6*****	0.3*****	5.7*****	-0.4*****	-14.0*****	-0.4								62.67	9.59	3.62	0.76	7.49	2.83
8645*****	7.8	11.8	4.2	-1.9	0.3	0.3	0.3*****	1.4	-6.8	-9.8	1.6	-3.2			62.24	7.34	2.12	0.50	5.83	1.68
8656*****	4.4*****	-1.0*****	5.8*****	5.6*****	*****	*****	*****	*****	*****	*****	*****	*****	*****	*****	65.16	10.09	5.05	3.69	3.20	1.60
8662*****	9.2*****	3.6*****	4.4*****	1.9*****	0.7*****	-8.7*****	-1.0								61.93	7.64	2.85	1.49	5.54	2.09
8692*****	7.3*****	4.8*****	0.2*****	-2.5*****	0.0*****	*****	*****	*****	*****	*****	*****	*****	*****	*****	66.11	8.93	3.95	1.95	3.98	1.78
8708*****	1.5*****	5.4*****	6.4*****	*****	*****	*****	*****	*****	*****	*****	*****	*****	*****	*****	69.48	6.88	3.97	4.42	2.59	1.50

Table 34b. 72 HR. 2500 RMS IMPACT ON EUROPE

EXP	8/20	8/21	8/22	8/23	8/24	8/25	8/26	8/27	8/28	8/29	8/30	8/31	9/1	9/2	*****EXPERIMENT*****			*****DIFF. FROM (7336)*****		
															AVE	SD	SE	AVE	SD	SE
7336	69.3	76.4	60.9	80.0	100.0	125.4	93.3	81.1	73.1	62.8	84.2	60.8	62.6	58.5	79.17	18.26	4.88	0.0	0.0	0.0
7854	14.0	7.7	-0.8	10.7	6.7	21.8	0.3	-0.9	6.9	12.2	-7.1	-18.4	-6.3	-4.3	76.57	14.22	3.80	2.60	10.34	2.76
7970	6.6	0.4	2.0	8.2	16.8	24.4	11.8	4.0	1.4	-0.1	-9.5	-9.6	31.1	5.7	72.38	17.37	4.64	6.79	11.62	3.10
8036	45.9	52.7	5.3	9.8	12.5	13.7	17.0	5.5	2.6	8.3	-0.9	-12.4	-8.2	6.2	67.89	23.46	6.27	11.28	16.03	4.82
8119	11.8	5.1	10.8	17.2	7.9	22.2	-2.4	9.7	-6.1	-18.3	-30.1	***	21.1	****	82.04	19.93	5.75	6.38	16.47	4.75
8130	5.4	22.3	4.0	6.4	16.6	38.4	24.3	1.1	6.5	-15.5	-42.6	-5.2	5.2	8.2	73.81	20.46	5.47	5.36	15.10	5.11
8637	****	10.2	****	3.8	****	3.0	****	22.4	****	-16.1	****	-36.0	****	3.0	82.12	24.72	9.34	-1.40	15.06	7.20
8645	4.1	14.2	12.2	4.8	8.1	9.9	9.6	20.4	-3.1	-8.6	-15.4	-17.0	-5.4	7.9	76.19	18.95	5.07	2.97	11.24	3.00
8656	****	11.3	****	16.4	****	8.3	****	26.8	****	****	****	****	****	****	75.05	28.50	14.25	15.70	8.14	4.07
8662	****	23.4	****	-1.4	****	3.5	****	10.5	****	-24.4	****	-18.0	****	-19.2	84.38	23.03	8.71	-3.67	17.62	6.66
8692	****	16.4	****	4.5	****	8.3	****	10.9	****	-18.6	****	-26.2	****	9.7	80.00	23.71	8.96	6.71	16.33	6.17
8708	****	12.2	****	17.1	****	24.6	****	27.9	****	1.2	****	-14.8	****	13.6	69.03	18.75	7.09	11.69	14.56	5.50

ORIGINAL PAGE IS  
OF POOR QUALITY

corresponding days. The first row contains actual skill score (or RMS) values for the NO SAT experiments 7336; the other rows contain the impacts determined by the differencing process described in Subsection 3.3.2.1.

Considering the results for each experiment, we notice great variations in the daily values of skill scores for all quantities (for both  $p_s$  and  $\phi$ , over both verification regions, and at both verification times); typically negative as well as positive impacts occur, and they are of varying magnitude. These variations can be attributed to a number of factors, among which the quality of the satellite data during the 48h preceding the given day figures prominently, along with the synoptic situation at the initial forecast time itself. Other factors can be simply assumed to generate random differences in the impacts.

A much more careful analysis than was possible up to the present would be needed to separate random influences on the impacts from those determined by the two factors we mentioned above. In the absence of such a separation, and in order to gain some overview of the experiments' impacts, we computed the results in the last six columns of the table. These computations were based on the assumption that all influences on the impacts, but that of the parameter varied from one experiment to the other (see Subsection 3.3.1.2), were random.

Let the entries in any of the Tables we discuss, in any of the columns labelled 8/20 through 9/2, be denoted by  $x_{ij}$ , with

$i$  the row number,  $0 \leq i \leq M$ ,  $M = 11$ , and  $j$  the column number,  $1 \leq j \leq N$ ,  $N = 14$ . Thus the actual skill scores for the NO SAT experiment are  $x_{0j}$ ,  $1 \leq j \leq N$ , while the skill score impacts for all the other experiments are  $x_{ij}$ ,  $1 \leq i \leq M$ .

The results in the three columns with the heading "Experiment" represent an overview of skill scores themselves, i.e., of  $x_{0j}$  for the first row,  $i=0$ , and of  $y_j = x_{0j} + x_{1j}$ , for the other rows,  $i \neq 0$ . The column headed "AVE" contains the averages  $\bar{x}_0 = \sum_{j=1}^N x_{0j}/N$  and  $\bar{y}_i = \sum_{j=1}^N y_{ij}/N$ ,  $i \neq 0$ , respectively; the column headed "SD" contains the standard deviations  $\delta_i$  of  $x_0$  or  $y_i$ , defined by  $\delta_i^2 = \sum_{j=1}^N (y_{ij} - \bar{y}_i)^2/N$ ,  $i \neq 0$ , and similarly for  $\delta_0$ . The column headed "SE" contains the so-called standard errors  $\hat{\delta}_i$  in estimating the means to  $\bar{x}_0$  and  $\bar{y}_i$ ,  $i \neq 0$ , respectively; it is computed as  $\hat{\delta}_i = \delta_i/\sqrt{N}$ .

The results in the three columns headed "Diff. from (7336)" represent an overview of the impacts  $x_{ij}$ ,  $0 \leq i \leq M$ . The entries in the first row are therefore clearly zero. The column headed "AVE" contains  $\bar{x}_i = \sum_{j=1}^N x_{ij}/N$ , column "SD" contains  $\sigma_i$ ,  $\sigma_i^2 = \sum_{j=1}^N (x_{ij} - \bar{x}_i)^2/N$ , and finally "SE" contains  $\hat{\sigma}_i = \sigma_i/\sqrt{N}$ .

We still see great differences between the results in the last three columns of Tables 27 through 34, from one Table to the other. A discussion very similar to the one concerning daily variations in results over the same area applies with respect to the variation in verification results over NA as compared to those over EU; the results of verification over these two regions can be considered as results of independent experiments in the case of 2-3 day forecasts. The

results for  $p_s$  on the other hand should be rather closely correlated to those for  $\phi$ , and so should the results for the same quantity at 48h and at 72h. We are not prepared at the present to make the finer distinctions alluded to above in our analysis of the experiments, and aim again for a "quick and dirty" overlook of all experimental results; a more rigorous analysis is in preparation.

The final overlook of  $S_1$  skill score results for our DST-5 experiments is given in Tables 35 and 36. In Table 35, the results in column "AVE DIFF" of Tables 27a through 34a are simply repeated, but as percentages of the value of  $\bar{x}_0$  in each Table, and with appropriate headings; let these entries be labelled  $\bar{x}_{ik}$ ,  $1 \leq k \leq 8$ . The last column of Table 35 then gives the "TOTAL" average  $S_1$  impact of each experiment,  $\bar{\bar{x}}_i = \sum_{k=1}^8 \bar{x}_{ik} / 8$ .

In Table 36 we have attempted to give a rough measure of the statistical significance of our experimental results. Such a measure has to be interpreted with caution, since the total number of forecasts for any given experiment is small, and some of the verified quantities for each forecast are not independent.

Without going into the details of statistical verification theory, and of hypothesis testing, we define our measure of statistical significance, or confidence in our results, in the following operational way: In each one of Tables 27a through 34a, compute  $\zeta_{ik} = \bar{x}_i / \hat{\sigma}_i$ ,  $1 \leq i \leq M$ ,  $1 \leq k \leq 8$ . These values  $\zeta_{ik}$  are entered under appropriate headings, which identify  $k$ , in columns 2 through 9 of Table 36; the first column identifies  $i$ , or the experiments, as in the previous tables. The "TOTAL" measure of significance of any given experiment  $i$  is

Table 35. Summary of percent impact in skill score.

EXPER	SLP		NA	Z500		SLP	ER	Z500		TOTAL
	48	72		48	72			48	72	
7336	0.0	0.0		0.0	0.0	0.0	0.0	0.0	0.0	0.0
7854	2.45	2.52		0.42	-1.13	2.32	3.61	2.51	0.77	1.69
7970	3.87	4.07		1.00	-0.71	2.50	3.49	2.89	2.06	2.40
8036	1.85	3.48		-0.27	0.16	1.83	3.87	0.47	1.74	1.64
8119	-0.96	-0.10		0.67	0.24	-3.44	-1.31	-8.64	-4.94	-2.31
8130	1.39	0.94		0.62	-1.73	-3.25	-1.44	-4.50	-0.48	-1.06
8637*	0.45	1.90		-2.61	-4.45	-0.87	1.47	-0.25	1.22	-0.32
8645*	1.12	3.06		0.56	-0.82	-0.52	-0.33	2.24	0.80	0.76
8656*	-7.95	-2.96		-4.42	-3.43	-1.70	-0.95	0.43	5.90	-1.89
8662*	-0.97	1.45		-1.77	-2.10	-0.13	0.74	1.42	2.39	0.13
8692*	2.34	3.50		2.46	-2.22	-0.20	-0.17	3.16	3.12	1.50
8708*	2.65	4.70		3.67	2.93	-5.46	-0.35	3.84	7.07	2.27
	* - INCOMPLETE									

Table 36. Average/standard error in skill score.

EXPER	SLP		NA	Z500		SLP		ER	Z500		TOTAL
	48	72		48	72	48	72		48	72	
7336	0.0	0.0		0.0	0.0	0.0	0.0		0.0	0.0	0.0
7854	1.88	1.64		0.22	-0.54	1.98	2.21		1.01	0.36	1.10
7970	2.59	2.34		0.48	-0.36	2.32	2.48		1.80	0.96	1.58
8036	1.84	2.23		-0.17	0.07	1.53	2.56		0.24	0.94	1.23
8119	-0.52	-0.05		0.21	0.08	-1.80	-0.45		-2.61	-1.53	-0.83
8130	0.63	0.40		0.23	-0.57	-1.14	-0.49		-1.29	-0.13	-0.29
8637*	0.17	0.56		-0.54	-1.94	-0.46	0.51		-0.03	0.27	-0.12
8645*	0.65	1.40		0.24	-0.38	-0.43	-0.24		1.10	0.30	0.38
8656*	-2.81	-1.15		-1.20	-0.83	-0.43	-0.52		0.11	2.31	-0.57
8662*	-0.36	0.51		-0.53	-1.15	-0.10	0.29		0.52	0.71	-0.01
8692*	0.86	1.27		0.64	-0.85	-0.15	-0.08		0.88	1.10	0.46
8708*	1.21	2.25		0.77	1.35	-2.26	-0.14		1.50	2.55	0.95

\* - INCOMPLETE



then given in the last column of the Table by simple averaging, as for Table 35,  $\bar{\zeta}_i = \sum_{k=1}^8 \zeta_{ik}/8$ . The values  $\bar{\zeta}_i$  are related to a standardized score, or z score, for the mean of the impacts, in terms of a probability distribution with zero mean and unit standard deviation. In this treatment we have neglected the uncertainty in estimating the standard deviation of the mean impact; this uncertainty would be taken into account in the careful application of a Student's t-test to the confidence limits of the mean. We hope to give a more detailed statistical analysis of our results in a future publication. At this point we would only like to remark that for a number of degrees of freedom  $\nu$ , or sample size  $N$ ,  $\nu = N-1 = 13$ , the t-distribution is practically undistinguishable from a standardized normal distribution; the remark is valid a fortiori if we are willing to grant that verification results over Europe are independent of those over North America, and hence  $\nu = N-1 = 23$ .

After these remarks we shall limit ourselves to saying that we have very little confidence in the results of a given experiment i if  $|\bar{\zeta}_i| \leq 0.5$ , reasonable confidence if  $0.5 < |\bar{\zeta}_i| \leq 2$ , and very high confidence if  $2 < |\bar{\zeta}_i|$ . It might be worthwhile to remember that the values 0.5, 1, 2 or  $z = \bar{\zeta}_i$  correspond to the following well known values of the cumulative distribution function  $F(z)$  of a normal distribution with zero mean and with standard deviation unity:

$$F(0.5) = 0.69, F(1) = 0.84, F(2) = 0.98 .$$

Having described the presentation of our results in the Tables, we proceed to their preliminary assessment. As indicated already in Subsection 3.3.1.1, some DST-5 experiments are still in progress; they use modifications of SAM which were based on intervening

experience with DST-6 experiments. We shall discuss only experiments 7854 through 8130, which have been completed.

A look at the last column of Table 36 indicates that the results of the two SAM experiments, 8119 and 8130, completed for the summer DST period, have at most marginal statistical significance. The bias removal described in Subsection 3.3.1.2 for 8119 did not seem to help. Columns 2 through 5 of Table 35 seem to give somewhat better skill score impacts over North America for 8130, but the results over Europe (columns 6 through 9) are negative for 8130 as well as 8119.

The statistical significance of the results for the two DIM experiments, 7854 and 7970, and of the SCM experiment 8036, seems reasonable good ( $\bar{\zeta}_i \geq 1.1$ ). The best total skill score impact obtains, surprisingly enough, for DIM experiment 7970, which utilized only data from one satellite, NIMBUS-6, processed by NESS. Neither the use of data from two satellites (7854), nor the use of SCM, a somewhat more sophisticated assimilation method (8036), yielded an improvement.

The interpretation of satellite-data impacts for the DST-5 period is made rather difficult, however, by the fact that, during that period, the synoptic situation was particularly sluggish (see, for instance, Subsection 3.2.6.2.4). This means that useful information from satellite data over the ocean basin upwind from a verification area does not reach that area in useful time, i.e., not before the information is completely distorted by the model's insufficient predictive capabilities during the assimilation process. It is therefore somewhat surprising that a positive impact, with moderate

Table 37. Summary of percent impact in rms errors.

EXPER	NCRTH AMERICA				EUROPE				TOTAL
	SLP		2500		SLP		2500		
	48	72	48	72	48	72	48	72	
7336	0.0	0.0	0.0	0.0	0.0	0.0	0.0	0.0	0.0
7854	6.12	7.00	4.86	6.52	14.14	9.08	10.06	3.28	7.63
7970	3.57	5.29	-0.05	0.53	11.22	9.18	11.17	8.58	6.19
8036	1.33	3.20	-2.17	-1.28	10.32	9.79	11.78	14.24	5.90
8119*	3.21	2.98	4.31	4.66	6.23	14.17	-4.68	0.48	3.92
8130	4.66	4.48	2.61	-5.08	12.52	12.17	5.52	6.77	5.46
8637*	-0.48	6.66	0.04	-5.59	-2.36	-7.57	8.81	-1.77	-0.26
8645	0.12	2.26	1.62	-2.80	5.24	3.18	11.48	3.76	3.11
8656*	-10.76	1.79	-23.57	-10.76	-4.65	-14.31	9.68	19.82	-4.10
8662*	-12.71	2.53	-5.29	-6.16	1.93	3.01	-0.32	-4.63	-2.71
8692*	4.33	4.32	6.58	-2.38	-1.98	-5.75	11.55	0.90	2.24
8708*	0.63	7.46	-1.86	-0.02	4.52*****		11.15	14.77	-23.31

\* - INCOMPLETE

Table 38. Statistical significance in rms error.

EXPER	NORTH AMERICA				EUROPE				TOTAL
	48	SLP 72	48	Z500 72	48	SLP 72	48	Z500 72	
7336	0.0	0.0	0.0	0.0	0.0	0.0	0.0	0.0	0.0
7854	2.13	2.38	1.46	1.62	7.44	4.03	3.84	0.94	2.98
7970	1.40	1.95	-0.02	0.15	6.68	3.27	3.38	2.19	2.32
8036	0.67	1.60	-0.28	-0.33	2.59	3.70	2.31	2.34	1.50
8119*	1.61	1.16	1.29	1.03	1.27	2.54	-1.06	0.08	0.99
8130	1.03	1.55	0.63	-0.76	2.03	1.86	1.18	1.05	1.07
8637*	-0.11	2.04	0.01	-0.82	-0.31	-1.80	1.70	-0.19	0.07
8645	0.03	0.64	0.44	-0.66	1.58	1.35	4.02	0.99	1.05
8656*	-2.00	0.24	-3.31	-0.75	-0.36	-1.23	1.44	3.86	-0.26
8662*	-1.55	0.38	-0.94	-0.86	0.33	1.40	-0.06	-0.55	-0.23
8692*	1.32	1.02	1.04	-0.46	-0.38	-1.67	1.82	0.12	0.36
8708*	0.18	1.92	-0.24	-0.00	0.62	-0.97	2.23	2.13	0.73

\* - INCOMPLETE

statistical significance, was obtained at all in the summer experiments.

The summary of rms results for DST-5 experiments is given in Tables 37 and 38: Table 37 contains average impacts, Table 38 displays their statistical significance. We notice immediately that both the impact itself and the confidence we can have in it are much better for the rms results than for the analogous  $S_1$  results; the reason for this is not clear. These rms results, are somewhat encouraging, but they cannot by themselves change our conclusions with respect to the summer experiments: we still have to regard them as inconclusive.

With this comment we turn to the presentation and discussion of results for the winter experiments.

### 3.3.2.3 DST-6 RESULTS

Results have been obtained, as of the time of this writing, for part of the DST-6 period, namely for January 30 through February 21. Since this period is somewhat longer than the DST-5 period, it was only feasible computationally to perform forecasts for every second day, starting with February 1, February 3, and so on, till February 21. Thus, eleven forecasts have been performed for each complete experiment.

The same quantities have been computed for each forecast as described in the Introduction (Subsection 3.3.2.1), and discussed in further detail in the previous Subsection (3.3.2.2). We present in Tables 39a-39h the  $S_1$  skill score results for  $p_s$  (SLP) and  $\phi$  (Z500) at 48h and 72h, over North America (NA) and over Europe (EU); this corresponds to Tables 27a, 28a, 29a, 30a, 31a, 32a, 33a, 34a of Subsection 3.3.2.2. The corresponding RMS results are given in

Table 39a. 48 HR. SLP SKILL SCORE IMPACT CN NORTH AMERICA

EXP	2/1	2/3	2/5	2/7	2/9	2/11	2/13	2/15	2/17	2/19	2/21	*****EXPERIMENT*****			*****DIFF. FROM (7578)*****				PRCNT. IMPACT
												AVE	SD	SE	AVE	SD	SE	AV/SE	
7578	78.8	53.4	72.1	88.2	81.0	84.2	74.0	70.0	59.8	73.6	64.9	72.73	10.43	3.15	0.0	0.0	0.0	0.0	0.0
8240	-6.1	2.2	-0.6	3.3	-0.2	2.2	7.2	-4.2	0.6	-3.4	-0.3	72.66	11.01	3.32	0.06	3.72	1.12	0.06	0.09
8497	-0.8	6.5	-1.5	3.0	*****	*****	*****	*****	*****	*****	*****	71.33	16.95	8.48	1.79	3.69	1.84	0.57	2.46
8310	-5.3	7.0	-4.0	10.6	8.2	7.8	5.9	0.7	-3.3	-8.8	0.3	70.97	10.60	3.19	1.75	6.51	1.96	0.89	2.41
8352	-4.3	6.7	0.8	10.4	2.8	4.3	6.6	0.3	4.6	-8.6	1.2	70.48	11.64	3.51	2.25	5.31	1.60	1.40	3.09
8405	-3.7	3.3	-2.6	5.1	1.3	1.4	3.6	-1.9	-2.2	-2.3	1.8	72.37	10.45	3.15	0.35	2.98	0.90	0.35	0.49
8447	-2.5	6.6	0.6	10.2	3.9	-1.4	7.0	-2.6	2.5	-9.4	-6.4	71.95	11.55	3.48	0.77	5.95	1.79	0.43	1.07
8472	-3.7	5.1	-1.4	10.0	6.3	0.5	9.1	-2.1	3.1	-13.0	1.2	71.35	11.91	3.59	1.38	6.53	1.97	0.70	1.90
8545	-2.9	6.7	-5.9	11.2	6.9	5.9	11.6	3.7	2.4	-0.8	1.2	69.64	11.21	3.38	3.09	6.26	1.89	1.64	4.25
8566	-5.6	8.4	-4.7	8.3	4.2	9.2	11.8	6.9	-0.1	-3.8	1.6	69.45	11.64	3.51	3.28	6.17	1.86	1.76	4.51
8574	-3.5	5.1	1.7	1.1	1.6	0.5	7.9	11.4	3.1	-3.5	-0.9	70.50	12.57	3.79	2.23	4.55	1.37	1.62	3.06
8581	-2.0	3.5	-5.1	*****	*****	*****	*****	*****	*****	*****	*****	69.28	16.91	9.76	-1.18	4.39	2.53	-0.47	-1.62
8593	-2.1	6.7	-5.2	9.1	7.1	7.2	11.7	5.4	4.5	-0.9	0.3	69.30	11.42	3.44	3.43	6.05	1.83	1.88	4.72
8695	-1.2	-1.3	-1.7	3.5	*****	*****	*****	*****	*****	*****	*****	73.29	13.19	6.59	-0.17	2.46	1.23	-0.14	-0.23
CAVE	-3.4	5.1	-2.3	7.1	4.2	3.8	8.2	1.8	1.5	-6.6	0.0								
ESGMA	1.6	2.5	2.4	3.5	2.7	3.5	2.6	4.7	2.6	3.2	2.3								
CSE	0.4	0.7	0.7	1.0	0.9	1.1	0.8	1.5	0.8	1.0	0.7								
CAVSE	-7.6	7.4	-3.4	7.1	4.9	3.4	9.9	1.2	1.9	-6.6	0.0								
CAVNS	-4.3	9.6	-3.2	8.1	5.2	4.5	11.1	2.5	2.5	-9.0	0.0								

3-142

C-2

ORIGINAL PAGE IS  
OF POOR QUALITY



Table 39b. 72 HR. SLP SKILL SCORE IMPACT ON NORTH AMERICA

EXP	2/1	2/3	2/5	2/7	2/9	2/11	2/13	2/15	2/17	2/19	2/21	*****EXPERIMENT*****	AVE	SD	SE	*****DIFF. FROM (7578)*****	AVE	SD	SE	AV/SE	PRCNT. IMPACT
7578	74.9	75.8	93.4	96.8	100.0	87.0	80.3	65.8	63.8	72.4	77.9	80.74	12.14	3.66	0.0	0.0	0.0	0.0	0.0	0.0	
8240	-8.0	-3.6	5.8	4.3	-1.0	12.0	7.3	-6.4	-2.0	4.0	-4.0	79.97	10.67	3.22	0.76	6.31	1.90	0.40	0.94		
8497	-1.2	1.0	5.0	-10.8	*****							86.48	15.20	7.60	-1.25	7.07	3.54	-0.35	-1.55		
8310	-7.1	9.4	2.6	9.3	17.8	14.9	4.7	-4.1	-14.7	-7.9	-7.6	79.16	7.59	2.29	1.57	10.57	3.19	0.49	1.95		
8352	-14.4	3.7	5.6	7.5	3.5	15.1	5.0	0.1	-9.7	-1.6	-4.8	79.82	9.72	2.93	0.91	6.29	2.50	0.37	1.13		
8405	-12.0	4.7	-2.8	0.3	1.4	-1.2	5.2	-3.7	-4.5	5.8	-4.3	81.75	12.24	3.69	-1.01	5.29	1.59	-0.64	-1.26		
8447	-7.9	2.8	6.0	8.4	5.6	8.0	8.1	-6.7	-7.8	-1.1	-12.7	80.12	7.97	2.40	0.61	8.13	2.45	0.25	0.76		
8472	-8.2	1.9	6.3	10.3	15.0	5.5	9.5	-0.1	-8.1	-15.6	-2.8	79.49	7.61	2.29	1.25	9.28	2.80	0.45	1.54		
8545	-3.7	8.1	3.9	12.7	10.9	7.2	11.8	-0.6	-5.7	-2.6	3.0	76.65	8.36	2.52	4.09	6.57	1.98	2.06	5.06		
8566	-4.9	8.4	-0.3	10.2	13.5	16.4	10.5	1.5	-5.7	-2.8	5.2	70.00	9.40	2.83	4.73	7.64	2.30	2.06	5.86		
8574	-8.0	-3.0	4.6	5.7	10.9	0.2	7.3	-1.0	4.8	-0.6	1.9	78.65	10.24	3.09	2.08	5.26	1.59	1.31	2.58		
8581	-1.3	4.2	-1.8	*****							81.02	12.54	7.24	0.35	3.37	1.95	0.18	0.43			
8593	-2.8	8.7	3.9	12.1	12.6	10.0	12.5	1.5	-4.2	-3.6	1.4	75.99	8.60	2.59	4.74	6.68	2.01	2.35	5.88		
8695	1.9	-8.2	10.6	-1.9	*****							84.63	10.61	5.30	0.59	7.83	3.92	0.15	0.73		
DAVE	-6.0	2.9	3.9	5.7	9.4	8.8	8.2	-1.9	-5.8	-2.6	-2.5										
CSGMA	4.4	5.1	3.5	6.6	5.8	5.8	2.7	2.9	4.8	5.7	5.2										
CSE	1.2	1.4	1.0	1.9	1.8	1.8	0.8	0.9	1.5	1.8	1.6										
CAVSE	-4.9	2.1	3.9	3.0	5.1	4.8	9.7	-2.1	-3.8	-1.4	-1.5										
CAVNS	-8.0	3.9	4.1	5.9	9.4	10.1	10.2	-3.0	-9.0	-3.6	-3.2										

ORIGINAL  
OF POOL

ORIGINAL PAGE IS  
OF POOR QUALITY





Table 39d. 72 HR. Z500 SKILL SCORE IMPACT ON NORTH AMERICA

EXP	2/1	2/3	2/5	2/7	2/9	2/11	2/13	2/15	2/17	2/19	2/21	*****EXPERIMENT*****			*****DIFF. FROM (7578)*****					PRCNT. IMPACT
												AVE	SD	SE	AVE	SD	SE	AV/SE		
7578	47.7	46.6	49.3	52.8	53.5	37.4	44.2	44.3	38.4	51.7	47.4	46.66	5.33	1.61	0.0	0.0	0.0	0.0	0.0	
8240	-3.8	-1.6	2.6	-0.6	-1.9	-2.3	4.3	-3.4	-0.1	4.1	-2.9	47.18	5.67	1.71	-0.52	2.94	0.89	-0.59	-1.11	
8497	-3.3	5.7	2.4	-8.4	*****							50.00	8.54	4.27	-0.90	6.22	3.11	-0.29	-1.93	
8310	4.5	11.0	1.2	-0.2	6.9	1.1	1.6	-1.9	-3.2	-0.9	4.5	44.25	5.62	1.69	2.41	4.43	1.34	1.81	5.17	
8352	-1.2	6.9	1.3	-2.8	5.1	0.9	2.5	-0.3	-2.9	2.4	-0.9	45.68	5.44	1.64	0.98	3.10	0.93	1.05	2.11	
8405	-3.5	3.4	0.8	-1.1	1.2	-2.1	1.1	-3.3	-1.8	3.9	-0.9	46.87	4.77	1.44	-0.20	2.50	0.75	-0.27	-0.43	
8447	0.7	7.5	0.5	-0.3	6.3	1.4	4.9	2.2	-1.6	4.5	0.8	44.22	5.21	1.57	2.44	2.92	0.88	2.77	5.23	
8472	0.1	4.8	2.1	2.5	5.6	0.8	4.9	1.6	-2.4	-3.8	3.9	44.48	5.36	1.62	2.19	3.69	1.11	1.96	4.69	
8545	3.0	9.7	-0.5	2.8	7.2	0.1	8.1	-0.4	-4.7	2.1	4.6	43.75	5.16	1.55	2.92	4.28	1.29	2.26	6.25	
8566	1.8	9.4	-2.2	0.7	7.8	5.9	6.8	1.9	-4.5	4.7	5.4	43.24	6.19	1.87	3.43	4.28	1.29	2.65	7.34	
8574	1.1	0.8	-0.2	-1.7	4.8	-2.8	4.9	-0.6	-1.5	*****		45.47	4.78	1.51	0.69	2.62	0.83	0.83	1.47	
8581	2.5	2.9	-3.5	*****								47.23	4.89	2.82	0.63	3.59	2.08	0.31	1.36	
8593	3.1	9.3	-0.4	3.2	7.7	1.9	7.8	0.1	-3.6	0.9	5.9	43.40	5.44	1.64	3.26	4.04	1.22	2.68	6.98	
8695	-3.7	-3.9	1.4	-2.7	*****							51.34	3.17	1.58	-2.24	2.46	1.23	-1.82	-4.79	
CAVE	0.1	5.1	0.4	-0.7	5.7	0.5	4.7	-0.4	-2.6	2.0	2.2									
DSGMA	2.8	4.4	1.7	3.0	3.4	2.4	2.3	1.5	1.4	2.7	2.9									
CSE	0.8	1.2	0.5	0.9	1.1	0.8	0.7	0.6	0.4	0.9	0.9									
CAVSE	0.1	4.2	0.9	-0.8	5.3	0.6	6.4	-0.7	-6.2	2.2	2.4									
CAVNS	0.2	10.5	0.9	-1.4	10.6	1.3	10.6	-0.5	-6.9	3.8	4.7									

ORIGINAL  
OF POOR

ORIGINAL PAGE IS  
OF POOR QUALITY

Table 39e. 48 HR. SLP SKILL SCORE IMPACT ON EUROPE

EXP	2/1	2/3	2/5	2/7	2/9	2/11	2/13	2/15	2/17	2/19	2/21	*****EXPERIMENT*****	AVE	SD	SE	*****DIFF. FROM (7578)*****	AVE	SD	SE	AV/SE	PRCNT. IMPACT
7578	64.7	74.4	55.7	57.9	57.5	64.0	50.1	66.1	61.1	60.9	69.1		61.95	6.73	2.03	0.0	0.0	0.0	0.0	0.0	
8240	-1.3	-0.5	2.6	2.6	-1.2	-1.9	-2.2	1.3	0.6	1.1	1.9		61.68	6.83	2.06	0.28	1.77	0.53	0.52	0.45	
8497	6.7	-4.6	13.1	0.9	*****							59.11	14.99	7.49	4.06	7.61	3.81	1.07	6.55		
8310	5.7	11.4	0.1	2.8	0.2	-5.9	1.4	0.4	9.2	1.4	0.6		59.47	6.74	2.03	2.48	4.77	1.44	1.72	4.00	
8352	-1.7	0.9	4.4	2.1	0.2	-5.1	1.7	2.7	2.2	2.9	1.1		60.91	7.82	2.36	1.04	2.57	0.78	1.35	1.69	
8405	0.7	3.5	5.7	2.6	-0.6	-1.5	-0.2	1.9	0.9	2.1	0.9		60.50	6.84	2.06	1.46	2.02	0.61	2.40	2.35	
8447	-0.0	-1.6	8.2	3.2	-2.4	-5.1	1.4	4.7	2.7	2.0	4.1		60.38	8.37	2.53	1.57	3.71	1.12	1.40	2.54	
8472	4.4	1.9	10.1	4.3	-0.9	-4.0	-0.5	0.1	9.2	1.8	4.4		59.15	8.23	2.48	2.81	4.26	1.28	2.19	4.53	
8545	0.7	0.7	5.5	5.5	-2.3	-4.4	1.6	-0.4	13.3	5.3	4.9		59.21	8.84	2.67	2.74	4.84	1.46	1.88	4.43	
8566	-2.2	1.1	7.1	4.3	-2.5	-4.1	1.6	0.3	13.6	0.7	1.7		60.00	9.16	2.76	1.95	4.96	1.49	1.31	3.15	
8574	-3.5	-2.4	-5.4	-1.5	-1.1	0.3	1.8	2.1	4.6	-0.9	1.7		62.35	7.29	2.20	-0.40	2.87	0.86	-0.46	-0.64	
8581	4.7	3.5	2.7	*****							61.31	9.01	5.20	3.62	0.98	0.57	6.41	5.85			
8593	1.7	1.3	6.9	4.9	-2.4	-4.4	1.8	0.6	12.1	3.8	3.9		59.21	8.63	2.60	2.74	4.46	1.34	2.04	4.43	
8695	3.9	-2.3	3.4	3.6	*****							61.01	11.05	5.53	2.16	2.96	1.48	1.46	3.49		
CAVE	1.5	1.0	5.0	2.9	-1.3	-3.6	0.8	1.4	6.9	2.0	2.5										
DSGMA	3.2	3.8	4.4	1.8	1.0	1.8	1.3	1.5	4.9	1.6	1.5										
CSE	0.9	1.0	1.2	0.5	0.3	0.6	0.4	0.5	1.6	0.5	0.5										
CAVSE	1.7	0.9	4.0	5.6	-4.1	-6.2	2.1	3.0	4.4	3.9	5.2										
CAVNS	2.4	1.3	6.9	5.1	-2.2	-5.7	1.7	2.1	11.2	3.3	3.6										

Table 39f. 72 HR. SLP SKILL SCORE IMPACT ON EUROPE

EXP												*****EXPERIMENT*****			*****DIFF. FROM (7578)*****			*****PRCNT. IMPACT*****	
	2/1	2/3	2/5	2/7	2/9	2/11	2/13	2/15	2/17	2/19	2/21	AVE	SD	SE	AVE	SD	SE	AV/SE	IMPACT
7578	74.6	73.7	65.5	75.8	55.5	61.8	66.4	75.7	53.1	68.1	75.1	69.97	9.71	2.93	0.0	0.0	0.0	0.0	0.0
8240	-1.8	-3.8	4.5	4.0	-2.7	0.6	-4.7	4.2	-3.1	3.3	6.6	69.31	8.51	2.57	0.66	4.01	1.21	0.54	0.94
8497	5.1	-8.7	8.4	10.8	*****	*****	*****	*****	*****	*****	*****	68.48	10.58	5.29	3.92	8.70	4.35	0.90	5.60
8310	8.1	20.2	-3.4	6.4	0.6	-12.7	-0.9	8.4	1.5	4.6	1.3	66.87	9.28	2.80	3.11	8.24	2.49	1.25	4.44
8352	2.8	-1.2	4.8	7.0	1.6	-4.6	-1.9	5.5	-2.5	3.4	5.4	68.14	8.08	2.44	1.84	3.86	1.16	1.58	2.62
8405	-0.7	2.7	5.7	3.8	-1.1	0.4	-0.7	1.6	2.3	5.9	1.6	68.01	8.97	2.71	1.96	2.45	0.74	2.66	2.81
8447	5.4	1.1	11.8	9.1	1.2	-5.7	-4.8	10.1	-1.2	0.5	7.1	66.77	9.49	2.86	3.20	5.94	1.79	1.79	4.57
8472	10.5	5.8	3.4	6.5	1.3	-3.7	-0.4	1.9	7.4	0.4	3.0	66.68	10.30	3.11	3.29	4.02	1.21	2.72	4.71
8545	2.6	5.9	4.5	8.6	-5.7	-4.7	3.5	-1.7	7.8	13.8	2.9	66.56	8.59	2.59	3.41	5.80	1.75	1.95	4.88
8560	1.9	6.7	6.3	8.3	-3.7	-6.1	4.5	2.4	5.8	0.3	-0.2	67.59	10.29	3.10	2.38	4.54	1.37	1.74	3.40
8574	-0.3	-2.4	2.8	-1.7	-2.9	-3.7	0.8	7.7	-0.2	5.9	3.0	69.15	8.32	2.51	0.82	3.68	1.11	0.74	1.18
8581	3.2	4.8	0.4	*****	*****	*****	*****	*****	*****	*****	*****	68.47	3.18	1.84	2.80	2.24	1.29	2.17	4.00
8593	5.0	6.7	3.0	8.2	-2.4	-5.1	4.2	-0.9	7.5	1.2	1.2	67.37	10.32	3.11	2.60	4.27	1.29	2.02	3.72
8695	5.1	-2.9	1.5	8.3	*****	*****	*****	*****	*****	*****	*****	69.39	5.29	2.64	3.01	4.81	2.41	1.25	4.30
CAVE	3.6	2.7	4.1	6.6	-1.3	-4.5	-0.0	3.5	2.5	3.9	3.2								
DSCMA	3.3	6.8	3.6	3.2	2.4	3.5	3.2	3.8	4.1	3.9	2.3								
CSE	6.9	1.9	1.0	0.9	0.8	1.1	1.0	1.2	1.3	1.2	0.7								
CAVSE	3.9	1.4	4.2	7.3	-1.7	-4.1	-0.0	3.3	2.0	3.2	4.4								
CAVNS	4.8	3.6	6.3	8.7	-2.2	-7.3	-0.1	5.2	4.8	4.5	4.3								

ORIGINAL PAGE IS  
OF POOR QUALITY



Table 39g. 48 HR. Z500 SKILL SCORE IMPACT ON EURCPE

EXP	2/1	2/3	2/5	2/7	2/9	2/11	2/13	2/15	2/17	2/19	2/21	*****EXPERIMENT*****			*****DIFF. FROM (7578)*****			PRCNT. IMPACT
												AVE	SD	SE	AVE	SD	SE	
7578	50.1	47.2	50.3	61.8	43.2	44.3	50.2	68.4	56.5	55.1	67.2	54.03	8.66	2.61	0.0	0.0	0.0	0.0
8240	-2.4	-0.2	1.1	1.2	-0.3	-2.0	-4.9	0.3	-0.0	1.0	8.3	53.84	7.15	2.16	0.19	3.26	0.98	0.19
8497	2.8	-0.9	4.2	3.3	*****							50.00	5.72	2.86	2.34	2.26	1.13	2.07
8310	6.1	5.8	-0.6	5.8	3.9	-12.1	0.2	-9.5	-0.6	3.4	7.8	53.10	10.58	3.19	0.93	6.49	1.96	0.47
8352	-1.3	0.9	2.6	1.8	-1.1	-7.9	1.4	2.2	-1.4	2.6	6.7	53.45	6.87	2.07	0.58	3.65	1.10	0.53
8405	1.4	3.0	1.1	3.0	-0.6	0.3	-0.8	1.8	-0.6	2.0	4.0	52.71	7.88	2.37	1.32	1.63	0.49	2.69
8447	0.1	0.4	4.3	4.6	-1.5	-6.9	2.2	3.4	0.7	2.5	7.8	52.43	6.33	1.91	1.60	3.81	1.15	1.39
8472	6.0	-1.9	3.4	6.7	2.6	-5.4	1.4	-3.7	1.9	1.6	5.7	52.36	8.69	2.62	1.67	3.95	1.19	1.40
8545	4.0	0.4	3.8	6.5	2.2	-5.4	4.2	-5.8	3.1	4.7	6.9	51.79	9.09	2.74	2.24	4.27	1.29	1.74
8566	4.4	0.6	4.2	4.9	2.1	-3.1	2.8	-5.6	4.2	2.8	4.6	52.05	9.41	2.84	1.98	3.44	1.04	1.91
8574	1.8	0.4	-3.6	-0.4	2.6	-1.5	1.5	-1.1	0.4	1.1	-0.4	53.95	9.25	2.79	0.07	1.74	0.53	0.14
8581	1.0	-1.1	0.8	*****								48.94	0.62	0.36	0.26	1.14	0.66	0.40
8593	5.5	1.3	3.5	6.0	1.6	-5.8	5.4	-5.6	2.4	4.3	6.2	51.78	9.30	2.61	2.25	4.29	1.29	1.74
8695	0.1	-3.6	0.0	1.9	*****							52.77	4.77	2.39	-0.42	2.32	1.16	-0.36
CAVE	2.3	0.4	1.9	3.8	1.2	-5.0	1.3	-2.4	1.0	2.6	5.8							
CSGMA	2.7	2.2	2.3	2.2	1.8	3.4	2.7	4.1	1.7	1.2	2.4							
CSE	0.7	0.6	0.6	0.6	0.6	1.1	0.9	1.3	0.5	0.4	0.8							
CAVSE	3.1	0.6	3.0	5.9	2.1	-4.6	1.6	-1.8	1.8	7.0	7.5							
CAVNS	4.5	0.8	3.8	6.1	2.7	-11.3	2.7	-3.5	1.8	4.7	8.6							

Table 39h. 72 HR. Z500 SKILL SCORE IMPACT ON EUROPE

EXP	2/1	2/3	2/5	2/7	2/9	2/11	2/13	2/15	2/17	2/19	2/21	*****EXPERIMENT*****	AVE	SD	SE	*****DIFF. FROM (7578)*****	AVE	SD	SE	AV/SE	PRCNT. IMPACT
7578	55.3	58.4	59.9	77.3	50.6	53.2	63.7	71.5	51.6	65.9	75.3	62.06	9.47	2.86	0.0	0.0	0.0	0.0	0.0	0.0	
8240	-2.2	-1.0	-0.5	2.4	-1.4	0.3	-4.8	0.2	-4.7	1.0	6.4	62.45	7.70	2.32	-0.39	3.16	0.95	-0.41	-0.63		
8497	0.1	-7.2	2.3	11.1	*****	*****	*****	*****	*****	*****	*****	61.18	5.58	2.79	1.55	7.53	3.77	0.41	2.49		
8310	-1.3	9.1	-8.2	9.9	3.8	-8.2	-5.1	-11.3	-9.6	2.5	7.9	63.02	9.94	3.00	-0.95	7.99	2.41	-0.40	-1.54		
8352	-0.8	-2.5	-1.0	7.8	-0.6	-6.4	-0.5	1.1	-10.8	2.5	3.7	62.74	6.17	1.86	-0.68	4.93	1.49	-0.45	-1.09		
8405	-0.6	3.1	1.4	4.2	-2.5	1.4	1.1	1.9	-2.4	1.2	2.8	61.02	7.93	2.39	1.04	2.13	0.64	1.63	1.68		
8447	2.3	0.2	8.2	6.7	-0.4	-4.6	-1.9	2.9	-6.2	8.9	5.9	60.06	7.26	2.19	2.00	5.08	1.53	1.30	3.22		
8472	6.2	0.2	-0.4	9.2	6.6	-2.9	0.0	-3.7	-7.9	2.1	1.2	61.10	9.50	2.86	0.97	4.97	1.50	0.65	1.56		
8545	1.5	1.3	1.8	9.9	5.6	-3.9	3.8	-3.4	0.9	7.0	3.3	59.53	8.90	2.68	2.54	4.13	1.25	2.04	4.09		
8566	3.4	1.4	1.7	8.8	5.8	-3.5	2.9	-3.6	-1.3	1.6	3.1	60.23	9.15	2.76	1.84	3.69	1.11	1.65	2.96		
8574	-2.8	-1.3	-2.7	0.1	3.1	-0.6	-0.5	0.3	0.0	3.3	1.7	62.00	9.30	2.80	0.07	2.02	0.61	0.11	0.11		
8581	-4.5	-0.4	-2.8	*****	*****	*****	*****	*****	*****	*****	*****	60.43	2.06	1.19	-2.57	2.06	1.19	-2.15	-4.14		
8593	3.4	2.5	2.1	9.2	7.5	-4.0	4.6	-2.8	-1.4	3.9	1.9	59.61	9.39	2.83	2.45	4.04	1.22	2.01	3.95		
8695	-0.5	-6.1	-0.8	6.6	*****	*****	*****	*****	*****	*****	*****	62.92	6.29	3.15	-0.19	5.22	2.61	-0.07	-0.31		
CAVE	0.3	-0.1	0.1	7.2	2.8	-3.2	-0.0	-1.6	-4.3	3.4	3.8										
OSOMA	2.8	3.9	3.6	3.2	3.5	2.8	3.1	3.5	3.9	2.5	2.1										
CSE	0.8	1.1	1.0	0.9	1.1	0.9	1.0	1.2	1.2	0.8	0.7										
CAVSE	0.4	-0.0	0.1	7.7	2.5	-3.7	-0.0	-1.5	-3.5	4.4	5.7										
CAVNS	0.6	-0.1	0.2	9.3	5.5	-6.1	-0.1	-2.6	-8.4	5.2	5.0										

ORIGINAL  
OF POO

ORIGINAL PAGE IS  
OF POOR QUALITY

Table 39i. 48 HR. SLP RMS IMPACT ON NORTH AMERICA

EXP	2/1	2/3	2/5	2/7	2/9	2/11	2/13	2/15	2/17	2/19	2/21	*****EXPERIMENT*****			*****DIFF. FROM (7578)*****				PRCNT.
												AVE	SD	SE	AVE	SD	SE	STSIG	IMPACT
7578	7.8	9.6	10.2	10.6	11.1	7.4	7.3	5.9	5.9	7.5	7.3	6.24	1.83	0.55	0.0	0.0	0.0	0.0	0.0
8240	-0.3	0.6	-0.2	1.0	-0.3	0.4	1.3	-0.5	-0.0	-0.1	0.7	7.99	1.86	0.56	0.25	0.60	0.18	1.38	3.05
8497	0.4	2.5	-0.1	-1.1	*****	*****	*****	*****	*****	*****	*****	9.11	2.24	1.12	0.43	1.51	0.76	0.57	5.22
8310	-0.3	1.5	-1.0	2.7	2.4	0.5	1.3	0.3	-0.2	-0.4	-0.8	7.70	1.56	0.47	0.4	1.26	0.38	1.43	6.61
8352	-0.2	2.6	-0.3	2.0	0.9	0.3	1.5	1.0	0.7	-0.7	0.1	7.52	1.84	0.55	0.72	1.03	0.31	2.31	8.69
8405	-0.2	0.5	-0.9	0.7	0.1	-0.4	0.6	0.1	-1.0	-1.0	0.3	6.35	1.75	0.53	-0.11	0.63	0.19	-0.56	-1.29
8447	0.1	2.7	-0.3	2.6	1.1	-0.2	1.4	-0.2	0.3	-0.6	-1.6	7.75	1.62	0.49	0.49	1.35	0.41	1.20	5.90
8472	-0.2	1.5	0.1	2.3	2.6	0.5	1.1	-0.2	0.2	-1.5	-0.0	7.66	1.35	0.41	0.58	1.20	0.36	1.62	7.09
8545	-0.1	2.1	-0.3	2.6	2.8	0.9	1.7	0.1	0.3	-0.4	0.6	7.29	1.43	0.41	0.95	1.16	0.33	2.85	11.58
8566	-0.3	2.7	0.1	1.7	2.5	0.6	1.0	1.0	-0.4	1.4	0.5	7.26	1.76	0.49	0.98	1.03	1.28	3.44	11.88
8574	-0.4	1.2	1.0	1.3	1.6	-0.4	1.0	1.8	0.7	0.4	*****	7.51	1.81	0.57	0.82	0.75	0.24	3.47	9.99
8581	0.4	-1.5	-2.0	*****	*****	*****	*****	*****	*****	*****	*****	10.24	2.53	1.46	-1.05	1.27	0.74	-1.42	-12.70
8593	-0.1	1.8	-0.6	2.0	2.9	1.3	1.7	1.1	0.8	-0.1	0.6	7.21	1.78	0.54	1.03	1.05	0.32	3.24	12.50
8695	0.0	-0.3	0.4	1.8	*****	*****	*****	*****	*****	*****	*****	9.04	0.97	0.48	0.50	0.93	0.46	1.08	6.07
DAVE	-0.1	1.4	-0.3	1.6	1.6	0.4	1.3	0.5	0.1	-0.3	0.1								
CSGMA	0.2	1.2	0.7	1.0	1.1	0.5	0.3	0.7	0.5	0.7	0.8								
CSE	0.1	0.3	0.2	0.3	0.3	0.2	0.1	0.2	0.2	0.2	0.3								
CAVSE	-1.3	4.1	-1.6	5.6	4.7	2.2	12.0	2.1	0.8	-1.3	0.3								
CAVNS	-1.1	14.5	-3.1	15.4	14.9	4.9	17.4	7.7	2.3	-4.2	1.0								



Table 39j. 72 HR. SLP RMS IMPACT ON NORTH AMERICA

EXP												*****EXPERIMENT*****			*****DIFF. FROM (7578)*****				PRCNT. IMPACT
	2/1	2/3	2/5	2/7	2/9	2/11	2/13	2/15	2/17	2/19	2/21	AVE	SD	SE	AVE	SD	SE	ST SIG	
7578	10.1	12.3	10.3	11.4	13.3	11.0	7.0	4.2	6.8	10.0	9.5	9.62	2.67	0.81	0.0	0.0	0.0	0.0	0.0
8240	0.7	-0.2	0.2	0.3	-0.0	2.3	1.0	-1.5	-0.1	1.3	-0.9	9.34	2.48	0.75	0.27	1.05	0.32	0.86	2.82
8497	1.9	1.3	-0.2	-1.3	*****	*****	*****	*****	*****	*****	*****	10.60	1.89	0.94	0.42	1.46	0.73	0.58	4.39
8310	0.1	2.6	-0.1	-0.4	3.6	3.5	0.4	-1.1	-0.5	0.4	-0.6	8.90	1.97	0.59	0.71	1.71	0.51	1.39	7.42
8352	-1.8	2.2	0.2	-1.5	2.2	2.6	0.7	-0.1	0.7	1.5	-0.5	9.04	2.65	0.80	0.57	1.50	0.45	1.27	5.98
8405	-1.4	1.2	-1.0	-0.5	0.1	-0.7	0.5	-1.0	-2.1	1.5	0.4	9.80	2.49	0.75	-0.28	1.12	0.34	-0.82	-2.87
8447	-0.4	1.6	0.4	-0.9	2.7	2.1	0.9	-1.0	-0.0	1.3	-2.2	9.21	2.34	0.70	0.41	1.49	0.45	0.91	4.22
8472	-0.3	2.3	-0.0	-0.5	3.3	1.8	0.3	-0.4	-0.1	-0.9	-1.0	9.21	2.21	0.67	0.41	1.43	0.43	0.95	4.25
8545	0.9	3.1	-0.6	-1.0	3.1	1.2	1.1	-0.8	-0.3	0.6	0.9	8.86	2.16	0.62	0.75	1.38	0.40	1.29	7.83
8566	0.6	4.0	-1.5	-2.4	3.9	2.7	0.8	-0.8	-1.2	3.2	2.4	8.55	2.49	0.69	1.06	2.14	0.59	1.79	11.07
8574	-1.5	0.2	-0.3	-2.1	2.1	-1.7	1.5	-1.1	0.5	1.9	*****	9.68	3.13	0.99	-0.05	1.55	0.49	-0.10	-0.50
8581	-0.4	-0.2	-1.3	*****	*****	*****	*****	*****	*****	*****	*****	11.54	1.02	0.59	-0.64	0.60	0.35	-1.26	-6.69
8593	1.3	3.1	-0.5	-1.9	3.5	1.5	1.2	-0.8	0.2	0.7	1.2	8.76	2.36	0.71	0.85	1.60	0.48	1.77	8.88
8695	0.8	-0.7	0.9	-1.1	*****	*****	*****	*****	*****	*****	*****	11.05	1.99	0.99	-0.02	1.04	0.52	-0.04	-0.23
CAVE	0.0	1.6	-0.3	-1.1	2.5	1.5	0.8	-0.5	-0.3	1.1	-0.1								
CSGMA	1.1	1.4	0.7	0.8	1.3	1.5	0.4	0.4	0.8	1.0	1.3								
CSE	0.3	0.4	0.2	0.2	0.4	0.5	0.1	0.1	0.2	0.3	0.4								
CAVSE	0.1	4.0	-1.6	-5.1	5.2	3.2	7.3	-7.5	-1.2	3.6	-0.1								
CAVNS	0.3	12.8	-2.8	-9.7	18.5	14.0	11.9	-20.6	-4.4	11.5	-0.5								

ORIGINAL PAGE IS  
OF POOR QUALITY

Table 39k. 48 HR. 2500 RMS IMPACT ON NORTH AMERICA

EXP	2/1	2/3	2/5	2/7	2/9	2/11	2/13	2/15	2/17	2/19	2/21	*****EXPERIMENT*****			*****DIFF. FROM (7578)*****				PRCNT.
												AVE	SD	SE	AVE	SD	SE	STS	IMPACT
7578	64.8	63.8	99.7	101.6	102.0	65.3	83.4	57.5	57.6	77.8	83.8	77.94	17.44	5.26	0.0	0.0	0.0	0.0	0.0
8240	0.8	-2.4	5.0	9.0	-4.0	-6.5	16.9	0.2	5.5	-0.3	2.9	75.47	16.78	5.06	2.46	6.55	1.97	1.25	3.16
8497	-4.1	13.1	-15.1	-26.2	*****	*****	*****	*****	*****	*****	*****	90.56	36.65	18.33	-8.09	16.74	8.37	-0.97	-10.38
8310	12.0	12.5	-4.8	17.3	26.6	-9.8	15.4	6.2	0.2	-1.4	-1.1	71.29	17.02	5.13	6.65	11.05	3.33	1.59	8.53
8352	12.3	9.5	3.3	15.6	16.0	-6.1	23.6	5.3	5.8	-0.1	5.6	69.67	16.26	4.90	8.26	8.29	2.50	3.31	10.60
8405	3.2	-0.9	2.4	4.6	1.4	1.8	5.6	-4.1	8.4	-7.9	-1.3	76.72	17.57	5.30	1.21	4.58	1.38	0.88	1.55
8447	8.0	9.8	-8.3	19.3	15.1	-6.1	25.8	-15.1	0.3	-5.2	12.5	72.82	16.49	4.97	5.11	12.87	3.88	1.22	6.56
8472	8.0	8.9	1.5	7.3	21.9	-6.0	27.6	11.6	-7.1	-10.3	4.9	71.72	17.53	5.29	6.21	11.69	3.52	1.76	7.97
8545	5.3	13.4	-2.6	15.6	26.5	7.3	31.7	-0.4	-2.2	-0.6	4.8	68.92	15.78	4.55	9.02	11.52	3.33	2.71	11.57
8566	1.4	6.3	7.5	12.0	25.3	-2.8	8.3	-6.0	-4.6	16.4	-8.0	72.85	12.65	3.65	5.09	9.97	2.88	1.77	6.53
8574	5.3	-5.7	4.3	12.0	16.7	-0.4	26.8	-4.1	-1.7	7.0	*****	71.32	13.92	4.40	6.03	10.15	3.21	1.88	7.73
8581	1.8	-18.8	-32.9	*****	*****	*****	*****	*****	*****	*****	*****	92.72	35.88	20.71	-16.62	17.44	10.07	-1.65	-21.33
8593	9.8	12.7	-9.9	8.9	22.0	5.2	30.8	7.4	0.9	3.3	6.0	69.11	19.53	5.89	8.83	10.67	3.22	2.74	11.33
8695	-15.4	-7.7	-12.9	-4.6	*****	*****	*****	*****	*****	*****	*****	92.62	19.89	9.94	-10.15	4.89	2.45	-4.13	-13.02
CAVE	3.7	3.9	-4.8	7.6	16.8	-2.3	21.3	0.1	0.6	0.1	2.9								
OSGMA	7.2	9.7	10.7	11.9	10.0	5.4	8.7	7.4	4.6	7.3	5.5								
CSE	2.0	2.7	3.0	3.4	3.2	1.7	2.8	2.4	1.5	2.3	1.8								
CAVSE	1.9	1.5	-1.6	2.2	5.3	-1.4	7.7	0.0	0.4	0.0	1.6								
CAVNS	5.8	6.1	-4.8	7.5	16.5	-3.6	25.5	0.2	1.0	0.1	3.5								



Table 391. 72 HR. 2500 RMS IMPACT ON NORTH AMERICA

EXP	2/1	2/3	2/5	2/7	2/9	2/11	2/13	2/15	2/17	2/19	2/21	*****EXPERIMENT*****			*****DIFF. FROM (7578)*****			*****	
												AVE	SD	SE	AVE	SD	SE	ST SIG	PRCNT. IMPACT
7578	80.4	119.2	117.4	118.4	136.0	74.4	70.9	68.3	56.3	99.9	90.0	93.75	26.03	7.85	0.0	0.0	0.0	0.0	0.0
8240	-4.8	-13.5	6.6	13.3	-8.8	-12.9	12.7	-9.5	8.1	14.1	-9.8	94.15	28.91	8.72	-0.41	11.32	3.41	-0.12	-0.43
8457	-9.2	5.0	-0.6	-35.2	*****							118.87	26.37	13.18	-10.02	17.79	8.90	-1.13	-10.69
8310	-8.4	24.9	-3.7	4.4	28.3	2.6	11.4	-5.5	1.5	2.7	3.8	88.12	21.59	6.51	5.93	11.68	3.52	1.60	6.00
8352	-17.1	17.1	-2.3	-0.2	17.7	0.0	16.3	-1.4	-0.2	6.9	-1.1	90.50	23.95	7.22	3.25	10.49	3.16	1.03	3.47
8405	-11.2	6.3	-0.9	-0.5	-3.9	-7.6	7.9	-10.5	0.8	1.6	1.5	95.25	25.56	7.71	-1.50	6.27	1.89	-0.79	-1.60
8447	-10.1	15.0	-2.1	4.6	15.8	10.9	17.4	-4.2	-15.3	26.4	-0.6	88.13	22.89	6.90	5.61	13.31	4.01	1.40	5.99
8472	70.1	20.8	-1.4	4.4	32.7	-7.8	28.5	10.5	-6.3	-8.6	7.4	80.08	33.81	10.20	13.66	23.52	7.09	1.93	14.57
8545	-17.3	33.7	-11.4	6.0	25.0	-4.9	26.4	-3.7	-14.8	1.2	20.0	88.27	23.13	6.68	5.48	17.26	4.98	1.10	5.84
8566	-9.2	42.7	-3.3	13.5	28.7	23.8	-6.9	-2.6	-19.0	31.0	19.4	83.00	19.94	5.76	10.74	19.26	5.56	1.93	11.46
8574	-13.5	-10.4	-4.2	11.8	17.2	-10.8	15.5	-0.7	-6.4	16.5	*****	92.62	25.97	8.21	1.50	12.43	3.93	0.38	1.60
8581	-33.2	-19.1	-26.1	*****							131.78	15.99	9.23	-26.12	7.02	4.05	-6.44	-27.86	
8593	-17.1	32.3	-12.0	2.9	28.8	-0.6	26.4	1.5	-9.4	-1.7	19.6	87.33	25.35	7.64	6.41	17.41	5.25	1.22	6.84
8695	-15.6	-24.8	-5.7	-1.8	*****							120.82	19.68	9.84	-11.97	10.36	5.18	-2.31	-12.77
CAVE	-7.4	10.0	-5.1	1.9	18.5	-0.7	15.6	-2.6	-6.1	9.0	6.7								
OSGMA	23.4	20.8	7.5	12.3	13.4	10.5	10.0	5.6	8.3	12.1	10.1								
CSE	6.5	5.8	2.1	3.5	4.2	3.3	3.2	1.6	2.6	3.8	3.4								
CAVSE	-1.1	1.7	-2.5	0.5	4.4	-0.2	4.9	-1.6	-2.3	2.4	2.0								
CAVNS	-9.2	8.4	-4.4	1.6	13.6	-1.0	22.0	-3.6	-10.8	9.0	7.4								

ORIGINAL  
OF POOL

ORIGINAL PAGE IS  
OF POOR QUALITY

Table 39m. 48 HR. SLP RMS IMPACT ON EUROPE

EXP	2/1	2/3	2/5	2/7	2/9	2/11	2/13	2/15	2/17	2/19	2/21	*****EXPERIMENT*****			*****DIFF. FROM (7578)*****			PRCNT. IMPACT
												AVE	SD	SE	AVE	SD	SE	
7578	5.2	8.5	7.7	7.4	7.7	7.0	9.0	8.8	5.6	6.2	11.9	7.73	1.86	0.56	0.0	0.0	0.0	0.0
8240	-0.4	0.4	1.4	0.9	-0.4	-0.7	-0.0	0.1	0.4	0.8	0.4	7.48	1.90	0.57	0.25	0.64	0.19	1.31
8497	1.0	0.7	2.1	0.1	*****	*****	*****	*****	*****	*****	*****	6.22	1.51	0.61	0.98	0.62	0.41	2.40
8310	0.8	2.8	1.4	1.6	0.0	-0.7	0.7	0.1	1.0	0.2	-1.6	7.15	2.55	0.77	0.58	1.17	0.35	1.63
8352	-0.6	0.3	1.4	0.9	-0.2	-0.4	0.5	1.1	0.4	0.9	-0.5	7.37	2.01	0.61	0.36	0.70	0.21	1.71
8405	-0.1	0.3	0.9	0.5	-0.1	-0.4	-0.1	0.1	0.5	0.5	-0.4	7.57	2.06	0.62	0.16	0.43	0.13	1.24
8447	0.1	1.0	-2.8	1.1	-1.2	-0.7	1.8	1.5	0.3	0.1	0.2	7.61	2.07	0.62	0.12	1.32	0.40	0.30
8472	0.5	1.4	1.8	1.0	-0.8	0.0	0.0	0.2	1.6	-0.2	1.3	7.12	1.94	0.58	0.62	0.84	0.25	2.44
8545	0.2	1.7	1.6	0.9	-2.8	-0.0	1.0	-0.1	1.7	0.2	0.2	7.32	3.09	0.86	0.42	1.17	0.33	1.28
8566	0.1	2.3	2.2	1.6	0.4	0.5	2.1	1.1	-0.4	2.3	-0.1	6.64	3.69	1.02	1.09	1.04	0.29	3.78
8574	-0.6	-0.9	-0.3	-0.9	-0.6	0.6	0.6	1.0	-0.5	-0.1	*****	7.51	1.24	0.39	-0.19	0.68	0.22	-0.68
8581	-0.9	-0.1	1.8	*****	*****	*****	*****	*****	*****	*****	*****	6.83	1.48	0.85	0.29	1.38	0.79	0.37
8593	0.8	2.0	1.5	1.9	-1.3	-0.4	0.5	0.6	1.6	0.1	-0.5	7.12	2.39	0.72	0.61	1.09	0.33	1.66
8695	0.0	0.2	0.5	0.2	*****	*****	*****	*****	*****	*****	*****	6.97	1.30	0.65	0.23	0.22	0.11	2.12
DAVE	0.1	0.9	1.0	0.8	-0.7	-0.2	0.7	0.6	0.7	0.5	-0.1							
DSGMA	0.6	1.0	1.3	0.7	0.9	0.5	0.7	0.5	0.7	0.7	0.8							
DSE	0.2	0.3	0.4	0.2	0.3	0.1	0.2	0.2	0.2	0.2	0.3							
CAVSE	0.4	3.3	2.9	3.6	-2.5	-1.5	3.2	3.3	2.8	2.2	-0.4							
CAVNS	1.1	11.0	13.5	11.1	-8.9	-3.2	7.8	6.4	11.7	7.8	-0.9							

Table 39n. 72 HR. SLP RMS IMPACT ON EUROPE

EXP	2/1	2/3	2/5	2/7	2/9	2/11	2/13	2/15	2/17	2/19	2/21	*****EXPERIMENT*****			*****DIFF. FROM (7578)*****			PRCNT.	
7578	6.4	8.6	11.0	7.6	5.0	8.5	13.8	10.6	6.1	10.1	17.5	AVE	SD	SE	AVE	SD	SE	ST SIG	IMPACT
7578	6.4	8.6	11.0	7.6	5.0	8.5	13.8	10.6	6.1	10.1	17.5	9.96	3.43	1.03	0.0	0.0	0.0	0.0	0.0
8240	-0.5	0.5	1.5	0.8	-1.2	0.5	0.1	1.0	0.8	0.6	0.1	9.57	3.51	1.06	0.39	0.75	0.23	1.74	3.93
8457	-0.4	-0.3	1.5	1.5	*****	*****	*****	*****	*****	*****	*****	7.84	1.64	0.62	0.57	1.11	0.55	1.63	5.72
8310	-1.2	3.1	0.3	0.3	-1.0	0.6	-1.4	-0.9	-1.3	-1.7	-3.2	10.54	4.45	1.34	-0.58	1.64	0.49	-1.17	-5.78
8352	-1.1	0.8	1.5	1.2	-0.6	2.4	0.4	1.2	0.4	0.8	-2.7	9.56	4.26	1.28	0.40	1.39	0.42	0.95	3.99
8405	-0.4	0.3	1.4	0.5	-0.4	0.2	-0.5	0.5	1.4	0.7	-0.0	9.63	3.64	1.10	0.33	0.65	0.20	1.69	3.32
8447	0.0	1.3	1.1	-0.1	-1.7	0.4	0.5	2.0	0.5	-0.9	-1.2	9.78	3.80	1.15	0.18	1.11	0.33	0.54	1.61
8472	1.0	1.9	1.5	0.8	0.1	1.6	0.4	-0.7	1.6	-0.5	-0.1	9.27	3.93	1.18	0.69	0.90	0.27	2.55	6.95
8545	-0.3	2.5	2.1	0.2	-2.3	0.6	1.9	-1.5	0.1	0.2	-1.8	9.79	4.22	1.17	0.17	1.45	0.40	0.41	1.66
8566	-0.2	3.1	2.1	1.0	1.3	1.5	2.8	0.7	-2.6	4.6	-2.3	8.97	4.16	1.15	0.99	2.18	0.61	1.44	9.98
8574	-2.5	-0.5	-0.2	-2.4	-1.4	0.6	0.7	1.4	-0.6	1.1	*****	9.54	1.76	0.56	-0.37	1.38	0.44	-0.86	-3.76
8581	-1.0	1.7	1.5	*****	*****	*****	*****	*****	*****	*****	*****	7.96	1.33	0.77	0.72	1.22	0.88	0.82	7.26
8593	0.8	3.1	2.0	1.4	-0.5	0.7	1.2	-0.6	-0.4	0.2	-2.6	9.49	4.32	1.30	0.47	1.12	0.46	1.04	4.76
8655	-0.9	-0.1	0.2	0.6	*****	*****	*****	*****	*****	*****	*****	8.46	1.72	0.86	-0.05	0.60	0.30	-0.16	-0.48
CAVE	-0.5	1.3	1.3	0.5	-0.8	0.9	0.6	0.3	-0.1	0.5	-1.5								
CSGMA	0.8	1.3	0.7	1.0	0.9	0.7	1.1	1.1	1.4	1.6	1.2								
DSE	0.2	0.4	0.2	0.3	0.3	0.2	0.3	0.3	0.5	0.5	0.4								
DAYSE	-2.2	3.8	6.6	1.7	-2.6	4.3	1.8	0.5	-0.2	1.0	-3.8								
DAYNS	-8.1	15.5	11.6	6.3	-8.6	10.6	4.4	3.1	-1.6	5.0	-8.5								

ORIGINAL  
OF POOR

ORIGINAL PAGE IS  
OF POOR QUALITY

Table 390. 48 HR. 2500 RMS IMPACT ON EUROPE

EXP	2/1	2/3	2/5	2/7	2/9	2/11	2/13	2/15	2/17	2/19	2/21	*****EXPERIMENT*****	*****DIFF. FROM (7578)*****	PRCNT.						
												AVE	SD	SE	AVE	SD	SE	STS	SIG	IMPACT
7578	53.1	56.0	78.6	82.1	67.4	42.6	76.7	111.6	55.7	50.7	93.5	65.85	20.94	6.31	0.0	0.0	0.0	0.0	0.0	0.0
8240	-3.8	0.8	8.2	8.3	-1.1	-10.6	-7.2	-1.7	1.4	4.8	17.0	62.40	18.98	5.72	1.46	7.81	2.35	0.62	2.09	
8457	4.3	7.9	32.5	23.6	*****	*****	*****	*****	*****	*****	*****	50.40	5.52	2.76	17.05	13.28	6.64	2.57	24.41	
8310	5.0	18.7	15.7	13.4	17.2	-13.6	10.3	-11.7	-4.3	5.3	22.7	62.69	22.70	6.85	7.16	12.34	3.72	1.92	10.25	
8352	-2.2	0.3	12.2	4.3	2.9	-12.5	7.1	10.2	-3.2	8.9	24.1	65.04	15.45	4.66	4.82	9.25	2.88	1.67	6.89	
8405	3.6	6.1	1.1	5.8	3.8	0.9	-0.3	2.9	1.2	4.3	6.1	66.29	21.16	6.38	3.57	2.72	0.82	4.35	5.11	
8447	-0.6	6.2	22.4	7.3	1.7	-8.8	21.5	12.8	1.9	4.3	27.6	61.09	15.05	4.54	8.76	11.14	3.36	2.61	12.54	
8472	4.3	-9.0	1.6	7.4	3.6	-20.1	-6.4	-4.4	-4.0	2.4	21.0	70.18	18.72	5.65	-0.32	10.47	3.16	-0.10	-0.46	
8545	7.8	1.5	22.4	17.7	26.4	-4.9	20.0	6.5	1.5	3.0	30.0	57.88	26.38	7.62	11.98	11.72	3.38	3.54	17.14	
8566	16.0	5.5	22.3	20.2	20.9	4.0	16.0	12.3	-7.5	-14.5	35.3	57.98	21.74	6.28	11.87	14.02	4.05	2.93	17.00	
8574	3.1	1.4	9.4	9.9	19.5	2.9	12.8	5.4	1.6	-1.6	*****	61.01	18.72	5.92	6.44	6.41	2.03	3.18	9.21	
8581	-6.9	-17.2	0.5	*****	*****	*****	*****	*****	*****	*****	*****	70.46	9.36	5.40	-7.89	8.89	5.13	-1.54	-11.29	
8593	14.3	4.9	20.9	14.4	15.4	-8.8	20.5	4.8	-1.9	5.0	22.0	59.63	18.07	5.45	10.23	10.17	3.07	3.33	14.64	
8655	-2.0	-12.9	-1.8	-3.5	*****	*****	*****	*****	*****	*****	*****	72.49	13.53	6.76	-5.04	5.28	2.64	-1.91	-7.21	
DAVE	3.3	1.1	12.9	10.7	11.1	-7.1	5.4	3.7	-1.3	2.6	23.0									
DSGMA	6.4	9.1	10.4	7.2	9.2	7.4	10.3	7.4	3.2	6.3	7.5									
CSE	1.8	2.5	2.9	2.1	2.9	2.4	3.3	2.2	1.0	2.0	2.6									
CAVSE	1.8	0.4	4.5	5.2	3.8	-3.0	2.9	1.6	-1.3	1.3	8.8									
CAVNS	6.2	2.0	16.4	13.1	16.5	-16.7	12.3	3.2	-2.4	5.1	24.5									



Table 39p. 72 HR. Z500 RMS IMPACT ON EUROPE

EXP	2/1	2/3	2/5	2/7	2/9	2/11	2/13	2/15	2/17	2/19	2/21	*****EXPERIMENT*****	AVE	SD	SE	*****DIFF. FROM (7578)*****	AVE	SC	SE	*****SYSTG*****	PRCNT. IMPACT
7578	59.3	60.0	96.0	92.5	76.1	65.3	131.2	142.5	58.3	63.0	149.4	92.15	33.99	10.25	0.0	0.0	0.0	0.0	0.0	0.0	
8240	-5.7	-0.6	6.6	11.6	-10.1	0.1	-14.8	3.3	2.1	11.0	11.9	96.75	34.37	10.36	1.40	8.89	2.68	0.52	1.51		
8497	-5.2	14.4	38.4	26.3	*****	*****	*****	*****	*****	*****	*****	63.49	3.99	1.99	18.46	18.57	9.29	1.55	20.03		
8310	-8.1	25.5	-3.1	20.4	-0.8	5.5	-8.2	-31.3	-9.0	-2.4	16.9	91.66	39.52	11.92	0.49	16.09	4.65	6.10	0.53		
8352	-7.3	-2.4	7.1	19.8	-3.8	11.9	7.2	8.5	0.5	13.3	7.8	86.47	32.60	9.83	5.68	8.14	2.45	2.31	6.16		
8405	0.4	3.7	1.0	13.4	2.0	1.5	2.8	4.6	7.4	11.5	10.8	86.78	33.57	10.12	5.37	4.65	1.40	3.83	5.82		
8447	-2.5	1.6	24.6	7.0	-4.3	4.7	19.2	130.3	3.0	4.8	17.5	73.43	31.21	9.41	18.72	38.13	11.50	1.63	20.31		
8472	3.2	-2.5	-4.9	17.2	2.9	-1.8	-2.3	-17.8	-15.4	1.5	13.9	92.68	35.00	10.55	-0.54	10.47	3.16	-0.17	-0.58		
8545	3.5	9.0	16.1	18.2	31.1	3.9	33.5	-0.7	14.9	7.2	21.0	77.81	37.08	10.70	14.33	11.49	3.32	4.22	15.56		
8566	12.9	8.9	10.8	18.0	20.3	13.8	34.2	7.1	-3.6	23.3	29.1	76.26	35.35	10.21	15.89	11.22	3.24	4.91	17.24		
8574	-8.0	1.0	5.6	-4.5	12.8	17.3	15.7	8.3	17.2	3.5	*****	79.53	29.80	9.42	6.89	9.00	2.85	2.42	7.48		
8581	-9.7	-4.5	-8.4	*****	*****	*****	*****	*****	*****	*****	*****	85.96	17.72	10.23	-7.53	2.74	1.58	-4.77	-8.17		
8593	9.0	14.9	16.3	20.6	9.4	6.8	31.6	-0.5	6.7	7.1	12.5	75.88	32.77	9.88	12.27	8.58	2.59	4.74	13.31		
8695	-7.0	-14.3	-7.3	3.9	*****	*****	*****	*****	*****	*****	*****	88.13	15.77	7.89	-6.18	7.50	3.75	-1.65	-6.70		
CAVE	-1.9	4.2	7.9	14.3	6.0	6.4	11.9	11.2	2.4	8.1	15.8										
CSGMA	6.9	9.9	13.0	8.2	12.0	5.9	16.9	41.5	9.5	6.8	6.0										
CSE	1.9	2.7	3.6	2.4	3.8	1.9	5.3	13.1	3.0	2.2	2.0										
CAVSE	-1.0	1.5	2.2	6.0	1.6	3.4	2.2	0.5	0.8	3.7	7.9										
CAVNS	-3.2	5.2	8.2	15.5	7.8	5.8	9.1	7.8	4.1	12.8	10.6										

OF DR

ORIGINAL PAGE IS  
OF POOR QUALITY

Table 40. Average/standard error for skill scores.

EXPER	SLP		Z500		SLP		Z500		TOTAL
	48	72	48	72	48	72	48	72	
7578	0.0	0.0	0.0	0.0	0.0	0.0	0.0	0.0	0.0
8240	0.06	0.40	0.32	-0.59	0.52	0.54	0.19	-0.41	0.13
8497*	0.97	-0.35	-1.00	-0.29	1.07	0.90	2.07	0.41	0.47
8310	0.89	0.49	1.29	1.81	1.72	1.25	0.47	-0.40	0.94
8352	1.40	0.37	2.30	1.05	1.35	1.58	0.53	-0.45	1.01
8405	0.39	-0.64	-0.31	-0.27	2.40	2.66	2.69	1.63	1.07
8447	0.43	0.25	1.55	2.77	1.40	1.79	1.39	1.30	1.36
8472	0.70	0.45	1.05	1.96	2.19	2.72	1.40	0.65	1.39
8545	1.64	2.06	1.92	2.26	1.38	1.95	1.74	2.04	1.94
8566	1.76	2.06	1.74	2.65	1.31	1.74	1.91	1.65	1.85
8574	1.62	1.31	0.57	0.83	-0.46	0.74	0.14	0.11	0.66
8581*	-0.47	0.16	0.18	0.31	6.41	2.17	0.40	-2.15	0.88
8593	1.88	2.35	1.72	2.66	2.04	2.02	1.74	2.01	2.05
8595*	-0.14	0.15	-2.23	-1.82	1.46	1.25	-0.36	-0.07	-0.22

\* - INCOMPLETE

Table 41. Summary of percent impact for skill scores.

EXPER	SLP		Z500		SLP		Z500		TOTAL
	48	72	48	72	48	72	48	72	
7578	0.0	0.0	0.0	0.0	0.0	0.0	0.0	0.0	0.0
8240	0.09	0.94	0.63	-1.11	0.45	0.94	0.35	-0.63	0.21
8497*	2.46	-1.55	-6.39	-1.93	6.55	5.60	4.34	2.49	1.45
8310	2.41	1.95	3.87	5.17	4.00	4.44	1.72	-1.54	2.75
8352	3.09	1.13	4.00	2.11	1.69	2.62	1.07	-1.09	1.83
8405	0.45	-1.26	-0.32	-0.43	2.35	2.81	2.44	1.68	0.97
8447	1.07	0.76	3.48	5.23	2.54	4.57	2.96	3.22	2.98
8472	1.90	1.54	2.88	4.69	4.53	4.71	3.09	1.56	3.11
8545	4.25	5.06	4.66	6.25	4.43	4.68	4.14	4.09	4.74
8566	4.51	5.86	4.62	7.34	3.15	3.40	3.66	2.96	4.46
8574	3.06	2.58	1.89	1.47	-0.64	1.18	0.14	0.11	1.20
8581*	-1.62	0.43	0.56	1.36	5.85	4.00	0.49	-4.14	0.87
8593	4.72	5.88	4.47	6.98	4.43	3.72	4.16	3.95	4.79
8695*	-0.23	0.73	-5.05	-4.79	3.49	4.30	-0.77	-0.31	-0.33

\* - INCOMPLETE

ORIGINAL PAGE IS  
OF POOR QUALITY

Tables 39i-39p; these are the analogs of Tables 27b, 28b, 29b, 30b, 31b, 32b, 33b, 34b given for DST-5. Table 40 presents our rough measure of statistical significance for the  $S_1$  results. Its entries were computed in the same way as those of Table 36 of the previous subsection. Table 41 is analogous to Table 35 of that Subsection and contains the mean percentual skill score impacts for each experiment.

Before discussing the results, it is important to remember that Experiment 8405 is a control experiment, as described in Subsection 3.3.1.3, and that all the results have to be gauged against those of Experiment 8405. We notice first in Table 40 that the measure of statistical significance for Experiment 8405 is  $\bar{\zeta}_5 = 1.07$ . Hence the results of the DIM experiment 8240, with  $\bar{\zeta}_1 = 0.13$ , have no confidence whatever attached to them (also  $\bar{\zeta}_1 < 0.5$ ), while those of the SCM experiments 8310, 8352, and 8447, with  $\bar{\zeta}_3 = 0.94$ ,  $\bar{\zeta}_4 = 1.01$ , and  $\bar{\zeta}_6 = 1.36$  respectively, can be considered as marginally significant:

$$\bar{\zeta}_3 \approx \bar{\zeta}_4 \approx 1 \approx \bar{\zeta}_5 < \bar{\zeta}_6 .$$

The corresponding mean percentual impacts from Table 41 are  $\bar{x}_5 = 0.97$  for the control experiment 8405, and  $\bar{x}_1 = 0.21$  for the DIM experiment 8240, which is practically negligible; they are  $\bar{x}_3 = 2.75$ ,  $\bar{x}_4 = 1.83$  and  $\bar{x}_6 = 2.98$  for the SCM experiments 8310, 8352, and 8447 respectively with  $\bar{x}_6 \approx \bar{x}_3 \approx 1.5\bar{x}_4$ ,  $\bar{x}_4 \approx 2\bar{x}_5$ . We already notice a strong correlation between measure of impact and measure of confidence. Moreover, the control experiment shows that the DIM experiment totally failed to produce favorable impacts, while the SCM experiments produced results considerably better than the performance level set by the control experiment, in fact twice as good, at least. Also Experiment 8310, which used a larger amount of data, obtained from two satellites, produced results which were 50 percent better in mean percentual impact than those of Experiment 8352, utilizing the same assimilation



method (SCM) but data from NIMBUS-6 only. Furthermore, Experiment 8447, in which no satellite data were inserted over land, reflecting higher reliance on conventional data, produced results comparable to and even better than those of Experiment 8310, while using only data from one satellite (NIMBUS 6).

We proceed now to discuss the SAM experiments, 8472 through 8695, i.e.,  $7 \leq i \leq 13$ , omitting, however, the incomplete ones, 8581 and 8695. The comparison of results, in both impact and significance, of Experiment 8574,  $i=10$ , which used only NOAA-4 data, Experiment 8472,  $i=7$ , which used the more abundant NIMBUS-6 data, and the remaining SAM experiments, 8545, 8566, and 8593,  $i = 8, 9$ , and  $12$ , which used data from both satellites, immediately shows the importance of data quantity, independently of the assimilation method. We have in fact  $\bar{\zeta}_{10} = 0.66 < \bar{\zeta}_7 = 1.39 < \bar{\zeta}_j$ ,  $j = 8, 9, 12$  with  $\bar{\zeta}_j \approx 2$ ; similarly  $\bar{x}_{10} = 1.20 < \bar{x}_7 = 3.11 < \bar{x}_j \approx 4.65$ . Thus Experiment 8472 is comparable to the best SCM experiment, 8310 or 8447, while Experiment 8574 produces somewhat poorer results.

The results of the three SAM experiments which utilized fully the available data, 8545, 8566, and 8593, are remarkably similar. We have  $\bar{\zeta}_8 = 1.94$ ,  $\bar{\zeta}_9 = 1.85$ , and  $\bar{\zeta}_{12} = 2.05$ ; these give us all high statistical confidence in the mean impacts, being very close to, and one even larger than, 2. The mean impacts are  $\bar{x}_8 = 4.74$ ,  $\bar{x}_9 = 4.46$ , and  $\bar{x}_{12} = 4.79$ , that is close to 5 percent. This is certainly not a very large impact, but is quite comparable to improvements in numerical weather prediction which have been considered as important over the last decade; it corresponds approximately to the ability of making a 60 h forecast of accuracy which equals that of today's operational 48 h forecast (see for instance Chapter 1 of this report.)

We remark in passing that the attempts at removing the bias, either at observation point (8566), or at the correction point (8593), did not make much difference in the results. The use of SAM itself, however, certainly did make a difference. It is very interesting to consider the SCM experiment which is similar in other respects to the three SAM experiments we are in the process of discussing, namely Experiment 8310; we immediately notice that the two quantities measuring results,  $\bar{\zeta}_3$  and  $\bar{x}_3$ , have a value which is almost exactly half the corresponding representative value for SAM,  $\bar{\zeta}_3 = 0.94$ , versus 2, and  $\bar{x}_3 = 2.75$ , versus 5. The values of  $\bar{\zeta}_1$  and  $\bar{x}_1$  for DIM experiment 8240 can be considered zero for all practical intents and purposes of this discussion. We observe at this point that, in a certain sense, SCM is a low-order approximation to SAM, in which the matrix  $\tilde{A}$  of Subsection 3.2.7.2 is approximated by a diagonal matrix (compare Rutherford, 1972).

The results for rms errors strongly support those presented here for skill scores; they are given in Tables 42 and 43: Table 42 contains mean rms impacts and Table 43 gives their statistical significance. The statistical significance of the rms results is influenced by data quantity and assimilation method in the same way as the  $S_1$  results, and so are the mean impacts; the values of rms mean impacts are of the order of 10 to 12 percent for the best SAM experiments, and 5 to 7 percent for the SCM experiments.

Furthermore, differences in initial states correlate well with impact on forecasts from those initial states. Our statistical measures of impact also correlate well with improvements in the capability of predicting local weather when using the large-scale numerically predicted fields for guidance (see Chapters 1 and 5 of this report).

Table 42. Summary of percent impact for rms errors.

EXPER	NORTH AMERICA				EUROPE				TOTAL
	48	SLP 72	48	Z500 72	48	SLP 72	48	Z500 72	
7578	0.0	0.0	0.0	0.0	0.0	0.0	0.0	0.0	0.0
8240	3.05	2.82	3.16	-0.43	3.28	3.93	2.09	1.51	2.43
8497*	5.22	4.39	-10.38	-10.69	12.74	5.72	24.41	20.03	6.43
8310	6.61	7.42	8.53	6.00	7.48	-5.78	10.25	0.53	5.13
8352*	8.69	5.98	10.60	3.47	4.67	3.99	6.89	6.16	6.31
8405	-1.29	-2.87	1.55	-1.60	2.07	3.32	5.11	5.82	1.51
8447	5.90	4.22	6.56	5.99	1.58	1.81	12.54	20.31	7.36
8472	7.09	4.25	7.57	14.57	7.98	6.95	-0.46	-0.58	5.97
8545	11.58	7.83	11.57	5.84	5.38	1.66	17.14	15.56	9.57
8566	11.68	11.07	6.53	11.46	14.15	9.98	17.00	17.24	12.41
8574*	9.59	-0.50	7.73	1.60	-2.46	-3.76	9.21	7.48	3.66
8581*	-12.70	-6.69	-21.33	-27.86	3.75	7.26	-11.29	-8.17	-9.63
8593	12.50	8.88	11.33	6.84	7.88	4.76	14.64	13.31	10.02
8695*	6.07	-0.23	-13.02	-12.77	2.57	-0.48	-7.21	-6.70	-3.92

\* - INCOMPLETE

ORIGINAL PAGE IS  
OF POOR QUALITY

Table 43. Statistical significance for rms errors.

EXPER	NORTH AMERICA				EUROPE				TOTAL
	48	SLP 72	48	Z500 72	48	SLP 72	48	Z500 72	
7578	0.0	0.0	0.0	0.0	0.0	0.0	0.0	0.0	0.0
8240	1.38	0.86	1.25	-0.12	1.31	1.74	0.62	0.52	0.94
8497*	0.57	0.58	-0.97	-1.13	2.40	1.03	2.57	1.99	0.88
8310	1.43	1.39	1.59	1.60	1.63	-1.17	1.92	0.10	1.11
8352*	2.31	1.27	3.31	1.03	1.71	0.95	1.67	2.31	1.82
8405	-0.56	-0.82	0.68	-0.79	1.24	1.69	4.35	3.83	1.23
8447	1.20	0.91	1.32	1.40	0.30	0.54	2.61	1.63	1.24
8472	1.62	0.95	1.76	1.93	2.44	2.55	-0.10	-0.17	1.37
8545	2.65	1.89	2.71	1.10	1.28	0.41	3.54	4.32	2.26
8566	3.44	1.79	1.77	1.93	3.78	1.64	2.93	4.91	2.77
8574*	3.47	-0.10	1.88	0.38	-0.88	-0.86	3.18	2.42	1.19
8581*	-1.42	-1.86	-1.65	-6.44	0.37	0.82	-1.54	-4.77	-2.06
8593	3.24	1.77	2.74	1.22	1.86	1.04	3.33	4.74	2.49
8695*	1.08	-0.04	-4.15	-2.31	2.12	-0.16	-1.91	-1.65	-0.88

\* - INCOMPLETE

ORIGINAL PAGE IS  
OF POOR QUALITY

This concludes the discussion of our DST-6 experiments, to the extent allowed by the framework of this report.

### 3.4 CONCLUSIONS AND RECOMMENDATIONS (M. Ghil)

During the 1976 Impact Test Project (April 1976 - April 1977), we have developed, tested and evaluated a number of methods for the four-dimensional (4-D) assimilation of satellite-derived temperature data. The methods were all local and time-continuous, using only data provided by satellites in a small interval of 10 minutes at a time. We applied a direct insertion method (DIM), a successive correction method (SCM), and a statistical assimilation method (SAM) to DST-5 and DST-6 data.

The results of the DST-5 experiments were inconclusive. This is probably due to two causes: (1) the synoptic situation during that summer period, and (2) the fact that our methods at the time when the experiments were carried out had not been perfected.

The results of the DST-6 experiments allow us to draw a number of conclusions: (1) satellite-derived temperature data can have a modest, but consistently positive impact on numerical weather forecasts, as verified over the continents of the Northern Hemisphere; (2) this impact is highly sensitive to the quantity of the data -- a two-satellite system is superior to one satellite by an amount roughly proportional to the quantity of data transmitted; (3) the assimilation method plays a major role in the level of impact for the same data -- direct insertion proved practically worthless, while SCM provided about half the impact obtained with SAM.

The impact for the best method and the best data was about 5 percent in  $S_1$  skill score and 12 percent in rms error; these correspond to an extension of about 8-12% in the usefulness of operational weather prediction (NWP) in the range between 48 h and 72 h. There are indications that local weather forecasts using large-scale NWP results as guidance can be similarly improved.

Our results seem to point to two major areas in which improvements can bring about larger impacts of asynoptic observing systems. The first is improving the accuracy of the observations themselves: in the presence of large errors (2-2.5°C rms errors in vertical temperature profiles derived from satellite radiance data), even as modest an impact as the one we obtained is surprising. The deficiencies in data quality can only partially be compensated for by large data quantities and by processing and assimilation methods. There is furthermore a major need for continued development of the processing methods and of the assimilation methods themselves, and also of a much closer interaction between the processing of raw data and the assimilation of the processed data.

The second area of improvement is in the numerical models themselves: for the asynoptic data to be successfully assimilated and contribute thus to a better approximation of initial states, it is necessary that the model used in the assimilation process be able to convey the information present in the data accurately over extended instances and periods of time. Model improvement can only proceed by a judicious combination of higher grid resolution, better numerical discretization methods, and better representation in the model of atmospheric processes.

We hope that the concerted effort in designing better observation instruments and systems, in refining the methods for processing and assimilating the observations, and in developing numerical models, will bring about the improvement in numerical weather prediction and in our understanding of the atmosphere which is the goal of the Global Atmospheric Research Program.

## REFERENCES

- Achtemeier, G. L. (1975). On the initialization problem: a variational adjustment method. Mon. Wea. Rev., 103, 1098-1103.
- Arakawa, A. (1972). Design of the UCLA General Circulation Model. Tech. Rep. No. 7, Dept. of Meteorology, UCLA, 115 pp.
- Bengtsson, L. (1975). Four-Dimensional Data Assimilation of Meteorological Observations. GARP publ. ser. No. 15, WMO/ICSU, Geneva, Switzerland, 76 pp.
- Bengtsson, L. and N. Gustavsson (1971). An experiment in the assimilation of data in dynamical analysis. Tellus, 23, 328-336.
- \_\_\_\_ (1972). Assimilation of non-synoptic observations. Tellus, 24, 383-399.
- Bergthorsson, P., and B. R. Döös (1955). Numerical weather map analysis. Tellus, 7, 329-340.
- Bolin, B. (1955). Numerical forecasting with the barotropic model. Tellus, 7, 27-49.
- \_\_\_\_ (1956). An improved barotropic model and some aspects of using the balance equation for three-dimensional flow. Tellus, 8, 61-75.
- Charney, J. G. (1955). The use of the primitive equations of motion in numerical prediction. Tellus, 7, 22-26.
- \_\_\_\_ (1962). Integration of the primitive and balance equations. Proc. Intern. Symp. Num. Wea. Pred., Tokyo, Meteor. Soc. Japan, 131-152.
- \_\_\_\_ (1963) A note on large scale motions in the tropics. J. Atmos. Sci., 20, 607-609.
- \_\_\_\_ (1973). Planetary fluid dynamics. Dynamic Meteorology, P. Morel, Ed., D. Reidel Publ. Co., Boston, 97-371.



- Cressman, G. P. (1959). An operational objective analysis system. Mon. Wea. Rev., 85, 367-374.
- Druyan, L. M. (1974). Short-range forecasts with the GISS model of the global atmosphere. Mon. Wea. Rev., 102, 269-279.
- Eliassen, A. (1954). Provisional report on calculation of spatial covariance and autocorrelation of the pressure field. Report No. 5, Inst. Weather and Climate Res., Acad. Sci., Oslo, 11 pp.
- Gandin, L. S. (1963). Objective Analysis of Meteorological Fields. Gidrometeorologicheskoe Izdatel'stvo (GIMIZ), Leningrad. English translation by Israel Program for Scientific Translations Jerusalem, 1965 [available from NTIS], 242 pp.
- Ghil, M. (1975). Initialization by compatible balancing. Report 75-16, Inst. Comp. Appl. Sci. Eng., NASA Langley Research Center, Hampton, VA 23665, 38 pp.
- Ghil, M., R. Dilling and H. Carus (1976a). Study and utilization of statistical error structure. The GISS Sounding Temperature Impact Test, Phase I Report. NASA Institute for Space Studies, Goddard Space Flight Center, New York, N. Y. 10025, 3.34-3.49.
- \_\_\_\_\_, (1976b). A time-continuous statistical assimilation method for satellite-derived temperatures. NASA Weather and Climate Program, Basic Science Review, Goddard Space Flight Center, Greenbelt, MD 20771, 42-47.
- Ghil, M. and M. Economedes (1976). Piece-wise linear fit to correlation data. The GISS Sounding Temperature Impact Test, Phase I Report. NASA Institute for Space Studies, Goddard Space Flight Center, New York, N. Y. 10025, 3.49-3.53.
- Ghil, M., and R. Mosebach (1976). A variational method for satellite-data assimilation. The GISS Sounding Temperature Impact Test, Phase I Report, NASA Institute for Space Studies, Goddard Space Flight Center, New York, N. Y. 10025, 3.67-3.71.

- Ghil, M. and B. Shkoller (1976). Wind laws for shockless initialization. Ann. Meteor. (Neue Folge), 11, 112-115.
- Ghil, M., B. Shkoller and V. Yangarber (1977). A balanced diagnostic system compatible with a barotropic prognostic model, Mon. Wea. Rev., in press.
- Isaacson, E., and H. B. Keller (1966). Analysis of Numerical Methods. Wiley, New York, 541 pp.
- Jastrow, R., and M. Halem (1973). Simulation studies and the design of the first GARP global experiment. Bull. Amer. Meteor. Soc., 54, 13-21.
- Kistler, R., and R. McPherson (1975). On the use of a local wind correction technique in four-dimensional data assimilation. Mon. Wea. Rev., 103, 445-449.
- Lewis, J. M., (1972). An operational upper air analysis using the variational method. Tellus, 24, 514-530.
- Lewis, J. M., and T. H. Grayson (1972). The adjustment of surface wind and pressure by Sasaki's variational matching technique. J. Appl. Meteor., 11, 586-597.
- Longuet-Higgins, M. S. (1968). The eigenfunctions of Laplace's tidal equations over a sphere. Phil. Trans. Roy. Soc. London, A262, 511-607.
- Masuda, Y. (1971). The use of non-geostrophic balance model for numerical weather prediction. J. Meteor. Soc. Japan, 49, Special Issue, 595-612.
- McPherson, R. D. (1975). Progress, problems, and prospects in meteorological data assimilation. Bull. Amer. Meteor. Soc., 56, 1154-1166.
- Monin, A. S. (1952). Pressure changes in a barotropic atmosphere.

Izv. Akad. Nauk. SSSR, Ser. Geofiz. No. 4, 76-85.

\_\_\_\_ (1958). Pressure changes in a baroclinic atmosphere.

Izv. Akad. Nauk. SSSR, Ser. Geofiz. No. 4, 280-286.

Moura, A. D. (1976). The eigensolutions of the linearized balance equations over a sphere. J. Atmos. Sci., 33, 877-907.

Murakami, T. (1972). Balance model in a conditional unstable tropical atmosphere. J. Atmos. Sci., 29, 463-487.

Phillips, N. (1976). The impact of synoptic observing and analysis systems on flow pattern forecast. Bull. Amer. Meteor. Soc., 57, 1225-1240.

Powell, M. J. D. (1964). An efficient method for finding the minimum of a function of several variables without calculating derivatives. The Computer Journal, 7, 155-162.

Russell, G. (1975). GISS Objective analysis. Meteorology Research Review 1975. NASA Institute for Space Studies, Goddard Space Flight Center, New York, N.Y. 10025, 16-25.

Rutherford, I. D. (1972). Data assimilation by statistical interpolation of forecast error fields. J. Atmos. Sci., 29, 809-815.

\_\_\_\_ (1973). Experiments in the updating of P. E. forecasts with real wind and geopotential data. Third Conference on Probability and Statistics in Atmospheric Science, Amer. Meteor. Soc., Boston, (Preprint) 198-201.

Sasaki, Y. (1958). An objective analysis based on the variational method. J. Meteor. Soc. Japan, 36, 1-12.

\_\_\_\_ (1969) Proposed inclusion of time variation terms, observational and theoretical, in numerical variational objective analysis. J. Meteor. Soc. Japan, 47, 115-124.

\_\_\_\_ (1970a) Some basic formalisms in numerical variational analysis. Mon. Wea. Rev., 98, 875-883.

- \_\_\_\_\_ (1970b). Numerical variational analysis formulated under the constraints as determined by longwave equations and a low-pass filter. Mon. Wea. Rev., 98, 884-898.
- \_\_\_\_\_ (1970c). Numerical variational analysis with weak constraint and application to surface analysis of severe storm gust. Mon. Wea. Rev., 98, 899-910.
- Smith, W. L. and H. M. Woolf (1976). The use of eigenvectors of statistical covariance matrices for interpreting satellite sounding radiometer observations. J. Atmos. Sci., 33, 1127-1140.
- Somerville, R. C. J., P. H. Stone, M. Halem, J. E. Hansen, J. S. Hogan, L. M. Druyan, G. Russell, A. A. Lacis, W. J. Quirk and J. Tenenbaum (1974). The GISS model of the global atmosphere. J. Atmos. Sci., 31, 84-117.
- Stephens, J. J., (1970). Variational initialization with the balance equation. J. Appl. Meteor., 9, 732-739.
- Stephens, J. J. and J. M. Stitt (1970). Optimum influence radii for interpolation with the method of successive corrections. Mon. Wea. Rev., 98, 680-687.
- Stone, P. H., L. C. Tsang and D. Schneider (1973). Balanced winds for assimilation of temperature and pressure data. GISS Research Review 1973, Part 2 (Applications), NASA Institute for Space Studies, Goddard Space Flight Center, New York, N. Y. 10025, 160-163.
- Thompson, P. D. (1956). A theory of large scale disturbances in non-geostrophic flow. J. Meteor., 13, 251-261.
- Tracton, M. S., and R. D. McPherson (1977). On the impact of radio-metric sounding data upon operational numerical weather prediction at NMC. Office Note 136, NOAA, National Weather Service, National Meteorological Center, Washington, D. C. 20233, 11 pp. and figures.

Tsang, L.C. and R. Karn (1973). A Documentation of the GISS Nine-Level Atmospheric General Circulation Model. Computer Sciences Corporation at NASA Institute for Space Studies, Goddard Space Flight Center, New York, N.Y. 10025, 236 pp.

## 4. FORECAST MODEL DEVELOPMENT

(W. Quirk, Scientist; Y. Sud, Manager)

### 4.1 APPROACH

From the start of this DST forecast impact project it was clear that the forecast models must be improved if satellite sounding data were to have its maximum impact. Current forecast models are of little operational use beyond 48 hours, however, satellite data has its greatest impact on weather prediction forecasts of 48 hours and longer (see Chapter 3: Analysis and Assimilation). Satellite data is of use primarily in defining the atmospheric state in data-sparse regions such as oceans, and by the time this weather influences conditions over populated regions the forecasts have already greatly deteriorated.

The deterioration of forecasts beyond 48 hours is believed to be due to three main causes: (1) forecast model inadequacies such as too coarse horizontal resolution, (2) the nonavailability or poor quality of data from certain regions, and (3) inadequate methods of data analysis and assimilation. Robert (1975) has estimated that almost 80 percent of the error in 36-hour forecasts comes from forecast model deficiencies, rather than errors in data. Since it is only at periods longer than 48 hours that satellite data become important for forecasts over populated areas, it is imperative to use better forecasting models. Only through a concentrated effort to improve all three areas can the most effective use be made of satellite data. *Only after the forecast models and methods of data*

*assimilation are improved and ways are found of getting high-quality data over the entire globe will forecasts of a week or more be possible.*

During 1976, the model development group considered the problem of how best to improve the forecast skill of the GISS GCM in time for use during the DST Impact Test Project. A number of improvements were made to the model physics in the areas of parameterization of clouds, radiation, hydrology, snow accumulation, and the planetary boundary layer; but these improvements showed little affect on model forecasts. A fourth-order differencing scheme was successfully developed and tested during the early phases of the Impact Test Project. While this model was a definite improvement over the standard GISS second-order model, in the few forecast tests conducted, the model was still in its developmental stage and could not be used operationally. Among other disadvantages, it ran two times slower than the second-order model. By using smoothed leap-frog time differencing the fourth-order model now uses only about 20 percent more CPU time than the second-order model, and should be ready in the near future for future forecast impact tests.

A decision was finally reached to develop a high resolution (ultrafine) 250 km grid version of the second-order model for use during the Impact Test Project. Preliminary results indicated the ultrafine model made substantially better forecasts than the fine model; for this reason a data assimilation and forecast experiment was initiated. However, as the final assimilation scheme was not fully tested with the fine model until late December, the ultrafine

test did not begin until early in January. The assimilation program proved to be extremely time consuming. New methods to speed up this program are being tried, but it still takes 6 hours to do one simulated day for an assimilation and nearly 10 hours for forecasts of 4 simulated days. Because of the large amount of computer time involved, only the No SAT assimilation run has been finished and analyzed. The satellite assimilation r-un is now in progress.

## 4.2 DEVELOPMENT OF THE ULTRAFINE MODEL

The current GISS Global Circulation Model (GCM) has a horizontal spacing of  $4^{\circ}$  in latitude by  $5^{\circ}$  in longitude; this grid yields horizontal resolution of about 400 km in midlatitudes. Theoretical studies (e.g., Grotjahn and O'Brien, 1976) have shown that with this resolution wave-lengths about the size of synoptic systems are poorly represented by the finite differencing scheme. In the GCM these systems propagate much more slowly than in nature and they do not strengthen as much as the observed highs and lows. Robert (1975) has estimated that almost 40 percent of the error in 36-hour forecasts is attributed to insufficient horizontal resolution.

NMC has developed the Limited Area Fine Mesh (LFM) model to increase its forecast skill without greatly increasing the computer time needed for a forecast. This model consists of a fine mesh



(200-km resolution) over the United States embedded in the standard 400-km grid. They have run the model for several years now and have found that about one-half the error in the propagation and deepening of low-pressure systems is eliminated by use of the LFM model (Brown 1975). The success of the LFM model is also shown in the statistical scores for sea-land pressure and 500-mb forecasts shown in Tables 1 and 2. (These tables were made available to us by Duane Cooley of NMC). The numbers in the columns headed by 6L PE give the S1 skill scores produced by the 6-level Primitive Equation model (400-km grid) for the last 16 months. The first column gives the average 12-hour forecasts skill during each of 16 months for the PE model, the second column gives the same statistics for the LFM model. The average scores for the last 12 months are also given. From the averages one can see that the improvement of the LFM over the PE in sea-level pressure skill is greatest at 48 hours. For the 500-mb skill the improvement is greatest at 24 hours, but there is still substantial skill improvement at 48 hours. It is surprising that the LFM model can make such good forecasts at 48 hours, given the smallness of the area that has a fine grid. NMC is now planning to implement a model with a hemispheric or global fine mesh so the time for which meaningful forecasts can be made will be extended.

It is of interest to note that this effort on the part of NMC is simultaneous with the acquisition of three IBM 370/195 computers. The improvement of weather forecasting models at NMC historically has occurred with the acquisition of new computer

systems. Figure 1 (from Fawcett, 1977) shows that the 500-mb 36-hour forecasts was greatly increased with the introduction of the barotropic model when the IBM 700 series was introduced, and the skill was greatly increased again with the introduction of the CDC 6600 and the 6-level PE model.

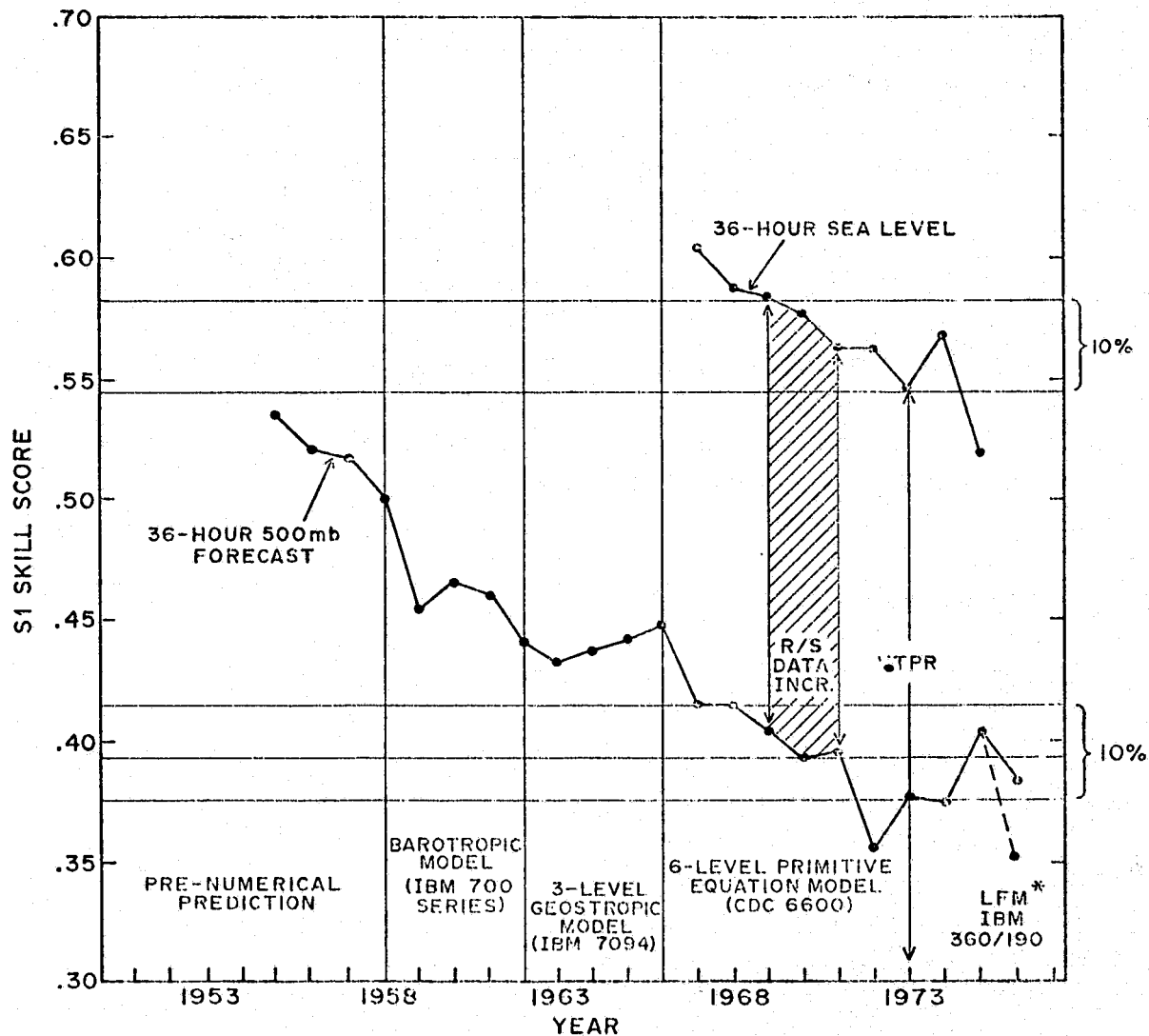
ORIGINAL PAGE IS  
OF POOR QUALITY

Table 1. SEA LEVEL PRESSURE

S1 Comparisons of the 6L PE and LFM for the contiguous United States.

	12-hr		24-hr		BAR	36-hr		48-hr	
	6L PE	LFM	6L PE	LFM		6L PE	LFM	6L PE	LFM
Oct 75	37.9	40.8	47.5	45.7	-	56.0	54.9	-	-
Nov 75	37.7	40.9	46.2	46.7	-	55.3	55.4	-	-
Dec 75	37.8	39.7	46.3	47.5	-	56.1	55.4	63.4	-
Jan 76	36.8	37.6	45.4	44.5	-	53.8	54.0	60.7	-
Feb 76	40.0	39.5	49.3	46.7	-	58.2	55.3	65.9	62.9
Mar 76	38.5	37.7	48.1	44.7	-	57.4	51.7	66.8	56.7
Apr 76	39.2	39.0	46.4	44.5	-	55.3	51.7	62.5	59.8
May 76	39.2	38.6	47.1	45.0	-	55.8	51.9	64.1	58.6
Jun 76	41.9	40.0	48.1	46.6	-	56.5	54.8	63.0	59.5
Jul 76	42.6	40.5	47.0	46.8	-	54.0	53.9	60.4	58.4
Aug 76	43.7	41.4	49.5	47.1	-	55.2	53.7	61.5	59.6
Sep 76	43.5	41.9	51.8	47.2	-	59.4	52.8	67.4	60.7
Oct 76	36.4	37.2	43.7	42.0	-	51.8	49.4	59.1	57.2
Nov 76	35.3	37.5	42.1	43.5	-	49.2	50.6	55.2	58.0
Dec 76	38.6	38.3	45.7	44.3	-	54.4	52.0	61.7	59.0
Jan 77	38.3	37.6	48.4	45.8	-	56.3	53.3	63.3	62.1
Average to Jan 77	39.8	39.1	47.3	45.4		55.3	52.6	62.6	59.4

# NATIONAL METEOROLOGICAL CENTER YEARLY SUMMARY S1 SKILL SCORE CENTERED ON JULY



\* Adjusted to same region

ORIGINAL PAGE IS  
OF POOR QUALITY

Table 2. 500 MBS

SI Comparisons of the 6L PE and LFM for the contiguous United States. The barotropic model (BAR) performance is included at 36 hours.

	12-hr		24-hr		BAR	36-hr		48-hr	
	6L PE	LFM	6L PE	LFM		6L PE	LFM	6L PE	LFM
Oct 75	23.3	18.7	31.7	25.5	44.5	38.7	34.7	-	-
Nov 75	21.9	18.1	29.4	25.2	-	36.5	33.8	-	-
Dec 75	20.9	16.4	28.4	22.8	39.4	35.1	29.9	40.1	-
Jan 76	20.6	15.6	26.9	22.5	37.6	33.8	30.5	38.4	-
Feb 76	20.2	15.7	26.5	21.2	36.7	32.0	28.0	37.3	36.1
Mar 76	19.7	15.8	26.8	21.8	37.8	34.0	28.8	40.0	34.2
Apr 76	24.3	21.0	32.1	27.7	42.1	40.6	36.3	47.3	46.0
May 76	24.9	20.0	31.4	26.4	42.8	39.2	34.6	47.1	42.0
Jun 76	26.7	22.3	32.1	28.1	44.8	37.6	36.2	43.9	43.3
Jul 76	26.8	22.9	31.7	28.0	42.4	38.5	34.6	44.6	42.2
Aug 76	25.2	22.1	31.7	27.5	42.0	38.2	34.6	44.7	42.3
Sep 76	23.6	20.5	29.9	25.1	43.8	36.1	32.7	42.6	39.2
Oct 76	20.7	18.0	27.3	23.5	39.2	32.9	31.3	38.7	37.8
Nov 76	19.6	16.3	25.3	21.8	33.9	30.6	28.9	35.5	35.5
Dec 76	18.9	15.0	25.5	20.2	36.1	31.3	26.5	36.8	32.7
Jan 77	20.6	16.9	28.4	24.4	40.3	35.1	31.7	41.0	38.4
Average to Jan 77	22.6	18.9	29.1	24.6	40.2	35.5	32.0	41.6	39.1

This points out the way that improvements in computing technology have gone hand in hand with the improvement of weather forecasts.

Because of the importance of long-term forecasts, accuracy for sounding impact development of a high-resolution GISS GCM model was given a high priority. The new model, called ultra-fine, has a resolution of 2.5° in latitude by 3° in longitude. Until the 1976 Impact Test Project, development of this model had not gone forward because of the limited computing resources. Only recently, with the addition of the AMDAHL computer dedicated

to the Global Atmospheric Research Programme (GARP) and the concentration of all resources on this effort, were we able to perform a limited number of high-resolution experiments.

Three major efforts in the development of the high-resolution model were performed during the Impact Test Project. First, a coding effort was required to reduce the core requirements for the model to run on the AMDAHL computer. Second, numerical techniques were developed to minimize finite amplitude stationary computational instabilities (e.g., checkerboard tendencies in the pressure fields). Both of these tasks were completed by June 1976, and limited forecast tests were carried out with summer DST data sets using the new high-resolution model. Third, a new topography had to be created for the ultrafine grid.

The model used for the DST experiments was somewhat different from the version described by Somerville et al. (1974). In this version, the numerical differencing near the poles was modified to obtain a nearly equal area mesh near the poles using the split grid technique described by Halem and Russell (1973). The use of the split grid technique allowed the model's time step to be 10 minutes instead of 5, so it effectively cut the computing time of the model in half. However, a problem arose, when we tried to extend this technique to an ultrafine resolution model.

The split grid technique was not amenable to using TASU (Time Alternating Space Uncentered), the method developed to prevent finite amplitude stationary computational instabilities. This did not matter for the fine model because no significant checkerboard

pressure patterns showed up in the forecasts, but checkerboard patterns of about 5 mb in magnitude showed up in the ultrafine forecasts. A method of eliminating such spurious checkerboard pattern has been developed by Shapiro (1970) and that method was used at GISS to eliminate the checkerboard. We used the 16th order version of Shapiro's filter. To 16th order it conserves energy and vorticity. It removes the checkerboard pattern only and does not otherwise affect the calculations.

The topography used by the ultrafine model was generated from the  $1^\circ \times 1^\circ$  terrain heights compiled at Scripps Institution of Oceanography as published by W.L. Gates and A.B. Nelson (1973). The heights were averaged to the GISS  $2.5^\circ$  by  $3^\circ$  grid to obtain GISS ultrafine topography.

#### 4.3 TESTING THE ULTRAFINE FORECAST MODEL (R. Atlas)

Two forecasts were made to evaluate the forecast skill of the new ultrafine high-resolution model. They were carried out using NMC analyses produced for the DST-5 period as initial conditions. Comparison of the skill scores of the new ultrafine model with the standard GISS fine model, and NMC's own model forecasts are shown in Figures 2 and 3. It should be noted here that the NMC model has a certain advantage in these comparisons in that it uses the same topography for both the analysis and forecasts, whereas the GISS topography is quite different so some errors may result from incorrect extrapolations to sea level.

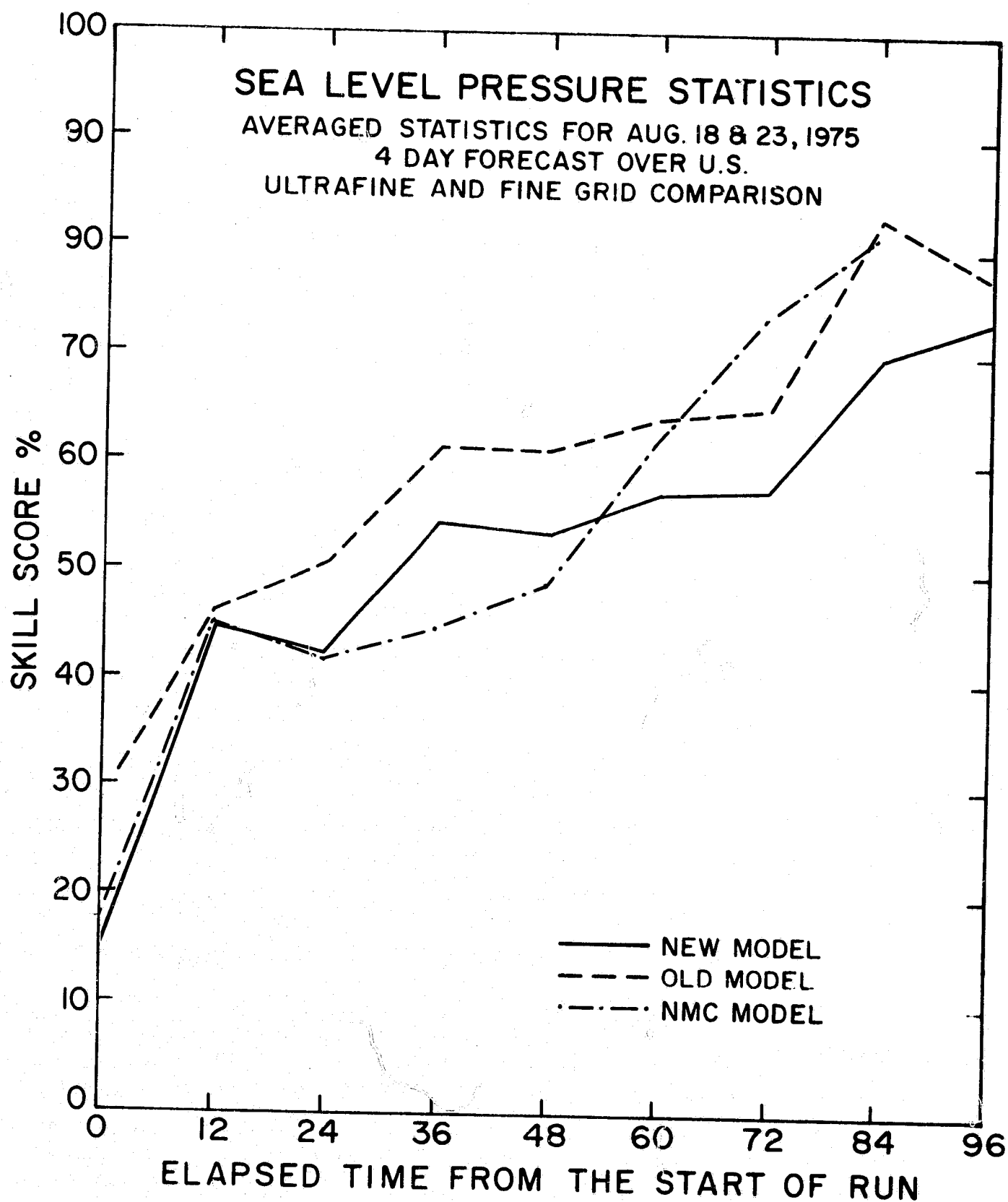


Figure 2. Sea-Level Pressure Statistics

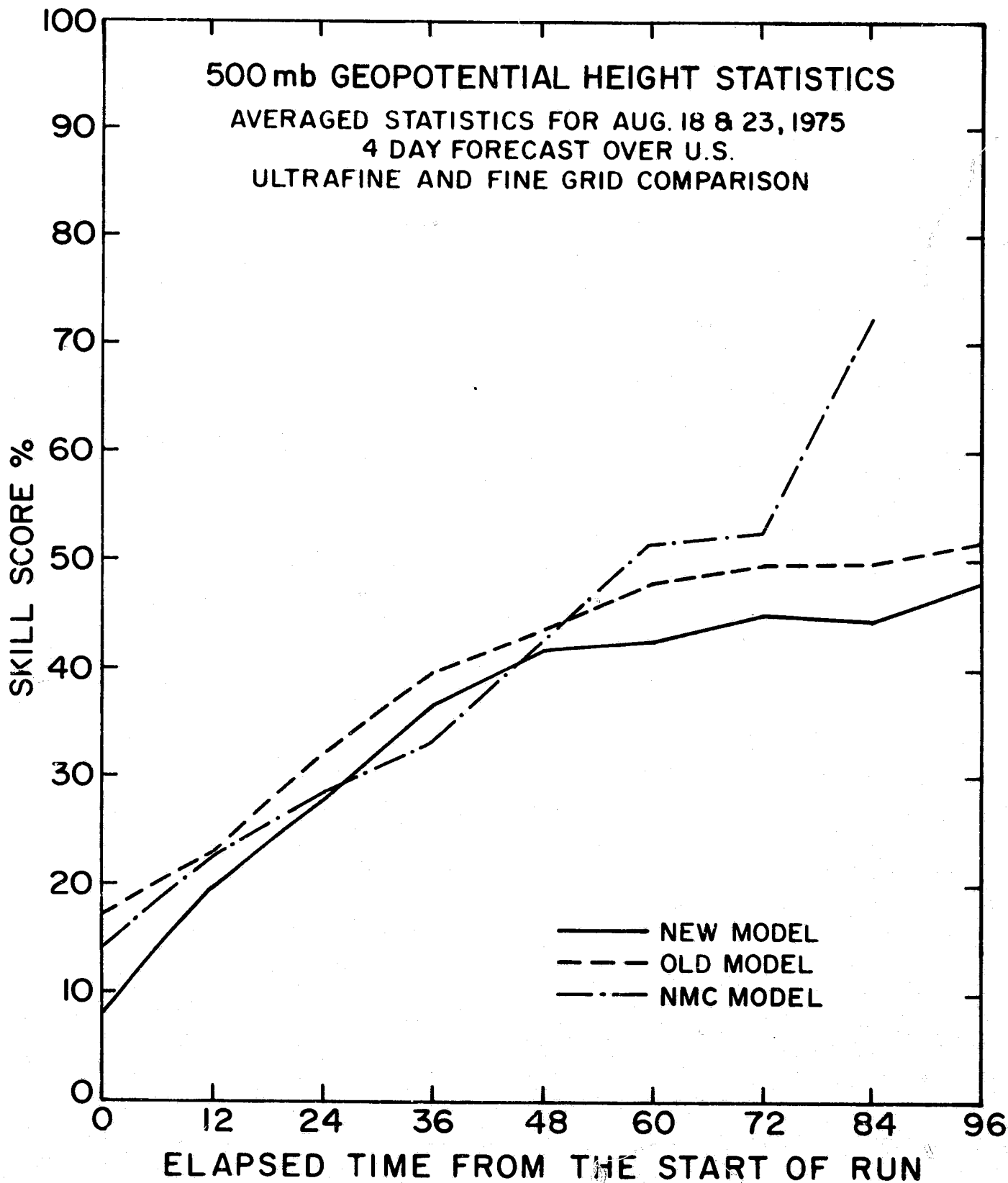


Figure 3. 500-mb Geopotential Height Statistics.



An additional test was made using the NMC analysis for 12Z May 10, 1976. This forecast was of special importance for the following reasons: on this date the forecast with the operational Primitive Equation (PE) model at NMC generated a physically unrealistic 36-hour, 300-mb isotach prediction. The operational PE forecast produced a significant ageostrophic flow leading to gross overestimation of the wind speeds over California. This problem has recurred often, and a decision was made to closely investigate this case. The forecast was redone with a hemispheric model developed by Dr. N. Philips of NMC which used the same resolution, and the problem was eliminated when a higher resolution embedded grid was introduced over the United States.

The experiment was repeated at GISS to determine if improvement in the forecast was due to the increase in resolution or if it was model- or data-dependent.

Fine ( $4^{\circ}$  by  $5^{\circ}$ ) resolution and ultrafine ( $2.5^{\circ}$  by  $3^{\circ}$ ) resolution models were used to generate a forecast from the operational analysis provided to GISS by NMC. The analysis data were valid for 12Z May 10, 1976. Initial data in the Southern Hemisphere and equatorial latitudes were not reasonable and were replaced by summer climatological fields. Examination of the forecasts indicated the following:

- (1) No significant cross geopotential flow occurred in the GISS fine or ultrafine predictions. Although a southerly extension of the Pacific isotach maxima does develop after 24 hours, these isotachs do conform with the general contour pattern associated with a weak Pacific ridge generated by the model, and isotachs are present in the verification. The results are in direct contrast to the NMC predictions, which had isotachs of high wind speed crossing geopotential contours at a large angle.
- (2) The GISS fine model (like the NMC model) was slow in its movement of a trough into Montana, as well as the movement of a weak high-pressure ridge over California; also it did not extend the high-pressure system at 130° longitude far enough north.
- (3) The GISS fine model did not sufficiently develop the isotach pattern over the northwestern United States.
- (4) The ultrafine version gave a significantly better set of predictions:
  - (a) The position of the trough in Montana is 5° in longitude closer to what was observed.
  - (b) The position of the ridge off California is also displaced further east by 5°.
  - (c) The isotach errors are much smaller. Differences of 20 knots can be noted at the center of the Pacific isotach maxima and over the northwestern United States.

- (5) Changes in the isotach strength at 300 mb appear to be related to changes in the vorticity gradient at that level. This may in part explain the decrease of isotach maxima speeds after 6 hours.

The tentative conclusions of the Forecast Model and Development Group were that better data specification over the oceans and low-latitude regions might have improved skills, but the problem in question is clearly model-dependent. The forecast was significantly improved when higher resolution was used.

The above findings show that the ultrafine model significantly improved forecast skill. Both skill score and forecasts of synoptic systems are improved. Therefore, efforts of the Forecast Model and Development Group were focused on a data assimilation and forecast experiment with the ultrafine model.

## 4.4 IMPLEMENTATION OF THE ULTRAFINE ASSIMILATION CYCLE WITH DST-6 DATA

### 4.4.1 INTRODUCTION

In the previous section it was shown that increasing the horizontal resolution of the model gave better forecasts. The next question to be answered was: Could using the ultrafine model for an assimilation cycle also improve the initial state? The importance of the initial state has been stressed in a paper by Baumhefner (1977). Baumhefner compared forecasts from an initial state prepared by the Working Group on Numerical Experimentation (WGNE) with forecasts made from an initial state prepared by NMC.

He found that the one-day forecasts made with the NMC initial states were 25 percent better than the forecasts made with the WGNE data. Since both groups used the same data in their analyses, this difference must be due to either differences in the first guess field (i.e., the 12-hour forecasts from the previous synoptic time) or their method of inserting data. In either case, it is evident that the method of arriving at an initial state is critical.

#### 4.4.2 ASSIMILATION AND FORECAST EXPERIMENTS USED TO TEST THE ULTRAFINE MODEL

There are two aspects of model skill that were tested using DST-6 data:

1. Was the forecast model improved by using ultrafine resolution?
2. Were the initial conditions improved by using the ultrafine model?

To answer these two questions three assimilation and forecast cycles were carried out:

1. A fine control experiment that consisted of a fine NO SAT assimilation cycle was carried out from January 29 to February 12, 1976. This experiment is described in Section 3.2. It used the direct insertion method (DIM) Section 3.2.1 of inserting observed data. Eleven forecasts were made from initial conditions taken from the assimilation run. The forecasts were for February 1, 3, 5, 7, 9, 11, 13, 15, 17, 19 and 21.

2. An ultrafine experiment that tested the full effects of using the high-resolution for both an assimilation run and for eleven forecasts for February 1, 3, to 21. This experiment differed in a few subtle ways from Experiment 1. First of all, the Successive Correction Method (SCM, see Section 3.2.4) was used to insert observed data during the assimilation run, since the paucity of observed data made it impossible to use the DIM method for the ultrafine model. This, however, should have no affect on our conclusions, since, as shown in Section 3.2.4 use of the SCM method has little affect on the fine model assimilation cycle. The other way that this experiment differed from the control was that the actual observed snow from the first week of February was used to estimate albedos, instead of using climatological albedos. This, however, had little affect on model predictions except for those of ground temperature. A fine control run using the SCM method and having February observed albedos is now being run, so that a more perfect control run will be available.
3. A set of eleven fine forecasts that used the ultrafine assimilation for initial conditions. This experiment tested how much of the improvement in the second experiment was from use of a better forecast model and how much was due to use of a better assimilation model.

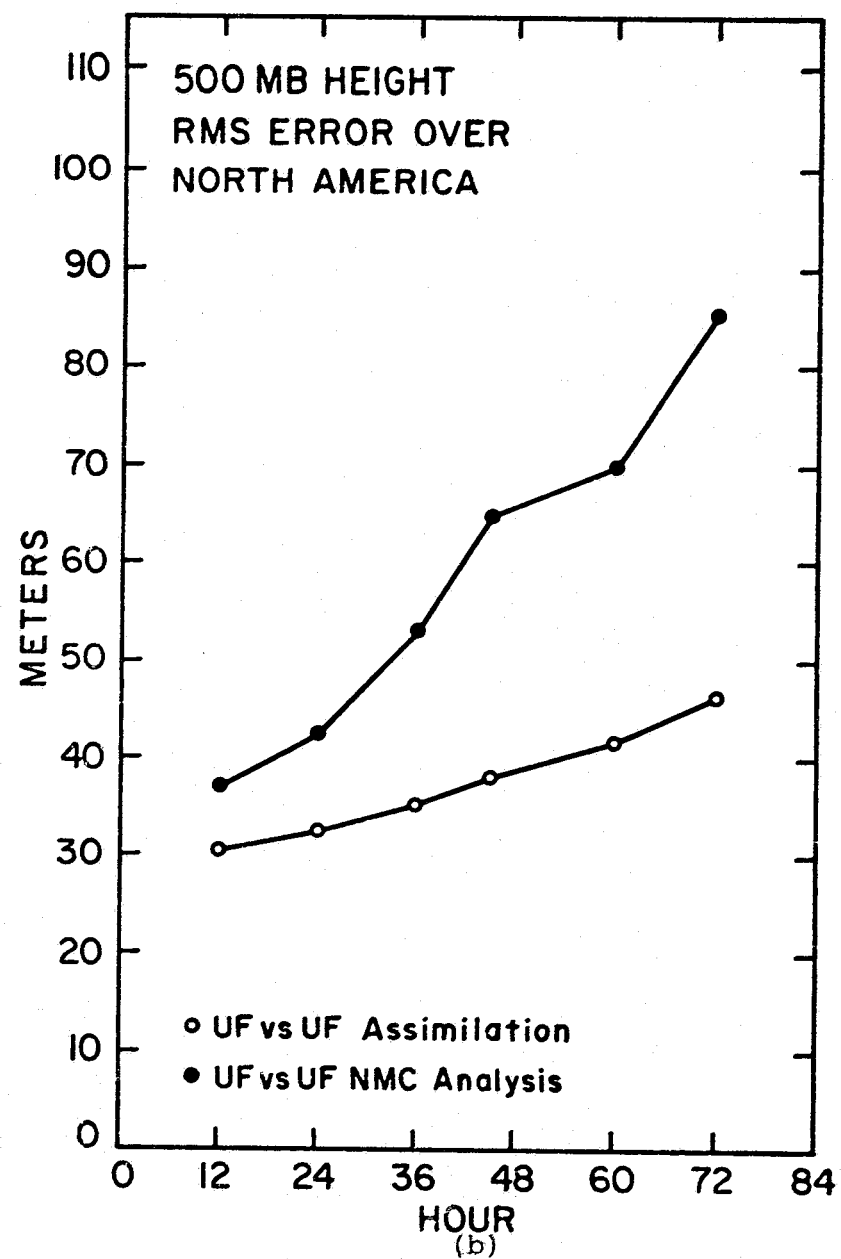
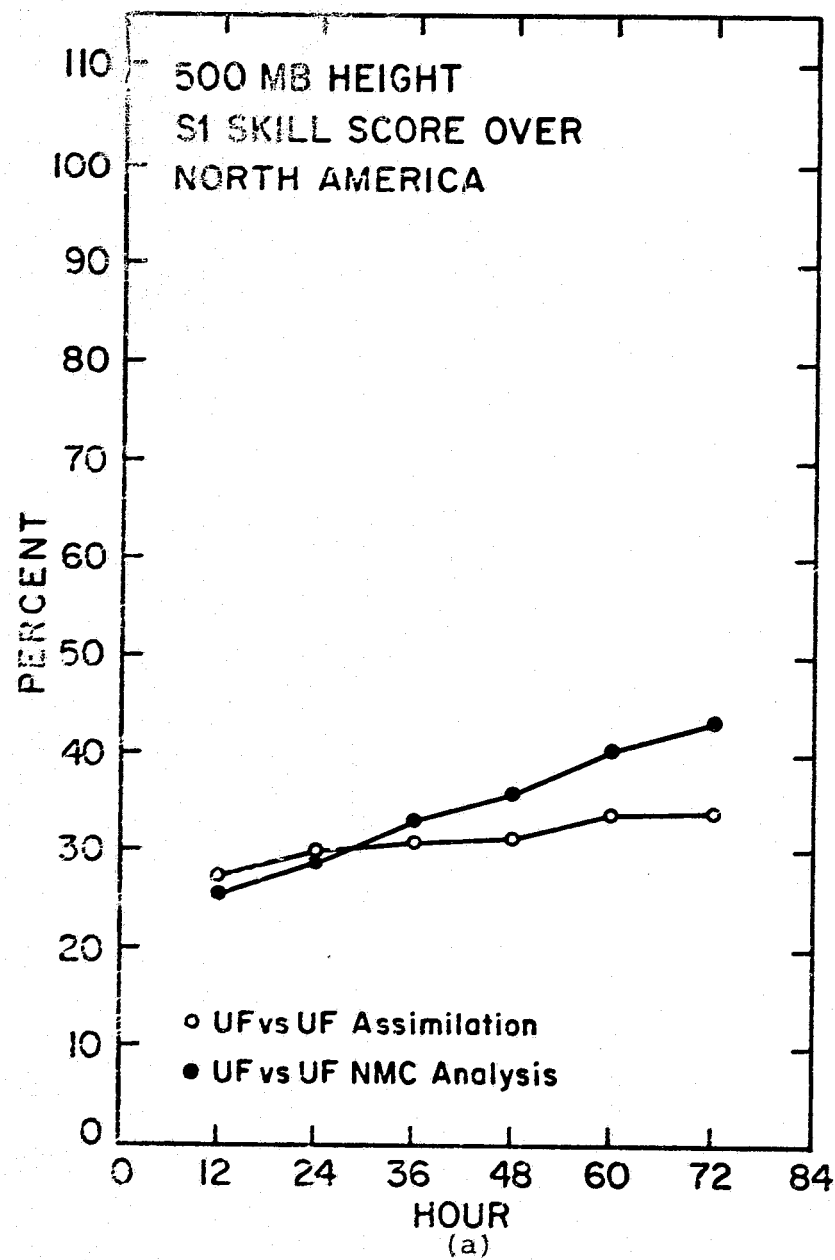


Figure 4

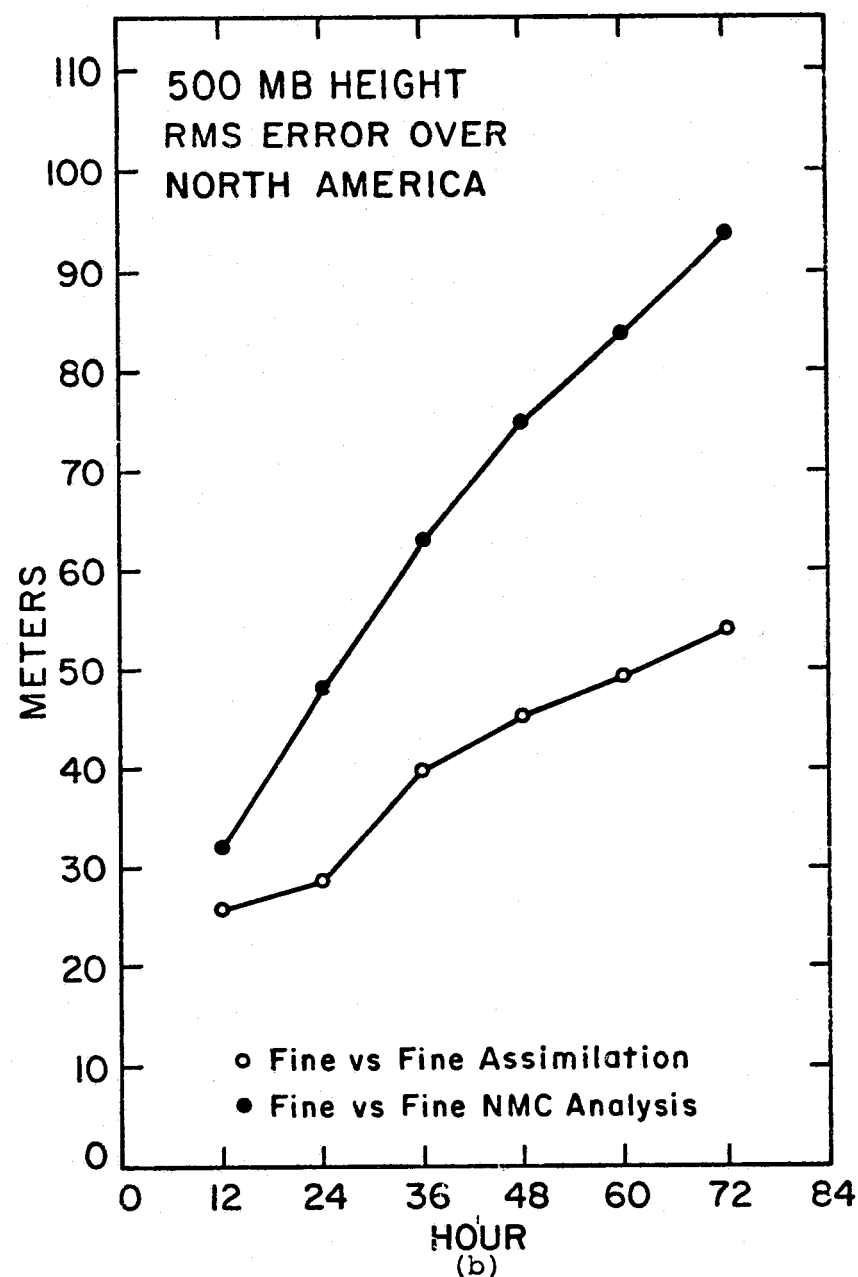
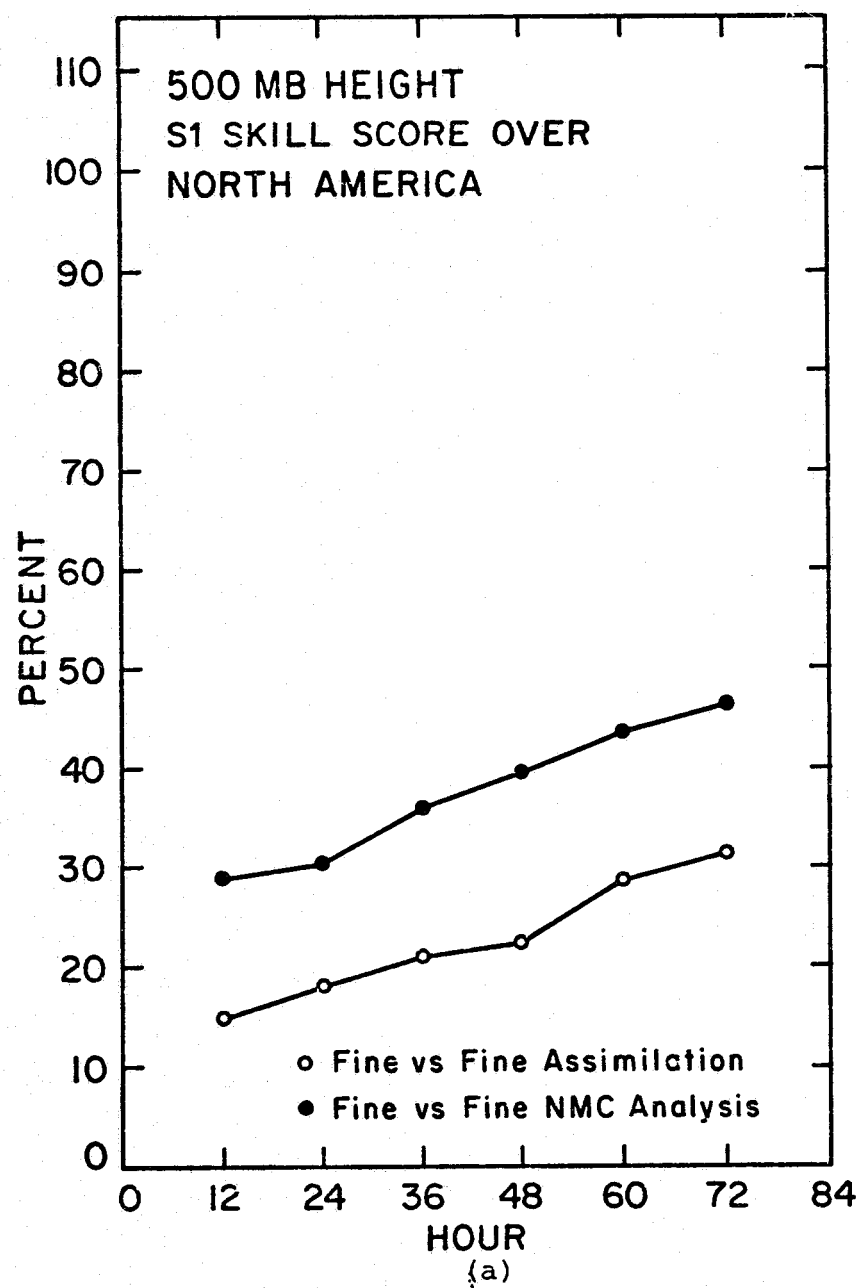


Figure 5

## 4.5 PROBLEMS OF STATISTICAL EVALUATION

A standard measure for evaluating the forecast skill of an assimilation experiment is to calculate the 12, 24, 36, 48, 60, and 72 hour forecast RMS errors and skills for each forecast made using the assimilation for an initial state. The scores for all the forecasts can then be averaged together to give average skill scores and RMS errors for each forecast interval.

A problem arises in computing RMS and S1 scores. There is an NMC analysis, a fine assimilation analysis, and an ultrafine assimilation analysis. Which analysis should be considered as the "truth?" It turns out that it makes a big difference. For example, Figure 1 shows two sets of S1 scores and RMS errors for 500-mb heights over North America. The upper set of curves (showing lower forecast skill) is the average of 11 ultrafine grid. The lower scores (higher forecast skill) were obtained by comparing the ultrafine forecasts with the ultrafine assimilation. Figure 5 shows S1 scores and RMS errors calculated by comparing the fine forecasts (Experiment 3) with the NMC analysis (upper curve worse skill) and the fine assimilation (lower curve better skill). This would seem to indicate that a forecast model would have an advantage in a comparison with another forecast model if an analysis generated from that particular model is used as the comparison. For the purpose of an impartial comparison of two models they should be compared with an analysis generated from an independent source.



## 4.6 STATISTICAL EVALUATION OF THE ULTRAFINE MODEL AND ASSIMILATION CYCLE

To make an impartial comparison of the three experiments described in Section 4.4.2, all three sets of forecasts were compared to the NMC DST-6 analyses interpolated to the GISS grids. The ultrafine model was compared on an ultrafine grid, and the fine model on a fine grid. Figure 6 shows RMS errors and S1 skill scores over the United States and Europe for 500-mb heights and sea-level pressures. The results shown were obtained by averaging together the scores for the eleven forecasts made for each experiment. Over Europe the ultrafine model does not show significant increase in forecast skill over the fine model; however, the increase in skill over North America is quite significant. It is not known why the forecast skill improvement is better over North America than over Europe.

The size of the improvement in skill score using the ultrafine model for forecasts and assimilation is so great that the 60-hour forecasts with the ultrafine model have as good a skill score as the 48-hour forecasts using the fine model. This equals all the improvements in the skill score made with NMC's forecast models during the 15 years from 1962 to 1976. The increase in skill shown here is almost twice those shown in Tables 1 and 2 for the LFM model. This may be due to two factors:

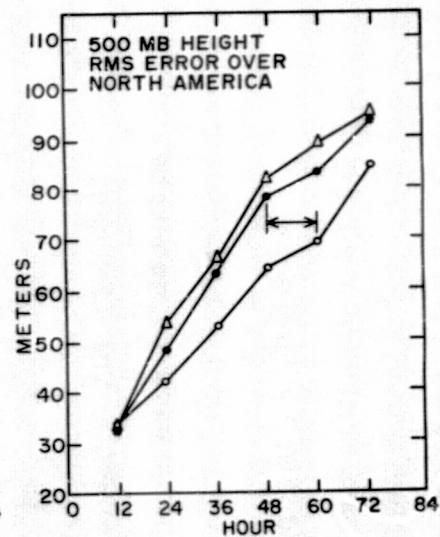
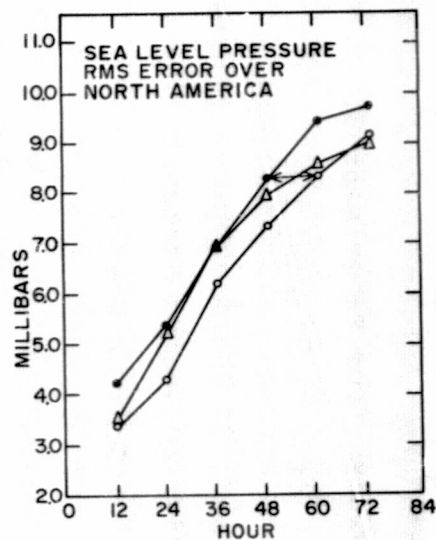
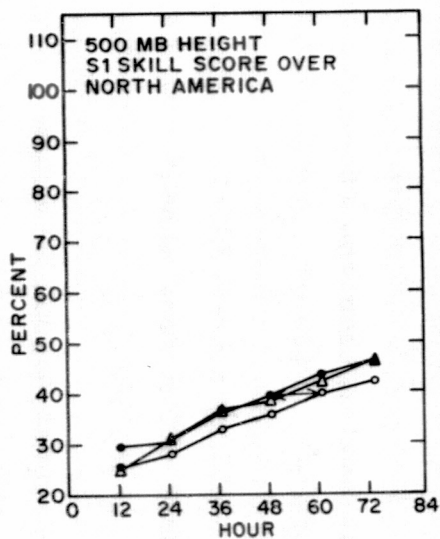
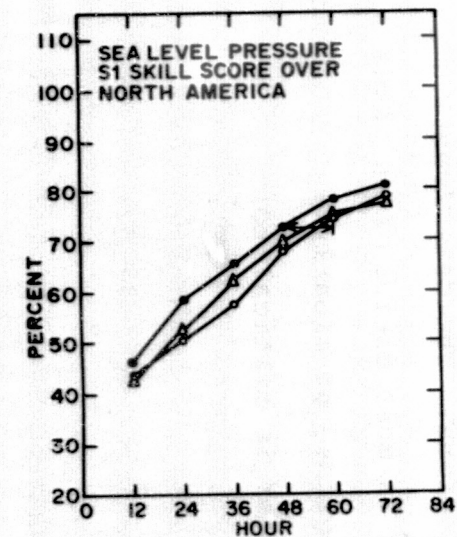
1. The ultrafine model is global so it does not have to

contend with any errors that are induced by having a nested mesh.

2. In Experiment 2 the ultrafine model was used to generate both the initial conditions and forecast. The LFM uses initial conditions that were generated by the same model that generated the PE initial conditions.

The second hypothesis is supported by the results from Experiment 3. The RMS and S1 skill scores obtained by doing fine forecasts, but using initial conditions generated by the ultrafine model (see Figure 6) show significantly better skill over the United States than the fine forecasts made from initial conditions generated by the fine model (Experiment 1).

If the improvement in skill score for the 60-hour forecast represents an equivalent increase in forecast skill, then the 60-hour forecast for the ultrafine would be equal in skill to the fine 48-hour forecast skill. This is critically important because it is agreed that the 48-hour operational forecast shows some useful skill and that there is little if any skill in the 60-hour forecast and beyond. Extending the useful forecasting range beyond 48 hours is particularly crucial for satellite applications. The data from unpopulated regions where the satellite data is most useful often takes 48 hours or longer to influence populated regions, so clearly a model that can forecast for 48 hours and longer is critical to satellite applications.



Legend

- UF versus NMC analysis (Experiment 2)
- Fine versus NMC analysis (Experiment 1)
- △ Fine from UF initial conditions (Experiment 3) versus NMC analysis

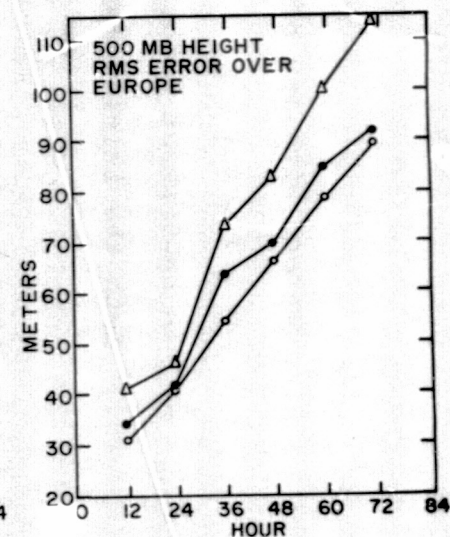
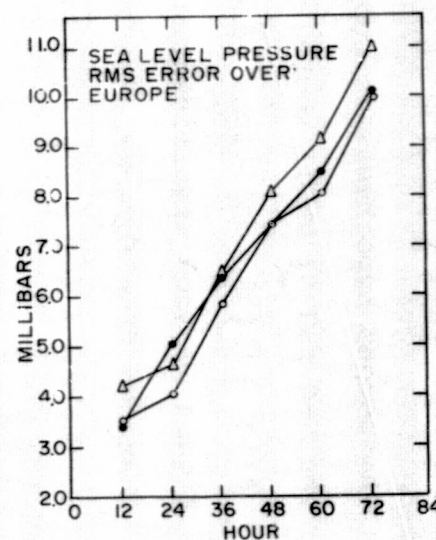
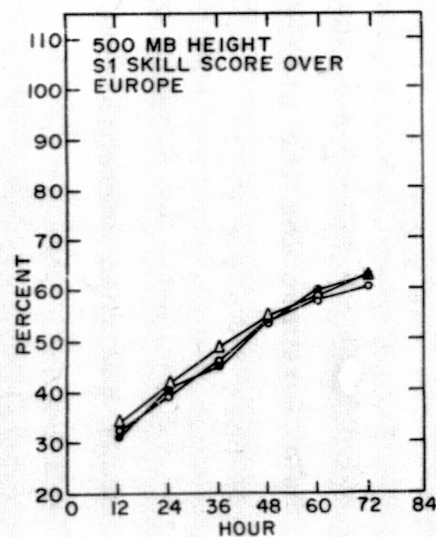
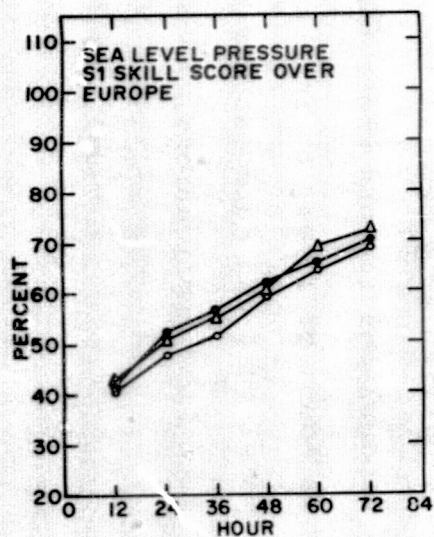


Figure 6

#### 4.7 SYNOPTIC EVALUATION OF ULTRAFINE FORECASTS (R. Atlas)

As a further evaluation of the ultrafine model, ultrafine forecasts of sea-level pressure and 500-mb heights have been subjectively compared to fine forecasts and the corresponding analyses. This comparison has shown that for sea-level pressure prognoses, significant improvements in the predicted displacement and intensification of individual pressure systems do occur. Along with these beneficial impacts, smaller negative impacts are also generated. These negative impacts sometimes take the form of small spurious pressure systems and may be the result of a certain degree of noise in the ultrafine version. Overall, however, the ultrafine model produces a significantly better and more useful sea-level pressure prognosis than does the fine. At 500-mb, the impact of the ultrafine model appears smaller. On the average, a small improvement in the prognostic flow patterns can be noted. However, at times the impact is negligible or even slightly negative.

One case study is presented below to illustrate the impact of the ultrafine model. This case is typical of the sample studied in that it depicts both positive and negative impacts in the prognoses. The results were compared to the NMC analyses interpolated to the GISS ultrafine grid rather than to the NMC fine analyses, because comparison of both analyses with NMC's hand-drawn analyses of surface stations showed this procedure to be more accurate.

Case I: Forecast From Feb. 1, 00Z

a) Sea Level Pressure

Figure 7a presents the initial conditions for this forecast; Figures 8a, 9a, and 10a are the 24, 48, and 72 hour fine forecasts; Figures 8b, 9b, and 10b are the 24, 48, and 72 hour ultrafine forecasts; the corresponding analyses are presented in Figures 8c, 9c, and 10c.

In this case, cyclogenesis occurs near the Gulf coast and this new cyclone merges with a low that had been moving toward the east coast from the west. This results in a large intensifying low over the eastern U.S. at the end of 24 hours.

The major differences between the fine and ultrafine 24-hour forecasts are the intensity of this eastern U.S. low, the position of the Canadian high approaching the Great Lakes, and the development of spurious pressure systems in each forecast. The fine model has correctly predicted the displacement of a low to the east of the Great Lakes but has failed to develop the new low or the merged system. This results in a much weaker cyclonic circulation than is observed. In addition, it is slow in its movement of a Canadian high towards the Great Lakes and develops a small high over Mexico and a weak low in Canadian Rockies which do not appear in the analysis.

The ultrafine model has correctly predicted the development of the large intensifying low over the eastern U.S. and has displaced a Canadian high much closer to the Great Lakes, in better agreement with reality. It did not develop the spurious high over Mexico, but

incorrectly did generate two low pressure centers on the lee side of the Rockies. Both models are similar in their failure to predict a cyclonic circulation entering southwest Canada, and in their positioning of a high pressure system over the northwestern U.S., although minor differences in these features do exist.

By 48 hours, large errors in both the fine and ultrafine predictions are evident. However, major differences between the two forecasts are apparent. Neither model has correctly predicted the intensity or position of the intense low now over southeast Canada. But the ultrafine prediction of this system is significantly better. The ultrafine model has forecast the central pressure of this low to be 12 mb deeper and the position of the low's center is also in better agreement with reality. This has resulted in a more accurate prediction of the pressure gradient over the northeastern U.S., even though the orientation of the isobars for both the fine and ultrafine predictions is in error in this region.

Over the remainder of the U.S. differences are more subtle. The ultrafine prediction depicts the isobaric pattern slightly better over southwestern Canada and the western U.S., but incorrectly depicts a more intense low in the central U.S.

At 72 hours, the improvement of the ultrafine prediction is evident even though significant errors are also present. The fine model predicts a closed high to be centered over the middle-Atlantic states, and a strong cyclonic circulation to be dominating the central and western U.S. It fails to predict the intense high pressure ridge

which extends from southwest Canada to the central plains. In contrast, the ultrafine model moves a high pressure center off the east coast of the U.S. and correctly indicates a high pressure ridge extending to the central plains. In addition, its representation of the complex low in the central U.S. appears closer to the observed situation.

(b) 500 Mb Heights

Figure 7b presents the initial condition for this forecast; Figures 11a, 12a, and 13a are the 24, 48, and 72 hour fine forecasts; Figures 11b, 12b, and 13b are the 24, 48, and 72 hour ultrafine forecasts; the corresponding analyses are presented in Figures 11c, 12c, and 13c.

In this case, a broad trough extending from the midwestern U.S. to the western Gulf of Mexico, intensifies as its southern end moves rapidly eastward during the first 24-hour period. At the same time a very slight flattening of the ridge over western North America occurs.

The 24-hour fine forecast correctly predicts the slight flattening of the ridge and the intensification of the trough, but has failed to move the southern end of the trough far enough east. As a result, the change in orientation of this trough is not predicted.

The 24-hour ultrafine forecast indicates the intensification of the trough correctly and moves the trough almost  $5^{\circ}$  of longitude further east (at  $30^{\circ}\text{N}$ ) in better agreement with reality. However,

the ultrafine's movement of the southern end of the trough is also slow, and thus the ultrafine has also failed to predict the change in orientation of the trough which has occurred. In addition, the ultrafine forecast depicts an excessive flattening of the western ridge.

By 48 hours, both the trough and the ridge have flattened considerably. Westerly flow dominates the eastern U.S. while northwest flow predominates over the remainder of the U.S. Both the fine and ultrafine 48-hour forecasts correctly indicate that northwest flow will dominate most of the U.S., but neither depicts the slight anti-cyclonic curvature of the contours over the Rockies, or the development of a closed low southeast of Hudson Bay. The major difference between the two forecasts is the position and structure of the trough which extends southward from Canada into the U.S. The ultrafine prediction depicts a sharper trough to be located further east and to have a more north-south orientation than that predicted by the fine model. One additional difference may be noted in the orientation of the 5700-m contour of the southwestern U.S. and northern Mexico. Here the fine model has incorrectly depicted a more cyclonic curvature of this contour.

By 72 hours, a radical re-orientation of the pattern has occurred. A new trough with an east-northeast to west-southwest orientation now extends from extreme south central Canada into the northwestern U.S. and west-to-east flow now predominates over the rest of the U.S. Both the fine and ultrafine models have failed to predict each of these features and it appears that the only major differences



SEA LEVEL PRESSURE (MB-1000.))

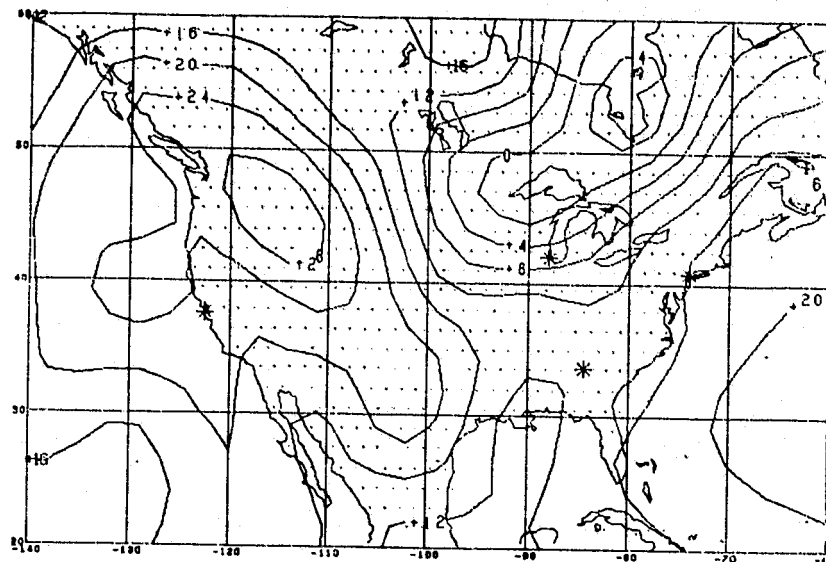


Figure 7a. Feb. 1 00Z Initial pressure distribution.

GEOPOTENTIAL HEIGHT SURFACE 500 M B

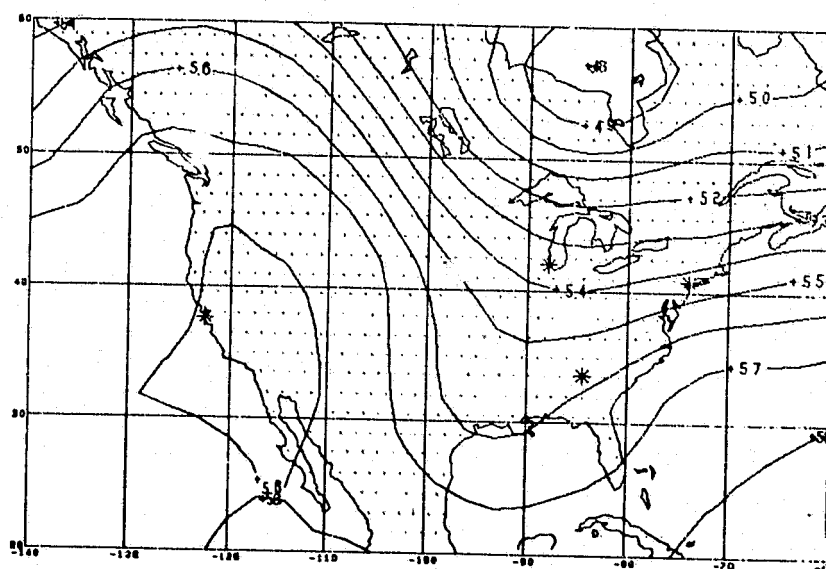
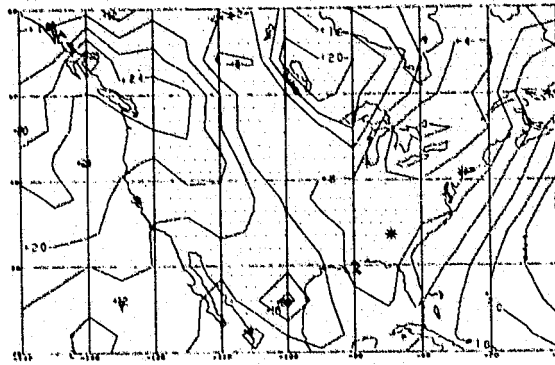


Figure 7b. Feb. 1 00Z Initial 500mb geopotential height in hundreds of meters.

ORIGINAL PAGE IS  
OF POOR QUALITY



A-29

4-30

SEA LEVEL PRESSURE (MB-1000.1)

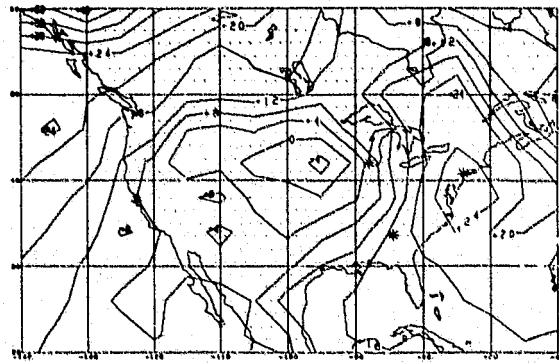


Figure 10a. Fine

ORIGINAL PAGE IS  
OF POOR QUALITY

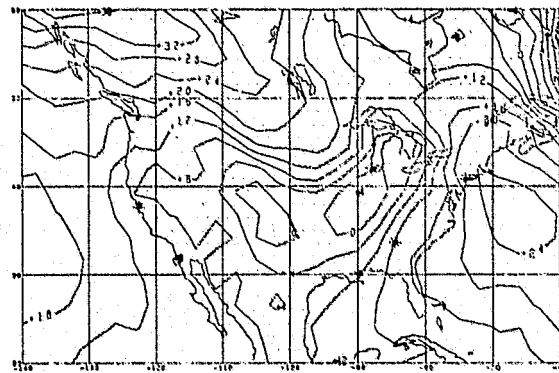


Figure 10b. Ultrafine

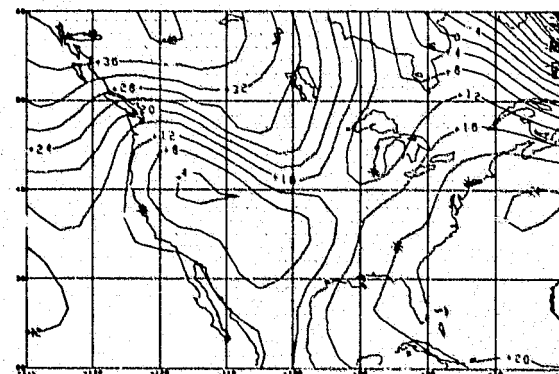


Figure 10c. Ultrafine Analysis  
Feb. 4 00Z

GEOPOTENTIAL HEIGHT SURFACE 500 M B  
(hundreds of meters)

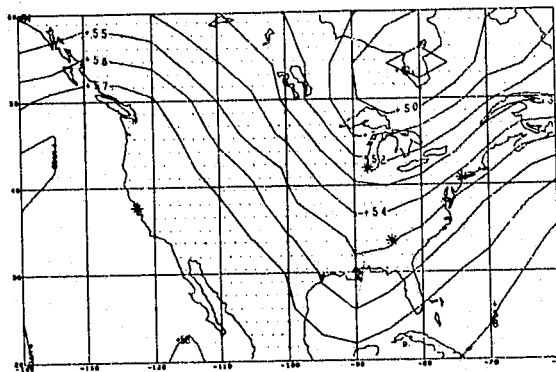


Figure 11a. Fine

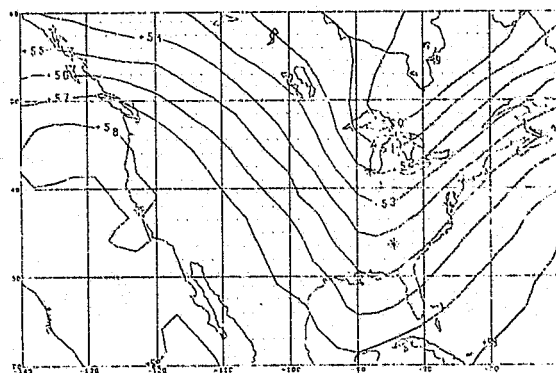


Figure 11b. Ultrafine

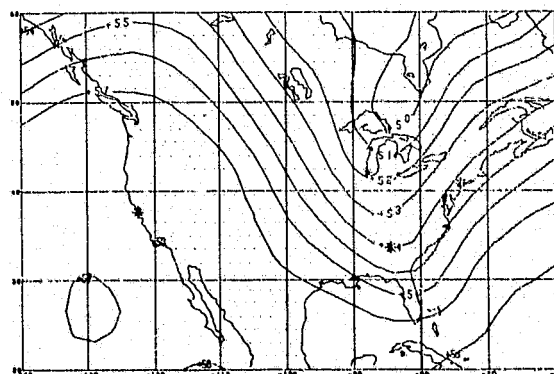


Figure 11c. Ultrafine Analysis  
Feb. 2 00Z

GEOPOTENTIAL HEIGHT SURFACE

500 M B

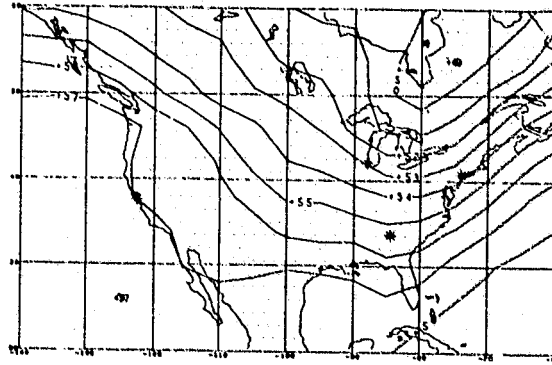


Figure 12a. Fine

ORIGINAL PAGE IS  
OF POOR QUALITY

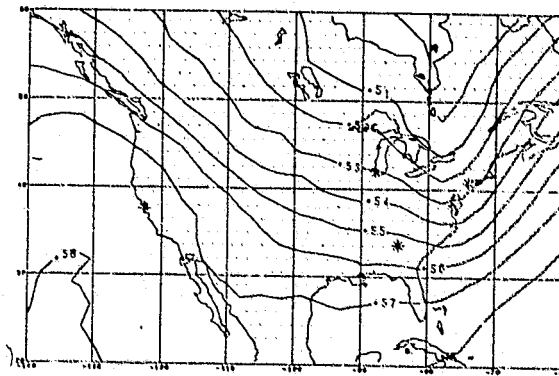


Figure 12b. Ultrafine

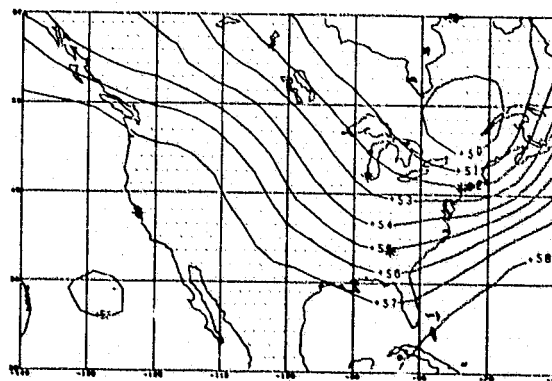


Figure 12c. Ultrafine Analysis  
Feb. 3 00Z

GEOPOTENTIAL HEIGHT SURFACE

500 M B

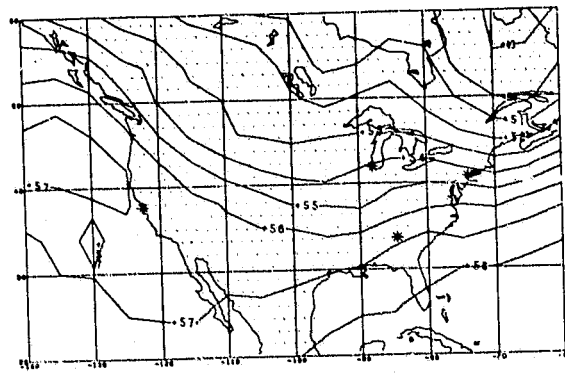


Figure 13a. Fine

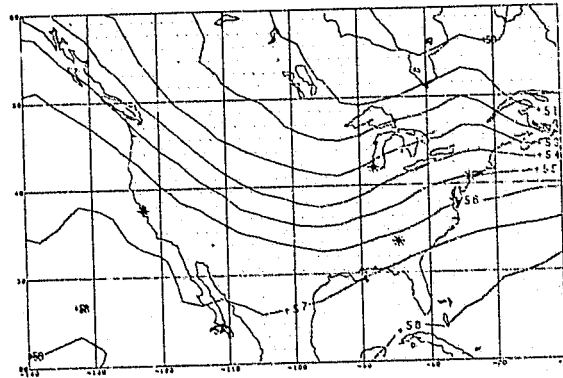


Figure 13b. Ultrafine

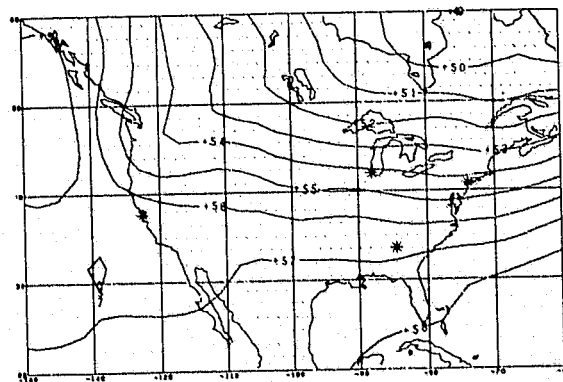


Figure 13c. Ultrafine Analysis

between the two forecasts are the positioning of a spurious short wave ridge in southeast Canada and the extent of troughing of the contours over the central United States.

## 4.8 CONCLUSIONS

1. Statistical analyses for 11 cases relative to the NMC analysis and synoptic evaluations show that assimilation experiments performed with the ultrafine model produce better forecasts than the experiments done with the fine model at all forecast intervals. It is necessary to use the ultrafine model for both the assimilation and the forecasts.

2. Use of the ultrafine model yields skill scores and rms comparisons with NMC analyses for 60-hour forecasts that are as good as the fine 48-hour forecasts. This is important for assessing the impact of satellite data, since it takes 48 hours for satellite data to make large impacts for forecasts over populated regions.

3. Only a 5-fold or larger increase in computing power can make use of the ultrafine model possible on a routine basis.

4. One must be very careful in evaluating statistical scores. If one model is used for both generating a forecast and the analysis to which the forecast is compared, it will have a big advantage over another model which is compared to the same analysis. Until this ambiguity is resolved it will be difficult to state quantitatively just how much the ultrafine model has improved over the fine model, but from both our synoptic studies and those of NMC it is obvious that use of higher resolution does improve forecast skill. So far it is the only known method of improving model forecasts.



## REFERENCES

- Baumhefner, David P. (1977). GARP Basic Data Set Forecast Experiments Generated from the NCAR and GISS Numerical Prediction Models. NCAR MS. 0501/77-1, 30 pp.
- Brown, Harry (1974). Listing of some specific performance characteristics of the 6L PE and LFM Models, Supplement to Bull. No. 107, Technical Procedures Branch, NOAA National Weather Service, 4 pp.
- \_\_\_\_\_ (1975). Comparison of the Position and Central Pressure Errors of East Coast Lows on 36-hour PE and LFM Prognoses, NMC Newsletter No. 75-4 Technical attachment, NOAA, National Weather Service.
- Brown, Harry E. and Edwin B. Fawcett (1975). Use of Numerical Guidance at the National Weather Services' National Meteorological Center, J. Appl. Meteor., 11, 1175-1182.
- Fawcett, Edwin B. (1977). Current capabilities in Prediction at the National Weather Service's National Meteorological Center. Bull. Amer. Meteor. Soc., 55, 1217-1227.
- Gates, W.L. and A.B. Nelson (1973). A New Tabulation of the Scripps Topography on a 1° Global Grid. Part 1; Terrain Heights. Available from Rand Corporation, Santa Monica, Ca. 90406. R-1276, ARPA Order No. 189-1.
- Grotjahn, Richard and James J. O'Brien (1976). Some inaccuracies in finite differencing hyperbolic equations, Mon. Wea. Rev., 104, 180-194.
- Halem, M. and G. Russell (1973). A Split-Grid Differencing Scheme for the GISS Model. Institute for Space Studies Research Review, 194-201.

Jensen, Clayton E. (1975). A Review of Federal Meteorological Programs for Fiscal Years 1965-1975, Bull. Amer. Meteor. Soc., 56, 208-224.

Robert, André (1975). Computational Resolution Requirements for Accurate Medium-Range Numerical Predictions, Proceedings of Symposium on Atmospheric and Oceanic Numeric Modeling, Novosibirsk. Published by the Computing Center of the Siberian Branch of the Academy of Science.

Shapiro, R. (1970). Smoothing, filtering and boundary effects. Rev. Geoph. and Space Phys., 8, 359-387.

Somerville, R.C.J., P.H. Stone, M. Halem, J.E. Hansen, J.S. Hogan, L.M. Druyan, G. Russell, A.A. Lacis, W.J. Quirk, J. Tenenbaum (1974). The Giss Model of the Global Atmosphere, 31, 84-117.

## Appendix A

### Definition of the Model Used for the GCM Experiment

(Chapter 4: Forecast Model Development)

## APPENDIX A

### DEFINITION OF THE MODEL USED FOR THE GCM EXPERIMENTS

The model used in this study is the same model as described in Somerville et al. (1974) with three exceptions:


1. The numerical differencing near the poles was modified so a nearly equal area mesh was used near the poles. This split-grid technique has been described by Halem and Russell (1973). The use of the split-grid technique allowed the model's time step to be 10 minutes instead of 5, so it affectively cut the computing time of the model in half (see Section 4.2).

2. The mountains over Greenland have only half the height prescribed in the topography given in Somerville et al. This was done because the split-grid model could not handle the flow over the steep mountains in Greenland. These mountains, which are near the pole, seemed twice as steep for the split-grid model as for the regular grid model since it only had half as many grid points at these latitudes.


3. A more realistic distribution of albedo was used. Instead of using an arbitrary latitude for the extent of snow to determine albedo and letting all other land have 14% albedo, climatologically realistic albedos were specified for all land areas. The global surface albedos were specified by using Posey and Clapp (1964) as compiled by Shutz and Gates (1972a and b).

## REFERENCES FOR APPENDIX

- Halem, M. and G. Russell (1973). A Split-Grid Differencing Scheme for the GISS Model. Institute for Space Studies Research Review, 194-201.
- Posey, J.W. and P.F. Clapp (1964). Global Distribution of Normal Surface Albedo, Geofisica Internacional, 4, 53-58.
- Schutz, C. and W.L. Gates (1972a). Global Climatic Data for Surface, 800 mb, and 400 mb: July. Available from Rand Corporation, Santa Monica, Ca. 90406. R-1029, ARPA Order No. 189-1.
- \_\_\_\_\_ (1972b). Supplemental Global Climatic Data: January. Available from Rand Corporation, Santa Monica, Ca. 90406. R-9 15/1, ARPA Order No. 189-1.
- Somerville, R.C.J., P.H. Stone, M. Halem, J.E. Hansen, J.S. Hogan, L.M. Druyan, G. Russell, A.A. Lacis, W.J. Quirk, J. Tenenbaum (1974). The GISS Model of the Global Atmosphere, J.A.S., 31, 84-117.



## CHAPTER V



## 5. EVALUATION AND VERIFICATION TESTS

(R. Atlas, Scientist; D. Sakal, Manager)

### 5.1 INTRODUCTION

The Evaluation and Verification Group (EVG) was organized to evaluate the forecasting impact of satellite data in support of the DST Impact Test Project. Traditional statistical measures of forecast accuracy have been the general tool used for this purpose. However, in recent years the value of interpreting these statistical measures in terms of actual improvements to weather prediction has been questioned by the meteorological community.

This report attempts to evaluate the impact of satellite data insertions in the context of a real-time forecasting operation; specifically to determine: (1) if the inclusion of satellite data results in significantly different analyses and prognostic flow patterns, (2) if the impact of satellite data is large enough to result in different actual weather forecasts, as might be prepared by a local weather forecaster, and (3) if this impact is beneficial.

For this purpose a prognostic plot package, similar to that distributed by NMC for use by local weather forecasters, has been developed and tested. Based on the subjective forecasting techniques which were applied to this plot package, a computerized forecasting model (CFM) was developed, which is capable of simulating the subjective forecasting process under very restrictive conditions. As a result of these tools, the evaluation of the forecasting impact of the satellite data can thus be expressed in terms of statistical scores,

differences in prognostic charts, and actual differences in local weather forecasts.

The major findings of the EVG for the winter DST-6 Impact Test are:

- (1) the impact of satellite sounding data over data-sparse regions is large enough to influence actual local weather forecasts,
- (2) significant differences in prognostic flow patterns occur as a result of the inclusion of satellite data,
- (3) significant impacts on prognostic vorticity and vorticity advection fields often occur, even when no impact is discernable in the contour field,
- (4) the inclusion of satellite soundings does not result in a systematic smoothing out of potential temperature gradients,
- (5) for the limited number of DST-6 cases studied, the evaluation techniques employed indicate that the impact is in general modest and favorable, and in several cases, large beneficial impacts occur.

In the following sections the results evaluating the impact of satellite sounding data on meteorological analyses and forecasts will be presented. Section 5.2 contains a review of the subjective evaluation of the DST-5 data set and the development of evaluation procedures. In Section 5.3, the nature and magnitude of the impact of satellite soundings on the initial states is presented. In Section 5.4, a statistical and synoptic evaluation of the impact of satellite soundings on prognostic flow fields is presented. In Section 5.5 the impact on actual local weather forecasts is described. Finally,



Section 5.6 contains our conclusions and recommendations for future research.

## 5.2 BACKGROUND

### 5.2.1 PRELIMINARY SUBJECTIVE EVALUATION

Prior to beginning the evaluation of the DST-6 data set, a preliminary subjective forecast experiment and a subjective evaluation of prognostic charts were carried out with DST-5 data. The preliminary subjective forecast experiment was conducted in the following manner: a set of SAT and NO SAT prognostic packages (consisting of sea-level pressure, 1000- to 500-mb thickness; 850-mb, 700-mb, and 500-mb geopotential heights; 850-mb temperatures and dewpoint depression; 500-mb absolute vorticity and vertical velocity; and 300-mb isotachs) were delivered to two human forecasters, without the corresponding analyses for verification. These forecasters would then note all of the major differences between SAT and NO SAT forecasts by comparing the maps for the United States and noting the meteorological variables at four different cities (New York, Chicago, Atlanta, and San Francisco) at 12-hour intervals for 84 hours. Finally, an actual weather forecast was issued for each of these cities at these times. Each forecast was based completely on the SAT or NO SAT prognostic charts (progs) without human modification.

Two of the 14 DST-5 forecasts, which were studied subjectively are presented below. Both of these forecasts were cases of

large positive statistical impact, but the extent to which the flow patterns and actual weather of the United States were affected was not known.

In the first forecast, from 00Z August 26 initial conditions, no significant impact on the flow patterns was initially obvious, and the actual weather forecasts for New York, Chicago, Atlanta, and San Francisco were the same for SAT and NO SAT predictions throughout the forecast period. However, initially small differences in the flow pattern increased in amplitude with time so that by 72 hours significant differences in the absolute vorticity pattern were evident. By 84 hours the vorticity differences were evident, even over the United States and Canada, and it is obvious that differences in weather would be expected from the SAT and NO SAT predictions for the affected regions.

Figures 1 and 2 illustrate these differences for the 84-hour forecast. On the maps, the solid lines represent isopleths of absolute vorticity, while the dashed lines represent the 500-mb contours for the same time. Areas in which the 500-mb contours are crossing vorticity isopleths from high to low values represent positive vorticity advection (PVA), and areas where the 500-mb contours are crossing vorticity isopleths from low to high values represent negative vorticity advection (NVA). These areas are important because PVA is normally associated with low-level convergence, upper-level divergence, rising motion, cloudiness, and precipitation, while NVA is normally associated with upper-level

convergence, low-level divergence, sinking, and clearing conditions. Note that the 500-mb flow as represented by the dashed lines is not significantly different for the SAT and NO SAT cases, while the vorticity patterns over the western United States, the extreme northeastern United States, and southeastern Canada are significantly different. In particular, note that the vorticity maximums in these two areas are displaced further east and are more intense for the SAT case. This results in strong PVA for the southwestern United States coast and extreme northeastern United States, strong NVA over the Pacific from 130°W to 125°W, and in portions of New England on the SAT forecast, while no significant vorticity advection is evident in the NO SAT forecast.

The second forecast, from 00Z August 31 initial conditions, produced a slightly different outcome. Once again the differences in flow patterns were initially small. However, in this case the small differences in the positions of pressure systems, atmospheric flow, and trends of variables for a particular area were evident over the United States and actually resulted in different subjective forecasts being issued. Table 1 shows the trend of vorticity at the four cities. Obvious differences may be noted for New York and San Francisco.

Table 1. Trend of Vorticity at Selected Cities

These forecasts were generated from 00Z August 31 initial conditions. Values indicate the absolute vorticity at each city for the SAT and NO SAT forecasts.

DAY		0	$\frac{1}{2}$	1	$1\frac{1}{2}$	2	$2\frac{1}{2}$	3	$3\frac{1}{2}$
New York	SAT	10	9	9.5	9.5	9.5	9	9	9
	NO SAT	10	9	9	9	9	8	7.5	6.5
Chicago	SAT	12	11	11	missing	8.5	5.5	4.5	5
	NO SAT	12	12	11	10	7.5	5	5	5
Atlanta	SAT	8	7	8	7	7.5	7.8	8	7.5
	NO SAT	8	8	8	8	8.5	8.5	8.5	8.5
San Francisco	SAT	7	6.5	7.5	8.5	9	9	9.5	9.5
	NO SAT	8	7	7	6	8	8.5	8	8

Differences in meteorological patterns may be noted after just 48 hours in this case. Figures 3 to 8 depict the 48-hour progs of sea-level pressure, 500-mb geopotential heights for the SAT and NO SAT cases. Two differences can be seen on the sea-level pressure map. There is a small high southeast of New York on the SAT progs which is missing on the NO SAT. This causes a change in the wind direction at New York City. Also the high-pressure ridge on the west coast of the United States and a small high center in the northern plains are not as well developed on the SAT as on the NO SAT progs.

At 500 mb the orientation and development of the trough in the northwestern United States and the adjacent ridge differ slightly between the two progs. This difference is more evident in the vorticity field, where a stronger vorticity minimum is evident on the SAT forecast.

These two cases demonstrated that the impact of satellite data can be large enough to influence subjective weather forecasts and prognostic flow patterns, as well as the importance of evaluating impact in terms of vorticity advection.

### 5.2.2 THE COMPUTERIZED FORECASTING MODEL

The computerized forecasting model (CFM) was designed to simulate the human forecaster's interpretation of a set of prognostic charts under the restrictive condition that no modification of the prognostic flow patterns (as forecast by the GISS model) can take place. It has two main advantages over the human forecaster approach:

(1) by use of the CFM, forecasts can be generated for any number of cities in a very short amount of time, and (2) the procedures that are applied to each set of prognostic charts will be uniform.

The major quantities forecast by the CFM are precipitation occurrence, type of precipitation, and 24-hour surface temperature change. Obviously the CFM cannot perform pattern recognition in the same manner as a human forecaster. But it can take account of most patterns in terms of the computed advection of certain quantities.

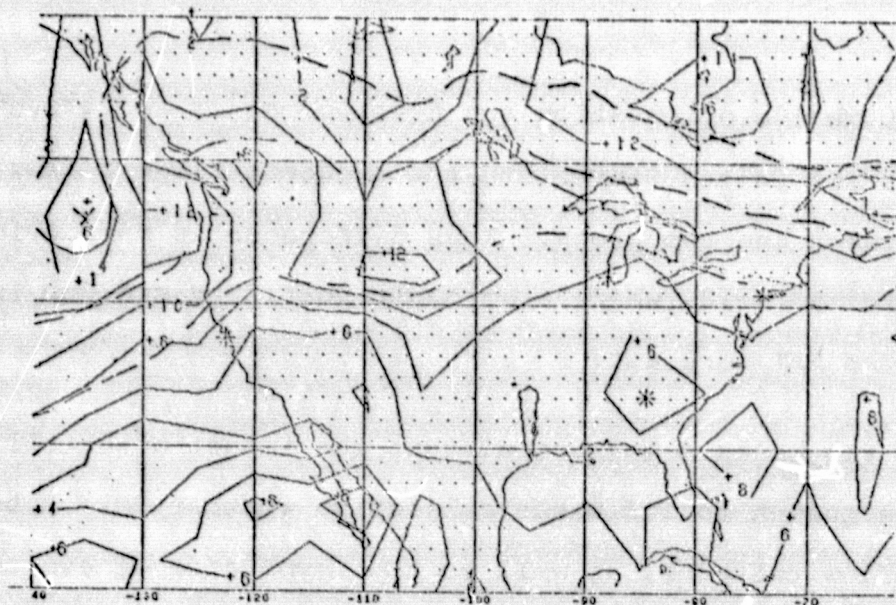


Figure 1. 84-Hour NO SAT Prediction of Vorticity Advection. Solid lines are isopleths of absolute vorticity; dashed lines are 500-mb geopotential height contours.

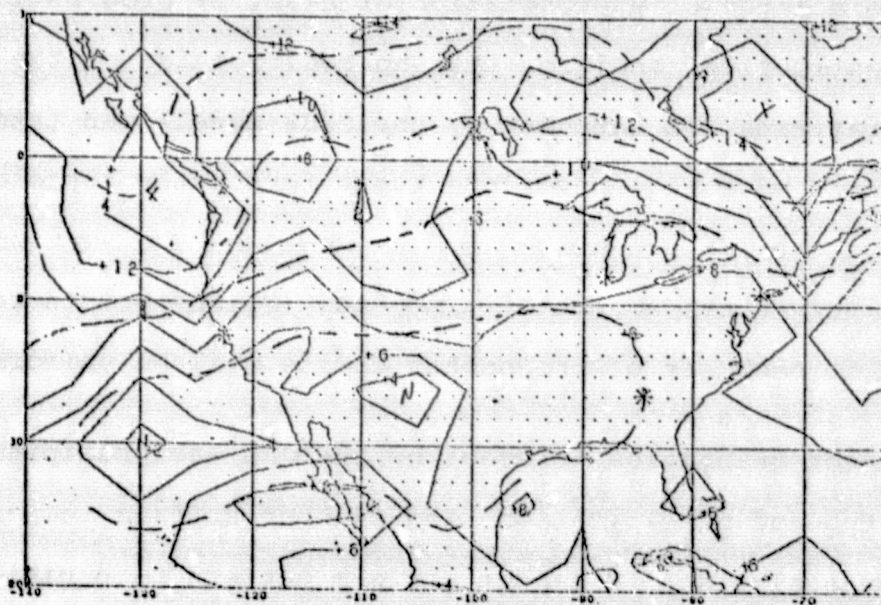


Figure 2. 84-Hour SAT Prediction of Vorticity Advection. Solid lines are isopleths of absolute vorticity; dashed lines are 500-mb geopotential height contours.



ORIGINAL PAGE IS  
OF POOR QUALITY

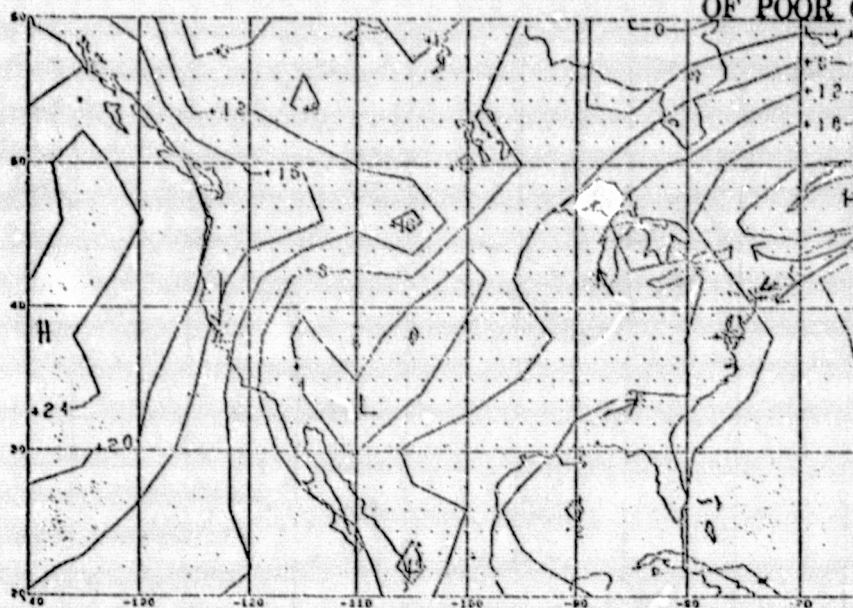


Figure 3. 48-Hour NO SAT Prediction of Sea-Level Pressure.

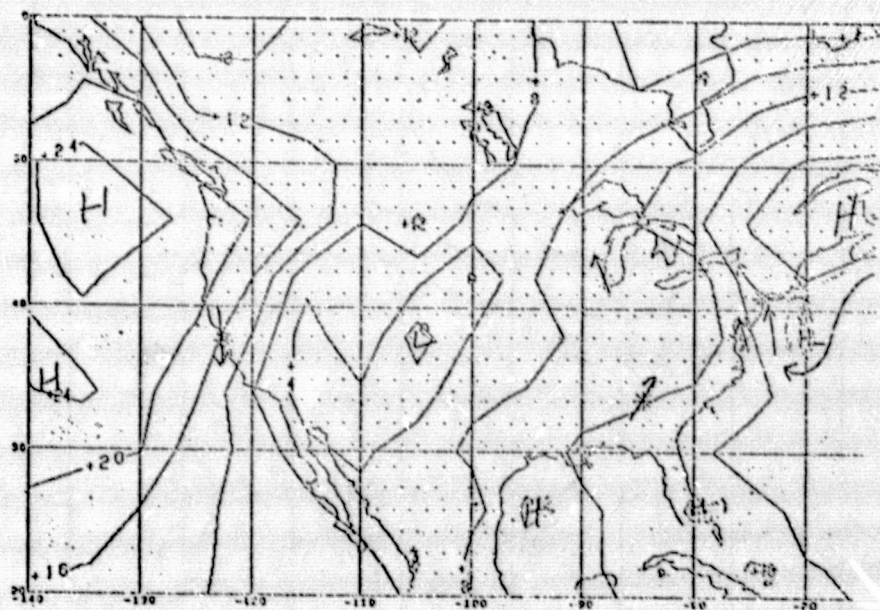


Figure 4. 48-Hour SAT Prediction of Sea-Level Pressure.

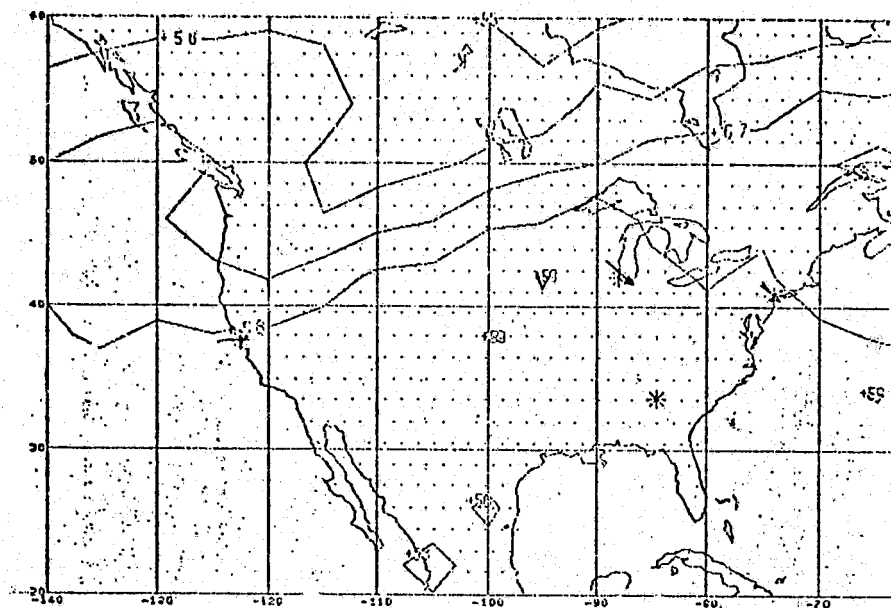


Figure 5. 48-Hour NO SAT Prediction of 500-mb Heights.

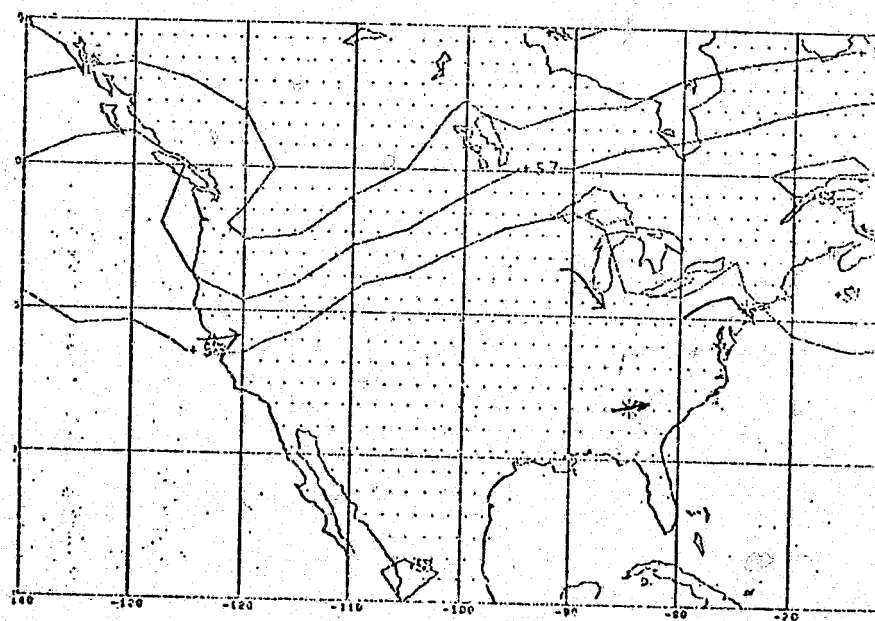


Figure 6. 48-Hour SAT Prediction of 500-mb Heights.



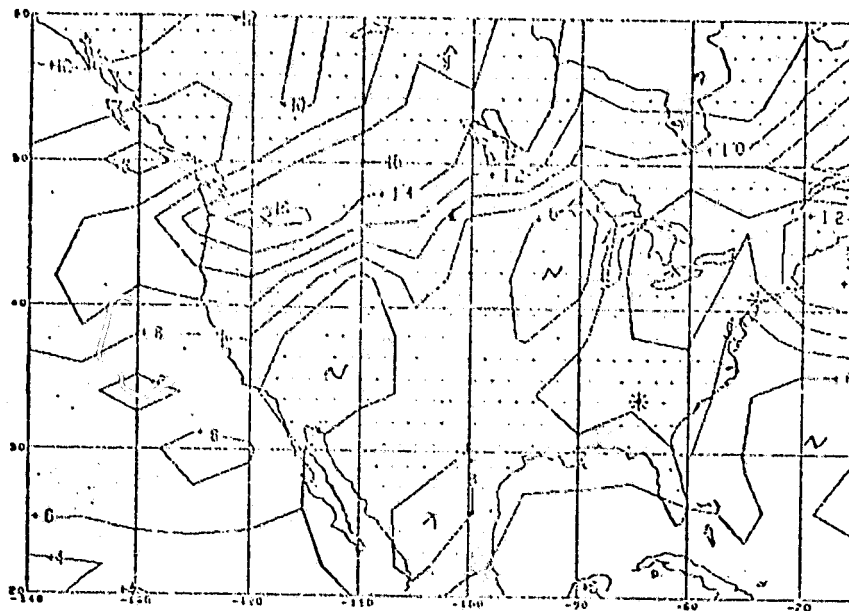


Figure 7. 48-Hour NO SAT Prediction of 500-mb Absolute Vorticity.

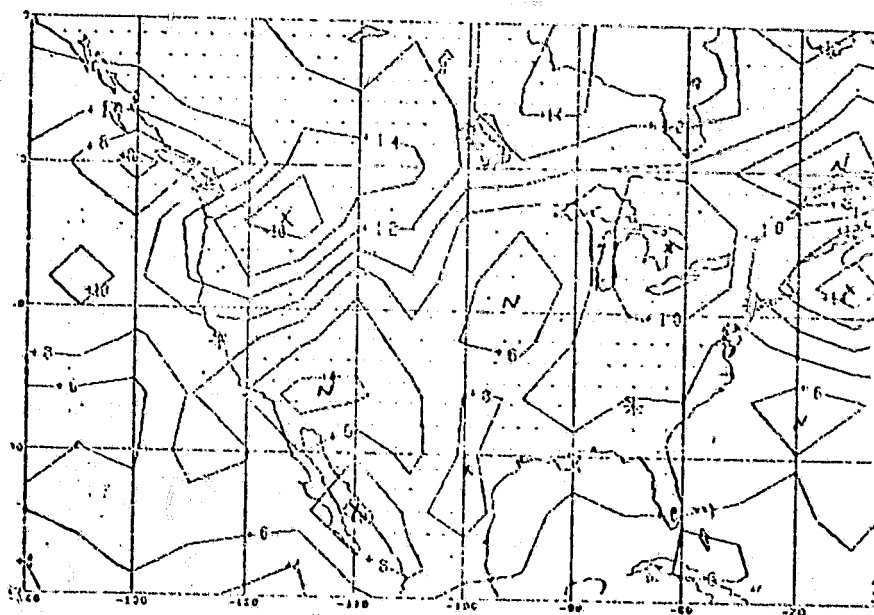


Figure 8. 48-Hour SAT Prediction of 500-mb Absolute Vorticity.

The first step of the CFM precipitation scheme is to compute and input the forecast parameters for every city at which the CFM is to be applied. These forecast parameters are listed in Table 2, and it can readily be seen that this list includes most of the basic tools that are used by operational forecasters to predict areas of large-scale precipitation.

The next step is to test the dewpoint depression to determine if there is sufficient moisture for precipitation. If this criteria is met, then we next test the vorticity advection field. As mentioned earlier, positive vorticity advection (PVA) is a strong indicator of upward vertical motion, whereas negative vorticity advection (NVA) is a strong indicator of downward vertical motion. Generally, if PVA is coupled with sufficient moisture, precipitation will occur. However, the effects of temperature advection must also be considered because strong cold advection can negate the effects of PVA, whereas warm advection will enhance it. The manner in which the CFM combines these quantities is illustrated in Figures 9 through 11.

Once the above precipitation calculation is completed, two additional tests for precipitation are performed. These include a test for cold frontal precipitation (Figure 12) and a gross check for the potential for showers (Figure 13). Finally, a test for the type of precipitation is made as illustrated in Figure 14. A sample of the CFM's output is presented in Figure 15.

**Table 2. Forecast Parameters**

VORTICITY ADVECTION	(VA)
TEMPERATURE ADVECTION	(TA)
THICKNESS ADVECTION	(THA)
MOISTURE ADVECTION	(MA)
DEWPOINT DEPRESSION	(DD)
WIND DIRECTION	(WD)
VERTICAL WIND SHEAR	(VWS)
850-MB TEMPERATURE	(850T)

# TEST DEWPOINT DEPRESSION

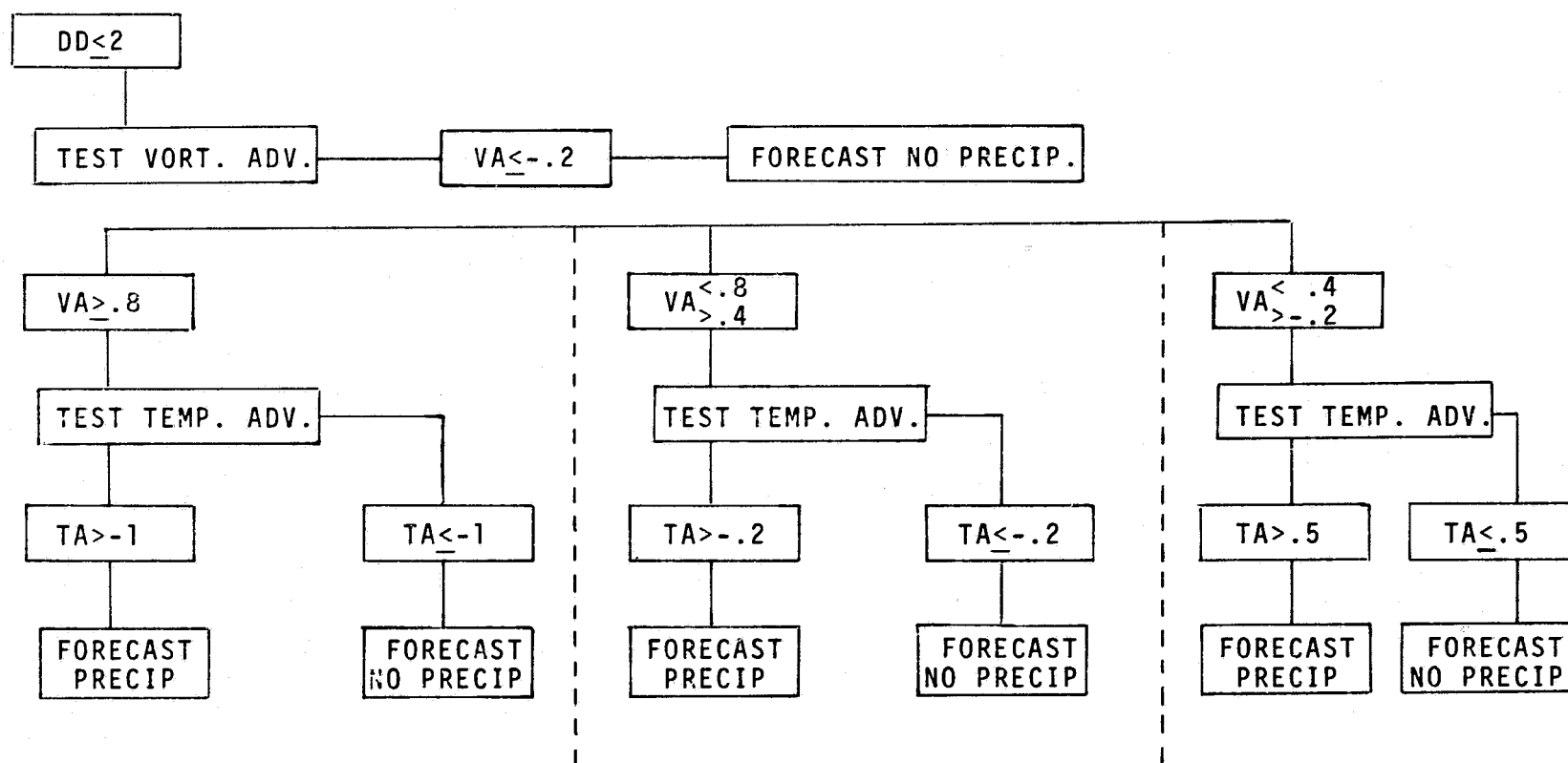


Figure 9

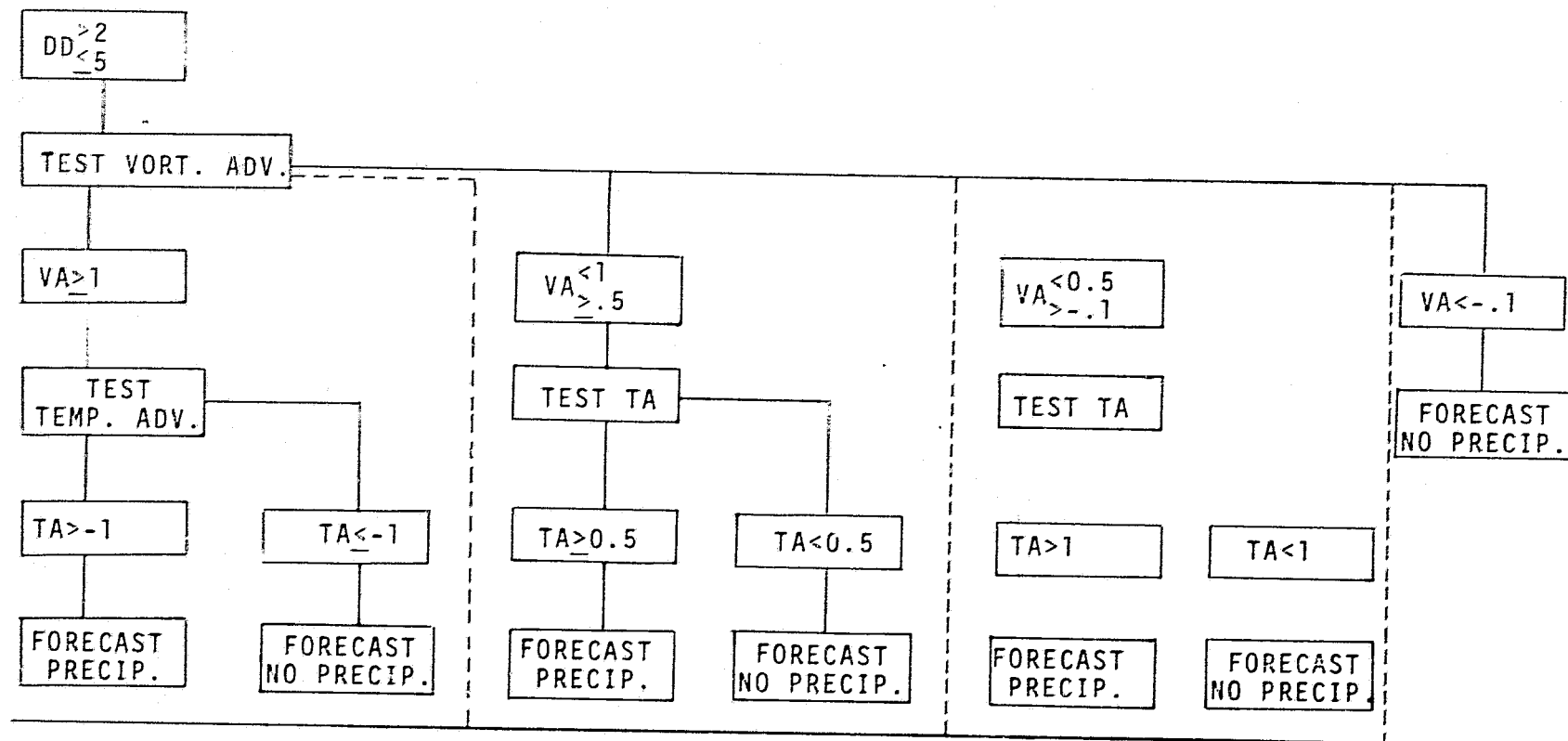
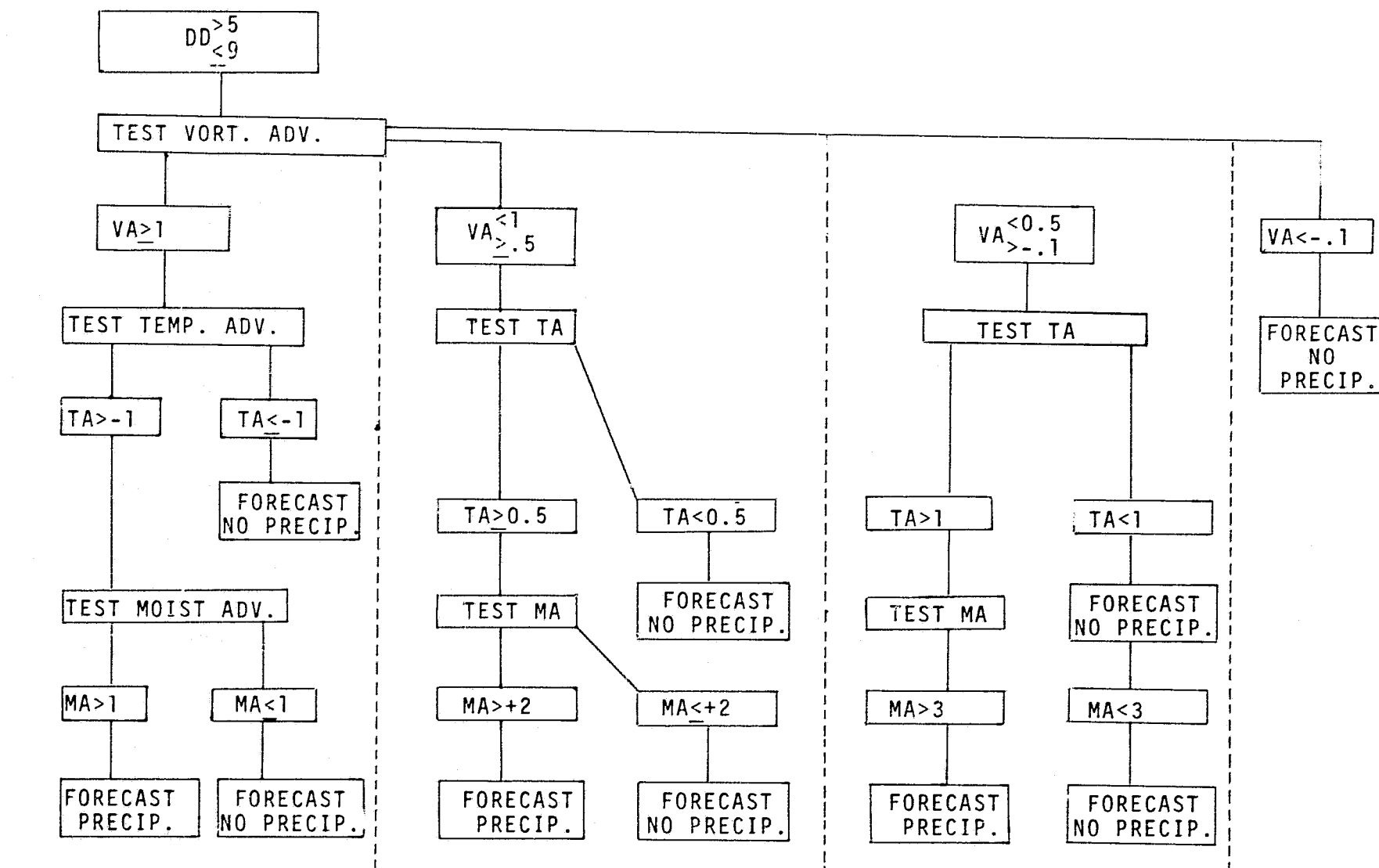


Figure 10

D.)  $DD > 9$ 

FORECAST NO PRECIP.

Figure 11

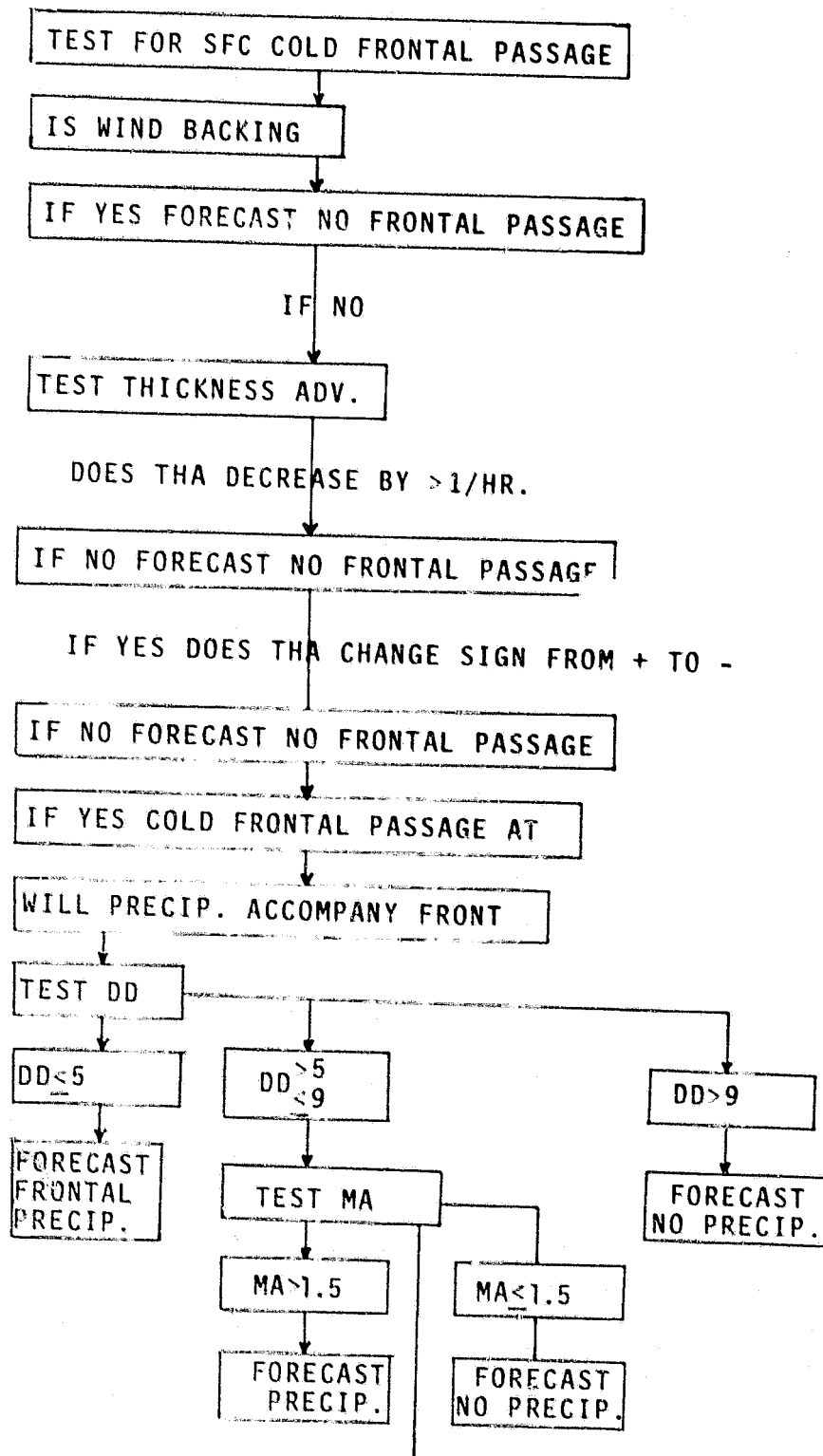


Figure 12

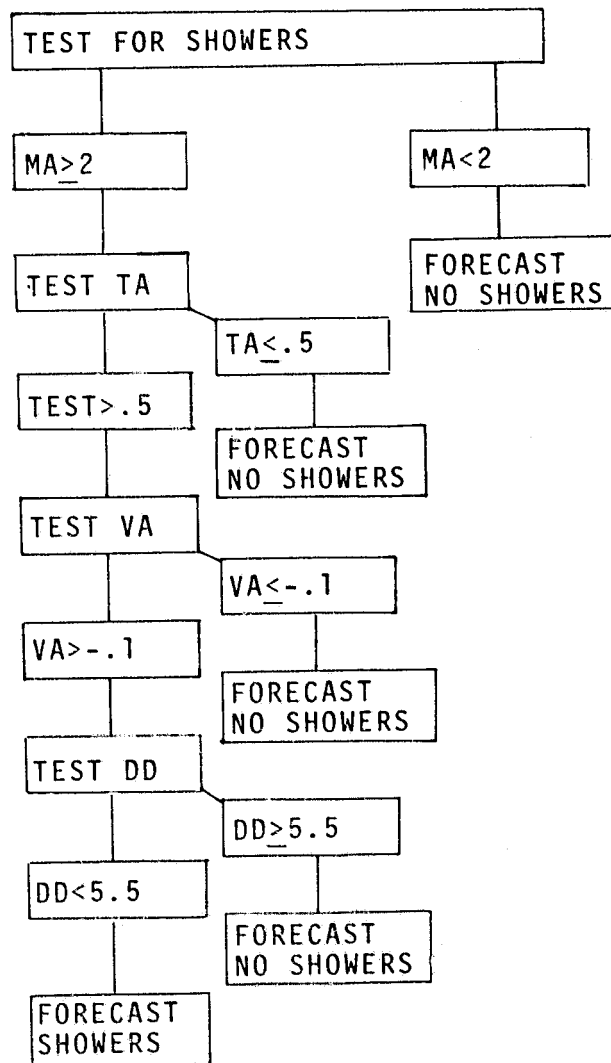


Figure 13



DETERMINE  
TYPE OF PRECIPITATION

TEST 850 MB T

$850T < -2$

SNOW

$850T \begin{matrix} > -2 \\ \leq 0 \end{matrix}$

MIXTURE OF  
RAIN & SNOW

$850T > 0$

RAIN

Figure 14

\*\*\* 24 HOUR SUMMARY \*\*\*

\*\*\*\*\*

NEW YORK

2 0Z	DD= 6.11	VA= -0.31	TA= 0.61	MA= 2.96	THADV= 5.08	VIRT= 10.44	T85C= 0.21	J= 13.14	V= 13.15	NO PRECIPITATION
2 4Z	DD= 4.22	VA= -0.07	TA= 0.37	MA= 1.98	THADV= -1.26	VIRT= 9.93	T85C= 0.08	J= 14.81	V= 10.51	SHOWERS
2 8Z	DD= 2.22	VA= 0.37	TA= 0.09	MA= 1.41	THADV= -3.24	VIRT= 9.66	T85C= -0.30	J= 12.12	V= 7.89	NO PRECIPITATION
212Z	DD= 1.18	VA= 0.99	TA= -0.24	MA= 0.33	THADV= -4.18	VIRT= 9.67	T85C= -0.76	J= 8.43	V= 3.03	RAIN & SNOW
216Z	DD= 0.31	VA= 1.28	TA= -0.62	MA= -1.03	THADV= -7.78	VIRT= 10.14	T85C= -1.52	J= 4.56	V= -1.99	RAIN & SNOW
220Z	DD= 0.17	VA= 1.04	TA= -0.98	MA= -2.51	THADV= -21.52	VIRT= 11.01	T85C= -2.25	J= 5.71	V= -7.70	SNOW

\*\*\* 12 HOUR PRECIPITATION FORECAST \*\*\*

\*\*\*\*\*

2 0Z SHOWERS

-----

212Z RAIN & SNOW

\*\*\*\*\*

\*\*\* FRONT FORECAST \*\*\*

NO FRONT PASSED	22Z +/- 2 HRS	PRECIP
FRONT PASSED	2Z +/- 2 HRS	
NO FRONT PASSED	6Z +/- 2 HRS	
NO FRONT PASSED	10Z +/- 2 HRS	
NO FRONT PASSED	14Z +/- 2 HRS	
NO FRONT PASSED	18Z +/- 2 HRS	

5-20

ORIGINAL PAGE 1  
OF POOR QUALITY

Figure 15

The CFM has been evaluated from two standpoints: (1) its accuracy when applied to a perfect prognostic chart (an analysis), and (2) its agreement with human forecasters. It has been found that for February 1976, the CFM was 93 percent accurate in correctly interpreting whether or not precipitation would occur, and 76 percent accurate in verifying a positive forecast of precipitation, and 76 percent accurate in accounting for precipitation which was actually observed. Its agreement with human forecasts was 94 percent for this period of time.

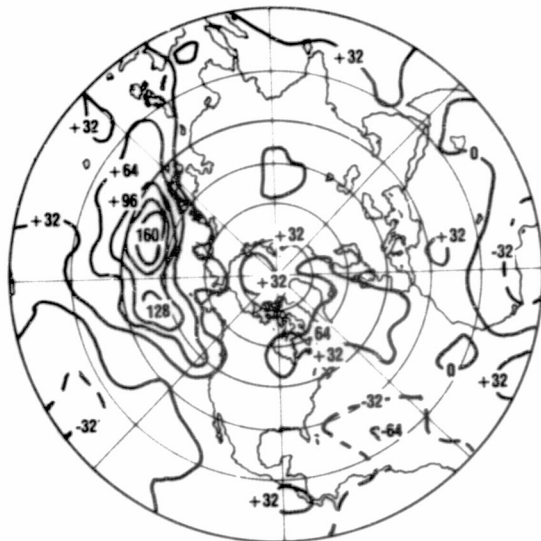
### 5.3 IMPACT OF SATELLITE DATA ON ANALYSES

If satellite soundings are to lead to improved or even distinct forecasts, then the origin of the forecast differences in the initial state conditions should at least be discernable. The initial state differences obtained in the impact test conducted for the period January 29 to February 21, 1976 are presented for all the sounding data which have thus far been processed. The method used to assimilate the sounding data was based on a four-dimensional optimal statistical interpolation procedure applied to both the NOAA 4 and Nimbus 6 satellites simultaneously.

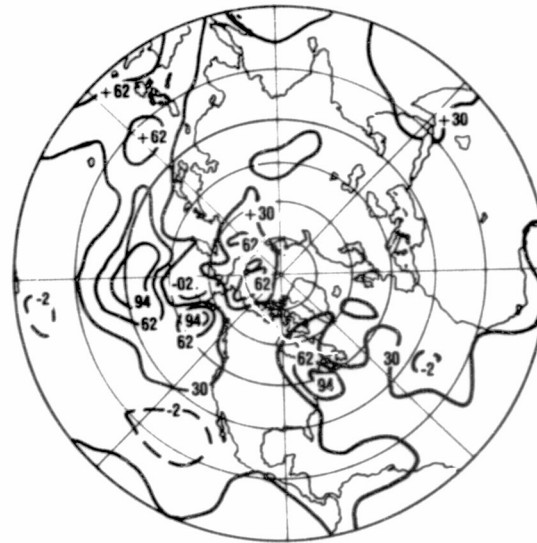
#### 5.3.1 INITIAL STATE DIFFERENCES (M. Halem)

Figures 16a and 16b show the 500-mb geopotential height difference fields for two analysis cycles, one including all the soundings from both satellites (called SAT) and the other withholding all satellite soundings (called NO SAT). The charts

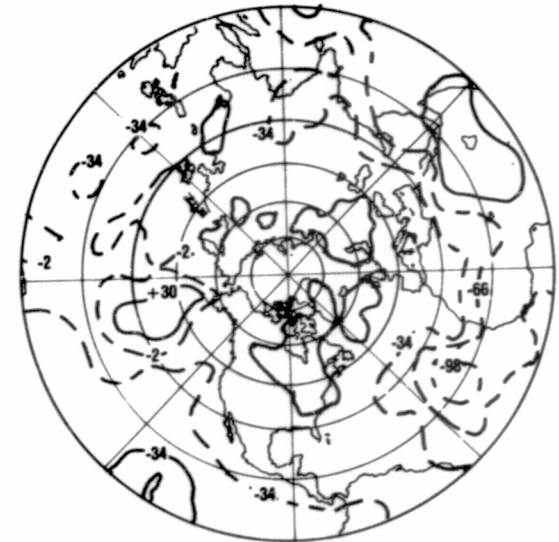
# GEOPOTENTIAL HEIGHT DIFFERENCE - 500 MB 2 SAT



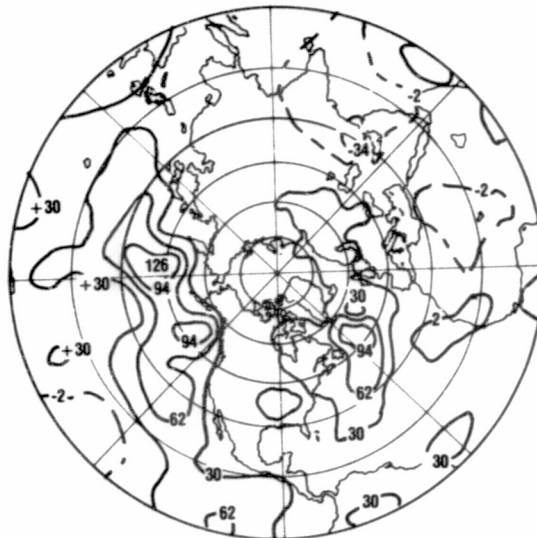
FEB 1



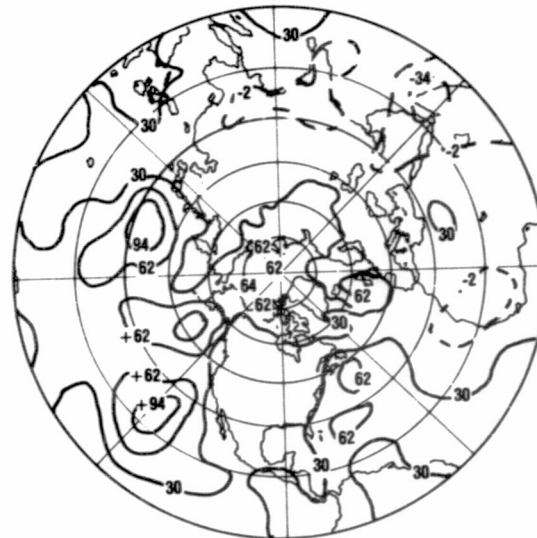
FEB 3



FEB 5



FEB 7



FEB 9



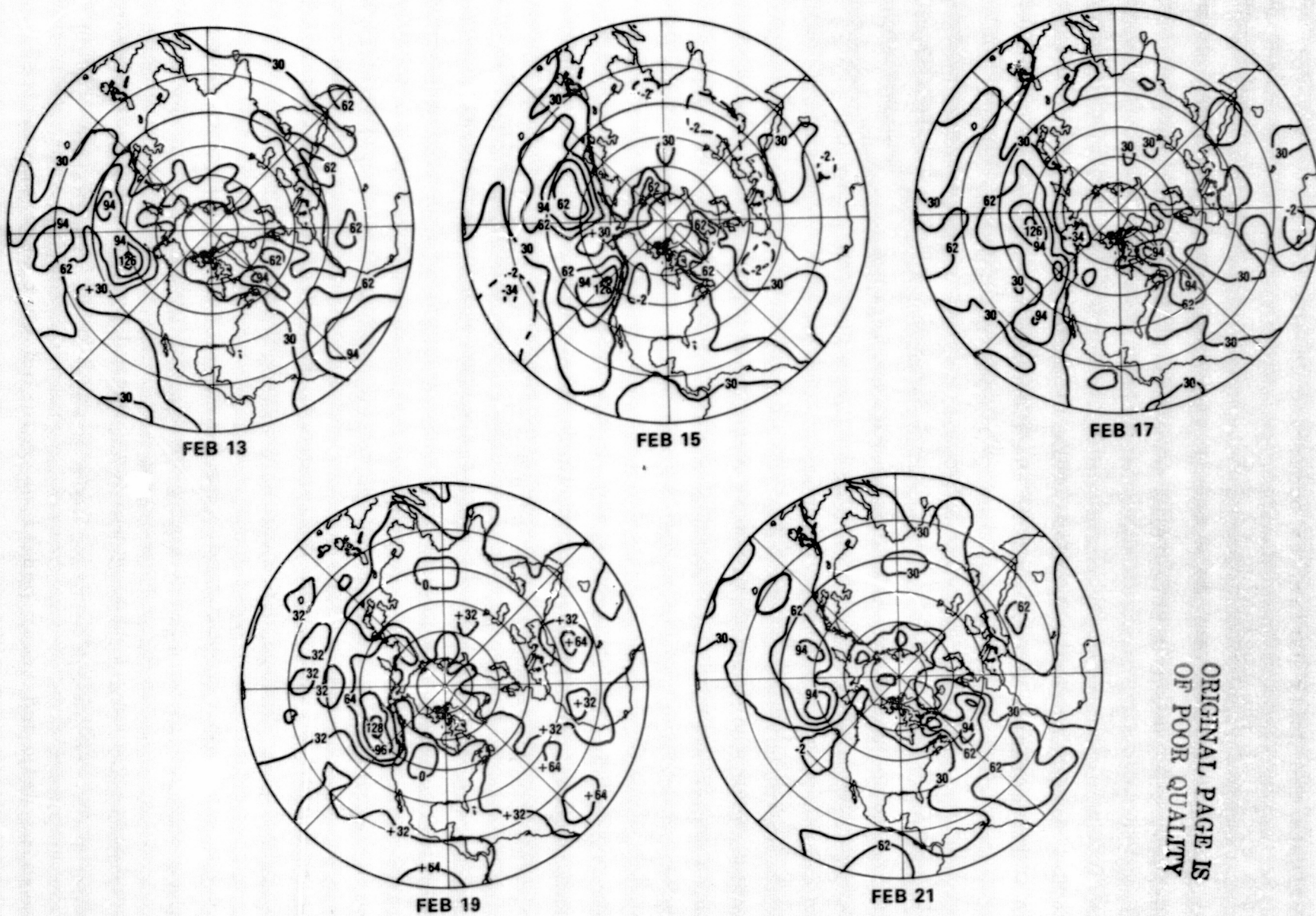
FEB 11

Fig. 16a

5-22

ORIGINAL PAGE IS  
OF POOR QUALITY

GEOPOTENTIAL HEIGHT DIFFERENCE - 500 MB  
2 SAT



ORIGINAL PAGE IS  
OF POOR QUALITY

Fig. 16-b

indicate the daily variations occurring in the initial states of each cycle at the beginning of each forecast period. The magnitudes of the differences vary as a result of variations in coverage, data quality, instrument difficulties encountered in processing the sounding data or just natural atmospheric variability. It is clear from the charts, that day after day, differences of the order of 30 - 120 meters are produced in the data-sparse regions of both the Pacific and Atlantic Oceans. Geopotential height differences of this magnitude correspond to 1.5° to 5°C temperature differences in the 1000- to 500-mb thickness. The variations are of both signs, although there seems to be a systematic tendency for warmer temperatures in the SAT system over most of this assimilation test. When the satellite tracks were superimposed, it was noticed that the largest differences occurred mainly in the data-sparse areas along the tracks where sounding data have recently been inserted. It was also observed that where the initial state differences are small (i.e., no differences of large areal extent at midlatitudes in the Pacific greater than 60 meters) the forecast impact in terms of statistical skill scores and rms scores is generally smaller as one might expect.

Upon closer examination of factors that might lead to weaker or stronger initial state differences, it was discovered that a lack of data coverage is sometimes responsible for certain cases where weak impacts occurred. For example, February 13 showed a weak impact and in fact 3 hours of data or nearly two orbits of sounding retrievals that would have passed over the Gulf of Alaska just prior to synoptic times were missing. An examination of all missing data and their positions revealed that several critical

gaps in coverage had a significant influence on the outcome of this test. In the case of February 13, when data were recovered the magnitude of the initial state impact increased in some regions by as much as 60 meters. As a result, gaps in the data were complete recovered and the DSI data were reprocessed to provide as complete data set as possible for conducting the impact test.

An additional factor influencing the magnitude of initial state differences resulting from the insertion of sounding data is the dependence of the analysis cycle on the method of assimilation. Studies show that the "optimal statistical weighting" approach suggested by N. Phillips, spreads the information over larger areas than other methods tested (e.g., local successive correction techniques) and through statistical corrections leads to better and more consistent impact results. The particular approach used by GISS takes advantage of the quantity of data available at each time interval using the statistical weights to improve the quality of the data.

From the nature of the initial state differences above, one cannot say, a priori, whether the satellite system would produce beneficial forecasts, but only that the magnitude of these differences are sufficiently large so that one would expect them to produce a significant number of distinct forecasts.

C-~~11~~5

### 5.3.2 ISENTROPIC CROSS SECTION ANALYSES

An evaluation of isentropic cross sections produced with and without the inclusion of satellite soundings was conducted in order to determine if systematic differences between the two analyses exist. In previous reports concerning the evaluation of satellite data at NMC, Tracton had stated: "the thermal structure of weather systems is systematically less in the analyses which incorporate satellite soundings than in those from which satellite data is excluded." In addition he presented an example of isentropic cross sections produced with and without satellite soundings to illustrate the systematic smoothing of intense gradients of potential temperature, which resulted from the inclusion of satellite data, at NMC.

The evaluation of isentropic cross section at GISS consisted of a subjective comparison of cross sections produced with and without satellite soundings, and an objective comparison of moderate to intense horizontal potential temperature gradients between the two fields. Isentropic cross sections were constructed for the GISS ( $4^{\circ}$ lat by  $5^{\circ}$ long) grid, along specific longitudes in the data sparse regions of the North Pacific, and also over the United States and Canada where radiosonde data is available. It should be noted that although the use of the GISS grid is adequate for determining the effect of satellite data on the initial states, it does not allow



for a direct comparison with the NMC cross sections analysis which were constructed from the raw data itself on a finer resolution.

Isentropic cross sections were evaluated for each of the eleven initial states which were described in Section 5.3.1. The subjective comparison of cross sections revealed that only very minor differences between the SAT and NO SAT analyses existed over the United States while larger and more significant differences were evident over the North Pacific. Several cases of weaker and stronger gradients of potential temperature in the SAT analysis occurred, and no systematic smoothing out of these gradients was observed. Figures 17a and 17b depict typical NO SAT and SAT cross sections over the United States. It is obvious that no significant differences between the two cross sections exist and that the inclusion of satellite data has not resulted in a degradation of the analysis. Figures 18a and 18b depict an example of NO SAT and SAT cross sections over the North Pacific. In this case, significant differences between the two cross sections are observed. For example, a more intense gradient of potential temperature in the low to middle troposphere and a more detailed thermal structure in the upper troposphere have resulted from the inclusion of satellite soundings. Although the impacts depicted in Figure 18 occurred near the 200mb and 600mb levels (which correspond to peaks of weighting functions for the microwave sounder), no tendency for impacts to occur at these levels was observed. The satellite soundings thus appear to be capable of resolving thermal structures over the ocean which are not otherwise observable.

The objective evaluation of isentropic cross sections consisted of a comparison of all moderate to intense horizontal gradients

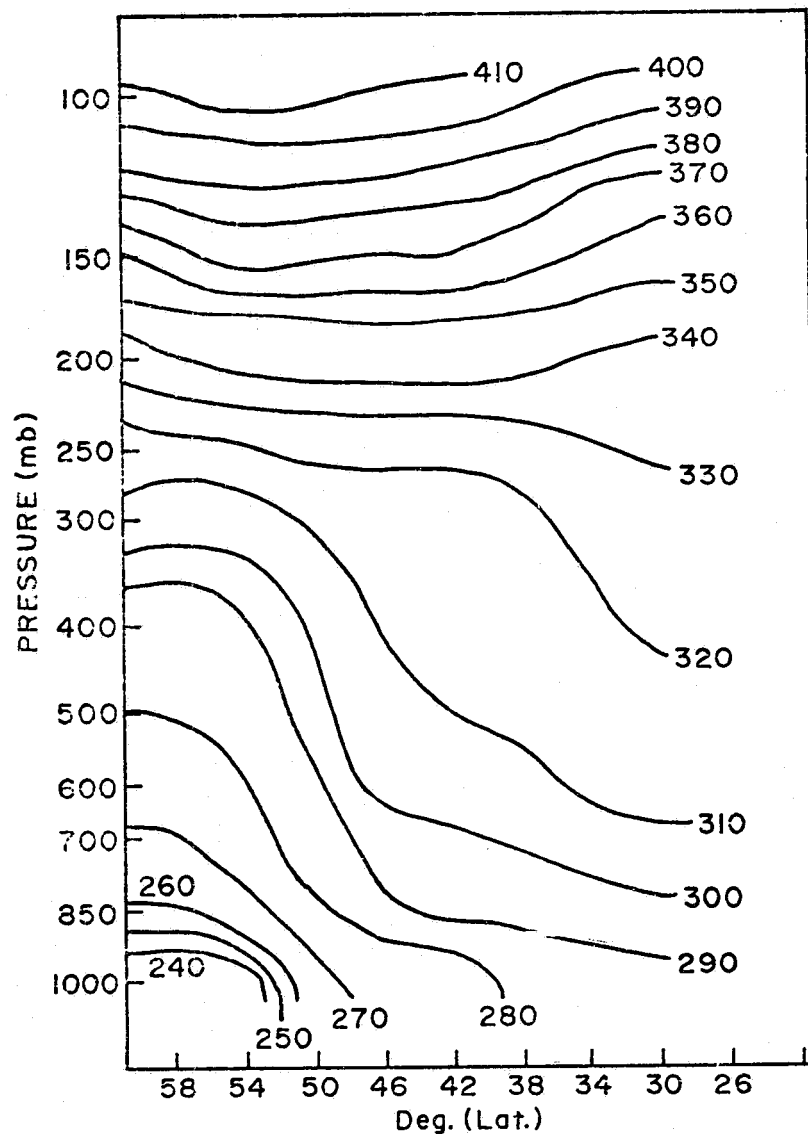


Figure 17a.

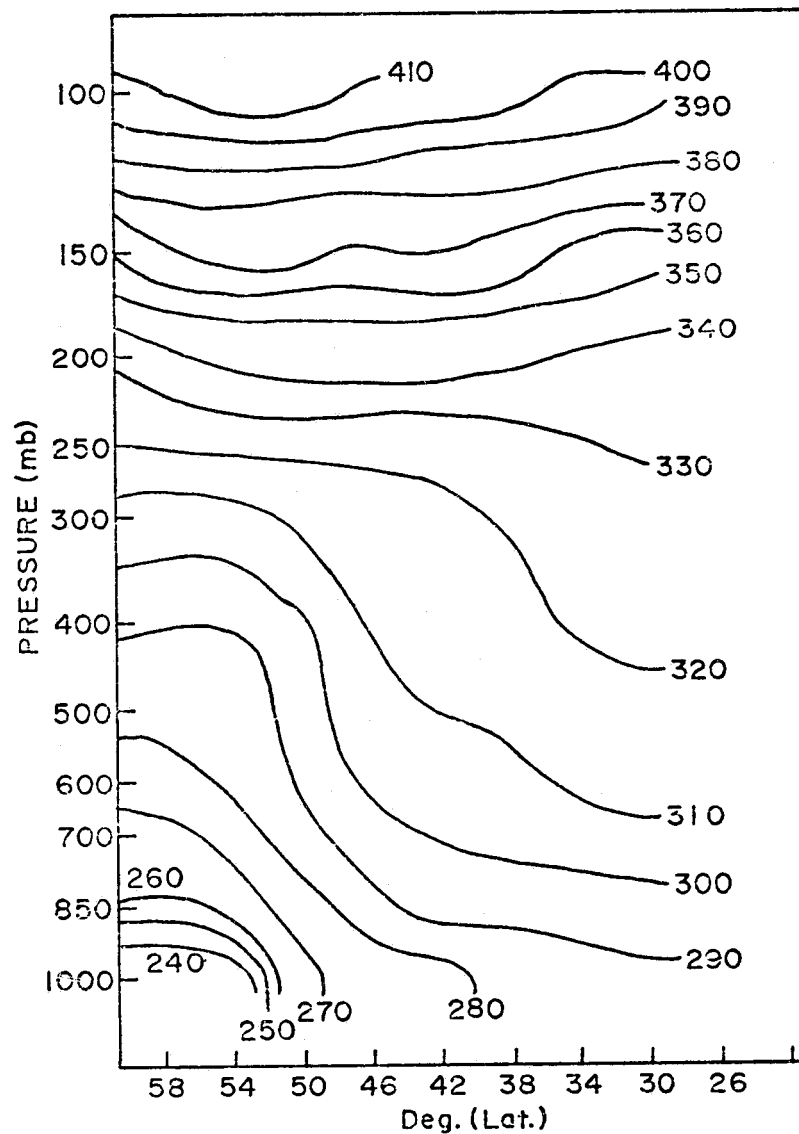


Figure 17b.

Figure 17. NO SAT (a) and SAT (b) Isentropic Cross Section,  
Along Longitude 85°W, for 00Z February 13.

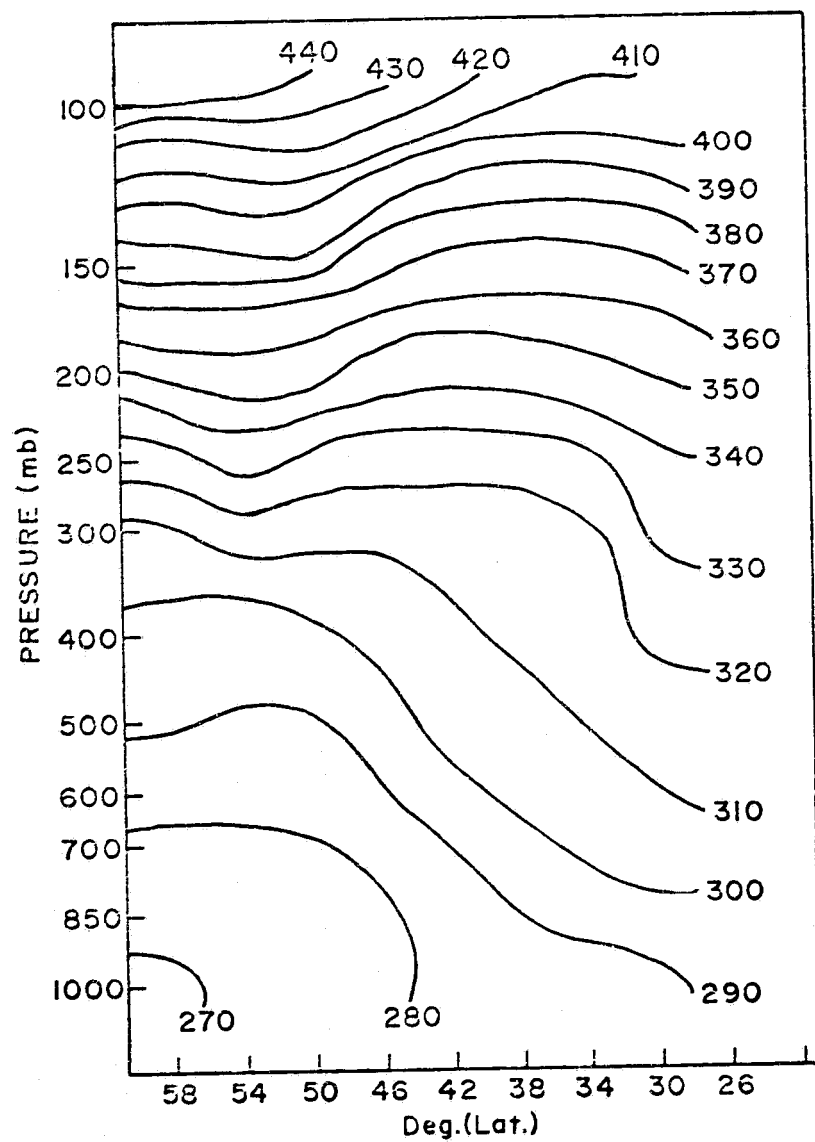


Figure 18a.

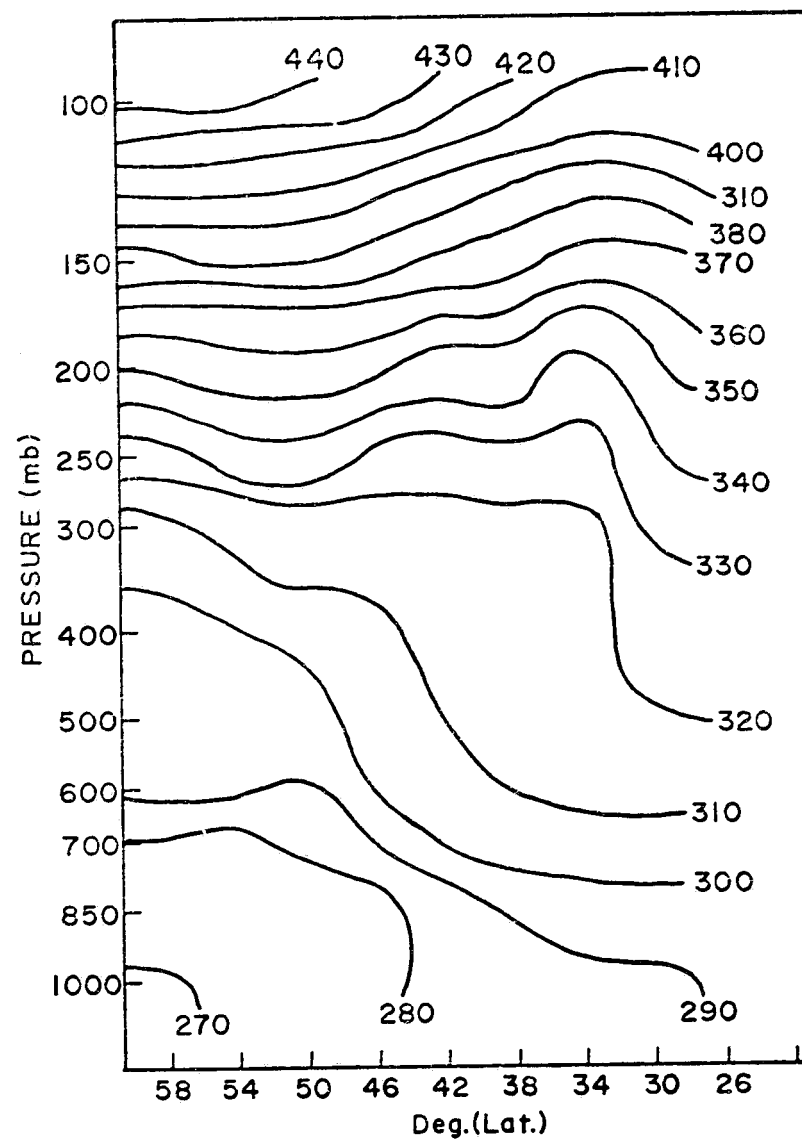


Figure 18b.

Figure 18. NO SAT (a) and SAT (b) Isentropic Cross Sections, Along Longitude 170°W for 00Z February 1e.

of potential temperature at all mandatory isobaric surfaces. Wherever a horizontal gradient of greater than  $8^{\circ}\text{K}$  between 2 gridpoints occurred in either the SAT or NO SAT systems, the gradients of each system were compared to determine if the SAT gradient was weaker, more intense, or approximately the same as the NOSAT gradient. Over the United States, 119 cases were compared. Of these the SAT gradients were weaker 27 percent of the time, more intense 8 percent of the time, and unchanged 65 percent of the time. Over the North Pacific 406 cases were compared. Of these the SAT gradients were weaker 40 percent of the time, more intense 24 percent of the time, and unchanged 36 percent of the time.

An objective comparison of potential temperature gradients along specific latitudes has also been conducted. Over the United States 174 cases of moderate to intense horizontal gradients of potential temperature were compared. Of these the SAT gradients were weaker 18% of the time, more intense 20% of the time, and unchanged 62% of the time. Over the North Pacific 482 cases were compared. Of these the SAT gradients were weaker 40% of the time, more intense 29% of the time and unchanged 31% of the time. In general a tendency toward warmer temperatures was observed in the SAT analysis but no systematic smoothing of potential temperature gradients was evident.

### 5.3.3 THE ENERGY SPECTRUM OF THE SATELLITE AND NO-SATELLITE ANALYSES (W. J. Quirk)

The energetics of the satellite and no satellite analyses produced by NMC have been analyzed by Steven Tracton of NMC and discussed in several widely circulated memos. Tracton has evaluated the eddy available potential energy of the analyses. The eddy available potential energy depends on two quantities, the departure of the temperatures at a given latitude  $[T - \bar{T}]$  and the departure of the vertical temperature gradient from an isentropic profile (See Peixoto, Jose P. and Abraham H. Oort, 1974. The annual distribution of atmospheric energy on a planetary scale, J. Geophys. Res., 79, 2149.)

Figure I is a graph produced by Tracton showing the day to day variation in eddy available potential energy above 30° latitude for a few days during DST 5. Tracton has pointed out that the satellite system has 10% less energy than the no satellite system. He has stated that this difference means that the satellite system must be making a systematic error that underestimates eddy energy which the no-satellite system calculates correctly. In fact only a very detailed study could determine whether it is the satellite or no satellite system which is correct.

To further verify and study Tracton's findings we have calculated the eddy available potential energy (north of the equator) for both the GISS SAT and NO SAT DIM assimilation, and for the NMC satellite analyses interpolated to the GISS grid (See Figure II). Note that our

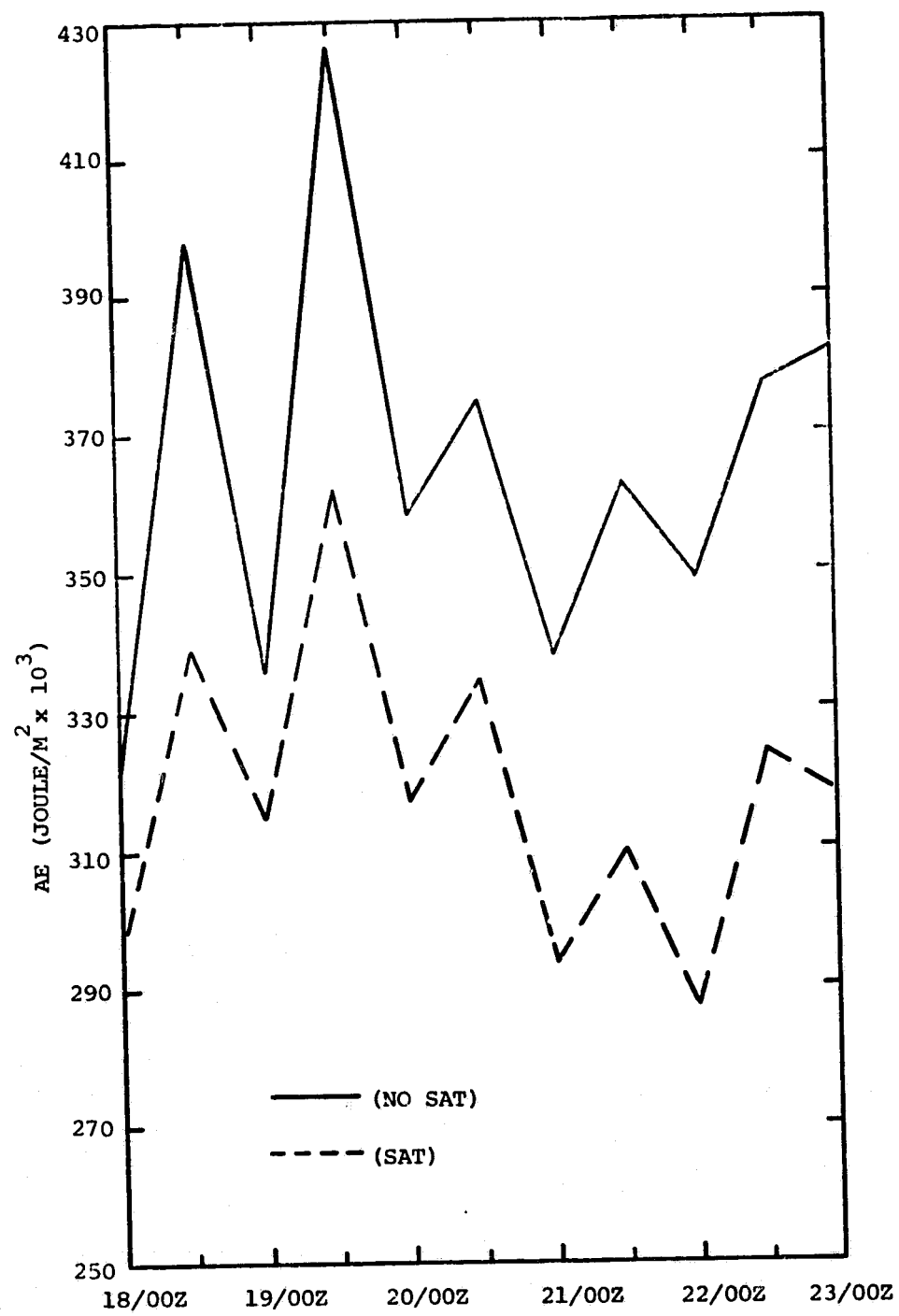
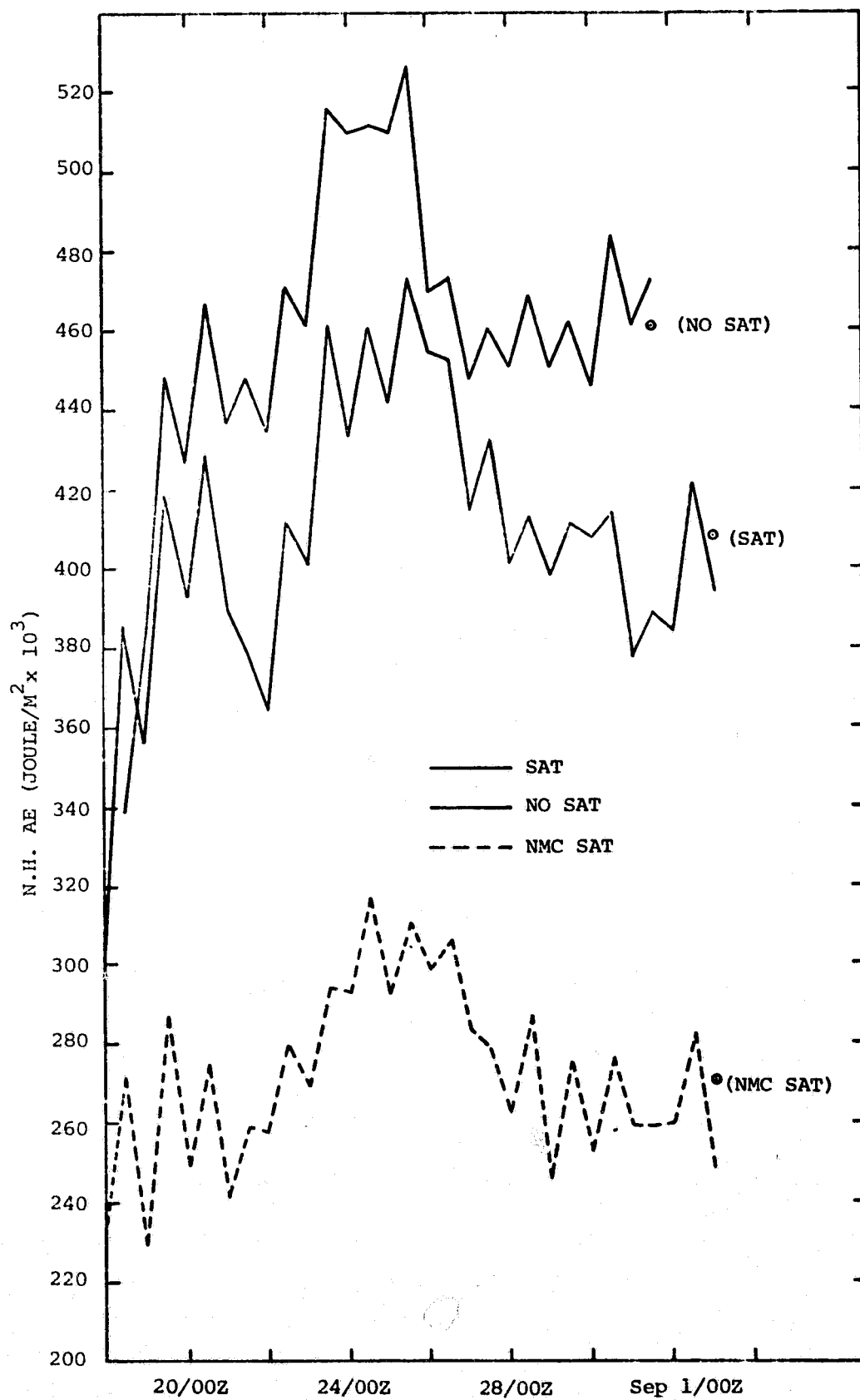


Figure I.



Aug, 1976

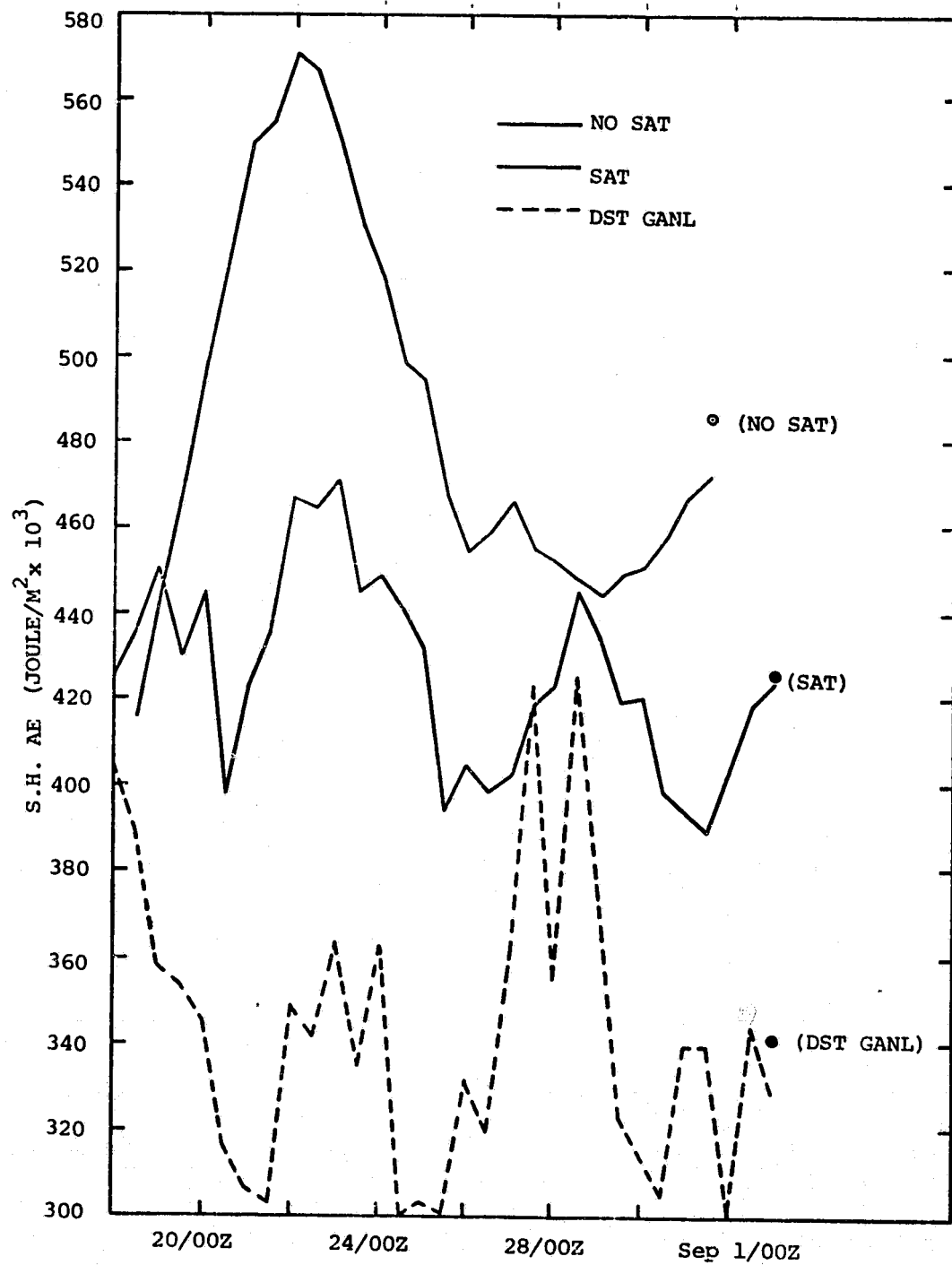
Figure II

calculation of the NMC eddy energy is lower than Tracton's calculation shown in Figure I. This is because almost all of the eddy energy is north of 20°N, but it was averaged over the whole hemisphere whereas Tracton averaged only above 20°N. Figure III shows the same quantities for DST 5, but for the Southern Hemisphere. Figures IV and V show the Northern and Southern Hemisphere quantities for DST 5 and 6. All 4 cases show that the satellite case has 10%-15% less energy than the no satellite case. However they also show that the GISS satellite analysis has 25%-50% more energy than the NMC satellite analysis.

Table A shows a spectral analysis of the Northern Hemisphere Available Potential Energy during DST 5. The first row gives available potential energy for wave numbers N for N=0 through 15 and the total eddy energy ( $\sum_{N=1}^{30}$ ) for the GISS NO SAT case. The second line gives the same quantities for the SAT case. The difference between the NO SAT and SAT cases are given on the next line. The fourth line gives a running sum of the sum from 1 to N of the difference between SAT and NO SAT.

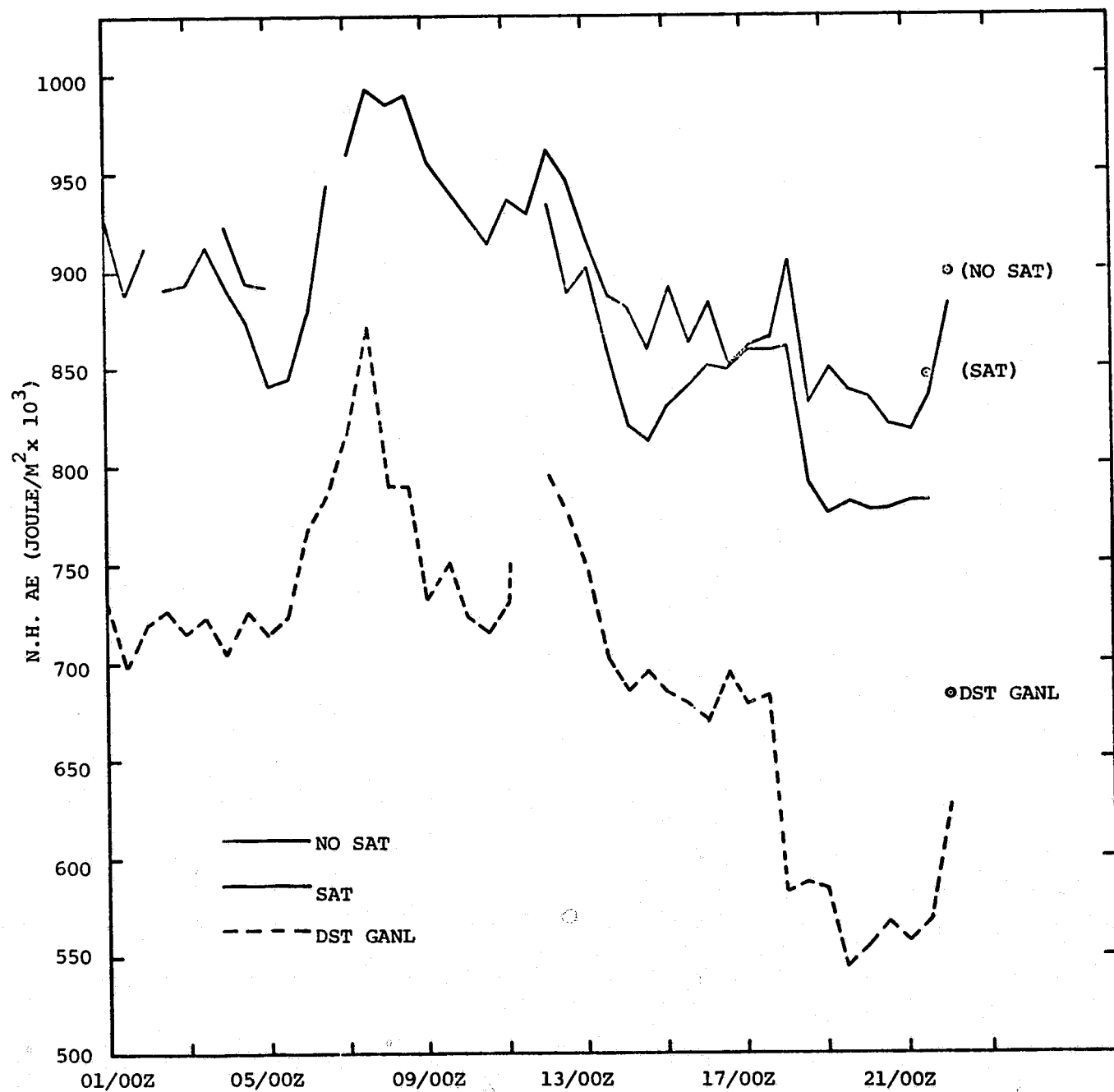
The running sums show that virtually all the differences between wave SAT and NO SAT are in wave numbers 1, 2, and 3. These differences were to have been expected from examination of SAT and NO SAT height fields difference maps. The difference between SAT and NO SAT height fields is primarily in definition of the Aleutian and North Pacific regions, areas where there is little conventional data. Comparisons between the GISS and NMC SAT cases show the NMC analysis is relatively low in eddy energy compared to GISS analysis at all wave numbers. Examination of plots (see Figure VI) of both analyses, reveals that the NMC analysis scheme has systematically smoother fields than the GISS analysis. Comparison of both of these maps with hand





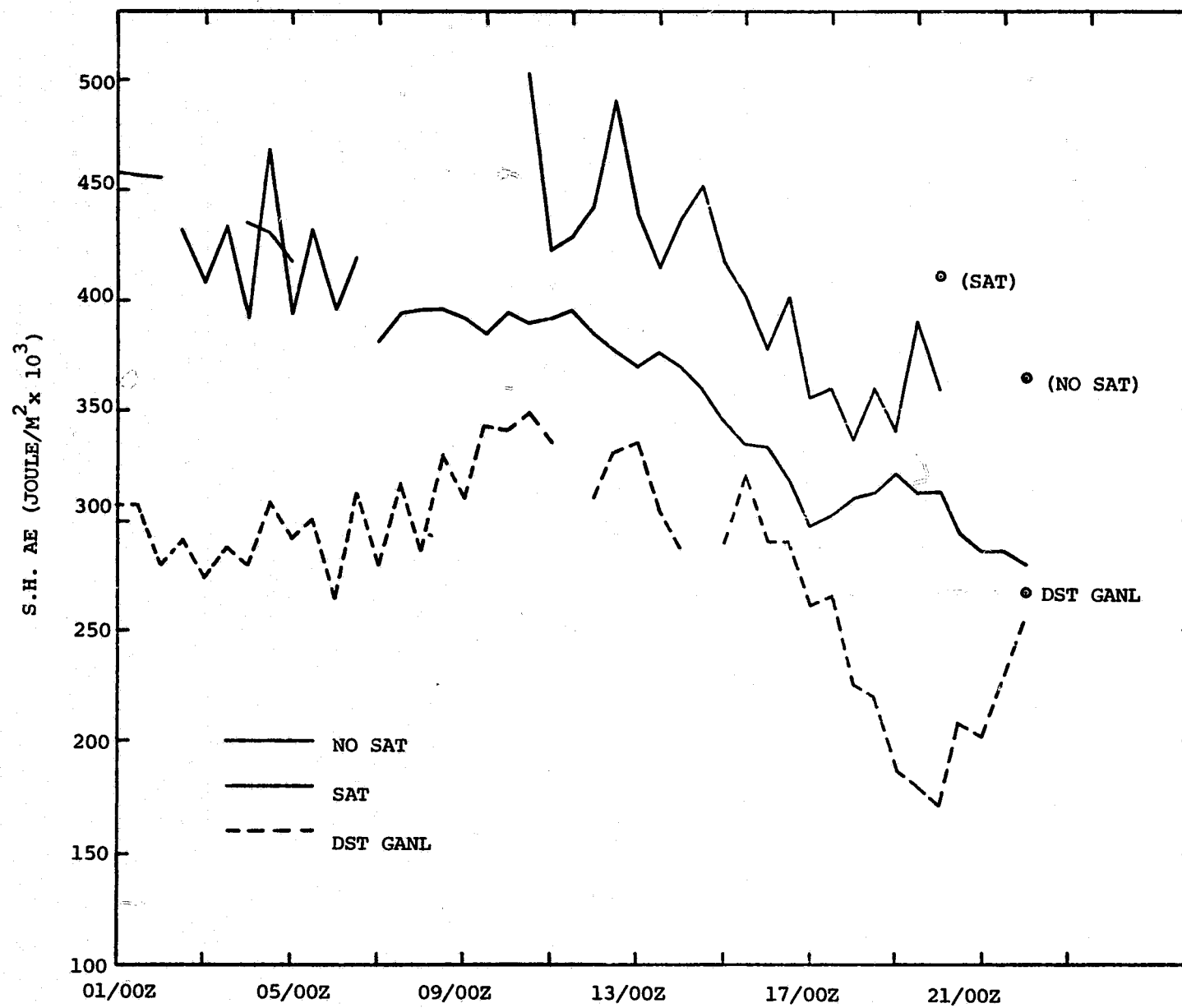
Aug, 1976

Figure III.



Feb., 1976

Figure IV.



Feb., 1976

Figure V.

Table A. Eddy Available Potential Energy

Wave Number N	0	1	2	3	4	5	6	7	8	9	10	11	12	13	14	15	$\sum_{1}^{30}$
GISS NO SAT	15.47	1.28	0.60	0.42	0.25	0.23	0.34	0.20	0.17	0.10	0.07	0.06	0.05	0.05	0.05	0.04	4.34
GISS SAT	15.60	1.09	0.54	0.36	0.24	0.23	0.34	0.22	0.16	0.10	0.07	0.06	0.05	0.05	0.05	0.04	3.99
GISS NO SAT - SAT	-0.13	0.19	0.06	0.06	0.01	0.00	0.00	-0.02	0.01	0.00	0.00	0.00	0.00	0.00	0.00	0.00	0.35
N $\sum_{1}^{N}$ GISS (NO SAT-SAT)		0.19	0.25	0.31	0.32	0.32	0.32	0.30	0.31	0.31	0.31	0.31	0.31	0.31	0.31	0.31	
NMC SAT	15.38	0.73	0.41	0.30	0.20	0.18	0.28	0.16	0.12	0.07	0.04	0.04	0.03	0.02	0.02	0.02	2.72
GISS NMC SAT - SAT	0.23	0.36	0.13	0.06	0.04	0.05	0.06	0.06	0.04	0.03	0.03	0.02	0.02	0.03	0.03	0.02	1.27
N $\sum_{1}^{N}$ (GISS SAT - NMC SAT)		0.36	0.49	0.55	0.59	0.64	0.70	0.76	0.80	0.83	0.86	0.88	0.90	0.93	0.96	0.98	

# Geopotential Height Surface

ORIGINAL PAGE IS  
OF POOR QUALITY

500 mb

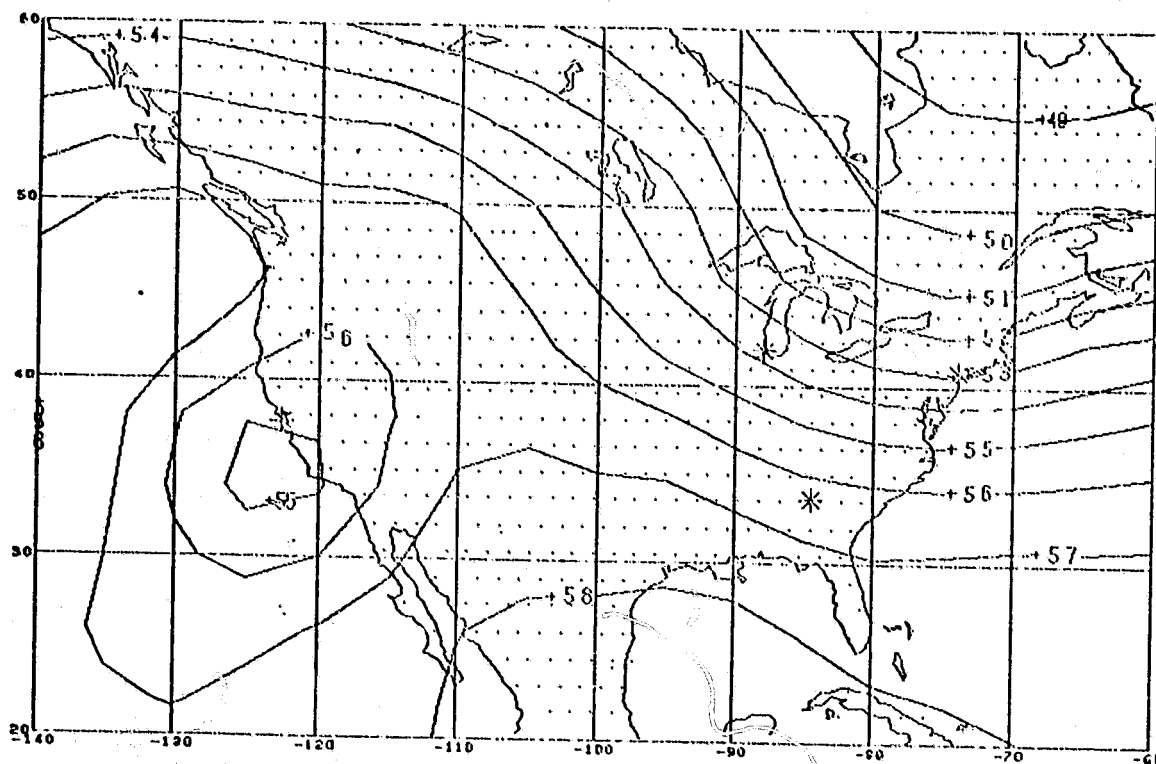


Figure VI-a. NMC Initial Conditions

# Geopotential Height Surface

500 mb

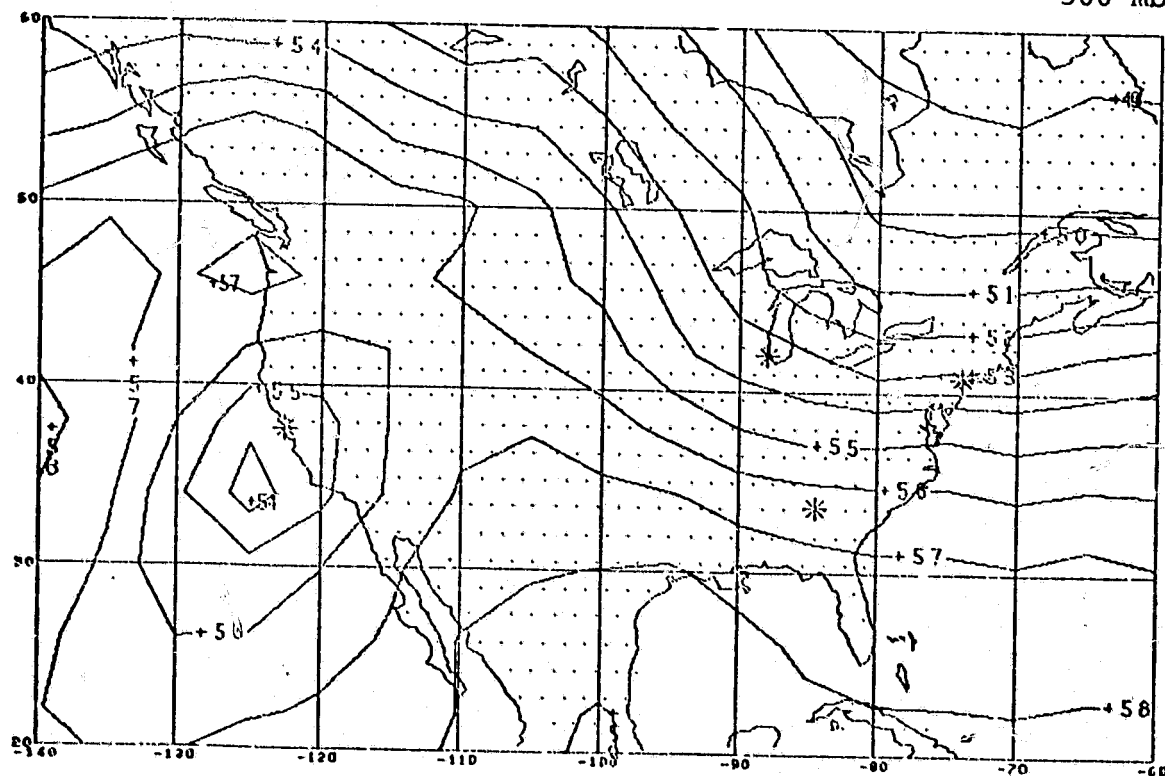


Figure VI-b. GISS Initial Conditions

drawn maps of station reports reveal the NMC maps to be systematically too smooth.

In conclusion it can be stated that the 10%-15% difference in eddy available potential energy between SAT and NO SAT analyses is primarily due to the differences in the Aleutian and North Pacific regions. To determine which analysis is correct a detailed study of these areas would be necessary. On the other hand the GISS and NMC analyses differ by 25% to 50%; and there are differences all over the globe. The NMC analysis scheme seems to significantly underestimate the energy in the atmosphere. This could be a significant source of error in NMC forecasts, if as Tracton and McPherson speculate (NMC office note 136), underestimation of the variance in the thermal structure of the atmosphere will act to the detriment of the analyses.

## 5.4 IMPACT OF SATELLITE DATA ON PROGNOSTIC FLOW PATTERNS

### 5.4.1 STATISTICAL COMPARISONS (M. Halem)

Two statistical measures commonly employed to estimate the accuracy of forecasts are S1 skill scores and rms differences in 500mb heights and sea-level pressures. In the GISS experiments, the SAT and NO SAT forecasts made from the GISS analysis and forecasts cycle were validated against NMC's analysis over North America. Table 3 shows the average impact for 11 separate forecasts spaced 2 days apart starting on February 1, for 48- and 72-hour sea-level pressure and 500mb heights, in terms of S1 scores and rms scores. The average impact in S1 scores is found to be about 5 percent in 48 hours and 7 percent in 72 hours for both quantities. RMS scores produce larger

Table 3. Average Statistical Impact Over North America (11 Cases),  
February 1 to February 21, 1976.

	<u>48 Hour</u>	<u>72 Hour</u>
Sea-Level Pressure	3.28 $\pm$ 1.9 (5%)	4.7 $\pm$ 2.3 (6%)
	.97 $\pm$ .3 (12%)	1.06 $\pm$ .7 (11%)
500-mb Heights	1.91 $\pm$ 1.1 (5%)	3.43 $\pm$ 1.3 (7%)
	5.1 $\pm$ 3.1 (7%)	10.74 $\pm$ 6 (11%)

Key

Skill score  $\pm$  Std. Err. (% impact)  
RMS Error  $\pm$  Std. Err. (% impact)

impacts on the order of 10 percent or more, respectively, for the same fields. The statistical error bounds indicate that the average impact is significant, being larger than twice the variance ( $\sigma$ ) for both the rms and skill score errors. Similar results with somewhat larger impacts occurred over Europe. Consideration of the results over Europe as an independent test region, the significance of the impact of these magnitudes would have a confidence probability of 99 percent.

Although similar positive impacts were obtained in the summer DST-5 experiments, the question still arises whether or not the impact is a fluke or the result of real information content stemming from satellite data. It is conceivable that these results are statistical fluctuations produced by the four-dimensional assimilation and balancing cycle. In order to test such a conjecture another experiment was set up in which the satellite data was replaced by "fabricated" satellite data and maintained all other assimilation processes identical to the experiment described above. The "fabricated" data were generated from the 12-hour forecasts based on the NO SAT system. The forecasts were used to interpolate to the positions of the satellite soundings and provide a temperature profile at all mandatory pressure levels corresponding to each satellite sounding that was available operationally during the test. The statistical bias, rms errors, and correlations were calculated for the differences between the original NESS soundings and the co-located radiosondes in a 3-hour window and 110-km region for each 10° latitude belt and every mandatory level. Correlations were also



calculated for the difference between the forecast temperature profiles and the radiosondes. Based on this pair of statistics, a random error and bias was added to the forecast profiles in order to generate "fabricated" sounding data having the identical statistical error structures that were measured for the DST-6 satellite soundings at the same positions. In this way, a new sounding tape was generated so that an outside user receiving this data set could not tell from the statistical properties or yield, whether the soundings were "real" or "fabricated."

These "fabricated" data were then fed into the control experiment and treated just as it was done in the case of the original sounding data. The forecast impacts for each of the 11 forecast periods are compared with the real-SAT system in Table 4. The largest positive impact in any forecast from the control experiment is a four-point S1 score which establishes the random background noise level due to modification of the analysis scheme by satellite data and balancing. The average 500-mb impact at 72 hours for the "fabricated" data is  $-.14$ , while for the satellite data the net impact is  $3.43$ . Similar results are shown in Table 4 for the sea-level pressure impact. Moreover, impacts of eight points or more occurred in the real system on February 3 and February 9, respectively, more than twice as large as anything produced in the control experiment. This experiment further confirms the conclusion that statistical impacts of this magnitude which seem to occur about one day in five are significantly above the random noise level. On other days the satellite soundings probably lie in the general realm of minor statistical fluctuations, although some might yet be significant.

Table 4. Individual Skill Score Impacts Over North America (Winter - 72 Hours)

<u>Date</u>	500 MB Heights		Sea Level Pressure	
	<u>2 SAT Impact</u>	<u>"Fabricated Data" Test</u>	<u>2 SAT Impact</u>	<u>"Fabricated Data" Test</u>
Feb. 1	1.8	-3.5	-4.9	-12.0
3	9.4	3.4	8.4	4.7
5	-2.2	0.8	-0.3	-2.8
7	0.7	-1.1	10.2	0.3
9	7.8	1.2	13.5	1.4
11	5.9	-2.1	16.4	-1.2
13	6.8	1.1	10.5	5.2
15	1.9	-3.3	1.5	-3.7
17	-4.5	-1.8	-5.7	-4.5
19	4.7	3.9	-2.8	5.8
21	5.4	-0.9	5.2	-4.3
	<u>3.43±1.3</u>	<u>-0.20±0.8</u>	<u>4.73±2.3</u>	<u>-1.01±1.6</u>

## 5.4.2 SYNOPTIC COMPARISONS

### 5.4.2.1 FORECAST DIFFERENCES (R. Atlas and W. Johnson)

A synoptic evaluation of the forecasting impact of the satellite-derived sounding data was performed by directly comparing the prognostic charts generated from SAT and NO SAT initial conditions with each other and with the corresponding NMC analyses for verification. Comparisons were made every 12 hours for all of the prognostic fields which were described in Section 5.2.1. However only the sea-level pressure and 500-mb height fields at the end of each 72-hour forecast will be discussed here.

Figures 19 to 40 depict the errors of the SAT and NO SAT sea-level pressure and 500 mb prognostic fields, as well as the differences between the SAT and NO SAT forecasts of these quantities. The error maps, (a) and (b) in Figures 19 to 40, were obtained by subtracting the NO SAT and SAT forecasts respectively from the NMC analysis interpolated to the GISS grid. The difference maps (c) were obtained by subtracting the SAT forecast from the corresponding NO SAT forecast. Moderate to large impacts of the satellite data are evident on most of the difference maps, and are summarized in Table 5.

This table was prepared by first noting the regions of moderate to large differences (8 mb or more at sea level or 96 meters or more at 500 mb) between the SAT and NO SAT prognostic fields, and then comparing the errors of each system in these regions.

From the table, it can be seen that moderate to large forecasting impacts occur in nine of the eleven cases and that 77% of these impacts are beneficial. As a result there is a 38-75% reduction of specific forecasting errors at 500 mb and a 40-100% reduction of specific errors in the sea level pressure forecast. It should be noted that these impacts refer only to the reduction of errors where the SAT and NO SAT prognoses are significantly different. The fact that these errors are reduced or increased (in the case of negative impacts) does not mean that the prognostic patterns have been significantly altered. In order to ascertain the predictive importance of the impact, it is necessary to compare the actual prognostic fields (rather than the difference plots). In the next section two case studies, in which a significant improvement of the 500 mb prognostic field occurred, will be presented.

#### 5.4.2.2 CASE STUDIES

I: 72-hour Forecast from Feb. 9, 00Z

This is a case in which a large positive impact is evident in the statistical scores or in the difference maps. Figure 34c shows that a large difference of 128 meters, between the NO SAT and SAT 500-mb forecasts, has occurred over the north central United States, while a comparison of Figures 34a and 34b reveals that this impact has resulted in a 50% reduction of the NO SAT 500-mb height errors in this region.

Figures 41 and 42 show the 72-hour 500-mb prognostic flow patterns for the NO SAT and SAT forecasts from February 9, respectively, while the corresponding NMC analysis is shown in Figure 43 for

verification. In the surface maps (not shown here) a low-pressure system, accompanied by moderate snowfall, was located in lower Canada at 55°N, 120°W (Alberta). A local forecaster, using the 500-mb contour patterns depicted in Figure 41 to steer the surface low, would forecast this low-pressure system to move southeastward into the central United States plains and would probably predict moderate to heavy snow over this area. If the forecaster used the steering patterns depicted in Figure 42 instead, he would forecast the surface low to move toward the Great Lakes and predict the snowfall to be further north along the border between the United States and Canada. The NMC analysis is in close agreement with the contour orientation of the SAT system and indeed the surface low and its associated snowfall did stay further north. The significant beneficial impact that is evident in this 500-mb contour pattern is also evident in the lower levels of the atmosphere (not shown), and it appears obvious that the inclusion of satellite data can result in decidedly different weather forecasts for large regions.

## II: 72-hour Forecast From Feb. 19, 00Z

This second case is one in which a significant difference in the prognostic pattern occurred even though a large statistical impact did not result. Figure 39c reveals that a large impact of 128 meters at 500 mb has occurred over the southwest United States while smaller differences exist elsewhere. From Figures 39a and 39b, it can be seen that this impact resulted in a 57% reduction of the NO SAT 500-mb height errors in this region.

Figures 44 and 45 depict the 72 hour 500-mb prognostic charts from February 19 for NO SAT and SAT cases respectively. The

corresponding NMC analysis is depicted in Figure 46. A comparison of these three charts reveals that the NO SAT prog is considerably slow in its movement of a trough into the midwest and a ridge off the east coast whereas both of these systems are displaced further east and in better agreement with the analysis in the SAT case.

ORIGINAL PAGE IS  
OF POOR QUALITY

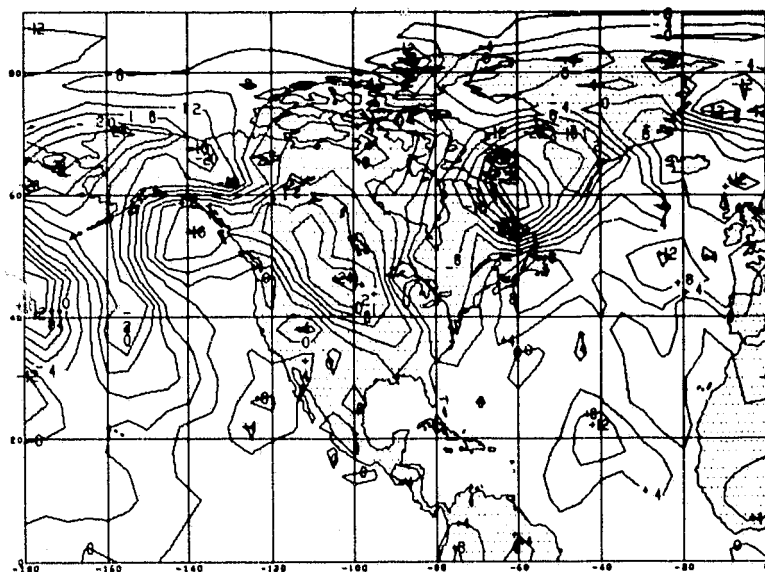


Figure 19a. 72-Hour  
Sea-Level Pressure NO  
SAT Error Map from  
February 1 00Z Initial  
Conditions.

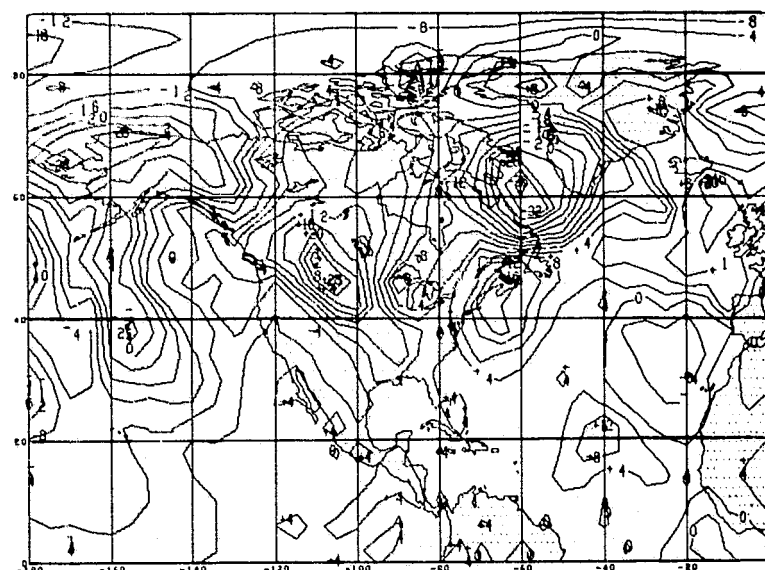


Figure 19b. 72-Hour  
SAT Error Map from  
February 1 00Z Initial  
Conditions.

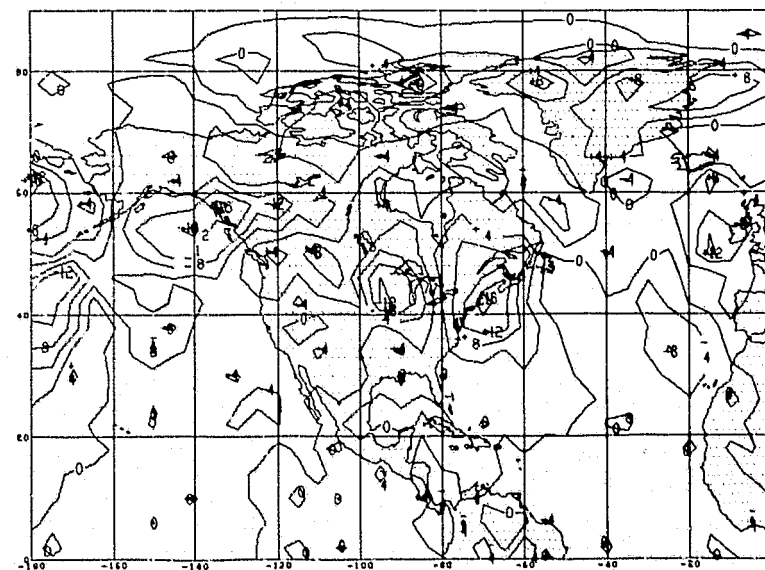


Figure 19c. 72-Hour  
NO SAT-SAT Difference  
Map from February 1 00Z  
Initial Conditions.

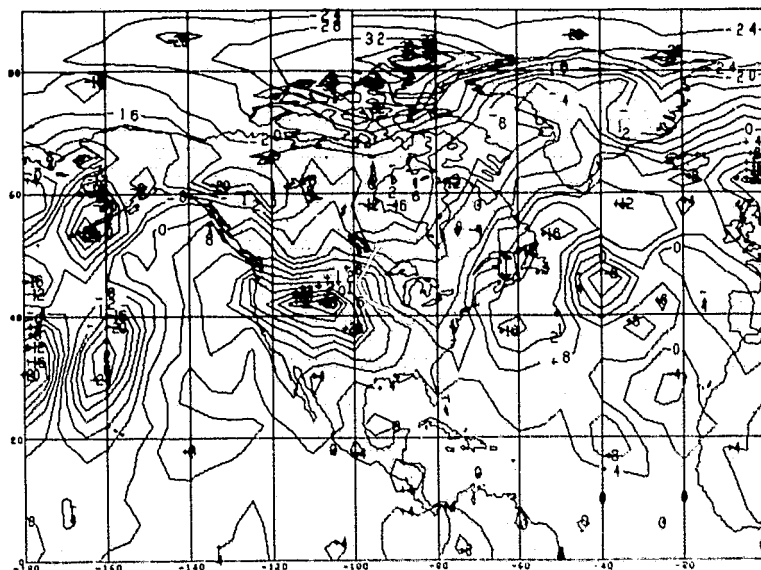


Figure 20a. 72-Hour  
Sea-Level Pressure NO  
SAT Error Map from  
February 3 00Z Initial  
Conditions.

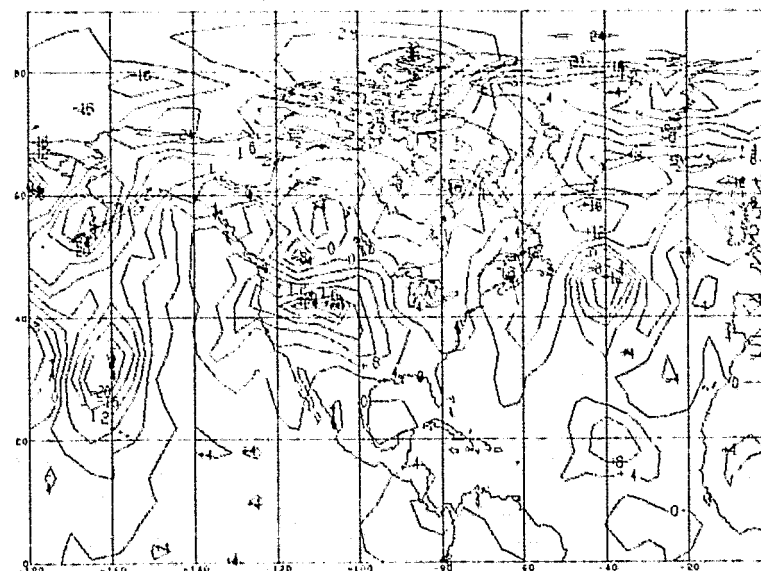


Figure 20b. 72-Hour  
SAT Error Map from  
February 3 00Z Initial  
Conditions.

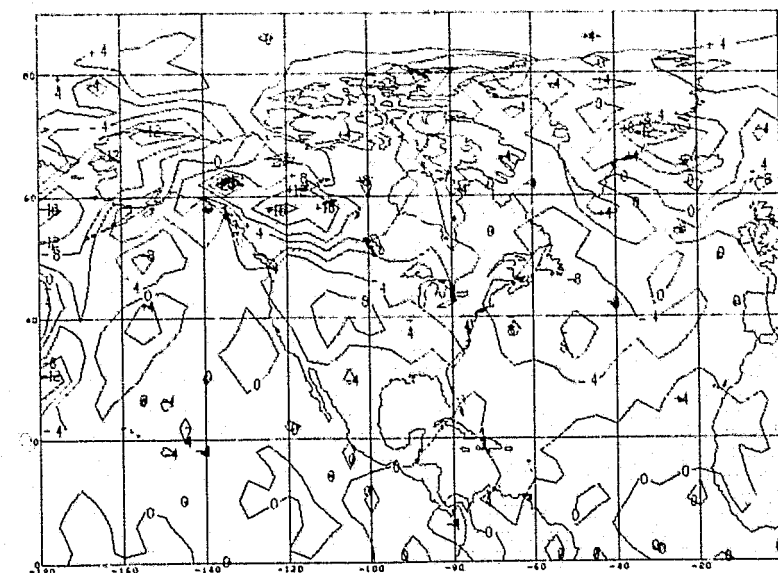


Figure 20c. 72-Hour  
NO SAT-SAT Difference  
Map from February 3 00Z  
Initial Conditions.



ORIGINAL PAGE IS  
POOR QUALITY

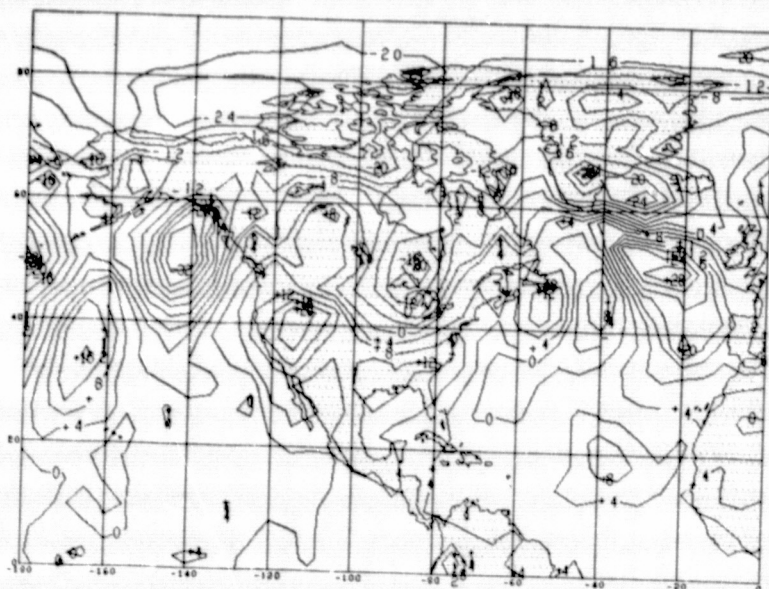


Figure 21a. 72-Hour  
Sea-Level Pressure NO  
SAT Error Map from  
February 5 00Z Initial  
Conditions.

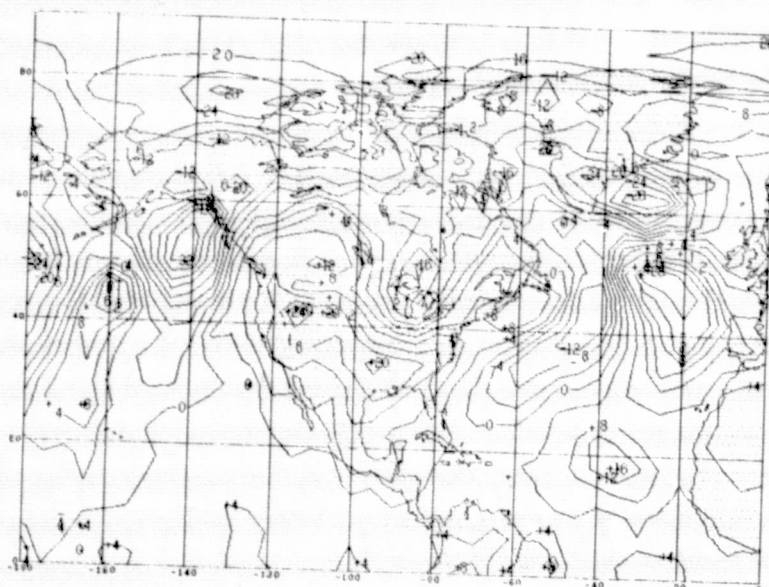


Figure 21b. 72-Hour  
SAT Error Map from  
February 5 00Z Initial  
Conditions.

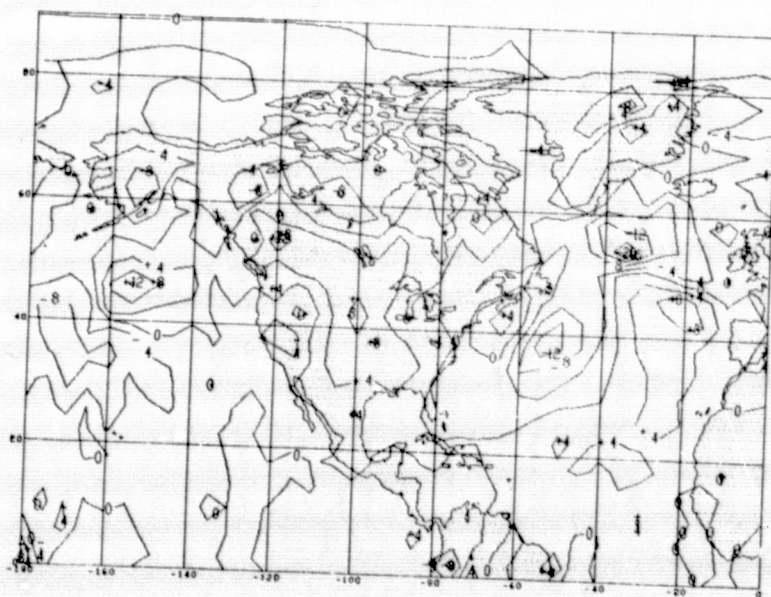


Figure 21c. 72-Hour  
NO SAT-SAT Difference  
Map from February 5 00Z  
Initial Conditions.

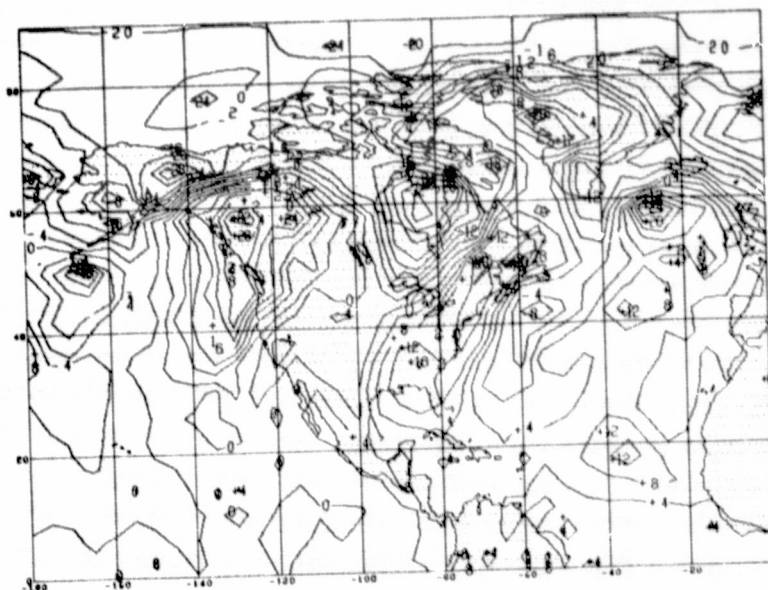


Figure 22a. 72-Hour  
Sea-Level Pressure NO  
SAT Error Map from  
February 7 00Z Initial  
Conditions.

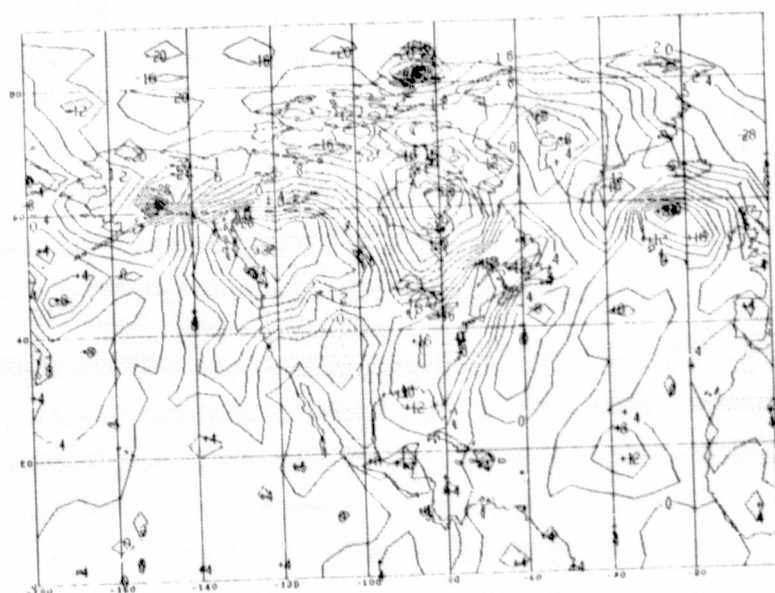


Figure 22b. 72-Hour  
SAT Error Map from  
February 7 00Z Initial  
Condition...

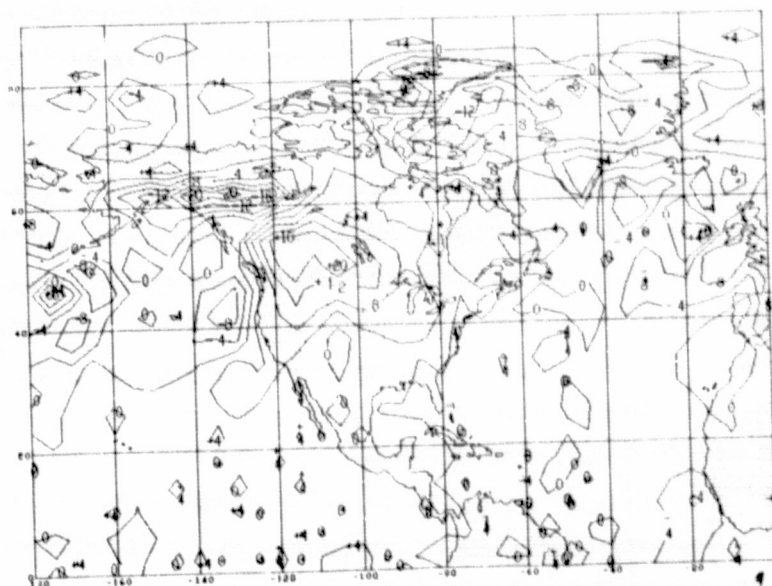


Figure 22c. 72-Hour  
NO SAT-SAT Difference  
Map from February 7 00Z  
Initial Conditions.

ORIGINAL PAGE IS  
OF POOR QUALITY

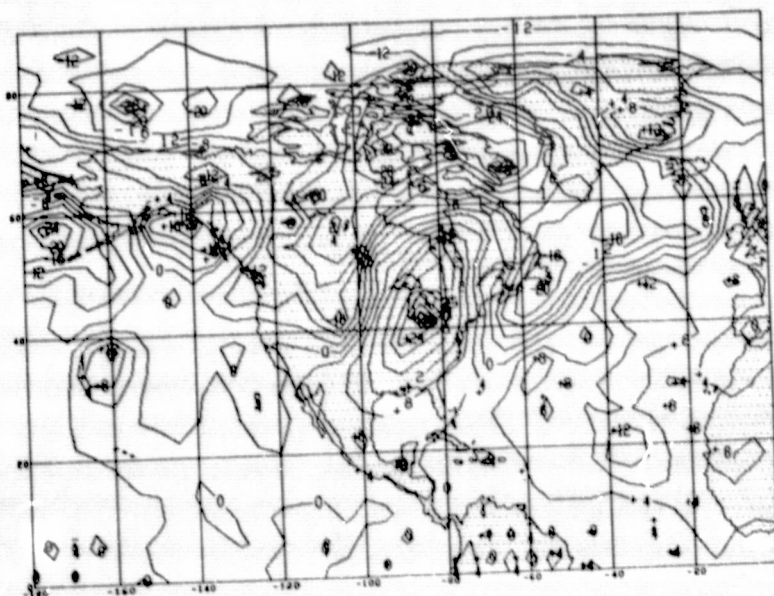


Figure 23a. 72-Hour  
Sea-Level Pressure  
NO SAT Error Map from  
February 9 00Z Initial  
Conditions.

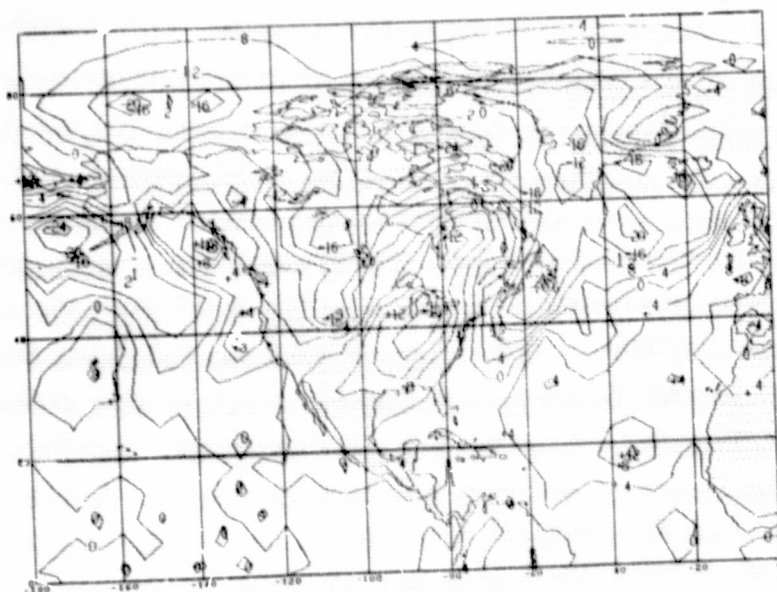


Figure 23b. 72-Hour  
SAT Error Map from  
February 9 00Z Initial  
Conditions.

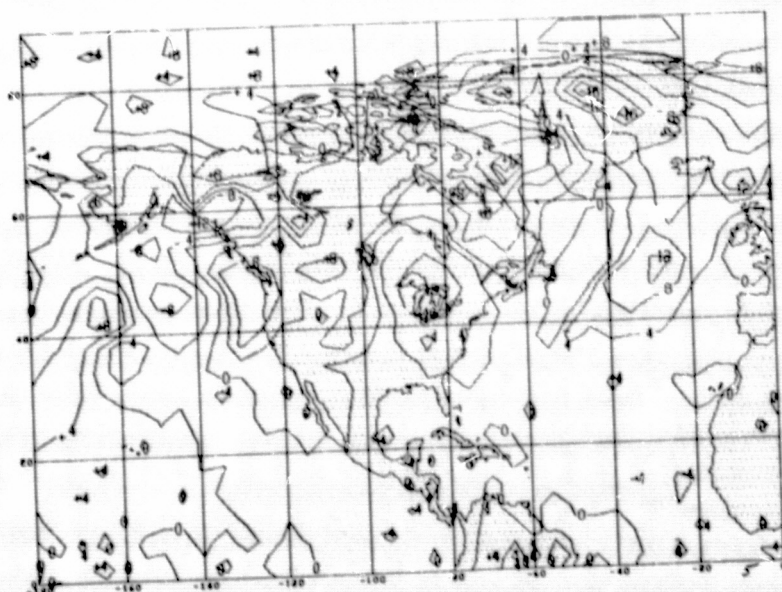


Figure 23c. 72-Hour NO  
SAT-SAT Difference Map  
from February 9 00Z  
Initial Conditions.



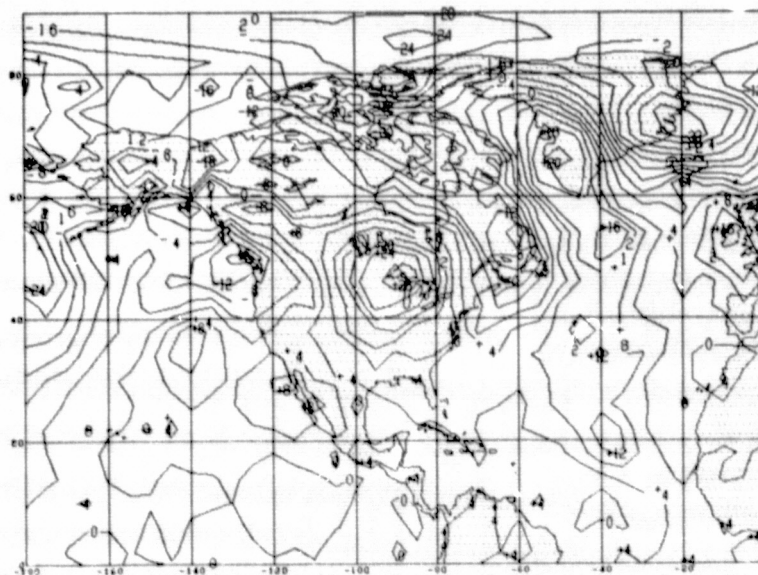


Figure 24a. 72-Hour  
Sea-Level Pressure  
NO SAT Error Map from  
February 11 00Z  
Initial Conditions.

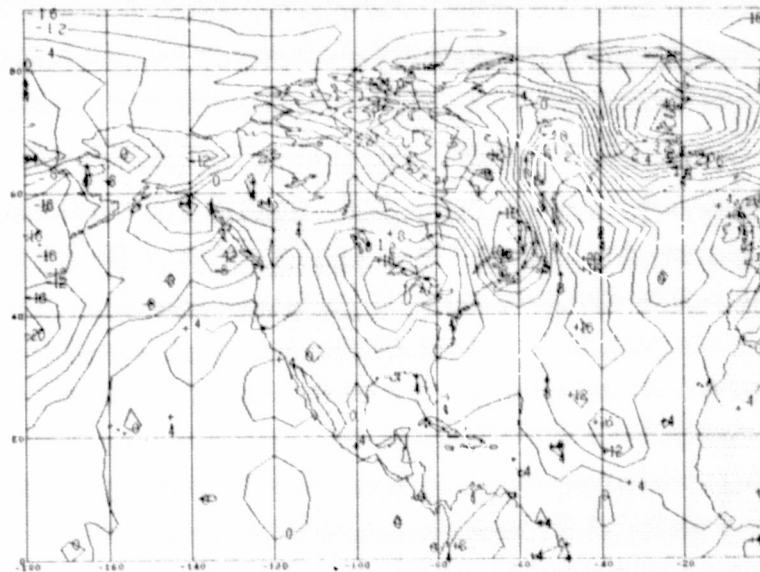


Figure 24b. 72-Hour  
SAT Error Map from  
February 11 00Z  
Initial Conditions.

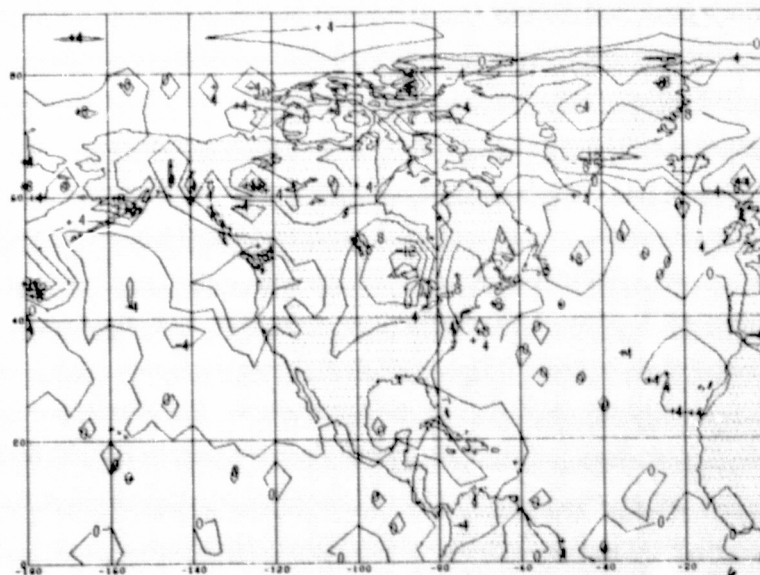


Figure 24c. 72-Hour  
NO SAT-SAT Difference  
Map from February 11  
00Z Initial Conditions

ORIGINAL PAGE IS  
OF POOR QUALITY

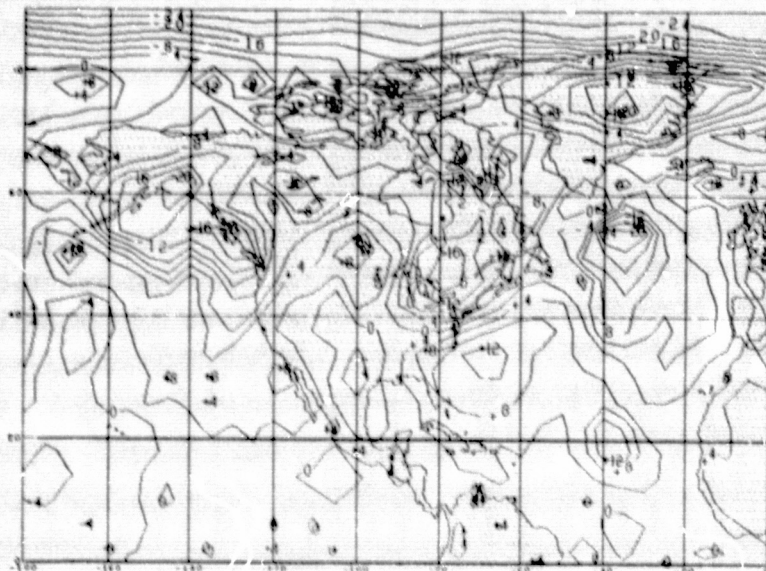


Figure 25a. 72-Hour  
Sea-Level Pressure  
NO SAT Error Map from  
February 13 00Z  
Initial Conditions.

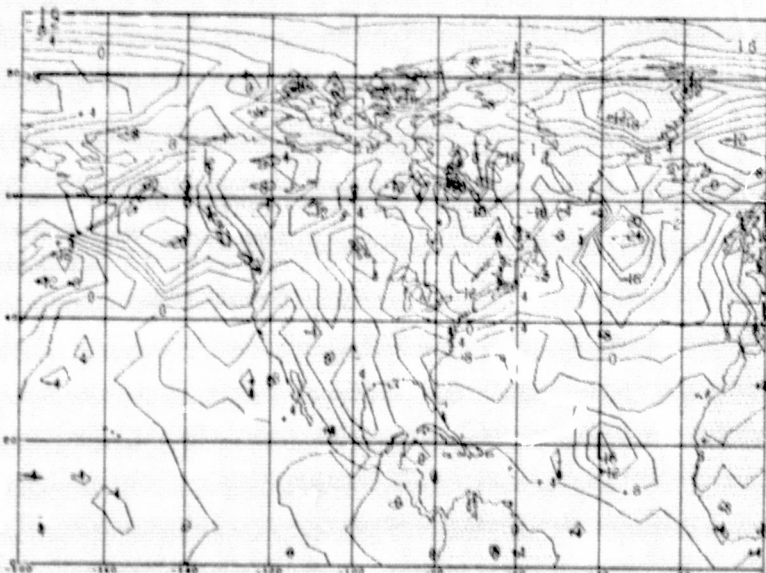


Figure 25b. 72-Hour  
SAT Error Map from  
February 13 00Z  
Initial Conditions.

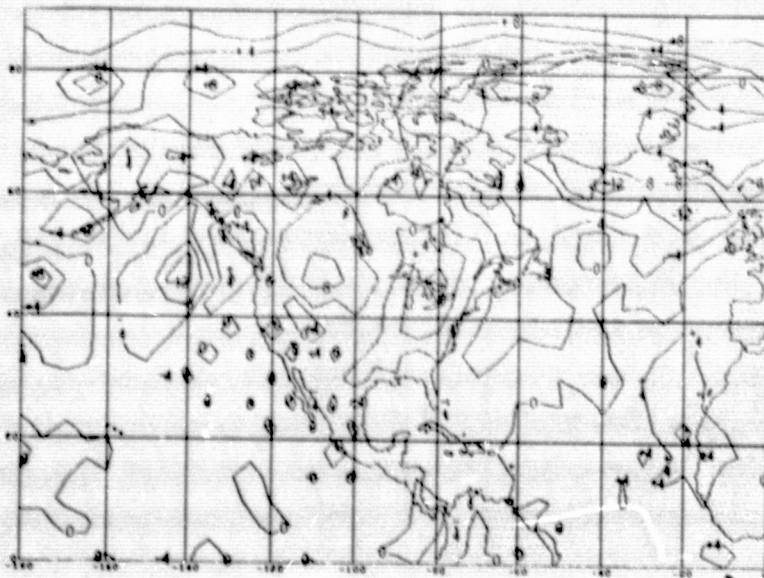


Figure 25c. 72-Hour NO  
SAT-SAT Difference Map  
from February 13 00Z  
Initial Conditions.



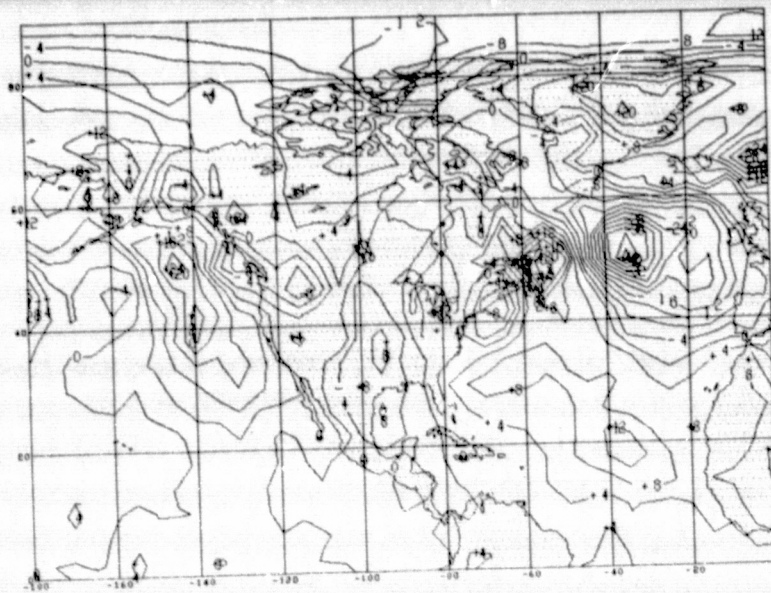


Figure 26a. 72-Hour  
Sea-Level Pressure  
NO SAT Error Map from  
February 15 00Z Initial  
Conditions.

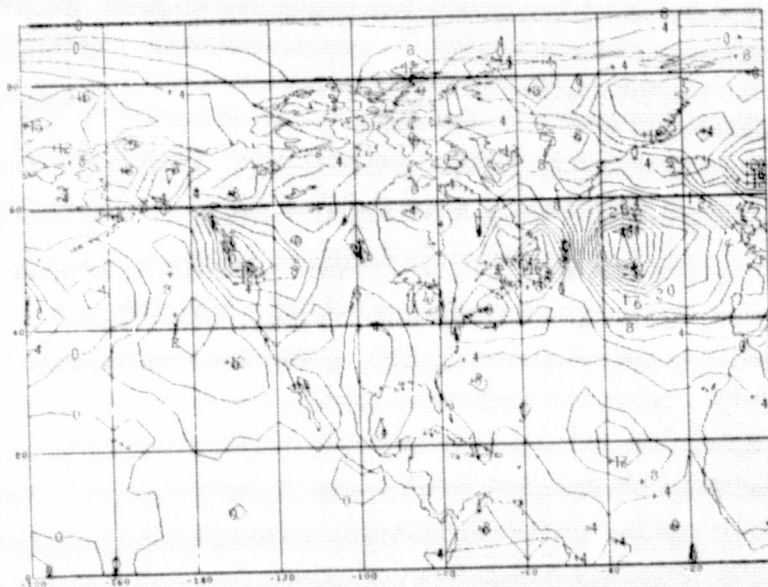


Figure 26b. 72-Hour  
SAT Error Map from  
February 15 00Z Initial  
Conditions.

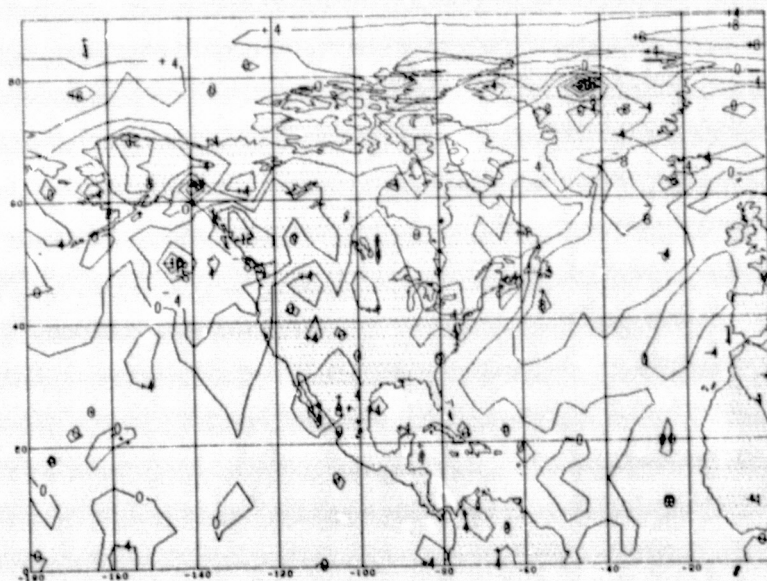


Figure 26c. 72-Hour NO  
SAT-SAT Difference Map  
from February 15 00Z  
Initial Conditions.

ORIGINAL PAGE IS  
OF POOR QUALITY

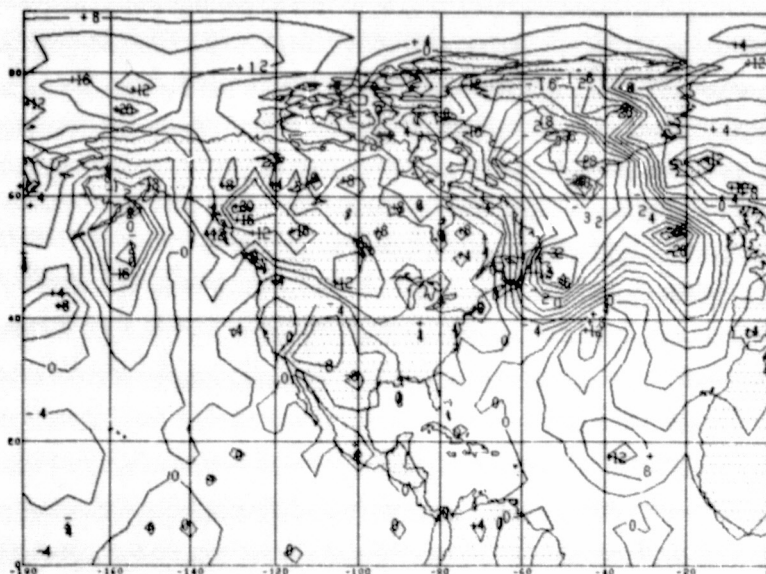


Figure 27a. 72-Hour  
Sea-Level Pressure  
NO SAT Error Map from  
February 17 00Z Initial  
Conditions.

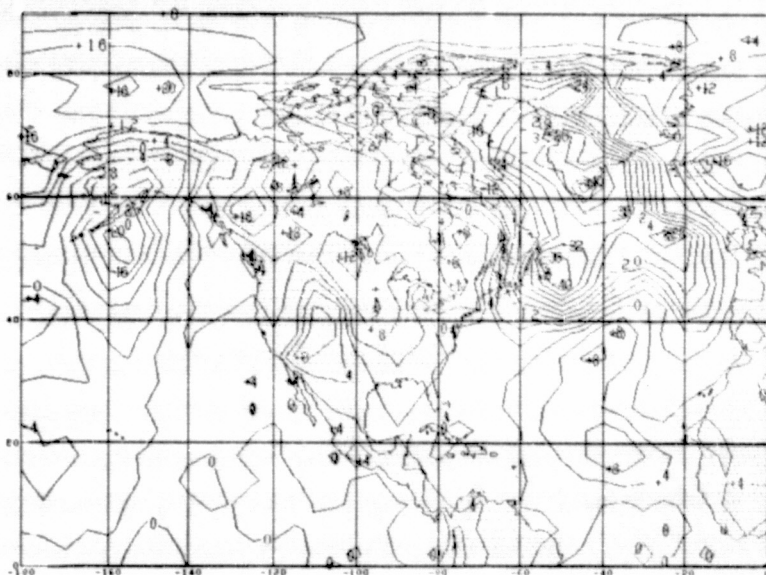


Figure 27b. 72-Hour  
SAT Error Map from  
February 17 00Z Initial  
Conditions.

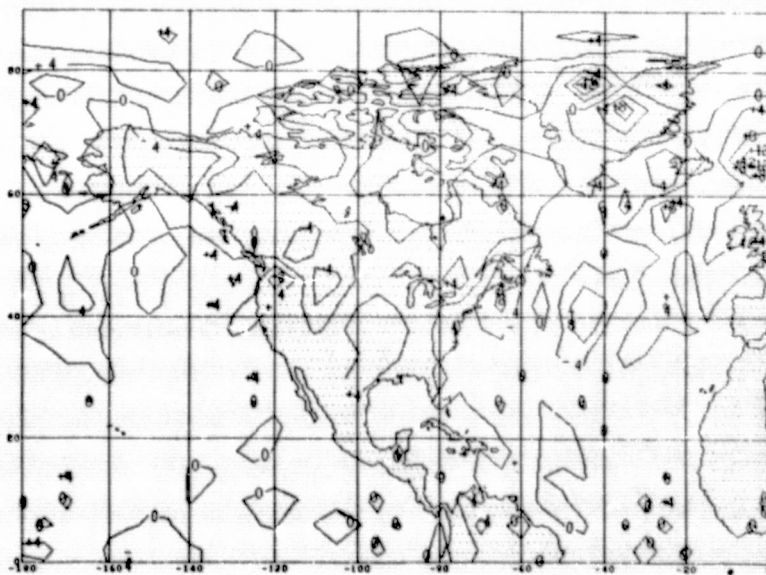
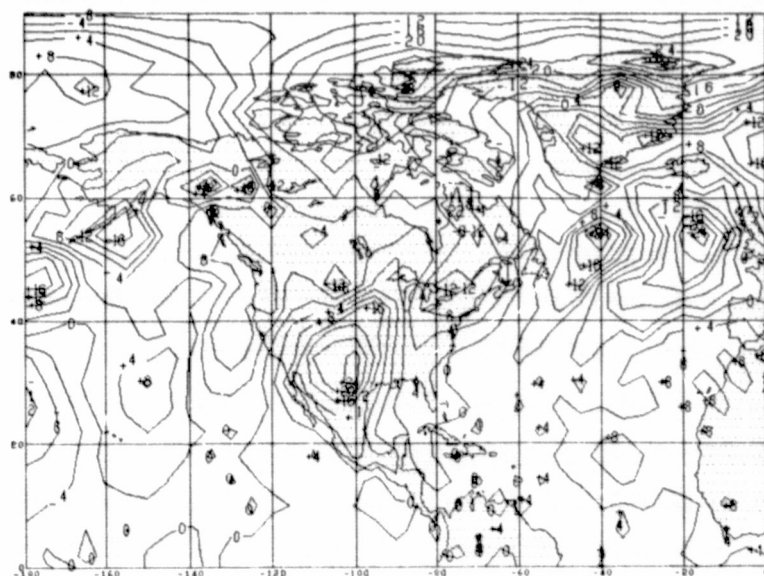
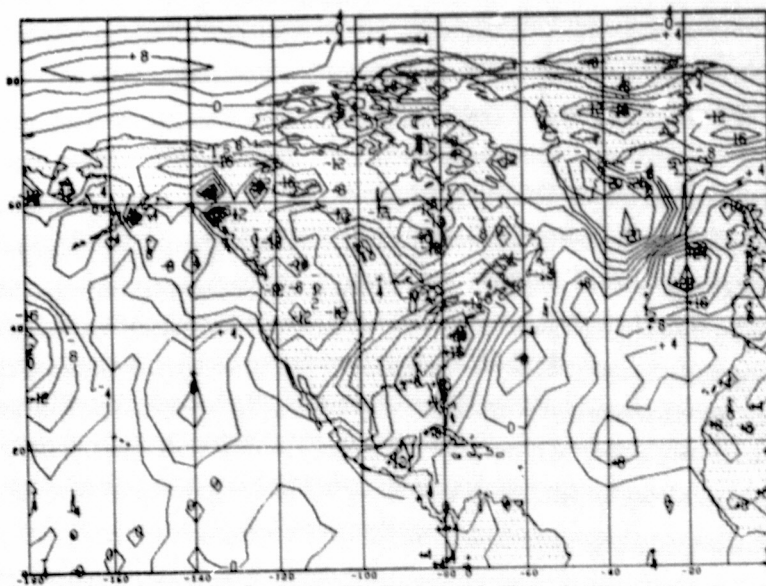


Figure 27c. 72-Hour NO  
SAT-SAT Difference Map  
from February 17 00Z  
Initial Conditions.







ORIGINAL PAGE IS  
OF POOR QUALITY

Figure 29a. 72-Hour  
Sea-Level Pressure  
NO SAT Error Map from  
February 21 00Z Initial  
Conditions.

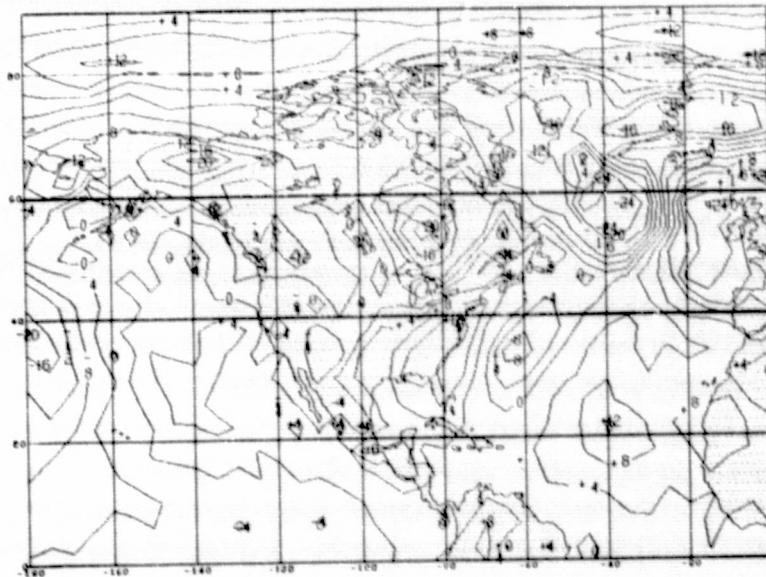


Figure 29b. 72-Hour  
SAT Error Map from  
February 21 00Z Initial  
Conditions.

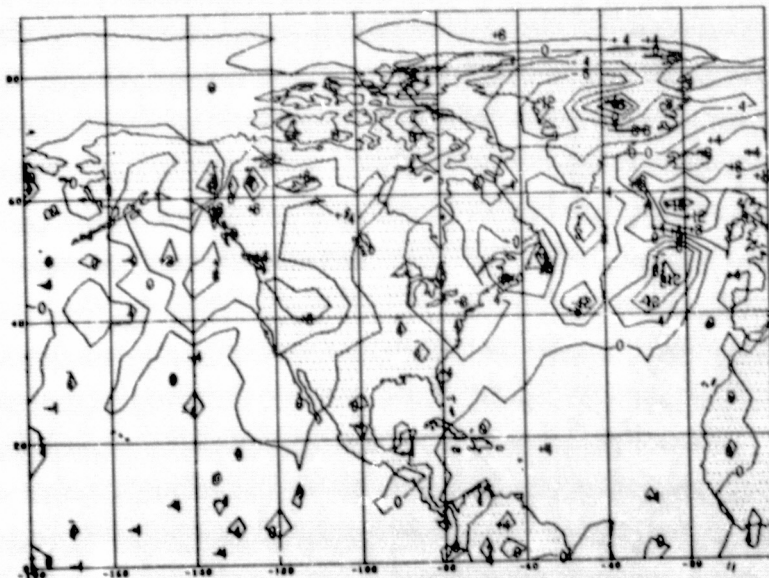
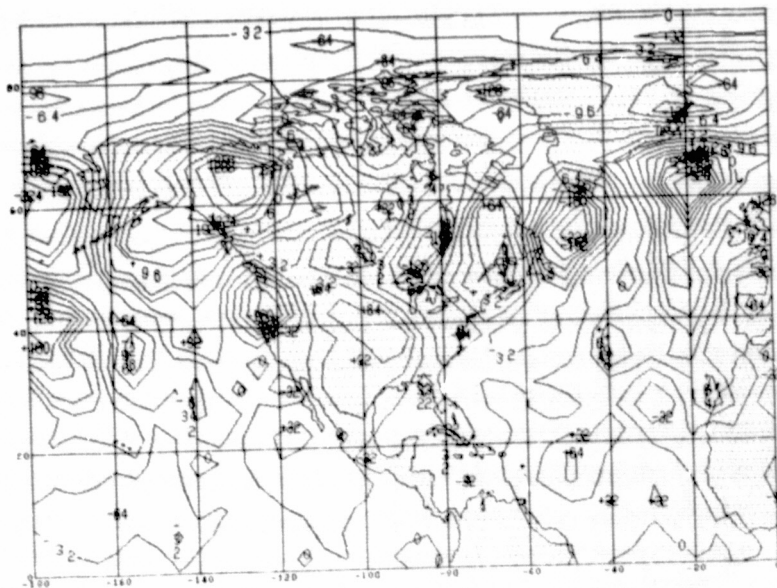


Figure 29c. 72-Hour NO  
SAT-SAT Difference Map  
from February 21 00Z  
Initial Conditions.





ORIGINAL PAGE IS  
OF POOR QUALITY

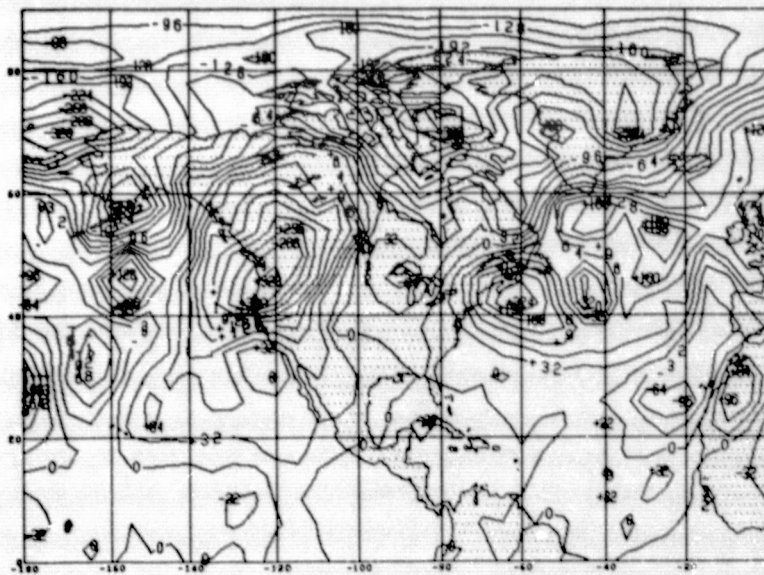


Figure 31a. 72-Hour  
500 mb NO SAT Error Map  
from February 3 00Z  
Initial Conditions.

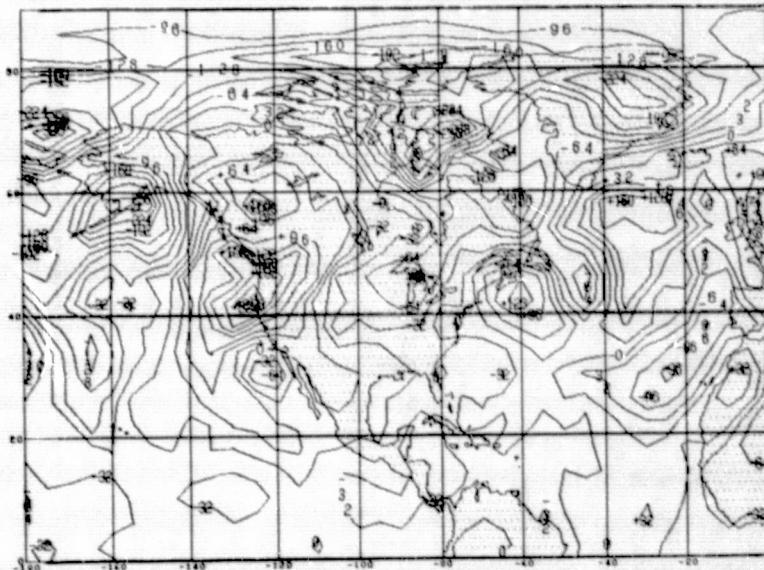


Figure 31b. 72-Hour  
SAT Error Map from  
February 3 00Z Initial  
Conditions.

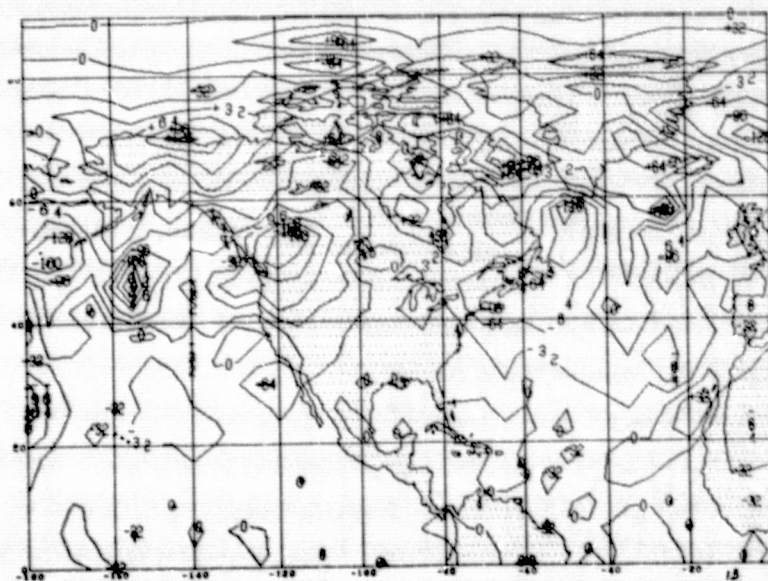


Figure 31c. 72-Hour NO  
SAT-SAT Difference Map  
from February 3 00Z  
Initial Conditions.

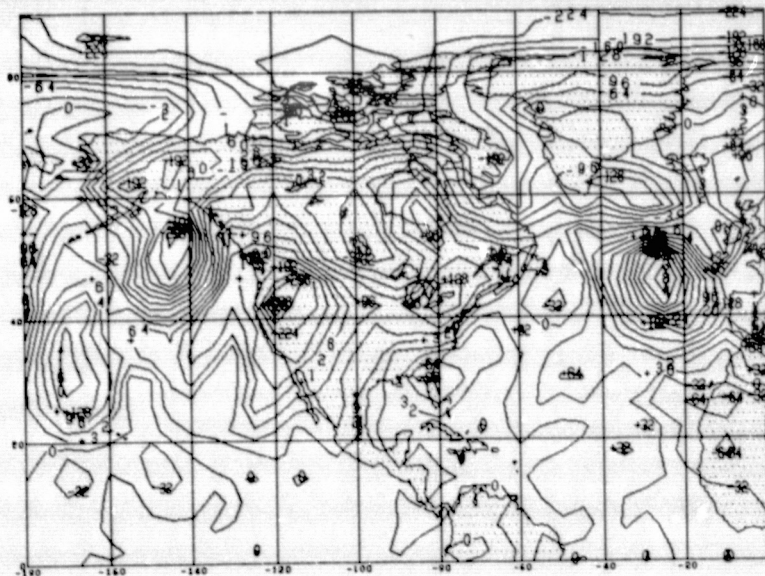


Figure 32a. 72-Hour  
500 mb NO SAT Error  
Map from February 5 00Z  
Initial Conditions.

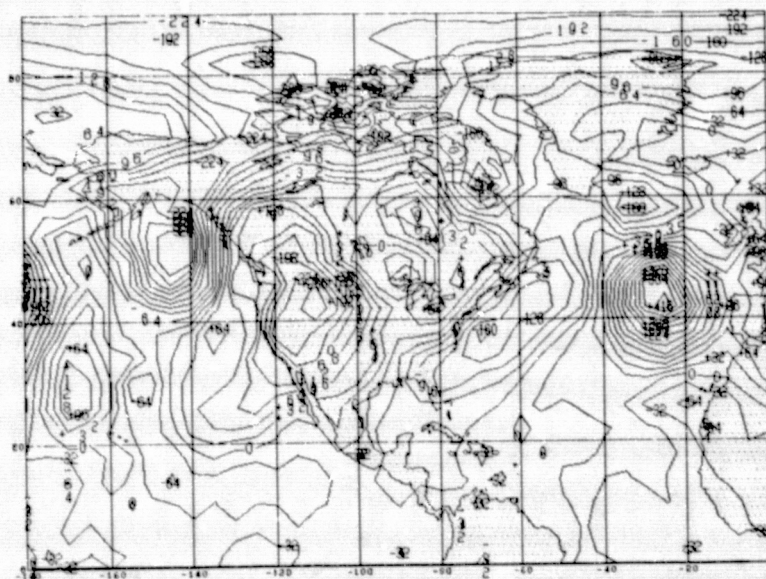


Figure 32b. 72-Hour  
SAT Error Map from  
February 5 00Z Initial  
Conditions.

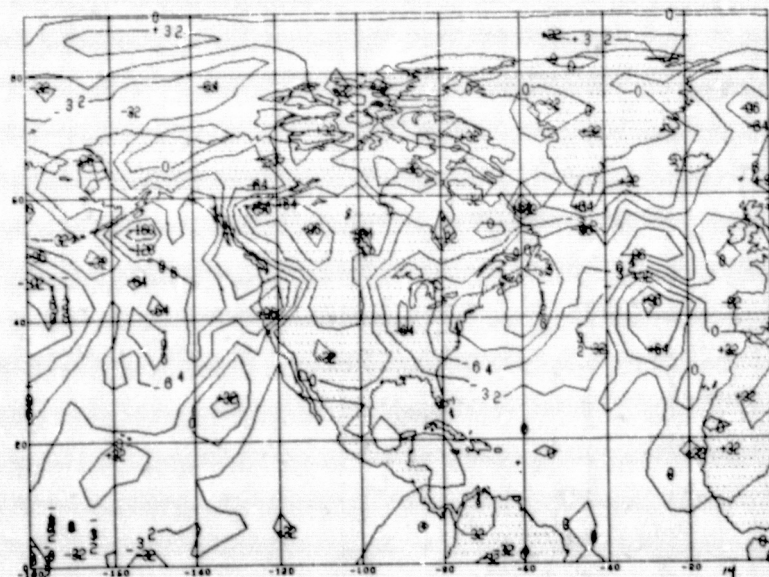


Figure 32c. 72-Hour NO  
SAT-SAT Difference Map  
from February 5 00Z  
Initial Conditions.



ORIGINAL PAGE IS  
OF POOR QUALITY

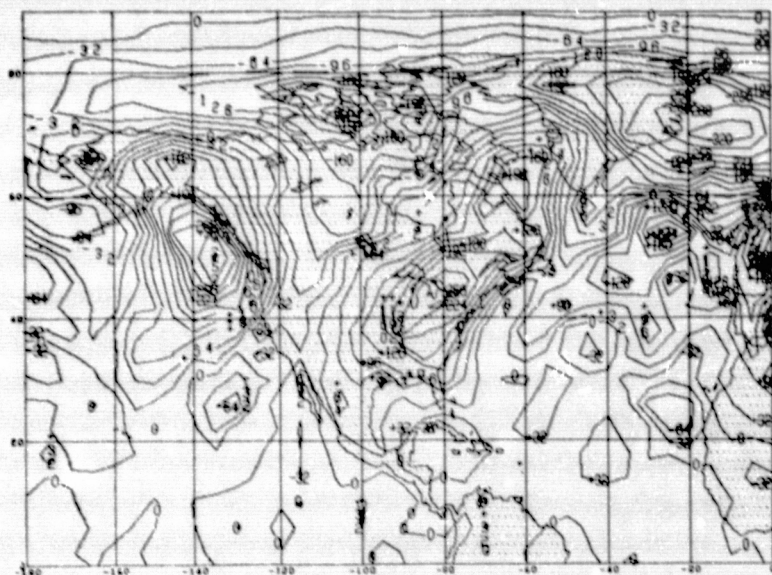


Figure 33a. 72-Hour  
500 mb NO SAT Error Map  
from February 7 00Z  
Initial Conditions.

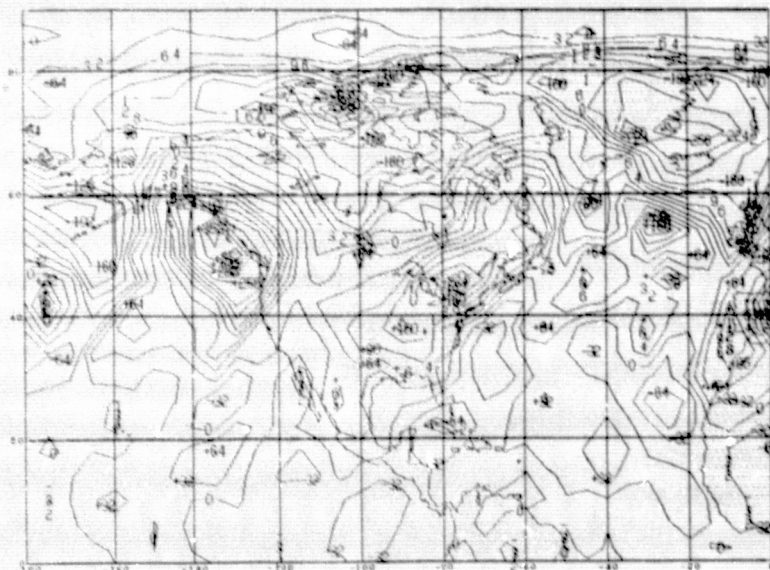


Figure 33b. 72-Hour  
SAT Error Map from  
February 7 00Z Initial  
Conditions.

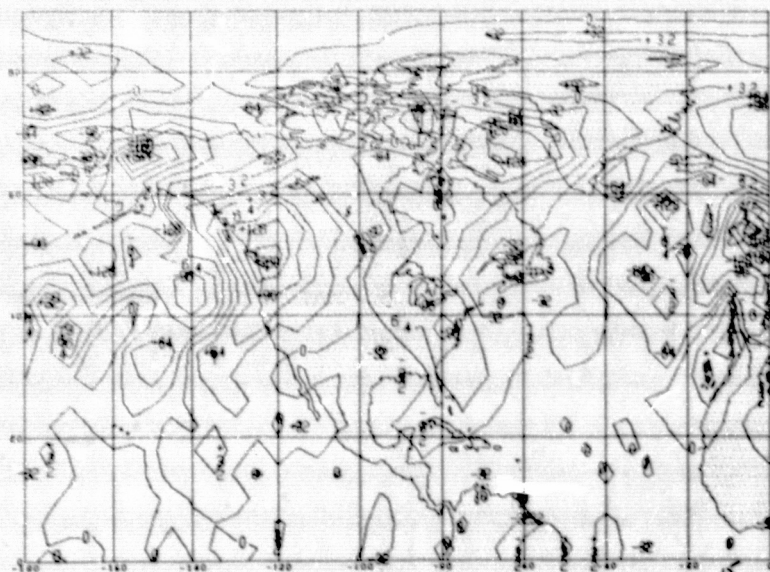


Figure 33c. 72-Hour NO  
SAT-SAT Difference Map  
from February 7 00Z  
Initial Conditions.

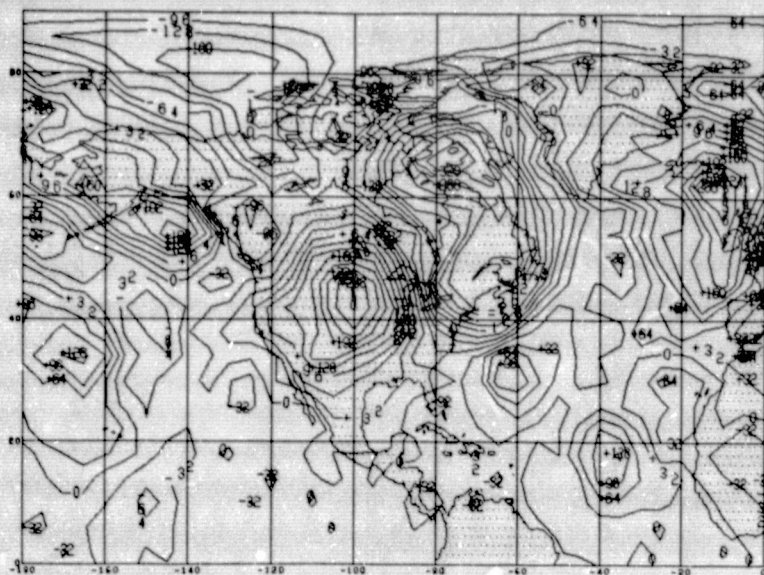


Figure 34a. 72-Hour  
500 mb NO SAT Error Map  
from February 9 00Z  
Initial Conditions.

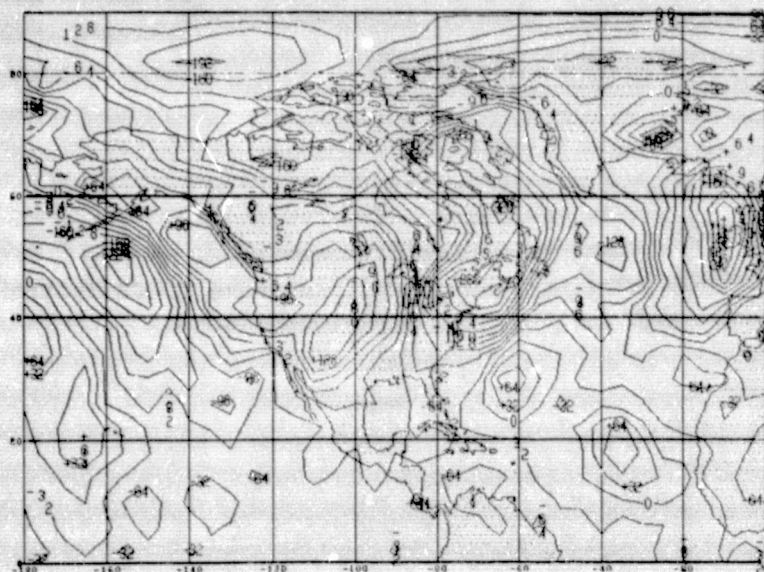


Figure 34b. 72-Hour  
SAT Error Map from  
February 9 00Z Initial  
Conditions.

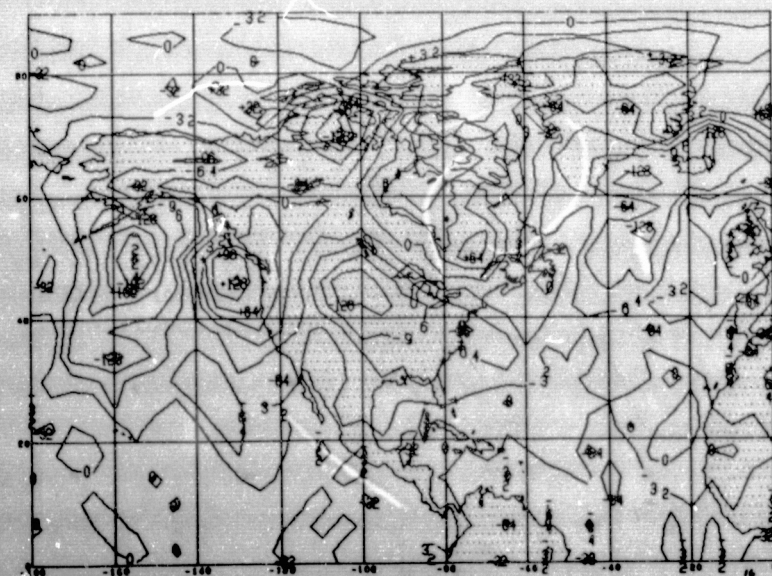
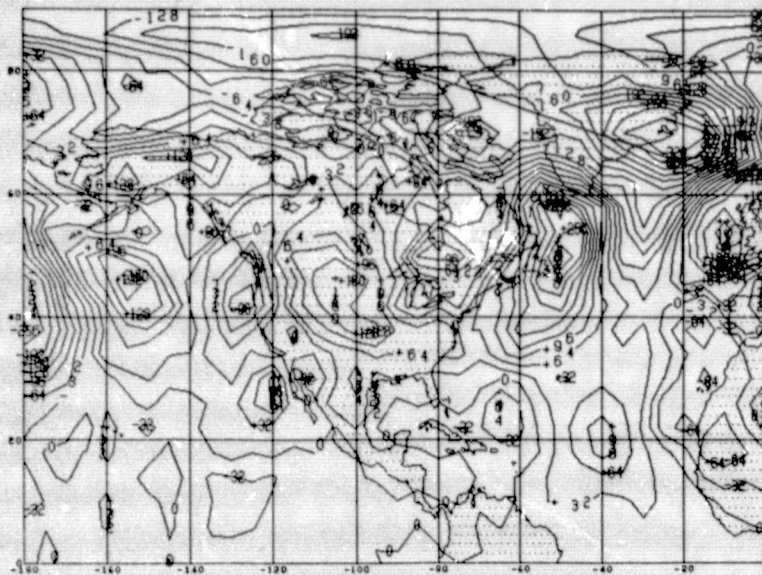


Figure 34c. 72-Hour NO  
SAT-SAT Difference Map  
from February 9 00Z  
Initial Conditions.





ORIGINAL PAGE IS  
OF POOR QUALITY

Figure 35a. 72-Hour  
500 mb NO SAT Error Map  
from February 11 00Z  
Initial Conditions.

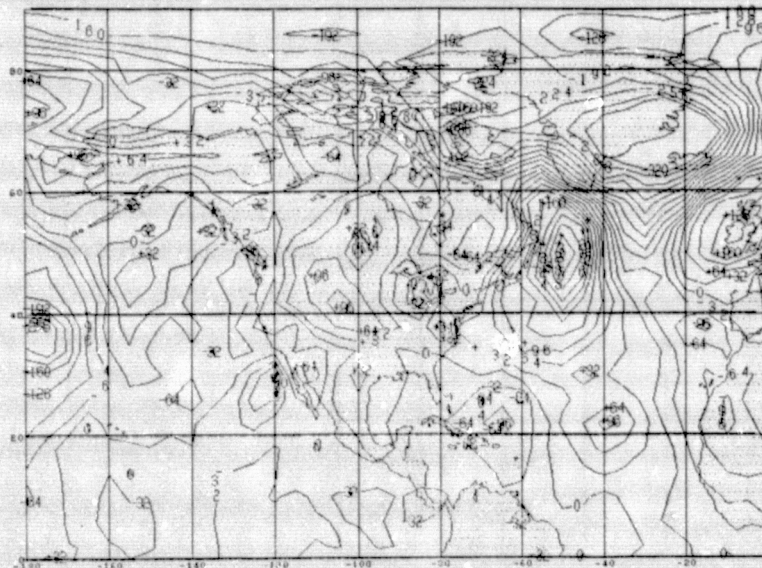


Figure 35b. 72-Hour  
SAT Error Map from  
February 11 00Z Initial  
Conditions.

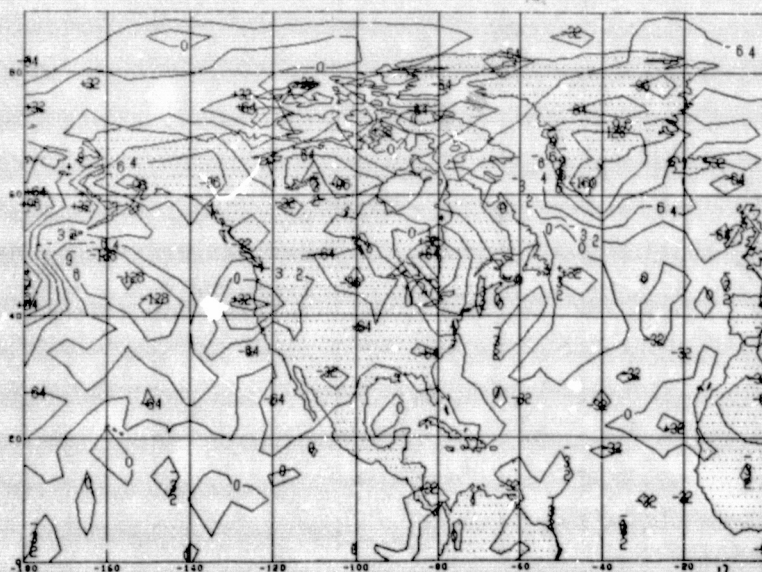


Figure 35c. 72-Hour NO  
SAT-SAT Difference Map  
from February 11 00Z  
Initial Conditions.

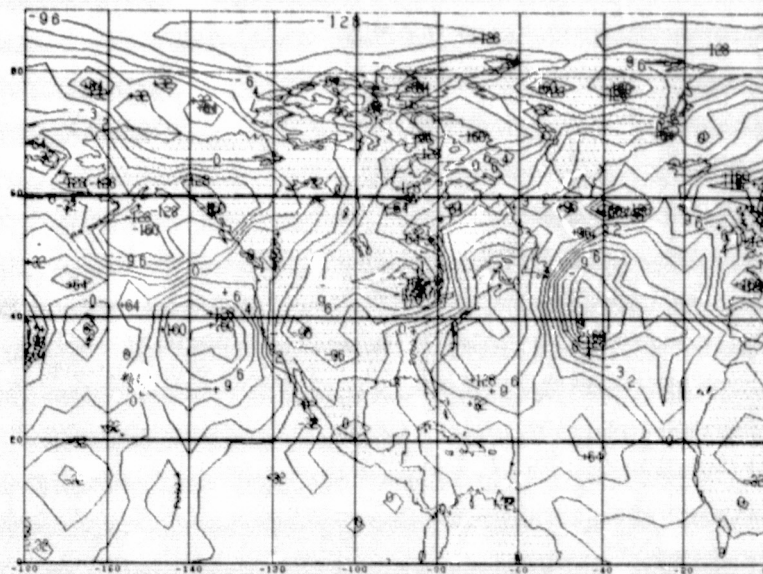


Figure 36a. 72-Hour  
500 mb NO SAT Error Map  
from February 13 00Z  
Initial Conditions.

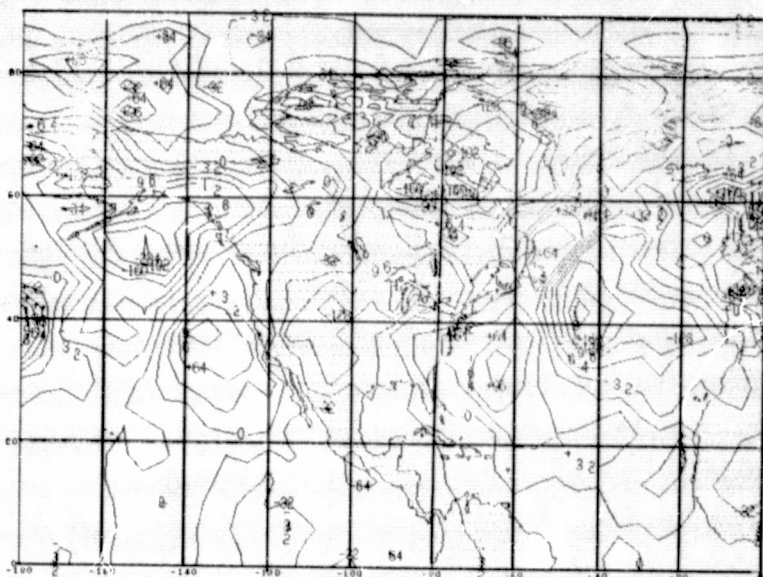


Figure 36b. 72-Hour  
SAT Error Map from  
February 13 00Z Initial  
Conditions.

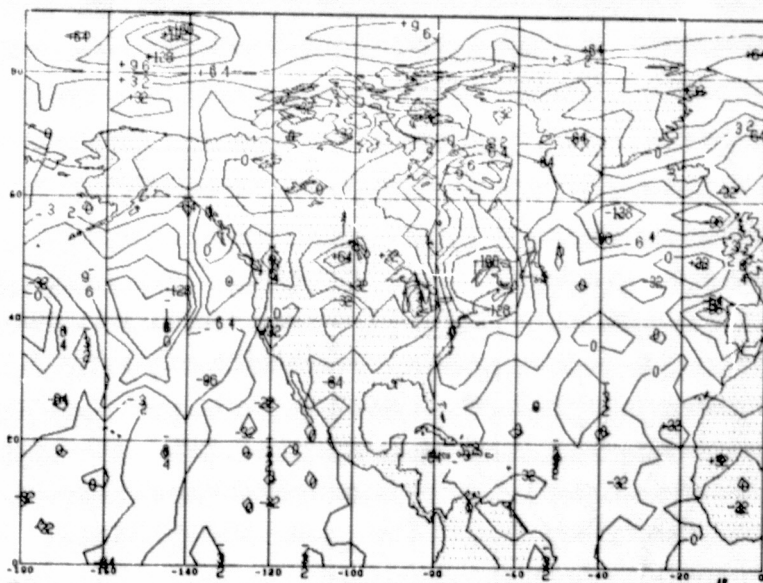


Figure 36c. 72-Hour NO  
SAT-SAT Difference Map  
from February 13 00Z  
Initial Conditions.



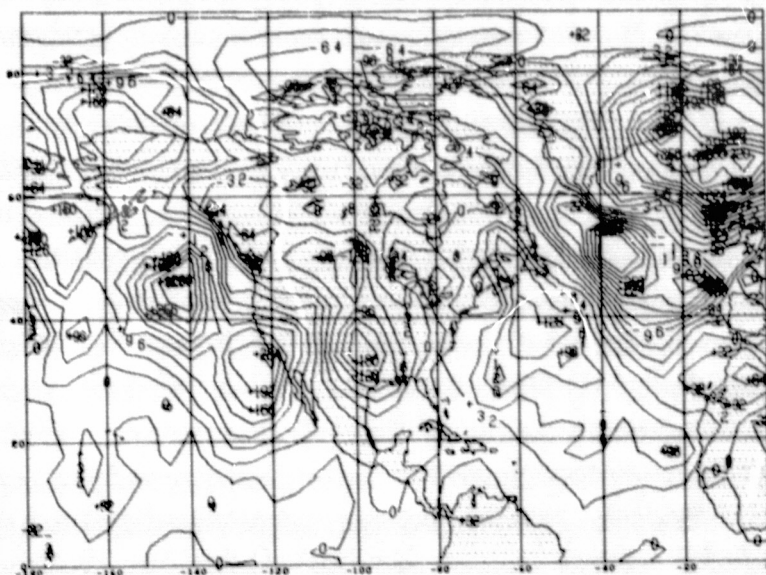


Figure 37a. 72-Hour  
500 mb NO SAT Error Map  
from February 15 00Z  
Initial Conditions.

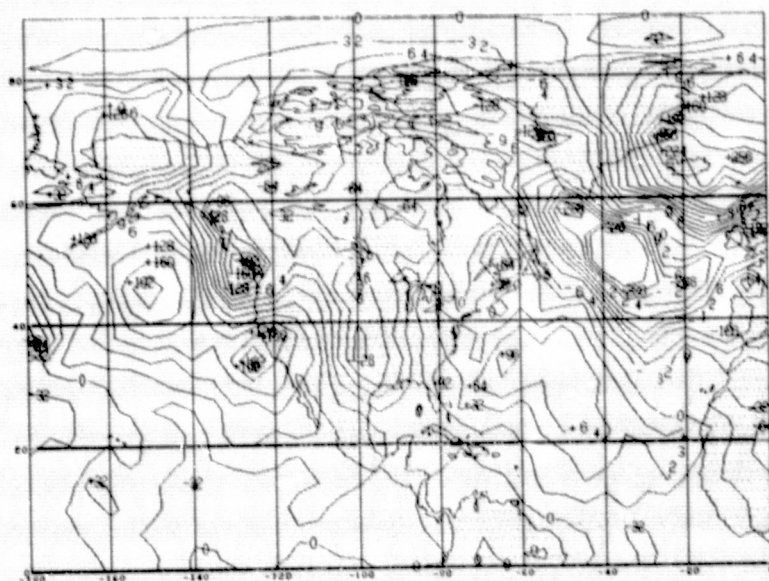


Figure 37b. 72-Hour  
SAT Error Map from  
February 15 00Z Initial  
Conditions.

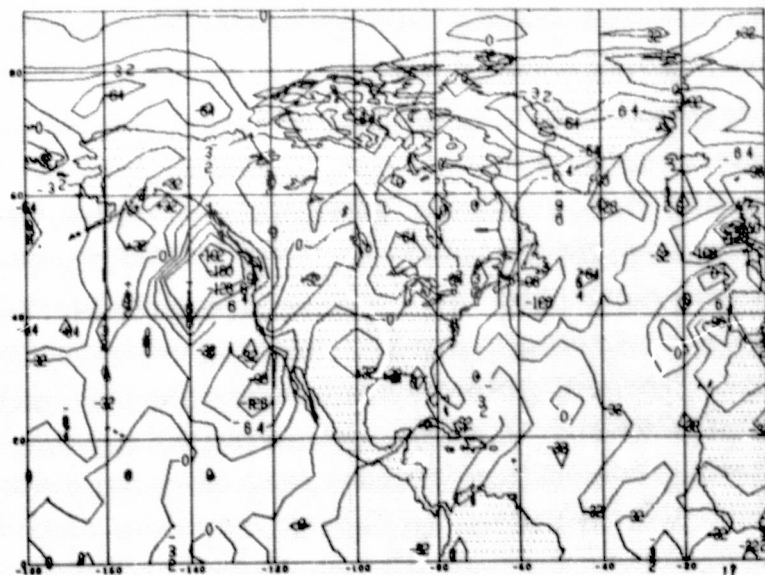


Figure 37c. 72-Hour NO  
SAT-SAT Difference Map  
from February 15 00Z  
Initial Conditions.

ORIGINAL PAGE IS  
OF POOR QUALITY

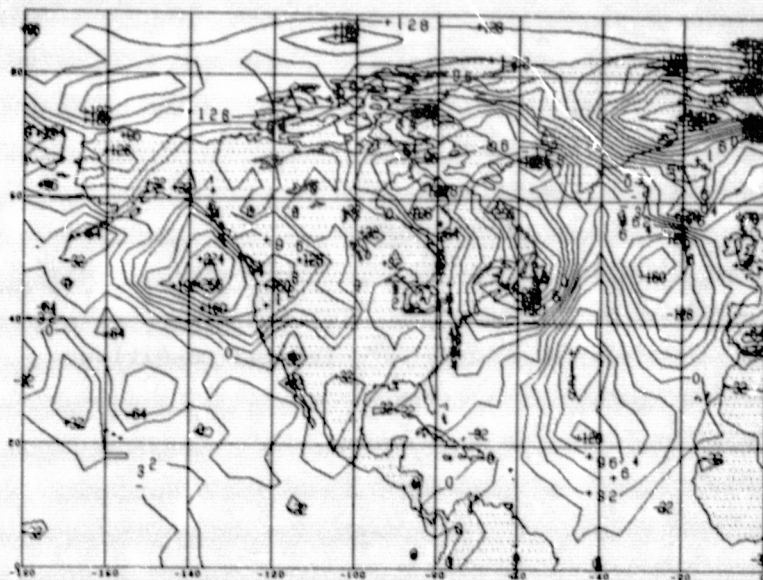


Figure 38a. 72-Hour  
500 mb NO SAT Error Map  
from February 17 00Z  
Initial Conditions.

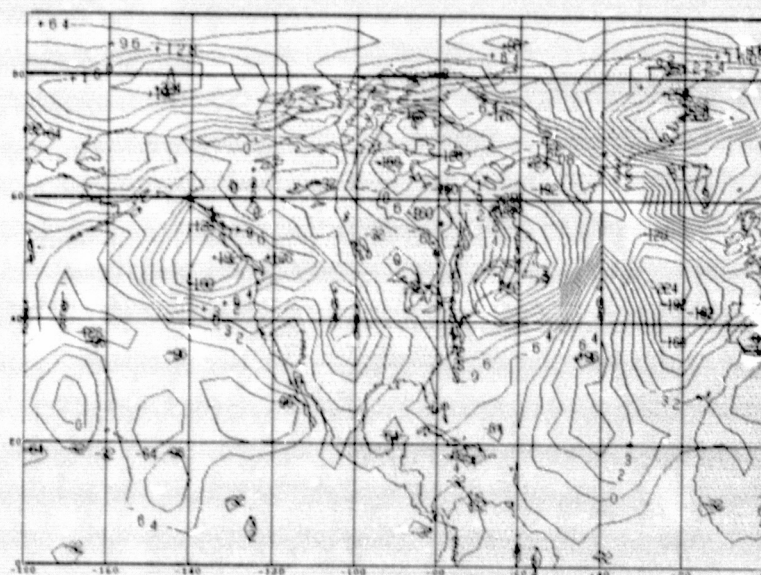


Figure 38b. 72-Hour  
SAT Error Map from  
February 17 00Z Initial  
Conditions.

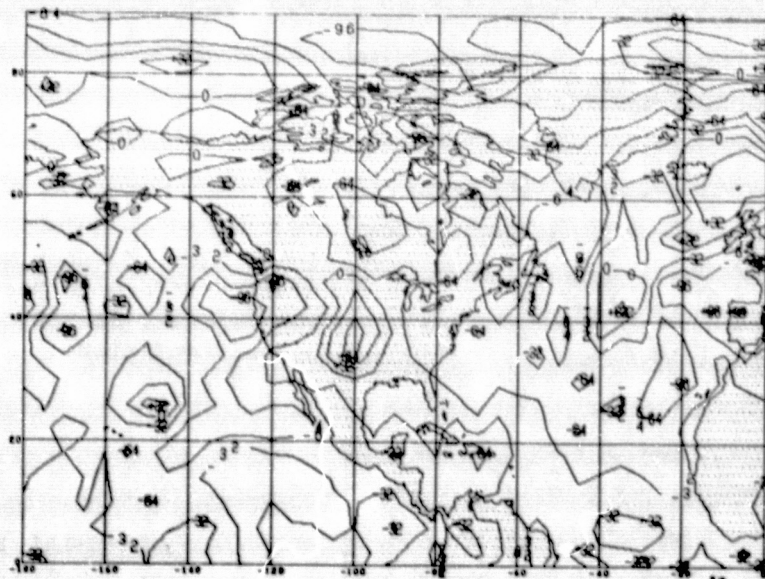


Figure 38c. 72-Hour NO  
SAT-SAT Difference Map  
from February 17 00Z  
Initial Conditions.



ORIGINAL PAGE IS  
OF POOR QUALITY

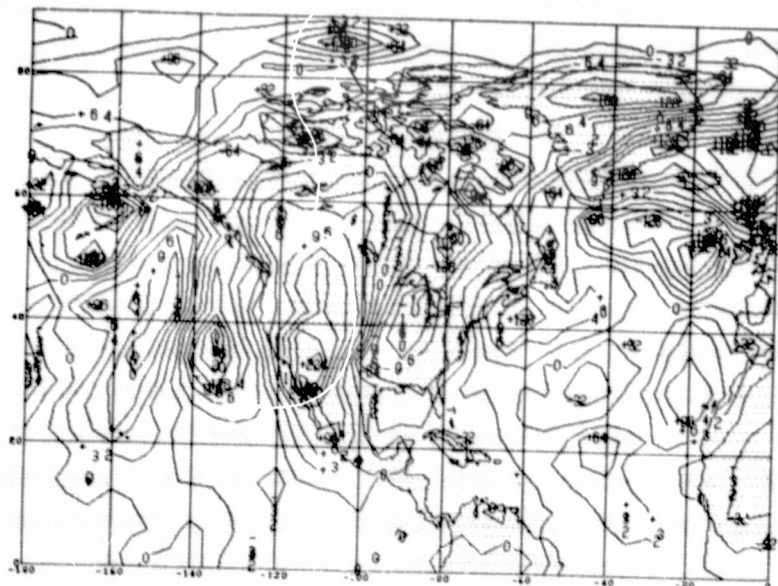


Figure 39a. 72-Hour  
500 mb NO SAT Error Map  
from February 19 00Z  
Initial Conditions.

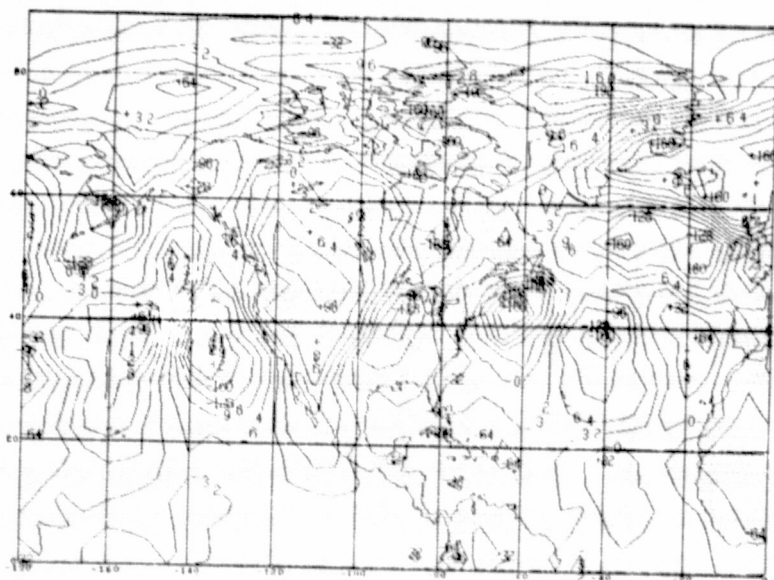


Figure 39b. 72-Hour  
SAT Error Map from  
February 19 00Z Initial  
Conditions.

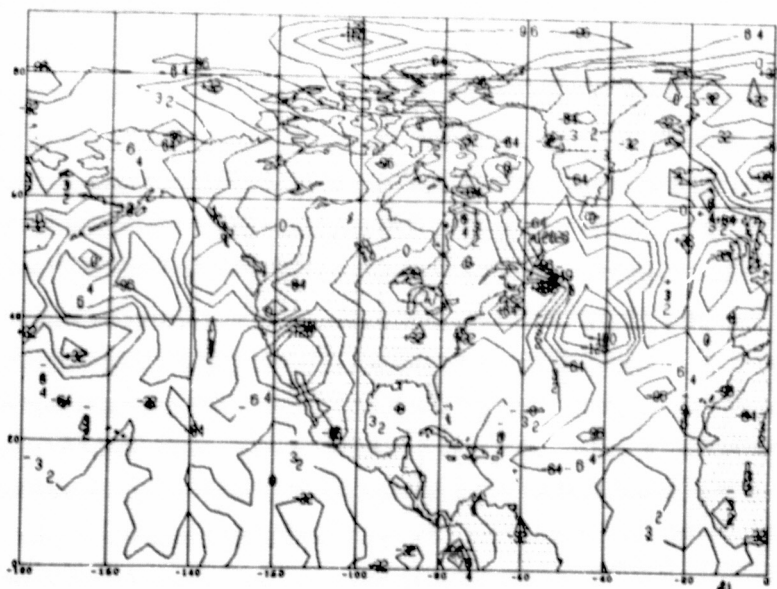


Figure 39c. 72-Hour NO  
SAT-SAT Difference Map  
from February 19 00Z  
Initial Conditions.

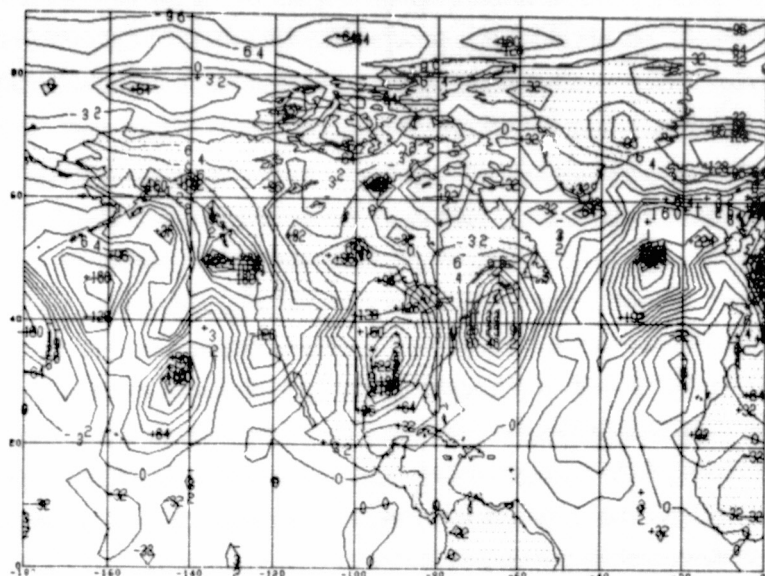


Table 5. Summary of Regional 72-hr Forecast Impacts\*  
Over North America

A) Sea Level Pressure

Forecast from	Beneficial Impacts (in mb)	Percent Correction of error	Negative Impacts (in mb)
Feb 1	+12	60%	
3	+ 8	40%	-12
3	+16	80%	
5			
7	+16	67%	- 8
9	+16	57%	-16
9	+ 8	50%	
11	+12	46%	
13	+ 8	50%	
19	+ 8	100%	
21	+ 8	67%	

B) 500mb

Forecast from	Beneficial Impacts (in mb)	Percent Correction of error	Negative Impacts (in meters)
Feb 1			
3	+160	56%	-96
5	+ 96	50%	
7			
9	+128	50%	-160
11	+ 96	60%	
13	+ 96	75%	
19	+128	57%	
21	+ 96	38%	

\*Only Impacts of 8mb or larger at sea-level or 96 meters  
or larger at 500mb have been included.

GEOPOTENTIAL HEIGHT SURFACE

500 M B UNSMOOTHED

NO SAT

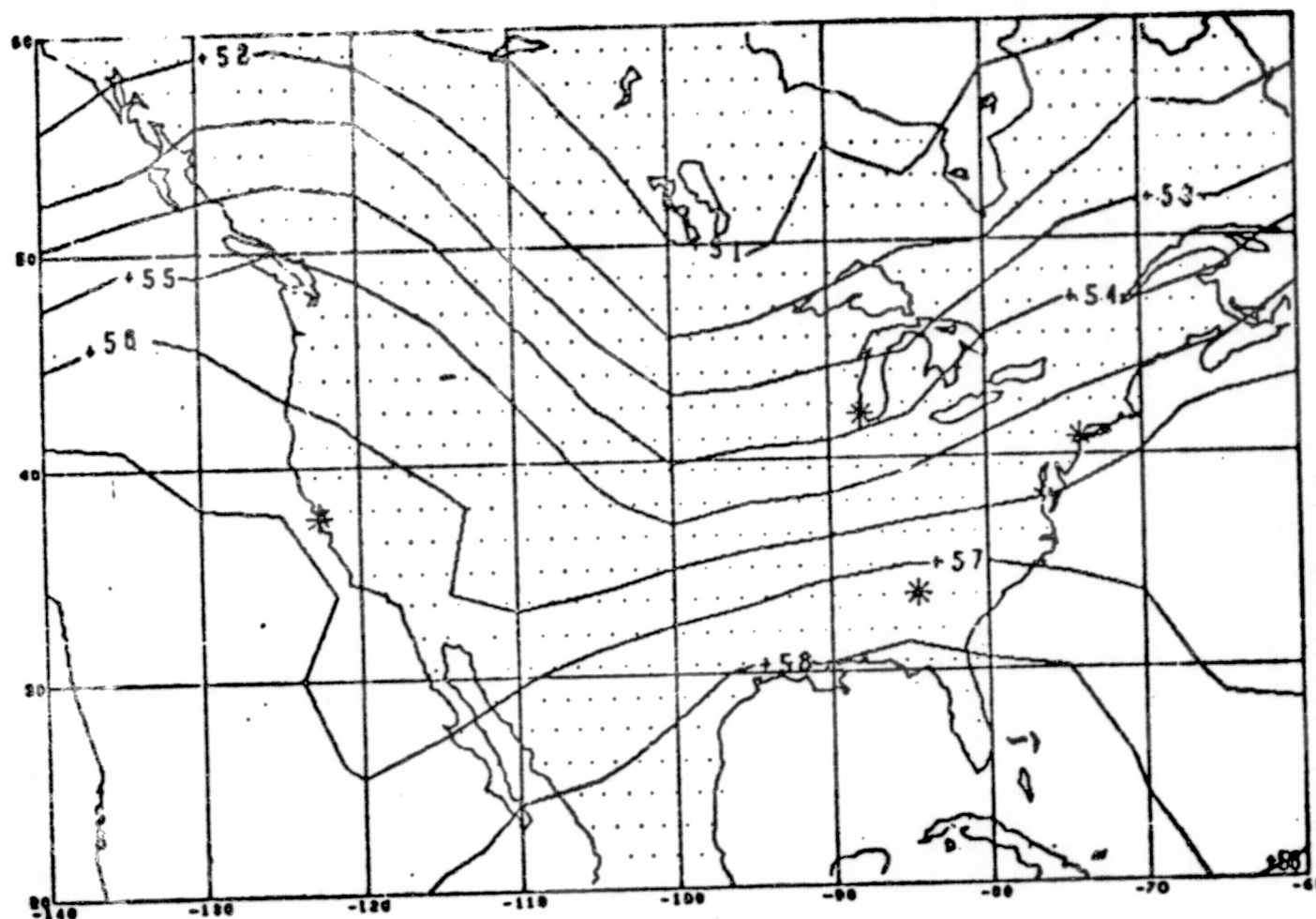


Figure 41

DAY 1201

HOUR 0.0

VALUES RANGE BETWEEN 49.00 AND 59.27

FOR CONTOUR INTERVALS OF 1.0

VERSION C DATE 05/17/76



GEOPOTENTIAL HEIGHT SURFACE

500 M B UNSMOOTHED

2 SATS

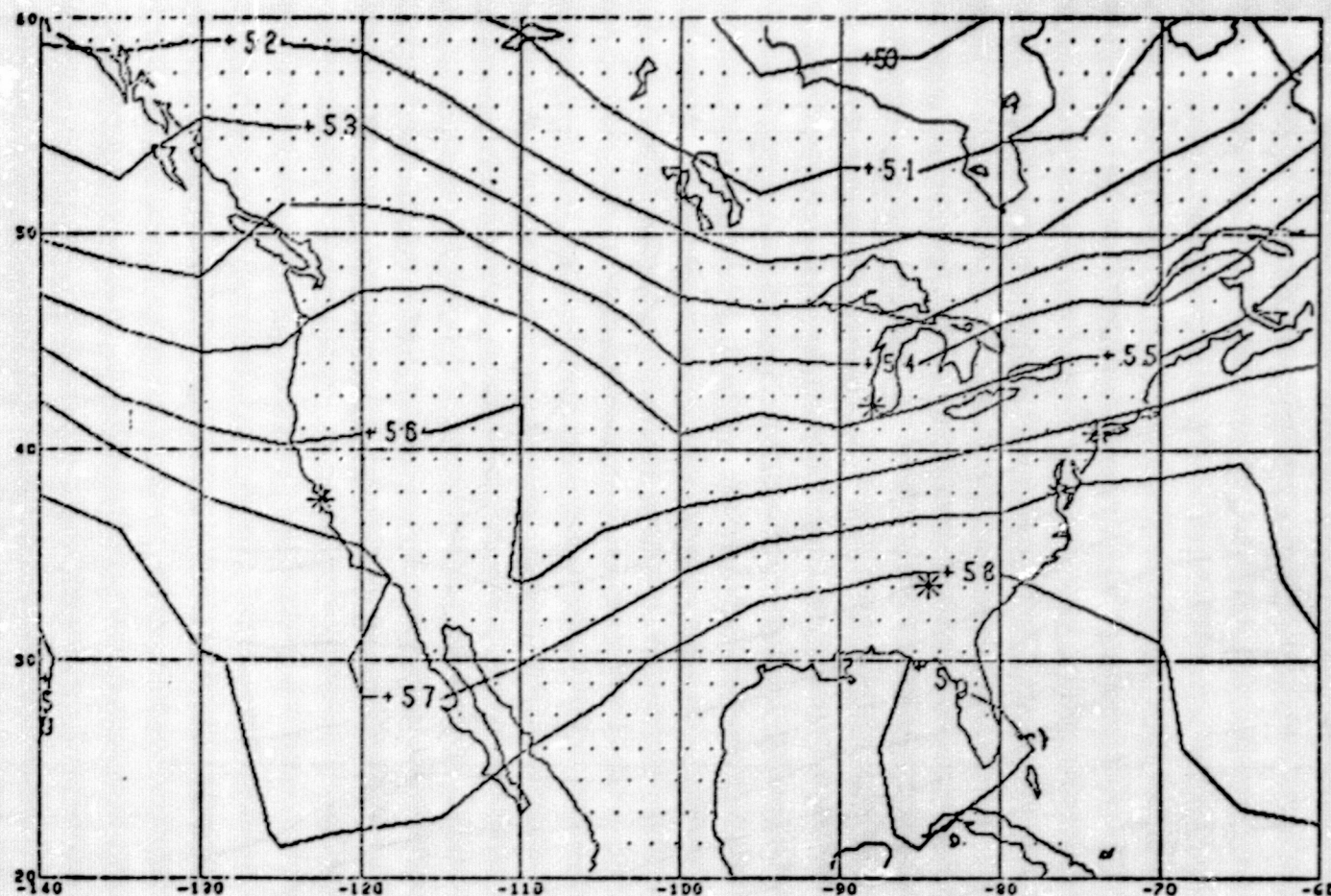


Figure 42

DAY 1201

HOUR 0.0

VALUES REFER TO 1000 FT 50.00 50.42

1000 CONTOUR INTERVALS OF 1.0

GEOPOTENTIAL HEIGHT SURFACE

ORIGINAL PAGE IS  
OF POOR QUALITY

5-73

GEOPOTENTIAL HEIGHT SURFACE

500 M B UNSMOOTHED

# ANALYSIS

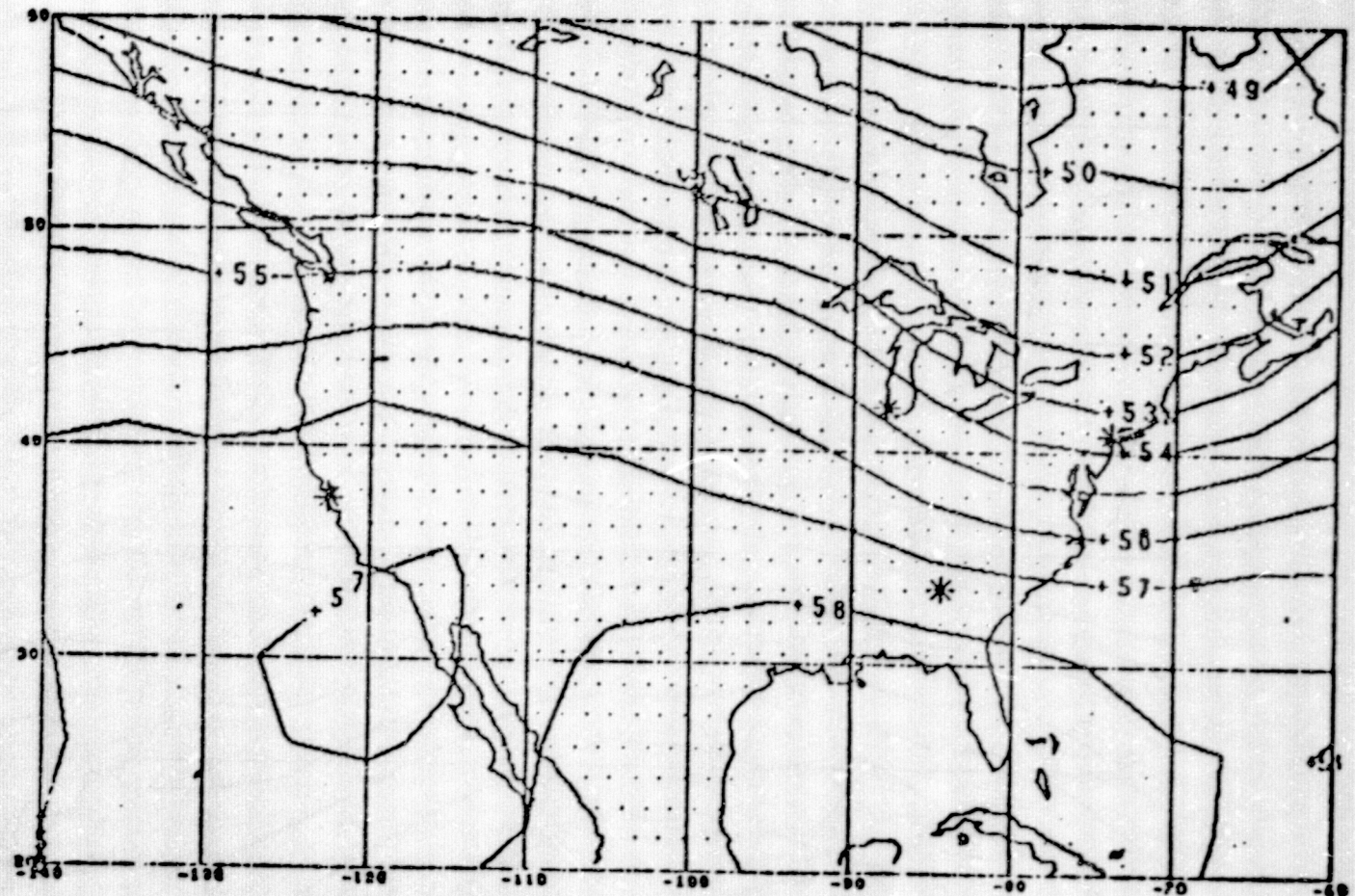


Figure 43

DAY 1201

HOUR 0.0

VALUES RANGE BETWEEN 47.00 AND 59.19

FOR CONTOUR INTERVALS OF 1.0

VERSION 2 DATE 02/01/76



GEOPOTENTIAL HEIGHT SURFACE 500 M B UNSMOOTHED  
NO SAT

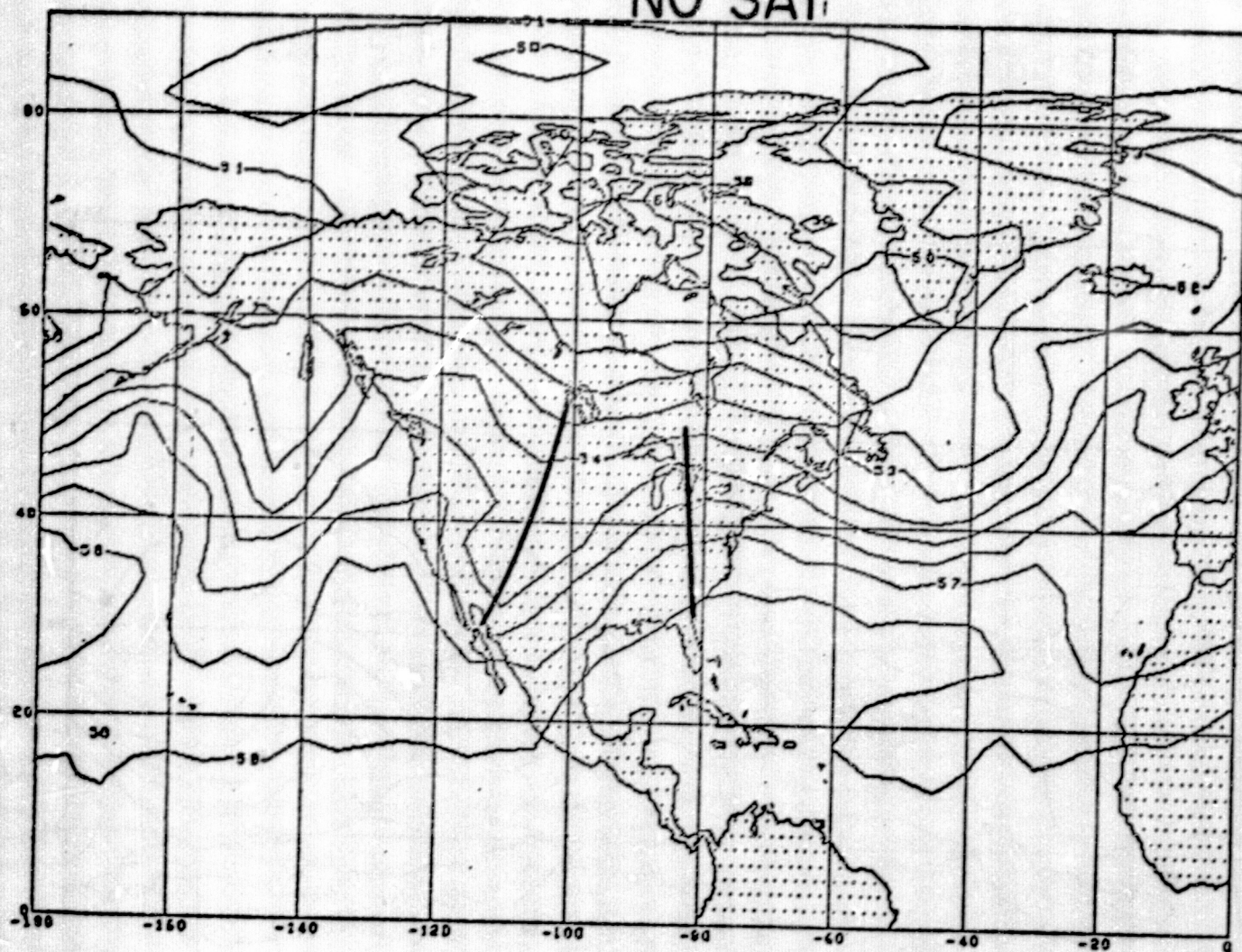


Figure 44

DAY 1211

HOUR 0.0

VALUES RANGE BETWEEN 50.00 AND 58.98

FOR CONTOUR INTERVALS OF 1.0

SECTION 4 DATE 01/19/76

ORIGINAL PAGE IS  
OF POOR QUALITY

GEOPOTENTIAL HEIGHT SURFACE

500 M B UNSMOOTHED

2 SATS

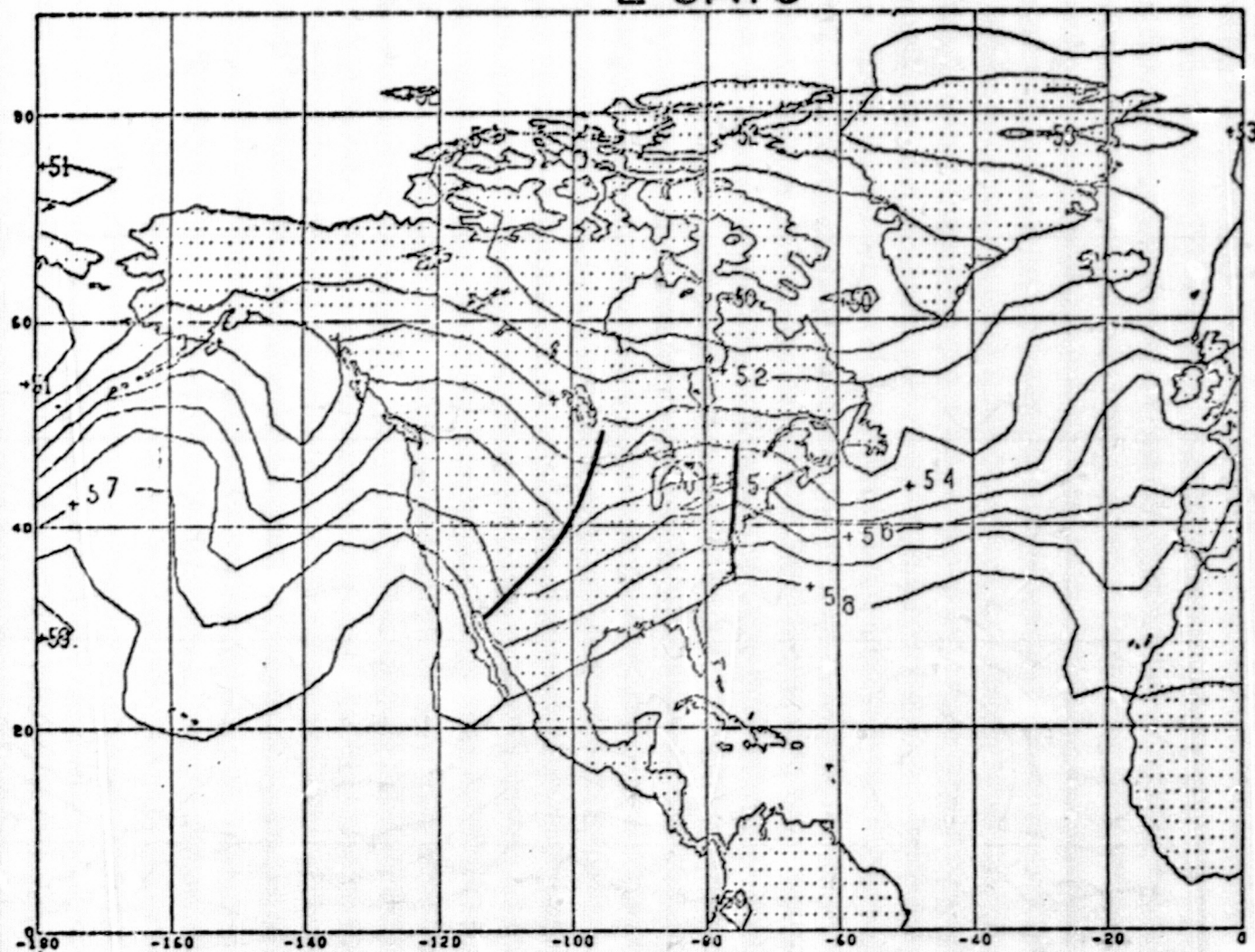


Figure 45

DAY 1211

HOUR 0.0

VALUES RANGE BETWEEN 50.00 AND 59.41

FOR COMPARISON INTERVALS OF 1.0



GEOPOTENTIAL HEIGHT SURFACE

500 M B UNSMOOTHED

ANALYSIS

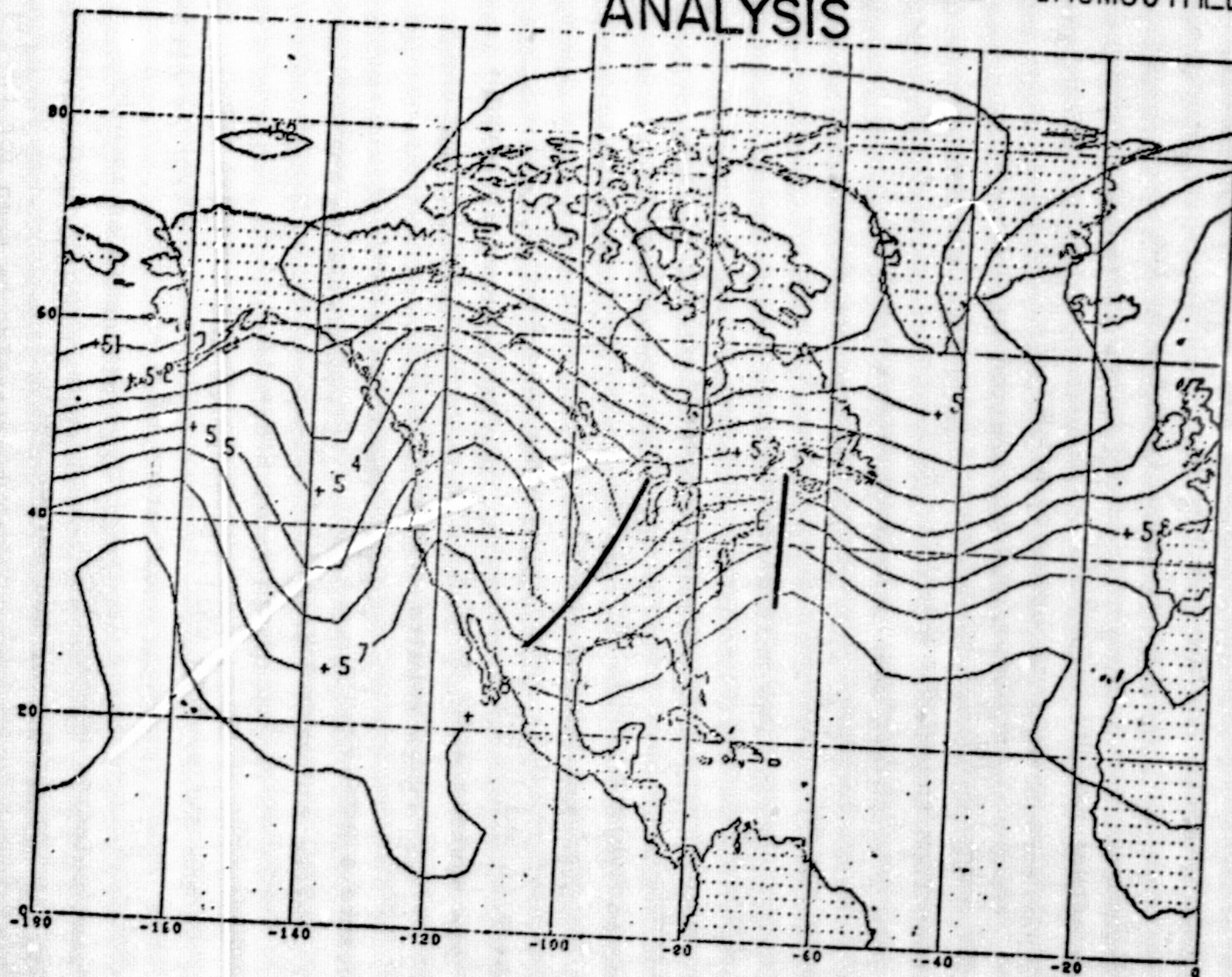


Figure 46

DAY 1211

HOUR 0.0

VALUES RANGE FROM 49.00 AND 50.20

FOR CONTOUR INTERVALS OF 1.0

UNIT: GEOPOTENTIAL HEIGHT

ORIGINAL PAGE IS  
OF POOR QUALITY

5-77

## 5.5 IMPACT OF SATELLITE DATA ON ACTUAL WEATHER FORECASTS

The ultimate objective in the evaluation of the impact of satellite data is to determine what it means in terms of the accuracy of the actual weather predictions that might be issued by a local weather forecaster. In order to assess this impact, the computerized forecasting model (CFM) was applied to the direct prognostic output from the GISS model for the DST-6 period. CFM local precipitation forecasts were generated from the eleven test periods for both the SAT and NO SAT systems for 128 cities uniformly distributed over the United States.

Comparisons of city precipitation forecasts for these cities are presented in Table 6. The total number of correct precipitation forecasts for the SAT and NO SAT systems are shown only for those cases in which the two systems gave rise to different forecasts. The systems differed over all cities in about 10 percent of all forecasts and these results cover cases when at least one system forecasts a precipitation event. The total number of different forecasts for each day is shown for 128 cities in the lower horizontal row. In 24 and 48 hours there is a 12 percent improvement in the SAT system, while in 72 hours the forecast improvement was 19 percent. Upon examination of a separate list of cities in the midwest selected because they are not influenced as much by coastal effects, mountains, or the warmer gulf convective systems, better than a two to one improvement in forecasting is seen for the 24 and 72 hours and a surprising eleven-fold improvement in 48 hours.

Table 6

## CITY PRECIPITATION FORECAST

	<u>24 HR</u>		<u>48 HR</u>		<u>72 HR</u>	
	"SAT" BETTER	"NO SAT" BETTER	"SAT" BETTER	"NO SAT" BETTER	"SAT" BETTER	"NO SAT" BETTER
MID WEST (17)	11	4	11	1	7	3
ALL US CITIES (128)	82	64	68	53	85	58

Daily examination of city forecast accuracies, as shown in Table 7 for specific forecasts such as those on February 9 or February 19, show major improvements in the 48 and 72 hour precipitation forecasts. Only on February 15 does a serious negative impact occur in 72 hours. This indicates that the increased accuracies in skill scores on a daily basis correlate well with improvements in local weather forecasts. However, such improvements can even occur in modest skill score impacts.

## 5.6 CONCLUSIONS AND RECOMMENDATIONS (R. Atlas and M. Halem)

The impact of satellite derived temperature measurements on medium-range (one to three day) weather forecasting was evaluated for eleven forecasts over a three-week winter period with regard to the following criteria:

- (1) Magnitudes and locations of initial-state differences in the analyzed fields produced with and without satellite data;
- (2) Statistical measures of forecast accuracy (i.e., SI-skill scores and rms errors) obtained from numerical integrations starting from these initial states prepared with and without satellite data;
- (3) Subjective comparisons of the usefulness and accuracy of prognostic charts generated from these initial states;
- (4) Verifications of precipitation forecasts as might be issued in local forecast operations based on forecast outputs with and without satellite data.

Table 7

## PRECIPITATION FORECAST OVER 128 CITIES

WINTER 1976

<u>DATE</u>	48 HOUR FORECASTS		72 HOUR FORECASTS	
	<u>'NO SAT'</u> <u>BETTER</u>	<u>'SAT'</u> <u>BETTER</u>	<u>'NO SAT'</u> <u>BETTER</u>	<u>'SAT'</u> <u>BETTER</u>
FEB 1	4	1	6	3
3	14	2	7	8
5	4	3	5	7
7	7	6	4	7
9	2	18	8	17
11	5	13	0	3
13	0	4	3	5
15	7	10	16	8
17	6	4	3	5
19	2	5	3	21
21	2	2	3	1
TOTALS	53	68	58	85

The impact was assessed for a combination of operational and experimental temperature sounders providing continuous coverage from two satellites, NOAA 4 and Nimbus 6. The impact of sounding data was found to be beneficial but modest for all the criteria listed above for the limited sample of cases examined in this study. Over the data-sparse regions, the magnitudes of the initial-state differences from day to day were generally large (90-120 meters in the 500-mb heights), while the average impact in skill scores and rms errors showed a 5-10 percent statistical improvement resulting from satellite data. The prognostic charts used in the precipitation forecasts showed many examples of better verifications of sea-level pressure and 500-mb heights. Actual precipitation forecasts made for specific cities were more favorable in 15 percent of the cases in which the forecasts for the two systems were substantially different. In particular, over the mid-west there was a striking improvement in precipitation forecasting.

A substantial positive impact (20 percent for SI scores and 30 percent or more for rms scores) occurred in a number of cases but a longer sequence of impact tests is needed to establish whether they are related to weather systems periodically missed in data-sparse regions. Furthermore, the experiments also confirm earlier simulation studies reported by GISS that soundings from a two-satellite system providing nearly continuous 6 hour coverage will produce larger and more consistently positive impacts than a single-satellite sounding system with twelve hour coverage.



The findings in this experiment are based on the global DST-data sets that have been jointly collected and processed by NOAA and NASA in a quasi-operational real-time test mode. The assimilation techniques developed and employed by GISS for this systems test are applicable operational forecasting practices. If these procedures were introduced into operational forecasting today, satellite sounding data of this quality and coverage might yield improvements of similar magnitudes.

The major limitations of this study have been the small number of cases studied and the inaccuracies of the forecast model. In order to rectify this situation additional cases are currently being generated and will be evaluated when available. In addition, the entire sample of cases will be re-evaluated utilizing the ultrafine version of the GISS model.

Additional modification to our evaluation systems are also being made. These include:

- (1) Statistical measures of the variance and eddy energy of analyses produced with and without the inclusion of satellite data;
- (2) Extension of the predictive capabilities of the CFM to include surface temperature change, convective precipitation, and quantitative precipitation amounts.